frontiers | Research Topics

Managing deep-sea and open ocean ecosystems at ocean basin scale, volume II

Edited by
J. Murray Roberts, Ellen Kenchington, Telmo Morato, Albertus J. Smit, Jose Angel Alvarez Perez and Stefán Áki Ragnarsson

Published in
Frontiers in Marine Science

ISSN 1664-8714
ISBN 978-2-8325-6312-0
DOI 10.3389/978-2-8325-6312-0

About Frontiers

Frontiers is more than just an open access publisher of scholarly articles: it is a pioneering approach to the world of academia, radically improving the way scholarly research is managed. The grand vision of Frontiers is a world where all people have an equal opportunity to seek, share and generate knowledge. Frontiers provides immediate and permanent online open access to all its publications, but this alone is not enough to realize our grand goals.

Frontiers journal series

The Frontiers journal series is a multi-tier and interdisciplinary set of open-access, online journals, promising a paradigm shift from the current review, selection and dissemination processes in academic publishing. All Frontiers journals are driven by researchers for researchers; therefore, they constitute a service to the scholarly community. At the same time, the *Frontiers journal series* operates on a revolutionary invention, the tiered publishing system, initially addressing specific communities of scholars, and gradually climbing up to broader public understanding, thus serving the interests of the lay society, too.

Dedication to quality

Each Frontiers article is a landmark of the highest quality, thanks to genuinely collaborative interactions between authors and review editors, who include some of the world's best academicians. Research must be certified by peers before entering a stream of knowledge that may eventually reach the public - and shape society; therefore, Frontiers only applies the most rigorous and unbiased reviews. Frontiers revolutionizes research publishing by freely delivering the most outstanding research, evaluated with no bias from both the academic and social point of view. By applying the most advanced information technologies, Frontiers is catapulting scholarly publishing into a new generation.

What are Frontiers Research Topics?

Frontiers Research Topics are very popular trademarks of the *Frontiers journals series*: they are collections of at least ten articles, all centered on a particular subject. With their unique mix of varied contributions from Original Research to Review Articles, Frontiers Research Topics unify the most influential researchers, the latest key findings and historical advances in a hot research area.

Find out more on how to host your own Frontiers Research Topic or contribute to one as an author by contacting the Frontiers editorial office: frontiersin.org/about/contact

Managing deep-sea and open ocean ecosystems at ocean basin scale, volume II

Topic editors

J. Murray Roberts — University of Edinburgh, United Kingdom
Ellen Kenchington — Bedford Institute of Oceanography (BIO), Canada
Telmo Morato — University of the Azores, Portugal
Albertus J. Smit — University of the Western Cape, South Africa
Jose Angel Alvarez Perez — Universidade do Vale do Itajaí, Brazil
Stefán Áki Ragnarsson — Marine and Freshwater Research Institute, Iceland

Citation

Roberts, J. M., Kenchington, E., Morato, T., Smit, A. J., Perez, J. A. A., Ragnarsson, S. Á., eds. (2025). *Managing deep-sea and open ocean ecosystems at ocean basin scale, volume II*. Lausanne: Frontiers Media SA. doi: 10.3389/978-2-8325-6312-0

Table of contents

frontiers in Marine Science

ORIGINAL RESEARCH
published: 05 November 2021
doi: 10.3389/fmars.2021.721062

Biomass Mapping for an Improved Understanding of the Contribution of Cold-Water Coral Carbonate Mounds to C and N Cycling

Laurence Helene De Clippele[1], Anna-Selma van der Kaaden[2], Sandra Rosa Maier[2], Evert de Froe[3] and J. Murray Roberts[1]*

[1] Changing Oceans Research Group, School of GeoSciences, The University of Edinburgh, Edinburgh, United Kingdom, [2] Royal Netherlands Institute for Sea Research, Department of Estuarine and Delta Systems (NIOZ-Yerseke), Den Burg, Netherlands, [3] Royal Netherlands Institute for Sea Research, Department of Ocean Systems (NIOZ-Den Burg), Den Burg, Netherlands

OPEN ACCESS

Edited by:
Ashley Alun Rowden, National Institute of Water and Atmospheric Research (NIWA), New Zealand

Reviewed by:
Gustavo Fonseca, Federal University of São Paulo, Brazil
Cécile Cathalot, Institut Français de Recherche pour l'Exploitation de la Mer (IFREMER), France

***Correspondence:**
Laurence Helene De Clippele
Laurence.de.clippele@gmail.com

Specialty section:
This article was submitted to Deep-Sea Environments and Ecology, a section of the journal Frontiers in Marine Science

Received: *05 June 2021*
Accepted: *11 October 2021*
Published: *05 November 2021*

Citation:
De Clippele LH, van der Kaaden A-S, Maier SR, de Froe E and Roberts JM (2021) Biomass Mapping for an Improved Understanding of the Contribution of Cold-Water Coral Carbonate Mounds to C and N Cycling. Front. Mar. Sci. 8:721062. doi: 10.3389/fmars.2021.721062

This study used a novel approach combining biological, environmental, and ecosystem function data of the Logachev cold-water coral carbonate mound province to predictively map coral framework (bio)mass. A more accurate representation and quantification of cold-water coral reef ecosystem functions such as Carbon and Nitrogen stock and turnover were given by accounting for the spatial heterogeneity. Our results indicate that 45% is covered by dead and only 3% by live coral framework. The remaining 51%, is covered by fine sediments. It is estimated that 75,034–93,534 tons (T) of live coral framework is present in the area, of which ∼10% (7,747–9,316 T) consists of C_{inorg} and ∼1% (411–1,061 T) of C_{org}. A much larger amount of 3,485,828–4,357,435 T (60:1 dead:live ratio) dead coral framework contained ∼11% (418,299–522,892 T) C_{inorg} and <1% (0–16 T) C_{org}. The nutrient turnover by dead coral framework is the largest, contributing 45–51% (2,596–3,626 T) C year^{-1} and 30–62% (290–1,989 T) N year^{-1} to the total turnover in the area. Live coral framework turns over 1,656–2,828 T C year^{-1} and 53–286 T N year^{-1}. Sediments contribute between 1,216–1,512 T C year^{-1} and 629–919 T N year^{-1} to the area's benthic organic matter mineralization. However, this amount is likely higher as sediments baffled by coral framework might play a much more critical role in reefs CN cycling than previously assumed. Our calculations showed that the area overturns 1–3.4 times the C compared to a soft-sediment area at a similar depth. With only 5–9% of the primary productivity reaching the corals via natural deposition, this study indicated that the supply of food largely depends on local hydrodynamical food supply mechanisms and the reefs ability to retain and recycle nutrients. Climate-induced changes in primary production, local hydrodynamical food supply and the dissolution of particle-baffling coral framework could have severe implications for the survival and functioning of cold-water coral reefs.

Keywords: biomass, ecosystem functions, carbon cycle, nitrogen cycle, predictive mapping, cold-water coral carbonate mound

INTRODUCTION

Cold-water coral (CWC) carbonate mounds are important marine ecosystems (Roberts et al., 2009). They are topographic seafloor structures that can be several hundreds of meters in height and have accumulated through successive periods of reef development, sedimentation and (bio)erosion over glacial-interglacial periods (Kenyon et al., 2003; Van Weering et al., 2003; Mienis et al., 2007; Roberts et al., 2009). They are hotspots of biomass and biodiversity and provide essential ecosystem functions through nutrient [Carbon (C) and Nitrogen (N)] cycling in a resource-limited deep sea (Henry and Roberts, 2007; van Oevelen et al., 2009; Armstrong et al., 2012). However, significant gaps remain in our understanding of the spatial distribution of their overall biomass and capacity to remineralise organic matter (OM) (De Clippele et al., 2021).

Cold-water coral reefs depend on OM produced at the ocean's surface to support their growth (Duineveld et al., 2004, 2007; Kiriakoulakis et al., 2005). This OM can be transported to the reef from surface waters through deposition, tidal downwelling, nepheloid layers and deep-water advection (Mienis et al., 2007; Davies et al., 2009; Findlay et al., 2013; Mohn et al., 2014; Soetaert et al., 2016). In addition, when reefs (tens of meters high) accumulate over time to form large CWC carbonate mounds (hundreds of meters high), they can induce a "topographically-enhanced carbon pump" (Soetaert et al., 2016). The mounds large size interrupts the currents, which creates downwelling events bringing OM from surface waters to the mound's summits and upper flanks (Guinan et al., 2009; Mohn et al., 2014; Rengstorf et al., 2014; Soetaert et al., 2016). Baffling of currents caused by the coral framework can also locally increase the POM concentration at the reefs (Soetaert et al., 2016).

The availability of this food is a major determinant controlling CWCs occurrence and the zonation of macrohabitats on the mounds (De Clippele et al., 2019; Maier et al., 2021). The mound bases are covered by sediments (bio- and siliciclastic sands), pebbles, cobbles and boulders (de Haas et al., 2009). Dense *Lophelia pertusa* patches characterize the summits of the carbonate mounds, while the flanks of the mounds are covered with patches of coral rubble, dead coral branches and living corals (Kenyon et al., 2003; Van Weering et al., 2003; de Haas et al., 2009; De Clippele et al., 2019; Maier et al., 2021). Dead coral framework is particularly biodiverse as it provides complex micro- and macrohabitats for diverse communities (Jonsson et al., 2004; Henry and Roberts, 2007). It is this living fauna (including e.g., anthozoans, hydroids, ophiuroids, and sponges) that contributes the most to a reef's capacity to mineralize OM (de Froe et al., 2019; Maier et al., 2019, 2020; De Clippele et al., 2021).

Knowing how much live and dead coral framework biomass is present on a CWC reef and their contribution toward OM mineralization is critical information to understand how well the reef is functioning. It also provides a baseline that can help us understand the extent of the potential effects of ocean acidification, warming and decreases in ocean O_2 levels on these vulnerable ecosystems (Hennige et al., 2014, 2015, 2020; Roberts and Cairns, 2014; Sweetman et al., 2017). To estimate biomass and OM mineralization on CWC carbonate mounds, we apply the novel approach by De Clippele et al. (2021). This approach uses surface area measurements of the coral *L. pertusa*, extracted from high-definition (HD) video frames and combines this with biomass and respiration data. We hypothesize that this method allows to map live and dead coral framework at the CWC Logachev Mound province (LMP) and quantify the ecosystem function of this area.

METHODOLOGY

Location

The LMP consists of a cluster of CWC carbonate mounds located on the south-eastern slope of Rockall Bank in the North-East Atlantic (Kenyon et al., 2003; **Figure 1**). The CWC carbonate mounds are between 5 and 360 m tall, up to a few kilometers long and located between 500 and 1,000 m depth (Kenyon et al., 2003; de Haas et al., 2009). The dominant current direction in the LMP is in a southwest direction, following from a clockwise circumventing flow around Rockall bank (Mienis et al., 2007), while the local diurnal barotropic tide causes cross slope transport in a northwest-southeast direction (Mienis et al., 2007; White, 2007).

Data

Biological Data

Eight HD video transects were recorded during the Changing Oceans 2012 expedition, RRS *James Cook* cruise 073 (Roberts, 2013), using the Remotely Operated Vehicle (ROV) Holland-1 (more details in De Clippele et al., 2019; **Table 1**). Using the software Photoshop CC 2018, video frames were extracted every 500th frame. The video frames were used to measure the surface area of live and dead coral framework (see Section "Biomass Estimation"). The remaining area (total area minus [dead + live] coral framework) was referred to as sediment. However, hard substrates such as pebbles, cobbles, boulders and lithified substrate can also be present (De Clippele et al., 2019; Maier et al., 2021). The ROV was equipped with two parallel pointers, marking a fixed distance of 10 cm on the video frames, which was used to scale the images.

In addition, data on the dry weight, C_{inorg} and C_{org} stock of the live and dead coral framework, collected with a NIOZ boxcorer (diameter: 50 cm; height 50 cm; surface area ~0.2 m^2) was used. Six cores were collected during the 2017 R/V *Pelagia* research cruise and used to derive *ex situ* benthic O_2 and N flux measurements of the CWC community (see Table 1 in de Froe et al., 2019). Photographs were taken of the core surface after sampling and used to calculate the surface area (m^2): dry weight (kg) ratio. The photographs were scaled using the dimensions of the boxcorer.

Environmental Data

Particulate organic matter (POM) concentrations were obtained from a POM model with a resolution of 250 m × 250 m (Soetaert et al., 2016). This model provides values that represent the concentration of reactive freshly-produced organic matter available in the water column. These are below the actual measured values of POM concentration, which additionally

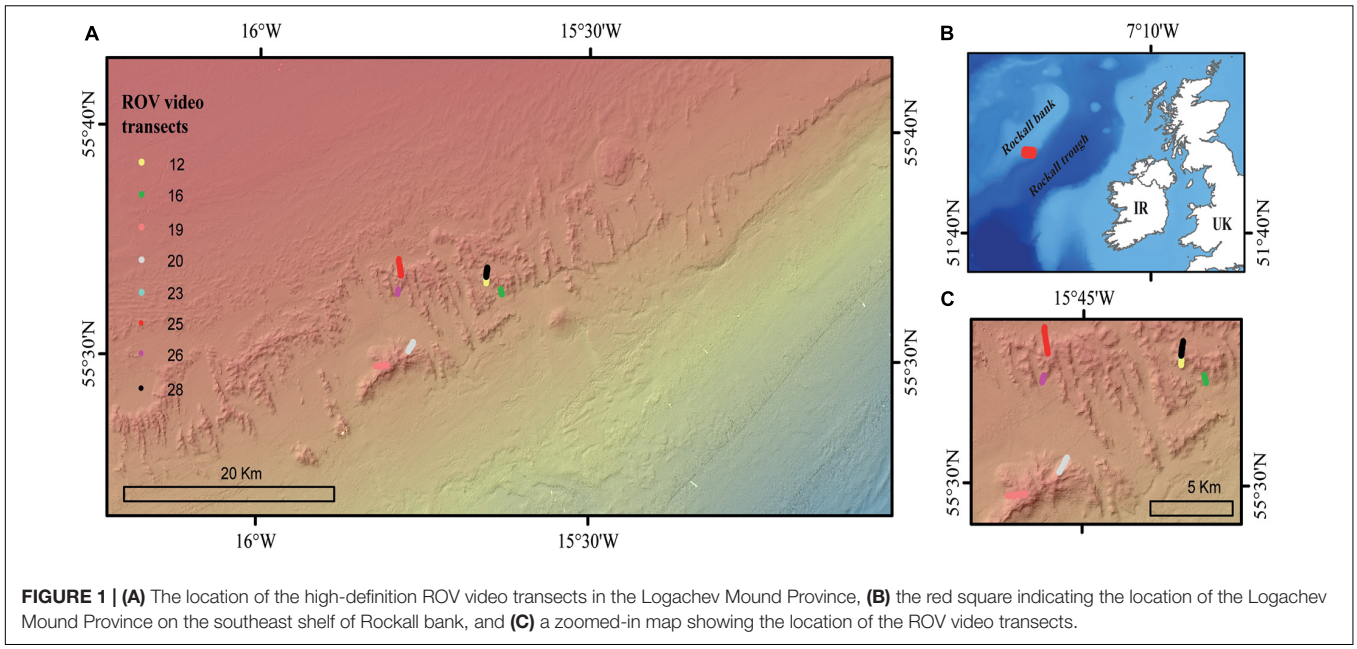

FIGURE 1 | (A) The location of the high-definition ROV video transects in the Logachev Mound Province, **(B)** the red square indicating the location of the Logachev Mound Province on the southeast shelf of Rockall bank, and **(C)** a zoomed-in map showing the location of the ROV video transects.

TABLE 1 | Dive number, location [longitude (Lon.) and latitude (Lat.)], depth range (m), and length (m) of ROV video transects.

Dive	Start Lon. (decimal degrees)	Start Lat. (decimal degrees)	End Lon. (decimal degrees)	End Lat. (decimal degrees)	Depth range (m)	Length (m)
12	−15.65523	55.55799	−15.65557	55.55567	[640;722]	200
16	−15.63350	55.55119	−15.63142	55.54744	[758;872]	240
19	−15.82089	55.49419	−15.80442	55.49478	[559;801]	880
20	−15.76447	55.51220	−15.77232	55.50529	[610;873]	360
23	−15.65630	55.55847	−15.65571	55.55965	[563;584]	40
25	−15.78718	55.57206	−15.78421	55.56013	[547;705]	1,040
26	−15.78795	55.55020	−15.78918	55.54672	[702;768]	360
28	−15.65585	55.56014	−15.65389	55.56674	[575;701]	240

include refractory organic matter (Soetaert et al., 2016). In addition, terrain variables were extracted from bathymetry data provided by the Irish National Seabed Survey program (INSS) at a 20 m × 20 m resolution. The following topographic terrain variables were derived from the bathymetry data using the ArcGIS 10.1, ESRI Software and the Benthic Terrain Modeller (Wright et al., 2005): depth, slope, aspect (eastness and northness), rugosity (calculated at two spatial scales, using a square kernel window of, respectively, 3 pixels × 3 pixels and 9 pixels × 9 pixels) and bathymetric positioning index (BPI; calculated at two spatial scales using an annulus kernel window with inner and outer radius of, respectively, 3 × 6 and 6 × 9 cells). More information on these variables is provided in De Clippele et al., 2019.

Oxygen and Nitrogen Data

O_2 consumption rates were obtained from *ex situ* boxcore incubations by de Froe et al. (2019). For live coral framework, an O_2 consumption rate of 6.39 ± 0.32 mmol O_2 kg^{-1} dry weight d^{-1} (*L. pertusa, Madrepora oculata,* and *Desmophyllum dianthus*) was found and for dead coral framework a 0.18 ± 0.01 mmol O_2 kg^{-1} dry weight d^{-1} was found. For sediment, an average O_2 consumption of 2.4 ± 0.59 mmol m^{-2} d^{-1} was used, based on the depth-based (500–800 m) turnover rates of O_2 by Glud (2008). Live coral framework released dissolved inorganic N (DIN) mostly as ammonium (NH^+_4) (Khripounoff et al., 2014), while dead coral framework mostly releases nitrate (NO^-_3) (Maier et al., 2021). For live corals we used an NH^+_4 release rate of 0.084 ± 0.017 NH_4^+ mmol kg^{-1} d^{-1} dry weight (Khripounoff et al., 2014) and for dead coral framework we used an NO^-_3 release rate of 0.053 ± 0.037 NO_3^- mmol kg^{-1} d^{-1} (Maier et al., 2021). Sediments baffled by coral framework in the LMP release 0.01 ± 0.06 NH_4^+ mmol m^2 d^{-1} and 0.64 ± 0.37 NO_3^- mmol m^2 d^{-1} while sediments on top of Rockall bank release 0.01 ± 0.06 NH_4^+ mmol m^2 d^{-1} and 0.52 ± 0.16 NO_3^- mmol m^2 d^{-1} (de Froe et al., 2019). These values are listed in **Table 2**.

Coral Presence Habitat

Our model area was defined by the habitat suitability model of CWC presence/absence produced by Rengstorf et al. (2014) and covers 253 km^2. This habitat suitability model was chosen as particulate organic matter (POM) is used as an environmental

TABLE 2 | Overview of the O_2 consumption and N values used in this study.

Functional group	Unit	Value	Source
Live coral framework	O_2 consumption	6.39 ± 0.32 mmol O_2 kg^{-1} dry weight d^{-1}	de Froe et al., 2019
Dead coral framework	O_2 consumption	0.18 ± 0.01 mmol O_2 kg^{-1} dry weight d^{-1}	de Froe et al., 2019
Sediments	O_2 consumption	2.4 ± 0.59 mmol O_2 m^{-2} d^{-1}	Glud, 2008
Live coral framework	N (NH^+_4 release)	0.084 ± 0.017 NH_4^+ mmol kg^{-1} d^{-1} dry weight	Khripounoff et al., 2014
Dead coral framework	N (NO^-_3 release)	0.053 ± 0.037 mmol NO_3^- kg^{-1} dry weight d^{-1}	Maier et al., 2021
Sediments	N (NH^+_4 release)	0.01 ± 0.06 mmol NH_4^+ kg^{-1} d^{-1} dry weight	de Froe et al., 2019
Sediments	N (NO^-_3 release)	0.64 ± 0.37 mmol NO_3^- kg^{-1} dry weight d^{-1}	de Froe et al., 2019

variable to explain the spatial variability in coral biomass. The POM was calculated by Soetaert et al. (2016) who used the above mentioned habitat suitability model to study benthic respiration and the amount of food supplied to the LMP (Rengstorf et al., 2014). Because the POM model assumed that OM deposition/uptake was increased by a constant factor in the presence of corals, we cannot compare coral-presence habitat with coral-absence habitat (Soetaert et al., 2016).

Biomass Estimation

Biomass is here defined as the live tissue of a specimen. In this study we therefore refer to "(bio)mass" to indicate the differentiation between measuring mass and biomass for, respectively, live and dead coral framework. The approach by De Clippele et al. (2021), was adapted due to a difference in coral morphologies, i.e., the presence of coral thickets at the LMP rather than the globular colonies at the Mingulay Reef (**Figure 2**). Here, to convert surface area to (bio)mass, (bio)mass data from boxcores collected at the LMP were used (de Froe et al., 2019). The steps are described in detail below and in **Figure 3**.

Image Analyses

Step 1

The video still frames from the HD videos (see Section "Biological Data") (**Figure 3A**), were imported in Adobe Photoshop. Bad quality images or images that overlapped were excluded from analyses. In Photoshop, the laser-scale dots, live and dead coral framework were labeled each with a unique color aided by Photoshop's "quick selection tool" (**Figure 3B**) (van der Kaaden and De Clippele, 2021). The benthic surface area covered by dead and live coral framework was calculated in R. An R-function (van der Kaaden and De Clippele, 2021) was used to semi-automatically calculate the percentage cover and image size from the labeled images, from which the surface area in m^2 could be calculated. This faster method is an alternative to the method proposed in De Clippele et al. (2021) where the open-source software ImageJ2 (Greene et al., 1999; Rueden et al., 2017) was used.

Predictive Mapping

Step 2

The surface area data points were imported in ArcGIS and combined in 20 m sub-samples (*x*-axis). The length of 20 m was chosen as this length gave the most accurate representation of the coral framework variability in relation to the multibeam grid cell size. Then, the ArcGIS Extract Values to Points tool was used to extract the environmental variables (i.e., depth, BPI, slope, rugosity, eastness, northness, and POM) (**Figure 3C**) associated with each sub-sample data point.

Step 3

The response (i.e., surface area) and explanatory (i.e., environmental) variables were then used to model a predictive map using the Random Forest approach (**Figure 3D**) with the randomForest package in R (Breiman, 2001). This supervised classification methodology is referred to as a regression tree with a number of simple decision trees. Each tree is based on a bootstrapped sample of the response and explanatory data set. This group of simple trees vote for the most popular class, which is capable of predicting a response when presented with a set of explanatory variables (Cutler et al., 2007; Rogan et al., 2008). Random Forest modeling is commonly used to produce predictive maps (Baccini et al., 2008; Wei et al., 2010; Zhang, 2015; Conti et al., 2019; De Clippele et al., 2021) and provides similar results to approaches using logarithmic regression and Deep Neural Networks (Conti et al., 2019). Here, the training dataset contained one-third of the total data points. This Random Forest model can then be applied to a new set of the same response variables to create a predictive map of the unseen data of the whole area. Correlated environmental variables (<0.5) were removed prior to analyses, using the cor test in R. The importance of the environmental variables in predicting surface area was assessed by calculating the Mean Decrease in Accuracy for each variable to indicate their contribution to the model performance.

To evaluate the uncertainty of the model outputs, we first used a bootstrap technique to produce estimates of model uncertainty (Rowden et al., 2017). This is done by repeating the Random Forest model one hundred times, with the same model but with a replacement random sample of the training data each time. This results in 100 estimates from which the coefficient of variance (CV) was calculated to examine the models output stability. This provides a range of how the Random Forest model output varies and is measured as the standard deviation/mean $\times$ 100 (Wei et al., 2010).

Biomass Calculation

Step 4

From the predictive *Lophelia* reef maps (see step 3), the total amount of live and dead coral framework surface area for the

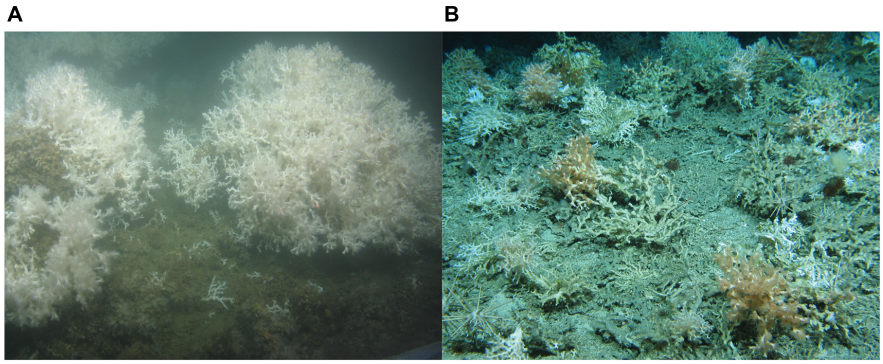

FIGURE 2 | (A) Globular, cauliflower-shaped *L. pertusa* colonies at the Mingulay Reef Complex sitting on a bed of dead framework and coral rubble, which is partially covered in white zoanthids. **(B)** Live pink, orange and white coral thickets of *L. pertusa* and *Madrepora oculata* at the Logachev Mound Province. The brown/beige colored framework is dead. Image credit: JC073 Changing Oceans Expedition 2012.

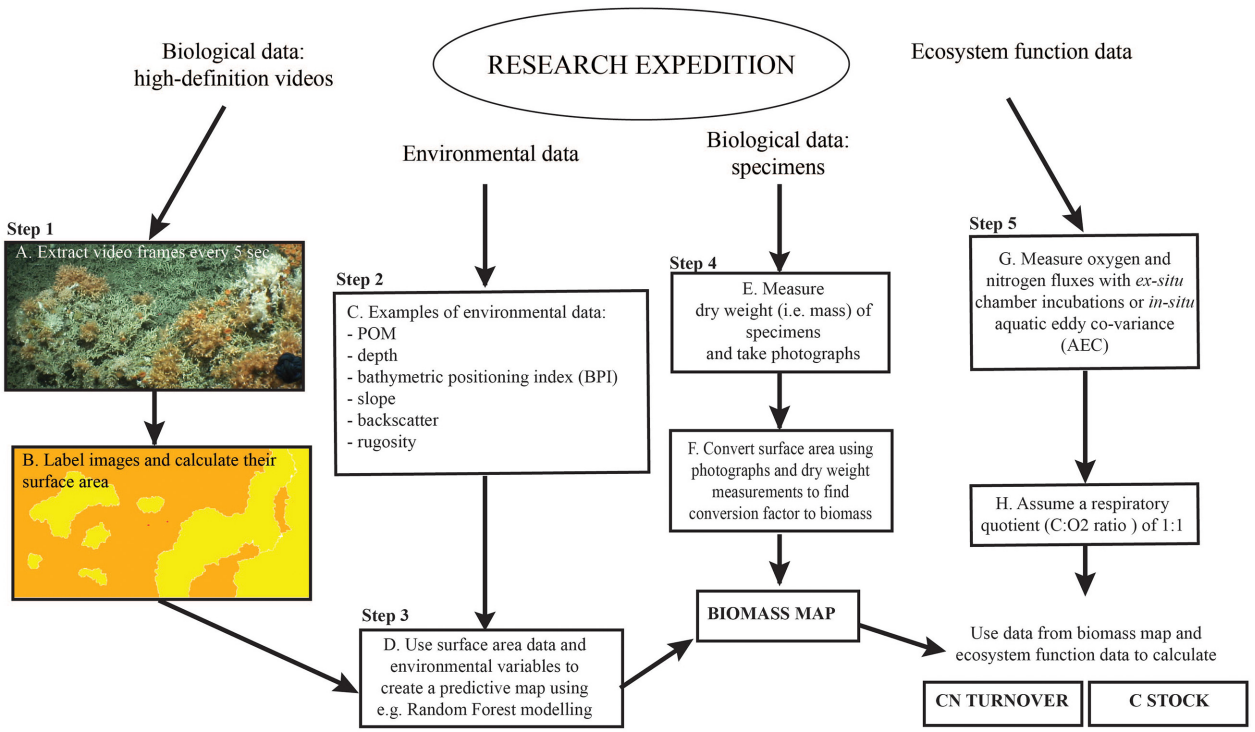

FIGURE 3 | Graphic overview of the approach used in this study. Adapted from Figure 2 in De Clippele et al. (2021).

whole habitat suitability area can be extracted and converted to bio(mass) in Excel. To convert live and dead coral framework to (bio)mass, data provided by de Froe et al. (2019) was used (**Figure 3E**). de Froe et al. (2019) reports the density (kg dry weight m^{-2}) of live and dead coral framework per boxcore sample (**Table 3**). From the known surface area of the boxcorer (see Section "Biological Data"), the dry weight of live and dead coral framework per boxcore sample was calculated (kg dry weight $boxcore^{-1}$). The benthic surface area of live and dead coral framework from boxcore photographs (**Supplementary Materials**) was then used to calculate a conversion factor of live/dead coral framework surface area to live/dead coral framework dry mass for each boxcore sample. The mean conversion factor of 8.01 ± 5.52 kg m^{-2} and 33.78 ± 6.27 kg m^{-2} for live and dead coral framework, respectively, was then used to convert benthic surface area measurements from the HD video extracted frames to skeletal dry weight (kg dry weight) (**Figure 3F**), i.e., dry weight (kg) = video surface area (m^2) × conversion factor (kg m^{-2}). From this, the biomass (live tissue mass) was calculated using the linear relationship between tissue dry weight and tissue and skeletal weight with the following equation from Hennige et al. (2014): TDW = 0.0415

TABLE 3 | Table showing the calculation of the average conversion values and standard deviations used in step 4 and step 5.

Live coral framework	SHM1	SHM2	FHM1	FHM2	OrM1	OrM2	Average	St. dev
Mass (kg dry weight)	0.0020	0.6800	0.0160	0.0000	0.1980	0.1000		
Surface area (m^2)	0.0000	0.0489	0.0072	0.0000	0.0435	0.0088		
Surface area conv. value (kg m^{-2})		13.9059	2.2222		4.5517	11.3636	8.0109	5.5217
C_{org} (kg^{-1} dry weight)	0.0000	0.0046	0.0001		0.0028	0.0014		
C_{org} conv. value (kg m^{-2})	0.0079	0.0067	0.0050		0.0143	0.0135	0.0095	0.0042
N_{org} (kg^{-1} dry weight)	0.0000	0.0012	0.0000		0.0007	0.0003		
N_{org} conv. value (kg m^{-2})		0.0019	0.0017	0.0007		0.0033	0.0019	0.0010
Dead coral framework								
Mass (kg dry weight)	1.1700	1.3900	3.9180	17.0000	1.9080	1.0000		
Surface area (m^2)	0.1895	0.0976	0.2052	0.1787	0.1598	0.0351		
Surface area conv. value (kg m^{-2})	6.1741	14.2418	19.0936	95.1315	11.9399	28.4900	33.7794	6.2651
C_{org} (kg^{-1} dry weight)	0.0014	0.0026	0.0055	0.0238	0.0027	0.0022		
C_{org} conv. value (kg m^{-2})	0.0012	0.0019	0.0014	0.0014	0.0014	0.0022	0.0016	0.0004
N_{org} (kg^{-1} dry weight)	0.0007	0.0011	0.0027	0.0119	0.0011	0.0009		
N_{org} conv. value (kg m^{-2})	0.0006	0.0008	0.0007	0.0007	0.0006	0.0009	0.0007	0.0001

*Surface area calculations based on the boxcore photographs (**Supplementary Materials**) and the live and dead coral framework mass (kg dry weight) present in the boxcore. The boxcore has a surface area of 0.2 m^2. The mass values were used from Table 3 in de Froe et al. (2019). Summit Haas Mound (SHM), Flank Haas Mound (FHM), Oreo Mound (OrM).*

(TWW + SDW) + 0.0849. With TDW = tissue dry weight (g) = SDW* 5%; TWW = tissue wet weight (g); SDW = skeletal dry weight (g) (De Clippele et al., 2021; Hennige et al., 2014). Sediment were calculated as the remainder (total area minus [dead + live] coral framework). The above conversion calculation was also used in the ArcGIS raster calculator tool to convert the surface area predictive map to a (bio)mass. The standard deviation of the conversion factors was used to calculate the absolute minimum, mean and maximum biomass (see the "Results" section and **Supplementary Materials**).

Carbon and Nitrogen Turnover and Stock

Step 5

The total biomass and sediment surface area data was used to calculate the yearly C and N turnover for the area, using O_2 consumption data reported in literature (**Table 2** and **Figure 3G**). Carbon and N turnover are here defined as the conversion of ingested food into biomass and loss by respiration as CO_2 and DIN. The C turnover is calculated from the total O_2 consumption assuming a respiratory quotient (C:O_2 ratio) of 1:1 (Glud, 2008) (**Figure 3H**). This does not account for temporal changes in O_2 consumption that the coral might experience during its lifetime, as this data is currently not available. The live and dead coral framework were multiplied with their respective DIN release rates. More details on this calculation can be found in Step 3 in De Clippele et al. (2021).

In **Table 3** by de Froe et al. (2019), the percentage of C_{org} and N_{org} of live and dead coral framework per boxcore sample are reported. The C_{org} and N_{org} stock of live and dead coral framework per boxcore sample was obtained by multiplying the percentage C_{org} and N_{org} content of live and dead coral framework with their total dry weight (C or N kg^{-1} dry weight). These values were used to calculate a mean conversion factor for the mass calculated in step 3 to C_{org} and N_{org} (**Table 3**). The C_{inorg} stock was calculated by multiplying the $CaCO_3$ mass by 0.12 (Windholz et al., 1983; De Clippele et al., 2021). To account for uncertainties the absolute minimum, mean and maximum CN turnover and C stock were calculated (see the "Results" section and **Supplementary Materials**).

RESULTS

Predictive Maps

Our model predicts live coral framework covering 8 km^2 (3%) and dead covering 115 km^2 (45%) of the CWC habitat area. The remaining 130 km^2 (51%) is therefore considered to consist of sediment.

The environmental variables used in the mean live coral framework Random Forest model explained 65.54% of the variation in the data. The environmental variables that contributed most to explaining the spatial variability in the amount of live coral framework were BPI (inner cell radius 6 × outer cell radius 9), POM concentration and rugosity (9 × 9 cells) (**Figure 4**). The live coral framework biomass map (**Figure 5**) illustrated that the highest live coral biomass is located on the summits of the mounds. The study area contained a total live coral framework skeletal mass of 64,054 T C_{inorg} (range: 62,280–77,635 T) and biomass of 13,117 T C_{org} (range: 12,754–15,899 T). Our model results showed highest uncertainty at deeper depths and at the most eastern mounds (**Figure 6**).

The environmental variables used in the mean dead coral framework Random Forest model explained 54.21% of the variation in the data. The environmental variables that contributed most to explaining the spatial variability in the dead coral framework were BPI, depth and POM (**Figure 4**). The dead coral framework predictive map (**Figure 7**) showed that the highest mass is located on the northeast flanks and on the summits of the mounds, and that it decreases with depth. The area has a total mean dead framework skeletal mass of 2,875,706 T C_{inorg} (range: 3,485,828–4,357,435 T) and variability was also here higher at depth and the most eastern mounds (**Figure 8**).

FIGURE 4 | Mean Decrease in Accuracy plots of the mean live and dead coral framework Random Forest model indicating what the contribution of each variable is to the model performance. When the Mean Decrease Accuracy value is higher for a certain variable, the removal of this variable from the model will decrease the model's performance.

Stock and Turnover of Carbon and Nitrogen

In the live coral framework a mean of 7,686 T C_{inorg} (range: 7,474–9,316 T), 607 T C_{org} (range: 330–1,061 T) and 122 T N_{org} (range: 119–148 T) is stored. The dead coral framework stores a mean of 465,085 T C_{inorg} (range: 418,299–522,892), 6 T C_{org} (range: 0–16 T), and 3 T N_{org} (range: 2–3 T). On average 0.3 kg m^{-2} dry weight of live coral framework and 15.3 kg m^{-2} dead coral framework is present in the area according to the predictive maps. Largest C_{inorg} turnover was found for the dead framework, reaching an annual rate of 3,056 T yr^{-1} (49%) (range: 2,596–3,626 T C yr^{-1}), followed by live coral framework with 1,793 T yr^{-1} (29%) (range: 1,656–2,828 T C yr^{-1}) (**Table 4**). The fine sediment area turned 1,386 T C_{inorg} yr^{-1} (22%) (range: 1,512–1,216). The total C_{inorg} turnover at the LMP is 6,235 T C $year^{-1}$ (range: 2,596–7,670 T C $year^{-1}$), corresponding to an O_2 consumption of 5.64 mmol m^{-2} d^{-1} (range: 5.21–6.44 mmol O_2 m^{-2} d^{-1}). Dead coral framework turned 290–1,989 T, sediments 432–919 T, and live framework 53–286 T N_{inorg} $year^{-1}$. The total at the LMP was 973–3,194 T N_{inorg} $year^{-1}$.

DISCUSSION

This study applied a new methodology to map live and dead coral framework biomass at the Logachev Mound Province. These biomass maps were used to estimate region-scale inorganic CN turnover, as well as the organic and inorganic CN standing stocks. Even though the reefs at the LMP occur in relatively deep and under food-limited waters compared to shallower inshore reefs (De Clippele et al., 2021) they contribute significantly to the global CN turnover and CN stock. This is as CWC mounds in the LMP, cover a large area and form big mounds due to their ability to persist over glacial-interglacial time scales. This work advances our growing knowledge of their significance to remineralise OM, a criteria used to define Ecologically or Biologically Significant Areas (EBSAs) (Titschack et al., 2015; Johnson et al., 2018).

Distribution of Dead and Live Coral Framework

Spatial differences in environmental conditions drive the small and large scale patterns in biomass observed at the LMP. This study showed that bathymetric positioning index (BPI) is the most important environmental predictor of both live and dead coral framework. This is as coral carbonate mounds form through periods of successive reef development (Roberts et al., 2009). When reef growth dominates over erosion, many small reefs will cover the surface of the mound before they merge and continue the development cycle (Roberts et al., 2009). These smaller reefs coincide with positive BPI values across the LMP (De Clippele et al., 2017). Our predictive biomass map also indicates that live coral framework is predominantly located on the summits of the mounds, which can largely be explained by the higher amount of available POM. In these relative food-limited waters, the supply of POM, i.e., their food, from surface water to the reefs is important to support the high metabolic C demand of the live coral framework (Davies et al., 2009; Roberts et al., 2009). Soetaert et al. (2016) suggest that the high elevation of the coral carbonate mounds induces downwelling and hence POM supply from the ocean surface, a concept described as topographically-enhanced carbon pump. The baffling created by the coral framework can locally increase the POM concentration measured on the reefs (Soetaert et al., 2016). These higher POM concentrations, in turn, can increase the biomass of the live coral framework. This positive feedback loop could explain why the prediction of live coral is strongly driven by POM concentration. The explanatory power of POM could increase even more if a higher resolution POM model would be used. Reduced POM supply linked with bio- and hydrodynamic erosion are the likely causes for the observed reduction in dead coral cover at greater depths (Roberts et al., 2009). This is also shown by Maier et al. (2021), where more degraded coral framework is found at deeper depths and less degraded framework at more shallow depths. Live corals form complex three-dimensional frameworks, and increase the local terrain roughness (Jenness, 2002). Rugosity, a measure of

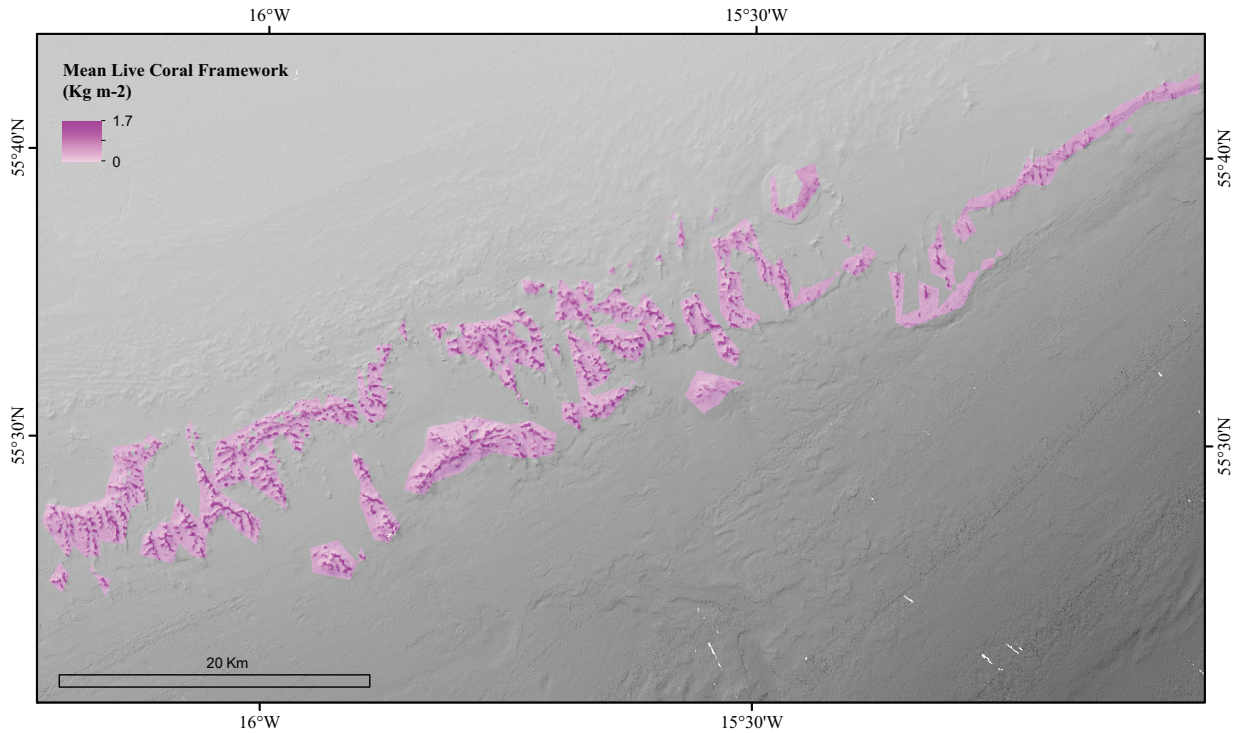

FIGURE 5 | Modeled amount of the mean biomass (Skeletal weight + live tissue weight) of live coral framework in the coral habitat suitability model area of the Logachev Mound Province.

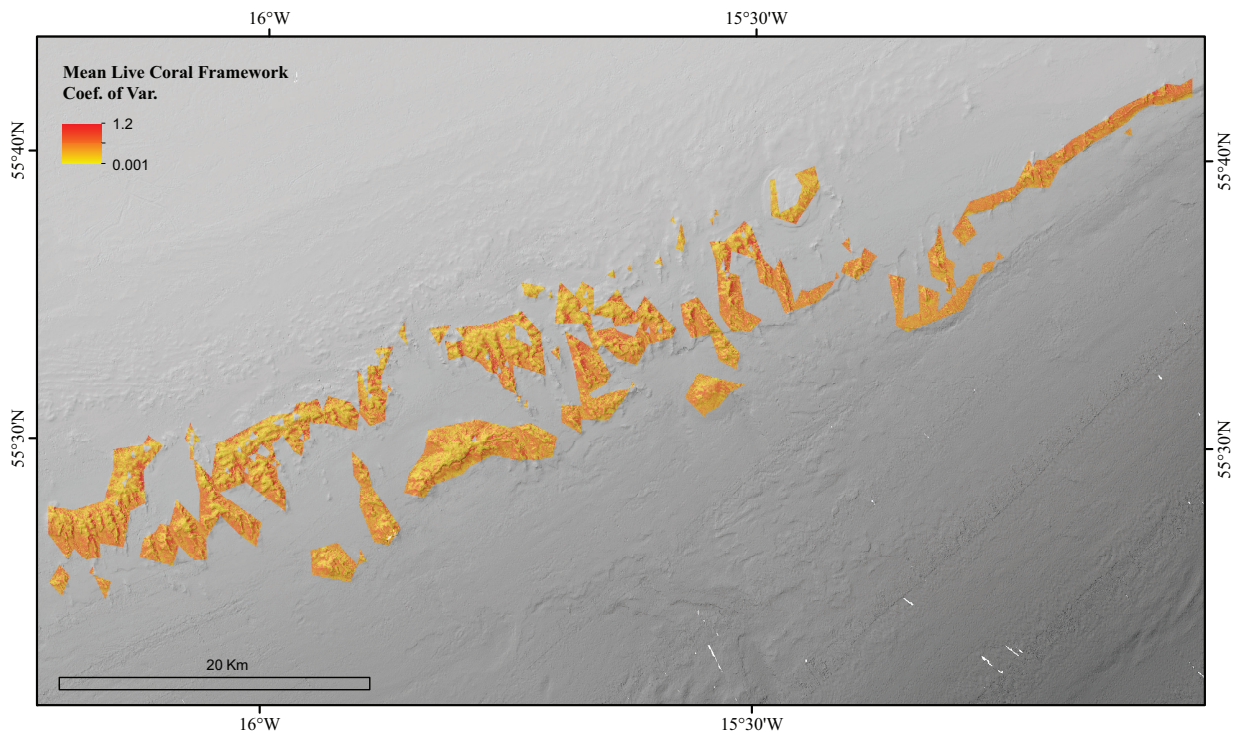

FIGURE 6 | The Coefficient of Variation for the Random Forest model of the mean biomass for live coral framework in the coral reef habitat area of the Logachev Mound Province.

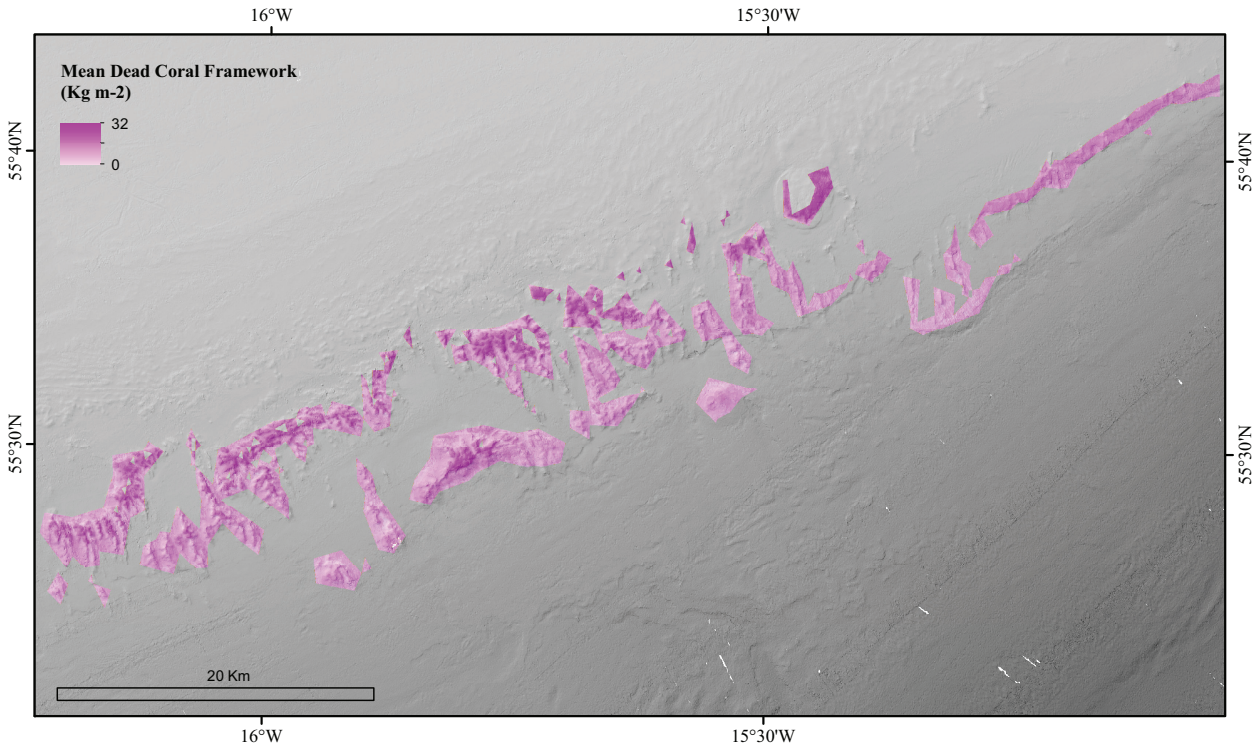

FIGURE 7 | Modeled amount of the mean biomass of dead coral framework in the coral habitat suitability model area of the Logachev Mound Province.

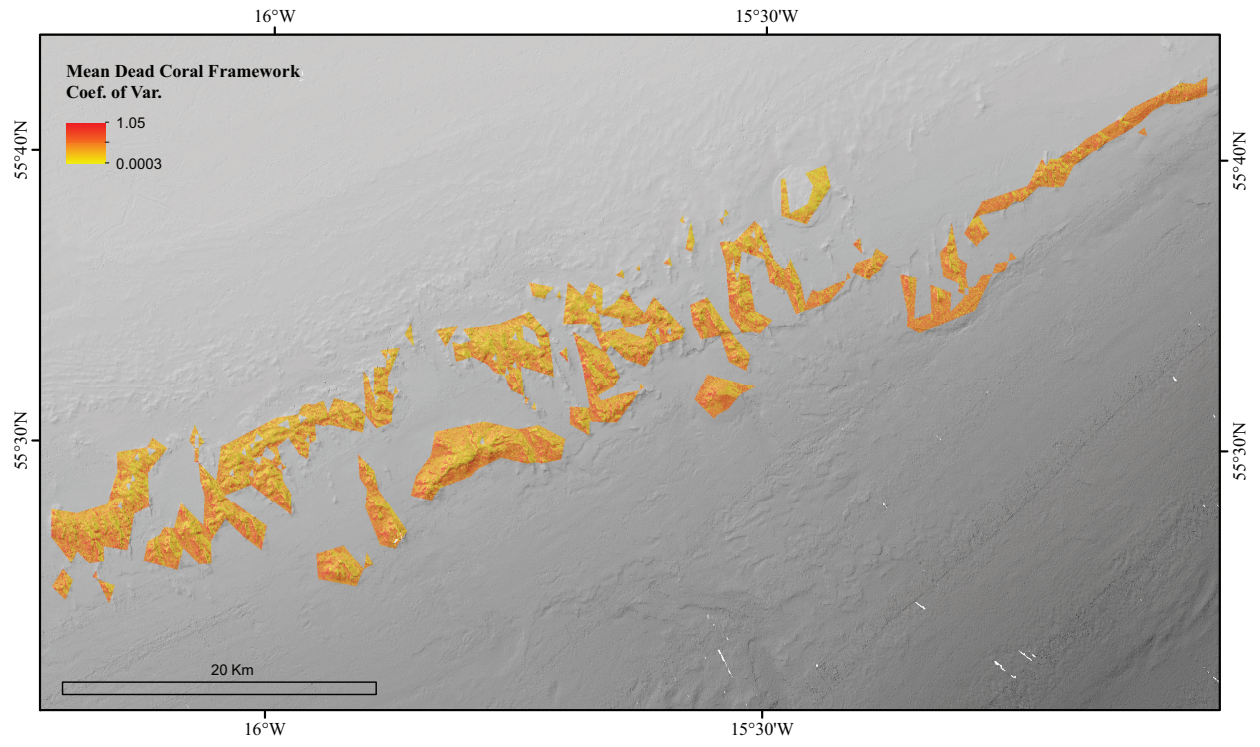

FIGURE 8 | The Coefficient of Variation for the Random Forest model of the mean biomass for dead coral framework in the coral reef habitat area of the Logachev Mound Province.

TABLE 4 | Overview of the minimum, mean and maximum (bio)mass, organic and inorganic carbon (C), organic nitrogen (N) stock masses, together with the mass of C and N turned over by live and dead coral framework and sediments.

		Live coral framework		Dead coral framework	Sediments	Total
		SDW	TWW	SDW		
Skeletal dry weight + tissue wet weight (T)	Min.	62,280	12,754	3,485,828	NA	3,560,861
	Mean	64,054	12,117	3,875,706	NA	3,951,877
	Max.	77,635	15,899	4,357,435	NA	4,450,969
C_{inorg} stock (T C)	Min.	7,474	NA	418,299	UN	425,773
	Mean	7,686	NA	465,085	UN	472,771
	Max.	9,316	NA	522,892	UN	532,208
C_{org} stock (T C)	Min.	411	NA	0	UN	411
	Mean	607	NA	6	UN	613
	Max.	1,061	NA	16	UN	1,076
N_{org} stock (T N)	Min.	119	NA	2	UN	122
	Mean	122	NA	3	UN	125
	Max.	148	NA	3	UN	151
C turnover per year (T C year $^{-1}$)	Min.	1,656	NA	2,596	1,512	5,763
	Mean	1,793	NA	3,056	1,386	6,235
	Max.	2,282	NA	3,626	1,216	7,124
N turnover per year (T N year $^{-1}$)	Min.	53	NA	290	629	973
	Mean	145	NA	1,046	431	1,623
	Max.	286	NA	1,989	919	3,194

Not Applicable (NA), Unknown (UN).

terrain roughness, therefore, represents the third most important variable explaining the prediction of live coral at the LMP.

Our model predicted more dead than live coral framework in the Logachev Mound Province, which is supported by previous studies on CWC reefs (De Clippele et al., 2019, 2021; de Froe et al., 2019; Maier et al., 2021). De Clippele et al. (2019) and Maier et al. (2021) calculated the percentage cover from ROV videos and found that dead coral framework covered 35–93% and live coral framework covered 3–25% of the transects at the LMP. This study found that dead coral framework surface area covered 45%, compared to live coral framework covering 3% of the area. Here, we report 60 times more dead framework mass than live coral mass in the area, which is twice as much as reported by earlier studies (27 times; de Froe et al., 2019). de Froe et al. (2019) based this difference in dry mass on collected boxcores, while here, the whole area is accounted for by means of predictive modeling. Other studies, such as Conti et al. (2019) have calculated the percentage of dead and live coral framework using video mosaic segmentation and classification approaches. They found that the Piddington Mound has 33–43% dead framework (rubble + dead coral framework), 2–3% live coral framework and 48–58% sediments (incl. dropstones) (Conti et al., 2019). While this is similar to what was found in our area, the Piddington mound has a spatial extent of approximately 40 m × 60 m and is one of the smaller mounds found in the Belgica Mound Province. The percentages of the substrates found will vary depending on the extent and the spatial heterogeneity of CWC reef area analyzed. The latter underlines the important contribution of representative sampling techniques and predictive models to more accurately represent CWC framework surface area coverage and biomass. Dead coral framework is important as it facilitates the high biodiversity typical of CWC reefs (Henry and Roberts, 2007) and contributes substantially more to reef fauna biomass and benthic fluxes (de Froe et al., 2019; De Clippele et al., 2021; Maier et al., 2021). Live corals protect themselves against colonization, for example by production of mucus (Freiwald, 2002; Wild et al., 2008; Buhl-Mortensen et al., 2010). In contrast, dead, unprotected coral framework is more easily colonized and provides the majority of micro- and macrohabitats in a CWC reef (Mortensen and Fosså, 2006; Buhl-Mortensen et al., 2010).

Oxygen Consumption and Nitrogen Release

Cold-water coral reefs are hotspots of O_2 consumption and N release, i.e., OM mineralization (van Oevelen et al., 2009; Cathalot et al., 2015; de Froe et al., 2019; De Clippele et al., 2021; Maier et al., 2021). The average C turnover at the LMP, which we derived from O_2 consumption measurements, was 1–3.4 times the global average for a soft-sediment area at the same depth (Glud, 2008). Dead coral framework contributed 49%, live coral framework 29%, and sediments 22% to the total C turnover of the area. At the same time, the reefs at the LMP released 1.9 times more DIN compared to adjacent soft-sediment grounds (de Froe et al., 2019). Here the majority of the DIN was released in the form of NO^-_3 by both dead coral framework (64% of the total N turnover) and sediments (27% of the total N turnover), while NH^+_4 was released by live coral framework (9% of the total N turnover). It should be noted that the partitioning of DIN release in NH_4^+ and NO_3^- originates from the model assumption, i.e., that live cold-water corals typically release ammonium as metabolic end product (Khripounoff et al., 2014), while dead framework and sediment release mostly nitrate, due to the activity of nitrifying microorganisms (de Froe et al., 2019;

Maier et al., 2021). Tidal induced upwelling of this nutrient-rich reef water could promote new phytoplankton primary production in the surface waters, which in turn would increase OM export to the reef (Davies et al., 2009; Eisele et al., 2011; Hebbeln et al., 2014; Soetaert et al., 2016). Such a loop has been suggested for cold-water coral ecosystems at the shallower Porcupine Bank (White et al., 2005) and could explain how cold-water coral reefs are sustained in the relative resource-poor deep sea. If such a loop is also present at the deeper LMP remains to be determined.

However, it is important to note that the C turnover reported in this study (5.21–6.44 mmol C m^{-2} d^{-1}) is 3–12 times lower than previously reported respiration measurements (van Oevelen et al., 2009; de Froe et al., 2019) (11–75 mmol C m^{-2} d^{-1}). There are three reasons why we might observe this difference. Firstly, in contrast to previous studies, our study accounted for the spatial variability in the biomass of the coral framework across the whole region and revealed that on average 51% is covered by sediments, 45% by dead coral framework, and 3% by live coral framework. Respiration measurements collected by Aquatic Eddy-Correlation (AEC) or boxcore samples are not able to grasp the spatial heterogeneity of such a large area (de Froe et al., 2019; De Clippele et al., 2021). Our study therefore provides a more accurate representation of the total C and N turnover in the area, as it accounts for the spatial complexity.

Secondly, our calculations might be an underestimation as the physical structure of the coral framework baffles sediment (de Haas et al., 2009; de Froe et al., 2019). This type of sediment has a higher OM concentration and C turnover rate (5.32 ± 0.59 mmol O_2 m^{-2} d^{-1}, de Froe et al., 2019) compared to non-reef sediments adjacent to the reefs (de Froe et al., 2019; de Haas et al., 2009). Given that the area that is covered by live and dead coral framework, it will also contain baffled sediment which could significantly increase the total OM mineralization capacity of the area (de Haas et al., 2009). To illustrate the potential contribution of the baffled sediments to the LMP carbon turnover, we assume the area covered by live and dead coral framework is also covered by baffled sediments and add this to our calculation. In this scenario, the result suggests that communities associated with dead coral branches would contribute a mean of 33% (3,056 T C $year^{-1}$), baffled sediments 33% (3,025 T C $year^{-1}$), sediments 15% (1,389 T C $year^{-1}$), and live coral framework 19% (1,793 $year^{-1}$) to the total benthic C turnover at the LMP. If we recalculate the C turnover per square meter for this new scenario, a total mean of 8.34 mmol C m^{-2} d^{-1} is found instead of a mean of 5.64 mmol C m^{-2} d^{-1}. This indicates that cold-water coral carbonate mound sediments might play a much more important role in the C turnover of CWC reefs and carbonate mounds than previously thought.

Thirdly, our predictive maps indicate that *in situ* measurements by de Froe et al. (2019) were deployed in areas with relatively high coral framework cover (**Figure 9**). This might provide an overestimation that does not reflect the spatial variability of the C turnover in the area. The Oreo Mound, where we found a particularly high live coral framework cover (**Figure 9A**), showed the highest AEC O_2 flux of 45.3 mmol m^{-2} d^{-1} (de Froe et al., 2019). In contrast, the Haas Mound, which contained a lower live coral framework coverage near the AEC deployment site (**Figure 9A**) showed an O_2 flux of 11.5–22.4 mmol m^{-2} d^{-1} (de Froe et al., 2019). This indicates that live coral patches are hotspots of metabolic activity within the reef and highlights the importance of understanding the spatial distribution of live and dead coral framework and sediments when planning research equipment deployments.

Similar to the Mingulay Reef, dead coral framework at the LMP contributes to the majority (49%) of the C turnover (De Clippele et al., 2021). This is expected as cold-water coral carbonate mounds consist of predominantly dead coral framework as discussed above. At the Mingulay Reef, the fauna associated with dead coral framework contributes ∼6 times more to C turnover compared to live coral framework. This is a larger difference compared to the LMP where the fauna associated with dead coral framework contributes only ∼1.7 times more. At Mingulay Reef, a higher biomass of fauna grows on the dead coral framework, hence turning over more C than the live corals (Kazanidis et al., 2016; De Clippele et al., 2021). This biomass difference may be caused by the reefs' shallower depth and the higher surface primary production above Mingulay Reef (0.048 g C_{org} m^{-3} d^{-1}), compared to the LMP (0.0067 g C_{org} m^{-3} d^{-1}) (Tyberghein et al., 2012; Assis et al., 2018; De Clippele et al., 2021) (**Table 5**). This results in an annual PP over the LMP of 6,194 T C $year^{-1}$ and 294 T C $year^{-1}$ at the Mingulay Reef (Tyberghein et al., 2012; Assis et al., 2018; De Clippele et al., 2021).

How Much Organic Matter Is Required to Sustain the Deep Reefs?

From the annual C and N turnover of the coral presence habitat in the LMP area, we estimate a minimum annual C requirement of 5,763–7,124 T C $year^{-1}$ and 973–3,194 T N $year^{-1}$. Using the parametrisation by Suess (1980), the amount of particulate organic carbon reaching the seafloor from the sea surface (annual primary production: 6,194 T C $year^{-1}$) via deposition was estimated to be 511–322 T C $year^{-1}$ for the shallowest (500 m) and deepest point (800 m) of LMP

TABLE 5 | Overview of key differences between the Mingulay reef (De Clippele et al., 2021) and the Logachev Mound Province.

	Mingulay reef	Logachev Mound Province
Area	1.7 km^2	253 km^2
Depth	120–190 m	500–1,000 m
Annual primary production	0.048 g C_{org} m^{-3} d^{-1}	0.0067 g C_{org} m^{-3} d^{-1}
Daily C turnover per square meter	32.37 mmol C m^{-2} d^{-1}	8.37 mmol C m^{-2} d^{-1}
Yearly C turnover for the whole area	241 T C yr^{-1}	9,260 T C yr^{-1}

The reported values of carbon (C) turnover are the mean values. The total C turnover at the Mingulay Reef is based on data from live Lophelia pertusa, the sponge Spongosorites coralliophaga and Aquatic Eddy-Correlation (AEC) data of the dead framework. The AEC measurements capture the oxygen consumption of the dead framework and baffled sediment community. The results on C turnover for Logachev include data of live and dead L. pertusa, sediments and baffled sediments (see Section "Oxygen Consumption and Nitrogen Release").

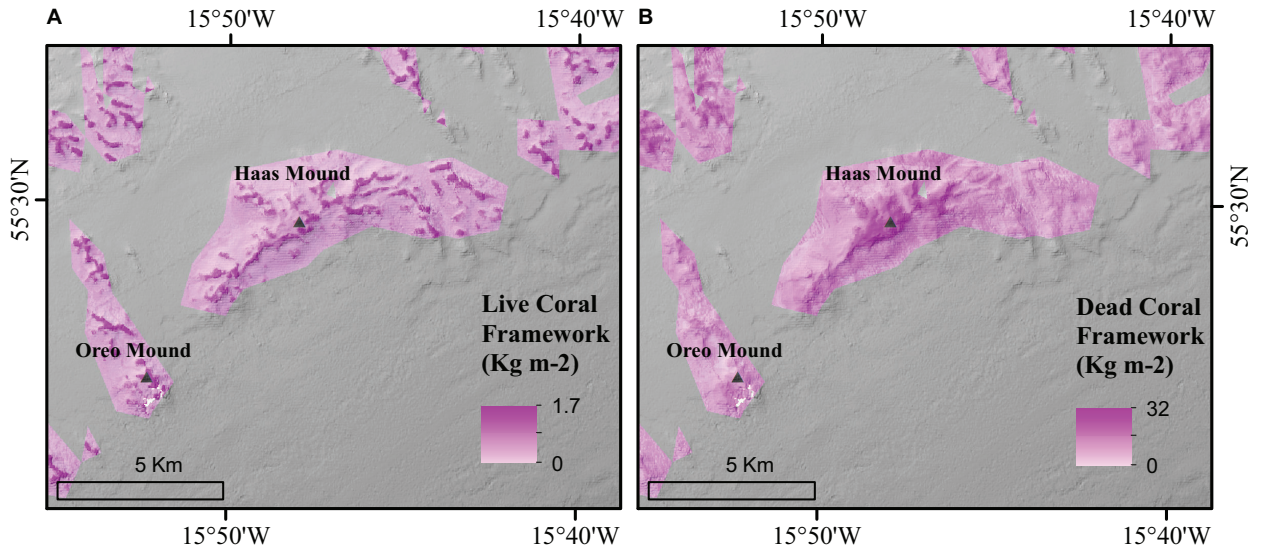

FIGURE 9 | Triangles represent the location of AEC deployment by de Froe et al. (2019) in both the predictive **(A)** live and **(B)** dead coral framework map.

reef habitat area, respectively. This indicates that almost the entire primary production, i.e., 91–95% (5,252–6,802 T C $year^{-1}$), would have to be supplied through tidal downwelling, nepheloid layers, lateral deep-water advection and/or by the topographically-enhanced carbon pump (Duineveld et al., 2004; White et al., 2005; Mienis et al., 2007; Soetaert et al., 2016). Our study suggests that the C requirement of the reef could be higher than the yearly PP over the area of 6,194 T C $year^{-1}$ (Tyberghein et al., 2012; Assis et al., 2018) depending on seasonal PP and/or biomass variability. This could mean that the PP right above the area might not be sufficient to sustain the reef and highlights the importance of the supply of food trough advection from the wider area, bottom currents together with material retention and recycling of waste material on the reef, in particular during winter food limitation (Maier et al., 2020, 2021). For example, studies have indicated that the reef could benefit from nitrification (re-utilization) of faunal-produced NH^{+}_{4} (Maier et al., 2020, 2021) and utilization of dissolved OM, which is produced by the corals as mucus (Wild et al., 2004). The dependence of the reef's function on these alternative supply mechanisms appears greater at the LMP compared to the Mingulay Reef (De Clippele et al., 2021) (**Table 5**), and is likely due to their location at greater depths with comparatively lower food flux. The supply of food needed to sustain the reef could be severely impacted by climate-induced changes in primary production, local hydrodynamical food supply, which could have severe implications for the survival and functioning of CWC reefs.

Conclusion

Biomass maps can guide sampling and monitoring expeditions and our current approach can be applied to other habitats, to provide large-scale maps of biomass, hotspots of metabolic activity and nutrient mineralization, in particular in the understudied, but large deep-sea realm. The predictive power of this approach can be improved by adding more coral surface area data, especially where the coefficient of variation of the map is higher. Additional local measurements on nutrient cycling, high resolution multibeam data (De Clippele et al., 2019) or more environmental variables (e.g., hydrodynamics) and the use of photo mosaics (Bodenmann and Thornton, 2017; Conti et al., 2019; Price et al., 2019) could further improve our understanding how complex habitats contribute to nutrient cycling. Biomass maps can also advice on the most optimal locations to collect AEC respiration data, to ensure a representative amount of habitat complexity is captured in the measurements (Rovelli et al., 2015; De Clippele et al., 2021). Alternatively, AEC deployments could be used to ground truth the biomass maps. Understanding how much dead and live coral framework is present in this area is especially important in deeper reefs such as the LMP, where ocean acidification threatens to dissolve dead coral framework (Hennige et al., 2015). If the dead coral framework dissolves, not only will the habitat of CWC reef organisms disappear (Kazanidis et al., 2016; Maier et al., 2021), but C and N demineralization, and sediment baffling will diminish. This may ultimately reduce primary production in surface waters, affecting the CO_2 being extracted from the atmosphere. Consequently, these effects will negatively impact the existence of the CWC mounds in the LMP and the overall functioning of the area.

DATA AVAILABILITY STATEMENT

The raw data supporting the conclusions of this article will be made available by the authors, without undue reservation, to any qualified researcher.

AUTHOR CONTRIBUTIONS

LDC: conceptualization, writing, and methodology. AVDK, SRM, and EDF: review and editing of the manuscript and methodology. JMR: review and editing of the manuscript. All authors contributed to the article and approved the submitted version.

FUNDING

LDC, EDF and JMR acknowledge funding from the EU Horizon 2020 ATLAS (Grant Agreement No. 678760 to JMR) and iAtlantic projects (Grant Agreement No. 818123 to JMR). SRM was funded by the Royal Netherlands Institute for Sea Research (Grant 864.13.007). AVDK was supported by collaboration funding between Utrecht University and the Royal Netherlands Institute for Sea Research.

ACKNOWLEDGMENTS

The ROV video and multibeam bathymetry used in this study was gathered during the JC073 expedition through the UK Ocean Acidification Research Programme benthic consortium (NERC grant NE/H017305/1 to JMR). We thank the captain and the crew of the RRS *James Cook* for assistance at sea.

SUPPLEMENTARY MATERIAL

The Supplementary Material for this article can be found online at: https://www.frontiersin.org/articles/10.3389/fmars.2021.721062/full#supplementary-material

REFERENCES

Armstrong, C. W., Foley, N. S., Tinch, R., and van den Hove, S. (2012). Services from the deep: steps towards valuation of deep sea goods and services. *Ecosyst. Serv.* 2, 2–13. doi: 10.1016/j.ecoser.2012.07.001

Assis, J., Tyberghein, L., Bosch, S., Verbruggen, H., Serr, E. A., and De Clerck, O. (2018). Bio-ORACLE v2 . 0?: extending marine data layers for bioclimatic modelling. *Glob. Ecol. Biogr.* 27, 277–284. doi: 10.1111/geb.12693

Baccini, A., Laporte, N., Goetz, S. J., Sun, M., and Dong, H. (2008). A first map of tropical Africa's above-ground biomass derived from satellite imagery. *Environ. Res. Lett.* 3:045011. doi: 10.1088/1748-9326/3/4/045011

Bodenmann, A., and Thornton, B. (2017). Generation of high-resolution three-dimensional reconstructions of the seafloor in color using a single camera and structured light. *J. Field Robot.* 34, 833–851. doi: 10.1002/rob.21682

Breiman, L. (2001). Random forests. *Mach. Learn.* 45, 5–32. doi: 10.1023/A:1010933404324

Buhl-Mortensen, L., Vanreusel, A., Gooday, A. J., Levin, L. A., Priede, I. G., Buhl-Mortensen, P., et al. (2010). Biological structures as a source of habitat heterogeneity and biodiversity on the deep ocean margins. *Mar. Ecol.* 31, 21–50. doi: 10.1111/j.1439-0485.2010.00359.x

Cathalot, C., Van Oevelen, D., Cox, T. J. S., Kutti, T., Lavaleye, M., Duineveld, G., et al. (2015). Cold-water coral reefs and adjacent sponge grounds: hotspots of benthic respiration and organic carbon cycling in the deep sea. *Front. Mar. Sci.* 2:37. doi: 10.3389/fmars.2015.00037

Conti, L. A., Lim, A., and Wheeler, A. J. (2019). High resolution mapping of a cold water coral mound. *Sci. Rep.* 9:1016. doi: 10.1038/s41598-018-37725-x

Cutler, D., Edwards, T. C., Beard, K., Cutler, A., Hess, K. T., and Gibson, J. C. (2007). Random forests for classification in ecology. *Ecology* 88, 2783–2792. doi: 10.1890/07-0539.1

Davies, A. J., Duineveld, G. C. A., Lavaleye, M. S. S., Bergman, M. J. N., Van Haren, H., and Roberts, J. M. (2009). Downwelling and deep-water bottom currents as food supply mechanisms to the cold-water coral *Lophelia pertusa* (Scleractinia) at the Mingulay reef complex. *Limnol. Oceanogr.* 54, 620–629. doi: 10.4319/lo.2009.54.2.0620

De Clippele, L. H., Gafeira, J., Robert, K., Hennige, S., Lavaleye, M. S., Duineveld, G. C. A., et al. (2017). Using novel acoustic and visual mapping tools to predict the small-scale spatial distribution of live biogenic reef framework in cold-water coral habitats. *Coral Reefs* 36, 255–268. doi: 10.1007/s00338-016-1519-8

De Clippele, L. H., Huvenne, V. A. I., Molodtsova, T. N., and Roberts, J. M. (2019). The diversity and ecological role of non-scleractinian corals (Antipatharia and Alcyonacea) on scleractinian cold-water coral mounds. *Front. Mar. Sci.* 6:184. doi: 10.3389/fmars.2019.00184

De Clippele, L. H., Rovelli, L., Kazanidis, G., Vad, J., Turner, S., Glud, R. N., et al. (2021). Mapping cold-water coral biomass: an approach to derive ecosystem functions. *Coral Reefs* 40, 215–231. doi: 10.1007/s00338-020-02030-5

de Froe, E., De, Rovelli, L., Glud, R. N., Maier, S. R., Duineveld, G., et al. (2019). Benthic oxygen and nitrogen exchange on a cold-water coral reef in the North-East Atlantic Ocean. *Front. Mar. Sci.* 6:665. doi: 10.3389/fmars.2019.00665

de Haas, H., Mienis, F., Frank, N., Richter, T. O., Steinacher, R., de Stigter, H., et al. (2009). Morphology and sedimentology of (clustered) cold-water coral mounds at the south Rockall Trough margins. NE Atlantic Ocean. *Facies* 55, 1–26.

Duineveld, G. C. A., Lavaleye, M. S. S., and Berghuis, E. M. (2004). Particle flux and food supply to a seamount cold-water coral community (Galicia Bank, NW Spain). *Mar. Ecol. Prog. Ser.* 277, 13–23. doi: 10.3354/meps277013

Duineveld, G. C., Lavaleye, M. S., Bergman, M. J., De Stigter, H., and Mienis, F. (2007). Trophic structure of a cold-water coral mound community (Rockall Bank, NE Atlantic) in relation to the near-bottom particle supply and current regime. *Bull. Mar. Sci.* 81, 449–467.

Eisele, M., Frank, N., Wienberg, C., Hebbeln, D., Correa, M. L., Douville, E., et al. (2011). Productivity controlled cold-water coral growth periods during the last glacial off Mauritania. *Mar. Geol.* 280, 143–149. doi: 10.1016/j.margeo.2010.12.007

Findlay, H. S., Artioli, Y., Moreno Navas, J., Hennige, S. J., Wicks, L. C., Huvenne, V. A. I., et al. (2013). Tidal downwelling and implications for the carbon biogeochemistry of cold-water corals in relation to future ocean acidification and warming. *Glob. Change Biol.* 19, 2708–2719. doi: 10.1111/gcb.12256

Freiwald, A. (2002). "Reef-forming cold-water corals," in *Ocean Margin Systems*, eds G. Wefer, D. Billet, and D. Hebbeln (Berlin: Springer), 365–385.

Glud, R. N. (2008). Oxygen dynamics of marine sediments. *Mar. Biol. Res.* 4, 243–289. doi: 10.1080/17451000801888726

Greene, H. G., Yoklavich, M. M., Starr, R. M., O'Connell, V. M., Wakefield, W. W., Sullivan, D. E., et al. (1999). A classification scheme for deep seafloor habitats. *Oceanologica Acta* 22, 663–678. doi: 10.1016/S0399-1784(00)88957-4

Guinan, J., Brown, C., Dolan, M. F. J., and Grehan, A. J. (2009). Ecological niche modelling of the distribution of cold-water coral habitat using underwater remote sensing data. *Ecol. Inform.* 4, 83–92. doi: 10.1016/j.ecoinf.2009.01.004

Hebbeln, D., Wienberg, C., Wintersteller, P., Freiwald, A., Becker, M., Beuck, L., et al. (2014). Environmental forcing of the Campeche cold-water coral province, southern Gulf of Mexico. *Biogeosciences* 11, 1799–1815. doi: 10.5194/bg-11-1799-2014

Hennige, S. J., Wicks, L. C., Kamenos, N. A., Bakker, D. C. E., Findlay, H. S., Dumousseaud, C., et al. (2014). Short-term metabolic and growth responses of the cold-water coral Lophelia pertusa to ocean acidification. *Deep Sea Res. Part II Top. Stud. Oceanogr.* 99, 27–35. doi: 10.1016/j.dsr2.2013.07.005

Hennige, S. J., Wicks, L. C., Kamenos, N. A., Perna, G., Findlay, H. S., and Roberts, J. M. (2015). Hidden impacts of ocean acidification to live and dead coral framework. *Proc. R. Soc. B* 282:20150990. doi: 10.1098/rspb.2015.0990

Hennige, S., Wolfram, U., Wickes, L., Murray, F., Roberts, J. M., Kamenos, N., et al. (2020). Crumbling reefs and coral habitat loss in a future ocean: evidence of 'coralporosis' as an indicator of habitat integrity. *Front. Mar. Sci.* 7:668. doi: 10.3389/fmars.2020.00668

Henry, L. A., and Roberts, J. M. (2007). Biodiversity and ecological composition of macrobenthos on cold-water coral mounds and adjacent off-mound habitat in the bathyal Porcupine Seabight, NE Atlantic. *Deep Sea Res. Part I Oceanogr. Res. Papers* 54, 654–672. doi: 10.1016/j.dsr.2007.01.005

Jenness, J. (2002). Surface Areas and Ratios from Elevation Grid (Surfgrids.avx) Extension for ArcView 3.x. Jenness Enterprises. Available Online at: www.jennessent.com/arcview/surface_areas.htm

Johnson, D., Adelaide Ferreira, M., and Kenchington, E. (2018). Climate change is likely to severely limit the effectiveness of deep-sea ABMTs in the North Atlantic. *Mar. Policy* 87, 111–122. doi: 10.1016/j.marpol.2017.09.034

Jonsson, L. G., Nilsson, P. G., Floruta, F., and Lundálv, T. (2004). Distributional patterns of macro-and megafauna associated with a reef of the cold-water coral Lophelia pertusa on the Swedish west coast. *Mar. Ecol. Prog. Ser.* 284, 163–171.

Kazanidis, G., Henry, L. A., Roberts, J. M., and Witte, U. F. M. (2016). Biodiversity of Spongosorites coralliophaga (Stephens, 1915) on coral rubble at two contrasting cold-water coral reef settings. *Coral Reefs* 35, 193–208. doi: 10.1007/s00338-015-1355-2

Kenyon, N. H., Akhmetzhanov, A. M., Wheeler, A. J., van Weering, T. C. E., de Haas, H., and Ivanov, M. K. (2003). Giant carbonate mud mounds in the southern Rockall Trough. *Mar. Geol.* 195, 5–30. doi: 10.1016/S0025-3227(02)00680-1

Khripounoff, A., Caprais, J., Bruchec, J., Le, Rodier, P., and Noel, P. (2014). Deep cold-water coral ecosystems in the Brittany submarine canyons (Northeast Atlantic): Hydrodynamics, particle supply, respiration, and carbon cycling. *Limnol. Oceanogr.* 59, 87–98. doi: 10.4319/lo.2014.59.1.0087

Kiriakoulakis, K., Fisher, E., Wolff, G. A., Freiwald, A., Grehan, A., and Roberts, J. M. (2005). "Lipids and nitrogen isotopes of two deep-water corals from the North-East Atlantic: initial results and implications for their nutrition," in *Cold-Water Corals and Ecosystems*, eds A. Freiwald and J. M. Roberts (Berlin: Springer), 715–729.

Maier, S. R., Kutti, T., Bannister, R. J., Fang, J. K. H., van Breugel, P., van Rijswijk, P., et al. (2020). Recycling pathways in cold-water coral reefs: use of dissolved organic matter and bacteria by key suspension feeding taxa. *Sci. Rep.* 10:9942.

Maier, S. R., Mienis, F., de Froe, E., Soetaert, K., Lavaleye, M., Duineveld, G., et al. (2021). Reef communities associated with 'dead' cold-water coral framework drive resource retention and recycling in the deep sea. *Deep Sea Res. Part I Oceangr. Res. Papers* 175:103574. doi: 10.1016/j.dsr.2021.103574

Maier, S. R., Kutti, T., Bannister, R. J., van Breugel, P., van Rijswijk, P., and Van Oevelen, D. (2019). Survival under conditions of variable food availability: resource utilization and storage in the cold-water coral Lophelia pertusa. *Limnol. Oceanogr.* 64, 1651–1671.

Mienis, F., de Stigter, H. C., White, M., Duineveld, G., De Haas, H., and van Weering, T. C. E. (2007). Hydrodynamic controls on cold-water coral growth and carbonate-mound development at the SW and SE Rockall Trough Margin, NE Atlantic Ocean. *Deep Sea Res. Part I Oceanogr. Res. Papers* 54, 1655–1674. doi: 10.1016/j.dsr.2007.05.013

Mohn, C., Rengstorf, A., White, M., Duineveld, G., Mienis, F., Soetaert, K., et al. (2014). Linking benthic hydrodynamics and cold-water coral occurrences: a high-resolution model study at three cold-water coral provinces in the NE Atlantic. *Prog. Oceanogr.* 122, 92–104. doi: 10.1016/j.pocean.2013.12.003

Mortensen, P. B., and Fosså, J. H. (2006). "Species diversity and spatial distribution of invertebrates on deep-water Lophelia reefs in Norway," in *Proceedings of 10th International Coral Reef Symposium* (Japan).

Price, D. M., Robert, K., Callaway, A., Hall, R. A., and Huvenne, V. A. (2019). Using 3D photogrammetry from ROV video to quantify cold-water coral reef structural complexity and investigate its influence on biodiversity and community assemblage. *Coral Reefs* 38, 1007–1021. doi: 10.1007/s00338-019-01827-3

Rengstorf, A. M., Mohn, C., Brown, C., Wisz, M. S., and Grehan, A. J. (2014). Predicting the distribution of deep-sea vulnerable marine ecosystems using high-resolution data: considerations and novel approaches. *Deep Sea Res. Part I* 93, 72–82. doi: 10.1016/j.dsr.2014.07.007

Roberts, J. M. (2013). *Changing Oceans Expedition 2013. RRS James Cook 073 Cruise Report*. Scotland: Heriot-Watt University.

Roberts, J. M., and Cairns, S. D. (2014). Cold-water corals in a changing ocean. *Curr. Opin. Environ. Sustain.* 7, 118–126. doi: 10.1016/j.cosust.2014.01.004

Roberts, J. M., Wheeler, A. J., Freiwald, A., and Cairns, S. D. (2009). *Cold-water Corals: The Biology and Geology of Deep-sea Coral Habitats*. Cambridge: Cambridge University Press. doi: 10.1017/CBO9780511581588

Rogan, J., Franklin, J., Stow, D., Miller, J., Woodcock, C., and Roberts, D. (2008). Mapping land-cover modifications over large areas: a comparison of machine learning algorithms. *Remote Sens. Environ.* 112, 2272–2283. doi: 10.1016/j.rse.2007.10.004

Rovelli, L., Attard, K. M., Bryant, L. D., Flögel, S., Stahl, H., Roberts, J. M., et al. (2015). Benthic O2 uptake of two cold-water coral communities estimated with the non-invasive eddy correlation technique. *Mar. Ecol. Prog. Ser.* 525, 97–104. doi: 10.3354/meps11211

Rowden, A. A., Anderson, O. F., Georgian, S. E., Bowden, D. A., Clark, M. R., Pallentin, A., et al. (2017). High-resolution habitat suitability models for the conservation and management of vulnerable marine ecosystems on the louisville seamount Chain, South Pacific Ocean. *Front. Mar. Sci.* 4:335. doi: 10.3389/fmars.2017.00335

Rueden, C. T., Schindelin, J., Hiner, M. C., DeZonia, B. E., Walter, A. E., Arena, E. T., et al. (2017). ImageJ2: imageJ for the next generation of scientific image data. *BMC Bioinformatics* 18:529. doi: 10.1186/s12859-017-1934-z

Soetaert, K., Mohn, C., Rengstorf, A., Grehan, A., and van Oevelen, D. (2016). Ecosystem engineering creates a direct nutritional link between 600-m deep cold-water coral mounds and surface productivity. *Sci. Rep.* 6:35057.

Suess, E. (1980). Particulate organic carbon flux in the oceans-surface productivity and oxygen utilisation. *Nature* 288, 260–263. doi: 10.1038/288260a0

Sweetman, A. K., Thurber, A. R., Smith, C. R., Levin, L. A., Mora, C., Wei, C. L., et al. (2017). Major impacts of climate change on deep-sea benthic ecosystems. *Elementa Sci. Anthropocene* 5:4. doi: 10.1525/elementa.203

Titschack, J., Baum, D., De Pol-Holz, R., Lopez Correa, M., Forster, N., Flögel, S., et al. (2015). Aggradation and carbonate accumulation of Holocene Norwegian cold-water coral reefs. *Sedimentology* 62, 1873–1898. doi: 10.1111/sed.12206

Tyberghein, L., Verbruggen, H., Pauly, K., Troupin, C., Mineur, F., and De Clerck, O. (2012). Bio-ORACLE?: a global environmental dataset for marine species. *Glob. Ecol. Biography* 21, 272–281. doi: 10.1111/j.1466-8238.2011.00656.x

van der Kaaden, A., and De Clippele, L. H. (2021). *AnnavdKaaden/ImageAnnotation: Image/Video Annotation and Analysis (Version v2). Zenodo*

van Oevelen, D., van, Duineveld, G., Lavaleye, M., Mienis, F., Soetaert, K., et al. (2009). The cold-water coral community as a hot spot for carbon cycling on continental margins: a food-web analysis from Rockall Bank (northeast Atlantic). *Limnol. Oceanogr.* 54, 1829–1844. doi: 10.4319/lo.2009.54.6.1829

Van Weering, T. C. E., De Haas, H., De Stigter, H. C., Lykke-Andersen, H., and Kouvaev, I. (2003). Structure and development of giant carbonate mounds at the SW and SE rockall Trough margins, NE Atlantic Ocean. *Mar. Geol.* 198, 67–81. doi: 10.1016/S0025-3227(03)00095-1

Wei, C., Rowe, G. T., Escobar-briones, E., Boetius, A., Soltwedel, T., Caley, J., et al. (2010). Global patterns and predictions of seafloor biomass using random forests. *PLoS One* 5:e15323. doi: 10.1371/journal.pone.0015323

White, M. (2007). Benthic dynamics at the carbonate mound regions of the Porcupine Sea Bight continental margin. *Int. J. Earth Sci.* 96, 1–9. doi: 10.1007/s00531-006-0099-1

White, M., Mohn, C., de Stigter, H., and Mottram, G. (2005). "Deep-water coral development as a function of hydrodynamics and surface productivity around the submarine banks of the Rockall Trough, NE Atlantic," in *Cold-Water Corals and Ecosystems*, ed. A. Freiwald and J. M. Roberts. (Berlin: Springer), 503–514.

Wild, C., Huettel, M., Klueter, A., Kremb, S. G., Rasheed, M. Y., and Jørgensen, B. B. (2004). Coral mucus functions as an energy carrier and particle trap in the reef ecosystem. *Nature* 428, 66–70. doi: 10.1038/nature02344

Wild, C., Mayr, C., Wehrmann, L., Schöttner, S., Naumann, M., Hoffmann, F., et al. (2008). Organic matter release by cold water corals and its implication

for fauna-microbe interaction. *Mar. Ecol. Prog. Ser.* 372, 67–75. doi: 10.3354/meps07724

Windholz, M., Budavari, S., Blumetti, R. F., and Otterbein, E. S. (1983). *The Merck Index, 10th Edn.* Rahway, NJ: Merck and Co., Inc.

Wright, D. J., Lundblad, E. R., Larkin, E. M., Rinehart, R. W., Murphy, J., Cary-Kothera, L., et al. (2005). *ArcGIS Benthic Terrain Modeler. Corvallis, Oregon, Oregon State University, Davey Jones Locker Seafloor Mapping/Marine GIS Laboratory and NOAA Coastal Services Center*. Available online at: http://maps.csc.noaa.gov/digitalcoast/tools/btm

Zhang, C. (2015). Applying data fusion techniques for benthic habitat mapping and monitoring in a coral reef ecosystem. *ISPRS J. Photogramm. Remote Sens.* 104, 213–223. doi: 10.1016/j.isprsjprs.2014.06.005

Author Disclaimer: This manuscript reflects the authors' view alone, and the European Union cannot be held responsible for any use that may be made of the information contained herein.

Conflict of Interest: The authors declare that the research was conducted in the absence of any commercial or financial relationships that could be construed as a potential conflict of interest.

Publisher's Note: All claims expressed in this article are solely those of the authors and do not necessarily represent those of their affiliated organizations, or those of the publisher, the editors and the reviewers. Any product that may be evaluated in this article, or claim that may be made by its manufacturer, is not guaranteed or endorsed by the publisher.

frontiers | Frontiers in Marine Science

ORIGINAL RESEARCH
published: 11 July 2022
doi: 10.3389/fmars.2022.863693

Climate-Change Refugia for the Bubblegum Coral *Paragorgia arborea* in the Northwest Atlantic

Shuangqiang Wang†, *F. Javier Murillo*† *and Ellen Kenchington* *

Department of Fisheries and Oceans, Ocean Ecology Section, Bedford Institute of Oceanography, Dartmouth, NS, Canada

The large, habitat-forming bubblegum coral, *Paragorgia arborea*, is a vulnerable marine ecosystem indicator with an antitropical distribution. Dense aggregations of the species have been protected from bottom-contact fishing in the Scotian Shelf bioregion off Nova Scotia, Canada in the northwest Atlantic Ocean. Recently, basin-scale habitat suitability ensemble modeling has projected an alarming loss of 99% of suitable habitat for this species across the North Atlantic by 2100. Here, a regional reassessment of the predicted distribution of this species in the bioregion, using both machine learning (random forest) and generalized additive model (GAM) frameworks, including projection to 2046–2065, was undertaken. Extrapolation diagnostics were applied to determine the degree to which the models projected into novel covariate space (i.e., extrapolation) in order to avoid erroneous inferences. The best predictors of the species' distribution were a suite of temporally-invariant terrain variables that identified suitable habitat along the upper continental slope. Additional predictors, projected to vary with future ocean climatologies, identified areas of the upper slope in the eastern portion of the study area that will remain within suitable ranges for *P. arborea* at least through to the mid-century. Additionally, 3-D Lagrangian particle tracking simulations indicated potential for both connectivity among known occurrence sites and existing protected areas, and for colonization of unsurveyed areas predicted to have suitable habitat, from locations of known occurrence. These results showed that extirpation of this iconic species from the Scotian Shelf bioregion is unlikely over the next decades. Potential climate refugia were identified and results presented in the context of protected area network design properties of representativity, connectivity, adequacy, viability and resilience.

Keywords: climate-change refugia, deep-sea coral, species distribution modeling, model transferability, lagrangian particle tracking, *Paragorgia arborea*, protected area design

OPEN ACCESS

Edited by:
Anna Metaxas,
Dalhousie University, Canada

Reviewed by:
Ashley Alun Rowden,
National Institute of Water and Atmospheric Research (NIWA), New Zealand
Rebecca E. Ross,
Norwegian Institute of Marine Research (IMR), Norway

***Correspondence:**
Ellen Kenchington
Ellen.Kenchington@dfo-mpo.gc.ca

†*These authors share first authorship*

Specialty section:
This article was submitted to Deep-Sea Environments and Ecology, a section of the journal Frontiers in Marine Science

Received: *27 January 2022*
Accepted: *03 June 2022*
Published: *11 July 2022*

Citation:
Wang S, Murillo FJ and Kenchington E (2022) Climate-Change Refugia for the Bubblegum Coral Paragorgia Arborea in the Northwest Atlantic. Front. Mar. Sci. 9:863693. doi: 10.3389/fmars.2022.863693

1 INTRODUCTION

The large, fan-shaped gorgonian octocorals of the genus *Paragorgia* Milne Edwards, 1857, known as 'bubblegum corals' (**Figure 1**), form ecologically significant habitats on hard substrates along the continental margins of eastern North America (Gass, 2002; Metaxas and Giffin, 2004; Mortensen and Buhl-Mortensen, 2004; Buhl-Mortensen and Mortensen, 2005; Gass and Willison, 2005; Leverette and Metaxas, 2005; Metaxas and Davis, 2005; Watling and Auster, 2005; Quattrini et al., 2015; Kenchington et al., 2019a), and elsewhere (Sánchez, 2005;

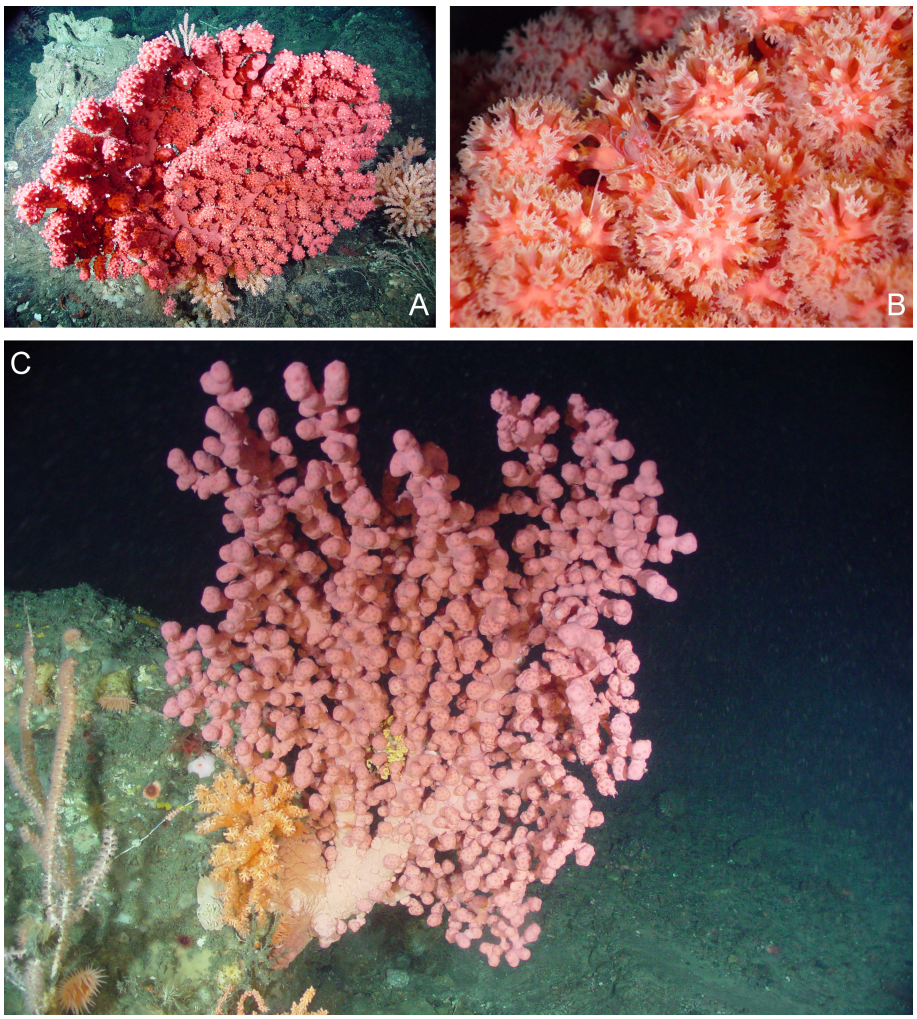

FIGURE 1 | *In situ* images of *Paragorgia arborea* from the Northeast Channel Coral Conservation Area. **(A)** Intact colony growing on bedrock; **(B)** Close up of polyps open for feeding; **(C)** Intact colony growing on a boulder.

Herrera et al., 2012; De Clippele et al., 2015; Morato et al., 2021). Of the 18 accepted species in the genus (Cordeiro et al., 2021), *P. arborea* (Linnaeus, 1758) and *P. johnsoni* Gray, 1862 are found on the continental slope off Nova Scotia, Canada, with *P. arborea* being the more frequently recorded (Cogswell et al., 2009; Strychar et al., 2011). In this region, both *Paragorgia* species are long-lived and slow-growing, attaining colony heights of 240 cm, and forming dense aggregations (Sherwood and Edinger, 2009; Watanabe et al., 2009). They are considered to be indicators of vulnerable marine ecosystems (ICES, 2021; NAFO, 2021), and are thereby linked to international conservation efforts advanced by the United Nations (FAO, 2016).

Thirteen bioregions, sub-divided into planning areas, have been delineated in Canadian waters to inform MPA network development (DFO, 2009; DFO, 2014). These biogeographic zones were delineated based primarily on a common set of ecological, oceanographic and bathymetric similarities (DFO, 2009). Among those, *Paragorgia* spp. are found in the Scotian Shelf bioregion within which is embedded the "Offshore Scotian Shelf" planning area, defined as extending from the 12-nautical mile limit of Canada's Territorial Sea to the 200-mile limit of its Exclusive Economic Zone (**Figure 2**), including parts of the Scotian Shelf itself, as well as portions of Georges Bank and the Gulf of Maine (DFO, 2014). A series of canyons incise the continental slope in that planning area, and provide habitat for bubblegum corals (Watanabe et al., 2009), some of which is subject to specific coral-protection measures. In 2002, Fisheries and Oceans Canada (DFO) established the Northeast Channel Coral Conservation Area to protect some of the region's largest aggregations of octocorals from the impacts of bottom-contact fishing gears (DFO, 2019). Smaller aggregations of *Paragorgia* spp. are similarly protected in the Corsair and Georges Canyons Conservation Area (Metaxas et al., 2019), in the Gully Marine Protected Area (Breeze and Fenton, 2007), and the *Lophelia* Coral Conservation Area, at the mouth of the Laurentian Channel (Beazley et al., 2021a).

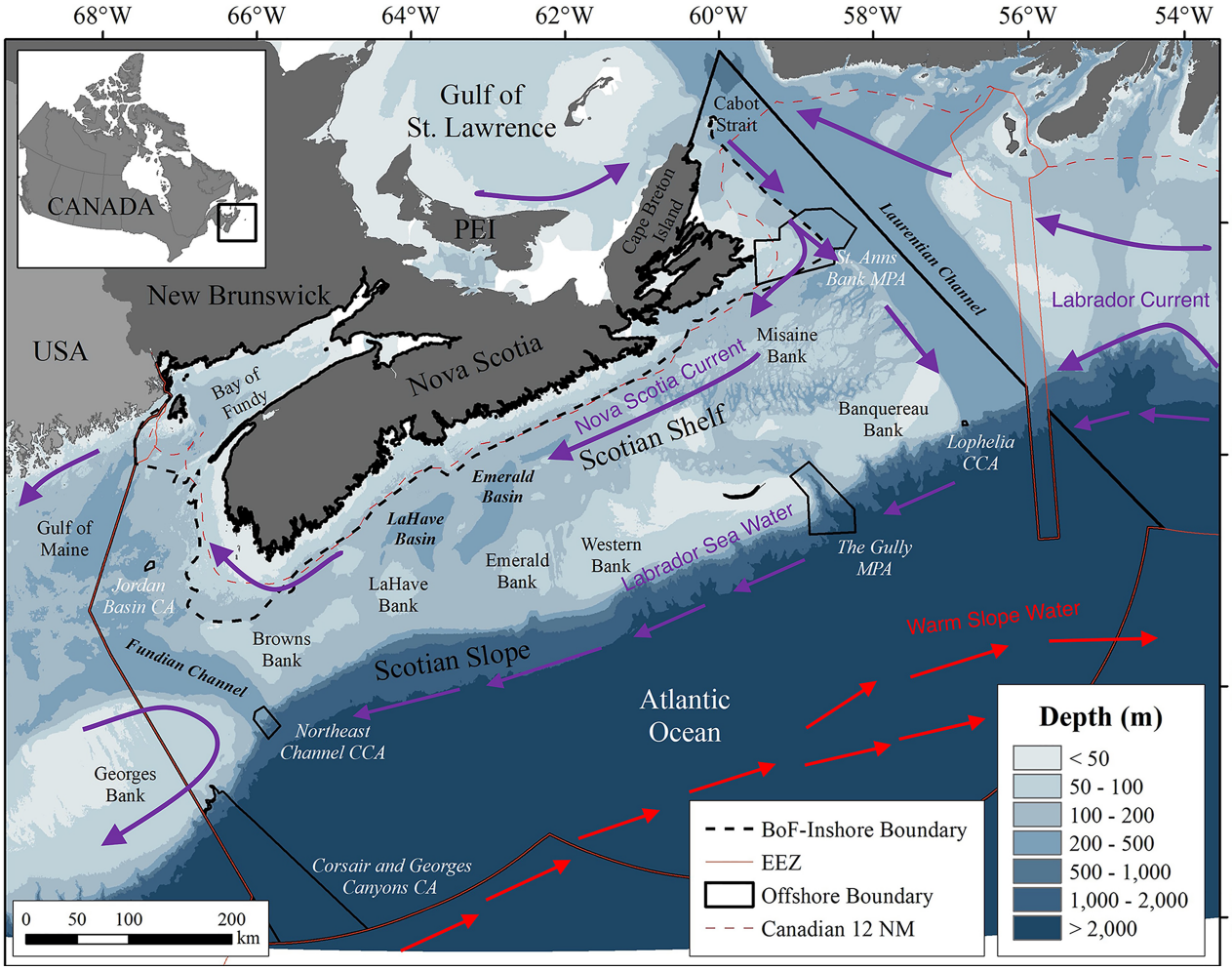

FIGURE 2 | Place names and locations of features in the Scotian Shelf bioregion study area (black perimeter). The six conservation areas within the study area but outside the 12 nm Territorial Sea (dashed line) are shown in black outline with their names in white lettering. The general location of currents and water masses influencing the region are indicated. CA, Conservation Area; CCA, Coral Conservation Area; MPA, Marine Protected Area.

Those protection areas were adopted independently, as aggregations were discovered and described. With the need to develop a network of protected areas in response to domestic (Oceans Act Section 35 (2)), and international (UN Convention on Biological Diversity, UN Sustainable Development Goals) policies, network properties such as representativity, connectivity, adequacy and viability must be considered (DFO, 2010; Garcia et al., 2021). Furthermore, with changing climatic conditions there is a need to consider climate resiliency in protected area network design (Brock et al., 2012; Simard et al., 2016).

Predictive models of species distributions, when presented with associated levels of uncertainty, enable managers to make informed decisions on the trade-offs implicit in marine spatial planning (Lester et al., 2013; Grorud-Colvert et al., 2014; Carr, 2019; Metaxas et al., 2019), while insight into the impacts of climate change on the size and configuration of suitable habitat, can improve network design (Santos et al., 2020). Meanwhile, Lagrangian particle tracking (LPT) models are valuable for assessing connectivity (e.g., Bracco et al., 2019; Kenchington et al., 2019b; Metaxas et al., 2019; Zeng et al., 2019; Wang et al., 2020; Wang et al., 2021), and can provide independent support for the evaluation of species distribution models (Kenchington et al., 2019b; Wang et al., 2021). In LPT models, virtual "particles" are advected by flow fields derived from numerical ocean models. Vertical behaviours can also be modeled through particle releases at different depths, and by incorporating vertical velocities into the tracking algorithms, such that the particles can mimic active drifters, enabling predictions of biophysical connectivity.

Recently, basin-scale distribution modeling of *P. arborea* habitat under present-day (1951–2000) and future (2081–2100) environmental conditions (the latter modeled as Intergovermental Panel on Climate Change (IPCC) Representative Concentration Pathway (RCP) 8.5, a "business-as-usual" scenario), projected an alarming loss of 99% of suitable habitat across the North Atlantic, including in the Offshore Scotian Shelf planning area (Morato et al., 2020). Consequently, a review of existing protections for

this species and of the properties required for a protected area network is needed, to support effective conservation efforts. That review must necessarily consider whether the results of basin-scale modeling of *P. arborea* habitat can be validly applied at the scale of the planning area.

Modeling of future ocean climate typically relies on low-resolution models designed to capture large-scale open-ocean properties (IPCC, 2013), the resulting products often being subsequently down-scaled for use in species distribution modeling. Such low-resolution models are inappropriate for capturing shelf-scale processes or for regions with sharp oceanographic boundaries, such as the Canadian Atlantic, where a higher native resolution is required to simulate ocean processes accurately, including under future projections (Stock et al., 2011; Brickman et al., 2016). Modeling over large spatial scales also increases the likelihood of both spatial autocorrelations in species-environmental relationships and the extrapolation of those relationships to non-analogous environments, which can lead to poorly-specified species distribution models with limited transferability to generate predictions for novel, including future, environments (Miller, 2012; Sequeira et al., 2018; Yates et al., 2018; Mannocci et al., 2020). In some situations, predicted distribution models are improved when they are calibrated within areas with a similar climate (Morán-Ordóñez et al., 2017; Qiao et al., 2018). For *Paragorgia* spp. in particular, heterogeneity in species/environment relationships over basin scales is indicated by the differences in relative importance of variables among studies by Bryan and Metaxas (2007), in the northwest Atlantic, and Sundahl et al. (2020), in the northeast. There are also regional differences in genetic composition of *P. arborea* within the North Atlantic (Herrera et al., 2012), potentially indicating differing environmental niches.

Metaxas et al. (2019) applied LPT hindcast models parameterized to the known biological traits of *P. arborea* and *Primnoa resedaeformis* to examine transborder connectivity among the canyons in the Corsair Canyon region along the slope of Georges Bank. A Finite-Volume Community Ocean Model (FVCOM) was used to generate velocity fields built across the Gulf of Maine. FVCOM models can have poor model accuracy in areas of steep slope (Feng et al., 2022), and the canyons in this region were poorly resolved (Metaxas et al., 2019). Nevertheless, there was evidence for connectivity to Corsair Canyon from the south, particularly from the two closest canyons, Georges in Canadian waters, and Heezen Canyon in US waters. Limited connectivity from the Northeast Channel Coral Conservation Area was observed in winter and spring, and it was suggested that future work should entail forward-tracking modeling to test hypotheses of dispersal trajectories emanating from Corsair Canyon and the Northeast Channel, specifically. In this study a similar approach was taken over a larger spatial extent, building on the demonstrated utility of applying LPT models to address issues of connectivity in *P. arborea*.

Here, a regional reassessment of both present-day and future distributions of *P. arborea* habitat in the Offshore Scotian Shelf planning area was undertaken, integrating the results of various species distribution and LPT models to evaluate the properties of representativity, connectivity, adequacy, viability and resiliency in relation to protected area network design (**Supplementary Table 1**). Models of the present-day distribution filled data gaps and supported evaluation of representativity. Climate resiliency was examined with additional models of the distributions of *P. arborea* habitat under climate projections for 2046–2065, assessed against a model built on the same variables but under 1990–2015 reference conditions, to allow examination of dynamic relationships among sites in time and space. Areas with projected conditions analogous to those of the reference period, representing potential climate refugia for long-lived *Paragorgia* spp., were identified.

The transferability of the species distribution models (Sequeira et al., 2018; Yates et al., 2018; Liu et al., 2020) was evaluated to determine their reliability (Mesgaran et al., 2014). For areas where suitable habitat was predicted but for which no presence records were available, the potential for larvae to colonize the areas from known populations using the LPT models was evaluated.

2 MATERIALS AND METHODS

2.1 Study Area

The study area, the Scotian Shelf bioregion (**Figure 2**), encompasses the marine waters of DFO's Maritimes Region, an administrative unit that includes the Bay of Fundy, parts of the Gulf of Maine, Georges Bank and the Laurentian Channel, plus the entire Scotian Shelf, the adjacent continental slope, rise and a portion of the abyssal plain, delimited to the southeast by the boundary of Canada's Exclusive Economic Zone. Within that area, a 5 km buffer drawn around all land was excluded from the analyses. The study area thus contains the Offshore Scotian Shelf planning area which informs marine planning exercises such as MPA network development.

The major current and water mass systems that influence the area occupied by *P. arborea* in the Scotian Shelf bioregion have been well-characterized. The Gulf Stream transports warm, saline water from the south and contributes to the formation of a warm and saline water mass, the Warm Slope Water (WSW) (**Figure 2**). This water mass extends from the surface to 400 m depth, bringing high nutrient concentrations below the surface (Townsend et al., 2015), and flows northeast between the shelf break and the north wall of the Gulf Stream to round Grand Bank (Csanady and Hamilton, 1988; Fratantoni and Pickart, 2007). South of Nova Scotia, WSW intermittently floods the area between two offshore banks, Emerald and LaHave (**Figure 2**), filling the depths of Emerald Basin with warm, saline water (Drinkwater et al., 2003).

The waters of the continental shelf originate in the Gulf of St. Lawrence, where a very cold, low-salinity Cold Intermediate Layer and, in summer, a warm surface layer, cross the shallow banks of the eastern Scotian Shelf (Han and Loder, 2003), flowing southwestwards with the Nova Scotia Current (**Figure 2**). These waters over the Scotian Shelf flow into the

Gulf of Maine, which also receives a deep inflow of WSW through the Northeast Channel (Townsend et al., 2015). Another branch of the Gulf of St. Lawrence outflow merges with cold, low salinity water from the north carried by the Labrador Current flowing southwestwards along the edge of the Scotian Shelf as a Shelf-Break Current (Han et al., 1999). This cold, less saline Labrador Sea Water is carried along the upper continental slope off Nova Scotia (**Figure 2**).

2.2 Species Distribution Modeling

Two fundamentally different modeling approaches were used to predict the probability of occurrence of *P. arborea*: random forest (RF), a non-parametric machine learning technique in which numerous regression or classification trees are built using random subsets of the data (Breiman, 2001), and generalized additive modeling (GAM), which uses smoothing functions applied to the input data to estimate non-linear effects of the covariates on the dependent variables (Wood, 2006; Conn et al., 2015). RF works well with high-dimensional data, including situations where the number of observations is much less than that of predictor variables, and is relatively insensitive to correlations among those variables (Díaz-Uriarte and Alvarez de Andrés, 2006; Biau, 2012; Biau and Scornet, 2016). GAMs are well-suited for capturing species-environment relationships and detecting trends in the data, however they are sensitive to nonlinear dependence, or concurvity, of the predictor variables (Amodio et al., 2014), and hence were used with a smaller number of poorly correlated predictors.

RF models were built in R version 4.0.4 (R Development Core Team, 2020) using the 'randomForest' package (Liaw and Wiener, 2002), with default parameter values, and the default 500 trees constructed for each model. The predictors were assessed using the 'importance' function of 'randomForest', which calculates the mean decrease in Gini index, or Gini impurity, for each variable. Probability of occurrence across environmental gradients was evaluated using functional response curves (Lopes et al., 2019). The probability of occurrence and the value of each environmental predictor for each raster cell were extracted and smoothed, using the loess method with span = 0.6 applied to each curve.

The GAMs were built with the 'mgcv' package (Wood, 2006) in R, and were based on the binomial error distribution. Model selection followed a backward, stepwise variable-selection approach. Preliminary analysis showed two different relationships between the response data and some environmental variables. The default number of knots (10) was used to capture this pattern.

2.2.1 Modeling Scenarios

A number of scenarios were modeled to address different aspects of the study (**Supplementary Table 1**). RF models, were constructed using both presence and assumed absence data, and initially with 47 environmental predictor variables representing contemporary conditions. The resulting prediction surfaces presented modeled distributions that were extrapolated over large areas, as a consequence of non-analogous conditions in some water-column variables. Following Mesgaran et al. (2014), those variables were removed and an alternative RF model was built using only the top 6 predictors from the first model, all of which were terrain variables. The outputs from those two models were used in assessing the representativity of the closures currently in place.

Examination of changes in the predicted distribution of *P. arborea* habitat across time required models constructed for each of two climate projections for 2046–2065. A subset of 8 projected predictors was available (see below) and was used in both RF modeling and GAMs. Models built under 1990–2015 reference conditions were used to project the future distributions using the same predictors.

2.2.2 Response Variables

Paragorgia spp. presence and absence records were obtained from various sources: DFO research-vessel bottom-trawl surveys conducted in the Maritimes Region during 2002–2019, DFO and Natural Resources Canada optical (camera/video) benthic surveys in 1967 and during 1997–2019, and a NOAA Okeanos Explorer ROV survey conducted in 2019 under the 'Deep Connections 2019: Exploring Atlantic Canyons and Seamounts of the United States and Canada' mission. Presence and assumed absence records (n=11 and 2982, respectively) were drawn from the trawl surveys, while only presence records (n=2366) were obtained from the other surveys. The trawl surveys followed a stratified-random sampling design (Halliday and Kohler, 1971), with fishing standardized as 30-minute tows at 3.5 knots using Western II-A bottom trawls (Tremblay et al., 2007). The starting position of each tow was used as its location, whereas *Paragorgia* spp. records from the benthic imagery were given their individual recorded locations. A 1 × 1 km grid was placed over the study area and the data reduced to recorded presence or assumed absence in each cell (3154 cells with data). In all, 115 of those cells had presence records, for a prevalence of 0.036 (**Figure 3**).

The two species of the genus found in the study area can co-occur (Cogswell et al., 2009), and can be difficult to identify in imagery. Of the 2377 presence records, 2124 were designated *P. arborea*, 11 were *P. johnsoni*, while the remainder could not be identified to species. All records identified as *P. johnsoni* fell within 2 grid cells, each of which also had *P. arborea*. Of the 242 records not identified to species, 14 were located in one cell which also had records of *P. arborea*. The remainder came from a single survey and fell within 4 cells, each less than 2 km from a *P. arborea* record. Therefore, with the dominance of *P. arborea* and the apparent overlapping environmental preferences of the two species, all presence records lacking species identifications are here treated as *P. arborea*.

Assessing accuracy and reliability of prediction models ideally requires data not used in model calibration (Liu et al., 2020). There are 94 records of *P. arborea* from the study area collected prior to 2002 that were not included in the response data for the models. Some were provided by fishermen and lacked either an exact location or confirmed species

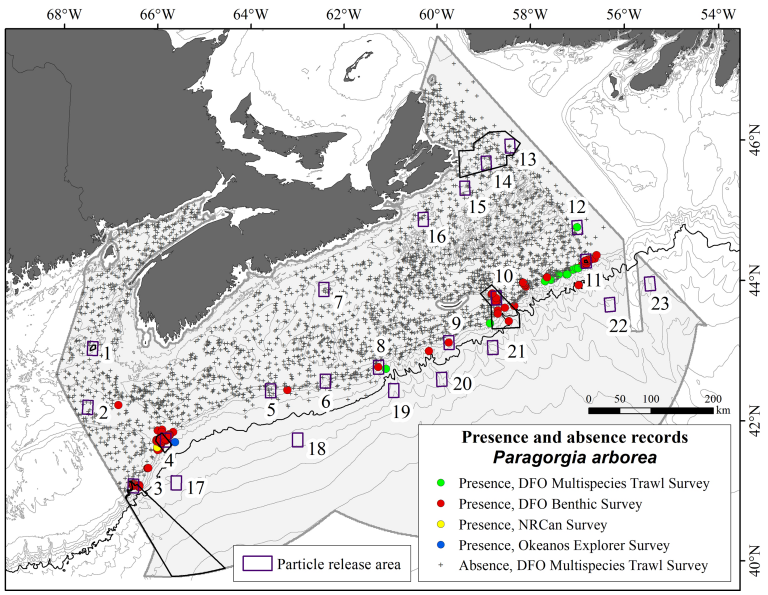

FIGURE 3 | Map of the study area showing the distribution of confirmed records of *Paragorgia arborea* presence and absence, and the locations of the source boxes used in LPT modeling (numbered). Bathymetric contours are shown at 50, 100, 200, and 500 m, and at 500 m below, with the 2000 m contour emphasized. The six conservation areas within the offshore extent of the study area are shown in black outline (see **Figure 2** for place names).

identification (Gass, 2002). Others were obtained from the Ocean Biodiversity Information System (OBIS: **Supplementary Figure 1**). Records from each of those sources were judged too uncertain for use in the modeling, but they were utilized in post-hoc evaluation of model performance. They documented presence only.

The presence and pseudo-absence data from the Scotian Shelf bioregion study area portion of the basin-scale study that were analyzed by Morato et al. (2020), were provided by Drs. T. Morato and J.-M. González-Irusta, and used in comparisons of the results of the two studies.

2.2.3 Environmental Predictor Variables

2.2.3.1 Contemporary Data

A suite of 35 environmental variables developed for modeling the distribution of the glass sponge *Vazella pourtalesii*, another deep-sea, sessile, filter-feeding species, on the Scotian Shelf (Beazley et al., 2018; Beazley et al., 2019; Beazley et al., 2021b; Beazley et al., 2021c) was used in representing contemporary environments. It included biologically-relevant measures associated with water masses and currents, food supply and fishing effort, and was supplemented with 13 additional terrain variables (**Supplementary Table 2**). Fishing effort may have shaped the distribution of *P. arborea* and could help to explain the observed patterns in the models, whereas terrain variables capture aspects of the canyon-channel systems that indent the Scotian Slope and were expected to have a strong influence on the distribution of *P. arborea*. Bathymetric Position Index (BPI) at fine- and broad-scale, eastness, northness and ruggedness were calculated using the ArcGIS Benthic Terrain Modeler (Wright et al., 2012; Walbridge et al., 2018), whereas SAGA (Conrad et al., 2015) was used to generate channel network base level, channel network distance, valley depth, relative slope position, LS-factor, positive and negative openness and the wind exposition index, following Kenchington et al. (2019a). (See **Supplementary Text 2.1** for further explanation of those terrain predictors.) Data on the physical-oceanographic predictors were drawn from the Bedford Institute of Oceanography North Atlantic Model (BNAM: Wang et al., 2018), an eddy resolving model of the North Atlantic based on Nucleus for European Modelling of the Ocean (NEMO) 2.3, with a nominal resolution of 1/12° (approximately 6 by 9 km in the study area). BNAM allows for a maximum of 50 depth layers, while a partial cell is introduced for the bottom layer, improving its representation. Biological and physical oceanographic variables (**Supplementary Table 2**) were spatially interpolated across the study area using ordinary kriging in ArcMap 10.2.2 software (ESRI, 2011) to create continuous data surfaces with a ~1 km grid size (more details in Beazley et al., 2017).

Biochemical variables, such as oxygen or nutrient concentrations, were not used because of very poor spatial coverage of the underlying source point data in the study area (Beazley et al., 2017). Other variables, such as depth, were considered but, following the approached of Beazley et al. (2018), were screened out because of high correlations with more biologically relevant alternatives. Amongst the original 35 predictors, bottom temperature range proved to be highly correlated with channel network base level and hence was excluded.

Long-term averages were used to reflect conditions across the lifespan of *Paragorgia* spp. The reference period for the

physical-oceanographic predictors was 1990–2015. Data availability constrained the periods for other variables. For the biological oceanographic predictors, it was 2002–2012, except that primary-production data were only available from 2006–2010. The reference period for the fishing-effort predictor was 2005–2014. It included only effort using mobile, bottom-tending gears.

The resulting 47 environmental layers were displayed in raster format with geographic coordinates using a WGS 1984 datum and had a cell size ~0.012° cell size (approximately equal to 1 km horizontal resolution). In addition, summary statistics (mean ± standard deviation) were created for each variable, based on their value in each of the 115 grid cells with confirmed *P. arborea* presence.

2.2.3.2 Data for Climate Change Projections

Modeling of the distribution of *P. arborea* under alternative climate scenarios (**Supplementary Table 1**) was restricted by data availability to the subset of the dynamic environmental variables used by Beazley et al. (2021b). These were mean temperatures, salinities and current speeds for both surface and seabed, plus mean maximum mixed-layer depth and seabed slope (data available at Beazley et al., 2021c). Most of the temporally invariant terrain variables were excluded as uninformative for projection purposes. Slope (**Supplementary Text 2.1**) was retained as it is expected to interact with bottom currents, has been shown to be very important in explaining the distribution of *Paragorgia* (Bryan and Metaxas, 2007; Sundahl et al., 2020), and as a static variable, it is expected to improve model predictive ability (Stanton et al., 2012).

Maximum mixed layer depth (MLD), the depth at which surface vertical mixing dissipates, is a near universal feature of the open ocean (de Boyer Montégut et al., 2004). Within this mixed layer, salinity, temperature, or density are nearly uniform, a phenomenon caused by surface forcing, lateral advection, and internal wave processes that vary on diurnal, intra-seasonal, seasonal, and inter-annual scales (de Boyer Montégut et al., 2004). The depth of this mixed zone can show large spatial variability, ranging from less than 20 m in the summer, to more than 500 m in the winter at subpolar latitudes (de Boyer Montégut et al., 2004). The MLD has a significant influence on primary production in the surface waters. As MLD increases it entrains nutrients from deeper waters below, supplying additional nutrients for primary production (Polovina et al., 1995; Carstensen et al., 2002). As data for the primary production variables used in the contemporary analyses were not available for assessing climate projections, MLD was used as a proxy variable.

A version of BNAM was developed (Brickman et al., 2016) to simulate climatology for 2046–2065, under IPCC (2013) RCP 4.5, an emission-stabilizing scenario, and RCP 8.5, a high-emission scenario in which radiative forcing increases through to 2100 (Moss et al., 2010; van Vuuren et al., 2011). Averaged annual anomalies for each of the dynamic variables noted above, representing the difference between present-day and future conditions, were extracted from those BNAM simulations and applied to the averaged contemporary climatology layers.

2.2.3.3 Environmental Variables Use in Previously Published Basin-Scale Study

Following collinearity analyses, Morato et al. (2020) used five variables (slope, BPI, particulate organic carbon (POC) flux to the seabed, seabed temperature and calcite saturation state) in their species distribution models for *P. arborea* at a cell size resolution of 3 × 3 km. To explore differences between basin-scale and regional models of *P. arborea* distribution, the same five variables were obtained for analyses in this study. Three of their variables had been made public through the PANGAEA data publisher portal (https://doi.org/10.1594/PANGAEA.911117), that is, POC flux, seabed temperature and calcite saturation state. Basin-scale rasters of BPI and depth were obtained directly from Drs. T. Morato and J.-M. González-Irusta, and slope was generated from their depth raster. Variables were available for both contemporary and 2100 RCP 8.5 climates. The five variables were subsequently masked to the spatial extent of the study area and rescaled to match our cell size resolution.

2.2.4 Model Performance

Model performance was assessed through three approaches: 1) 10-fold random cross-validation, 2) 5-fold spatial block cross-validation (recommended for spatially autocorrelated data: Roberts et al., 2017), and 3) evaluation of the accuracy of model predictions using data not used in model calibration (Liu et al., 2020). The spatial cross-validation was calculated with the 'spatialBlock' and 'spatialAutoRange' functions in the R package 'blockCV' (Valavi et al., 2019), with three measures of accuracy: sensitivity (the proportion of accurately predicted presences), specificity (the proportion of accurately predicted absences), and Area under the Receiver Operating Characteristic Curve (AUC). Sensitivity and specificity were derived by summing the predicted outcomes across the 2 × 2 confusion matrices generated for each of the model cross-validation runs, whereas AUC was calculated for each cross-validation run. The True Skill Statistic (TSS) was determined from sensitivity and specificity. From those measures, the overall accuracy of the model prediction in geographic space was considered to be good when AUC > 0.9 and TSS > 0.6 (Landis and Koch, 1977; Jones et al., 2010).

Because the response dataset for *P. arborea* has a high number of absences relative to presences, a threshold based on species prevalence was used to define which class probability was considered a presence when converting them into binary predicted outcomes, that were then summarized in the 2 × 2 confusion matrices. That approach has been shown to produce constant error rates and optimal model accuracy measures compared to alternatives (Liu et al., 2005; Hanberry and He, 2013). The AUC is considered threshold-independent (Fawcett, 2006).

For the GAMs, Pearson residuals were plotted against both the fitted values and each covariate included in the model, and the spatial autocorrelation of those residuals assessed. The most parsimonious GAM was selected, following the Akaike information criterion (AIC).

2.2.5 Identification of Non-Analogous Environments

In common with other tree-based models, the reliability of predictions from RF modeling rapidly decreases in areas of

extrapolation outside of the domain of the environmental predictors (Liu et al., 2020), though the emergence of non-analogous environments is highly informative, both for evaluating the reliability of models of present-day distributions and for interpreting climate projections (Mahony et al., 2017). The Extrapolation Detection (ExDet) tool, based on Euclidean and Mahalanobis distances was used, as implemented in the 'dsmextra' R package (Bouchet et al., 2020), to characterize both univariate and combinatorial extrapolation of the environmental data sets used here (Mesgaran et al., 2014), and also to assess the transferability of the model projections (Yates et al., 2018). Cells with non-analogous environments are novel because they are outside the range of individual covariates (univariate) or they are within the univariate range but constitute novel combinations between covariates not found in the reference data set (see **Figure 2** in Mesgaran et al., 2014). Cells that are both outside the univariate range and forming novel combinations are included in the former. In univariate extrapolation if more than one variable lies outside of the range, the covariate that has the greatest univariate distance is identified as the most influential covariate for the cell. Identification of covariates contributing most to the new combinatorial environments is made by quantifying the covariate that when omitted (while retaining all others) makes the largest reduction in the Mahalanobis distance to the centroid of the reference data (Bouchet et al., 2020). The number of cells and their percentage are tabulated for each type of environment (analogous, non-analogous (univariate, combinatorial)) and the most influential covariate in each of the non-analogous classes identified. Extrapolation diagnostics in the 'dsmextra' package include maps of '% Nearby' (the percentage of data nearby) which draw on Gower's distance to calculate the proportion of reference data lying within a given radius of any prediction point in the multivariate environmental space (Bouchet et al., 2020). Following Mannocci et al. (2018) the neighbourhood for % Nearby was defined as a radius of one geometric mean Gower's distance.

These extrapolation diagnostics were applied using two types of response data for determining environmental envelopes: 1) presence and absence data (N=3154); 2) presence-only data (N=115). Presence and absence data were used to identify areas of extrapolation in the RF and GAM species distribution models under present-day and future climate conditions (**Supplementary Table 1**), and to inform variable elimination in RF models (Mannocci et al., 2018). The presence-only data was used to identify climate refugia (see Section 2.2.5.1).

The same diagnostics were applied to the variables used by Morato et al. (2020) at both the basin- and regional-scales under present-day and future (2100; RCP 8.5) environmental conditions to explore the reasons for differences in model outputs between the basin-scale study and the regional-scale study presented herein (**Supplementary Table 1**).

2.2.5.1 Identification of Climate Refugia

The extrapolation diagnostics were also applied to the 8 environmental covariates in the 115 grid cells containing *P. arborea*, to conservatively characterize their present-day environments. The outcome was used to identify which of those cells are expected to still experience similar conditions under the RCP 4.5 2046–2065 climate projections and that, therefore, represent climate refugia for *P. arborea*. Grid cells having projected future environmental conditions analogous to those currently experienced in occupied grid cells anywhere in the study area were identified, but also, and separately, those expected to have conditions similar to current ones either east or west of 60°W.

2.3 Lagrangian Particle Tracking

Three-dimensional passive-particle tracking experiments (**Supplementary Tables 1**, **3** and **4**), extending across the study area and surrounding region, were prepared using the Parcels framework version 2.2 (Lange and van Sebille, 2017; Delandmeter and van Sebille, 2019) with current velocities extracted from the BNAM ocean model (Wang et al., 2018; see **Supplementary Text 2.2** for the selection of the ocean model). For the principal experiments, the LPT models were run in forward-tracking mode.

The spawning season for *Paragorgia* spp. is unknown (see literature review of relevant biological traits for LPT modeling of gorgonian corals in Kenchington et al., 2019b). Hence, experiments were performed using monthly-averaged currents within each of: Winter (January, February, March); Spring (April, May, June); Summer (July, August, September); Autumn (October, November, December), extending the examination of seasonality in LPT models for *P. arborea* reported in Metaxas et al. (2019) to include the autumn period.

Pelagic larval duration (PLD) is also unknown for *Paragorgia* spp. (Kenchington et al., 2019b). Experiments were therefore run for 2 weeks, 1 month and 3 months (Wang et al., 2020) to encompass all likely durations. Hilario et al. (2015) report a range of maximum PLD for five alcyonacean corals, including one gorgonian species, of 7 to 90 days, consistent with this selection of time frames. Metaxas et al. (2019) chose an intermediate 60 day PLD for their hindcast LPT models of *P. arborea*. Modeled particles were released from the seafloor to mimic natural release depth. However, as larval vertical migration, buoyancy and swimming ability are unknown for *Paragorgia* spp., particles were also released in mid-water and at the surface, to represent active vertical ascent from seabed release.

Random horizontal particle movement was modeled by a horizontal diffusivity constant, K_h, based on Okubo's (1971) 4/3 power law relationship:

$$K_a = 0.0103 l^{4/3}$$

where K_α and l are in units of $cm^2\ s^{-1}$ and cm, respectively. l, the scale of diffusion, depends on the spatial resolution of the ocean model. For BNAM on the Scotian Shelf:

$$K_h = 0.0103 \times 600000^{4/3} = 521239\ cm^2 s^{-1} = 52.1239\ m^2 s^{-1}$$

In each experiment, model particles were seeded in 23 'source boxes', each 0.1° × 0.1° in extent, with some of them selected

within the known or predicted distributions of *P. arborea*, and others positioned where needed to examine various connectivity hypotheses (**Figure 3** and **Supplementary Table 4**). Source Boxes 1, 3, 4, 10, 11, and 13 and 14, were placed in, respectively, the Jordan Basin, Corsair and Georges Canyons, and Northeast Channel Coral Conservation Areas, the Gully MPA, the *Lophelia* Coral Conservation Area, and the St. Anns Bank MPA. In each model day, 121 particles were released in each source box, seeded uniformly across its area. Each seasonal model had 90 daily releases for a total of 10,890 particles per source box. Following Le Corre et al. (2020), the proportion of particles passing over or terminating in another source box was presented as a connectivity matrix for each model run. Shading on the major diagonal of the matrices was separately calculated and indicates the proportion of particles in the source box at the end of the PLD.

In addition to the principal experiments, potential source populations outside the eastern boundary of the study area were investigated through additional simulations, run in hindcast mode from single particle releases in each of Source Boxes 11, 13 and 14. Those used only monthly-averaged water movements for the spring season.

To examine inter-annual variability in connectivity, two individual years were selected, and the modeling repeated for each, for comparison of outputs with those generated from 1990–2015 averages (**Supplementary Table 3**). The selected years, 1993 and 2015, were chosen for their expression of particular features (Wang et al., 2021): 1993 fell during a period when the winter North Atlantic Oscillation (NAO) index was high and the influence of the Atlantic Meridional Overturning Circulation (AMOC) strong; 2015 saw high values of the winter NAO index, and the AMOC was weaker than in 1993.

3 RESULTS

3.1 Regional-Scale Modeling of Contemporary Distributions

3.1.1 Representations of Contemporary Distribution

All RF models achieved 'good' performance by the AUC and TSS criteria. In the RF model with all 47 environmental predictors, sensitivity and specificity were 0.99 and 0.95 respectively (TSS = 0.94), and the AUC was 0.99 ± 0.02 (SD). The high sensitivity indicates that the mean values of each of the 47 predictor variables in the 115 grid cells where *P. arborea* presence has been confirmed (**Supplementary Table 5**) provide a good description of the species' habitat within the study area (**Supplementary Figure 2**). The seven most influential of them, in terms of mean decrease in Gini value, concerned terrain morphology (**Supplementary Figures 3, 4**). They were followed by maximum surface temperature and minimum bottom salinity, then an array of lesser variables.

The most important variable in the model was ruggedness, a measure of bathymetric complexity in a rectangle of approximately 46 km^2 around each point for which it was quantified, the probability of presence of *P. arborea* increasing rapidly with even small positive values. Ruggedness was high in the canyon areas along the continental slope (**Supplementary Text 2.1**). It was followed by positive topographic openness, for which higher probabilities of presence were associated with values of openness < 1.50, representing upward slopes of at least 15° from the quantified point, hence such topographies as gully bottoms or walls. The probability of presence was likewise high where negative topographic openness was < 1.50, meaning where there were downward slopes of at least 15°, hence on ridges and steep slopes. Both openness indices indicated very low probability of presence on extensive horizontal seabeds. Higher probabilities of presence were also associated with slopes of > 5°, with longer and steeper gradients, and in valleys with depths (below adjacent ridges) of > 200 m (**Supplementary Text 2.1**).

The RF model with 47 predictors produced a high probability of presence across a broad swath, extrapolated across the continental rise and abyssal plain (**Supplementary Figures 2A, B**). Extrapolation diagnostics showed that the area of univariate extrapolation was 49.78%, while combinatorial extrapolation was only 0.01%, indicating that nearly half of the spatial extent fell outside the range of one of the covariates found in the reference data. The area of that extrapolation was largest over the deeper water, and in an area along the coast off southwest Nova Scotia (**Supplementary Figure 2**). Channel network base level and the water column covariates contributed most to the extrapolation extent, with the first, the most important covariate in 34% of the cells with non-analogue conditions, followed by maximum surface temperature in 11%. The alternative RF model (**Figure 4**), using only the top 6 environmental prediction layers, reduced the area of extrapolation to 0.31% of the cells, leaving analogous conditions over 99.69% of the spatial extent, indicating that the input data for the RF models sampled the range of terrain predictors found in the study area. Model performance was only slightly reduced: sensitivity and specificity were each 0.90 (TSS = 0.80), and the AUC was 0.96 ± 0.02 (SD). The order of importance of the variables was the same, except for LS-factor taking second importance over positive topographic openness, which fell to third position. The elimination of variables contributing to the extrapolation prior to running the alternative RF models allowed for reliable predictions in deeper parts of the study area, revealing extensive unsuitable habitat, likely mischaracterized by the extrapolation in the model with 47 variables.

3.1.2 Contemporary Distribution for Comparison With Climate Projections

The RF model for present-day conditions built on the 8 environmental predictors available for the era of projected climate (**Figure 5**) had sensitivity and specificity using 10-fold cross-validation of 0.97 and 0.90 respectively (TSS = 0.88), while AUC was 0.98 ± 0.01 (SD), indicating good model performance. Similar values were obtained using 5-fold spatial blocking possibly indicating that either a dependence structure was not a prominent feature of the data or that the algorithm was able to cope with that structure (**Supplementary Table 6**). Slope, mean surface temperature and mean bottom salinity were the top three most important variables influencing the model (**Supplementary Figure 5**).

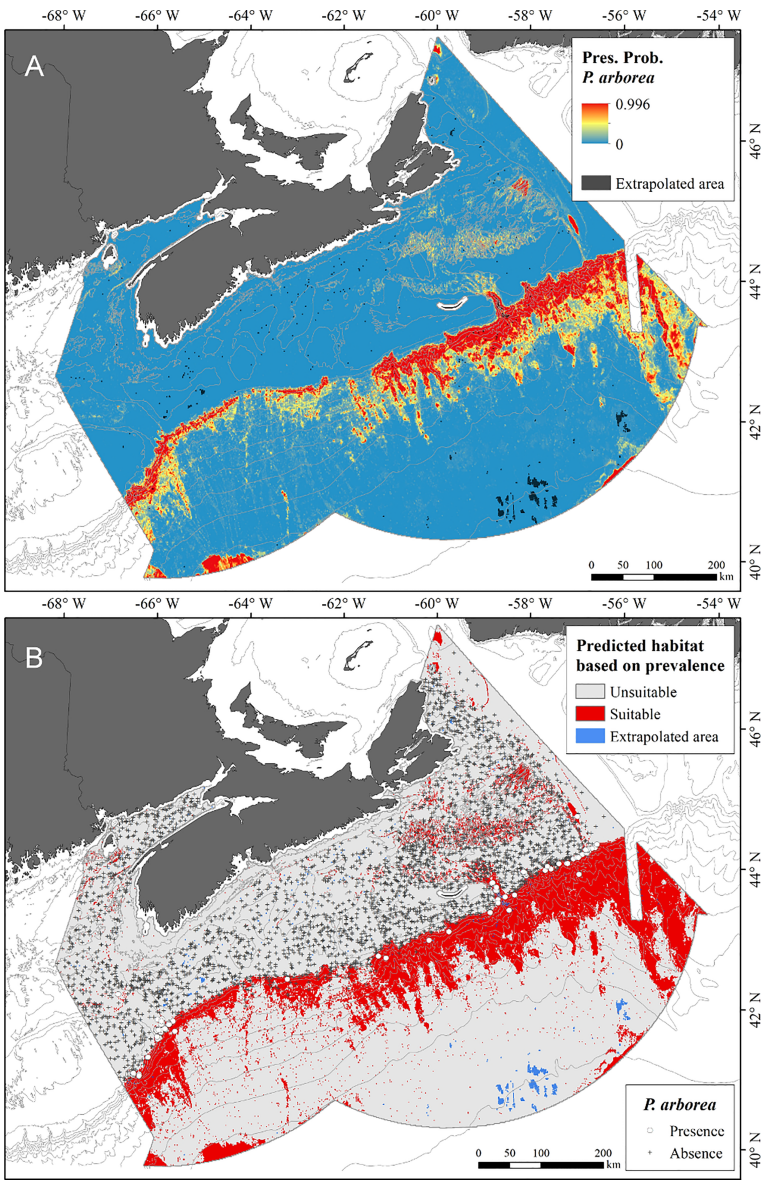

FIGURE 4 | (A) Probability of occurrence of *Paragorgia arborea* under present-day conditions, based on RF model constructed using 6 terrain predictors; **(B)** Predicted distribution of suitable and unsuitable habitat following a prevalence threshold of 0.036, overlain with locations of presence and absence response data. (Note: the combined shadings indicating extrapolated areas of predicted suitable habitat appear dark red.).

A GAM fit to the same suite of 8 environmental predictors (**Supplementary Figure 6**), explained 39% of the variability in the data (**Table 1**). The most parsimonious GAM included only five variables, with slope and mean surface temperature the most important. Cross-validation using 5-fold spatial blocking with random assignment of blocks into folds showed poor sensitivity compared with other accuracy measures indicating a poorer ability to correctly predict presence records (**Supplementary Table 6**). Specificity was high indicating that a higher proportion of absence records were correctly predicted but TSS was poor and together with the lower AUC indicated non-independence of hold-out data from the training data and suggested that the GAMs were not as reliable as the AUC indicated. However the spatial blocks appear to have introduced extrapolated conditions between cross-validation folds, causing predictions for the hold-out data to be outside the range of data in the training folds causing the poor sensitivity (Roberts et al., 2017).

The functional response curves for environmental variables in the RF and GAM models (**Figure 6**) show very similar predictive relationships for the variables they had in common, explained by the general similarity of their predicted distributions under present-day conditions (**Figure 5A, E**). The bimodal distribution of some of the variables was verified to be

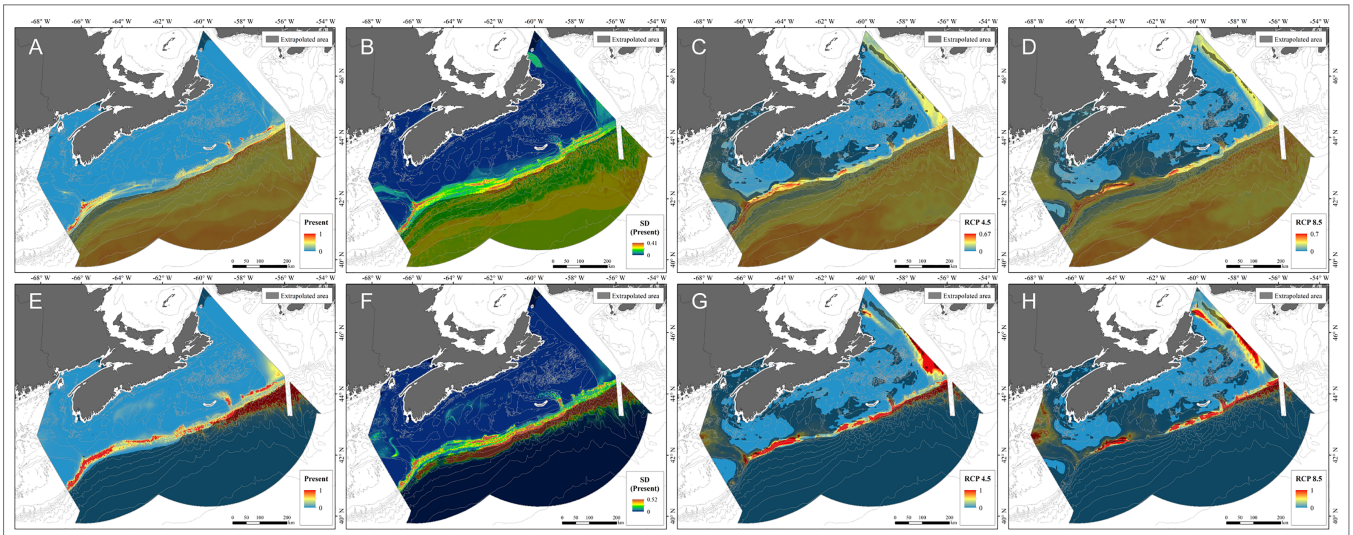

FIGURE 5 | Probability of occurrence of *Paragorgia arborea* from RF models **(A–D)** and GAMs **(E–H)** under present-day **(A, E)**, RCP 4.5 **(C, G)** and RCP 8.5 **(D, H)**, as predicted by models constructed using 8 environmental predictors, with model uncertainty for present-day predictions **(B, F)** generated from the standard deviation created from 5-fold spatial block cross-validation. Areas of model extrapolation are shown on each map as a transparent overlay and were created using both presence and absence data.

TABLE 1 | Parametric coefficients and approximate probability of smooth terms in the GAMs.

	Parametric terms			
		Estimate	**SE**	**Probability**
	(intercept)	-143.070	28.410	4.77x10-7
	Bottom salinity mean	3.034	0.770	8.21x10-5
GAM	**Approximate significance of smooth terms**			
R^2 (adj.) = 0.39		**edf**		**Probability**
	s(Bottom current mean)	2.753		3.07x10-5
	s(Mixed layer depth)	2.292		0.016
	s(Surface temperature mean)	6.004		< 2x10-16
	s(Slope)	2.695		< 2x10-16

SE, standard error; edf, estimated degrees of freedom; adj., adjusted.

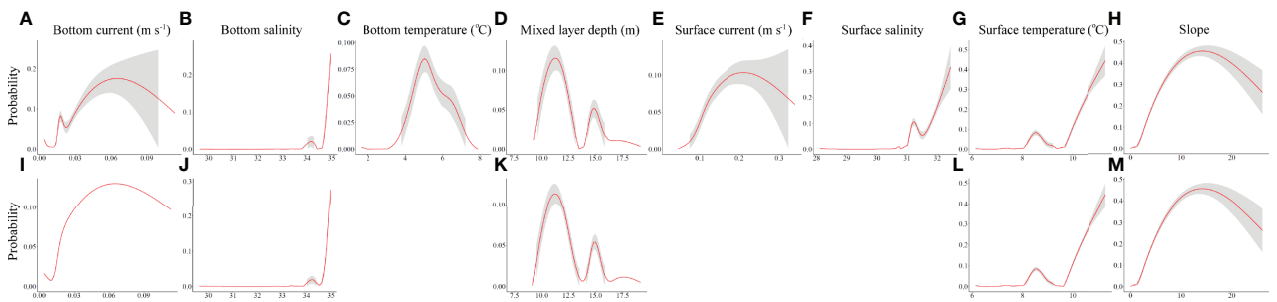

FIGURE 6 | Functional response curves for RF models **(A–H)** and GAMs **(I–M)** constructed using 8 environmental predictors, under present-day conditions. (Three predictors not included in the GAMs are left blank). Shaded regions represent approximate 95% confidence intervals. All curves and confidence intervals were bounded at zero probability. (MLD, mixed layer depth. Units are as in **Supplementary Table 2**).

explained by spatial differences in environmental conditions. RF and GAMs each identified areas of high probability of *P. arborea* presence along the Scotian Slope and in the Northeast Channel, associated with high standard deviations in that probability (**Figure 5A, B, E, F**). Analogous environmental conditions were found over most of these areas (**Figure 7A**) and in 51.56% of the full study area (**Table 2**), associated with high percentages of proximate data (**Figure 7C**). In contrast to the RF model using 47 predictors, the extent of extrapolation could not be mitigated through variable

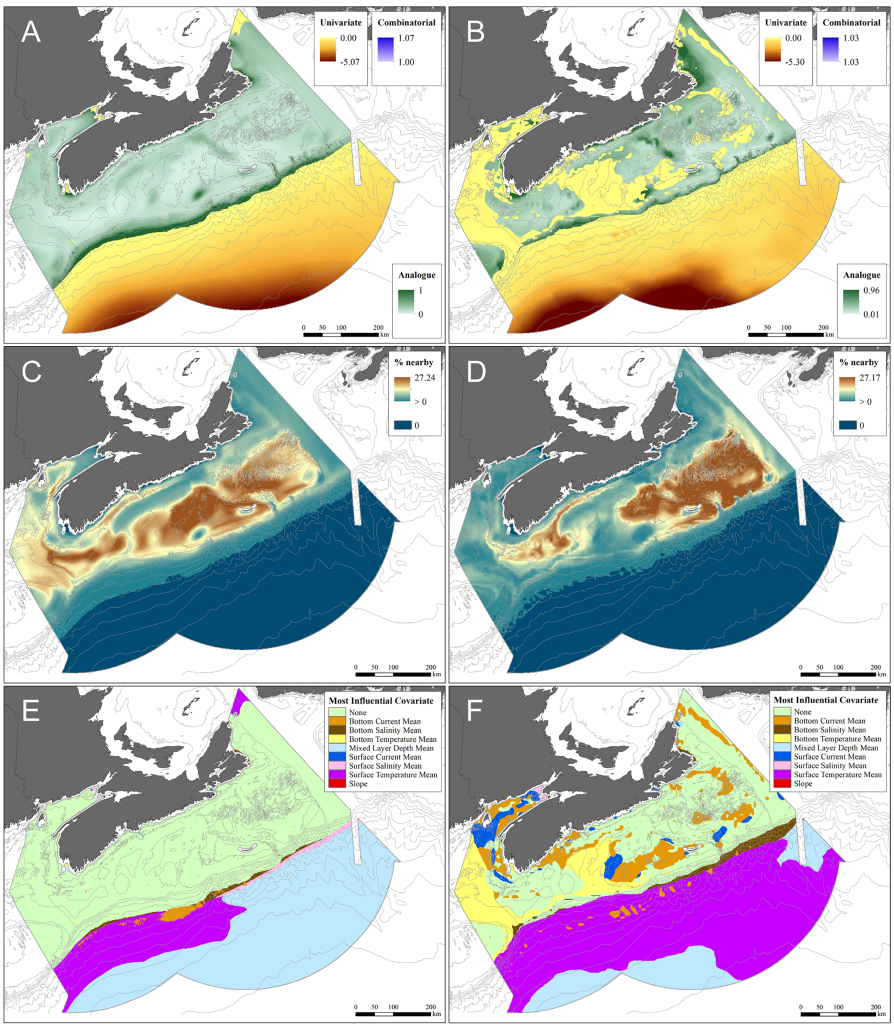

FIGURE 7 | Areas of extrapolation defined by eight input covariates under present-day **(A, C, E)** and 2046–2065 RCP 4.5 **(B, D, F)** conditions, using both presence and absence data. **(A, B)** Extrapolation quantified by the Extrapolation Detection tool (ExDet); **(C, D)** Percentage of data nearby (% Nearby), with areas where predictions are potentially unreliable shaded in dark blue; **(E, F)** Areas of extrapolation identified by their most influential covariate. (Areas with analogous conditions are shaded light green).

elimination, as most of the available predictors were water-column variables – appropriately so for climate projections – which if removed would nullify the analysis. Instead we relied on spatial mapping to identify areas of extrapolation. Binary classification of habitat predictions based on prevalence showed that the RF model likely wrongly predicted extensive areas of suitable habitat in the areas of extrapolation over deep water (**Supplementary Figure 7A**), where those predictions were associated with high standard deviations (**Figure 5B**), while the GAM was able to classify most of the deep-water area as unsuitable (**Supplementary Figure 7D**), with low standard deviations in probability of presence (**Figure 4F**). In the deep-water extrapolated area, mixed layer depth, and to the west, mean surface temperature contributed most to the extrapolation (**Table 2**). Along the shallow boundary of the extrapolated area, on the upper continental slope where predicted presence was high (**Figures 5A, D**), mean surface and bottom salinity and mean bottom currents contributed the most to the extrapolation (**Table 2** and **Figure 7E**).

Interestingly, the predicted distribution of binary-classified suitable habitat outside areas of extrapolation produced similar predictions among contemporary models constructed using the 6 terrain variables (**Figure 4**) and those constructed using the 8 environmental predictors that were mostly water column variables (**Supplementary Figure 7**). All models predicted suitable habitat along the upper continental slope. Their similarity is best explained by the importance of the slope variable in all of the models, as correlations between water column and terrain variables were generally low (< 0.50).

3.1.3 Assessment of Model Predictions Against Independent Response Data

Of the 44 OBIS records, 86% fell within areas of predicted presence of *P. arborea* (**Supplementary Table 7**) in both

TABLE 2 | Spatial extent (in number of grid cells) of extrapolation for single covariates and combinations of covariates under present-day and future climatologies based on presence and absence data for *Paragorgia arborea*.

	Count	Percentage	Count	Percentage	Count	Percentage
This Study	**Present-Day**		**2046–2065, RCP 4.5**		**2046–2065, RCP 8.5**	
Mixed Layer Depth	112,631	34.51	31,785	9.74	36,718	11.25
Mean Surface Temperature	37,280	11.43	131,776	40.39	131,608	40.34
Mean Surface Salinity	2,962	0.91	405	0.12	418	0.13
Mean Bottom Current	2,506	0.77	25,956	7.96	24,923	7.64
Mean Bottom Salinity	2,424	0.74	6,091	1.87	5,494	1.68
Mean Bottom Temperature	103	0.03	25,394	7.78	36,629	11.23
Slope	74	0.02	58	0.02	56	0.02
Mean Surface Current	41	0.01	7,802	2.39	7,233	2.22
Sub-Total Univariate	158,021	48.43	229,267	70.27	243,079	74.50
Slope	14	0.00	–	–	–	–
Mean Bottom Current	4	0.00	2	0.00061	2	0.00061
Sub-Total Combinatorial	18	0.01	2	0.00061	2	0.00061
Total	158,039	48.44	229,269	70.27	243,081	74.50
Analogue	168,242	51.56	97,012	29.73	83,200	25.50
Variables from Morato et al. (2020)	**Present-Day**				**2100, RCP 8.5**	
BPI	8,218	2.52			6,594	2.02
Calcium saturation	5,037	1.54			15,256	4.68
Bottom temperature	2,129	0.65			152,361	46.70
POC flux	890	0.27			39,413	12.08
Slope	411	0.13			303	0.09
Sub-Total Univariate	16,685	5.11			213,927	65.57
Calcium saturation	12	0.0037			25	0.01
BPI	–	–			22,939	7.03
Slope	–	–			651	0.20
Bottom temperature	–	–			78	0.02
Sub-Total Combinatorial	12	0.0037			23,693	7.26
Total	16,697	5.12			237,620	72.83
Analogue	309,584	94.88			88,661	27.17

Analogous conditions are determined from the environments experienced by the response data. Equivalent extents, recalculated for the Scotian Shelf bioregion study area, from the data used in Morato et al. (2020) are also shown. The Most Influential Covariates contributing to the extrapolations are indicated.

RF and GAM models, which was relatively consistent with the sensitivity of the RF models (0.99 with all 47 variables, 0.97 with the 8 variables used for the present-day climate baseline). Some records shared positional information with others. Removing those reduced the data-set to 23 unique positions, 19 of which (83%) were found in areas of predicted presence.

The records extracted from Gass' (2002) compilation of historical reports of coral occurrence did not map well against the areas of suitable habitat identified by either the RF or GAM models for current environmental conditions, only 24% falling within areas deemed as having suitable habitat (**Supplementary Table 7**). Concordance with the predictions was highest for records from the Scotian Slope. Some eastern Scotian Shelf records were from locations very close to small areas of predicted suitable habitat near the Laurentian Channel (**Supplementary Figures 1C, D**), such that their poor concordance may result from imprecise positional information in original records. Other cases may have arisen from misidentifications. Therefore the poor match of those data with areas of predicted presence of *P. arborea* is not necessarily indicative of model performance.

3.2 Predicted Distribution Under Climate Projections

Under projected (2046–2065) environmental conditions, RF modeling predicted both increased probability of occurrence and a considerable expansion of the extent of suitable habitat for *P. arborea*, especially in the Fundian and Laurentian Channels, along the slope in general, and even onto Georges Bank (**Figures 5C, D**; **Supplementary Figures 7B, C**). Although the GAM also predicted some increased probability of occurrence in both channels (**Figures 5G, H; Supplementary Figures 7E, F**), the predicted expansion in suitable habitat was less than that of the RF models. The Fundian and Laurentian Channels were each associated with higher residuals in the GAM, indicating a poorer fit in those areas (**Supplementary Figure 6C**).

Extrapolation diagnostics applied to prediction modeling under future environmental conditions, identified extrapolation areas extending from deep ocean into the Northeast Channel, Fundian Channel, Jordan Basin, Emerald and La Have Basins and onto Emerald Bank (**Figure 7B**). Those areas occupied 70% (RCP 4.5) and 74.5% (RCP 8.5) of the spatial extent of the study area (**Table 2**). RF predictions in

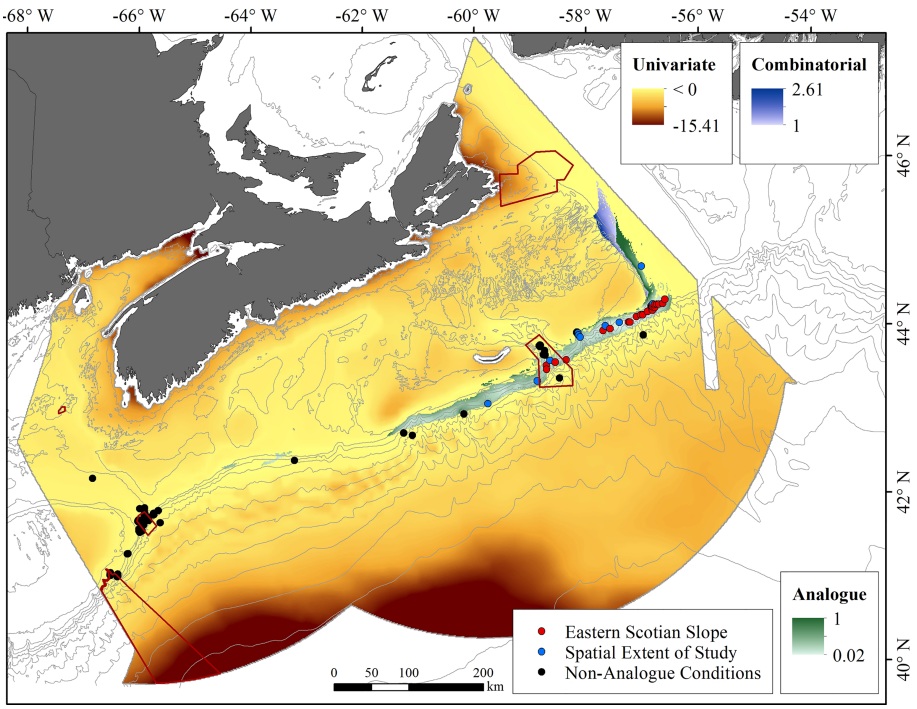

FIGURE 8 | Areas of analogous and non-analogous conditions under RCP 4.5 climate projections for 2046-2065, defined by eight input covariates, showing the locations of confirmed records of *Paragorgia arborea* coded by the projected future status of environmental conditions at those sites and existing conservation areas (in red outline). Locations of existing records that are projected to retain conditions analogous to those where the species presently occurs on the eastern Scotian Slope are shown in red. Locations which will retain, or change to, conditions analogous to those under which the species is presently found west of 60°W are shown in blue. Black dots mark records in areas projected to change to non-analogous conditions.

those areas are unreliable, though the extent of extrapolation from present-day values varies. In the Northeast Channel (**Figure 7B**), where *P. arborea* occurs under present-day conditions (**Figure 3**), univariate extrapolation is near zero, indicating that the environmental variables creating the extrapolation (mean bottom temperature and salinity, **Figure 7F**) are close to the range found in the reference data.

The relative magnitude of univariate and combinatorial extrapolation in the future distribution models associated with different sets of the 8 predictor variables (**Table 2**), show that the extent of extrapolation was much larger with individual variables than with combinations of them. Small areas of combinatorial extrapolation were found in the Gully MPA and adjacent Shortland Canyon. Closer examination of those areas showed that the combination of variables creating the novel environments (**Table 2**) was restricted to two grid cells in the former and one grid cell in the latter, both at the canyon heads.

In summary, the predicted distributions under projected climates appear reliable along the upper Scotian Slope and the wall of the Laurentian Channel (**Supplementary Figure 7**), if not necessarily so elsewhere. Within that restricted area, RF and GAMs produced similar predictions of future distributions, both suggesting the presence of suitable habitat in 2046–2065, including potential for habitat expansion.

3.3 Identification of Potential Climate Refugia

Of the 115 grid cells currently known to contain *P. arborea*, 39 are expected to retain similar conditions to those seen in presently-occupied cells (**Supplementary Table 8**), under climate projections for 2046–2065. Most lie along the Scotian Slope east of 60°W (**Supplementary Figure 8** and **Figure 8**). There, 23 of 58 grid cells with *P. arborea* present today will remain within the range of existing environmental conditions seen in that sub-region, indicating that those cells may contain climate refugia for this species over the next decades. Another 16 of those 58 cells are projected to have future environments similar to present-day conditions in the Northeast Channel, but with one or more variables outside the ranges experienced by extant colonies in the eastern sub-region (**Figure 8**).

The 57 grid cells west of 60°W that are known to have *P. arborea* today all lie in areas of univariate extrapolation under future conditions (**Figure 8**), meaning that one or more of the 8 environmental variables is projected to fall outside its present-day range seen in occupied grid cells in the study area by 2046–2065 (**Supplementary Table 8**). That was a consequence of, primarily, higher projected mean surface temperatures, which will affect 55 of the cells, making the predictions in this area unreliable.

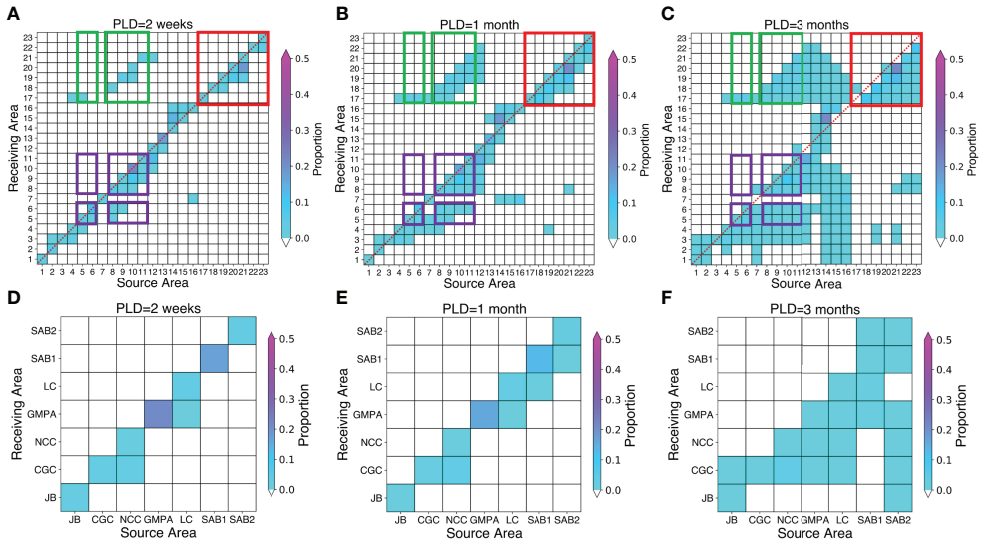

FIGURE 9 | (A–C) Proportions of virtual particles released from each source box, in ensembles of seasonal LPT simulations using long-term averaged currents, that pass over or terminate in each source box (termed: "Receiving Area"), during 2-week (left column), 1-month (centre column) and 3-months (right column) PLDs. Shading on the major diagonal indicates particle retention in the source box at the end of the PLD. Red outlines indicate deep-slope source boxes; purple outlines indicate upper-slope source boxes; green outlines indicate connectivity from upper-slope to deep-slope source boxes. **(D–F)** Extracts from the above matrices, showing connectivity among source boxes in conservation areas: 1, Jordan Basin Conservation Area, JB; 3, Corsair and Georges Canyons Conservation Area, CGC; 4, Northeast Channel Coral Conservation Area, NCC; 10, Gully MPA, GMPA; 11, Lophelia Coral Conservation Area, LC; 13, 14, St. Anns Bank MPA, SAB1, SAB2.

Given the large areas of extrapolation shown in both the contemporary and future predictive models (Section 3.2) this use of the extrapolation diagnostic tool to identify climate refugia is more reliable than identification of common habitat between contemporary and future prediction surfaces.

3.4 Comparison With Results of Basin-Scale Modeling

Extrapolation diagnostics for the suite of response and predictor variables used by Morato et al. (2020), applied within the Scotian Shelf bioregion study area, identified analogous conditions over most of its spatial extent under present-day conditions (94.88%; **Table 2**), except for some areas of univariate extrapolation in BPI in the canyon areas (**Supplementary Figure 9** and **Table 2**). Under future climate projections (2100, RCP 8.5), large areas of the Scotian Shelf and continental rise were projected to lie in areas of extrapolation, the most important variables being bottom temperature, POC flux and calcite saturation at the seafloor (**Table 2**). New combinatorial areas on the Scotian Slope were identified, with BPI accounting for most of the extrapolation there. Only the deep continental slope and upper rise were projected to retain analogous conditions (**Supplementary Figure 9**).

3.5 Regional-Scale Connectivity Patterns

In all seasons and for all particle release depths, connectivity increased with PLD (**Supplementary Figures 10–21**), that trend being particularly pronounced in autumn and winter, at mid-water and seabed release depths. Connectivity between source boxes was highly and consistently clustered (**Figure 9**). Down-stream connectivity amongst deep-slope source boxes (Source Boxes 17–23: **Figure 3**) was observed across all seasons and particle release depths, being particularly strong with mid-water and seabed releases and a PLD of 3 months, which enabled the more distant connections. Similarly, upper-slope down-stream connectivity (Source Boxes 5, 6, 8–11) was observed across all seasons and depths to varying degrees, and was also particularly strong with mid-water and seabed releases and a 3 month PLD. Source Box 10 in the Gully MPA emerged as a potential seed source for the largest number of other Source Boxes, while Source Box 19 showed the greatest redundancy, receiving particles from the largest number of other source boxes.

Connectivity among the source boxes on the inner Scotian Shelf (Source Boxes 7, 13–16) was observed in all seasons and was less influenced by PLD. Among the source boxes at the westward end of the study area, the greatest connectivity was observed between Source Boxes 4 and 3, where connections were made regardless of PLD, season or release depth. Connectivity was also high from the Fundian Channel to the eastern slope of Georges Bank (Source Boxes 1, 2 to 3, 4) with connections in all seasons, but most commonly in spring at all release depths and PLD. Source Boxes 3 and 17 were the least connected to others within the study area, larvae from there perhaps drifting to *Paragorgia* habitat in waters of the USA, although Source Box 17 did connect eastward to Source Box 18 in autumn releases at the surface with a 3-month PLD.

Connectivity between the clusters of connected source boxes described above was most prevalent between the upper- and deep-slope groups (**Figure 9**), with connections in the down-slope direction at all release depths in both summer and autumn, but only with surface and mid-water releases in winter and spring. The particle drifts were never made down-slope but rather combined along-slope movements with entrainment of water from the shelf-break current into the east-going offshore flow. Connectivity in the up-slope direction was less common, being observed only in mid-water releases with longer PLDs in summer, autumn and winter (**Supplementary Figures 17, 20, 11** respectively). Connections between the source boxes on the inner Scotian Shelf with those on the continental slope were observed, primarily with surface releases in the spring, with deep-slope connections also observed in winter at the surface, and upper-slope connections in autumn at mid-water and surface release depths.

Potential upstream source areas for Source Box 11 (located in the *Lophelia* Coral Conservation Area) that were identified by hindcast LPT models, included waters from coastal Newfoundland and the Tail of Grand Bank to the Cabot Strait (**Supplementary Figure 22**). OBIS records (**Supplementary Figure 1**) showed that *Paragorgia* spp. do occur in that area, potentially providing a supply of larvae to the populations on the Scotian Slope.

Source Boxes 13 and 14 were situated in the St. Anns Bank MPA, an area where *P. arborea* has not been observed but is projected to occur in its deeper extent, along the slope of the Laurentian Channel (**Supplementary Text 2.1**), in future. Hindcast LPT modeling for spring releases (**Supplementary Figure 22**) identified potential source areas primarily in the Cabot Strait and southern Gulf of St. Lawrence.

Consistent with expectations, particle retention within source boxes decreased with increasing PLD. It was most common in seabed releases in summer, autumn and winter, when it was often the predominant outcome (**Supplementary Figures 18, 21, 12**). Source Box 3 and to a lesser extent, Source Box 17, which had poor connectivity, showed more particle retention. Elsewhere, retention was commonly seen with PLDs of 2 weeks or 1 month, in all source boxes, and 13 of them showed some retention even after 3 months (**Figure 9**).

3.5.1 Inter-Annual Variability in Connectivity Patterns

The LPT simulations using monthly-averaged currents for 1993 and 2015 showed generally less difference in connectivity and retention than was seen amongst different PLDs or seasons with the long-term averaged current data, and were consistent with the connectivity patterns observed in simulations using those data (**Supplementary Figures 10–21**). However, some particular differences were observed. With releases in the winter at the surface, there was greater connectivity among upper-slope source boxes in 1993 than in 2015, for example, whereas mid-water and seabed releases in winter, summer surface releases, plus surface and seabed releases in autumn, showed more connectivity in 2015 than 1993.

3.6 Connectivity Between Conservation Areas in the Offshore Scotian Shelf Planning Area

Some particles released in the Jordan Basin Conservation Area (Source Box 1) in all seasons were retained there, particularly those from seabed and mid-water releases (**Figure 9**). With 3-month PLD, that area also has direct, down-stream connections to the Corsair and Georges Canyons Conservation Area (Source Box 3) in the spring at all release depths, and for surface releases only, in summer. *P. arborea* has not been confirmed for this area, although another coral often found with *P. arborea*, *Primnoa resedaeformis* occurs there (**Supplementary Table 4**) and the conservation area is identified as having suitable habitat under climate projection (**Supplementary Figure 7**).

Source Box 3, in the Corsair and Georges Canyons Conservation Area, did not have downstream connections to other Canadian conservation areas in the simulations based on long-term averaged currents (**Figure 9**). It was, however, connected to the Northeast Channel Coral Conservation Area (Source Box 4) in both 1993 and 2015, for mid-water releases in summer with PLDs of 1 and 3 months, and in 2015 also in winter under the same conditions. With those same PLDs, Source Box 3 was additionally connected to the deep-slope Source Boxes 17, 18, 19 and 23 in individual years in summer and autumn of 1993 and 2015. There was also particle retention in Source Box 3 in summer, autumn and winter with mid-water and seabed release simulations. The Northeast Channel Coral Conservation Area likewise had particle retention in those seasons and release depths, as well as the strong downstream connections to the Corsair and Georges Canyons Conservation Area noted above.

To the east, Source Box 10 in the Gully MPA is well-connected to the deep-slope cluster with 3-month PLD (**Figure 9**). It also has downstream connections with the Northeast Channel Coral Conservation Area and Corsair and Georges Canyons Conservation Area (**Figure 9**), both under simulations using long-term averaged currents and in individual years, and in all seasons. However, those connections were typically restricted to mid-water and seabed particle releases. More connections were seen in 2015 than in 1993. Other particles were retained within Box 10 in both individual years and under long-term averaged conditions, particularly with winter releases as well as those seabed releases in summer and autumn with PLDs of 2 weeks or 1 month. Under those conditions, particle retention was on the order of 50% (**Supplementary Figures 12, 18, 21**). Similarly high retention was seen in 2015 only in the spring under the same LPT parameters. The Gully MPA also had connections to the *Lophelia* Coral Conservation Area (Source Box 11) with mid-water releases in spring 2015 and a PLD of 3 months, plus surface and mid-water releases in summer, regardless of the chosen PLD, and in seabed releases with PLDs of 1 and 3 months.

The *Lophelia* Coral Conservation Area (Source Box 11) also had particle retention in all seasons both under averaged conditions and in individual years. Retention was more

common under shorter PLDs (2 weeks, 1 month), and in releases from the mid-water and seabed depths. This area was connected to three other downstream conservation areas, especially the Gully MPA, to which connections were found in all seasons, both in individual years and under long-term averaged conditions. In winter and spring, there were connections at all three release depths, while in the summer they were restricted to surface and mid-water releases, and in autumn to mid-water and seabed releases. The *Lophelia* Coral Conservation Area was also connected to the Northeast Channel Coral Conservation Area and Corsair and Georges Canyons Conservation Area in the autumn, winter and spring but not the summer. Connections were mostly from mid-water releases with a PLD of 3 months.

On the Scotian Shelf, Source Box 13 in the St. Anns Bank MPA, has a very high retention of 50% of particles released at the seabed in all seasons, with PLDs of 2 weeks or 1 month (**Figure 9**). Retentions were also seen with a PLD of 3 months but with a lower proportion of particles being retained. There were connections to both the Gully MPA and the *Lophelia* Coral Conservation Area, with more connections to the latter. Those connections were found in all seasons and predominantly in surface and mid-water releases with 1- and 3-month PLDs. Source Box 14, also in the St. Anns Bank MPA but further to the west of Source Box 13 (**Figure 3**), is the most highly connected with particles reaching nineteen other source boxes and all protected areas except for the *Lophelia* Coral Conservation Area when PLD was set to 3 months (**Figure 9**). The highest connectivity was with Source Box 15 to the west just outside the MPA boundary, but eastward connections to Source Box 13 inside the MPA were observed with 1- and 3-month PLDs. At 1-month PLD particles connected westward along the shelf to Source Boxes 15, 16 and 7, connecting only to Source Boxes 15 and 16 with 2-week PLD (**Figure 9**). As for the Jordan Basin Conservation Area, the St. Anns Bank MPA includes suitable habitat for *P. arborea* under climate projection models to mid-century (**Supplementary Figure 7**).

4 DISCUSSION

This study combined regional species distribution models of the present-day and future distributions of the deep-sea coral *P. arborea* with particle tracking models that were used to evaluate the likelihood of colonization for areas of predicted habitat and to assess connectivity among areas closed to protect this and other deep-sea coral species. Extrapolation diagnostics proved to be a useful tool for reducing the degree of extrapolation in the species distribution models and for spatially assessing the reliability of model outputs. The results have led to the identification of mid-century climate refugia along the upper slope in the eastern part of the Scotian Shelf bioregion, contrary to projections inferred from models performed at a basin-scale across the North Atlantic. Collectively these results have enabled a first review of the current set of closed areas with respect to fulfilling the expected properties of a protected area network.

4.1 Distribution of *Paragorgia arborea* in the Study Area

Restricting the RF model from the full complement of 47 predictors to the top six allowed us to reliably exclude large expanses of extrapolated habitat unsuitable for *P. arborea* over the continental rise and abyssal plain, without compromising model performance. The six were terrain variables which had not previously been used for predictive habitat modeling of benthic species in the study region (e.g., Bryan and Metaxas, 2007; Beazley et al., 2018; Beazley et al., 2021b), but to our knowledge proved to be effective predictors of *P. arborea* habitat. They identified steep and rugged areas, suitable for the species, along the upper continental slope, reflecting variability in seafloor elevation and steep slopes at scales of kilometres and tens of square kilometers, as well as vertical relief of hundreds of metres. The available variables do not capture micro-relief but rather such geomorphic features as ridges, gullies and moraines (Sowers et al., 2020).

Within those areas of predicted suitable habitat, *P. arborea* will be confined to the hard surfaces it requires for attachment; surfaces which may be provided by bedrock, boulders in glacial till, or drop stones (Mortensen and Buhl-Mortensen, 2004). The upper Scotian Slope is underlain by till, though at water depths < 300 m that is mostly covered by mobile fine sand in the east, and coarser sand and gravel in the west, while ice-berg pits and scours expose underlying harder substrata (Piper and Campbell, 2002). Low ridges and patches of boulders, which provide suitable settlement substrates for *P. arborea*, are common and contribute to the ruggedness. Ridges and canyons extend down the Slope. Apart from The Gully's, the heads of the canyons are mostly choked with sand, although some mudstone outcrops emerge on their walls, creating potential settlement substrate. Hard surfaces in deeper water are typically coated with a layer of fine sediment, and so may not support *P. arborea* settlement, but the canyon walls have a steep "ridge and gully" topography (Piper and Campbell, 2002), which may promote water flows that maintain exposure of bedrock outcrops. Below 1000 m depth, the continental slope and rise are typically covered with bioturbated mud, consistent with predictions of low probabilities of *P. arborea* occurrence over much of that area.

Particle tracking models showed potential for biophysical connectivity along that strip of predicted *P. arborea* habitat on the upper slope, mediated by the Shelf-Break Current, the principal water flow on the Scotian Shelf (Han et al., 1999; Hannah et al., 2001), at all times of year and independent of larval vertical behaviour — hence a conclusion not constrained by limited available knowledge of the species' reproductive biology. LPT modeling also demonstrated that the areas of suitable habitat identified at greater depths, where the species has yet to be found, could receive recruitment from upper-slope populations and once established, could support other deep-slope populations through passive larval dispersal.

Hindcast LPTs showed potential for recruitment to present or future suitable habitat in the eastern part of the study area from populations in Newfoundland waters and as far east as the Tail of Grand Bank.

The greatest uncertainty influencing the degree of connectivity concerned pelagic larval duration, which will profoundly affect dispersal. Two broad classes of sexual reproduction are known in octocorals: either broadcast spawning, with fertilization and development in the water column, or fertilization and subsequent brooding of embryos internally or externally on the maternal colony. Embryos develop into planula larvae, which are either crawling or ciliated and the minimum time to settlement competency is less than 1 week for the few species studied (Simpson, 2006). Even if *P. arborea* is a broadcast spawner, its PLD is likely short, two weeks or less (Lacharité and Metaxas, 2013). LPT models indicate that, with such short durations, most *P. arborea* larvae are retained in the immediate environs of their parent colonies. Ensembled connectivity patterns for 2-week PLD (**Figure 9**) show retention in all source boxes, supporting a hypothesis of primarily localized recruitment, while connections were mostly between adjacent source boxes (**Supplementary Figure 23**).

4.2 Predicted Distribution Under Climate Change Projections

Because of extrapolation uncertainties, the predicted distributions of *P. arborea* under climate projections for 2046–2065 are only reliable for the upper continental slope and portions of the eastern Scotian Shelf. Within that limitation, the RF models and GAMs showed very similar predictions (**Figure 5**), with common areas of suitable habitat expected along the upper slope. In contrast, the predicted areas of suitable habitat in Jordan Basin, on the flanks of Georges Bank, in parts of the Laurentian Channel, and in some areas on the continental slope, cannot be reliably confirmed due to the novel environmental conditions projected to occur there. Nevertheless, a substantial portion of the present-day predicted distribution is projected to persist through to 2046–2065, using models with good performance and reliability.

That limited impact of climate change on *P. arborea* in the Scotian Shelf bioregion study area conflicts with conclusions from basin-scale modeling of the same species (Morato et al., 2020). Both studies agreed on the existence of suitable habitat along the continental slope under present-day conditions, but they differed widely in their future projections, where the regional models showed an increase in suitable habitat in contrast to the loss of habitat projected in the basin-scale models (Morato et al., 2020). Without access to BNAM outputs for the 2081–2100 period, results directly comparable to those from the basin-scale analyses were not generated. However, trends in regional oceanography during the second half of the century are expected to be similar to those in the first, with no sharp increases anticipated (Shackell and Loder, 2012; Brickman et al., 2016). Thus, the limited projected change in the distribution of suitable habitat for *P. arborea* through to 2046–2065 should continue until 2100.

The causes of the conflicting results merit closer examination. Extrapolation diagnostics showed that, in both studies and despite their different suites of predictors, much of the study area falls within swaths with non-analogous environmental conditions (**Figure 7** and **Supplementary Figure 9**), where habitat predictions are unreliable. With the predictors used in the basin-scale study applied to the Scotian Shelf bioregion, the continental slope was included in an area of extrapolation, whereas in this study much of the predicted suitable future habitat on the slope had analogous conditions. Hence, the results presented herein are the more confident.

Differences between the basin-scale study and the regional study presented here were also a byproduct of the resolution of the oceanographic models used to create the environmental predictors. In the study area, ocean-climate variability is determined by a complex of atmospheric forcing and solar heating, interactions between the Gulf Stream and Labrador Current and local factors, including tides, river discharge and seabed topography (Brickman et al., 2016). The physical oceanographic variables used in this study came from BNAM, a basin-scale ocean model that has been rigorously tested against observational data in the region (Wang et al., 2018; Wang et al., 2019). In contrast, the basin-scale study (Morato et al., 2020) used output from the Earth System Grid Federation (ESGF) Peer-to-Peer System, which was specifically developed for global-scale studies in support of the IPCC Coupled Model Intercomparison Project 5 (Cinquini et al., 2012). It is well known that those models do not well capture details of the study region (Stock et al., 2011; Saba et al., 2016), and do not resolve the bathymetry of the Scotian Shelf, nor the spatial structure of the ocean overlying the shelf. Neither do they properly resolve the Gulf Stream separation off Cape Hatteras (Saba et al., 2016). It is, therefore, unsurprising that the two studies differ markedly in their predictions (**Supplementary Figure 24**; **Supplementary Text 2.3**), while the BNAM-based analysis must be considered the more realistic for the Scotian Shelf bioregion.

The two studies also used different environmental variables as predictors. In the basin-scale study, POC flux to the seafloor and calcite saturation state there, were the most important of five predictors in RF and Maxent models, whereas calcite saturation was the most important in a GAM (Morato et al., 2020). In this study, slope, mean surface temperature and mean bottom salinity were the three most important variables of eight influencing the RF model, while the GAM relied most on slope and mean surface temperature. The only predictor common to both studies was (temporally invariant) slope (**Supplementary Text 2.1**).

While all of the variables used by both studies are assumed to have biological relevance, very little is known about the threshold limits, tolerance or adaptive capacity of *P. arborea* or any other deep-water non-symbiotic gorgonian (Schubert et al., 2017; Gugliotti et al., 2019). Without that understanding, the alternative models are correlative, rather than built on causal relationships, limiting the interpretations needed to give preference to one study over the other based on their predictor

variables. Of the various predictors, biological response to calcite saturation has received the most attention. The saturation state of seawater for $CaCO_3$ (Ω) is a measure of its potential to corrode the calcitic sclerites found in *P. arborea* and other gorgonians. When $\Omega < 1$, seawater is corrosive to calcifying organisms (Azetsu-Scott et al., 2010). Experimental evidence suggests that gorgonian coral sclerites are somewhat protected from corrosive environments by their thick, fleshy coenenchyme tissue (Gabay et al., 2014; Gómez et al., 2015) and so *P. arborea* may be able to tolerate the degree of ocean acidification expected by the end of this century.

4.3 Implications for Conservation

Conservation of the iconic and ecologically significant bubblegum coral, *P. arborea*, has been a priority for ocean management in Atlantic Canada for over two decades (ESSIM Planning Office, 2006). Indeed, the Northeast Channel Coral Conservation Area was established in June 2002 with the purpose of protecting the largest known concentrations of *P. arborea* in the region from the harmful effects of bottom-contact fishing gears. Shortly thereafter, the Gully MPA was designated under Canada's Oceans Act in May 2004. The first such MPA in Canadian Atlantic waters, it was intended (in part) to protect rich aggregations of cold water corals, including *P. arborea* (Breeze and Fenton, 2007). The species is also found in the *Lophelia* Coral Conservation Area (Korabik et al., 2021). More recently, the Corsair and Georges Canyons Conservation Area was created in 2016 to protect a wide variety of coral species living on the canyon walls, including *P. arborea* (Metaxas et al., 2019). Those four protection areas were not originally planned as a network of protected areas nor have they been collectively evaluated for network properties such as representativity, connectivity, adequacy, viability and climate resiliency. The results of this study enable a first assessment of those areas for the suite of protected area network properties as they pertain to *P. arborea*.

The concept of "representativity" in protected area network design applies to different spatial scales and biogeographic subdivisions (DFO, 2010). The Northeast Channel Coral Conservation Area, the Corsair and Georges Canyons Conservation Area, the Gully MPA and the *Lophelia* Coral Conservation Area, together create a protected area network for *P. arborea* spanning from east to west along the upper continental slope within the Offshore Scotian Shelf planning area. The most reliable species distribution models (**Figure 4**) showed that most of the unexplored deep-water area is unlikely to provide suitable habitat for this species and so the nominal network currently in place has good representation and replication of *P. arborea* habitat. The areas where predicted suitable habitat extends into deeper waters identify targets for future exploration to determine whether or not the species is present. As noted above, the LPT modeling suggested that those areas have potential for colonization from areas of known presence. If *P. arborea* is confirmed in the deep-slope areas additional closed areas would need to be established to maintain representativity in the protected area network.

Amongst the four closed areas within the putative network where *P. arborea* has been observed, LPT analyses demonstrated the potential for connectivity, and extensive connectivity between the protected areas within that network with adjacent habitats outside the closures (**Figure 9** and **Supplementary Figure 23**). The *Lophelia* Coral Conservation Area, despite being the smallest of the closures at 15 km^2, has large potential as a seed source to all of the other protected areas in the network and to adjacent habitats on the Scotian Slope. Increasing its size would render further protection to this area which also protects the only known cold-water coral reef in eastern Canada (Beazley et al., 2021a). Metaxas et al. (2019) showed connectivity to the Corsair and Georges Canyons Conservation Area from canyons to the south, hypotheses not tested in this analysis. Limited connectivity between the Northeast Channel Coral Conservation Area and the Corsair and Georges Canyons Conservation Area was observed in winter and spring using the FVCOM ocean products (Metaxas et al., 2019). Connectivity between those two conservation areas was consistently observed in this study using BNAM ocean products, with connections made under all PLD scenarios, release depths and seasons using both long-term averaged currents (**Figure 9**) and currents extracted for individual years — the only exceptions being for 2 week PLD in 1993 in summer mid-water (**Supplementary Figure 17**) and autumn seabed releases (**Supplementary Figure 21**). Different ocean models are known to produce different connectivity trajectories (Wang et al., 2019; **Supplementary Text 2.2**), and given other differences between the studies (forward vs. hindcast modeling, particle release numbers, PLD etc.) these differences are not surprising. Collectively they show that the nominal protected area network for *P. arborea* has potential for strong connectivity between component closed areas either effected in a single spawning event or through stepping stone links where colonies occur along the connectivity trajectories.

The Jordan Basin Conservation Area and the St. Anns Bank MPA at the western and eastern extent of the planning area respectively, may prove to support *P. arborea*. Although neither area was identified as having suitable habitat in our contemporary models, both were identified as potentially having suitable habitat in mid-century projections under RCP 4.5 and RCP 8.5, albeit for Jordan Basin Conservation Area in areas of extrapolated environmental conditions (**Supplementary Figure 7**). Jordan Basin has validated presence of *Primnoa resedaeformis*, a species found co-occurring with *P. arborea* in the Northeast Channel. LPT modeling indicated that St. Anns Bank MPA connects with the *Lophelia* Coral Conservation Area under some scenarios and to other closed areas with 3 month larval duration (**Figure 9**). Assuming that the current velocities are not strongly altered in future, St. Anns Bank MPA should connect to the putative network. Should *P. arborea* be discovered in the Jordan Basin Conservation Area, the dependence of that area on larval retention would warrant an increase in its size which is currently 49 km^2.

Adequacy and viability of a protected-area network should be evaluated relative to the likely effectiveness of each closed area in achieving its objectives (DFO, 2010). If one objective is to maintain and enhance populations of *P. arborea*, the ability of populations to self-recruit will support effectiveness. All four closed areas have strong potential for larval retention if, as expected, PLD is short. However, increasing the size of the protected areas would improve that potential still further.

Identification of climate refugia is an important element in marine spatial planning (Johnson and Kenchington, 2019). The Gully MPA, the *Lophelia* Coral Conservation Area and other areas along the Scotian Slope east of Sable Island, some with records of *P. arborea* presence and others with predicted presence, have potential as climate refugia, where environmental conditions important to the species are projected to remain stable through to 2046–2065 at least (**Figure 8**). Priority should be given to reducing cumulative stressors on gorgonians, including bottom contact fishing, in those areas. Some other locations along the eastern Scotian Slope, including Shortland Canyon, will experience conditions that the species tolerates in the western sub-area (including the Northeast Channel), but for which the populations further east may not be adapted. Meanwhile, the dense aggregations of *P. arborea* in the Northeast Channel may experience novel environmental conditions by 2046–2065, indicated in the analyses primarily by warmer mean surface temperatures. However, the projected differences from present-day conditions in that area are not large and colonies already established there may be able to adapt. Management measures to reduce cumulative stresses on *P. arborea* throughout those areas could support survival in the face of pending environmental change.

DATA AVAILABILITY STATEMENT

The datasets presented in this study can be found in online repositories. The names of the repository/repositories and accession number(s) can be found below:

The 3-D Lagrangian particle simulator (Parcels) is freely available (https://www.oceanparcels.org); Monthly mean currents from the Bedford Institute of Oceanography North Atlantic Model (BNAM) results averaged over the 1990 to 2015 period for the Northwest Atlantic Ocean, are available online on the Federal Government of Canada Open Data Portal (https://open.canada.ca/data/en/dataset/dd5ef0d6-d588-4f4f-99e5-27c4bdfddf6a). The GLORYS12V1 ocean products with daily-means for the surface are publicly available from the Copernicus Marine Service data portal. Environmental data layers used for modeling present and future distributions are available from Mendeley Data as cited in the text.

AUTHOR CONTRIBUTIONS

SW and FM performed the analyses and produced the tables and figures. All authors designed the experiments and contributed to the writing of the manuscript, take responsibility for the content, and approved the submitted version.

ACKNOWLEDGMENTS

We thank Drs. Zeliang Wang and David Brickman at the Bedford Institute of Oceanography (BIO), Dartmouth, Nova Scotia, Canada for providing the BNAM ocean model products for this study, and Dr. Trevor Kenchington, also of BIO, for providing helpful comments on successive drafts of our manuscript. We thank Drs. Telmo Morato and José-Manuel González-Irusta for providing us with regional data used in their analyses which allowed us to interpret our results with greater insight. Dr. González-Irusta also kindly provided comments on a first draft of our manuscript. The authors acknowledge input and discussions within Work Package 2 of the EU Horizon 2020 iAtlantic project (Grant Agreement No. 818123). This publication is a Canadian contribution for Case Study 4 under that Work Package. SW was hired through the Competitive Science Research Fund and FM was hired through the Marine Spatial Planning program, both administered within Fisheries and Oceans Canada.

SUPPLEMENTARY MATERIAL

The Supplementary Material for this article can be found online at: https://www.frontiersin.org/articles/10.3389/fmars.2022.863693/full#supplementary-material

REFERENCES

Amodio, S., Aria, M. and D'Ambrosio, A. (2014). On Concurvity in Nonlinear and Nonparametric Regression Models. *Statistica* 74, 81–94. doi: 10.6092/issn.1973-2201/4599

Azetsu-Scott, K., Clarke, A., Falkner, K., Hamilton, J., Jones, E. P., Lee, C., et al. (2010). Calcium Carbonate Saturation States in the Waters of the Canadian Arctic Archipelago and the Labrador Sea. *J. Geophys. Res.* 115, C11021. doi: 10.1029/2009JC005917

Beazley, L., Guijarro, J., Lirette, C., Wang, Z. and Kenchington, E. (2017). Characteristics of Environmental Data Layers for Use in Species Distribution Modelling in the Maritimes Region. *Can. Tech. Rep. Fish. Aquat. Sci.* 3212, vii + 327.

Beazley, L., Kenchington, E., Korabik, M., Fenton, D. and King, M. (2021a). Other Effective Area-Based Conservation Measure Promotes Recovery in a Cold-Water Coral Reef. *Glob. Ecol. Conserv.* 26, e01485. doi: 10.1016/j.gecco.2021.e01485

Beazley, L., Kenchington, E., Murillo, F. J., Brickman, D., Wang, Z., Davies, A. J., et al. (2021b). Climate Change Winner in the Deep Sea? Predicting the Impacts of Climate Change on the Distribution of the Glass Sponge *Vazella Pourtalesii*. *Mar. Ecol. Prog. Ser.* 657, 1–23. doi: 10.3354/meps13566

Beazley, L., Kenchington, E., Murillo, F. J., Brickman, D., Wang, Z., Davies, A. J., et al. (2021c). Data From: Climate Change Winner in the Deep Sea? Predicting the Impacts of Climate Change on the Distribution of the Glass Sponge *Vazella pourtalesii*. *Mendeley Data* V1. doi: 10.17632/vm4bjn7g74.1

Beazley, L., Wang, Z., Kenchington, E., Yashayaev, I., Rapp, H. T., Xavier, J. R., et al. (2018). Predicted Distribution of the Glass Sponge *Vazella pourtalesi* on the Scotian Shelf and its Persistence in the Face of Climatic Variability. *PLoS One* 13, e0205505. doi: 10.1371/journal.pone.0205505

Beazley, L., Wang, Z., Kenchington, E., Yashayaev, I., Rapp, H. T., Xavier, J. R., et al. (2019). Data From: Predicted Distribution of the Glass Sponge *Vazella pourtalesi* on the Scotian Shelf and its Persistence in the Face of Climatic Variability. *Mendeley Data* V2. doi: 10.17632/zg8k3mchgx.2

Biau, G. (2012). Analysis of a Random Forests Model. *J. Mach. Learn. Res.* 13, 1063–1095. doi: 10.5555/2188385.2343682

Biau, G. and Scornet, E. (2016). A Random Forest Guided Tour. *TEST* 25, 197–227. doi: 10.1007/s11749-016-0481-7

Bouchet, P. J., Miller, D. L., Roberts, J. J., Mannocci, L., Harris, C. M. and Thomas, L. (2020). Dsmextra: Extrapolation Assessment Tools for Density Surface Models. *Methods Ecol. Evol.* 11, 1464–1469. doi: 10.1111/2041-210X.13469

Bracco, A., Liu, G., Galaska, M., Quattrini, A. M. and Herrera, S. (2019). Integrating Physical Circulation Models and Genetic Approaches to Investigate Population Connectivity in Deep-Sea Corals. *J. Mar. Syst.* 198, 103189. doi: 10.1016/j.jmarsys.2019.103189

Breeze, H. and Fenton, D. (2007). Designing Management Measures to Protect Cold-Water Corals Off Nova Scotia, Canada. *Bull. Mar. Sci.* 81, 123–133.

Breiman, L. (2001). Random Forests. *Mach. Learn.* 45, 5–32. doi: 10.1023/A:1010933404324

Brickman, D., Wang, Z. and DeTracey, B. (2016). High Resolution Future Climate Ocean Model Simulations for the Northwest Atlantic Shelf Region. *Can. Tech. Rep. Hydrogr. Ocean. Sci.* 315, xiv + 143.

Brock, R. J., Kenchington, E. and Martínez-Arroyo, A. (Eds.) (2012). *Scientific Guidelines for Designing Resilient Marine Protected Area Networks in a Changing Climate* (Montreal, Canada: Commission for Environmental Cooperation). Available at: http://www.cec.org/files/documents/publications/10820-scientific-guidelines-designing-resilient-marine-protected-area-networks-in-changing-en.pdf.

Bryan, T. and Metaxas, A. (2007). Predicting Suitable Habitat for Paragorgiidae and Primnoidae on the Atlantic and Pacific Continental Margins of North America. *Mar. Ecol. Prog. Ser.* 330, 113–126. doi: 10.3354/meps330113

Buhl-Mortensen, L. and Mortensen, P. B. (2005). "Distribution and Diversity of Species Associated With Deep-Sea Gorgonian Corals Off Atlantic Canada" in *Cold-Water Corals and Ecosystems*. Eds. Freiwald, A. R. and Roberts, J. M. (Berlin: Springer-Verlag), 849–879.

Carr, L. M. (2019). Marine Spatial Planning in a Climate of Uncertainty – An Irish Perspective. *Irish. Geogr.* 52, 1–20. doi: 10.6092/issn.1973-2201/4599.

Carstensen, J., Conley, D. J., Lophaven, S., Danielsson, Å., Rahm, L., Toompuu, A., et al. (2002). "Statistical Analysis and Modelling of Phytoplankton Dynamics," in *Exploitation of Data in the Nordic and Baltic Monitoring Programs* Copenhagen: (Nordic Council of Ministers).

Cinquini, L., Crichton, D. J., Mattmann, C., Bell, G. M., Drach, B., Williams, D., et al. (2012). The Earth System Grid Federation: An Open Infrastructure for Access to Distributed Geospatial Data. *Future Gener. Comput. Syst.* 36, 1–10. doi: 10.1109/eScience.2012.6404471

Cogswell, A. T., Kenchington, E. L. R., Lirette, C. G., MacIsaac, K., Best, M. M., Beazley, L. I., et al. (2009). The Current State of Knowledge Concerning the Distribution of Coral in the Maritime Provinces. *Can. Tech. Rep. Fish. Aquat. Sci.* 2855, v + 66.

Conn, P. B., Johnson, D. S. and Boveng, P. L. (2015). On Extrapolating Past the Range of Observed Data When Making Statistical Predictions in Ecology. *PLoS One* 10 (10), e0141416. doi: 10.1371/journal.pone.0141416

Conrad, O., Bechtel, B., Bock, M., Dietrich, H., Fischer, E., Gerlitz, L., et al. (2015). System for Automated Geoscientific Analyses (SAGA) V. 2.1.4. *Geosci. Model. Dev.* 8, 1991–2007. doi: 10.5194/gmd-8-1991-2015

Cordeiro, R., McFadden, C., van Ofwegen, L. and Williams, G. (2021)World List of Octocorallia. In: *Paragorgia Milne Edward* (World Register of Marine Species) (Accessed September 28, 2021).

Csanady, G. T. and Hamilton, P. (1988). Circulation of Slopewater. *Cont. Shelf Res.* 8, 565–624. doi: 10.1016/0278-4343(88)90068-4

de Boyer Montégut, C., Madec, G., Fischer, A. S., Lazar, A. and Iudicone, D. (2004). Mixed Layer Depth Over the Global Ocean: An Examination of Profile Data and a Profile-Based Climatology. *J. Geophys. Res.* 109, C12003. doi: 10.1029/2004JC002378

De Clippele, L. H., Buhl-Mortensen, P. and Buhl-Mortensen, L. (2015). Fauna Associated With Cold Water Gorgonians and Sea Pens. *Cont. Shelf Res.* 105, 67–78. doi: 10.1016/j.csr.2015.06.007

Delandmeter, P. and van Sebille, E. (2019). The Parcels V2.0 Lagrangian Framework: New Field Interpolation Schemes. *Geosci. Model. Devel.* 12, 3571–3584. doi: 10.5194/gmd-12-3571-2019

DFO (2009). Development of a Framework and Principles for the Biogeographic Classification of Canadian Marine Areas. *DFO Can. Sci. Advis. Sec. Sci. Advis. Rep*. 2009/056.

DFO (2010). Science Guidance on the Development of Networks of Marine Protected Areas (MPAs). *DFO Can. Sci. Advis. Sec. Sci. Advis. Rep*. 2009/061.

DFO (2014) *Regional Oceans Plan - Scotian Shelf, Atlantic Coast, Bay of Fundy. Background and Program Description* (Halifax: Fisheries and Oceans Canada. Regional Oceans Plan (dfo-mpo.gc.ca) (Accessed October 5, 2021).

DFO (2019)Northeast Channel Coral Conservation Area (Restricted Bottom Fisheries Zone). In: *Northeast Channel Coral Conservation Area (Restricted Bottom Fisheries Zone)* (dfo-mpo.gc.ca) (Accessed October 4, 2021).

Díaz-Uriarte, R. and Alvarez de Andrés, S. (2006). Gene Selection and Classification of Microarray Data Using Random Forest. *BMC Bioinf.* 7, 3. doi: 10.1186/1471-2105-7-3

Drinkwater, K., Petrie, B. and Smith, P. (2003). Climate Variability on the Scotian Shelf During the 1990s. *ICES Mar. Sci. Symp.* 219, 40–49.

ESRI (2011). *ArcGIS Desktop: Release 10* (Redlands, CA: Environmental Systems Research Institute).

ESSIM Planning Office (2006). Coral Conservation Plan. Maritimes Region, (2006-2010). *Oceans. Coast. Mgt. Rep.* 2006, 01.

FAO (2016). *Vulnerable Marine Ecosystems: Processes and Practices in the High Seas*. Eds. Thompson, A., Sanders, J., Tandstad, M., Carocci, F. and Fuller, J. (Rome, Italy: FAO).

Fawcett, T. (2006). An Introduction to ROC Analysis. *Pattern Recog. Lett.* 27, 861–874. doi: 10.1016/j.patrec.2005.10.010

Feng, T., Stanley, R. R. E., Wu, Y., Kenchington, E., Xu, J. and Horne, E. (2022). A High-Resolution 3-D Circulation Model in a Complex Archipelago on the Coastal Scotian Shelf. *J. Geophys. Res. Oceans.* 127, e2021JC017791. doi: 10.1029/2021JC017791

Fratantoni, P. S. and Pickart, R. S. (2007). The Western North Atlantic Shelfbreak Current System in Summer. *J. Phys. Oceanogr.* 37, 2509–2533. doi: 10.1175/JPO3123.1

Gabay, Y., Fine, M., Barkay, Z. and Benayahu, Y. (2014). Octocoral Tissue Provides Protection From Declining Oceanic pH. *PLoS One* 9 (4), e91553. doi: 10.1371/journal.pone.0091553

Garcia, S. M., Rice, J., Charles, A. and Diz, D. (2021) *OECMs in Marine Capture Fisheries: Systematic Approach to Identification, Use and Performance Assessment in Marine Capture Fisheries (Version 2)* (Brussels, Belgium: Fisheries Expert Group of the IUCN Commission on Ecosystem Management, Gland, Switzerland. European Bureau of Conservation and Development). Available at: https://ebcd.org/oecms-in-marine-capture-fisheries/ (Accessed December 14, 2021).

Gass, S. E. (2002). *An Assessment of the Distribution and Status of Deep-Sea Corals in Atlantic Canada by Using Both Scientific and Local Forms of Knowledge. [MES Thesis]* (Halifax, Canada: Dalhousie University).

Gass, S. E. and Willison, J. H. M. (2005). "An Assessment of the Distribution of Deep-Sea Corals in Atlantic Canada by Using Both Scientific and Local Forms of Knowledge" in *Cold-Water Corals and Ecosystems*. Eds. Freiwald, A. R. and Roberts, J. M. (Berlin: Springer-Verlag), 223–245.

Gómez, C. E., Paul, V. J., Ritson-Williams, R., Muehllehner, N., Langdon, C. and Sánchez, J. A. (2015). Responses of the Tropical Gorgonian Coral *Eunicea fusca* to Ocean Acidification Conditions. *Coral Reefs.* 34, 451–460. doi: 10.1007/s00338-014-1241-3

Grorud-Colvert, K., Claudet, J., Tissot, B. N., Caselle, J. E., Carr, M. H., Day, J. C., et al. (2014). Marine Protected Area Networks: Assessing Whether the Whole is Greater Than the Sum of its Parts. *PLoS One* 9, e102298. doi: 10.1371/journal.pone.0102298

Gugliotti, E. F., DeLorenzo, M. E. and Etnoyer, P. J. (2019). Depth-Dependent Temperature Variability in the Southern California Bight With Implications for the Cold-Water Gorgonian Octocroal *Adelogrogia phyllosclera*. *J. Exp. Mar. Biol. Ecol.* 514 (515), 118–126. doi: 10.1016/j.jembe.2019.03.010

Halliday, R. G. and Kohler, A. C. (1971). Groundfish Survey Programmes of the St. Andrews Biological Station, Fisheries Research Board of Canada – Objectives and Characteristics. *ICNAF. Res. Doc.* 71, 35.

Hanberry, B. B. and He, H. S. (2013). Prevalence, Statistical Thresholds and Accuracy Assessment for Species Distribution Models. *Web Ecol.* 13, 13–19. doi: 10.5194/we-13-13-2013

Han, G. and Loder, J. W. (2003). Three-Dimensional Seasonal-Mean Circulation and Hydrography on the Eastern Scotian Shelf. *J. Geophys. Res.* 108 (C5), 3136. doi: 10.1029/2002JC001463

Han, G., Loder, J. W. and Smith, P. C. (1999). Seasonal-Mean Hydrography and Circulation in the Gulf of St. Lawrence and on the Eastern Scotian and Southern Newfoundland Shelves. *J. Phys. Ocean.* 29, 1279–1301. doi: 10.1175/1520-0485(1999)029<1279:SMHACI>2.0.CO;2

Hannah, C. G., Shore, J. A., Loder, J. W. and Naimie, C. E. (2001). Seasonal Circulation of the Western and Central Scotian Shelf. *J. Phys. Ocean.* 31, 591–615. doi: 10.1175/1520-0485(2001)031<0591:SCOTWA>2.0.CO;2

Herrera, S., Shank, M. and Sánchez, J. A. (2012). Spatial and Temporal Patterns of Genetic Variation in the Widespread Antitropical Deep-Sea Coral *Paragorgia arborea*. *Mol. Ecol.* 21, 6053–6067. doi: 10.1111/mec.12074

Hilário, A., Metaxas, A., Gaudron, S. M., Howell, K. L., Mercier, A., Mestre, N. C., et al. (2015). Estimating Dispersal Distance in the Deep Sea: Challenges and Applications to Marine Reserves. *Front. Mar. Sci.* 2. doi: 10.3389/fmars.2015.00006

ICES (2021). "EU Request to Advise on the List of Areas Where VMEs are Known to Occur or are Likely to Occur and on the Existing Deep-Sea Fishing Areas (Ref. (EU)2016/2336.)" in *Report of the ICES Advisory Committe* (Copenhagen: ICES Advice), sr.2021.01. doi: 10.17895/ices.advice.7507

IPCC (2013). *Climate Change 2013: The Physical Science Basis. Contribution of Working Group I to the Fifth Assessment Report of the Intergovernmental Panel on Climate Change* (Cambridge, UK: Cambridge University Press).

Johnson, D. and Kenchington, E. (2019). Should Potential for Climate Change Refugia be Considered as an Eighth Criterion for Describing EBSAs? *Conserv. Lett.* 12 (4), e12634. doi: 10.1111/conl.12634

Jones, C. C., Acker, S. A. and Halpern, C. B. (2010). Combining Local- and Large-Scale Models to Predict the Distributions of Invasive Plant Species. *Ecol. Appl.* 20, 311–326. doi: 10.1890/08-2261.1

Kenchington, E., Lirette, C., Murillo, F. J., Beazley, L. and Downie, A.-L. (2019a). Vulnerable Marine Ecosystems in the NAFO Regulatory Area: Updated Kernel Density Analysis of Vulnerable Marine Ecosystem Indicators. *NAFO. SCR. Doc.*, 68. https://www.nafo.int/Portals/0/PDFs/sc/2019/scr19-058.pdf. 19/058, Serial No. N7030.

Kenchington, E., Wang, Z., Lirette, C., Murillo, J. F., Guijarro, J., Yashayaev, I., et al. (2019b). Connectivity Modelling of Areas Closed to Protect Vulnerable Marine Ecosystems in the Northwest Atlantic. *Deep-Sea. Res. I* 143, 85–103. doi: 10.1016/j.dsr.2018.11.007

Korabik, M., Baker, E., Beazley, L., Thompson, S., Bouchard Marmen, M. and Kenchington, E. (2021). A Pictorial Guide to the Epibenthic Megafauna of the Lophelia Coral Conservation Area Identified From *In Situ* Benthic Images. *Can. Tech. Rep. Fish. Aquat. Sci.* 3430, v + 142.

Lacharité, M. and Metaxas, A. (2013). Early Life History of Deep-Water Gorgonian Corals may Limit Their Abundance. *PLoS One* 8 (6), e65394. doi: 10.1371/journal.pone.0065394

Landis, J. R. and Koch, G. G. (1977). The Measurement of Observer Agreement for Categorical Data. *Biometrics* 33, 159–174. doi: 10.2307/2529310

Lange, M. and van Sebille, E. (2017). Parcels V0.9: Prototyping a Lagrangian Ocean Analysis Framework for the Petascale Age. *Geosci. Model. Devel.* 10, 4175–4186. doi: 10.5194/gmd-10-4175-2017

Le Corre, N., Pepin, P., Burmeister, A. D., Walkusz, W., Skanes, K., Wang, Z., et al. (2020). Larval Connectivity of Northern Shrimp (*Pandalus borealis*) in the Northwest Atlantic. *Can. J. Fish. Aquat. Sci.* 77, 1332–1347. doi: 10.1139/cjfas-2019-0454

Lester, S. E., Costello, C., Halpern, B. S., Gaines, S. D., White, C. and Barth, J. A. (2013). Evaluating Tradeoffs Among Ecosystem Services to Inform Marine Spatial Planning. *Mar. Policy* 38, 80–89. doi: 10.1016/j.marpol.2012.05.022

Leverette, T. L. and Metaxas, A. (2005). "Predicting Habitat for Two Species of Deep-Water Coral on the Canadian Atlantic Continental Shelf and Slope" in *Cold-Water Corals and Ecosystems*. Eds. Freiwald, A. and Roberts, J. M. (Berlin: Springer-Verlag), 467–479.

Liaw, A. and Wiener, M. (2002). Classification and Regression by randomForest. *R News* 2, 18–22.

Liu, C., Berry, P. M., Dawson, T. P. and Pearson, R. G. (2005). Selecting Thresholds of Occurrence in Prediction of Species Distribution. *Ecography* 28, 385–393. doi: 10.1111/j.0906-7590.2005.03957.x

Liu, C., Wolter, C., Xian, W. and Jeschke, J. M. (2020). Species Distribution Models Have Limited Spatial Transferability for Invasive Species. *Ecol. Lett.* 23, 1682–1692. doi: 10.1111/ele.13577

Lopes, P. F. M., Verba, J. T., Begossi, A. and Pennino, M. G. (2019). Predicting Species Distribution From Fishers' Local Ecological Knowledge: A New Alternative for Data-Poor Management. *Can. J. Fish. Aquat. Sci.* 76, 1423–1431. doi: 10.1139/cjfas-2018-0148

Mahony, C. R., Cannon, A. J., Wang, T. and Aitken, S. N. (2017). A Closer Look at Novel Climates: New Methods and Insights at Continental to Landscape Scales. *Glob. Change Biol.* 23, 3934–3955. doi: 10.1111/gcb.13645

Mannocci, L., Roberts, J. J., Halpin, P. N., Authier, M., Boisseau, O., Nejmeddine Bradai, M., et al. (2018). Assessing Cetacean Surveys Throughout the Mediterranean Sea: A Gap Analysis in Environmental Space. *Sci. Rep.* 8, 3126. doi: 10.1038/s41598-018-19842-9

Mannocci, L., Roberts, J. J., Pedersen, E. J. and Halpin, P. N. (2020). Geographical Differences in Habitat Relationships of Cetaceans Across an Ocean Basin. *Ecography* 43, 1–10. doi: 10.1111/ecog.04979

Mesgaran, M. B., Cousens, R. D. and Webber, B. L. (2014). Here be Dragons: A Tool for Quantifying Novelty Due to Covariate and Correlation Change When Projecting Species Distribution Models. *Diversity Distrib.* 20, 1147–1159. doi: 10.1111/ddi.12209

Metaxas, A. and Davis, J. (2005). Megafauna Associated With Assemblages of Deep-Water Gorgonian Corals in Northeast Channel, Off Nova Scotia, Canada. *J. Mar. Biolog. Assoc. U.K.* 85, 1381–1390. doi: 10.1017/S0025315405012567

Metaxas, A. and Giffin, B. (2004). Dense Beds of the Ophiuroid *Ophiacantha abyssicola* on the Continental Slope Off Nova Scotia, Canada. *Deep-Sea. Res. I* 51, 1307–1317. doi: 10.1016/j.dsr.2004.06.001

Metaxas, A., Lacharité, M. and de Mendonça, S. N. (2019). Hydrodynamic Connectivity of Habitats of Deep-Water Corals in Corsair Canyon, Northwest Atlantic: A Case for Cross-Boundary Conservation. *Front. Mar. Sci.* 6. doi: 10.3389/fmars.2019.00159

Miller, J. A. (2012). Species Distribution Models: Spatial Autocorrelation and non-Stationarity. *Prog. Phys. Geogr. Earth Environ.* 36, 681–692. doi: 10.1177/0309133312442522

Morán-Ordóñez, A., Lahoz-Monfort, J. J., Elith, J. and Wintle, B. A. (2017). Evaluating 318 Continental-Scale Species Distribution Models Over a 60-Year Prediction Horizon: What Factors Influence the Reliability of Predictions? *Glob. Ecol. Biogeogr.* 26, 371–384. doi: 10.1111/geb.12545

Morato, T., Dominguez-Carrió, C., Mohn, C., Ocaña Vincente, O., Ramos, M., Rodrigues, L., et al. (2021). Dense Cold-Water Coral Garden of *Paragorgia johnsoni* Suggests the Importance of the Mid-Atlantic Ridge for Deep-Sea Biodiversity. *Ecol. Evol.* 00, 1–8. doi: 10.1002/ece3.8319

Morato, T., González-Irusta, J.-M., Dominguez-Carrió, C., Wei, C.-L., Davies, A., Sweetman, A. K., et al. (2020). Climate-Induced Changes in the Suitable Habitat of Cold-Water Corals and Commercially Important Deep-Sea Fishes in the North Atlantic. *Glob. Change Biol.* 26, 2181–2202. doi: 10.1111/gcb.14996

Mortensen, P. B. and Buhl-Mortensen, L. (2004). Distribution of Deepwater Gorgonian Corals in Relation to Benthic Habitat Features in the Northeast Channel (Atlantic Canada). *Mar. Biol.* 144, 1223–1238. doi: 10.1007/s00227-003-1280-8

Moss, R. H., Edmonds, J. A., Hibbard, K. A., Manning, M. R., Rose, S. K., van Vuuren, D. P., et al. (2010). The Next Generation Scenarios for Climate Change Research and Assessment. *Nature* 463, 747–756. doi: 10.1038/nature08823

NAFO (2021) *Northwest Atlantic Fisheries Organization Conservation and Enforcement Measures 2021. Serial No. N7153. NAFO/COM Doc. 21-01*. Available at: https://www.nafo.int/Portals/0/PDFs/COM/2021/comdoc21-01.pdf.

Okubo, A. (1971). Oceanic Diffusion Diagrams. *Deep-sea. Res.* 18, 789–802. doi: 10.1016/0011-7471(71)90046-5

Piper, D. J. W. and Campbell, D. C. (2002). Surficial Geology of the Scotian Slope, Eastern Canada. *Geol. Surv. Can. Curr. Res.* 2002, E15.10.

Polovina, J. J., Mitchum, G. T. and Evans, G. T. (1995). Decadal and Basin-Scale Variation in Mixed Layer Depth and the Impact on Biological Production in the Central and North Pacific 1960-88. *Deep-Sea. Res.* 42, 1701–1716. doi: 10.1016/0967-0637(95)00075-H

Qiao, H., Feng, X., Escobar, L. E., Peterson, A. T., Soberón, J., Zhu, G., et al. (2018). An Evaluation of Transferability of Ecological Niche Models. *Ecography* 42, 521–534. doi: 10.1111/ecog.03986

Quattrini, A. M., Nizinski, M. S., Chaytor, J. D., Demopoulos, A. W., Roark, E. B., France, S. C., et al. (2015). Exploration of the Canyon-Incised Continental Margin of the Northeastern United States Reveals Dynamic Habitats and Diverse Communities. *PLoS One* 10, e0139904. doi: 10.1371/journal.pone.0139904

R Development Core Team (2020). *R: A Language and Environment for Statistical Computing* (Vienna, Austria: R Foundation for Statistical Computing).

Roberts, D. R., Bahn, V., Ciuti, S., Boyce, M. S., Elith, J., Guillera-Arroita, , et al. (2017). Cross-Validation Strategies for Data With Temporal, Spatial, Hierarchical, or Phylogenetic Structure. *Ecography* 40, 913–929. doi: 10.1111/ecog.02881

Saba, V. S., Griffies, S. M., Anderson, W. G., Winton, M., Alexander, M. A., Delworth, T. L., et al. (2016). Enhanced Warming of the Northwest Atlantic Ocean Under Climate Change. *JGR. Oceans.* 121, 118–132. doi: 10.1002/2015JC011346

Sánchez, J. A. (2005). Systematics of the Bubblegum Corals (Cnidaria: Octocorallia: Paragorgiidae) With Description of New Species From New Zealand and the Eastern Pacific. *Zootaxa* 1014, 1–72. doi: 10.11646/zootaxa.1014.1.1

Santos, C., Agardy, T., Andrade, F., Calado, H., Crowder, L. B., Ehler, C. N., et al. (2020). Integrating Climate Change in Ocean Planning. *Nat. Sust.* 3, 1–12. doi: 10.1038/s41893-020-0513-x

Schubert, N., Brown, D. and Rossi, S. (2017). "Symbiotic Versus Non-Symbiotic Octocorals: Physiological and Ecological Implications" in *In Marine Animal Forests*. Eds. Rossi, S., Bramanti, L., Gori, A. and Orejas Saco del Valle, C. (Berlin: Springer-Verlag), 1–32. doi: 10.1007/978-3-319-17001-5_54-1

Sequeira, A. M. M., Bouchet, P. J., Yates, K. L., Mengersen, K. and Caley, M. J. (2018). Transferring Biodiversity Models for Conservation: Opportunities and Challenges. *Methods Ecol. Evol.* 9, 1250–1264. doi: 10.1111/2041-210X.12998

Shackell, N. and Loder, J. W. (2012). "Climate Change and Its Effects on Ecosystems, Habitats and Biota," in *Atlantic Coastal Zone Information Steering Committee*, Publisher is Coastal & Ocean Information Network Atlantic (COINAtlantic) based in Halifax, NS, Canada: Mailing Address: COINAtlantic Dalhousie University 6414 Coburg Road PO Box 15000 Halifax, NS B3H 4R2 29 p. Available at: https://0fb5ebe8ca924c3c9170ef778a77f76e.filesusr.com/ugd/cf2ff9_af28b1c825d943a6b204777ac87c0873.pdf.

Sherwood, O. A. and Edinger, E. N. (2009). Ages and Growth Rates of Some Deep-Sea Gorgonian and Antipatharian Corals of Newfoundland and Labrador. *Can. J. Fish. Aquat. Sci.* 66, 142–152. doi: 10.1139/F08-195

Simard, F., Laffoley, D. and J.M, B. (Eds.) (2016). *Marine Protected Areas and Climate Change: Adaptation and Mitigation Synergies, Opportunities and Challenges. Full Report* (Gland, Switzerland: IUCN).

Simpson, A. (2006) *Reproduction in Octocorals (Subclass Octocorallia): A Review of Published Literature*. Available at: https://userweb.ucs.louisiana.edu/~scf4101/Bambooweb/reviewrepro.pdf (Accessed December 14, 2021).

Sowers, D. C., Masetti, G., Mayer, L. A., Johnson, P., Gardner, J. V. and Armstrong, A. A. (2020). Standardized Geomorphic Classification of Seafloor Within the United States Atlantic Canyons and Continental Margin. *Front. Mar. Sci.* 7. doi: 10.3389/fmars.2020.00009

Stanton, J. C., Pearson, R. G., Horning, N., Ersts, P. and Reşit Akçakaya, H. (2012). Combining Static and Dynamic Variables in Species Distribution Models Under Climate Change. *Methods Ecol. Evol.* 3, 349–357. doi: 10.1111/j.2041-210X.2011.00157.x

Stock, C. A., Alexander, M. A., Bond, N. A., Brander, K. M., Cheung, W. W. L., Curchitser, E. N., et al. (2011). On the Use of IPCC-Class Models to Assess the Impact of Climate on Living Marine Resources. *Prog. Oceanogr.* 88, 1–27. doi: 10.1016/j.pocean.2010.09.001

Strychar, K. B., Kenchington, E. L., Hamilton, L. C. and Scott, D. B. (2011). Phylogenetic Diversity of the Cold Water Octocoral *Paragorgia Arborea* (Linnaeus 1758) Off the East Coast of Canada. *Int. J. Biol.* 3, 3–22. doi: 10.5539/ijb.v3n1p3

Sundahl, H., Buhl-Mortensen, P. and Buhl-Mortensen, L. (2020). Distribution and Suitable Habitat of the Cold-Water Corals *Lophelia pertusa*, *Paragorgia Arborea*, and *Primnoa resedaeformis* on the Norwegian Continental Shelf. *Front. Mar. Sci.* 7. doi: 10.3389/fmars.2020.00213

Townsend, D. W., Pettigrew, N. R., Thomas, M. A., Neary, M. G., McGillicuddy, D. J., Jr. and O'Connell, J. (2015). Water Masses and Nutrient Sources to the Gulf of Maine. *J. Mar. Res.* 73, 93–122. doi: 10.1357/002224015815848811

Tremblay, M. J., Black, G. A. P. and Branton, R. M. (2007). The Distribution of Common Decapod Crustaceans and Other Invertebrates Recorded in Annual Ecosystem Surveys of the Scotian Shelf 1999-2006. *Can. Tech. Rep. Fish. Aquat. Sci.* 2762, iii + 74.

Valavi, R., Elith, J., Lahoz-Monfort, J. J. and Guillera-Arroita, G. (2019). BlockCV: An R Package for Generating Spatially or Environmentally Separated Folds for K-Fold Cross-Validation of Species Distribution Models. *Methods Ecol. Evol.* 10, 225–232. doi: 10.1111/2041-210X.13107

van Vuuren, D. P., Edmonds, J., Kainuma, M., Riahi, K., Thomson, A., Hibbard, K., et al. (2011). The Representative Concentration Pathways: An Overview. *Clim. Change* 109, 5. doi: 10.1007/s10584-011-0148-z

Walbridge, S., Slocum, N., Pobuda, M. and Wright, D. J. (2018). Unified Geomorphological Analysis Workflows With Benthic Terrain Modeler. *Geosciences* 8, 94. doi: 10.3390/geosciences8030094

Wang, Z., Brickman, D. and Greenan, B. J. W. (2019). Characteristic Evolution of the Atlantic Meridional Overturning Circulation From 1990 to 2015: An Eddy-Resolving Ocean Model Study. *Deep. Sea. Res. I* 149, 103056. doi: 10.1016/j.dsr.2019.06.002

Wang, S., Kenchington, E., Wang, Z. and Davies, A. J. (2021). Life in the Fast Lane: Modeling the Fate of Glass Sponge Larvae in the Gulf Stream. *Front. Mar. Sci.* 8. doi: 10.3389/fmars.2021.701218

Wang, S., Kenchington, E. L., Wang, Z., Yashayaev, I. and Davies, A. J. (2020). 3-D Ocean Particle Tracking Modeling Reveals Extensive Vertical Movement and Downstream Interdependence of Closed Areas in the Northwest Atlantic. *Sci. Rep.* 10, 21421. doi: 10.1038/s41598-020-76617-x

Wang, Z., Lu, Y., Greenan, B. and Brickman, D. (2018). BNAM: An Eddy-Resolving North Atlantic Ocean Model to Support Ocean Monitoring in *Can. Tech. Rep. Hydrogr. Ocean Sci*, 327 vii + 18.

Wang, S., Wang, Z., Lirette, C., Davies, A. and Kenchington, E. (2019). Comparison of Physical Connectivity Particle Tracking Models in the Flemish Cap Region. *Can. Tech. Rep. Fish. Aquat. Sci.* 3353, v + 39.

Watanabe, S., Metaxas, A., Sameoto, J. and Lawton, P. (2009). Patterns in Abundance and Size of Two Deep-Water Gorgonian Octocorals, in Relation to Depth and Substrate Features Off Nova Scotia. *Deep-Sea. Res. I: Oceanogr. Res. Pap.* 56, 2235–2248. doi: 10.1016/j.dsr.2009.09.003

Watling, L. and Auster, P. J. (2005). "Distribution of Deep-Water Alcyonacea Off the Northeast Coast of the United States" in *Cold-Water Corals and Ecosystems*. Eds. Freiwald, A. R. and Roberts, J. M. (Berlin: Springer-Verlag), 279–296.

Wood, S. N. (2006). *Generalized Additive Models: An Introduction With R* (Boca Raton, Florida: Chapman & Hall/CRC Press).

Wright, D. J., Pendleton, M., Boulware, J., Walbridge, S., Gerlt, B., Eslinger, D., et al. (2012) *ArcGIS Benthic Terrain Modeler (BTM), V. 3.0* (Massachusetts Office of Coastal Zone Management: Environmental Systems Research Institute, NOAA Coastal Services Center) (Accessed October 4, 2021).

Yates, K. L., Bouchet, P. J., Caley, M. J., Mengersen, K., Randin, C. F., Parnell, S., et al. (2018). Outstanding Challenges in the Transferability of Ecological Models. *Trends Ecol. Evol.* 33, 790–802. doi: 10.1016/j.tree.2018.08.001

Zeng, X., Adams, A., Roffer, M. and He, R. (2019). Potential Connectivity Among Spatially Distinct Management Zones for Bonefish (*Albula Vulpes*) *via* Larval Dispersal. *Environ. Biol. Fish.* 102, 233–252. doi: 10.1007/s10641-018-0826-z

Conflict of Interest: The authors declare that the research was conducted in the absence of any commercial or financial relationships that could be construed as a potential conflict of interest.

frontiers | Frontiers in Marine Science

PERSPECTIVE
published: 15 July 2022
doi: 10.3389/fmars.2022.878077

The Need for a Global Ocean Vision Within Biodiversity Beyond National Jurisdiction: A Key Role for Strategic Environmental Assessment

Maria Adelaide Ferreira[1]*, *David E. Johnson*[2] and *Francisco Andrade*[1,3]

[1]Marine and Environmental Sciences Centre – Lisbon University (MARE-UL), Lisboa, Portugal, [2]Seascape Consultants, Ltd., Romsey, United Kingdom, [3]Faculty of Sciences of the University of Lisbon, Lisboa, Portugal

An ecosystem-based forward-looking vision for the global ocean, encompassing ocean health and productivity, ecosystem integrity and resilience, incorporating area beyond national jurisdiction, is fundamental. A vision which is holistic and universally acceptable to guide future sustainable ocean policies, plans and programmes (PPPs). We argue that Strategic Environmental Assessment (SEA) is the best available framework to develop such a vision and its suitability for this purpose should be recognised within the on-going process to negotiate an International Legally Binding Instrument (ILBI) for the conservation and sustainable use of Biodiversity Beyond National Jurisdiction (BBNJ Agreement). This perspective paper justifies why such an ecosystem-based Global Ocean Vision is essential. It then describes the key characteristics it must integrate and how it can be elaborated in the framework of a collective SEA within the BBNJ process. We advocate expanding text in Part I General Provisions of the draft BBNJ Agreement to include development of such a global ocean vision. We conclude by highlighting the opportunity and timeliness of this proposal, with the fifth session of the IGC of BBNJ tentatively scheduled for August 2022.

Keywords: ecosystem-based approach, global ocean vision, strategic environmental assessment, UNCLOS, BBNJ Agreement

OPEN ACCESS

Edited by:
J. Murray Roberts, University of Edinburgh, United Kingdom

Reviewed by:
Glen Wright, Institut du Développement Durable et des Relations Internationales, France

***Correspondence:**
Maria Adelaide Ferreira
maferreira@fc.ul.pt

Specialty section:
This article was submitted to Deep-Sea Environments and Ecology, a section of the journal Frontiers in Marine Science

Received: *17 February 2022*
Accepted: *09 June 2022*
Published: *15 July 2022*

Citation:
Ferreira MA, Johnson DE and Andrade F (2022) The Need for a Global Ocean Vision Within Biodiversity Beyond National Jurisdiction: A Key Role for Strategic Environmental Assessment. Front. Mar. Sci. 9:878077. doi: 10.3389/fmars.2022.878077

INTRODUCTION – THE NEED FOR AN ECOSYSTEM BASED GLOBAL OCEAN VISION UNDER BBNJ

The ocean is the largest ecosystem on Earth, covering more than two thirds of the planet's surface and encompassing 99% of all the habitable space for life on Earth (IPCC, 2019a). We rely on the continued supply of ecosystem services provided by a healthy ocean (e.g., IPBES, 2019; SCBD, 2020; UN, 2021), whose use must take place within the planetary boundaries of a sustainable development for humankind (Rockström et al., 2009), ensuring ocean ecosystems remain sufficiently intact and resilient to human disturbance (Rockström et al., 2021). However, that is not our current global trajectory (Steffen et al., 2015). The ocean is changing fast in the Anthropocene: warming, deoxygenating and acidifying. Eutrophication and other types of pollution, changing oceanographic conditions, and concomitant effects on biotic communities, such as species migrations and die-off, are increasingly evident as a direct combined result of human activities (UN, 2021; United Nations Environment Programme, 2021; IOC-UNESCO, 2022). The growing range of maritime economic sectors with a direct or indirect link to the

ocean (e.g., Boschen-Rose et al., 2020), is further contributing to increased and cumulative pressures on the ocean, including overexploitation of living (and non-living) marine resources, chemical and physical pollution (including noise), the spread of invasive alien species, and physical destruction of habitats (UN, 2021). These combined pressures on the ocean ecosystem, namely on marine biodiversity, are impairing (and even threatening) the continued delivery of essential ecosystem services throughout the water column, all the way down to the deep sea and ocean floor (e.g., Levin and Le Bris, 2015), making the need to safeguard marine biodiversity ever more urgent (Johnson et al., 2019; Johnson et al., 2018).

The United Nations Convention on the Law of the Sea is the international agreement that establishes a legal framework for all marine and maritime activities. Conceived in the 1970s and signed in 1982, Part XII of UNCLOS contains special provisions for protection of the marine environment. However, our understanding of the complexity of the biosphere and the climate-ocean nexus, as well as humanity's collective ocean literacy, has evolved. This has raised awareness of important governance gaps concerning the protection of marine biodiversity particularly in areas beyond national jurisdiction (e.g., Druel and Gjerde, 2014; Warner, 2014). In 2017 the UN General Assembly established an Intergovernmental Conference to negotiate an International Legally Binding Instrument under UNCLOS on the conservation and sustainable use of marine biological diversity of areas beyond national jurisdiction (BBNJ) (General Assembly resolution 72/249). Negotiations are ongoing but the latest draft text of an agreement includes a short General objective in Article 2 stating that "The objective of this Agreement is to ensure the [long-term] conservation and sustainable use of marine biological diversity of areas beyond national jurisdiction through effective implementation of the relevant provisions of the Convention and further international cooperation and coordination." (UNGA, 2019).

Our contention is that this negotiation, and an expansion of the draft General objective specifically, is a golden opportunity to articulate a global ecosystem-based ocean vision, to guide any and all human activities in the ocean, as the common denominator for future policies, strategies, plans (including those resulting from marine spatial planning (MSP), programmes and projects, involving maritime activities. It would enhance their mutual coherence, framing the 'new narrative for the ocean' that the ocean is 'too big to ignore', called for by Lubchenko and Gaines (2019), and establishing the foundation for future ocean stewardship ensuring sustainable active management of the ocean ecosystem to promote multi-generational human wellbeing, as proposed by Rockström and co-authors (2021).

PROPOSED TENETS OF AN ECOSYSTEM-BASED GLOBAL OCEAN VISION

A global ocean vision will be a picture of a desired future ocean (Lukic et al., 2018; Stuchtey et al., 2020): an image of what the marine environment should look like to be able to deliver to humanity the ecosystem services it relies on in a predefined but dilated timeline. Given that such a holistic and overarching future vision for the ocean must be capable of underpinning any and all relevant future global policies, plans and programmes, it must integrate key considerations such as global ecosystem scale, dilated time scale, a rapidly changing environment, globally agreed principles, and 'strategicness':

- global ecosystem scale (not always captured by framework conventions or lines on maps): this vision must assume an ocean basin scale as the only appropriate scale able to cover/integrate global ocean ecosystem level information (such as ecological connectivity (Harrison et al., 2018)) and all ocean uses and governance scales (jurisdictions), ranging from that of small local MPAs to national marine spaces, to regional seas and all the way through to ocean basins integrating areas beyond national jurisdiction (ABNJ), including the high-seas and the subjacent seafloor, a.k.a., the Area. Global ecosystem scale is in fact the one at which phenomena such as major ocean migrations or the global ocean circulation that cross the whole range of existing jurisdictions and corresponding borders can be understood and sustainably managed;

- dilated time scales: time scales at stake also span a wide range, from seasonal or yearly licensing of fisheries quotas through multidecadal concessions for exploitation of non-living marine resources or the installation of fixed infrastructures, e.g., for renewable energies production (e.g., Ferreira & Andrade, 2021). For these reasons, a useful vision must be able to see beyond multiple decades (and correspondingly encompass a transgenerational horizon);

- rapidly changing environment/shifting baselines in the Anthropocene: a useful future global ocean vision must integrate current planetary ocean-climate and marine biodiversity trends (IPBES, 2019; IPCC, 2019b; Sweetman et al., 2017; Steneck and Pauly, 2019; Paulus, 2021) to be able to provide a realistic backdrop to the visioning process;

- globally agreed-principles: such as the so called 'modern conservation principles', which include the ecosystem approach and the precautionary approach, integrated and adaptive management, use of best available scientific information and application of best practices and technologies, stakeholder consultation, etc. (Gjerde et al., 2008)[1]. This is consistent with the call for a precautionary approach enshrined in many international instruments [e.g., ITLOS Advisory opinion in para. 131-135 (ITLOS, 2011) and UN Fish Stocks Agreement Art. 6 (UNGA, 1995)];

- 'strategicness': refers to a holistic, anticipatory, prospective, all-encompassing integrative approach/framework to address the planning and management of these global environmental challenges, and to assess the effectiveness of the measures adopted (Stoeglehner, 2020). Such a strategic approach must be capable of guiding all vested interests towards a sustainable ocean economy; setting a general direction towards robust ocean health; building and promoting a culture of sustainability; serving both the short- and the long-term interests which will likely cover decadal time spans; and achieving delivery of lasting wellbeing.

[1] *Included in Article 5 of the draft BBNJ Agreement.*

DISCUSSION - BUILDING THE ECOSYSTEM-BASED GLOBAL OCEAN VISION UNDER BBNJ - A KEY ROLE FOR SEA

Strategic Environmental Assessment (SEA), "a process to facilitate strategic decisions toward sustainability" (Noble and Nwanekezie, 2017), is an approach for future visions development and evaluation, and has been considered the best option for the delivery of lasting wellbeing, building a culture of sustainability, and serving the long and the short-term interest (Gibson et al., 2016). It has been mooted as a "modern conservation tool", together with other instruments, alongside MSP or networks of representative MPAs, that apply to human activities or to their effects in the ocean (Gjerde et al., 2008). We argue below how an SEA approach could inform the BBNJ Agreement, specifically its General objective text.

Potential of SEA in BBNJ: From EIA-Based to Strategy-Based

SEA is still predominantly applied as an Environmental Impact Assessment (EIA)-based approach to the identification and evaluation of the environmental consequences of policies, plans or programmes[2] (PPP), differing from the traditional EIA of projects (see Glasson and Therivel, 2019) [3] mainly in terms of its scope (Noble & Nwanekezie, 2017). Under this understanding SEA is commonly used as a post-evaluation procedure whose main aim is to ensure the formal consistency of the high-level management instrument it applies to with environmental requirements (*ibid*.) (**Figure 1**). As such, although it may contribute to "greening" such instruments (CEC, 2009, 10), it is often seen as a 'necessary evil' to be hurdled to enable economic endeavours or "a simple procedural box-ticking requirement" (EC, 2017, 10). Even where efforts are being made to introduce SEA at the earliest stages of planning processes (see European MSP Platform, 2021; UNESCO-IOC/European Commission, 2021), its role is still limited to addressing "the environmental impacts of regional planning and sectoral plans as well as planning alternatives" (ibid., 113). In this 'EIA-based' application of SEA, as a process used to review predefined proposals after key strategic decisions have been taken, SEA has value but its contribution to the decision-making process is effectively limited and relevant opportunities are lost (Gibson et al., 2016). This EIA-based SEA is the model adopted by the Convention on Biological Diversity [see COP 6 Decision VI/7 (CBD, 2002)] and is the sense in which it is included in the current draft of the International Legally Binding Instrument (ILBI) on BBNJ [see articles 28 and 42 (UNGA, 2019)].

Conversely, adoption of SEA as a strategy-based[4] or proactive approach opens up for new opportunities, able to reconcile multiple ambitions and perspectives. With such an approach SEA becomes a process for driving the decision-making process and institutional change. Use of strategy-based SEA has been advocated in the context of the Convention for Biodiversity Sustainable Ocean Initiative (CBD/SOI, n.d.) and within the BBNJ agreement/negotiations, to promote cooperation and conservation (e.g., Doelle & Sander, 2020; Hassanali and Mahon, 2022; WWF, 2019; Hills, 2020). WWF (2019) suggested that States should be required to conduct a 'collective' SEA, which would act as a warrant of environmental oversight and as an "exercise in 'enhanced cooperation'", and Hill (2020, p. 27), reporting on the results of a 2020 EC workshop on EIAs and SEAs in ABNJ, noted 'the need to harmonise processes to create a cooperative and integrated approach'. Doelle & Sander (2020) listed the basic building blocks of next generation environmental assessments (including SEA) that need to be in place under Hassanali and Mahon (2022) detailed the components of a proactive process for conservation of BBNJ with an SEA track informing subsequent region-specific policies and plans (including MSP).

An obligation for States to undertake SEA of "plans and programmes relating to activities" is currently given a place holder (Article 28) in the revised draft text of the BBNJ Implementing Agreement (A/CONF.232/2020/3) (UN, 2020). This was considered at the fourth substantive session (IGC4) of the Intergovernmental Conference held from 7-18 March 2022. During IGC4 there was no consensus on SEA with mixed opinions regarding its application and some States continuing to promote voluntary application. However, this interpretation relates to instruments meeting set criteria (yet to be agreed), albeit supporting the use of SEA to address cumulative pressures, instead of addressing/pursuing an overarching holistic future vision.

Employing a Strategy-Based SEA to Reach a Global Ocean Vision Within BBNJ

We specifically argue that a strategy-based SEA could inform the BBNJ Agreement General objective text, framing the development of an ecosystem-based global ocean vision that can guide and support the development of any subsequent (related) instruments and of their corresponding assessments (**Figure 2**). Expanding text in Part I General Provisions of the draft BBNJ Agreement – for example in Article 2 General Objective, or in a new Article 2 *bis*, or strengthening Article 5 (General principles and approaches) – could, in succinct terms, incorporate a vision resulting from a strategy-based SEA approach. Contributions to a virtual dialogue convened from 29-31 March 2022 (i.e., shortly after IGC4) by the STRONG High Seas Project[5] underlined the benefits of a

[2] *In EU member-states, under Directive 2001/42/EC, SEA only applies to plans and programmes.*

[3] *'EIA is a process, a systematic process that examines the environmental consequences of development actions, in advance.' (Glasson and Therivel, 2019).*

[4] *For an in-depth discussion of the gradient from less to more strategic aspects that SEA can assume, see Noble and Nwanekezie, 2017.*

[5] *https://www.prog-ocean.org/our-work/strong-high-seas/.*

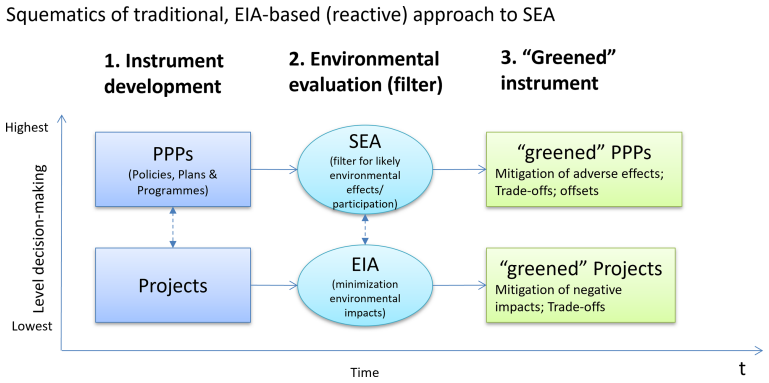

FIGURE 1 | Traditional, EIA-based (reactive) approach to SEA, where SEA is at best a greening mechanism of a corresponding high-level management instrument. indicates potential connections.

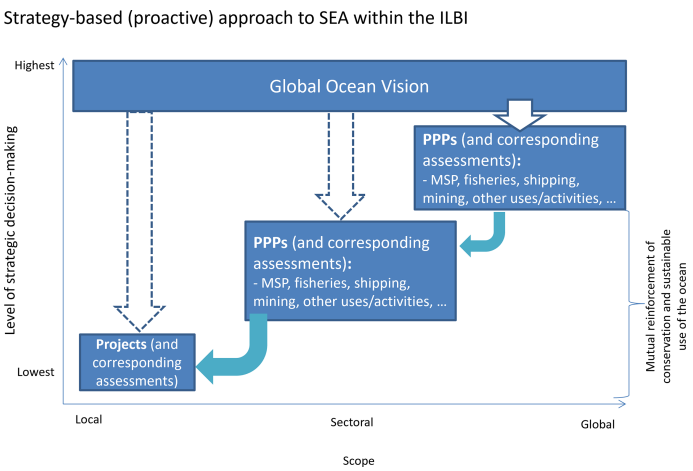

FIGURE 2 | Proactive strategy-based SEA positioning within the ILBI.

common goal or purpose; an overarching set of principles, and more explicit State obligations to cooperate.

Building, agreeing and ratifying such an all-encompassing global ocean vision is a complex task, with multiple and interlinking layers. To use a theatrical analogy, some key elements need to be considered:

- Selling the concept: understanding and incorporating the tenets described above as the backdrop (scenario) for developing the vision;

- Writing the script: a clear, simple, synthetic, consensual message that can be used to guide action (the vision);

- Casting: carefully identifying the full range of actors that need to be won over and involved, across all geographic scales and sectors of society. This translates into a major challenge in view of the diversity of interests and of stakeholders at play: from states, to regional bodies and to international organisations; from individuals to NGOs, business companies, investors;

- Setting the scenario: ensuring incorporation of the strongly stated pre-condition of the BBNJ negotiation that it should 'not undermine existing relevant legal instruments and frameworks and relevant global, regional and sectoral bodies' (UN, 2019) (see below);

- Connecting with the audience (society and its various elements) and its needs: well-being, health, prosperity,… and scope, from humankind (for the High Seas or the Area) to the individual (e.g., a fisherman).

Various methods could be used to operationalise this proposal. A conceptual flexible framework for SEA has been laid out by Partidário (2012), with a set of key structural elements to be combined in the best adapted way, including the identification of internal and external driving forces, either drivers of change or inhibitors; establishing priority/determinant environmental and sustainability issues; identifying government and non-governmental organizations and institutions; and establishing a network of relevant stakeholders. Base information to underpin such an SEA process is now increasingly available as a result of comprehensive, basin scale research (Cf. **Supplementary Material**: North Atlantic case study). Also, an emerging scenario building methodological framework that could be employed to

TABLE 1 | Examples of existing Ocean Visions.

Source	Vision
Ocean Panel, n.d.	A Vision of Protection, Production and Prosperity: In a sustainable ocean economy, effective protection, sustainable production and equitable prosperity go hand in hand to create a triple win for people, nature and the economy.
Gobierno de Chili, 2021	"In search of a healthy ocean as an object of its protection and conservation; benefactor in its economic and social dimension; safe for the different activities that take place within it; formative to strengthen its quality of natural laboratory and of academic development; inspiring as a national cultural heritage; and predictable in terms of the phenomena that affect it, both natural and anthropogenic" (our translation from Spanish original)
Republic of Fiji, (2020)	"A healthy Ocean that sustains the livelihoods and aspirations of current and future generations of Fiji."
New Zealand Government (2021)	Ensuring the long-term health and resilience of ocean and coastal ecosystems, including the role of fisheries.
Governo de Portugal, (2021)	Promoting healthy ocean in order to maximize sustainable blue development and the well-being of Portuguese people, setting Portugal as a leader in science-based ocean governance.
DEFRA, (2019)	Clean, healthy, safe, productive and biologically diverse ocean and seas

establish this type of forward-looking vision is the Nature Futures Framework Approach (NFF), which shifts the traditional scenario building focus from exploring impacts of society on nature, to nature-centred visions and pathways (Pereira et al., 2020).

A major role should be attributed to participatory approaches in strategic contexts to contribute to the new consistent narrative underlying construction of the global ocean vision. Abundant guidance is available on participatory processes and stakeholder involvement[6]. In the context of on-going negotiations, this could be coordinated by any new BBNJ Scientific and Technical Body perhaps as an Annex to the Agreement.

Inspiration could be drawn from The Protocol on Environmental Protection to the Antarctic Treaty[7]. The Protocol is a significant, high ambition and long-standing binding instrument[8]. Article 3 of the Protocol covers Environmental Principles relating to human activities. In effect, this Article takes an SEA stance: prioritizing protection, placing limitations on activities that could cause adverse impacts, insisting on informed decision-making and risk assessment, and establishing monitoring obligations. Articles 4, 5 and 6 cover context (i.e., relationship with other components of the Antarctic Treaty System), consistency with other components (of the Antarctic Treaty System) and Co-operation.

Opportunity and Timeliness

IGC4 did not conclude negotiations, with States requesting a fifth negotiating session. Following IGC4, Article 2 of the draft BBNJ Agreement remains unchanged although many delegations called for streamlining text on international cooperation and Treaty. Recognition of the 'not undermining principle'[9]. This is further reflected in language pertaining to international cooperation and coordination of Area-Based Management Tools stressing the need to recognise their coherence and complementarity. Several commentators have also reflected on implications of this principle for institutional arrangements of the new Agreement (e.g., Clark, 2020; Berry, 2021) and global cooperation (Friedman, 2019). Considerable discussion was devoted to cross-cutting issues such as the remit of the Conference of the Parties (COP) and subsidiary bodies that the COP could establish.

An 'environment for well-being' approach (Ntona and Morgera, 2018) enshrined in a globally shared normative framework would reflect high-level commitments made in a range of international policy processes (Pretlove and Blasiak, 2018). Such an approach would explicitly align a BBNJ instrument with the 2030 Sustainable Development Agenda and SDG 14 (UNGA, 2015) while maintaining consistency with the Convention on Biological Diversity (Article 5) and the United Nations Fish Stocks Agreement and the mandate of Regional Fisheries Management Organizations.

Our proposal has strong synergy with the 'New Action Agenda' of the Ocean Panel that seeks a vision for protection, production and prosperity in national waters[10], and complements national visions, such as those published by Chili, Fiji, New Zealand, Portugal and the UK (**Table 1**) (Gobierno de Chili, 2021; DEFRA, 2019; Republic of Fiji, 2020; Governo de Portugal, 2021; New Zealand Government, 2021). The One Ocean Summit (9-11 February 2022, in Brest, France) highlighted multiple non-coherent talks taking place in different sectoral initiatives and called for simpler

[6] *e.g., CBD SOI training modules (https://www.cbd.int/soi/training/soi-training-modules).*
[7] *https://www.ats.aq/e/protocol.html.*
[8] *Until 2048 the Protocol can only be modified by unanimous agreement of all Consultative Parties to the Antarctic Treaty*

9The 'not undermining' principle is a key issue and relates to achieving a harmonious coexistence between the BBNJ Agreement and existing instruments. Article 4, para 3 (as currently drafted) affirms that the ILBI: "…does not undermine existing relevant legal instruments and frameworks and relevant global, regional and sectoral bodies".
[10] *The High-Level Panel for a Sustainable Ocean Economy (The Ocean Panel), co-chaired by Norway and Palau, have set out a vision for how to build a sustainable ocean economy (https://www.oceanpanel.org/).*

governance to involve civil society and preserve global commons, a notion that has synergy with an overall global ocean vision.

A global ocean vision as envisaged here is timely as 2022 marks the 40th anniversary of UNCLOS, the legal framework that, to date, has successfully provided the foundation for cooperation and consistency in terms of global multilateralism for all marine and maritime activities[11]. A fifth session of the IGC of BBNJ is tentatively scheduled for August 2022 at which it is hoped that the implementing agreement will be concluded, so this critical negotiation can provide a final chance to implement the suggestion we are promoting here.

DATA AVAILABILITY STATEMENT

The original contributions presented in the study are included in the article/**Supplementary Material**. Further inquiries can be directed to the corresponding author.

AUTHOR CONTRIBUTIONS

All authors listed have made a substantial, direct, and intellectual contribution to the work and approved it for publication.

[11] This stance is consistent with Arvid Pardo's inspiration in the 1960s to look at the ocean's problems as a whole (UNGA, 1967; UN, 1999), that represented the underlying rationale of UNCLOS, whose preamble acknowledges that 'the problems of ocean space are closely interrelated and need to be considered as a whole'.

FUNDING

DEJ is funded by the Global Ocean Biodiversity Initiative (GOBI). GOBI is supported by the International Climate Initiative (IKI). The German Federal Ministry for the Environment, Nature Conservation and Nuclear Safety (BMU) supports this initiative on the basis of a decision adopted by the German Bundestag.

ACKNOWLDGMENTS

With grateful thanks to Phil Weaver for his contribution on the International Seabed Authority's Regional Environmental Management Plan for the Mid Atlantic Ridge in the Atlantic case study (see **Supplementary Material**). The authors are grateful to the anonymous reviewers for their constructive comments which prompted a radical revision of the manuscript and greatly improved its coherence.

SUPPLEMENTARY MATERIAL

The Supplementary Material for this article can be found online at: https://www.frontiersin.org/articles/10.3389/fmars.2022.878077/full#supplementary-material

REFERENCES

Berry, D. S. (2021). Unity or Fragmentation in the Deep Blue: Choices in Institutional Design for Marine Biological Diversity in ABNJ. *Front. Mar. Sci.* 8. doi: 10.3389/fmars.2021.761552

Boschen-Rose, R. E., Ferreira, M. A., Johnson, D. E. and Gianni, M. (2020). "Engaging With Industry to Spur Blue Growth," in *Proceedings From the International Coastal Symposium (ICS) 2020 (Seville, Spain*. Eds. Malvárez, G. and Navas, F. (Coconut Creek (Florida: Journal of Coastal Research). ISSN 0749-0208.

CBD/SOI *Strategic Environmental Assessment: A Strategic Thinking Framework for Achieving Sustainable Development*. Available at: https://www.cbd.int/marine/soi/soi-training-modules/SOI-SEA_Training-Guide-en.pdf.

CBD (2002) *COP6 Decision VI/7. Identification, Monitoring, Indicators and Assessments*. Available at: https://www.cbd.int/decision/cop/?id=7181.

CEC (2009). *Final Report From the Commission to the Council, the European Parliament, the European Economic and Social Committee and the Committee of the Regions on the Application and Effectiveness of the Directive on Strategic Environmental Assessment*, Directive 2001/42/EC). COM(2009) 469.

Clark, N. A. (2020). Institutional Arrangements for the New BBNJ Agreement: Moving Beyond Global, Regional and Hybrid. *Mar. Policy* 122, 104143. doi: 10.1016/j.marpol.2020.104143

DEFRA (2019) *Marine Strategy Part One: UK Updated Assessment and Good Environmental Status*. Available at: https://assets.publishing.service.gov.uk/government/uploads/system/uploads/attachment_data/file/921262/marine-strategy-part1-october19.pdf.

Doelle, M. and Sander, G. (2020). Next Generation Environmental Assessment in the Emerging High Seas Regime? An Evaluation of the State of the Negotiations. *Int. J. Mar. Coast. Law* 35, 498–532. doi: 10.1163/15718085-BJA10022

Druel, E. and Gjerde, K. (2014). Sustaining Marine Life Beyond Boundaries: Options for an Implementing Agreement for Marine Biodiversity Beyond National Jurisdiction Under the United Nations Convention on the Law of the Sea. *Mar. Policy* 49, 90–97. doi: 10.1016/j.marpol.2013.11.023

EC (2017). *COM, (2017) 234 Final REPORT FROM THE COMMISSION TO THE COUNCIL AND THE EUROPEAN PARLIAMENT Under Article 12(3) of Directive 2001/42/EC on the Assessment of the Effects of Certain Plans and Programmes on the Environment. Brussels: European Commission.*

European MSP Platform (2021) *Strategic Environmental Assessment (SEA)*. Available at: https://www.msp-platform.eu/faq/strategic-environmental-assessment-sea.

Ferreira, M. A. and Andrade, F. (2021). "A Protecção do Mar E O Ordenamento do Espaço Marítimo," in *Ministério do Mar 2021. Proteger O Mar. IPMA, I.P*, 200 pp. Available at: https://www.ipma.pt/resources.www/docs/publicacoes.site/Proteger-O-Mar-Eletronico.pdf, ISBN: ISBN: 978-972-9083-24-2. Lisboa, IPMA - Instituto Português do Mar e da Atmosfera, I.P.

Friedman, A. (2019). Beyond "Not Undermining": Possibilities for Global Cooperation to Improve Environmental Protection in Areas Beyond National Jurisdiction. *ICES J. Mar. Sci.* 76 (2), 452–456. doi: 10.1093/icesjms/fsy192

Gibson, R. B., Doelle, M. and Sinclair, A. J. (2016). Fulfilling the Promise: Basic Components of Next Generation Environmental Assessment. *J. Environ. Law Pract*. 29, 251-276.

Gjerde, K. M., et al. (2008). *Options for Addressing Regulatory and Governance Gaps in the International Regime for the Conservation and Sustainable Use of Marine Biodiversity in Areas Beyond National Jurisdiction* (IUCN, Gland, Switzerland), + 20.

Glasson, J. and Therivel, R. (2019). *Introduction to Environmental Impact Assessment (5th Edition)* (Routledge), 394 pages. Oxon and New York

Gobierno de Chili (2021) *Política Oceánica Nacional De Chile*. Available https://www.acanav.cl/wp-content/uploads/2021/07/poli__tica_ocea__nica_nacional_de_chile_ok-1.pdf

Governo de Portugal (2021) *National Ocean Strategy 2021-2030*. Available at: https://www.dgpm.mm.gov.pt/_files/ugd/eb00d2_066d6252d6f84342aa34d8f9f301ae32.pdf.

Harrison, A.-L., Costa, D.P., Winship, A.J., Benson, S.R., Bograd, S.J., Antolos, M., et al. (2018). The Political Biogeography of Migratory Marine Predators. *Nat. Ecol. Evol.* 2, 1571–1578. doi: 10.1038/s41559-018-0646-8

Hassanali, K. and Mahon, R. (2022). Encouraging Proactive Governance of Marine Biological Diversity of Areas Beyond National Jurisdiction Through

Strategic Environmental Assessment (SEA). *Mar. Policy* 136, 104932. doi: 10.1016/j.marpol.2021.104932

Hills, J. M. (2020). *Report of the Workshop "Environmental Impact Assessments and Strategic Environmental Assessments in Areas Beyond National Jurisdiction"* (Brussels, Belgium: European Commission). 28-29 January 2020.

IOC-UNESCO (2022). *Multiple Ocean Stressors: A Scientific Summary for Policy Makers*. Ed. Boyd, P. W. (Paris, UNESCO: IOC Information Series, 1404), 20 pp. doi: 10.25607/OBP-1724

IPBES (2019). *Summary for Policymakers of the Global Assessment Report on Biodiversity and Ecosystem Services of the Intergovernmental Science-Policy Platform on Biodiversity and Ecosystem Services*. Eds. Díaz, S., Settele, J., E. S. Brondízio, E. S., Ngo, H. T., Guèze, M., Agard, J., Arneth, A., Balvanera, P., Brauman, K. A., Butchart, S. H. M., Chan, K. M. A., Garibaldi, L. A., Ichii, K., Liu, J., Subramanian, S. M., Midgley, G. F., Miloslavich, P., Molnár, Z., Obura, D., Pfaff, A., Polasky, S., Purvis, A., Razzaque, J., Reyers, B., Chowdhury, R.R., Shin, Y. J., Visseren-Hamakers, I. J., Willis, K. J. and Zayas, C. N., 56 pages, IPBES secretariat, Bonn, Germany.

IPCC (2019a). Annex I: Glossary [Weyer, N.M. (ed.)]. In: IPCC Special Report on the Ocean and Cryosphere in a Changing Climate [H.-O. Pörtner, D.C. Roberts, V. Masson-Delmotte, P. Zhai, M. Tignor, E. Poloczanska, K. Mintenbeck, A. Alegría, M.Nicolai, A. Okem, J. Petzold, B. Rama, N.M. Weyer (eds.)]. Cambridge University Press, Cambridge, UK and New York, NY,USA, pp. 677 -702. https://doi.org/10.1017/9781009157964.010.

IPCC (2019b). Summary for Policymakers. In: IPCC Special Report on the Ocean and Cryosphere in a Changing Climate[H.-O. Pörtner, D.C. Roberts, V. Masson-Delmotte, P. Zhai, M. Tignor, E. Poloczanska, K. Mintenbeck, A. Alegría, M. Nicolai, A. Okem, J. Petzold, B. Rama, N.M. Weyer (eds.)]. Cambridge University Press, Cambridge, UK andNew York, NY, USA, pp. 3 -35. https://doi.org/10.1017/9781009157964.001

ITLOS (2011). *Responsibilities and Obligations of States Sponsoring Persons and Entities With Respect to Activities in the Area, Advisory Opinion, 1 February 2011*. Hamburg, Germany: International Tribunal for the Law of the Sea. p.10.

Johnson, D. E., Barrio-Frojan, C., Bax, N., Dunstan, P., Woolley, S., Halpin, P., et al. (2018a). The Global Ocean Biodiversity Initiative: Promoting Scientific Support for Global Ocean Governance. *Aquat. Conserv. Special Issue*. 29(S2): 162–169. doi: 10.1002/aqc.3024

Johnson, D., Ferreira, M. A. and Kenchington, E. (2019). Climate Change is Likely to Severely Limit the Effectiveness of Deep-Sea ABMTs in the North Atlantic. *Mar. Policy* 87, 111/122. doi: 10.1016/j.marpol.2017.09.034

Levin, L. A. and Le Bris, N. (2015). Deep Oceans Under Climate Change. *Science* 350, 766–768. doi: 10.1126/science.aad0126

Lubchenko, J. and Gaines, S. (2019). A New Narrative for the Ocean. *Science* 364, 6444. doi: 10.1126/science.aay2241

Lukic, I., Schultz-Zehden, A. and de Grunt, L. S. (2018). "Handbook for Developing Visions in MSP," in *Technical Study Under the Assistance Mechanism for the Implementation of Maritime Spatial Planning*. Brussels: European Commission.

New Zealand Government (2021) *Government Adopts Oceans Vision. 26 June 2021*. Available at: https://www.beehive.govt.nz/release/government-adopts-oceans-vision.

Noble, B. and Nwanekezie, K. (2017). Conceptualizing Strategic Environmental Assessment: Principles, Approaches and Research Directions. *Environ. Impact Assess. Rev*. 61: 165-173. doi: 10.1016/j.eiar.2016.03.005

Ntona, M. and Morgera, E. (2018). Connecting SDG14 With Other SDGs Through Marine Spatial Planning. *Mar. Policy* 93, 214–222. doi: 10.1016/j.marpol.2017.06.020

Ocean Panel, n.d. A Vision of Protection, Production and Prosperity. Available at https://www.oceanpanel.org/. Accessed 22.06.2022

Pacific Regional Ocean Policies (2017) *Our Sea of Islands Our Livelihoods Our Oceania*. Available at: http://www.forumsec.org/wp-content/uploads/2018/03/Overview-of-Pacific-Islands-Forum-Ocean-Policies-2017.pdf.

Partidário, M. R. (2012). *Strategic Environmental Assessment Better Practice Guide - Methodological Guidance for Strategic Thinking in SEA* (Lisboa: Agência Portuguesa do Ambiente e Redes Energéticas Nacionais).

Paulus, E. (2021). Shedding Light on Deep-Sea Biodiversity—A Highly Vulnerable Habitat in the Face of Anthropogenic Change. *Front. Mar. Sci.* 8. doi: 10.3389/fmars.2021.667048

Pretlove, B. and Blasiak, R. (2018) *Mapping Ocean Governance and Regulation. Working Paper for Consultation for UN Global Compact Action Platform for Sustainable Ocean Business*. Available at: https://www.unglobalcompact.org/library/5710.

Pereira, L.M., Davies, K.K., den Belder, E., Ferrier, S., Karlsson-Vinkhuyzen, S., Kim, H., et al. 2020. Developing Multiscale and Integrative Nature–Peoplescenarios Using the Nature Futures Framework. *People Nat*. 2, 1172–1195. doi: 10.1002/pan3.10146.

Republic of Fiji (2020) *National Ocean Policy. To Secure and Sustainably Manage All of Fiji's Ocean and Marine Resources*. Available at: https://drive.google.com/file/d/1w7skJdv7PvZ0cUYfZxKSanMLQDEA3Sip/view.

Rockström, J., Beringer, T., Griscom, B., Mascia, M. B., Folke, C. and Creutzig, F. (2021). Opinion: We Need Biosphere Stewardship That Protects Carbon Sinks and Builds Resilience. *Proc. Natl. Acad. Sci. Sep 2021* 118 (38), e2115218118. doi: 10.1073/pnas.2115218118

Rockström, J., Steffen, W., Noone, K., Persson, A., Chapin, F. S., Lambin, E. F., et al. (2009). A Safe Operating Space for Humanity. *Nature* 461, 472–475. doi: 10.1038/461472a

SCBD (2020). *Global Biodiversity Outlook 5* (Montreal : Secretariat of the Convention on Biological Diversity). Available at: www.cbd.int/GBO5.

Steffen, W., Broadgate, W., Deutsch, L., Gaffney, O. and Ludwig, C. (2015). The Trajectory of the Anthropocene: The Great Acceleration. *Anthropocene Rev.* 2 (1), 81–98. doi: 10.1177/2053019614564785

Steneck, R. and Pauly, D. (2019). Fishing Through the Anthropocene. *Curr. Biol.* 29, R942–R995. doi: 10.1016/j.cub.2019.07.081

Stoeglehner, G. (2020). Strategicness – the Core Issue of Environmental Planning and Assessment of the 21st Century. *Impact Assess. Project Appraisal* 38 (2), 141–145. doi: 10.1080/14615517.2019.1678969

Stuchtey, M. R., Vincent, A., Merkl, A., Bucher, M., Haugan, P.M., Lubchenco, J., et al. (2020). *Ocean Solutions That Benefit People, Nature and the Economy* (Washington, DC: World Resources Institute). Available at: www.oceanpanel.org/ocean-solutions.

Sweetman, A. K., Thurber, A. R., Smith, C. R., Levin, L. A., Mora, C., Wei, C.-L., et al.(2017). Major Impacts of Climate Change on Deep-Sea Benthic Ecosystems. *Elementa: Sci. Anthropocene* (2017)5, 4. doi: 10.1525/elementia.203

UN (1982) *United Nations Convention on the Law of the Sea*. Available at: https://www.un.org/depts/los/convention_agreements/texts/unclos/unclos_e.pdf.

UN (1999). *DR. ARVID PARDO, 'Father OF LAW OF SEA Conference'DIES AT 85, IN HOUSTON* (TEXAS: Press Release SEA/1619). Available at: https://www.un.org/press/en/1999/19990716.SEA1619.html.

UN (2019) *Revised Draft Text of an Agreement Under the United Nations Convention on the Law of the Sea on the Conservation and Sustainable Use of Marine Biological Diversity of Areas Beyond National Jurisdiction*. United Nations, New York. Available at: https://www.un.org/bbnj/sites/www.un.org.bbnj/files/revised_draft_text_a.conf_.232.2020.11_advance_unedited_version.pdf.

UN (2020). *Textual Proposals Submitted by Delegations by 20 February 2020, for Consideration at the Fourth Session of the Intergovernmental Conference on an International Legally Binding Instrument Under the United Nations Convention on the Law of the Sea on the Conservation and Sustainable Use of Marine Biological Diversity of Areas Beyond National Jurisdiction (the Conference), in Response to the Invitation by the President of the Conference in Her Note of 18 November 2019*, (A/CONF.232/2020/3).

UN (2021). *The Second World Ocean Assessment* Vol. 2 (New York), ISBN: ISBN: 978-92-1-1-130422-0.

UNESCO-IOC/European Commission (2021). *MSPglobal International Guide on Marine/Maritime Spatial Planning* (Paris: UNESCO). IOC Manuals and Guides no.89.

UNGA (1967). *Official Records of the United Nations General Assembly Twenty-Second Meeting. First Committee 1515th Meeting, 1 November 1967* (New York : United Nations General Assembly). Available at: https://www.un.org/depts/los/convention_agreements/texts/pardo_ga1967.pdf.

UNGA (1995). *Agreement for the Implementation of the Provisions of the United Nations Convention on the Law of the Sea of 10 December 1982 Relating to the Conservation and Management of Straddling Fish Stocks and Highly Migratory Fish Stocks*, United Nations, New York A/CONF.164/37.

UNGA (2015). *70/1. Transforming Our World: The 2030 Agenda for Sustainable Development. Resolution Adopted by the General Assembly on 25 September 2015*, A/RES/70/1.

UNGA (2019) *Revised Draft Text of an Agreement Under the United Nations Convention on the Law of the Sea on the Conservation and Sustainable Use of*

Marine Biological Diversity of Areas Beyond National Jurisdiction. Available at: https://undocs.org/en/a/conf.232/2020/3.

UNGA (2021). *Singapore Draft Decision: Intergovernmental Conference on an International Legally Binding Instrument Under the United Nations Convention on the Law of the Sea on the Conservation and Sustainable Use of Marine Biological Diversity of Areas Beyond National Jurisdiction*, A/75/L.96. 9 June 2021.

United Nations Environment Programme (2021). *Making Peace With Nature: A Scientific Blueprint to Tackle the Climate, Biodiversity and Pollution Emergencies. Nairobi: United Nations Rnvironment Programme*

Warner, R. M. (2014). Conserving Marine Biodiversity in Areas Beyond National Jurisdiction: Co-Evolution and Interaction With the Law of the Sea. *Front. Mar. Sci.* 1 doi: 10.3389/fmars.2014.00006

WWF (2019) *Strategic Environmental Assessments in the Context of the BBNJ ILBI. A Webinar for Delegates Produced by WWF, With the Collaboration of the UK Government, the Government of Sweden, the University of Waterloo and the University of Lisbon. July 2019*. Available at: https://wwf.zoom.us/recording/play/m6w1wFMND5TPHjc3HNiYQ-KWfvUp9omR3mssYJdzRZzmnaK7nLqy1JGzk93lkExk?continueMode=true.

Conflict of Interest: Author DeJ is employed by the company Seascape Consultants, Ltd. The remaining authors declare that the research was conducted in the absence of any commercial or financial relationships that could be construed as a potential conflict of interest.

The handling Editor JMR declared a past collaboration with the author DEJ.

frontiers | Frontiers in Marine Science

TYPE Methods
PUBLISHED 15 August 2022
DOI 10.3389/fmars.2022.936095

OPEN ACCESS

EDITED BY
Albertus J. Smit,
University of the Western Cape,
South Africa

REVIEWED BY
Lissette Victorero,
Norwegian Institute for Water Research (NIVA), Norway
Fabian J. Tapia,
University of Concepcion, Chile

*CORRESPONDENCE
Mia Schumacher
mschumacher@geomar.de

SPECIALTY SECTION
This article was submitted to Deep-Sea Environments and Ecology, a section of the journal Frontiers in Marine Science

RECEIVED 04 May 2022
ACCEPTED 08 July 2022
PUBLISHED 15 August 2022

CITATION
Schumacher M, Huvenne VAI, Devey CW, Arbizu PM, Biastoch A and Meinecke S (2022) The Atlantic Ocean landscape: A basin-wide cluster analysis of the Atlantic near seafloor environment.
Front. Mar. Sci. 9:936095.
doi: 10.3389/fmars.2022.936095

The Atlantic Ocean landscape: A basin-wide cluster analysis of the Atlantic near seafloor environment

Mia Schumacher[1]*, Veerle A. I. Huvenne[2], Colin W. Devey[1,3], Pedro Martínez Arbizu[4], Arne Biastoch[1,3] and Stefan Meinecke[5]

[1]GEOMAR Helmholtz Centre for Ocean Research Kiel, Kiel, Germany, [2]National Oceanography Centre, Southampton, United Kingdom, [3]Kiel University, Kiel, Germany, [4]Senckenberg am Meer, German Center for Marine Biodiversity Research (DZMB), Wilhelmshaven, Germany, [5]Research Vessel, Sonne, Briese Research, Briese Schiffahrts GmbH & Co KG, Leer, Germany

Landscape maps based on multivariate cluster analyses provide an objective and comprehensive view on the (marine) environment. They can hence support decision making regarding sustainable ocean resource handling and protection schemes. Across a large number of scales, input parameters and classification methods, numerous studies categorize the ocean into seascapes, hydro-morphological provinces or clusters. Many of them are regional, however, while only a few are on a basin scale. This study presents an automated cluster analysis of the entire Atlantic seafloor environment, based on eight global datasets and their derivatives: Bathymetry, slope, terrain ruggedness index, topographic position index, sediment thickness, POC flux, salinity, dissolved oxygen, temperature, current velocity, and phytoplankton abundance in surface waters along with seasonal variabilities. As a result, we obtained nine seabed areas (SBAs) that portray the Atlantic seafloor. Some SBAs have a clear geological and geomorphological nature, while others are defined by a mixture of terrain and water body characteristics. The majority of the SBAs, especially those covering the deep ocean areas, are coherent and show little seasonal and hydrographic variation, whereas other, nearshore SBAs, are smaller sized and dominated by high seasonal changes. To demonstrate the potential use of the marine landscape map for marine spatial planning purposes, we mapped out local SBA diversity using the patch richness index developed in landscape ecology. It identifies areas of high landscape diversity, and is a practical way of defining potential areas of interest, e.g. for designation as protected areas, or for further research. Clustering probabilities are highest (100%) in the center of SBA patches and decrease towards the edges (< 98%). On the SBA point cloud which was reduced for probabilities <98%, we ran a diversity analysis to identify and highlight regions that have a high number of different SBAs per area, indicating the use of such analyses to automatically find

potentially delicate areas. We found that some of the highlights are already within existing EBSAs, but the majority is yet unexplored.

KEYWORDS

marine landscape, unsupervised learning, machine learning (ML), multivariate analysis, biogeographic provinces, marine protection, marine habitat connectivity, landscape ecology metrics

1 Introduction: landscape maps and the need for objectivity

The ocean environment is perceived as vast and seemingly endlessly variable, and so are its inhabitants. It may be argued that breaking it down into a handful of distinct classes does not account for its diversity. However, if we aim to develop sustainable practices, particularly those grounded in ecosystem-based management (typically using area-based management tools, [e.g., IUCN, 2018)], there is a need to condense this variability into spatially explicit delineations of biological and environmental entities. As such, there is a need to classify the marine ecosystem into 'provinces', 'landscapes', or 'habitats' (Roff et al., 2003). Indeed, Kavanaugh et al. (2016) summarize that, 'landscapes are conceptual models of systems shaped by the local geomorphology, environmental conditions and biological processes.'

Most classifications to date either start from a biological point of view, based on the knowledge of species distributions and leading to the delineation of biomes or biogeographic provinces (e.g., Watling et al., 2013), or from the physiographic point of view, deploying a classification of the physical environment as a proxy for species niches and habitats (e.g., Harris et al., 2014). Unfortunately, due to the remoteness and challenging sampling conditions in the deep and open ocean, our knowledge of species distributions in the marine realm is still very limited, creating considerable uncertainties in biogeographic classifications of the ocean (e.g. Tyler et al., 2016) despite the significant progress achieved by large research programs such as the Census of Marine Life (Snelgrove, 2010). Predictions of the distribution patterns of species and biomass are typically made using physical environmental variables as predicting factors, given the fact that, particularly at broad scales, the physical environment is one of the main drivers for species occurrence and community composition, and is commonly better known or observed than the species themselves (Gille et al., 2004; Wei et al., 2010; Watling et al., 2013; Morato et al., 2021). This means that the large-scale ecosystem classifications of the oceans (i.e. the European Nature Information System (hereafter EUNIS) by Davies et al., 2004, the Global Seascape Map by Harris and Whiteway, 2009, the Global Open Ocean and Deep Seabed (hereafter GOODS) biogeographic classification by the Intergovernmental Oceanographic Commission (hereafter IOC), 2009, the Global Seafloor Features Map (hereafter GSFM) by Harris et al., 2014, and the Environmental Marine Units (hereafter EMU) by Sayre et al., 2017) typically start with broad divisions of the physical environment, based on key parameters that influence species' physiology, distribution, and behavior (e.g., depth, temperature, oxygen concentration, and food availability). They provide a first-level insight into the spatial structure of ocean ecosystems and serve as a tool to indicate ecosystem connectivity or patchiness, as well as supporting marine protected area networks assessments (e.g. McQuaid et al., 2020, Popova et al., 2019) or other aspects of marine spatial planning and conservation (Combes et al., 2021).

Since there are already multiple large scale (e.g. Vasquez et al., 2015, Verfaille et al 2009) or even global ocean classifications, an important question could be: 'why do we need yet another?'. The answer to this is neither exhaustive nor trivial: there is a need for enhanced objectivity when talking about classifications, as well as for the use of updated and recent data.

Classifying the ocean environment using thresholds that are based on human interpretation of what exists on the seafloor bears the risk of overlooking specific types of marine landscapes by considering only a few aspects of the environment each time and may introduce artificial divisions because of the way people historically looked at ocean maps and biological data (Howell, 2010). In reality, the physical environment is a multivariate continuum. Ideally, all aspects of its character should, *a priori*, be considered simultaneously and equally weighted when delineating significantly different environmental entities or landscapes. Multivariate data analysis techniques are capable of this, and can take marine landscape classification beyond the initial, manual approach (Kavanaugh et al., 2016). To our knowledge, only two studies exist that have applied this to the global marine environment: the Global Seascapes by Harris & Whiteway (2009) and the Environmental Marine Units (EMU) by Sayre et al. (2017), which aim to take an objective approach using unsupervised classification techniques on datasets that

include hydrographic, morphological, and biological variables on a global scale. Harris and Whiteway (2009, their Figure 10) applied an unsupervised isoclass technique, which is comparable to a stepwise (cascaded) K-Means, on six biophysical variables (i.e., depth, seabed slope, sediment thickness, primary production, bottom water dissolved oxygen, and bottom temperature). Sayre et al. (2017) chose the k-means clustering algorithm in their work. Within this study, we aim to expand the range of input variables, including the latest data from recent and fine-scale ocean models. Using density estimation and model-based clustering, we try to overcome shortcomings of the widely used K-Means, or of similar algorithms (e.g. isoclass), such as their sensitivity to the initial cluster centre placement, fixed number of clusters, limitation to spherically shaped clusters, etc. (Press et al., 2007; Sayre et al. 2017).

1.1 Making use of marine landscape maps

As pressures on the ocean floor from e.g., climate change, overfishing and mining increase, it is becoming increasingly urgent to protect key regions by declaring them marine protected areas (MPA). Less than 10% of the ocean realm is under any form of protection today (IUCN, 2021) although there is agreement that protecting 30% of global land and ocean would be beneficial not only for ecosystem and biodiversity recovery but also for the financial and non-monetary economic sector. This has been widely examined in the 30x30 study by Waldron et al. (2020). And although in 2010, the World Park Congress recommended a protection of 30% by 2014, it is widely known that even today this is by far not the case (e.g. O'Leary et al., 2016; IUCN, 2021).

Out of the existing MPAs, only 31% (less than 2% of the entire ocean) enjoy full protection. The remaining 69% are still open to some extent of fishing activities (Turnbull et al., 2021; IUCN, 2021), although No-Take areas, regions that are fully protected, have shown the greatest effectiveness in preserving marine biodiversity and also a capability of re-establishing the complexity of marine ecosystems (Sala & Giakoumi, 2017). Often, a lack of basic knowledge about the deep-sea ecosystems in a particular region of the deep sea can result in it not being considered for protection. Landscape maps may be an aid with this problem, as they highlight, on an ocean basin scale, both coherent marine areas that may have been unknown so far (e.g. Magali et al., 2021) and also regions of high landscape variability. The latter are particularly relevant, because a major criterion for the designation of MPAs or the definition of EBSAs (Ecologically or Biologically Significant Areas) is the assessment of the local environment's diversity and variability (IUCN, 2018, CBD 2009). EBSAs are defined by experts, based on seven parameters (Uniqueness or Rarity, Special importance for life history stages of species, Importance for threatened, endangered or declining species and/or habitats, Vulnerability, Fragility, Sensitivity, or Slow recovery, Biological Productivity, Biological Diversity, Naturalness) (CBD 2019). Often, EBSAs can be found in combination with rough topography, for example along seamount chains (e.g. Walvis ridge) or large fracture zones (e.g La Romanche), but also associated to upwelling and open water regions (Convention on Biological Diversity (CBD), 2009). Translated to the landscape map, these would be regions with a high density of different landscapes. We therefore further demonstrate a prospective use of classifications like this by running a quantitative landscape analysis over the final cluster map. It highlights areas of high cluster diversity density and therewith potential regions of interest for future studies or candidates for marine protected area designation.

2 Methods – processing steps

With this study, we aim to reduce human subjectivity in ecosystem classification as far as possible by avoiding setting thresholds between classes and applying an unsupervised multivariate statistical approach. Unsupervised in this sense means that the clustering procedure is an automatic process that recognizes patterns in an unlabeled dataset. This kind of multivariate statistical clustering scheme treats all input variables equally. We believe that this is a more objective way to describe the ocean environment than weighting individual variables.

2.1 Data selection

Deciding on the right input parameters is as fundamental as it is challenging. In an unsupervised cluster analysis, it is this part which can be influenced by human subjectivity the most, with incorrect choices at this stage potentially rendering biased results (Roff et al., 2003; Harris and Whiteway, 2009). We selected data based on the following: ecological understanding described in literature and existing classifications (e.g., Harris and Whiteway, 2009; IOC, 2009; Howell, 2010; Watling et al., 2013; Harris et al., 2014; Sayre et al. 2017; Morato et al., 2021), spatial coverage, resolution, data access, and data format to have a representative sample of ecological determinants and a good exemplification of the seafloor habitat. In our aim to map hydro-morphological provinces of the Atlantic seafloor, the spatial availability of input data is constrained to the Atlantic geographical boundary and further excluded data from the sea surface and the water column (except for the bottom water). Hence in the deep sea, where data presence is scarce (e.g. Clark et al., 2016) and the major area to be classified is below 1,000m water depth, we relied on models and data compilations that are available in full coverage and not in single scattered sample points. We chose the Copernicus Mercator model (hereafter

CMEMS) (EU Copernicus Marine Service, 2021) for hydrographic variables and the Satellite Radar Topography Mission version 2 (hereafter SRTM) 15+V2 data (Tozer et al., 2019a) for geomorphological parameters. Furthermore, also GlobSed (Updated Total Sediment Thickness in the World's Oceans, Straume et al., 2019) and Particulate Organic Carbon (POC) flux (Lutz 2007) were chosen as determinant variables. All data were unprojected and were referenced to World Geodetic System (WGS) 84.

2.2 Data acquisition and description

2.2.1 CMEMS data products

Global physical and biochemical data from satellite observations, ocean models, and *in-situ* samples are combined and published on a regular basis by CMEMS and provide information on the physical and biochemical state, dynamics, and variability of the ocean ecosystem. All data products are freely available to the public (EU Copernicus Marine Service, 2021).

The data used for this study are based on numerical models (NEMO 3.1, ORCA12) and data assimilation techniques (reduced order Kalman filter) (Lellouche et al., 2018). From these, we extracted the following parameters:

* Bottom temperature in [°C] (physical), resolution 1/12°
* Salinity in [psu] (physical), resolution 1/12°
* East (uo) and north (vo) components of ocean currents in [m/s] (physical), resolution 1/12°
* Oxygen in [mmol/m^3] (biochemical), resolution ¼ °
* Phytoplankton in [mol] (biochemical) expressed as carbon in sea water, resolution ¼ °

CMEMS provides all hydrographic data products *via* FTP server download as global multiband and multi - dimensional NetCDF files. The dimensions are time, latitude, longitude, depth (50 layers), and 11 value variables (salinity, oxygen, etc.).

The physical data product (GLOBAL_ANALYSIS_FORECAST_PHY_001_024_monthly) is based on the PSY4V3 Mercator system of the NEMO 3.1 model and amongst others contains 3D monthly mean fields for temperature, salinity, and current velocity. These data have a horizontal resolution of 1/12° (approximately 8 km at the equator) with 50 depth levels and a vertical resolution of 1m at the sea surface and 450m at the seafloor depth level (Lellouche et al., 2018; Tressol et al., 2020; Chune et al., 2020).

The biochemical data products (GLOBAL_ANALYSIS_FORECAST_BIO_001_028) are based on the PISCES-v2 (Pelagic Interactions Scheme for Carbon and Ecosystem Studies volume 2) model within NEMO 3.6 which simulates biochemical and lower trophic levels of marine ecosystems, as well as carbon and main nutrient cycles (Aumont et al., 2015). It also contains 3D monthly mean fields for oxygen and phytoplankton and comes with a horizontal resolution of ¼° (approximately 24 km at the equator). Similar to the physical data, it has 50 depth levels at a vertical resolution of 1m on the sea surface and 450 m at the seafloor depth level (Paul, 2019).

For our analysis, the selected hydrographic data were reduced to seafloor level (i.e., taking the CMEMS depth layers closest to seafloor), averaged over three years (2018 - 2020) and, additionally, three years' seasonal variability was calculated. We considered three years a reasonable time scale to capture annual changes and seasonal variability at the same time. An overview of all input variables and their main statistics is listed in the supplementary material. A detailed description of the data preparation and processing is given in sections 2.3 & 2.4.

2.2.2 SRTM15+ V2

The latest Shuttle Radar Topography Mission (SRTM) version 2 digital topographic dataset released by NASA in 2015 is the basis to the topography determinants in our classification. Depending on the satellites' track spacing, latitude, and water depth, the resolution of the predicted bathymetry is approximately 6 km (Tozer et al., 2019a).

The SRTM15+ V2 grid is available *via* OpenTopography (https://opentopography.org) as a global NetCDF. It is a data compilation built by Tozer et al. (2019a) of the SRTM predicted ocean depth complemented by shipborne MBES bathymetry at 15" (1/240°) resolution. To avoid bias towards higher resolution data during the classification, the SRTM15+ V2 has been down-sampled to the CMEMS data product resolution of 1/12° (Yesson et al., 2011a, b). The bathymetry grid by Tozer et al. (2019b) was used. Slope, terrain ruggedness (after Riley et al., 1999) and topographic position index (a landform analysis where each data point's altitude is evaluated to its surrounding neighbors, after Weiss, 2001) were calculated from the depth grid.

2.2.3 Global sediment layer thickness and POC flux

The latest compilation for sediment thickness data GlobSed (Straume et al., 2019) was selected as a further determining variable as sedimentation is a crucial indicator for ecosystem types and biodiversity (e.g., Snelgrove, 1999; Zeppilli et al., 2016). It was also used as a proxy for the sedimentation rate since there is currently no Atlantic-wide full-coverage dataset that reflects sedimentation rate across the basin. GlobSed is the most updated version of global sedimentation information and has been constructed at the same resolution as the CMEMS data (1/12°). Particulate Organic Carbon (POC) flux (Lutz et al., 2007) has further been chosen as a proxy for food availability at the seafloor in addition to phytoplankton (from CMEMS) (e.g.

Kharbush et al., 2020). The original grid of resolution of 1/11° was rescaled to 1/12°.

2.3 Data pre-processing

The pre-processing was carried out using gdal (GDAL/OGR 2021), Python V3.7 (Van Rossum & Drake, 2009), and GMT Generic mapping Tools V6.1.1 (Wessel et al., 2019). The results were visualized with QGIS V3.16 (Hannover) (QGIS Development Team, 2020). The following pre-processing steps were made:

1. Apply scale factor and offset to unpack real values from packed netCDF file format (Chune et al., 2020)
2. Create a seafloor layer, if necessary (from those data including the entire water column, e.g. salinity). Resample each input raster at an equal resolution of 1/12° using the grdsample algorithm within GMT.
3. For bathymetry only: calculate derivatives slope, TPI, TRI
4. For partial current velocity components: Calculate absolute velocity using:
   v = sqrt(uo2 + vo2)
   where vo, uo are north and east current velocity components, respectively
5. For non-static variables: Calculate three-years mean using: [(Jan18 + Jan19 + Jan20) + (Feb18 +)… + (Dec20)]/36
6. For non-static variables: Calculate seasonal variability as: |summer – winter| where: Summer = (June + July + Aug.)/3 and Winter = (Dec. + Jan. + Feb.)/3
7. 'Nan out' landmass: Uniquely fill land areas with NaNs to indicate a lack of relevant oceanic data here and so exclude them from the analysis.

2.4 Data clustering

To find and define clusters, we applied a density estimation and model-based clustering method that is implemented by (finite) Gaussian mixture models (GMM) in R v4.1 (R Core Team 2018). This technique reveals latent structures within the dataset by seeking an optimal number of Gaussian distributions that sufficiently represent the dataset (Hastie et al., 2001). The distributions are fitted iteratively with maximum likelihood implemented by Expectation Maximization (EM) methods. For each point of the dataset, the probability of it belonging to a certain cluster of distributions is estimated (expectation, E-step) using each distribution's current mean, its covariance matrix, and a hidden mixing probability coefficient as fitting parameters. The expectation step is then repeated (maximization, M-step) until convergence (stabilization of the model) occurs (Hastie et al., 2001; Scrucca and Raftery, 2014). The optimum model (= best number of clusters) is selected by the Bayesian Information Criterion (BIC) index which is known to be robust against overfitting (Press et al., 2007). The E-M-step is somewhat analogous to calculating the distance of each point to the cluster center for a data point in KMeans. In fact, KMeans is a special, simplified case of GMM (Press et al., 2007). GMM however has advantages over KMeans: The number of clusters does not have to be known à priori; GMM takes clusters of various shape, volume, and orientation and is not sensitive to the initial placement of cluster centres, whereas KMeans only accepts spherically shaped clusters. Given that it is based on probability, GMM cluster boundaries are not sharp (i.e. either a point belongs to a cluster or not) but soft, meaning that there is a certain probability that a data point is part of a cluster.

To assess whether to include or exclude variables as input parameters, the variable selection algorithm clustvarsel v2.3.4 (Scrucca & Raftery, 2018) is run before the actual clustering. It examines the differences of BIC indices depending on whether a variable has clustering properties or not. Based on this, a variable is accepted or rejected. A large positive BIC difference indicates high clustering properties (Scrucca and Raftery, 2014). The algorithm accepted all input variables as input parameters, hence this step will not be further discussed. The main steps of the clustering process are listed below.

1. The input parameters were scaled to avoid bias towards extreme values and obtain zero mean and unit variance.
2. A variable selection algorithm ('clustvarsel' v2.3.4) (Scrucca and Raftery, 2018) was applied on the input parameters to identify an optimal subset based on their clustering properties.
3. According to its result, all variables were accepted as input for the clustering.
4. The Gaussian mixture modelling algorithm 'mclust' v 5.4.6. (Fraley & Raftery, 2003; Scrucca et al., 2016) was applied on the entire input variable dataset.
5. The mclust result was exported as a text file along with the clustering uncertainties of each point.
6. Boxplots were created using 'ggplot2' v3.3.5 (Whickham, 2016) and the 'RcolourBrewer' (Brewer, 2013) library.

3 Results: The Atlantic seabed areas

The statistical analysis revealed nine clusters derived from the input variables. We named the clusters 'seabed areas (SBAs)'. In the following the expressions 'clusters' and 'SBA', will be used as synonyms, whereas cluster will be used as a technical term, SBAs will be referred to in an interpretational context. The

shapefile containing the SBA outlines will be published on the iAtlantic Geonode (geonode.iatlantic.eu/).

A map showing the nine SBAs found in the analysis is shown in Figure 1. The majority of the SBAs are located in the deep sea in Areas beyond national jurisdiction ('ABNJs') and only two SBAs define coast-adjacent and continental shelf regions.

To understand what distinguishes the SBAs and what are the dominating factors, a look at the boxplots below is of use (Figure 2). They give quantitative information, outlining the characteristics of each cluster and indicating which parameter describes the respective cluster in the first order. The boxes contain 50% of the data. The 'whiskers' (straight lines below and above the box) denote minimum and maximum data values, respectively, such that box and whiskers include 95% of the data. The larger the box, the wider is the value span or variation of the respective input variable across a cluster. The median (central horizontal line inside the box) is another important measure when interpreting boxplots. It shows the middle quartile of the data set and, opposite to the mean or average, it is not sensitive to outliers. A mean value (dot inside the box) that is far away from the median indicates a bias towards the direction of displacement. The most illustrative boxplots are presented below (Figure 2). The complete set of boxplots for all input variables can be found in the Supplementary Material F1. A summary of the cluster statistics is listed in Tables A1, A2 of the supplementary material. A detailed boxplot assessment and boxplots including extreme values are given in the Supplementary Material F2, T1.

Although we see from the box-plots that there is seldom a single environmental variable that describes a particular SBA, we can make some general statements about their most defining characteristics. Table 1 presents a short outline along with the area covered by each SBA.

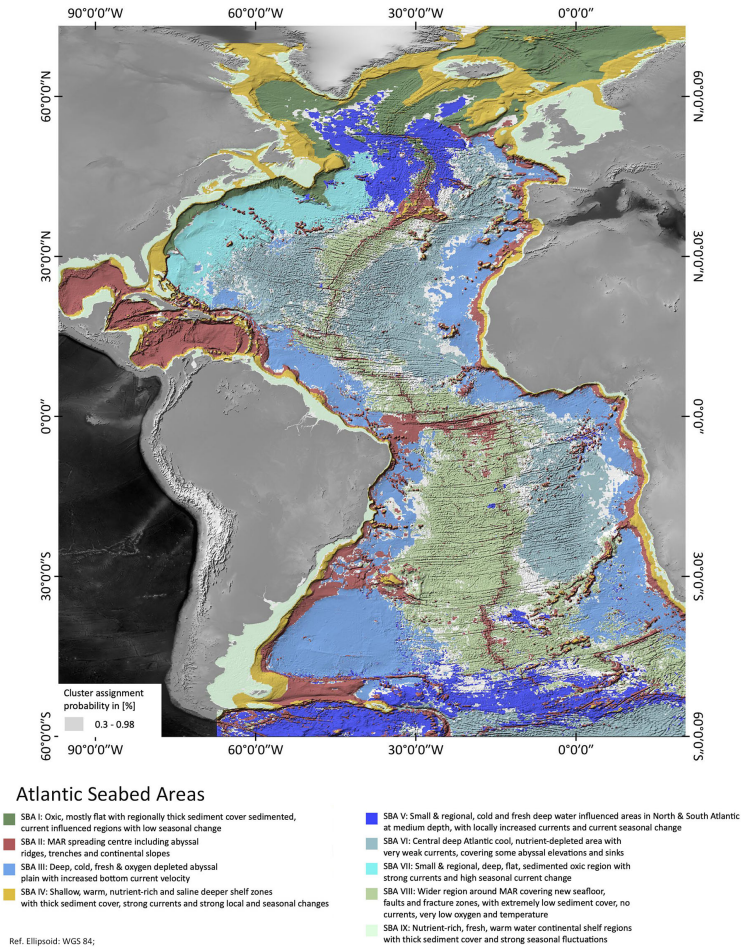

FIGURE 1
Atlantic Seabed Areas as identified by the Gaussian Mixture Model analysis along with cluster probabilities. Areas of saturated colors have a probability of >98% of being classified correctly. Especially at the cluster boundaries, probability decreases.

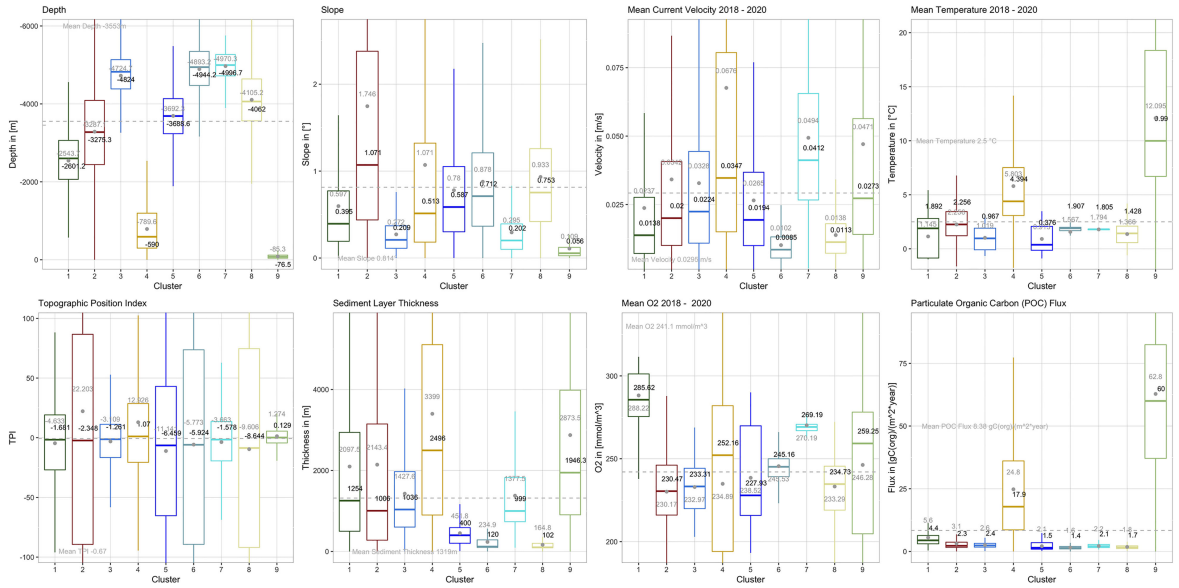

FIGURE 2
Boxplots outlining the SBA characteristics. The boxes comprise the groups' interquartile ranges, i.e. between the upper (75%) and lower (25%) quartiles and contain the central 50% of the data. The 'whiskers' (straight lines below and above the box) denote minimum and maximum data values, and together with the boxes make up 95% of the data set. The remaining 5% are extreme values, which for better visibility are not shown here. They can be found in boxplots of the supplementary material F2. The colored lines/grey dots inside the boxes indicates the groups' median/mean, whereas the grey dashed line is the overall data set's median.

3.1 Cluster probability

As the clustering is based on the probability of any one 1/12°x 1/12° cell being classified into one of the nine SBAs, a 'hard boundary' - map showing all cells in the colour corresponding to their most probable cluster could be misleading if many cells had quite similar probabilities for a number of clusters. To test how robust the classification is, we examined the absolute values of the dominant cluster probability, hereafter referred to as probability. A cumulative curve of the classification probabilities [plotted as "probability = 1 – uncertainty" as of Fraley & Raftery (2003)] is shown in Figure 3. On Figure 1, the grey colours illustrate probabilities of less than 98%, those were excluded. We see from Figure 3 that more than 85% of the cells are assigned to a

TABLE 1 SBA description summary ordered by area covered (from smallest to largest).

SBA	Depth (quartile range) in [-m]	Area [km2]	Description
1	2064 - 3063	3,998,145	SBA I: Oxic, mostly flat with regionally thick sedimented coverage current influenced regions with low seasonal change
2	2443 - 4090	11,967,939	SBA II: MAR spreading center including abyssal ridges, trenches, seamounts and continental slopes as well as the Gulf of Mexico.
3	4385 - 5135	14,990,027	SBA III: Deep, cold, fresh and oxygen-depleted abyssal plain with increased bottom current velocity
4	300 - 1395	5,216,720	SBA IV: Shallow, warm, nutrient-rich and saline deeper shelf/upper slope zones with thick sediment cover, strong currents and strong local and seasonal changes
5	3236 - 4135	6,002,183	SBA V: Small and regional, cold and fresh deep water influenced areas in North and South Atlantic at medium depth, with locally increased currents and current seasonal change
6	4473 - 5347	15,508,117	SBA VI: Central deep Atlantic cool, nutrient-depleted area with very weak currents, covering some abyssal elevations and sinks
7	4720 - 5268	3,472,998	SBA VII: Small and regional, deep, flat, sedimented oxic region with strong currents and high seasonal current change
8	3563 - 4640	16,128,258	SBA VIII: Wider region around MAR covering new seafloor, faults and fracture zones, with extremely low sediment cover, no currents, very low oxygen and temperature
9	39 - 119	5,945,256	SBA IX: Nutrient-rich, fresh, warm water continental shelf regions with thick sediment cover and strong seasonal fluctuations

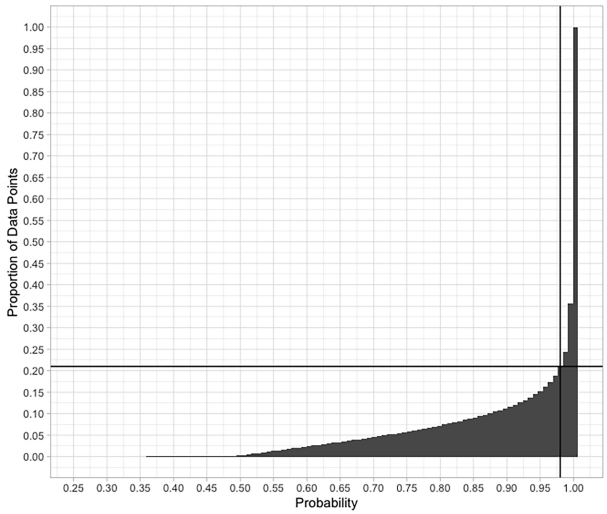

FIGURE 3
A plot of cumulative frequency of observed probabilities in the classification of individual grid cells into one of the nine SBAs. The lines indicate the 98% probability threshold that includes 79% of the data. Over 85% of the cells are classified with > 95% certainty.

dominant cluster with a probability of > 95% (uncertainty < 0.05). Only around 2% of the cells lie in a transition zone of 40-60% probability. Figure 1 shows that these higher-uncertainty cells mainly lie at SBA boundaries, presumably reflecting the regions where environmental variables are in transition between one SBA and another. The cells which are classified with 0 uncertainty generally lie in the centre of an SBA patch, classified as belonging to just one SBA.

3.2 Landscape diversity

To highlight the diversity of the Atlantic sea floor landscape, we ran a moving window analysis based on landscape ecology principles (e.g. Swanborn et al., 2022) that automatically identifies areas where several cluster boundaries meet. Regions of high diversity are at the same time those with the highest classification uncertainties. To be confident that our search for areas of high landscape diversity is not weakened by these poorly-classified cells, we included only points with classification probabilities of >= 98% in the analysis. This still amounted to about 80% of the data but significantly reduced the data density in cluster boundary regions.

The diversity analysis was executed using the package 'landscapemetrics' (Hesselbarth et al., 2019). A major part of it is based on FRAGSTATS (McGarigal et al., 2012), a program that automatically quantifies landscape structure and has been implemented in R by Hesselbarth et al. (2019). In combination with a moving window, we used patch richness (PR) index, a simple diversity indicator that counts the number of different patch types within a given area (McGarigal et al., 2012). A patch describes the local area covered by a single SBA: Hence, the more patches of different SBAs in an area, the higher the PR and local diversity. As we did not want to fix patch sizes in advance by defining a search radius, we chose a cell-wise moving window approach with a window size of 3x3, including only one cell and its direct neighbours. This approach catches even the smallest region of high diversity. The PR index expresses the numbers of different neighbours of a cell, with a minimum to maximum count of one to four neighbours.

Figure 4 is a heatmap showing the patch richness as a result of the diversity analysis. Regions of large densities of high SBA diversity are highlighted as indicated by the red colours. The highlights must be understood as a count of the different neighbours per area – the more cells with a high number of different neighbours in a region, the more intense the yellow/red colour. The highlighted areas are well spread across the central Atlantic basin, less in the Northern Atlantic. They correspond in parts with the latest EBSAs as defined by the Convention of Biological Diversity (CBD) 2019. Most of them are associated with and around SBA II, which is the sparsest of all SBAs, hence with most cluster boundaries. Many of the highlights are found around small-scaled patches. Only few are in the vicinity of one large patch of a single SBA, which is why in the region > 55°, where large patches prevail, there is less patch diversity. We chose two regions on Figure 5 for a detailed inspection to highlight what this patch richness means in terms of landscape variability.

Figure 5 shows the Namibia abyssal plain and Cape Basin, as well as the southern edge of Walvis ridge, with red outlines

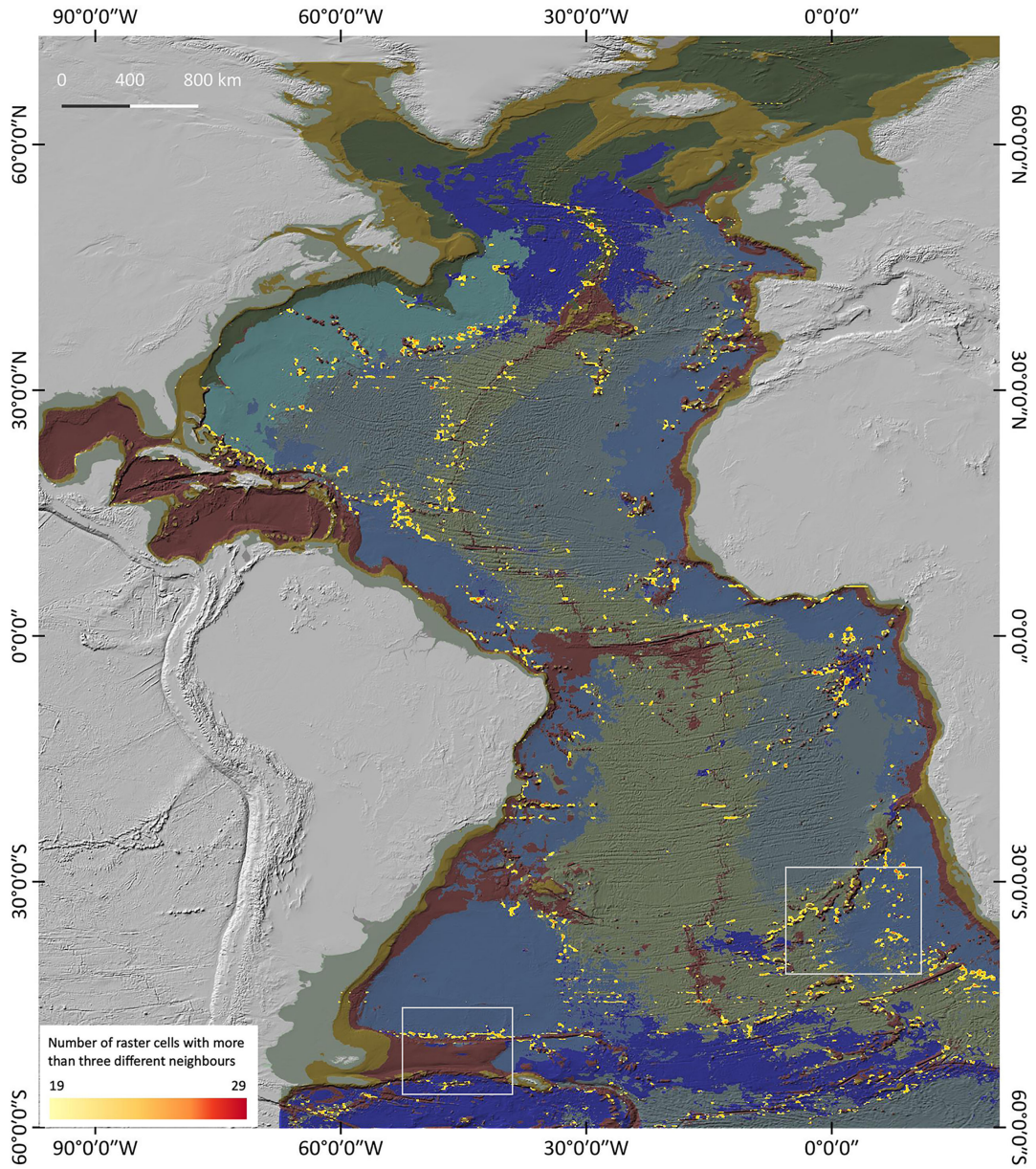

Atlantic Seabed Areas

- SBA I: Oxic, mostly flat with regionally thick sediment cover sedimented, current influenced regions with low seasonal change
- SBA II: MAR spreading centre including abyssal ridges, trenches and continental slopes
- SBA III: Deep, cold, fresh & oxygen depleted abyssal plain with increased bottom current velocity
- SBA IV: Shallow, warm, nutrient-rich and saline deeper shelf zones with thick sediment cover, strong currents and strong local and seasonal changes
- SBA V: Small & regional, cold and fresh deep water influenced areas in North & South Atlantic at medium depth, with locally increased currents and current seasonal change
- SBA VI: Central deep Atlantic cool, nutrient-depleted area with very weak currents, covering some abyssal elevations and sinks
- SBA VII: Small & regional, deep, flat, sedimented oxic region with strong currents and high seasonal current change
- SBA VIII: Wider region around MAR covering new seafloor, faults and fracture zones, with extremely low sediment cover, no currents, very low oxygen and temperature
- SBA IX: Nutrient-rich, fresh, warm water continental shelf regions with thick sediment cover and strong seasonal fluctuations

Ref. Ellipsoid: WGS 84;

FIGURE 4
Atlantic Seabed Area diversity density. A patch richness analysis map highlighting areas of high SBA diversity. The boxed areas of Walvis ridge and Falkland Plateau are discussed in more detail below in Figures 5 and Figure 6.

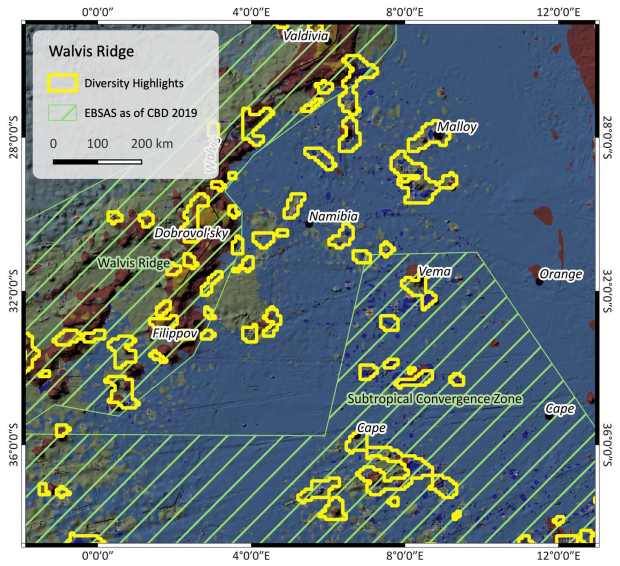

FIGURE 5
Patch richness near Walvis ridge. The outlines are the highlighted regions as found by the patch richness analysis. The map also shows EBSAs (green stripes) as of CBD 2019. For SBA color legend, please refer to Figure 1.

indicating regions of high SBA diversity. SBA III prevails, along with several patches of SBA VII and seamounts covered by SBA II. Besides the presence of seamounts, the input data suggest deep and cold abyssal plain under the influence of strong currents. The oxygen is slightly higher within the Walvis ridge EBSA than in the Subtropical Convergence Zone EBSA and the Namibian abyssal plain in between. Also, currents are locally stronger, e.g. south of the Walvis ridge line and weaker in the deeper basin. Here, the highlighted areas along Walvis ridge correspond to the Walvis Ridge EBSA patch, but not so well to the Subtropical Convergence Zone EBSA further south.

Figure 6 shows the Falkland escarpment north of the Falkland plateau and the Tehuelche fracture zone south of the plateau. At the escarpment, the highlights mainly include SBAs II & III and some small patches of SBA V. At Tehuelche fracture zone, these are SBAs II, V and VIII. The input data indicate higher current speeds and increased seasonal change north than south of the plateau and especially along the Falkland escarpment which can be associated with the influence of the Malvinas current and the Argentine gyre (Yu et al., 2018).

4 Discussion

4.1 How the SBAs relate to existing data and publications

The unsupervised clustering of the Atlantic seabed environment resulted in nine seabed areas, with characteristics summarised in Table 1. To interpret the SBAs, we compared them to published oceanographic patterns such as large currents, upwelling systems and water-mass formation zones as well as to predicted seamounts (Yesson et al., 2011a; Yesson et al., 2011b), and hydrothermal vent locations (Beaulieu and Szafrański, 2020). Many of the SBAs are influenced by currents, water masses and water formation zones. A striking example for this is SBA VII which is confined to one region: the major spreading path of NADW through the North Atlantic deep abyssal plain (e.g. Gary et al., 2011). High oxygen concentrations, cold water, very strong currents and high seasonal change support the interpretation as a highly ventilated region (Figure 1 in Rahmstorf, 2006). The partitioning into a Northern and a Southern compartment of SBA V can be related to the influence of Labrador Sea Water (LSW) formation taking place in the deep convection zone of the Labrador basin (Koelling et al., 2022), which spreads out into the central Atlantic Ocean as part of the North Atlantic Deep Water (NADW), as well as to Antarctic Bottom Water (AABW) in the Weddell Sea (Figure 1 in Rahmstorf, 2006). This is underpinned by the expert knowledge-based GOODS classification whose authors found a strong division into North and South Atlantic, too (Supplementary Material Table T4, IOC, 2009; Morato et al., 2021).

SBA IV encloses the Atlantic's deeper shelf zones and regions of strong local (boundary) current systems with a high seasonal variability, such as the East Greenland current or overflow areas such as the Greenland-Scotland-ridge complex (Mauritzen, 1996; Rahmstorf, 2006; Våge et al., 2011; Semper

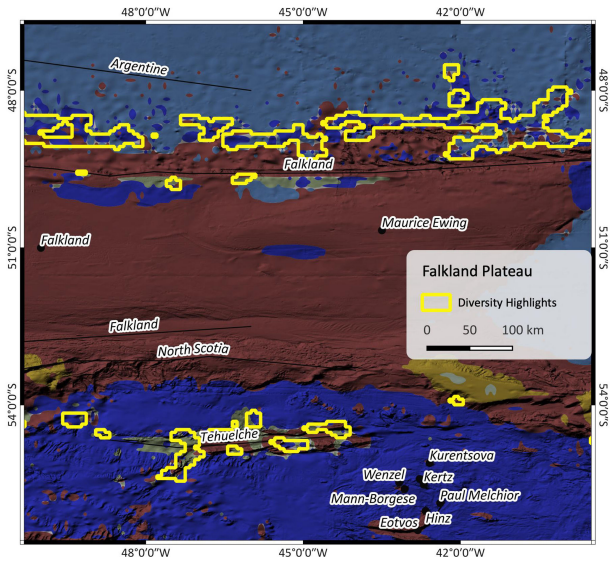

FIGURE 6
Patch richness at Falkland fracture Zone. The outlines are the highlighted regions as found by the patch richness analysis. For SBA color legend, please refer to Figure 1.

et al., 2020). Similar to this but in shallower regions is SBA I, strongly influenced by water formation zones in the Labrador and Greenland Sea as well as by the boundary and overflow currents. SBAs I, IV and VII show an increased oxygen concentration, emphasising the influence of mixing processes. Lower oxygen concentrations in moderate depths (SBA V) may be attributed to enhanced biological productivity (e.g. (Sigman and Hain, 2012; Schmidtko et al., 2017), oxygen depletion during the spreading of water masses, like e.g. the AABW on its way up North (Menezes et al., 2017) or oxygen minimum or even dead zones (Diaz et al., 2013; Rabalais, 2021). SBA II sticks out as it seems to be mainly defined by topography, covering areas of rough terrain and corresponding well with the spreading center of the MAR. It is the patchiest of all SBAs. In major parts, SBA II agrees with listed hydrothermal vent fields (Beaulieu & Szafrański, 2020) and seamounts (Yesson et al., 2011a; Yesson et al., 2011b).

4.2 Comments on the seascapes, GOODS and EMUs

We further compared the SBAs to the seascapes described by Harris and Whiteway (2009), to the GOODS biogeographic provinces (IOC, 2009) and to the Ecological Marine Units ('EMUs') found by Sayre et al. (2017). The latter have also been used by Morato et al. (2021) to assess their suitability for a species distribution model (SDM). Harris and Whiteway (2009) used a clustering approach (isoclass) on seafloor data which is most similar to ours. Sayre et al. (2017) also used a similar technique (KMeans), applied in 3D on the water column. Their EMUs are three-dimensional entities, vertically comprising water column layers rather than separating the seafloor from the water body above which makes it difficult to directly compare to our seafloor-only zones. The same applies to GOODS, which moreover is purely expert-based and hence subjective. Table A3 in the supplementary material lists the SBAs we found against the classes of Harris and Whiteway (2009), Sayre et al. (2017) and GOODS to give an approximate conversion. Also, only major matching areas are included; those that have minor overlap are left out to avoid confusion. In Table A4, the input parameters and methods of all aforementioned classifications are listed.

When comparing the SBAs we identified to the seascapes by Harris & Whiteway (2009), some (esp. SBAs III, V, VII) can be 'translated' into one single seascape (10), others (e.g. SBA VIII) correspond to more than one seascape (5, 7 and 9). This might be because we used additional non-morphologic parameters like current speed, POC flux, etc., higher resolution data (1/12° for SBAs, 1/10° for seascapes), and more recent data. We have not included primary production in the classification, as it is a variable mostly determining the ocean surface and the upper water column until a depth of around -350 m (CMEMS, 2021). Instead, we used POC flux to the sea floor. On the other hand, Harris and Whiteway (2009) did not take into account seasonal variability, a measure we considered crucial for currents, salinity, temperature, and oxygen concentration. They further excluded salinity, arguing that its variation at seafloor depths is very low.

This may be correct in the deeper parts of the Atlantic, but our results show that salinity values and seasonal variability do play a role, for example, in the shallower SBA IX region, a region that was excluded on their seascape map. In addition, the seascapes of Harris & Whiteway (2009) were defined on a global scale and, depending on the principal parameters that defined the respective seascape, those may have varied across the global ocean compared to the Atlantic basin. Another difference is that we applied a different clustering technique, one which allows for cluster shapes other than only spherical.

The other two mentioned classifications GOODS (IOC, 2009) and EMU (Sayre et al. (2017)) follow different approaches: GOODS is a purely expert-based (subjective) classification without automated or computer-based process. EMUs are three-dimensional entities, vertically comprising water column layers rather than separating the sea floor from the water body above.

The non – comparability of marine classifications is, according to Lecours (2017), a significant drawback regarding their use. Table A3 in the supplementary material shows that, except for the smaller SBAs I and VII, all SBAs correspond to more than one biogeographic region. As both EMUs and the GOODS areas have a large extent, several of those regions are almost as large as the entire Atlantic basin. Nevertheless, in marine spatial planning or MPA network designation processes, for example, it might be extremely useful to consult more than one classification to illuminate several aspects of the same area (e.g. Lecours et al., 2017).

The use of ocean landscape maps with regard to conservation targeted decision making is pointed out by Lecours (2017) as being somewhat like the classic problem of comparing apples and pears: There is a lack of uniformity concerning input data selection, standardised clustering techniques and algorithms. Furthermore, quality assessment widely differs and there is no method yet to combine the uncertainties and errors that occur during a mapping process into one ultimate uncertainty estimation. Visualising mapping results in e.g. interactive GIS is a first step to tackle those challenges, but in the long run, standardising determining variables, methods and error estimation might become inevitable (Lecours 2017).

4.3 Seabed areas and marine life

It is difficult to state whether the environmental clusters identified here contain distinct species assemblages: in addition to physical conditions, life-history traits and biological interactions will influence biogeographic patterns. Even if the physical environment is similar, species and assemblages may differ.

While individuals may not be the same, species with similar traits and functional behaviour could populate areas with comparable physical environments (e.g., burrowing fauna in heavily sedimented areas or filter-feeders in complex, rocky environments) (e.g. McGill et al., 2006; Zeng et al., 2020). From a biodiversity management perspective, such spatially explicit delineation of potential ecosystem functions (and therefore services) is of high value even if the exact species occupying the particular environment are not known. Quantitative metrics like the patch richness index to calculate diversity can discover those regions automatically and objectively.

Morato et al. (2021) have made steps towards integrating biogeographic province maps into environmental niche modelling (e.g. species distribution models (SDM) or habitat suitability models (HSM)). In their work, they compare the two seafloor bioregion models EMU and GOODS to an SDM. Although their results show only very little to hardly any agreement of the SDM's with the bioregions' boundaries, they still outline a valuable approach and a possibility of implementing those kinds of classifications into species prediction related work. Nevertheless, to effectively predict and relate species to environmental conditions, classifications and data at a finer scale must be available (Lim et al., 2021). The combination of high-resolution classifications and SDMs or HSMs is a very promising task, capable of supporting marine area-based management and spatial planning work (Lim et al., 2021; Morato et al., 2021).

At the same time, it is crucial to keep in mind that the map presented here is based on the current environmental conditions. As a result of climate change, seabed environments will change (e.g. rising temperatures, reducing oxygen content of the bottom waters), and so may the SBAs. The SBAs may change in shape and extent, or in characteristics. A next step may be to create similar marine landscape maps based on future predictions of the seafloor environment under different climate scenarios, in order to provide policy-makers with a forward look in addition to the comprehensive description of the present-day situation presented here.

4.4 Automatically finding areas of interest - interpretation of the patch richness analysis in relation to EBSAs

The results of such patch richness analyses ought to make it easier to identify potential areas of interest. Because they are based on a multivariate cluster analysis, they combine complex ensembles of multiple influencing parameters, a process which is challenging for a human brain but simple for machine algorithms. The highlights shall draw our attention to areas where special conditions prevail, and which might be worth to have a closer look at. In the case of the Falkland region (Figure 6), the Falkland plateau seems to be a barrier between two areas that are under the influence of different variables as

shown by the altered composition of neighbouring SBAs. The highlights in Figure 5 mostly cover seamounts or other subsea features, which, with regard to the Walvis Ridge where highlights and EBSA largely correspond, confirms that this is an area of significance.

From Figures 4–6, we see that landscape diversity hotspots are often found on and around seamounts or regions of strongly varying topography. This is perhaps not surprising as they are the regions where the physico-chemical conditions in the ocean are known to change significantly over small spatio-temporal extents. It is for this reason that research has often been concentrated there (e.g. Clark et al., 2011). Over the Atlantic basin, the identified regions of high landscape diversity correspond in parts with the latest EBSAs. As EBSAs need a certain amount of ground-truth data for their definition, our landscape diversity map could be useful to concentrate research in presently unstudied areas which may harbour significant landscape diversity.

EBSAs are defined on a solid data basis which is why there may be a bias towards well investigated regions. This may be the fact in the Walvis ridge region (Figure 5) – with Walvis ridge itself being significantly more examined than the surrounding environment. The EBSA patch covers the entire Walvis ridge and the area around Cape basin but only some of the nearby seamounts – besides other reasons probably due to insufficient existing data. It is not easy to find proof for this assumption. A search in Google scholar in April 2022 however yields over 300 hits for publications containing Walvis Ridge in their title, over 500 containing Cape basin and 25 for Vema seamount, but none for e.g. Malloy seamount. This could be an indicator for unbalanced data distribution and research effort between these areas.

Furthermore, EBSA definition is based on multiple criteria where (biological) diversity is just one of them. In addition to the sea floor, the water column is taken into consideration, too. It is hence obvious, that the EBSAs only partially agree with the highlights: For example in areas like the Labrador Sea, whose sea floor is defined by only one SBA, the water column however is highly dynamic due to deep water convection, making it a unique spot and EBSA candidate (CBD 2021). On the other hand, there are numerous highlights that are not within existing EBSAs or MPAs, like e.g. in the basins of Guiana or Newfoundland. This might be due to a lack of ground truth data needed for EBSA designation. It may also be because some regions we highlighted fail on other EBSA criteria. It has to be noted, though, that currently, some regions still lack EBSA expert workshops and do hence not have any EBSAs at all, like e.g. the Argentine basin. Also, to date, the North-East Atlantic most recent EBSAs have not been published yet, so there is a lack of coverage here, too. Nevertheless, the highlights of diversity in combination with the SBA map pinpoint towards regions of interest and can help finding and defining new research areas, e.g. to support cruise proposals or contribute to marine protection-based decision making, regarding location and extent of potential MPAs or new EBSAs. They may be able to support entire stages of EBSA identification without introducing too much subjectivity.

Methodological constraints, potential errors and data limitation

Despite the fact that multivariate clustering techniques are more objective than hierarchical methods, unsupervised analyses can still bear error sources that may not be visible at first sight but must be considered when using them.

Resolution

Although a density estimation and model-based clustering approach seems suitable for this kind of high dimensional and complex data, it is the input data quality that needs to be looked at. The most prominent quality-reducing factors are differences in resolution, especially when dealing with multiple data sources. This holds true for vertical as well as for horizontal resolution. At depths > 1000 m, CMEMS model data products have a very low vertical resolution of about 450 m (Lellouche et al., 2019). Hence, they only give a very rough approximation of the conditions prevailing in those depths or at the seafloor. Local small-scale (vertical) variations (e.g., in temperature, caused, for example, by hydrothermal vent fields) or the few-meters thick bottom boundary layer will not be resolved. Given that ground truth seafloor data are scarce in the deep sea, we considered for our analysis the last depth level as defined by CMEMS to be representing seafloor conditions. This induces a huge vertical uncertainty, which cannot be resolved with the present data and models. Bathymetry, on the other hand, is a seafloor layer by nature, and can have a much higher vertical resolution. Tozer et al. (2019a) state +/- 150m for the satellite data, but e.g. bathymetry acquired from multibeam systems may reach an order of metres to tens of metres. Hence in places, we are aligning data from nominally different depths: those directly at the seafloor (e.g., bathymetry), and the others in a vertical range between seafloor level and 450 m above it (CMEMS model data).

Horizontal resolution is another constraint and mainly attributed to limited data availability. For this analysis, we re-sampled all data layers to the CMEMS physical data product resolution of 1/12° (around 8 km at the equator (Lellouche et al., 2019)), which required downscaling the CMEMS biological product and upscaling the bathymetry data. Another option would have been to upscale all data to the lowest resolution, which in this case was ¼° (of the CMEMS biological product). However, we dismissed this option, as the information loss would have been intolerably high considering the fact that oxygen and phytoplankton are the only data of this low resolution. Notably, even 1/12°, or 8 km, is a very coarse scale which does not resolve small scale variations or features that

might be of importance, like e.g. submarine volcanoes or small oxygen dead zones. Local hydrodynamic and morphologic conditions are important drivers for food flux and organic matter transport to the seabed. These processes however typically operate at the scale of an offshore bank or seamount, i.e. at a resolution of maximum several hundreds of metres, and might hence not captured within this study.

Both downscaling from low to high resolution as well as the reverse can be critical; this is because high-resolution data naturally inherit more parameter variance that is passed on when resampled to coarser resolution than data that was collected at a coarse resolution in the first place, thus affecting the analysis. To at least partially accommodate this in our analysis, we scaled the data and chose model-based clustering, as it is robust towards different variances (e.g., Scrucca et al., 2016).

An approach to obviate these deficiencies could be using nested classifications, running multiple cluster algorithms on the existing classes as performed in Hogg et al. (2016). This would refine the original clusters and split them into smaller parts, but would, of course, not change the initial data resolution. Such nesting of classifications, on an ocean basin scale, would however result in complex clusters with multiple hierarchical levels which would be unwieldy to analyse.

Higher resolution ocean models (e.g. VIKING20X (Biastoch et al., 2021) or INALT (Schwarzkopf et al., 2019)), if available down to the km-scale on a basin-wide or even global scale, would significantly improve this kind of seabed clustering. To date, such models usually have a very fine resolution at the sea surface which also becomes coarse towards the seafloor. In our approach we preferred the CMEMS product, even though it has the same limited vertical resolution at depth. However, because CMEMS used an assimilation towards observational data (despite the fact that these are sparse at depth) we aimed at a more realistic representation of the hydrography.

Variable selection

Another limitation which may influence the classification result is the predictor variable selection itself. This issue has been widely discussed (e.g., Harris and Whiteway, 2009; Howell, 2010; Watling et al., 2013) and several determinants have been agreed as being good representatives of the ocean environment. In this study, we focussed on morphological and hydrographical parameters, largely leaving out biologic measures, as our aim was to define submarine landscapes (e.g. Pearman et al., 2020). However, the ocean and its inhabitants form a coherent system and likewise, human impacts (e.g., mining, fishing, etc.) have a severe influence on these ecosystems. Hence, in the future data selection will have to be expanded to encompass the full range of factors that affect the seafloor habitat. A more holistic approach, also with respect to marine protected area designation, would not only be to include a larger span of environmental data, but also information on natural resources abundances, fishing grounds, etc., such as bottom-trawling fishing activities that negatively impact the benthic environment (Eggleton et al., 2018; Ferguson et al., 2020). Visalli et al., 2020 for example worked out a data-driven spatial planning tool aiming to highlight priority regions in the ABNJ for protection. For the whole-Atlantic approach targeted here, the data layers necessary for this extended type of analysis are, sadly, simply not available at present.

Conclusion

This work presents a marine landscape map of the Atlantic seafloor based on an unsupervised, multivariate statistics cluster analysis. We found nine seabed areas in total, each of them being unique and differently defined by oceanographic and morphologic determinants. Unsupervised cluster analyses have the advantage of providing an objective view on the ocean environment, stepping away from human-defined hierarchical categorisations towards an unbiased understanding of seafloor ecosystem coherence.

Generally, depending on the clustering technique applied and the selection of input parameters, the results can be very different, highlighting the complexity and variability of the ocean. As there is not the one 'true' arrangement of marine bio-physio-chemical-morphologic regimes, verification can only take place *via* ground truthing – and even this may not catch the entire complex diversity. Hence, depending on the purpose, a combination of several existing models may be more useful than one single classification. Automated landscape analyses can help to understand the classifications better, and subsequent quantitative metrics will help to identify biodiversity hotspots and vulnerable habitats by pointing out new complex regions of interest. Studies like this and in combination with other, also smaller-scaled classifications can be used e.g. for protection-targeted decision making. Our SBAs for example have been implemented into the designation process for the new NACES MPA and acts as one of the knowledge bases to the local prevailing conditions.

A valuable future task would be to assess whether species distribution patterns can be further related to the SBAs we found. Also collating more ground truth data and a detailed assessment of the diversity highlighted regions shall support decisions about protection objectives.

Data availability statement

Publicly available datasets were analyzed in this study. This data can be found here: World data Service for Geophysics: https://ngdc.noaa.gov/mgg/sedthick/, Copernicus Marine Data Service: https://resources.marine.copernicus.eu/products, Shuttle Radar Topography Mission/Opentopography: https://opentopography.

org. The resulting cluster shape file can be found here: https://doi.pangaea.de/10.1594/PANGAEA.946690: or directly under: http://www.geonode.iatlantic.eu/layers/geonode:AtlanticSeabedAreas_WGS84.

Author contributions

MS, VH, CD, AB, and PM contributed to conception and design of the study. MS, PM, AB, and SM organized the data and performed the statistical analysis. MS prepared the figures and wrote the first draft of the manuscript. VH and CD wrote sections of the manuscript. AB gave input to oceanic models and error analysis and CD gave input to the use of the analysis. All authors contributed to manuscript revision, read, and approved the submitted version.

Funding

This work was supported by the iAtlantic project, funded by EU/HORIZON 2020, Blue Growth (grant agreement No 818123). The results are hosted on the iAtlantic Geonode (geonode.iatlantic.eu/). The authors owe gratitude to the oceanography group at GEOMAR, Helmholtz Centre for Ocean Research, for providing help with oceanographic model know-how.

Acknowledgments

Special thanks to Iason Gazis from Geomar for their help during the process of clustering model selection. We are further grateful to Catherine Wardell from National Oceanography Centre and to Anne-Cathrin Wölfl form GEOMAR for support in R scripting. We would also like to thank the reviewers for their valuable and friendly comments and their support.

Conflict of interest

Author SM was employed by the company Briese Schiffahrts GmbH & Co.

The remaining authors declare that the research was conducted in the absence of any commercial or financial relationships that could be construed as a potential conflict of interest.

Publisher's note

Supplementary material

The Supplementary Material for this article can be found online at: https://www.frontiersin.org/articles/10.3389/fmars.2022.936095/full#supplementary-material

References

Aumont, O., Ethé, C., Tagliabue, A., Bopp, L., and Gehlen, M. (2015). PISCES-v2: an ocean biogeochemical model for carbon and ecosystem studies. *Geoscientific Model. Dev.*8, 2465–2513. doi: 10.5194/gmd-8-2465-2015

Beaulieu, S. E., and Szafrański, K. M. (2020). *InterRidge global database of active submarine hydrothermal vent fields version 3.4* (www.pangaea.de). doi: 10.1594/PANGAEA.917894

Biastoch, A., Schwarzkopf, F. U., Getzlaff, K., Rühs, S., Martin, T., Scheinert, M., et al. (2021). Regional imprints of changes in the Atlantic meridional overturning circulation in the eddy-rich ocean model VIKING20X. *Ocean. Sci.*17, 1177–1211. doi: 10.5194/os-17-1177-2021

Brewer, C., and Harrower, M. (2021) *ColourBrewer, the Pennsylvania state university*. Available at: https://colorbrewer2.org/ (Accessed August 2021).

British Oceanographic Data Centre (2020) *Gebco gridded global bathymetry data*. Available at: https://www.gebco.net/data_and_products/gridded_bathymetry_data/gebco_2020/ (Accessed August 2021).

CBD Secretariat (2009). "Azores Scientific criteria and guidance," in *For identifying ecologically or biologically significant marine areas and designing representative networks of marine protected areas in open ocean waters and deep sea habitats*. CBD: Secretariat of the Convention on Biological Diversity:Montreal, Canada

Convention on Biological Diversity (CBD) Secretariat. (2021) *Ecologically or biologically significant marine areas - special places in the world's oceans*. Available at: https://www.cbd.int/ebsa/ (Accessed March 2022).

Chune, S. L., Nouel, L., Fernandez, E., Derval, C., Tressol, M., and Dussurget, R. (2020). *Product user manual for global biogeochemical analysis and forecast product GLOBAL_ANALYSIS_FORECAST_PHY_001_024. EC Copernicus marine environment monitoring service 1.6*. 34 Copernicus Marine Environment Monitoring Service, implemented by Mercator Ocean International (MOi): Toulouse, France, Public Ref.: CMEMS-GLO-PUM-001-024.

Clark, M. R., Consalvey, M., and Rowden, A. A. (2016). *Biological sampling in the deep Sea. 1. Edition* (New York:John Wiley & Sons), 472 Pages. doi: 10.1002/9781118332535

Clark, M. R., Watling, L., Rowden, A. A., Guinotte, J. M., and Smith, C. R. (2011). A global seamount classification to aid the scientific design of marine protected area networks. *Ocean Coast. Manage.*54, 19–36. doi: 10.1016/j.ocecoaman.2010.10.006

Combes, M., Vaz, S., Grehan, A., Morato, T., Arnaud-Haond, S., Dominguez-Carrió, C., et al. (2021). Systematic conservation planning at an ocean basin scale: Identifying a viable network of deep-Sea protected areas in the north Atlantic and the Mediterranean. *Front. Mar. Sci.*8. doi: 10.3389/fmars.2021.611358

Davies, C. E., Moss, D., and Hill, M. O. (2004). *EUNIS habitat classification revised 2004* (Paris: European Topic Centre on Nature Protection and Biodiversity), 127–143. Available at: http://eunis.eea.europa.eu/upload/EUNIS_2004_report.pdf.

Diaz, R. J., Eriksson-Hägg, H., and Rosenberg, R. (2013). "Chapter 4 – hypoxia," in *Managing ocean environments in a changing climate*. Eds. K. J. Noone, U. R. Sumaila and R. J. Diaz (Burlington MA, USA:Elsevier Inc.,), 67–96. doi: 10.1016/B978-0-12-407668-6.00004-5

Eggleton, J. D., Depestele, J., Kenny, A. J., Bolam, S. G., and Garcia, C. (2018). How benthic habitats and bottom trawling affect trait composition in the diet of seven demersal and benthivorous fish species in the north Sea. *J. Sea Res.*142, 132–146. doi: 10.1016/j.seares.2018.09.013

EU Copernicus Marine Service*Operational Mercator biochemical global ocean analysis and forecast system, GLOBAL_ANALYSIS_FORECAST_BIO_001_028*. Available at: https://resources.marine.copernicus.eu/?option=com_csw&view=details&product_id=GLOBAL_ANALYSIS_FORECAST_BIO_001_028 (Accessed February 2021).

EU Copernicus Marine Service*Operational Mercator global ocean analysis and forecast system, GLOBAL_ANALYSIS_FORECAST_PHYS_001_024*. Available at: https://marine.copernicus.eu/node/173 (Accessed February 2021).

Ferguson, A. J. P., Oakes, J., and Eyre, B. D. (2020). Bottom trawling reduces benthic denitrification and has the potential to influence the global nitrogen cycle. *Limnol. Oceanog.*5, 237–245. doi: 10.1002/lol2.10150

Fraley, C., and Raftery, A. E. (2003). SOFTWARE REVIEW: Enhanced model-based clustering, density estimation, and discriminant analysis software: MCLUST. *J. Classification*20, 263–286. doi: 10.1007/s00357-003-0015-3

Gary, S. F., Lozier, M. S., Böning, C. W., and Biastoch, A. (2011). Deciphering the pathways for the deep limb of the meridional overturning circulation. *Deep Sea Res. Part II*58, 1781–1797. doi: 10.1016/j.dsr2.2010.10.059

GDAL/OGR contributors (2021) *GDAL/OGR geospatial data abstraction software library* (Open Source Geospatial Foundation). Available at: https://gdal.org (Accessed August 2021).

Gille, S. T., Metzger, E. J., and Tokmakian, R. (2004). Seafloor topography and ocean circulation. *Oceanography* 17. doi: 10.5670/oceanog.2004.66

Harris, P. T., MacMillan-Lawler, M., Rupp, J., and Baker, E. K. (2014). Geomorphology of the oceans. *Mar. Geology*352, 4–24. doi: 10.1016/j.margeo.2014.01.011

Harris, P. T., and Whiteway, T. (2009). High seas marine protected areas: Benthic environmental conservation priorities from a GIS analysis of global ocean biophysical data. *Ocean Coast. Manage.*52, 22–38. doi: 10.1016/j.ocecoaman.2008.09.009

Hastie, T. J., Tibshirani, R. J., and Friedman, J. H. (2001). "The elements of statistical learning: data mining, inference, and prediction," in *Springer series in statistics* (New York, New York, USA: Springer).

Hesselbarth, M. H. K., Sciaini, M., With, K. A., Wiegand, K., and Nowosad, J. (2019). Landscapemetrics: an open-source r tool to calculate landscape metrics. *Ecography*42, 1648–1657. doi: 10.1111/ecog.04617

Hogg, O. T., Huvenne, V. A. I., Griffiths, H. J., Dorschel, B., and Linse, K. (2016). Landscape mapping at sub-Antarctic south Georgia provides a protocol for underpinning large-scale marine protected areas. *Sci. Rep.*6, 33163. doi: 10.1038/srep33163

Howell, K. L. (2010). A benthic classification system to aid in the implementation of marine protected area networks in the deep/high seas of the NE Atlantic. *Biol. Conserv.*143, 1041–1056. doi: 10.1016/j.biocon.2010.02.001

IHO-IOC*GEBCO gazetteer of undersea feature names*. Available at: https://www.ngdc.noaa.gov/gazetteer/ (Accessed August 2021).

Intergovernmental Oceanographic Commission (IOC) (2009). "Global open oceans and deep seabed (GOODS) – biogeographic classification," Eds.M. Vierros, I. Cresswell, E. Escobar Briones, J. Rice and J Ardron. *J. IOC Technical Series 84*, 96pp (UNESCO-IOC:Paris, France).

IUCN (2018). *Area based management tools, including marine protected areas in areas beyond national jurisdiction* (Gland, Switzerland: IUCN Headquarters), 9–11.

IUCN (2021)Marine protected areas and climate change. In: *Issues brief*. Available at: https://www.iucn.org/resources/issues-briefs/marine-protected-areas-and-climate-change (Accessed December 21).

Kavanaugh, M. T., Oliver, M. J., Chavez, F. P., Letelier, R. M., Muller-Karger, F. E., and Doney, S. C. (2016). Seascapes as a new vernacular for pelagic ocean monitoring, management and conservation. *ICES J. Mar. Sci.*73, 1839–1850. doi: 10.1093/icesjms/fsw086

Kharbush, J. J., Close, H. G., Van Mooy, B. A. S., Arnosti, C., Smittenberg, R. H., Le Moigne, F. A. C., et al. (2020). Particulate organic carbon deconstructed: Molecular and chemical composition of particulate organic carbon in the ocean. *Front. Mar. Sci.*7. doi: 10.3389/fmars.2020.00518

Koelling, J., Atamanchuk, D., Karstensen, J., Handmann, P., and Wallace, D. W. R. (2022). Oxygen export to the deep ocean following Labrador Sea water formation. *Biogeosciences*19, 437–454. doi: 10.5194/bg-19-437-2022

Lecours, V. (2017). On the Use of Maps and Models in Conservation and Resource Management (Warning:Results May Vary). *Front. Mar. Sci* 4, 288. doi: 10.3389/fmars.2017.00288

Lellouche, J. M., Greiner, E., Le Galloudec, O., Garric, G., Regnier, C., Drevillon, M., et al. (2018). Recent updates to the Copernicus marine service global ocean monitoring and forecasting real-time 1/12° high-resolution system. *Ocean Sci.*14, 1093–1126. doi: 10.5194/os-14-1093-2018

Lellouche, J. M., Le Galloudec, O., Regnier, C., Levier, B., Greiner, E., and Drevillion, M. (2019). *Quality information document for global Sea physical analysis and forecasting product GLOBAL_ANALYSIS_FORECAST_PHY_001_024* Copernicus Marine Environment Monitoring Service, implemented by Mercator Ocean International (MOi):Toulouse, France, Public Ref.: CMEMS-GLO-QUID-001-024.

Lim, A., Wheeler, A. J., and Conti, L. (2021). Cold-water coral habitat mapping: Trends and developments in acquisition and processing methods. *Geosciences*11, 9. doi: 10.3390/geosciences11010009

Lutz, M. J., Caldeira, K., Dunbar, R. B., and Behrenfeld, M. J. (2007). Seasonal rhythms of net primary production and particulate organic carbon flux to depth describe the efficiency of biological pump in the global ocean. *J. Geophys. Res.*112, C10011. doi: 10.1029/2006JC003706

Magali, C., Vaz, S., Grehan, A., Morato, T., Arnaud-Haond, S., Dominguez-Carrió, C., et al. (2021). Systematic conservation planning at an ocean basin scale: Identifying a viable network of deep-Sea protected areas in the north Atlantic and the Mediterranean. *Front. Mar. Sci.*8. doi: 10.3389/fmars.2021.611358

Matano, R., Palma, E., and Piola, A. (2010). The influence of the Brazil and malvinas currents on the southwestern Atlantic shelf circulation. *Ocean Sci. Discussions*6, 983–995. doi: 10.5194/os-6-983-2010

Mauritzen, C. (1996). Production of dense overflow waters feeding the north Atlantic across the Greenland-Scotland ridge. part 1: Evidence for a revised circulation scheme. *Deep Sea Res. Part I: Oceanog. Res. Papers*43, 769–806. doi: 10.1016/0967-0637(96)00037-4

McGarigal, K., Cushman, S. A., and Ene, E. (2012) *FRAGSTATS v4: Spatial pattern analysis program for categorical and continuous maps. computer software program produced by the authors at the university of Massachusetts, Amherst*. Available at: http://www.umass.edu/landeco/research/fragstats/fragstats.html.

McGill, B. J., Enquist, B. J., Weiher, E., and Westoby, M. (2006). Rebuilding community ecology from functional traits. *Trends Ecol. Evol.*21, 178–185. doi: 10.1016/j.tree.2006.02.002

McQuaid, K. A., Attrill, M. J., Clark, M. R., Cobley, A., Glover, A. G., Smith, C. R., et al. (2020). Using habitat classification to assess representativity of a protected area network in a Large, data-poor area targeted for deep-Sea mining. *Front. Mar. Sci.*7. doi: 10.3389/fmars.2020.558860

Menezes, V. V., Macdonald, A. M., and Schatzman, C. (2017). Accelerated freshening of Antarctic bottom water over the last decade in the southern Indian ocean. *Sci. Adv.*3, e1601426. doi: 10.1126/sciadv.1601426

Morato, T., González-Irusta, J. M., Dominguez-Carrió, C., Wei, C. L., Davies, A., Sweetman, A. K., et al. (2021). *EU H2020 ATLAS deliverable 3.3: Biodiversity, biogeography and GOODS classification system under current climate conditions and future IPCC scenarios* (zenodo.org). doi: 10.5281/zenodo.4658502

O'Leary, B. C., Winther-Janson, M., Bainbridge, J. M., Aitken, J., Hawkins, J. P., and Roberts, C. M. (2016). Effective coverage targets for ocean protection. *Conserv. Lett.*9, 398–404. doi: 10.1111/conl.12247

Paul, J. (2019). *Product user manual for global biogeochemical analysis and forecast product GLOBAL_ANALYSIS_FORECAST_BIO_001_028* Copernicus Marine Environment Monitoring Service, implemented by Mercator Ocean International (MOi):Toulouse, France, Public Ref.: CMEMS-GLO-PUM-001-028.

Pearman, T. R. R., Robert, K., Callaway, A., Hall, R., Lo Iacono, C., and Huvenne, V. A. I. (2020). Improving the predictive capability of benthic species distribution models by incorporating oceanographic data – towards holistic ecological modelling of a submarine canyon. *Prog. Oceanog.*184, 102338. doi: 10.1016/j.pocean.2020.102338

Popova, E., Vousden, D., Sauer, W. H., Mohammed, E. Y., Allain, V., Downey-Breedt, N., et al (2019). Ecological connectivity between the areas beyond national jurisdiction and coastal waters: safeguarding interests of coastal communities in developing countries. *Mar. Policy*) 104, 90–102. doi: 10.1016/j.marpol.2019.02.050

Press, W. H., Teukolsky, S. A., Vetterling, W. T., and Flannery, B. P. (2007). "Section 16.1. Gaussian mixture models and k-means clustering," in *Numerical recipes: The art of scientific computing* (Cambridge, United Kingdom: Cambridge University Press).

QGIS Development Team (2020)QGIS geographic information system. In: *Open source geospatial foundation project*. Available at: http://qgis.osgeo.org (Accessed August 2021).

Rabalais (2021) *Gulf of Mexico hypoxia*. Available at: https://gulfhypoxia.net/.

Rahmstorf, S. (2006). "Thermohaline ocean circulation," in *Encyclopedia of quaternary sciences*. Ed. S. A. Elias (Amsterdam, Netherlands: Elsevier).

R Core Team (2018). *R: A language and environment for statistical computing* (Vienna, Austria: R Foundation for Statistical Computing).

Riley, S., Degloria, S., and Elliot, S. D. (1999). A terrain ruggedness index that quantifies topographic heterogeneity. *Intermountain J. Sci.*5, 23–27. https://www.researchgate.net/publication/259011943_A_Terrain_Ruggedness_Index_that_Quantifies_Topographic_Heterogeneity.

Roff, J. C., Taylor, M. E., and Laughren, J. (2003). Geophysical approaches to the classification, delineation and monitoring of marine habitats and their communities. *Aquat. Conservation: Mar. Freshw. Ecosyst.*13, 77–90. doi: 10.1002/aqc.525

Sala, E., and Giakoumi, S. (2017). No-take marine reserves are the most effective protected areas in the ocean. *ICES J. Mar. Sci.*75, 1166–1168. doi: 10.1093/icesjms/fsx059

Sayre, R. G., Wright, D. J., Breyer, S. P., Butler, K. A., Van Graafeiland, K., Costello, M. J., et al. (2017). A three- dimensional mapping of the ocean based on environmental data. *Oceanography*30, 90–103. doi: 10.5670/oceanog.2017.116

Schmidtko, S., Stramma, L., and Visbeck, M. (2017). Decline in global oceanic oxygen content during the past five decades. *Nature*542, 335–339. doi: 10.1038/nature21399

Schwarzkopf, F. U., Biastoch, A., Böning, C. W., Chanut, J., Durgadoo, J. V., Getzlaff, K., et al. (2019). The INALT family – a set of high-resolution nests for the agulhas current system within global NEMO ocean/sea-ice configurations. *Geoscientific Model. Dev.*12, 3329–3355. doi: 10.5194/gmd-12-3329-2019

Scrucca, L., Fop, M., Murphy, T. B., and Raftery, A. E. (2016). Mclust 5: clustering, classification and density estimation using Gaussian finite mixture models. *R J.* 8, 289–317. doi: 10.32614/RJ-2016-021

Scrucca, L., and Raftery, A. E. (2014). Clustvarsel: A package implementing variable selection for model-based clustering in r. *J. Stat. Software* 84, 1. doi: 10.18637/jss.v084.i01

Scrucca, L., and Raftery, A. E. (2018). Clustvarsel: A package implementing variable selection for Gaussian model-based clustering in r. *J. Stat. Software*84 (1), 1–28. doi: 10.18637/jss.v084.i01

Semper, S., Pickart, R. S., and Våge, K. (2020). The Iceland-faroe slope jet: a conduit for dense water toward the faroe bank channel overflow. *Nat. Commun.*11, 5390. doi: 10.1038/s41467-020-19049-5

Sigman, D. M., and Hain, M. P. (2012). The biological productivity of the ocean. *Nat. Educ. Knowledge*3 (10), 21.

Snelgrove, P. V. R. (1999). Getting to the bottom of marine biodiversity: Sedimentary habitats. *BioScience*49, 129–138. doi: 10.2307/1313538

Snelgrove, P. V. R. (2010). "Discoveries of the Census of Marine Life - Making Ocean Life Count," (Cambridge, United Kingdom: Cambridge University Press).

Straume, E. O., Gaina, C., Medvedev, S., Hochmuth, K., Gohl, K., Whittaker, J. M., et al. (2019). GlobSed: Updated total sediment thickness in the world's oceans. *Geochem. Geophys. Geosystems*20, 1756–1772. doi: 10.1029/2018GC008115

Swanborn, D. J. B., Huvenne, V. A. I., Pittman, S. J., and Woodall, L. C. (2022). Bringing seascape ecology to the deep seabed: a review and framework for its application. *Limnol. Oceanog.*67, 66–88. doi: 10.1002/lno.11976

Tozer, B., Sandwell, D. T., Smith, W. H. F., Olson, C., Beale, J. R., and Wessel, P. (2019a)Global bathymetry and topography at 15 arc sec: SRTM15+ (Accessed May 2021).

Tozer, B., Sandwell, D. T., Smith, W. H. F., Olson, C., Beale, J. R., and Wessel, P. (2019b). Global bathymetry and topography at 15 arc sec: SRTM15+. *Earth Space Sci.*6, 1847–1864. doi: 10.1029/2019EA000658

Turnbull, J. W., Johnston, E. L., and Clark, G. F. (2021). Evaluating the social and ecological effectiveness of partially protected marine areas. *Conserv. Biol* 35(3), 921–932. doi: 10.1111/cobi.13677

Tyler, P. A., Baker, M., and Ramirez-Llodra, E. (2016). "Deep-Sea benthic habitats," in *Biological sampling in the deep Sea*. Eds. M. R. Clark, M. Consalvey and A. A. Rowden (New York:John Wiley & Sons Ltd,) , 1–15. doi: 10.1002/9781118332535.ch1

Våge, K., Pickart, R. S., Spall, M. A., Valdimarsson, H., Jónsson, S., Torres, D. J., et al. (2011). Significant role of the north icelandic jet in the formation of Denmark strait overflow water. *Nat. Geosci.*4, 723–727. doi: 10.1038/ngeo1234

Van Rossum, G., and Drake, F. L. (2009). *Python 3 reference manual* (Scotts Valley, California, USA: Createspace Independent Pub).

Vasquez, M., Mata Chacón, D., Tempera, F., O'Keeffe, E., Galparsoro, I., Sanz Alonso, J. L., et al. (2015). Broad-scale mapping of seafloor habitats in the north-east Atlantic using existing environmental data. *J. Sea Res.*100, 120–132. doi: 10.1016/j.seares.2014.09.011

Verfaillie, E., Degraer, S., Schelfaut, K., Willems, W., and Van Lancker, V. A. (2009). A protocol for classifying ecologically relevant marine zones, a statistical approach. *Estuarine Coast. Shelf Sci.*83, 175–185. doi: 10.1016/j.ecss.2009.03.003

Visalli, M. E., Best, B. D., Cabral, R. B., Cheung, W. W. L., Clark, N. A., Garilao, C., et al. (2020). Data-driven approach for highlighting priority areas for protection in marine areas beyond national jurisdiction. *Mar. Policy*122, 103927. doi: 10.1016/j.marpol.2020.103927

Waldron, A., Adams, V., Allan, J., Arnell, A., Asner, G., Atkinson, S., et al. (2020). *Protecting 30% of the planet for nature: costs, benefits and economic implications. working paper analysing the economic implications of the proposed 30% target forareal protection in the draft post-2020 global biodiversity framework*.

Watling, L., Guinotte, J., Clark, M. R., and Smith, C. R. (2013). A proposed biogeography of the deep ocean floor. *Prog. Oceanog.*111, 91–112. doi: 10.1016/j.pocean.2012.11.003

Wei, C-L, Rowe, G. T., Escobar-Briones, E., Boetius, A., Soltwedel, T., Caley, M. J., et al. (2010). Global Patterns and Predictions of Seafloor Biomass Using Random Forests. *PLoS ONE* 5 (12), e15323. doi: 10.1371/journal.pone.0015323

Weiss, A. (2001)Topographic position and landforms analysis. In: *The nature conservancy*. Available at: http://www.jennessent.com/downloads/tpi-poster-tnc_18x22.pdf (Accessed May 2021).

Wessel, P., Luis, J. F., Uieda, L., Scharroo, R., Wobbe, F., Smith, W. H. F., et al. (2019). The generic mapping tools version 6. *Geochem. Geophys. Geosystems*20, 5556–5564. doi: 10.1029/2019GC008515

Whickham, H. (2016). *ggplot2: Elegant graphics for data analysis* (New York, USA: Springer-Verlag).

Yesson, C., Clark, M. R., Taylor, M., and Rogers, A. D. (2011a). *Lists of seamounts and knolls in different formats* (PANGAEA). doi: 10.1594/PANGAEA.757564

Yesson, C., Clark, M. R., Taylor, M., and Rogers, A. D. (2011b). The global distribution of seamounts based on 30 arc seconds bathymetry data. *Deep Sea Res. Part I: Oceanog. Res. Papers*58, 442–453. doi: 10.1016/j.dsr.2011.02.004

Yu, Y., Chao, B. F., Garcia-Garcia, D., and Luo, Z. (2018). Variations of the Argentine gyre observed in the GRACE time-variable gravity and ocean altimetry measurements. *J. Geophysical Res. Oceans* 123(8), 5375–87. doi: 10.1029/2018JC014189

Zeng, C., Rowden, A. A., Clark, M. R., and Gardner, J. P. A. (2020). Species-specific genetic variation in response to deep-sea environmental variation amongst vulnerable marine ecosystem indicator taxa. *Sci. Rep.*10, 2844. doi: 10.1038/s41598-020-59210-0

Zeppilli, D., Pusceddu, A., Trincardi, F., and Danovaro, R. (2016). Seafloor heterogeneity influences the biodiversity–ecosystem functioning relationships in the deep sea. *Sci. Rep.*6, 26352. doi: 10.1038/srep2635

frontiers | Frontiers in Marine Science

TYPE Original Research
PUBLISHED 13 September 2022
DOI 10.3389/fmars.2022.941793

OPEN ACCESS

EDITED BY
Albertus J. Smit,
University of the Western Cape,
South Africa

REVIEWED BY
Fannie W. Shabangu,
Department of Forestry, Fisheries and the Environment, South Africa
Yoko Mitani,
Kyoto University, Japan

*CORRESPONDENCE
Lea-Anne Henry
L.Henry@ed.ac.uk

SPECIALTY SECTION
This article was submitted to Deep-Sea Environments and Ecology, a section of the journal Frontiers in Marine Science

RECEIVED 11 May 2022
ACCEPTED 23 August 2022
PUBLISHED 13 September 2022

CITATION
Narganes Homfeldt T, Risch D, Stevenson A and Henry L-A (2022) Seasonal and diel patterns in singing activity of humpback whales migrating through Bermuda. *Front. Mar. Sci.* 9:941793. doi: 10.3389/fmars.2022.941793

Seasonal and diel patterns in singing activity of humpback whales migrating through Bermuda

Tamara Narganes Homfeldt[1,2], Denise Risch[3], Andrew Stevenson[4] and Lea-Anne Henry[2*]

[1]Department of Migration, Max Planck Institute of Animal Behavior, Radolfzell, Germany, [2]School of GeoSciences, University of Edinburgh, Edinburgh, United Kingdom, [3]Scottish Association for Marine Science, Oban, United Kingdom, [4]Whales Bermuda, Pembroke, Bermuda

Humpback whales (*Megaptera novaeangliae*) produce song and non-song vocalisations, which allows their presence to be detected through passive acoustic monitoring. To determine the seasonal and diel acoustic presence and acoustic behaviour of humpback whales at the migratory stopover site off Bermuda, three hydrophones were deployed between March 2018 and April 2019 on Challenger Bank and the Bermuda platform. Song was the predominant vocalisation type encountered, with 65% of song recordings containing whale chorus and a clear seasonal trend of humpback whale occurrence in the spring and winter months from late December to mid-May. A strong diel pattern in singing activity was detected. Singing activity significantly increased at night relative to the daytime ($p<0.01$), whilst twilight periods were characterised by intermediate levels of singing. The song structure encountered in spring 2018 consisted of 18 units, 6 themes and 5 transitional phrases. The high occurrence of whale chorus and the strong seasonal and diel patterns of male humpback whale singing activity highlights the importance of Bermuda not just on their northward migration during spring, as described historically, but also on their southward migration during winter. Bermuda therefore constitutes a two-way migratory stopover site for humpback whales. The present study also provides Bermuda's planning authorities with better constraints on the duration and intensity of anthropogenic activities in these waters.

KEYWORDS

North Atlantic humpback whale, Bermuda, song, seasonality, diel pattern, passive acoustic monitoring, management

Introduction

Humpback whales (*Megaptera novaeangliae*) are one of the large baleen whales best known for their extremely variable vocal behaviour. "Song of the Humpback Whale", recorded off Bermuda in the 1950s by Frank Watlington, was the first recording of humpback whale song worldwide and initiated an era of humpback whale research off Bermuda throughout the 1960s and 1970s (Payne and Payne, 1985). While humpback whales produce unstructured non-song vocalisations year-round in different behavioural contexts (Silber, 1986; Dunlop et al., 2007; Rekdahl et al., 2015), humpback whale song is the most dominant vocal display of the species. Humpback whale song is displayed exclusively by males (Herman et al., 2013), and is thought to be a multi-message reproductive display (Murray et al., 2018) involved in both inter- (Smith et al., 2008) and intra-sexual interactions (Darling and Berube, 2001; Cholewiak et al., 2018b). However, the exact function of the song remains uncertain (Herman, 2017).

Humpback whale songs differ across ocean basins, due to the geographic isolation of the three recognised humpback whale subspecies (Baker et al., 1990; Bettridge et al., 2015; Cooke, 2018), and to some extent within an ocean basin, but are the same within a breeding population (Murray et al., 2012; Garland et al., 2013; Nikšić, 2014; Darling et al., 2019). Song is defined as a repetitive, stereotyped vocal display with a hierarchical structure (Payne and McVay, 1971; Cholewiak et al., 2013). A humpback whale "song" or "song cycle" is repeated for the duration of a "song session", i.e., the time period an individual whale sings continuously, which has been shown to last up to 22 hours (Winn and Winn, 1978). A song can be subdivided into a hierarchical order of several distinct "themes", each of which consists of repeated "phrases", which in turn consist of a sequence of individual "units" (Payne and McVay, 1971; Cholewiak et al., 2013). Along with songs produced by bowhead whales (*Balaena mysticetus*), humpback whale song is considered the most complex (Janik, 2009; Stafford et al., 2018). A population's song undergoes constant and progressive changes through time, a phenomenon referred to as song evolution (or song revolution in the case of sudden changes) (Winn and Winn, 1978; Payne and Payne, 1985; Noad et al., 2000; Garland et al., 2011; Garland et al., 2017).

North Atlantic humpback whales undertake extensive seasonal migrations between high latitude summer feeding grounds – off northern Norway and Iceland (referred to as eastern feeding grounds), as well as western Greenland, eastern Canada and the northeastern United States (referred to as western feeding grounds) – and low latitude winter breeding grounds around the West Indies and Cape Verde (Stevick et al., 2003; Reeves et al., 2004; Wenzel et al., 2009; Ruegg et al., 2013; Bettridge et al., 2015). However, fluke identification matches now suggest that the Caribbean breeding ground might be further subdivided, as humpback whales wintering in the southeast Caribbean are behaviourally distinct from those wintering in the northwest Caribbean, in two ways (Stevick et al., 2016). First, humpback whales winter in the northwestern Caribbean between January–April with peaks between February–March, while those wintering in the southeastern Caribbean do so a bit later between March–May with peaks in April (Charif et al., 2001; Stevick et al., 2003; Gandilhon, 2012; Stevick et al., 2018; Heenehan et al., 2019). Second, re-sightings of individuals revealed a strong tendency for southeastern Caribbean humpback whales to migrate to eastern North Atlantic feeding grounds, while whales from northwestern Caribbean breeding grounds tend to migrate to western feeding grounds (MacKay, 2015; Stevick et al., 2018), causing some genetical differentiation (partly due to feeding ground destination in humpback whales showing strong maternally-directed fidelity) (Baker et al., 1990; Palsboll et al., 1995; Weinrich, 1998). However, some individuals have been matched between Cape Verde and the southeastern Caribbean, as well as between the southeastern and northwestern Caribbean, demonstrating that the population units and boundaries are not as clear as previously thought (Stevick et al., 2016; MacKay et al., 2019). While the western North Atlantic humpback whale population has been increasing in recent years after the cessation of whaling, the Cape Verde population is still of considerable concern (Wenzel et al., 2020).

Although historically believed to exclusively occur on breeding grounds (Winn and Winn, 1978), humpback whale song has been increasingly recorded on their feeding grounds during the breeding season, which suggests that some males may not migrate at all but instead remain year-round in their feeding grounds (Mattila et al., 1987; Vu et al., 2012; Baumgartner et al., 2019; Magnúsdóttir and Lim, 2019; Kowarski et al., 2021; Tyarks et al., 2021). In the North Atlantic, humpback whales start singing in early autumn (around September) and continue singing through winter, stopping in late spring (around June) (Mattila et al., 1987; Vu et al., 2012; Kowarski et al., 2019; Kowarski et al., 2021). Transitions between song and "non-song" periods at the start and end of summer are dominated by "song fragments", i.e., only a short part of the complete song is sung (Mattila et al., 1987; Vu et al., 2012; Kowarski et al., 2019; Kowarski et al., 2021). The seasonal singing behaviour displayed by males is thought to underlie a hormonally triggered physiological mechanism (Wright and Walsh, 2010; Vu et al., 2012), as the males' testosterone levels are the lowest during the summer months and highest during the winter months, i.e., during the breeding season (Cates et al., 2019). Thus, song fragments could be the result of spring decreases and autumnal increases in testosterone levels (Cates et al., 2019; Kowarski et al., 2019).

Notably, most of what is known about North Atlantic humpback whales and their vocalisations has come from coastal studies on feeding and breeding grounds. Thus, their migration routes and mid-ocean behaviours, including

vocalisations, with the exception of a few studies tracking individual whales with satellite tags (Kennedy et al., 2014; Kennedy and Clapham, 2017), remain vastly understudied or unknown (Reeves et al., 2004; MacKay, 2015; Kowarski et al., 2018). Bermuda, being an oceanic migratory stopover site for North Atlantic humpback whales on their northward migration (Payne and McVay, 1971; Stone et al., 1987; Stevenson and Stevick, 2009), provides a unique opportunity to study vocalisations of migrating humpback whales. Individuals observed off Bermuda have been re-sighted in the northwestern Caribbean breeding grounds and to a much lesser extent in the southeastern Caribbean, as well as, in all major feeding grounds (with the exception of Norway) (Stone et al., 1987; Beaudette et al., 2009; Stevenson, 2010; MacKay, 2015; Stevenson, unpublished data), but predominantly in western North Atlantic feeding grounds (Stone et al., 1987; Beaudette et al., 2009; Kennedy et al., 2014). Thus, the waters around Bermuda most likely represent an oceanic migratory stopover site between the northwestern Caribbean breeding grounds and higher latitude western feeding grounds. While in Bermuda, humpback whales have been observed to linger for several days whilst aggregating into large groups, accompanied by male singing (Payne and McVay, 1971; Payne and Payne, 1985; Stevenson, 2011), before continuing their northward migration.

Recordings of humpback whales off Bermuda led to the first formal description and definition of humpback whale song (Payne and McVay, 1971), which is now fundamental to the field of humpback whale song research. However, there has been no acoustic recording or analysis of whale vocalisations in Bermuda since 1976 (Winn and Winn, 1978; Payne and Payne, 1985) and these initial studies did not use long-term Passive Acoustic Monitoring (PAM) deployments that permit year-round data collection (under all weather conditions and overnight) of the marine soundscape and therefore year-round acoustic detection of vocal species like humpback whales (Johnson et al., 2009; Rafter et al., 2018). Thus, in stark contrast to a good baseline knowledge of the seasonal occurrence of humpback whale vocalisations from North Atlantic feeding and breeding grounds, the acoustic presence of humpback whales at their stopover site off Bermuda has not yet been analysed.

Such knowledge on the temporal presence of whales off Bermuda is urgently needed to address potential threats posed by increasing human activities. The Government of Bermuda has enacted some protection for humpback whales under its Fisheries Act 1972 (Government of Bermuda, 1978) and its Protected Species Act 2003 (Government of Bermuda, 2003; Minister of Health Seniors and Environment, 2016) and there are voluntary whale-watching guidelines (Department of Environment and Natural Resources, 2017). Bermuda's Exclusive Economic Zone (EEZ) is also an important migratory corridor and stopover location for various cetacean species (Klatsky et al., 2007; Hallett, 2011; Hoyt, 2011) and was designated as a Marine Mammal Sanctuary but this designation only offers data-sharing opportunities and comes with no management or protection measures (NOAA and Government of Bermuda, 2012). With Bermuda becoming popular as a megafauna "hotspot", as a cruise destination and sites for various international sporting events, the tourism industry including the whale-watching industry (O'Connor et al., 2009) is anticipated to further develop in line with Bermuda's six-year National Tourism Plan 2015–2023 (Bermuda Tourism Authority, 2019). New legislation under the Superyachts and Other Vessel (Miscellaneous) Act 2019 now also allows more large yachts (>24 meters length) to secure cruising and charter permits. Thus, growth in Bermuda's tourism industry will increase vessel traffic of all kinds (cruise liners, freight, superyachts, whale-watching boats and smaller recreational craft).

Increased vessel traffic and marine tourism can have various negative impacts on humpback whales, from behavioural disturbance, increased stress levels and physical injuries, to disturbing their crucial auditory sensory system and communication (Au and Green, 2000; Cholewiak et al., 2018a; Fiori et al., 2020; Sprogis et al., 2020; Currie et al., 2021). Humpback whales produce low to mid frequency vocalisations (ranging from 0.01-28 kHz), but like all baleen whales most energy is produced in the lower frequencies (below 2 kHz), which can propagate across an entire ocean basin (Payne and Webb, 1971; Hannay et al., 2013; Cerchio et al., 2014; Huang et al., 2016; Cholewiak et al., 2018a; Davis et al., 2020). However, vessel-generated noise, the most prevalent anthropogenic underwater noise (Cato, 2014), overlaps in frequency (Clark et al., 2009; Rolland et al., 2012) and thus interferes with the acoustic detection of mysticetes non-song and song vocalisations ("masking") (André, 2018; Dooling and Leek, 2018) and reduces the distance over which they are able to acoustically communicate (Clark et al., 2009; Rolland et al., 2012; Cato, 2014; Cholewiak et al., 2018a; Dunlop, 2019). Thus, to mitigate impacts of increased anthropogenic noise levels on humpback whales migrating through Bermuda, knowledge of spatiotemporal patterns of humpback whale presence and vocalisations needs to be gathered and integrated by ocean planners and authorities into planning and management scenarios and decisions for sustainable developments.

The present study is the first long-term PAM study of humpback whale vocalisations in Bermuda. The aim is to investigate their seasonal and diel acoustic presence and acoustic behaviour at this migratory stopover site. To facilitate future comparisons of song structures across the North Atlantic, as well as within Bermuda (determining inter-annual song variation), the song structure encountered in spring 2018 will be described in detail at the unit, phrase and theme level.

Materials and methods

Study area and acoustic data collection

Bermuda forms part of a small mid-ocean seamount chain of volcanic origin rising abruptly from the deep abyssal plain of the Sargasso Sea (Figure 1) (Stone et al., 1987; Vogt and Jung, 2007). Besides the topographic highs of the inhabited Bermuda platform, Bermuda's EEZ has three large submerged seamounts, which are known for their high biodiversity: Bowditch Seamount, Challenger Bank (CB) and Plantagenet Bank (Figure 1) (Vogt and Jung, 2007; Hallett, 2011). CB and Sally Tucker (ST; located at the southwest edge of the Bermuda platform), which are 13 km apart, were chosen as recording sites for the present study (Figure 1).

Two Autonomous Multichannel Acoustic Recorders (AMAR G3A; JASCO Applied Sciences) equipped with M36-V35-100 omnidirectional hydrophones (-165 ± 4 dB re 1 V/µPa sensitivity) (Supplementary Figure 1) were deployed from 31 March to 6 September 2018 on CB at a water depth of 45.7 m at 32.08746, -65.05373 and from 31 March to 10 September 2018 on ST at a water depth of 40.2 m at 32.19605, -64.99133. The AMARs were programmed to record 30 minutes of every hour. Another AMAR equipped with M36-V35-900 omnidirectional hydrophone (-165 ± 4 dB re 1 V/µPa sensitivity) was deployed on CB at a water depth of 47.7 m from 10 September 2018 to 23 April 2019 at 32.08725, -65.05386, and programmed to record 30 minutes every 75 minutes. All three hydrophones located on the seafloor recorded 29 minutes at a sampling rate of 16 kHz (24 bit resolution) and 1 minute at a sampling rate of 250 kHz (16 bit resolution). These sampling rates were chosen to detect the lower frequency vocalisations of baleen whales (Kowarski et al., 2018), as well as high-frequency clicks and whistles produced by toothed whale (Edds-Walton, 1997). For the present study, only the 29-minute recordings were analysed. Due to technical failure of the recording device, recordings from 20 September 2018 to 1 November 2018 were not usable. The AMARs were retrieved from anchors using an acoustic release (Supplementary Figure 1).

Acoustic analysis

All recordings were manually scanned for humpback whale sounds using spectrograms generated with Raven Pro 1.6 sound analysis software (fast Fourier transformation [FFT] size: 2048 points, 75% overlap, Hann window, frequency resolution: 7.8 Hz, time resolution: 32 ms) (Center for Conservation Bioacoustics, 2019). As most humpback whale vocalisations are detected below 2 kHz (Silber, 1986; Cerchio et al., 2014; Huang et al., 2016), the 29-minute-long recordings were viewed zooming into the frequency band of 0–2 kHz.

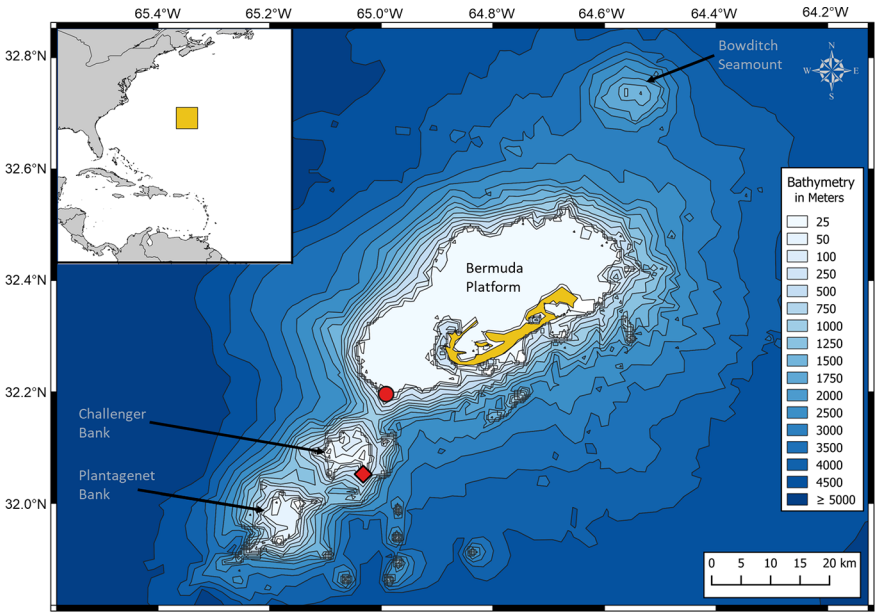

FIGURE 1
Map of the study area, showing Bermuda (in yellow) and the three seamounts Bowditch Seamount, Challenger Bank and Plantagenet Bank. The three hydrophones were deployed on Challenger Bank (red rhombus) and Sally Tucker (red circle), which are 13 km apart. The map was created in QGIS 3.2 software (QGIS Development Team, 2016) using the coordinate reference system WGS 84, EPSG: 4326 and a world (source: Natural Earth) and bathymetry map (source: Open Digital Elevation Model, 2019).

Every 29-minute recording was first scanned for humpback whale song. If no song was detected then the recording was re-scanned for other humpback whale vocalisations (non-song vocalisations) to capture the acoustic presence of whales, in absence of song. Each recording was classified into one of three whale sound categories: song (song fragments were also allocated to this category), calls, and no vocalisation.

Second, all recordings allocated to the song category were re-analysed to assess the minimum number of singing whales ("singers") per hour. Spectrograms of song-containing recordings were scanned for the first 10 minutes (Cerchio et al., 2014; Cholewiak et al., 2018b) of song detection to determine the highest number of overlapping singers in that period. Number of singers was determined by visually counting (i) overlapping units, (ii) overlapping phrases and (iii) differences in sound intensity (Cerchio et al., 2014; Magnúsdóttir and Lim, 2019) from the spectrogram (Figure 2). This is because song structures overlapping in time cannot be produced by the same whale and therefore indicate the number of simultaneously singing whales at one moment in time (Magnúsdóttir and Lim, 2019), while sounds of different intensities indicate multiple vocalising whales at different distances from the hydrophone (Cerchio et al., 2014). Up to five simultaneously singing whales could be differentiated confidently in the present dataset. Therefore, every recording was allocated the minimum number of simultaneous singers, ranging from 0 to 5 (Figure 2). In instances where five or more singers were detected, they could not be further differentiated and were allocated the category "5".

Third, all 29-minute recordings where only one whale was singing one entire song cycle were graded into low, medium, and high-quality recordings (Supplementary Figure 2). Only recordings in the high-quality category were considered for the detailed 2018 Bermuda song description. To ensure consistency throughout the acoustic analysis, all recordings were analysed and categorised into vocalisation type, number of singers and quality by a single person (the first author).

Analysis of seasonal and diel patterns in singing activity

Temporal patterns of humpback whale song based on the numbers of singing whales were statistically analysed in R version 3.6.2 (R Core Team, 2019), with figures created using the R-package ggplot2 (Wickham, 2016). To explore diel

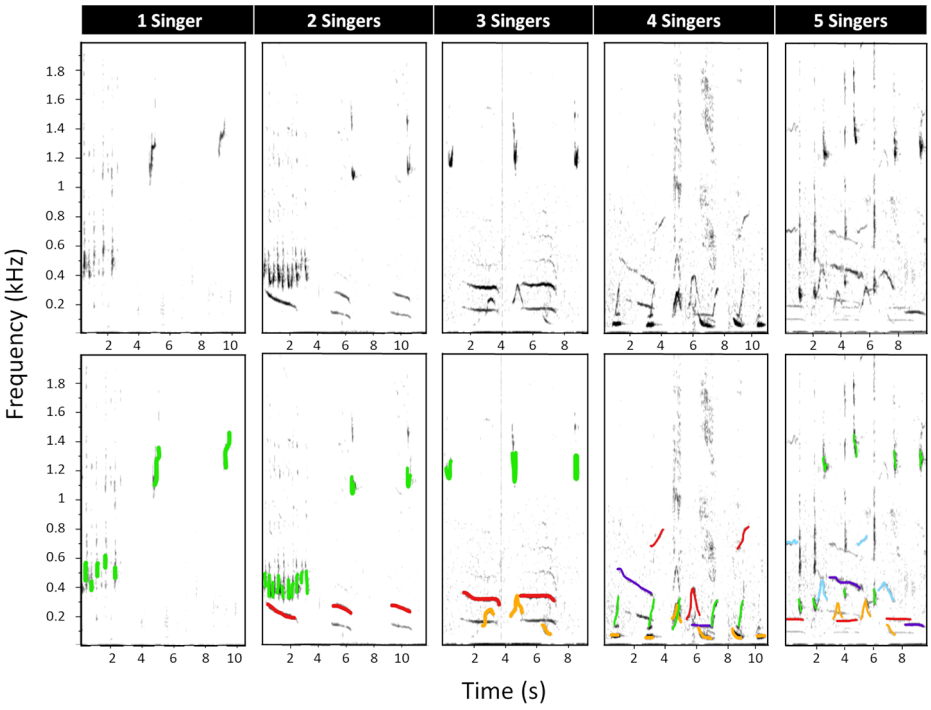

FIGURE 2
Spectrograms of multiple humpback whales signing, showing five different recordings that vary in their number of simultaneously singing humpback whales. In the lower panel, every singer has been allocated a colour to visualise overlapping units and/or overlapping phrases. Only the fundamental units were coloured. Differences in sound intensity can be seen in the upper panel by the darkness of a unit. Spectrogram parameters: fast Fourier transform (FFT) size = 2048 points, overlap = 75%, sample rate = 16000 Hz, frequency resolution = 7.8 Hz and time resolution = 32 ms.

patterns, the entire dataset was shifted to Atlantic Standard Time (UTC -4, Bermudas standard time zone) and every day was split into four light conditions in accordance with previous studies (Cholewiak, 2008; Kowarski et al., 2018; Ryan et al., 2019): nighttime, dawn, daytime and dusk. To accommodate for the variation in day and night length over the study period, the corresponding time intervals defined by nautical dawn, sunrise, sunset and nautical dusk were determined separately for each day. The four variables were obtained from https://www.timeanddate.com/ (Time and Date, 2019a) and uniformly transformed to UTC -4. Then, the 29-minute-long audio files recorded during the around one-hour long dawn and dusk periods were allocated to the appropriate light level and the remaining recordings to the daytime or nighttime category accordingly. To further explore seasonal patterns, the entire study period was split into astronomical seasons, i.e., as defined by equinoxes and solstices (Time and Date, 2019b), giving rise to four datasets: ST-spring-2018, CB-spring-2018, CB-winter-2018/19 and CB-spring-2019.

Statistical analysis of diel patterns in singing activity focussed exclusively on days with song-containing recordings. As humpback whale songs can be detected over greater distances than the distance between CB and ST (Cholewiak et al., 2018a), we cannot exclude that individual whales were recorded simultaneously during overlapping time frames between the two sites. Given the unequal sample sizes between the light categories and seasons, the data not being normally distributed and the spring 2018 datasets potentially being dependent of each other, each dataset was analysed individually with a non-parametric Kruskal-Wallis test to determine if the mean number of singing whales significantly differed between different light conditions, to determine any diel variation. Consequently, Bonferroni *post-hoc* tests were conducted to identify specific pairs of conditions that differed.

Humpback whale song description

Phrase and theme allocation in humpback whale song analysis is most often conducted through the subjective manual analysis of spectrograms (Cholewiak et al., 2013; Nikšić, 2014; Garland et al., 2017; Magnúsdóttir, 2017; Hauer-Jensen, 2018). Thus, it is recommended to base the song description on the review of multiple song recordings from different individuals (Cholewiak et al., 2013). Only the CB recordings from spring 2018 were used for the song description. By going through every song-containing recording (n = 777) in detail to determine the number of singers, the typical song structure became rapidly evident. Seven high-quality song recordings (Narganes Homfeldt et al., 2022), each around a week apart from the next, were chosen to describe the song in more detail. This interval was chosen to minimise the chances of describing the vocal display of the same individual (Kowarski et al., 2019; Magnúsdóttir and Lim, 2019), given that some individuals are sighted for eight consecutive days off Bermuda (Stevenson, 2011). The methodology to describe the songs generally followed approaches adopted in previous humpback whale song analyses (Nikšić, 2014; Garland et al., 2017; Magnúsdóttir, 2017; Darling et al., 2019; Kowarski et al., 2019) and is summarised below.

The seven songs were viewed as spectrograms (FFT size: 2048 points, 75% overlap, Hann window, frequency resolution: 7.8 Hz, time resolution: 32 ms) and each full song cycle was delineated at the unit and phrase level, based on aural and visual spectrographic characteristics. Distinct units and phrases were identified and allocated an alphanumeric code: units (a,b,c); phrases (1,2,3). As a theme is defined as a repeated sequence of the same or similar phrases (Payne and McVay, 1971; Cholewiak et al., 2013; Magnúsdóttir, 2017), themes were allocated the same numerical code as the phrase type it contained, e.g., phrase 1 is repeated within theme 1. The identified characteristic unit sequences were then grouped into phrases and phrase types into themes. Any natural variation in the characteristic unit sequences through addition, deletion or replacement of individual units within a phrase that would generate imperfect replicas of a phrase type (Payne and McVay, 1971; Cholewiak et al., 2013) were considered to be the same phrase type. In addition, there were "transitional phrases", which are sometimes encountered at the transition between two subsequent themes and contain units from both themes (Payne and Payne, 1985; Garland et al., 2017). For example, a transitional phrase between themes 2 and 3 would be referred to as phrase 2/3. All seven songs were transcribed into alphanumerical sequences to facilitate the identification of the songs' theme order.

Given the subjective nature of the song delineation process, Cholewiak et al. (2013) advised to support the alphanumerical classification with exemplar spectrograms to illustrate at least part of the song structure to the humpback whale song research field. Thus, in the present study, exemplars of the identified unit, phrase and theme order were illustrated (see Results).

Results

The present study analysed a total of 347 days of continuous recording [excluding a 43-day period with no available recordings (Figure 3)] from 2018 and 2019 across two locations off Bermuda, scanning a total of 5417 hours of acoustic data for humpback whale vocalisations. Besides humpback whale song and non-song vocalisations, an unusually long, tonal baleen whale vocalisation, lasting for 18-seconds, was detected in the presence of multiple humpback whale singers (Supplementary Figure 3). Also, other biotic sounds emitted by dolphins (and possibly other cetacean

10.3389/fmars.2022.941793

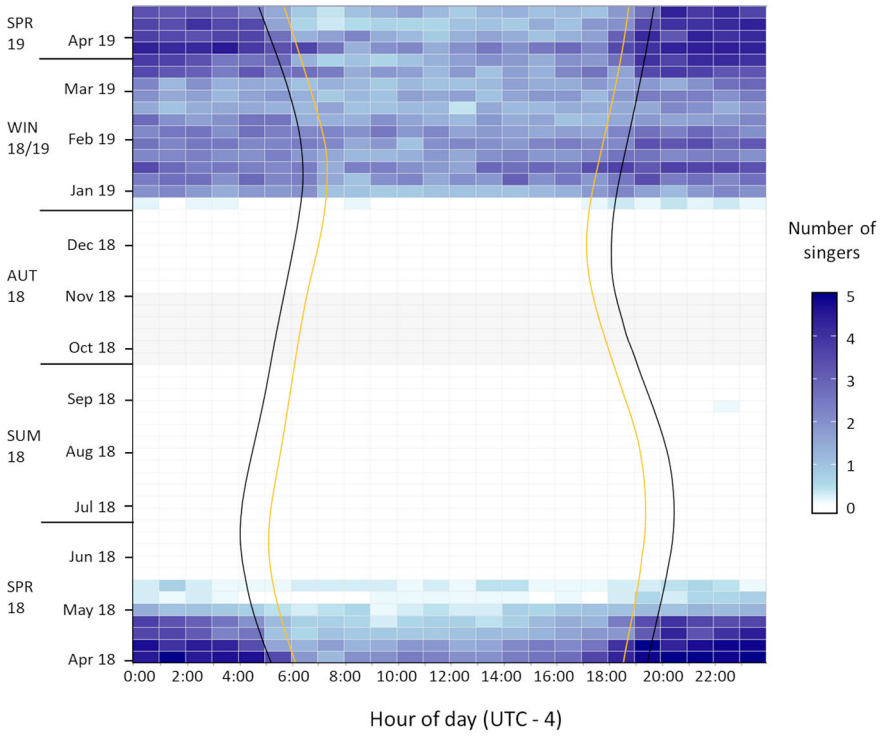

FIGURE 3
Seasonal occurrence and diel pattern of humpback whale song on Challenger Bank encountered across 55 weeks between 2018 and 2019. Sunset to sunrise (yellow lines) defines daytime, dusk to dawn (black lines) defines nighttime and the two remaining time intervals define the twilight periods. Grey shaded fields indicate no available recordings due to technical failure of the recording device.

species), fish and invertebrates, as well as anthropogenic sounds from vessels and echosounders, were regularly detected in recordings.

Seasonality of vocalisations and singing activity

Humpback whale vocalisations were heard in 32% (1733 h) of recordings. All acoustic detections occurred on 48% (166 days) of recording days, whereby social calls were only detected on days when song, the predominant vocalisation type (97%), was present too. Thus, non-song vocalisations were neglected for determining the seasonality of humpback whale vocalisations. Humpback whales were exclusively heard between 31 March (start of study) and 19 May 2018 (across both sites), as well as 26 December 2018 and 23 April 2019 (end of study) (Figure 4). There was one exception on 31 August 2018 (Figure 3) when a single song fragment was documented on CB. Overall, acoustic presences across the three deployments indicated a clear seasonal trend of humpback whale occurrence off Bermuda in the spring and winter months, ranging from late December to mid-May, hereafter referred to as "whale season" (Figures 3, 4). Notably, 65% of song recordings contained whale chorus (≥ 2 singers).

Singing activity, as quantified by the numbers of simultaneously singing whales, starts in late December and reaches the daily average across the whale season (1.7 ± 1.5 singers) quite quickly (Figure 4). The daily averages of simultaneously singing whales recorded at CB during the two spring seasons (1.921 ± 1.385 singers) and the winter season (1.926 ± 1.388 singers) were nearly identical, indicating that the intra-seasonal variation might be bigger than inter-seasonal variation. By mid-February to early March, fewer male humpback whales were recorded singing (Figures 3, 4). The highest average number of singers was detected in January, March and early April (in both 2018 and 2019 data) (Figure 4). In May, consecutive recordings were often characterised by a single singer and similar intensities, which likely represent a single male's song session lasting several hours. Thus, although still singing for most hours of the day, the acoustic density of singing males fell below daily average in late April and ceased entirely by mid-May (Figures 3, 4). Days without song presence during the whale season only occurred at the start (27

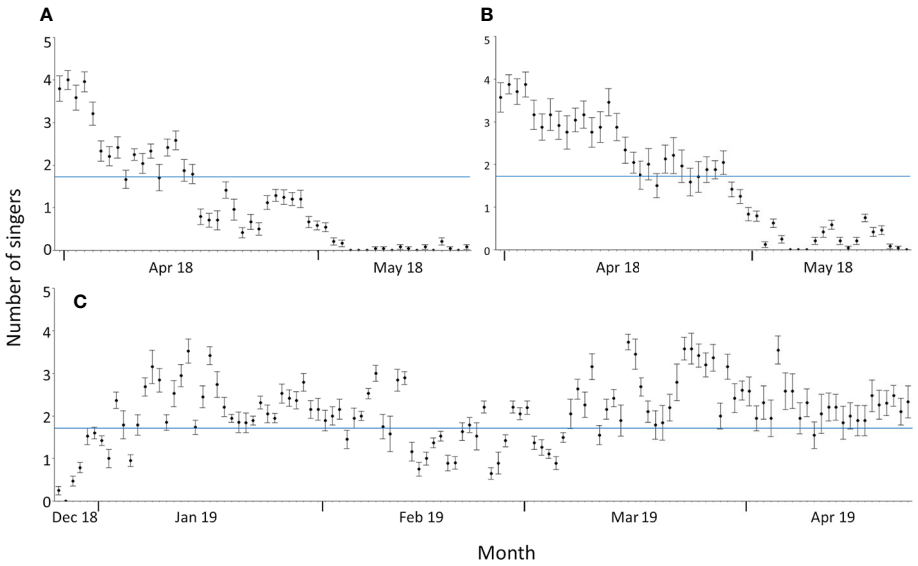

FIGURE 4
Daily mean number of singers during the whale season at Sally Tucker **(A)** and Challenger Bank between 31 March and 19 May 2018 **(B)** and between 26 December 2018 and 23 April 2019 **(C)**. Error bars are ± 1 standard error. The average number of singers across the entire whale season (1.73 singers; blue line) is illustrated as a reference.

December 2018) and end of the whale season at both CB (5-7 and 19 May 2018) and ST (5-7, 10, 13, 15, 18 May 2018) (Figure 4).

ST and CB showed broadly similar patterns in singing activity in spring 2018 (Figure 4). The concentration of singers was higher at CB, with the last humpback whale song being recorded on 18 May 2018, whilst singing activity at ST had already decreased below average by mid-April, with the last humpback whale song being recorded on 19 May 2018 (Figure 4). Therefore, humpback whale singing activity in Bermuda showed a strong seasonal pattern in the spring and winter months but with reduced activity towards the start and end of the whale season, as well as mid-season from February to early March.

Diel patterns in singing activity

Throughout the whale season moderate singing activity was detected during daylight hours and high levels of whale chorusing during the night (Figure 3). A statistically significant difference in the mean number of singing whales was detected between light conditions for all four datasets (Kruskal-Wallis; ST-spring-2018: χ^2 = 13.9; df = 3; p = 0.003; CB-spring-2018: χ^2 = 27.2; df = 3;

p = 5.4 x 10 $^{-6;}$ CB-winter-2018/19: χ^2 = 26.7; df = 3; p = 6.7 x 10 $^{-6}$; CB-spring-2019: χ^2 = 55.0;

df = 3; p = 6.9 x 10 $^{-12}$), with the number of singers being significantly lower during daytime than nighttime (ST-spring-2018: p = 0.0011; CB-spring-2018: p = 3.5 x 10 $^{-5}$; CB-winter-2018/19:

p = 7.7 x 10 $^{-7}$; CB-spring-2019: p = 2.1 x 10 $^{-11}$) (Figure 5). At CB, the number of singers across the seasons was also significantly lower during dawn than nighttime (CB-spring-2018: p = 0.013; CB-winter-2018/19: p = 0.013; CB-spring-2019: p = 0.0053) (Figure 5). In both spring seasons at CB there was a significantly lower number of singers during daytime than dusk (CB-spring-2018:

p = 6.5 x 10 $^{-4}$; CB-spring-2019: p = 6.5 x 10 $^{-6}$) and in spring 2019 during daytime than dawn

(p = 3.3 x 10 $^{-5}$) (Figure 5). Across all datasets the mean number of singers during the twilight periods did not differ significantly from each other (Figure 5). In addition, the single song fragment encountered in late August was also recorded during nighttime (Figure 3). Therefore, humpback whale singing activity in Bermuda showed a diel pattern across spring and winter months with significantly increased singing at night relative to the daytime and with twilight periods characterised by intermediate levels of singing (Figures 3, 5).

Song structure

The detailed analysis of the seven humpback whale songs that were transcribed at the unit and phrase level contained 14

10.3389/fmars.2022.941793

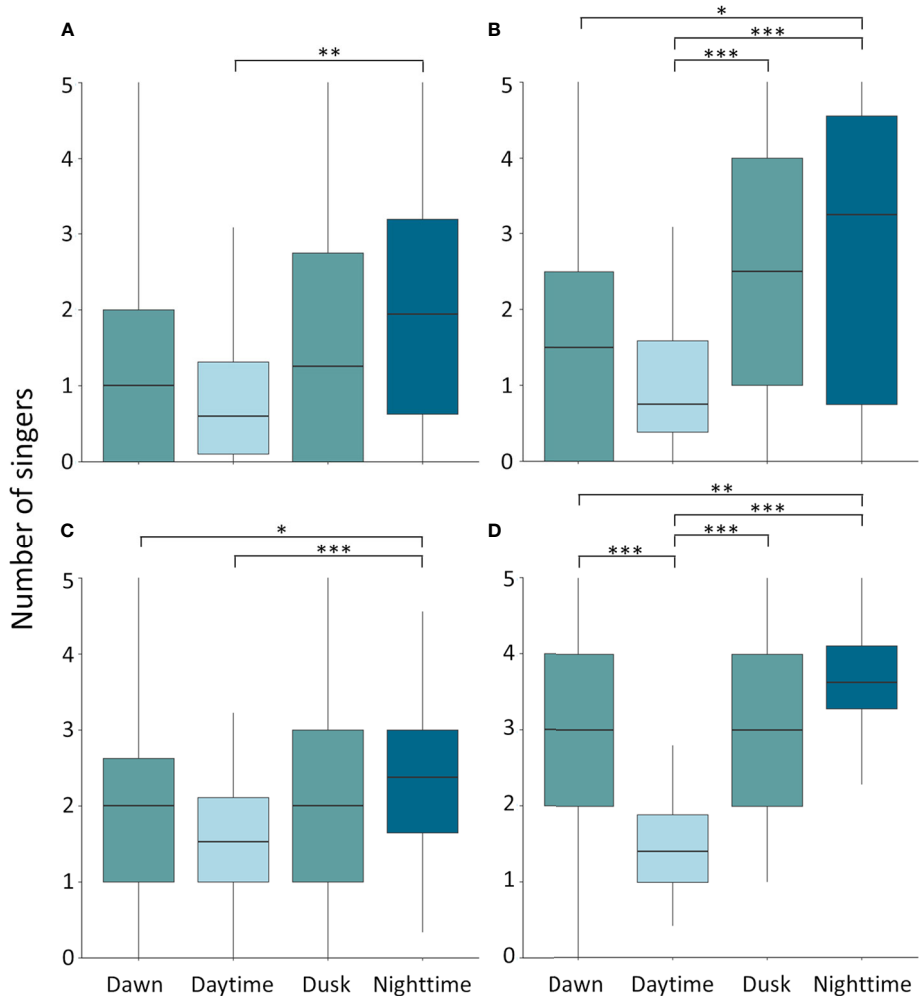

FIGURE 5
Diel patterns of humpback whale singing activity at Sally Tucker in spring 2018 **(A)** and Challenger Bank in spring 2018 **(B)**, winter 2018/19 **(C)** and spring 2019 **(D)**. The median number of singers (horizontal black line) varied significantly between daytime and nighttime in all four datasets. Boxes indicate the interquartile range and the vertical lines indicate the range of daily averages in the number of singers. Significance levels are illustrated with stars (*p < 0.05; **p < 0.01; ***p < 0.001).

full song cycles (Supplementary Table 1). The coded songs revealed the stereotypical song structure of the whales migrating through Bermuda in spring 2018, consisting of: 18 distinctive unit types (Supplementary Figure 4), making up 6 phrase types and consequently 6 themes, and 5 transitional phrases (Table 1; Figure 6).

Every song cycle, even from the same individual, showed small unit variations within the same phrase type. These variations were still considered the same phrase and thus part of the same theme (Table 1). In particular, units b, c, f, p, q seemed to act as synonyms and be interchangeable to some extent within various phrase types (Table 1). Also, the amount of unit repetitions within the same phrase sequence varied (Supplementary Table 1).

All seven whales sung the theme order: 1-1/2-2-2/3-3-3/4-4-4/5-5-5/1-1 (Figure 6), which repeated itself through various song cycles (Supplementary Table 1). However, in 4 of the 14 analysed song cycles, although the transitional phrases 2/3 and 3/4 occurred, phrase 3 was not sung (Supplementary Table 1). Every song cycle contained the five transitional phrases once, while the non-transitional phrase types were repeated to a varying extent, even within an individual's song session (Supplementary Table 1). This variation in phrase repetitions resulted in a large range of song cycle duration, ranging from 4.05 to 16.15 min for the same theme frequency (Supplementary Table 1).

Notably, phrase 6, the only phrase containing unit m (Table 1), was only sung by three of the seven whales (on 27

TABLE 1 Unit sequences of phrase types.

Phrase Type	Characteristic Unit Sequence	Derived Unit Sequence (s)
1	acacde	c replaced by: bc; cb; p; q; cc - a + ac
1/2	acacdecg	c replaced by: bc; p; cc - a + h
2	fcg[h]	fc replaced by: cc; c; f; bc
2/3	fcg[i][jr]	fc replaced by: cc; bc - r
3	[i][jr]	- r
3/4	[i][jr][jrk]	+/- j; r; k
4	lk[jrk]	+/- j; r; k
4/5	l[o]	ln[o]
5	n[o]	
5/1	ncde	c replaced by: o; p + d
6	l[k[m]]	- k

Unit sequences derived from the characteristic unit sequences through unit replacement, deletion (-) or addition (+) were still allocated to the same phrase type. Square brackets ([]) indicate that the unit(s) were repeated multiple times before the following unit, phrase repetition or phrase type occurred. Every distinctive and characteristic unit sequence, represented by an alphabetical code, was allocated to a different phrase type and a corresponding numerical code. If unit sequences of two phrase types overlapped, the unit sequence was allocated as a transitional phrase (/).

April, 3 and 18 May), and two of these did not sing phrase 6 in every song cycle either (Supplementary Table 1). Phrase 6 either replaced phrase 4 or occurred after phrase 4, and was always followed by the transitional phrase 4/5 (Figure 6; Supplementary Table 1). All other phrases remained stable throughout the whale season.

Discussion

Vocalisations at Challenger Bank and Sally Tucker's

As all recordings obtained from the fixed AMARs contained high levels of singing activity throughout the whale season (Figures 3, 4), CB and ST seem to be an important singing habitat and stopover site for male humpback whales on their annual migrations. Seamounts with shallow summits like CB are generally known as hotspots for aggregations of migratory megafauna (Morato et al., 2008) and are considered important offshore habitats for humpback whales worldwide, on their breeding grounds but also as key sites along their trans-oceanic migration routes (Garrigue et al., 2015; MacKay, 2015; Derville et al., 2020). Garrigue et al. (2015) suggests that humpback whales visit seamounts on their migration to rest, to use them as navigational landmarks, and potentially as opportunistic feeding areas. These habitat uses could all be applicable to Bermuda (Stevenson, 2011). The Bermuda platform (ST), which is shallower and has calmer waters than CB, represents the typical protected nearshore habitat in which mother-calf pairs are frequently encountered in other regions (MacKay, 2015; Indeck et al., 2021). Although ST and CB thus might form different habitats for humpback whales, both locations showed a very similar pattern in singing activity in spring 2018 (Figure 4). However, singing activity was most prevalent at CB, which might indicate that the more sheltered waters of ST are visited less by male singers and might in fact be used more by mothers and calves (Stevenson, unpublished data).

Finally, the present study detected a long tonal vocalisation of unknown origin on 8 April 2018 within the presence of humpback whale chorus (Supplementary Figure 3). This type of vocalisation is not part of humpback whales' described call repertoire in either the North Pacific (Fournet, 2018), Southern Hemisphere (Dunlop et al., 2007; Recalde-Salas et al., 2020; Ross-Marsh et al., 2022) or the North Atlantic (Stimpert et al., 2011). The "long cry" as defined in the repertoire of humpback whales in Western Australia is typically only 3 seconds long (Recalde-Salas et al., 2020), compared to the 18-second-long cry documented in this present study (Supplementary Figure 3). Therefore, if produced by humpback whales, this very long cry could be a rare vocalisation (from calves, females and/or males), and may serve a highly specialised, but rarely required, function. Alternatively, it could have been emitted by another baleen species, such as Bryde's whale (*Balaenoptera edeni*), who are known for long moans that are in this range of duration (Rice et al., 2014) but who have not so far been recorded off Bermuda (Stevenson, unpublished data).

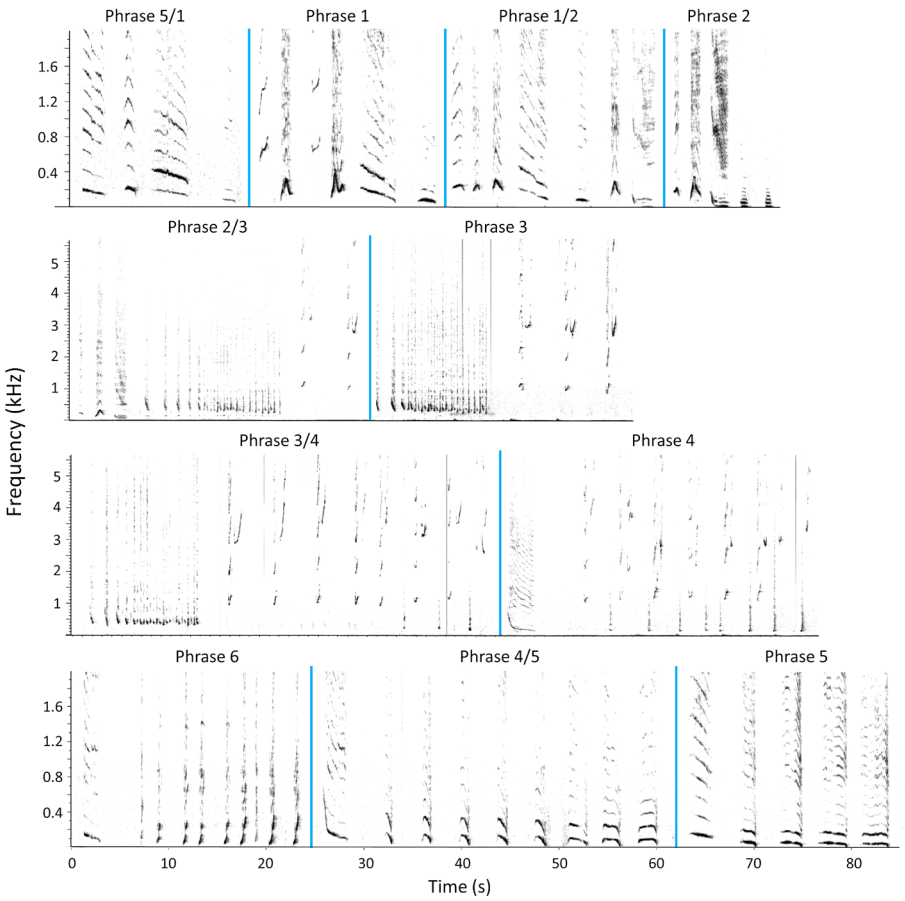

FIGURE 6
Humpback whale song type encountered in spring 2018 at Challenger Bank, Bermuda. A representative phrase for each theme and transitional phrase (/) is shown. The phrases are in cyclical order 5/1-1-1/2-2-2/3-3-3/4-4-6-4/5-5. Phrase 6 did not occur in every analysed song cycle. The vertical blue lines indicate divisions between phrase types. Spectrogram parameters: fast Fourier transform (FFT) size = 2048 points, overlap = 75%, sample rate = 16000 Hz, frequency resolution = 7.8 Hz and time resolution = 32 ms.

Seasonality and migration pattern

The present study identified a strong seasonal pattern of humpback whale singing activity, with a moderately high occurrence of chorusing whales, off Bermuda in the spring and winter months, ranging from late December to mid-May (Figure 3). This is in line with boat-based observations from Whales Bermuda (Stevenson and Stevick, 2009; Stevenson, 2011) and the historic records of humpback whales (Stone et al., 1987) and their songs being recorded off Bermuda in January, April and May (Payne and McVay, 1971; Payne and Payne, 1985). Fluctuations in numbers of singers throughout the spring and winter months (Figure 4) suggest that male humpback whales migrate through Bermuda in waves and do not stay for longer periods of time. This theory is supported by visual boat-based observations made by Whales Bermuda and studies showing North Atlantic humpback whales lingering for several days up to two weeks and aggregating around Bermuda before continuing their northward migrations in large groups (Payne and Payne, 1985; Stevenson, 2008; Stevenson and Stevick, 2009; Stevenson, 2011). Humpback whales overwintering in the northwestern Caribbean are sighted at their breeding grounds between January–April with peaks between February–March, while those wintering in the southeastern Caribbean do so a bit later between March–May with peaks in April (Charif et al., 2001; Stevick et al., 2003; Gandilhon, 2012; Stevick et al., 2018; Heenehan et al., 2019). In Bermuda, reduced singing activity was observed between mid-February to early March (Figures 3, 4), which is in line with the northwestern Caribbean peak. Detecting humpback whale song from late December onwards and to a lesser extent during the northwestern Caribbean peak breeding season (Figure 3), as well as the observed higher intra- than inter-seasonal variation in average number of singers, suggests that Bermuda, previously described as a one-way stopover on their northward migration during the spring months (Payne and McVay, 1971; Stone et al.,

1987; Stevenson and Stevick, 2009) also acts as a migratory stopover site on their southward migration during the winter months.

The humpback whales recorded in the present study could have migrated to and from either Caribbean breeding ground, given the temporal overlap in both breeding grounds. However, as Bermuda's whale season starts just before the northwestern Caribbean whale season and the northwestern peak aligns with reduced singing in Bermuda (Figure 3), it is more likely that humpback whales migrate to and from the northwestern Caribbean through Bermuda. Both, satellite-tagging (Kennedy et al., 2014) and fluke identification matches support this theory (Stone et al., 1987; Beaudette et al., 2009; MacKay, 2015). However, in 2017, humpback whales were heard singing until 13 May on the northwestern Caribbean breeding ground and until 27 May on the southeastern Caribbean breeding ground (Heenehan et al., 2019). Thus, it is possible, that humpback whales recorded towards the end of Bermuda's whale season (Figure 3) could also be originating from the southeastern breeding ground.

The single song fragment heard on 31 August 2018 (Figure 3) matches temporarily with song fragments only starting to become more frequent from late August onwards in feeding grounds (Vu et al., 2012; Baumgartner et al., 2019). However, North Atlantic humpback whales are thought to leave their feeding grounds and start their southward migrations much later than August, usually in late autumn to early winter, or, for some whales from the eastern feeding grounds, even in late winter (Stevick et al., 2018; Heenehan et al., 2019; Kowarski et al., 2019; Magnúsdóttir and Lim, 2019). Bermudian fishermen have reported sightings of humpback whales in September (Stevenson, unpublished data). This suggests that a few individuals in some years could start their migration earlier than previously expected and the present acoustic study confirms the presence of such an individual at this time in 2018. Although no acoustic presence of humpback whales was evident in June 2018 (Figure 3), a humpback whale was observed breaching at CB two years later on 15 June 2020 (Stevenson, unpublished data). Thus, inter-annual variability of occasional single individuals migrating through Bermuda seems to occur off-season, e.g., on 31 August 2018 and 15 June 2020.

Diel pattern in singing activity

The diel singing pattern observed in our study, with peak singing activity at nighttime (Figure 3; 5), has been observed in all three humpback whale subspecies on feeding (Magnúsdóttir et al., 2014; Huang et al., 2016; Kowarski et al., 2018) and breeding (Au et al., 2000; Cholewiak, 2008; Cerchio et al., 2014; Kobayashi et al., 2021) grounds, as well as migration routes (Ryan et al., 2019; Shabangu and Kowarski, 2022), and is thus suggested to be a species-wide characteristic (Kowarski et al., 2019). Au et al. (2000) suggested that the diel pattern results from humpback whales relying on visual and acoustic cues during the day, but solely on acoustic cues during the night. For the singing whale, this means that nighttime is the most efficient time to send out the signal and may explain why the diel trend is observed across different breeding, feeding and migratory habitats and why even most non-song vocalisations increase at night (Parks et al., 2014; Huang et al., 2016; Kowarski et al., 2018). In other baleen species, diel variations in vocal activity have been linked to diel distribution in their prey: when prey aggregate, foraging becomes most efficient and whales vocalise less, unless the vocalisation is directly associated to foraging (Wiggins et al., 2005; Baumgartner and Fratantoni, 2008; Širović et al., 2013). However, this hypothesis would not explain why humpback whale singing activity also peaks at nighttime on breeding grounds where they are not exhibiting any feeding behaviour (Cholewiak, 2008). Thus, reliance on visual cues during daytime, as suggested by Au et al. (2000) is currently considered the most plausible explanation for the observed diel patterns in humpback whale singing activity.

Future anthropogenic noise mitigation measures

The present study reveals the importance of Bermuda's waters for migrating humpback whales throughout the spring and winter months. However, the high volume of vessel traffic and underwater noise that accompanies expansion of Bermuda's tourism industry could become a key issue (Jones, 2011; Lester et al., 2016; Bermuda Tourism Authority, 2019). Bermuda's lucrative cruise tourism season currently operates from May to October (Jones, 2011) but could be extended to last from April to December (Bermuda Tourism Authority, 2019). The presence of humpback whales, being continuously present from late December until mid-May (Figure 3), already coincides with the start of the current cruise season; should the new cruise season be rolled out, this temporal overlap will increase. Besides increased risks from ship strikes and behavioural disturbance from prolonged and more intense whale-watching, cruise and freight passages through Bermuda, growth in the tourism sector will further elevate ambient noise levels (e.g., through coastal infrastructure construction and increased vessel noise) which reduce humpback whales' communication space (Au and Green, 2000; Jones, 2011; Micheli et al., 2012; Dunlop, 2016; Lester et al., 2016; Cholewiak et al., 2018a; Gabriele et al., 2018; Sprogis et al., 2020; Currie et al., 2021). In response to elevated noise levels male humpback whales have been shown to cease their song (Sousa-Lima and Clark, 2008; Risch et al., 2012; Cerchio et al., 2014; Tsujii et al., 2018), lengthen their song cycle (Miller et al., 2000) and amplify their vocalisation display, exhibiting the Lombard effect (Guazzo et al., 2020). Given that the present study detected humpback whales frequently chorusing, the

masking of these displays by anthropogenic noise could negatively impact this behaviour in Bermuda, with currently unknown consequences on the population.

In light of this, we advocate authorities to consider precautionary and mitigation measures (Currie et al., 2021; Pires et al., 2021; Risch et al., 2021) during the whale season (December–May). The heavy cruise and shipping traffic lanes operating near CB and the Bermuda platform (ST) could be re-routed given the authorisation by the International Maritime Organization (IMO, 2014), similar to the implementation at the sister Marine Mammal Sanctuary around the Dominican Republic (Kennedy and Clapham, 2017; Heenehan et al., 2019). Dredging and construction of critical marine infrastructure to support the shipping and tourism sectors could be avoided during the night, when humpback whale vocal activity is at its highest (Figure 5), or during the whale season entirely. In addition, moving towards more sustainable noise-reduction vessel designs (Arranz et al., 2021) and implementing a 10 knot vessel speed limit across Bermuda's EEZ for the duration of the whale season could significantly reduce noise levels and reduce masking for both mysticetes and odontocetes (IMO, 2014; Pensieri and Bozzano, 2017; Williams et al., 2019; Aschettino et al., 2020; ZoBell et al., 2021). The latter measure, would also reduce the risk of vessel collisions and cut down on the vessel's carbon emissions (Laist et al., 2001; Lack and Corbett, 2012).

Although these precautionary measures will reduce anthropogenic noise for humpback whales when migrating through Bermuda, year-round implementation of any measure to reduce cetacean disturbance, collision risk and anthropogenic noise would benefit other marine species in Bermuda's EEZ including the resident bottlenose dolphin (*Tursiops truncatus*) population (Klatsky et al., 2007), Cuvier's beaked whales (*Ziphius cavirostris*) and occasional passing sperm whales (*Physeter macrocephalus*) (Hallett, 2011; Stevenson, unpublished data).

Bermuda's song and future song comparisons

The present study characterised Bermuda's humpback whale song structure, encountered in spring 2018, for the first time since 1976. As phrase 6 occurred less frequently than other phrase types and was increasingly present at the end of the 2018 spring season (Supplementary Table 1), it may represent a new phrase type that evolved in late April from phrase 4 and was slowly being introduced into the song repertoire of the predominant breeding population (northwestern Caribbean) migrating through Bermuda across the whale season. Alternatively, phrase 6 could represent the song repertoire of the southeastern breeding population migrating through Bermuda later in the spring season. Therefore, further research should compare the song type described in the present study to acoustic recordings obtained between 2017 and 2019 across the full North Atlantic humpback whale range including off Cape Verde, the southeastern and northwestern Caribbean, Bermuda, the migratory corridor off the British Isles and eastern and western feeding grounds. Analysing and identifying similarities and differences in song structure of all the above listed habitats within the same song season would help elucidate North Atlantic humpback whales' population structure (Murray et al., 2012; Archer et al., 2020), migration paths and the role of Bermuda as a migratory stopover for both the northwestern and southeastern breeding population, which is important information required for the conservation management of this migratory species.

Conclusion

The present acoustic study represents the first long-term PAM study of humpback whale vocalisations off Bermuda. Our results highlight the importance of Bermuda as a key two-way migration stopover site for male North Atlantic humpback whales. They primarily display nocturnal singing activity in the spring and winter months from late December until mid-May. The strong seasonal and diel pattern of whale chorus observed in this study provides new evidence to aid Bermuda's planning authorities with sustainable marine development around Bermuda and the wider Sargasso Sea.

Data availability statement

The original contributions presented in the study are included in the article/Supplementary Material and an additional data publication is archived with PANGAEA at https://doi.pangaea.de/10.1594/PANGAEA.946517. Further inquiries can be directed to the corresponding author.

Ethics statement

The animal study was reviewed and approved by School of GeoSciences, University of Edinburgh.

Author contributions

AS and L-AH contributed to the conception of the study. AS conducted all fieldwork. TNH and DR designed the study. TNH processed the data, performed the analysis, created the figures and took the lead in writing the manuscript. DR and L-AH supervised the project and provided critical feedback throughout

the study. All authors contributed to the article and approved the submitted version.

Funding

This study has received funding from the Atlantic Conservation Partnership and the European Union's Horizon 2020 research and innovation programme under grant agreement No. 818123 for the iAtlantic project. This output reflects only the authors' views and the European Union cannot be held responsible for any use that may be made of the information contained therein.

Acknowledgments

We thank JASCO Applied Sciences (Canada) Ltd. for providing the measurement equipment for the data collection and to Katie Kowarksi for discussions on data analysis and interpretation of humpback song. Data for this study were collected under a Protected Species Licence (License no: 18-12-18-73) for Scientific Research Activities issued by the Department of Environment and Natural Resources, Government of Bermuda.

Conflict of interest

The authors declare that the research was conducted in the absence of any commercial or financial relationships that could be construed as a potential conflict of interest.

Publisher's note

Supplementary material

The Supplementary Material for this article can be found online at: https://www.frontiersin.org/articles/10.3389/fmars.2022.941793/full#supplementary-material

References

André, M. (2018). Ocean noise: Making sense of sounds. *Soc Sci. Inf.* 57, 483–493. doi: 10.1177/0539018418793052

Archer, F. I., Rankin, S., Stafford, K. M., Castellote, M., and Delarue, J. (2020). Quantifying spatial and temporal variation of north pacific fin whale (*Balaenoptera physalus*) acoustic behavior. *Mar. Mammal Sci.* 36, 224–245. doi: 10.1111/mms.12640

Arranz, P., de Soto, N. A., Madsen, P. T., and Sprogis, K. R. (2021). Whale-watch vessel noise levels with applications to whale-watching guidelines and conservation. *Mar. Policy* 134, 104776. doi: 10.1016/j.marpol.2021.104776

Aschettino, J. M., Engelhaupt, D. T., Engelhaupt, A. G., DiMatteo, A., Pusser, T., Richlen, M. F., et al. (2020). Satellite telemetry reveals spatial overlap between vessel high-traffic areas and humpback whales (Megaptera novaeangliae) near the mouth of the Chesapeake bay. *Front. Mar. Sci.* 7. doi: 10.3389/fmars.2020.00121

Au, W. W. L., and Green, M. (2000). Acoustic interaction of humpback whales and whale-watching boats. *Mar. Environ. Res.* 49, 469–481. doi: 10.1016/S0141-1136(99)00086-0

Au, W. W. L., Mobley, J., Burgess, W. C., Lammers, M. O., and Nachtigall, P. E. (2000). Seasonal and diurnal trends of chorusing humpback whales wintering in waters off western Maui. *Mar. Mammal Sci.* 16, 530–544. doi: 10.1111/j.1748-7692.2000.tb00949.x

Baker, C. S., Palumbi, S. R., Lambertsen, R. H., Weinrich, M. T., Calambokidis, J., and O'Brien, S. J. (1990). Influence of seasonal migration on geographic distribution of mitochondrial DNA haplotypes in humpback whales. *Nature* 344, 238–240. doi: 10.1038/344238a0

Baumgartner, M. F., Bonnell, J., Van Parijs, S. M., Corkeron, P. J., Hotchkin, C., Ball, K., et al. (2019). Persistent near real-time passive acoustic monitoring for baleen whales from a moored buoy: System description and evaluation. *Methods Ecol. Evol.* 10, 1476–1489. doi: 10.1111/2041-210X.13244

Baumgartner, M. F., and Fratantoni, D. M. (2008). Diel periodicity in both sei whale vocalization rates and the vertical migration of their copepod prey observed from ocean gliders. *Limnol. Oceanogr.* 53, 2197–2209. doi: 10.4319/lo.2008.53.5_part_2.2197

Beaudette, A., Allen, J., Bort, J., Stevenson, A., Stevick, P., and Stone, G. (2009) *Movement patterns of north Atlantic humpback whales identified at Bermuda.* Available at: http://www.whalesbermuda.com/whale-diary/60-2009-diary/506-2009-10-12-presentation-to-biennial-meeting-of-the-society-for-marine-mammology (Accessed July 24, 2020).

Bermuda Tourism Authority (2019). *Bermuda National tourism plan 2019-2025* (Hamilton, Bermuda: BTA). Available at: https://www.gotobermuda.com/bta.

Bettridge, S., Baker, C. S., Barlow, J., Clapham, P. J., Ford, M., Gouveia, D., et al. (2015). *Status review of the humpback whale (Megaptera novaeangliae) under the endangered species act.* (Southwest Fisheries Science Center, Miami, FL: National Oceanic and Atmospheric Administration, NOAA Fisheries)

Cates, K. A., Atkinson, S., Gabriele, C. M., Pack, A. A., Straley, J. M., and Yin, S. (2019). Testosterone trends within and across seasons in male humpback whales (Megaptera novaeangliae)from Hawaii and Alaska. *Gen. Comp. Endocrinol.* 279, 164–173. doi: 10.1016/j.ygcen.2019.03.013

Cato, D. H. (2014) *Shipping noise impacts on marine life. in 43rd international congress and exposition on noise control engineering (Internoise 2014): Improving the world through noise control* (Melbourne, VIC, Australia). Available at: http://www.acoustics.asn.au/conference_proceedings/INTERNOISE2014/papers/p888.pdf# (Accessed May 15, 2020).

Center for Conservation Bioacoustics (2019) *Raven pro: Interactive sound analysis software (Version 1.6.1).* Available at: http://ravensoundsoftware.com/.

Cerchio, S., Strindberg, S., Collins, T., Bennett, C., and Rosenbaum, H. (2014). Seismic surveys negatively affect humpback whale singing activity off northern Angola. *PloS One* 9:e86464. doi: 10.1371/journal.pone.0086464

Charif, R. A., Clapham, P. J., and Clark, C. W. (2001). Acoustic detections of singing humpback whales in deep waters off the British isles. *Mar. Mammal Sci.* 17, 751–768. doi: 10.1111/j.1748-7692.2001.tb01297.x

Cholewiak, D. M. (2008). *Evaluating the role of song in the humpback whale (Megaptera novaeangliae) breeding system with respect to intra-sexual interactions.* (Cornell, NY: Faculty of the Graduate School of Cornell University)

Cholewiak, D. M., Cerchio, S., Jacobsen, J. K., Urbán-R., J., and Clark, C. W. (2018b). Songbird dynamics under the sea: acoustic interactions between humpback whales suggest song mediates male interactions. *R. Soc Open Sci.* 5, 171298. doi: 10.1098/rsos.171298

Cholewiak, D., Clark, C. W., Ponirakis, D., Frankel, A., Hatch, L. T., Risch, D., et al. (2018a). Communicating amidst the noise: Modeling the aggregate influence of ambient and vessel noise on baleen whale communication space in a national marine sanctuary. *Endanger. Species Res.* 36, 59–75. doi: 10.3354/ESR00875

Cholewiak, D. M., Sousa-Lima, R. S., and Cerchio, S. (2013). Humpback whale song hierarchical structure: Historical context and discussion of current classification issues. *Mar. Mammal Sci.* 29, 312–332. doi: 10.1111/mms.12005

Clark, C., Ellison, W., Southall, B., Hatch, L., Van Parijs, S., Frankel, A., et al. (2009). Acoustic masking in marine ecosystems: intuitions, analysis, and implication. *Mar. Ecol. Prog. Ser.* 395, 201–222. doi: 10.3354/meps08402

Cooke, J. G. (2018). Megaptera novaeangliae. *IUCN Red List Threat. Species 2018*, e.T13006A50362794. doi: 10.1016/B978-0-12-373553-9.00135-8

Currie, J. J., McCordic, J. A., Olson, G. L., Machernis, A. F., and Stack, S. H. (2021). The impact of vessels on humpback whale behavior: The benefit of added whale watching guidelines. *Front. Mar. Sci.* 8. doi: 10.3389/fmars.2021.601433

Darling, J. D., Acebes, J. M. V., Frey, O., Jorge Urbán, R., and Yamaguchi, M. (2019). Convergence and divergence of songs suggests ongoing, but annually variable, mixing of humpback whale populations throughout the north pacific. *Sci. Rep.* 9, 1–14. doi: 10.1038/s41598-019-42233-7

Darling, J. D., and Berube, M. (2001). Interactions of singing humpback whales with other males. *Mar. Mammal Sci.* 17, 570–584. doi: 10.1111/j.1748-7692.2001.tb01005.x

Davis, G. E., Baumgartner, M. F., Corkeron, P. J., Bell, J., Berchok, C., Bonnell, J. M., et al. (2020). Exploring movement patterns and changing distributions of baleen whales in the western north Atlantic using a decade of passive acoustic data. *Glob. Change Biol.* 26, 4812–4840. doi: 10.1111/gcb.15191

Department of Environment and Natural Resources (2017) *Whale watching guidelines*. Available at: https://environment.bm/whale-watching-guidelines.

Derville, S., Torres, L. G., Zerbini, A. N., Oremus, M., and Garrigue, C. (2020). Horizontal and vertical movements of humpback whales inform the use of critical pelagic habitats in the western south pacific. *Sci. Rep.* 10, 1–13. doi: 10.1038/s41598-020-61771-z

Dooling, R. J., and Leek, M. R. (2018). Communication masking by man-made noise, in *Effects of anthropogenic noise on animals* (New York, NY: Springer). doi: 10.1007/978-1-4939-8574-6_2

Dunlop, R. A. (2016). The effect of vessel noise on humpback whale, megaptera novaeangliae, communication behaviour. *Anim. Behav.* 111, 13–21. doi: 10.1016/j.anbehav.2015.10.002

Dunlop, R. A. (2019). The effects of vessel noise on the communication network of humpback whales. *R. Soc Open Sci.* 6, 190967. doi: 10.1098/rsos.190967

Dunlop, R. A., Noad, M. J., Cato, D. H., and Stokes, D. (2007). The social vocalization repertoire of east Australian migrating humpback whales (Megaptera novaeangliae). *J. Acoust. Soc Am.* 122, 2893. doi: 10.1121/1.2783115

Edds-Walton, P. L. (1997). Acoustic communication signals of mysticete whales. *Bioacoustics* 8, 47–60. doi: 10.1080/09524622.1997.9753353

Fiori, L., Martinez, E., Orams, M. B., and Bollard, B. (2020). Using unmanned aerial vehicles (UAVs) to assess humpback whale behavioral responses to swim-with interactions in vava'u, kingdom of Tonga. *J. Sustain. Tour.* 28, 1743–1761. doi: 10.1080/09669582.2020.1758706

Fournet, M. E. H. (2018). *Humpback whale (Megaptera novaeangliae) calling behavior in southeast Alaska: A study in acoustic ecology and noise acoustic spyglass view project rapunzel project: investigating non-song vocalizations in southeast Alaska view project* (Corvallis, OR: Oregon State University). doi: 10.13140/RG.2.2.35810.43200

Gabriele, C. M., Ponirakis, D. W., Clark, C. W., Womble, J. N., and Vanselow, P. B. S. (2018). Underwater acoustic ecology metrics in an Alaska marine protected area reveal marine mammal communication masking and management alternatives. *Front. Mar. Sci.* 5. doi: 10.3389/fmars.2018.00270

Gandilhon, N. (2012). *Contribution au recensement des cétacés dans l'archipel de Guadeloupe*. (Antilles-Guyane)

Garland, E. C., Goldizen, A. W., Rekdahl, M. L., Constantine, R., Garrigue, C., Hauser, N. D., et al. (2011). Dynamic horizontal cultural transmission of humpback whale song at the ocean basin scale. *Curr. Biol.* 21, 687–691. doi: 10.1016/j.cub.2011.03.019

Garland, E. C., Noad, M. J., Goldizen, A. W., Lilley, M. S., Rekdahl, M. L., Garrigue, C., et al. (2013). Quantifying humpback whale song sequences to understand the dynamics of song exchange at the ocean basin scale. *J. Acoust. Soc Am.* 133, 560–569. doi: 10.1121/1.4770232

Garland, E. C., Rendell, L., Lamoni, L., Poole, M. M., and Noad, M. J. (2017). Song hybridization events during revolutionary song change provide insights into cultural transmission in humpback whales. *Proc. Natl. Acad. Sci. U. S. A.* 114, 7822–7829. doi: 10.1073/pnas.1621072114

Garrigue, C., Clapham, P. J., Geyer, Y., Kennedy, A. S., and Zerbini, A. N. (2015). Satellite tracking reveals novel migratory patterns and the importance of seamounts for endangered south pacific humpback whales. *R. Soc Open Sci.* 2, 150489. doi: 10.1098/rsos.150489

Government of Bermuda (1978) *Bermuda Fisheries (Protected species) order 1978. BR8 / 1978*. Available at: http://www.bermudalaws.bm/laws/ConsolidatedLaws/Fisheries(ProtectedSpecies)Order1978.pdf.

Government of Bermuda (2003) *Bermuda Protected species act 2003*. Available at: http://www.bermudalaws.bm/laws/ConsolidatedLaws/ProtectedSpeciesAct2003.pdf.

Guazzo, R. A., Helble, T. A., Alongi, G. C., Durbach, I. N., Martin, C. R., Martin, S. W., et al. (2020). The Lombard effect in singing humpback whales: Source levels increase as ambient ocean noise levels increase. *J. Acoust. Soc Am.* 148, 542–555. doi: 10.1121/10.0001669

Hallett, J. (2011). *The importance of the Sargasso sea and the offshore waters of the bermudian exclusive economic zone to Bermuda and its people.*

Hannay, D. E., Delarue, J., Mouy, X., Martin, B. S., Leary, D., Oswald, J. N., et al. (2013). Marine mammal acoustic detections in the northeastern chukchi Sea, September 2007-July 2011. *Cont. Shelf Res.* 67, 127–146. doi: 10.1016/j.csr.2013.07.009

Hauer-Jensen, M. (2018). *Analysis of humpback whale songs: Applying the traditional method*. (Scripps College: MBARI)

Heenehan, H., Stanistreet, J. E., Corkeron, P. J., Bouveret, L., Chalifour, J., Davis, G. E., et al. (2019). Caribbean Sea Soundscapes: Monitoring humpback whales, biological sounds, geological events, and anthropogenic impacts of vessel noise. *Front. Mar. Sci.* 6. doi: 10.3389/fmars.2019.00347

Herman, L. M. (2017). The multiple functions of male song within the humpback whale (*Megaptera novaeangliae*) mating system: review, evaluation, and synthesis. *Biol. Rev.* 92, 1795–1818. doi: 10.1111/brv.12309

Herman, L. M., Pack, A. A., Spitz, S. S., Herman, E. Y. K., Rose, K., Hakala, S., et al. (2013). Humpback whale song: who sings? *Behav. Ecol. Sociobiol.* 67, 1653–1663. doi: 10.1007/s00265-013-1576-8

Hoyt, E. (2011). *Marine protected areas for whales, dolphins and porpoises: A world handbook for cetacean habitat conservation and planning* (New York, US: Earthscan, Taylor & Francis Ltd).

Huang, W., Wang, D., and Ratilal, P. (2016). Diel and spatial dependence of humpback song and non-song vocalizations in fish spawning ground. *Remote Sens* 8, 712. doi: 10.3390/rs8090712

IMO (2014) *Guidelines for the reduction of underwater noise from commercial shipping to address adverse impacts on marine life*. Available at: http://docs.nrdc.org/water/files/wat_14050501a.pdf.

Indeck, K. L., Noad, M. J., and Dunlop, R. A. (2021). The conspecific avoidance strategies of adult female-calf humpback whales. *Behav. Ecol.* 32, 845–855. doi: 10.1093/beheco/arab031

Janik, V. M. (2009). Whale song. *Curr. Biol.* 19, R109–R111. doi: 10.1016/j.cub.2008.11.026

Johnson, M., Aguilar de Soto, N., and Madsen, P. (2009). Studying the behaviour and sensory ecology of marine mammals using acoustic recording tags: a review. *Mar. Ecol. Prog. Ser.* 395, 55–73. doi: 10.3354/meps08255

Jones, R. (2011). Environmental effects of the cruise tourism boom: Sediment resuspension from cruise ships and the possible effects of increased turbidity and sediment deposition on corals (Bermuda). *Bull. Mar. Sci.* 87, 659–679. doi: 10.5343/bms.2011.1007

Kennedy, A. S., and Clapham, P. J. (2017). From whaling to tagging: The evolution of north Atlantic humpback whale research in the West indies. *Mar. Fish. Rev.* 79, 23–37. doi: 10.7755/MFR.79.2.2

Kennedy, A. S., Zerbini, A. N., Vásquez, O. V., Gandilhon, N., Clapham, P. J., and Adam, O. (2014). Local and migratory movements of humpback whales (Megaptera novaeangliae) satellite-tracked in the north Atlantic ocean. *Can. J. Zool.* 92, 8–17. doi: 10.1139/cjz-2013-0161

Klatsky, L. J., Wells, R. S., and Sweeney, J. C. (2007). Offshore bottlenose dolphins (tursiops truncatus): Movement and dive behavior near the Bermuda pedestal. *J. Mammal.* 88, 59–66. doi: 10.1644/05-mamm-a-365r1.1

Kobayashi, N., Okabe, H., Higashi, N., Miyahara, H., and Uchida, S. (2021). Diel patterns in singing activity of humpback whales in a winter breeding area in okinawan (Ryukyuan) waters. *Mar. Mammal Sci.* 37, 982–992. doi: 10.1111/mms.12790

Kowarski, K., Cerchio, S., Whitehead, H., and Moors-Murphy, H. (2021). Where, when, and why do western north Atlantic humpback whales begin to sing? *Bioacoustics* 31: 450–69. doi: 10.1080/09524622.2021.1972838

Kowarski, K., Evers, C., Moors-Murphy, H., Martin, B., and Denes, S. L. (2018). Singing through winter nights: Seasonal and diel occurrence of humpback whale (megaptera novaeangliae) calls in and around the Gully MPA,offshore eastern Canada. *Mar. Mammal Sci.* 34, 169–189. doi: 10.1111/mms.12447

Kowarski, K., Moors-Murphy, H., Maxner, E., and Cerchio, S. (2019). Western North Atlantic humpback whale fall and spring acoustic repertoire: Insight into

onset and cessation of singing behavior. *J. Acoust. Soc Am.* 145, 2305–2316. doi: 10.1121/1.5095404

Lack, D. A., and Corbett, J. J. (2012). Black carbon from ships: a review of the effects of ship speed, fuel quality and exhaust gas scrubbing. *Atmos. Chem. Phys.* 12, 3985–4000. doi: 10.5194/acp-12-3985-2012

Laist, D. W., Knowlton, A. R., Mead, J. G., Collet, A. S., and Podesta, M. (2001). Collisions between ships and whales. *Mar. Mammal Sci.* 17, 35–75. doi: 10.1111/j.1748-7692.2001.tb00980.x

Lester, S. E., White, C., Mayall, K., and Walter, R. K. (2016). Environmental and economic implications of alternative cruise ship pathways in Bermuda. *Ocean Coast. Manage.* 132, 70–79. doi: 10.1016/j.ocecoaman.2016.08.015

MacKay, M. (2015). *Occurence patterns and social behaviors of humpback whales (Megaptera novaeangliae) wintering off Puerto Rico, USA*. (Corpus Christi, TX: Texas A&M University)

MacKay, M. M., Bacon, C. E., Bouveret, L., Fossette, S., and Stevick, P. T. (2019). Humpback whale (Megaptera novaeangliae) Intra/Inter-seasonal exchanges between Puerto Rico and the southeastern Caribbean. *Anim. Behav. Cogn.* 6, 98–104. doi: 10.26451/abc.06.02.02.2019

Magnúsdóttir, E. E. (2017). *The singing behaviour of humpback whales (Megaptera novaeangliae) in subarctic waters*. (University of Iceland: Faculty of Life and Environmental Science)

Magnúsdóttir, E. E., and Lim, R. (2019). Subarctic singers: Humpback whale (Megaptera novaeangliae) song structure and progression from an icelandic feeding ground during winter. *PloS One* 14, 1–26. doi: 10.1371/journal.pone.0210057

Magnúsdóttir, E. E., Rasmussen, M. H., Lammers, M. O., and Svavarsson, J. (2014). Humpback whale songs during winter in subarctic waters. *Polar Biol.* 37, 427–433. doi: 10.1007/s00300-014-1448-3

Mattila, D. K., Guinee, L. N., and Mayo, C. A. (1987). Humpback whale songs on a north Atlantic feeding ground. *J. Mammal.* 68, 880–883. doi: 10.2307/1381574

Micheli, F., Saenz-Arroyo, A., Greenley, A., Vazquez, L., Espinoza Montes, J. A., Rossetto, M., et al. (2012). Evidence that marine reserves enhance resilience to climatic impacts. *PloS One* 7, e40832. doi: 10.1371/journal.pone.0040832

Miller, P. J. O., Biassoni, N., Samuels, A., and Tyack, P. L. (2000). Whale songs lengthen in response to sonar. *Nature* 405, 903. doi: 10.1038/35016148

Minister of Health Seniors and Environment (2016) *Bermuda Protected species amendment order 2016. gov. Bermuda BR4 / 2016*. Available at: http://www.bermudalaws.bm/laws/AnnualLaws/2016/StatutoryInstruments/ProtectedSpeciesAmendmentOrder2016.pdf.

Morato, T., Varkey, D., Damaso, C., Machete, M., Santos, M., Prieto, R., et al. (2008). Evidence of a seamount effect on aggregating visitors. *Mar. Ecol. Prog. Ser.* 357, 23–32. doi: 10.3354/meps07269

Murray, A., Cerchio, S., McCauley, R., Jenner, C. S., Razafindrakoto, Y., Coughran, D., et al. (2012). Minimal similarity in songs suggests limited exchange between humpback whales (Megaptera novaeangliae) in the southern Indian ocean. *Mar. Mammal Sci.* 28, E41–E57. doi: 10.1111/j.1748-7692.2011.00484.x

Murray, A., Dunlop, R. A., Noad, M. J., and Goldizen, A. W. (2018). Stereotypic and complex phrase types provide structural evidence for a multi-message display in humpback whales (megaptera novaeangliae). *J. Acoust. Soc Am.* 143, 980–994. doi: 10.1121/1.5023680

Narganes Homfeldt, T., Risch, D., Stevenson, A., and Henry, L.-A. (2022). Spectrograms of singing humpback whales migrating through Bermuda. *PANGAEA*. doi: 10.1594/PANGAEA.946517

Natural Earth. *Features*. Available at: http://www.naturalearthdata.com/features/ (Accessed July 13, 2020).

Nikšić, S. (2014). *Analysis of humpback whale song from the Eastern Caribbean*. (Zagreb, Croatia: University of Zagreb)

NOAA and Government of Bermuda (2012) *Memorandum of understanding between the united states of America, U.S. department of commerce national oceanic and atmospheric administration, national ocean service, office of marine sanctuaries - and the government of Bermuda, ministry of the environmen. MOA-2012-0*. Available at: https://nmsstellwagen.blob.core.windows.net/stellwagen-prod/media/archive/sister/pdfs/bermuda_moa12.pdf.

Noad, M. J., Cato, D. H., Bryden, M. M., Jenner, M. N., and Jenner, K. C. S. (2000). Cultural revolution in whale songs: Humpbacks have picked up a catchy tune sung by immigrants from a distant ocean. *Nature* 408, 537. doi: 10.1038/35046199

O'Connor, S., Campbell, R., Knowles, T., and Cortez, H. (2009). Whale watching worldwide: tourism numbers, expenditures and expanding economic benefits, a special report from the international fund for animal welfare228. doi: 10.1115/89GT251

Open Digital Elevation Model (2019) *Bathymetry*. Available at: https://opendem.info/download_bathymetry.html (Accessed July 12, 2020).

Palsboll, P. J., Clapham, P. J., Mattila, D. K., Larsen, F., Sears, R., Siegismund, H. R., et al. (1995). Distribution of mtDNA haplotypes in north Atlantic humpback whales: The influence of behaviour on population structure. *Mar. Ecol. Prog. Ser.* 116, 1–10. doi: 10.3354/meps116001

Parks, S. E., Cusano, D. A., Stimpert, A. K., Weinrich, M. T., Friedlaender, A. S., and Wiley, D. N. (2014). Evidence for acoustic communication among bottom foraging humpback whales. *Sci. Rep.* 4, 1–7. doi: 10.1038/srep07508

Payne, R. S., and McVay, S. (1971). Songs of humpback whales. *Sci. (80-.).* 173, 585–597. doi: 10.1126/science.173.3997.585

Payne, K., and Payne, R. (1985). Large Scale changes over 19 years in songs of humpback whales in Bermuda. *Z. Tierpsychol.* 68, 89–114. doi: 10.1111/j.1439-0310.1985.tb00118.x

Payne, R., and Webb, D. (1971). Orientation by means of long range acoustic signaling in baleen whales. *Ann. N. Y. Acad. Sci.* 188, 110–141. doi: 10.1111/j.1749-6632.1971.tb13093.x

Pensieri, S., and Bozzano, R. (2017). "Active and passive acoustic methods for in-situ monitoring of the ocean status,"," in *Advances in underwater acoustics* (InTechOpen). doi: 10.5772/intechopen.68998

Pires, A. L. M. S., de Sá Maciel, I., dos Santos Alves, M. A., and Tardin, R. H. (2021). The effects of anthropogenic noise on cetaceans in Brazil: the need to consider recent scientific advances in environmental licensing. *J. Coast. Conserv.* 25, 45. doi: 10.1007/s11852-021-00832-5

QGIS Development Team (2016). "QGIS geographic information system (Version 3.2.0)," in *Open source geospatial found*. (Open Source Geospatial Foundation Project) Available at: http://qgis.osgeo.org.

Rafter, M. A., Frasier, K. E., Trickey, J. S., Hildebrand, J. A., Rice, A. C., Thayre, B. J., et al. (2018). *Passive acoustic monitoring for marine mammals at Norfolk canyon April 2016 - June 2017* (San Diego, California: Marine Physical Laboratory).

R Core Team (2019) *R: A language and environment for statistical computing*. Available at: https://www.r-project.org/.

Recalde-Salas, A., Erbe, C., Salgado Kent, C., and Parsons, M. (2020). Non-song vocalizations of humpback whales in Western Australia. *Front. Mar. Sci.* 7. doi: 10.3389/fmars.2020.00141

Reeves, R. R., Smith, T. D., Josephson, E. A., Clapham, P. J., and Woolmer, G. (2004). Historical observations of humpback and blue whales in the north Atlantic ocean: Clues to migratory routes and possibly additional feeding grounds. *Mar. Mammal Sci.* 20, 774–786. doi: 10.1111/j.1748-7692.2004.tb01192.x

Rekdahl, M. L., Dunlop, R. A., Goldizen, A. W., Garland, E. C., Biassoni, N., Miller, P., et al. (2015). Non-song social call bouts of migrating humpback whales. *J. Acoust. Soc Am.* 137, 3042–3053. doi: 10.1121/1.4921280

Rice, A. N., Palmer, K. J., Tielens, J. T., Muirhead, C. A., and Clark, C. W. (2014). Potential bryde's whale (balaenoptera edeni) calls recorded in the northern gulf of Mexico. *J. Acoust. Soc Am.* 135, 3066–3076. doi: 10.1121/1.4870057

Risch, D., Calderan, S., Leaper, R., Weilgart, L., and Werner, S. (2021). Current knowledge already justifies underwater noise reduction. *Trends Ecol. Evol.* 36, 381–382. doi: 10.1016/j.tree.2020.12.010

Risch, D., Corkeron, P. J., Ellison, W. T., and van Parijs, S. M. (2012). Changes in humpback whale song occurrence in response to an acoustic source 200 km away. *PloS One* 7e29741. doi: 10.1371/journal.pone.0029741

Rolland, R. M., Parks, S. E., Hunt, K. E., Castellote, M., Corkeron, P. J., Nowacek, D. P., et al. (2012). Evidence that ship noise increases stress in right whales. *Proc. R. Soc B Biol. Sci.* 279, 2363–2368. doi: 10.1098/rspb.2011.2429

Ross-Marsh, E. C., Elwen, S. H., Fearey, J., Thompson, K. F., Maack, T., and Gridley, T. (2022). Detection of humpback whale (megaptera novaeangliae) non-song vocalizations around the vema seamount, southeast Atlantic ocean. *JASA Express Lett.* 2, 041201. doi: 10.1121/10.0010072

Ruegg, K., Rosenbaum, H. C., Anderson, E. C., Engel, M., Rothschild, A., Baker, C. S., et al. (2013). Long-term population size of the north Atlantic humpback whale within the context of worldwide population structure. *Conserv. Genet.* 14, 103–114. doi: 10.1007/s10592-012-0432-0

Ryan, J. P., Cline, D. E., Joseph, J. E., Margolina, T., Santora, J. A., Kudela, R. M., et al. (2019). Humpback whale song occurrence reflects ecosystem variability in feeding and migratory habitat of the northeast pacific. *PloS One* 14, e0222456. doi: 10.1371/journal.pone.0222456

Shabangu, F. W., and Kowarski, K. A. (2022). The beat goes on: Humpback whale song seasonality in Antarctic and south African waters. *Front. Mar. Sci.* 9. doi: 10.3389/fmars.2022.827324

Silber, G. K. (1986). The relationship of social vocalizations to surface behavior and aggression in the Hawaiian humpback whale (megaptera novaeangliae). *Can. J. Zool.* 64, 2075–2080. doi: 10.1139/z86-316

Širović, A., Williams, L. N., Kerosky, S. M., Wiggins, S. M., and Hildebrand, J. A. (2013). Temporal separation of two fin whale call types across the eastern north pacific. *Mar. Biol.* 160, 47–57. doi: 10.1007/s00227-012-2061-z

Smith, J. N., Goldizen, A. W., Dunlop, R. A., and Noad, M. J. (2008). Songs of male humpback whales, megaptera novaeangliae, are involved in intersexual interactions. *Anim. Behav.* 76, 467–477. doi: 10.1016/j.anbehav.2008.02.013

Sousa-Lima, R. S., and Clark, C. W. (2008). Modeling the effect of boat traffic on the fluctuation of humpback whale singing activity in the abrolhos national marine park, Brazil. *Can. Acoust.* 36, 174–181.

Sprogis, K. R., Videsen, S., and Madsen, P. T. (2020). Vessel noise levels drive behavioural responses of humpback whales with implications for whale-watching. *Elife* 9, e56760. doi: 10.7554/eLife.56760

Stafford, K. M., Lydersen, C., Wiig, Ø., and Kovacs, K. M. (2018). Extreme diversity in the songs of spitsbergen's bowhead whales. *Biol. Lett.* 14, 20180056. doi: 10.1098/rsbl.2018.0056

Stevenson, A. (2008)Whale behaviour in Bermuda. In: *Whales Bermuda*. Available at: http://www.whalesbermuda.com/all-about-humpbacks/whale-behaviour/46-general/217-whale-behaviour-in-bermuda (Accessed May 17, 2020).

Stevenson, A. (2010)Fluke ID matches. In: *Whales Bermuda*. Available at: https://www.whalesbermuda.com/fluke-ids/57-whale-id-flukes/131-using-fluke-shots-to-identify-whales (Accessed July 18, 2020).

Stevenson, A. (2011) *Humpback whale research project, bermuda. Sargasso Sea alliance science report series*. Available at: www.sargassoalliance.org (Accessed July 26, 2020).

Stevenson, A., and Stevick, P. T. (2009) *Habitat use of humpback whales at Bermuda*. Available at: http://www.whalesbermuda.com/whale-diary/60-2009-diary/506-2009-10-12-presentation-to-biennial-meeting-of-the-society-for-marine-mammology.

Stevick, P. T., Allen, J., Bérubé, M., Clapham, P. J., Katona, S. K., Larsen, F., et al. (2003). Segregation of migration by feeding ground origin in north Atlantic humpback whales (*Megaptera novaeangliae*). *J. Zool.*), 259. doi: 10.1017/S0952836902003151

Stevick, P. T., Berrow, S. D., Bérubé, M., Bouveret, L., Broms, F., Jann, B., et al. (2016). There and back again: Multiple and return exchange of humpback whales between breeding habitats separated by an ocean basin. *J. Mar. Biol. Assoc. United Kingdom* 96, 885–890. doi: 10.1017/S0025315416000321

Stevick, P. T., Bouveret, L., Gandilhon, N., Rinaldi, C., Rinaldi, R., Broms, F., et al. (2018). Migratory destinations and timing of humpback whales in the southeastern Caribbean differ from those off the Dominican republic. *J. Cetacean Res. Manage.* 18, 127–133.

Stimpert, A. K., Au, W. W. L., Parks, S. E., Hurst, T., and Wiley, D. N. (2011). Common humpback whale (megaptera novaeangliae) sound types for passive acoustic monitoring. *J. Acoust. Soc Am.* 129, 476–482. doi: 10.1121/1.3504708

Stone, G. S., Katona, S. K., and Tucker, E. B. (1987). History, migration and present status of humpback whales megaptera novaeangliae at Bermuda. *Biol. Conserv.* 42, 133–145. doi: 10.1016/0006-3207(87)90019-X

Time and Date (2019a) *Hamilton, Bermuda – sunrise, sunset and daylength 2018*. Available at: https://www.timeanddate.com/sun/bermuda/hamilton?month=5&year=2018 (Accessed July 20, 2020).

Time and Date (2019b) *Solstices & equinoxes for Hamilton (Surrounding 10 years)*. Available at: https://www.timeanddate.com/calendar/seasons.html?n=38 (Accessed July 28, 2022).

Tsujii, K., Akamatsu, T., Okamoto, R., Mori, K., Mitani, Y., and Umeda, N. (2018). Change in singing behavior of humpback whales caused by shipping noise. *PloS One* 13 e0204112. doi: 10.1371/journal.pone.0204112

Tyarks, S. C., Aniceto, A. S., Ahonen, H., Pedersen, G., and Lindstrøm, U. (2021). Humpback whale (Megaptera novaeangliae) song on a subarctic feeding ground. *Front. Mar. Sci.* 8. doi: 10.3389/fmars.2021.669748

Vogt, P. R., and Jung, W.-Y. (2007). Origin of the Bermuda volcanoes and the Bermuda rise: History, observations, models, and puzzles, in *Plates, plumes and planetary processes* (Boulder, CO: Geological Society of America), 553–591. doi: 10.1130/2007.2430(27

Vu, E., Risch, D., Clark, C., Gaylord, S., Hatch, L., Thompson, M., et al. (2012). Humpback whale song occurs extensively on feeding grounds in the western north Atlantic ocean. *Aquat. Biol.* 14, 175–183. doi: 10.3354/ab00390

Weinrich, M. (1998). Early experience in habitat choice by humpback whales (Megaptera novaeangliae). *J. Mammal.* 79, 163–170. doi: 10.2307/1382851

Wenzel, F. W., Allen, J., Berrow, S., Hazevoet, C. J., Jann, B., Seton, R. E., et al. (2009). Current knowledge on the distribution and relative abundance of humpback whales (Megaptera novaeangliae) off the cape Verde islands, Eastern north Atlantic. *Aquat. Mamm.* 35, 502–510. doi: 10.1578/AM.35.4.2009.502

Wenzel, F. W., Broms, F., López-Suárez, P., Lopes, K., Veiga, N., Yeoman, K., et al. (2020). Humpback whales (Megaptera novaeangliae) in the cape Verde islands: Migratory patterns, resightings, and abundance. *Aquat. Mamm.* 46, 21–31. doi: 10.1578/AM.46.1.2020.21

Wickham, H. (2016) *ggplot2: Elegant graphics for data analysis*. Available at: https://ggplot2.tidyverse.org.

Wiggins, S. M., Oleson, E. M., McDonald, M. A., and Hildebrand, J. A. (2005). Blue whale (Balaenoptera musculus) diel call patterns offshore of southern California. *Aquat. Mamm.* 31, 161–168. doi: 10.1578/am.31.2.2005.161

Williams, R., Veirs, S., Veirs, V., Ashe, E., and Mastick, N. (2019). Approaches to reduce noise from ships operating in important killer whale habitats. *Mar. pollut. Bull.* 139, 459–469. doi: 10.1016/j.marpolbul.2018.05.015

Winn, H. E., and Winn, L. K. (1978). The song of the humpback whale megaptera novaeangliae in the West indies. *Mar. Biol.* 47, 97–114. doi: 10.1007/BF00395631

Wright, A. J., and Walsh, L. A. (2010). Mind the gap: Why neurological plasticity may explain seasonal interruption in humpback whale song. *J. Mar. Biol. Assoc. United Kingdom* 90, 1489–1491. doi: 10.1017/S0025315410000913

ZoBell, V. M., Frasier, K. E., Morten, J. A., Hastings, S. P., Peavey Reeves, L. E., Wiggins, S. M., et al. (2021). Underwater noise mitigation in the Santa Barbara channel through incentive-based vessel speed reduction. *Sci. Rep.* 11, 18391. doi: 10.1038/s41598-021-96506-1

frontiers | Frontiers in Marine Science

TYPE Original Research
PUBLISHED 06 January 2023
DOI 10.3389/fmars.2022.971801

OPEN ACCESS

EDITED BY
Albertus J. Smit,
University of the Western Cape,
South Africa

REVIEWED BY
Simon Elwen,
Stellenbosch University, South Africa
Leah M. Crowe,
Integrated Statistics, United States

*CORRESPONDENCE
Thomas Grove
tomgrove20@yahoo.co.uk

SPECIALTY SECTION
This article was submitted to Deep-Sea Environments and Ecology, a section of the journal Frontiers in Marine Science

RECEIVED 17 June 2022
ACCEPTED 09 December 2022
PUBLISHED 06 January 2023

CITATION
Grove T, King R, Stevenson A and Henry L-A (2023) A decade of humpback whale abundance estimates at Bermuda, an oceanic migratory stopover site. *Front. Mar. Sci.* 9:971801. doi: 10.3389/fmars.2022.971801

A decade of humpback whale abundance estimates at Bermuda, an oceanic migratory stopover site

Thomas Grove[1,2*], Ruth King[3], Andrew Stevenson[4] and Lea-Anne Henry[1]

[1]School of GeoSciences, University of Edinburgh, Edinburgh, United Kingdom, [2]Whale Wise, Swansea, United Kingdom, [3]School of Mathematics and Maxwell Institute for Mathematical Sciences, University of Edinburgh, Edinburgh, United Kingdom, [4]WhalesBermuda, Hamilton, Bermuda

We constructed annual abundance of a migratory baleen whale at an oceanic stopover site to elucidate temporal changes in Bermuda, an area with increasing anthropogenic activity. The annual abundance of North Atlantic humpback whales visiting Bermuda between 2011 and 2020 was estimated using photo-identification capture-recapture data for 1,204 whales, collected between December 2009 and May 2020. Owing to a sparse data set, we combined a Cormack-Jolly-Seber (CJS) model, fit through maximum likelihood estimation, with a Horvitz-Thompson estimator to calculate abundance and used stratified bootstrap resampling to derive 95% confidence intervals (CI). We accounted for temporal heterogeneity in detection and sighting rates *via* a catch-effort model and, guided by goodness-of-fit testing, considered models that accounted for transience. A model incorporating modified sighting effort and time-varying transience was selected using (corrected) Akaike's Information Criterion (AICc). The survival probability of non-transient animals was 0.97 (95% CI 0.91-0.98), which is comparable with other studies. The rate of transience increased gradually from 2011 to 2018, before a large drop in 2019. Abundance varied from 786 individuals (95% CI 593-964) in 2016 to 1,434 (95% CI 924-1,908) in 2020, with a non-significant linear increase across the period and interannual fluctuations. These abundance estimates confirm the importance of Bermuda for migrating North Atlantic humpback whales and should encourage a review of cetacean conservation measures in Bermudian waters, including area-based management tools. Moreover, in line with the time series presented here, regional abundance estimates should be updated across the North Atlantic to facilitate population monitoring over the entire migratory range.

KEYWORDS

baleen whale, humpback whale, *Megaptera novaeangliae*, abundance, capture-recapture, migratory stopover

1 Introduction

Abundance time series are critical to wildlife management as they can inform conservation status and determine underlying drivers of observed trends (Lawton, 1993; Taylor and Gerrodette, 1993; Mace et al., 2008). As a population metric, abundance is relatively easy to understand and interpret, and values can be compared across different time periods (Moore and Barlow, 2011), populations (Barlow et al., 2011), and species (Víkingsson et al., 2015). Further, variation in abundance may relate to other population-scale changes (Madon et al., 2013). For example, temporal trends in baleen whale abundance have been related to variation in mortality, body condition, reproductive rates, and species range shifts (Moore, 2005; Patrician and Kenney, 2010; Ramp et al., 2014; Becker et al., 2019; Simard et al., 2019; Kügler et al., 2020). Combined, such indices allow an integrated assessment of population responses to environmental change and stressors (Hazen et al., 2019), and inform local-regional marine management (Gabriele et al., 2017).

The abundance of baleen whales is frequently estimated through capture-recapture (CR) methods (Hammond et al., 2021). Applied to humpback whales (*Megaptera novaeangliae* [Borowski 1781]), this typically involves photo-identification of naturally occurring markings on tail flukes to determine individual sighting histories over time (e.g., Katona and Whitehead, 1981; Franklin et al., 2020). Values for parameters including survival, detection and abundance are then estimated. To minimize bias of abundance estimates, analyses may account for heterogeneity in survival and detection, including features such as: transient animals, which are only available within the study system once across the study period (Pradel et al., 1997; Madon et al., 2013); temporal heterogeneity due to variable sighting effort (Marucco et al., 2009; Monnahan et al., 2019); and individual detection heterogeneity (IDH), where detection varies as a function of individual attributes and habitat features (Hammond, 1990; Cubaynes et al., 2010). CR methods have been used to construct humpback whale abundance time series at local, regional, and basin scales (e.g., Barlow et al., 2011; Madon et al., 2013; Monnahan et al., 2019). These have been used to inform conservation status for the global and regional populations (Bettridge et al., 2015; Cooke, 2018) and to inform species management (International Whaling Commission, 2009).

Abundance estimates for humpback whales rarely incorporate all parts of a population's range. Like other mysticetes, humpback whales are capital breeders, undertaking long-distance annual migrations between low-latitude winter breeding grounds and high-latitude summer feeding grounds (Mackintosh, 1946; Carwardine, 2019). During this migration, animals may use stopover sites as transitory stops, from days to weeks, for activities such as feeding, resting, socializing or information gathering (Linscott and Senner, 2021). Stopover sites can be coastal, such as Hervey Bay in East Australia (Franklin et al., 2021), but are often oceanic, such as the Kermadec Islands in Oceania (Owen et al., 2019) and the Rio Grande Rise in the Southwest Atlantic (Horton et al., 2020). To date, whale abundance time series have been largely derived for the 'end points' of migration – feeding and breeding grounds (e.g., Chaloupka et al., 1999; Schleimer et al., 2019). These abundance estimates are crucial to monitor population size (Stevick et al., 2003; Punt et al., 2006). In contrast, there are few abundance estimates or time series for stopover sites, particularly mid-ocean areas, which may provide more information about migratory patterns in space and time (Findlay et al., 2011).

In the present study, we investigate humpback whale abundance around Bermuda, a North Atlantic mid-ocean stopover site (Figure 1; Payne and McVay, 1971; Stevenson, 2011). The North Atlantic is considered to be a discrete population of humpback whales (Cooke, 2018) with two distinct population segments (DPS), listed as 'not at risk' in the Caribbean breeding area and 'endangered' at Cape Verde (NOAA, 2016). The Caribbean DPS is subdivided into northern and southeastern Caribbean breeding grounds; and the principal feeding grounds are the Gulf of Maine, eastern Canada, West Greenland, Iceland, and north of Norway (Smith et al., 1999; Reeves et al., 2002; Stevick et al., 2003; Stevick et al., 2018; Wenzel et al., 2020), with each feeding ground considered as a separate management unit (International Whaling Commission, 2002; Hayes et al., 2019). Long-distance migration routes in the North Atlantic are not coastal (Stevick et al., 2006; Kennedy et al., 2014) and there are few mid-ocean migratory stopovers, including Bermuda and the Azores (Visser et al., 2011; Cucuzza et al., 2015). Following extensive commercial hunting in the 19th and 20th centuries (Smith and Reeves, 2010) and a commercial whaling ban in 1955 (Best, 1993), the population size of North Atlantic humpback whales steadily increased through the end of the 20th century (Punt et al., 2006). From CR analysis, modeled annual increase ranged from 1.2% to 3.1% in the principal breeding ground in the northern Caribbean, 1979-1992 (Stevick et al., 2003; Punt et al., 2006). Rates of annual increase varied widely across feeding grounds, from 3% in the Gulf of Maine, 2009-2016, determined by CR (Robbins and Pace, 2018); to ~15% in Icelandic waters, 1987-2001 (Pike et al., 2005), and a sharp decline in the West Greenland feeding ground, 2007-2015 (Heide-Jørgensen and Laidre, 2015; Hansen et al., 2018), determined by line transect sampling. Total abundance in the North Atlantic is still thought to be far below pre-exploitation population size (Punt et al., 2006; Ruegg et al., 2013), although the carrying capacity may have changed due to environmental shifts (Tulloch et al., 2019). To our knowledge, abundance estimates have not been provided for any part of this population more recently than 2016 (Robbins and Pace, 2018). Moreover, in 2018, the International Whaling Commission (IWC) recommended a range-wide, in-depth assessment for North Atlantic humpback whales, including abundance (International Whaling Commission, 2019).

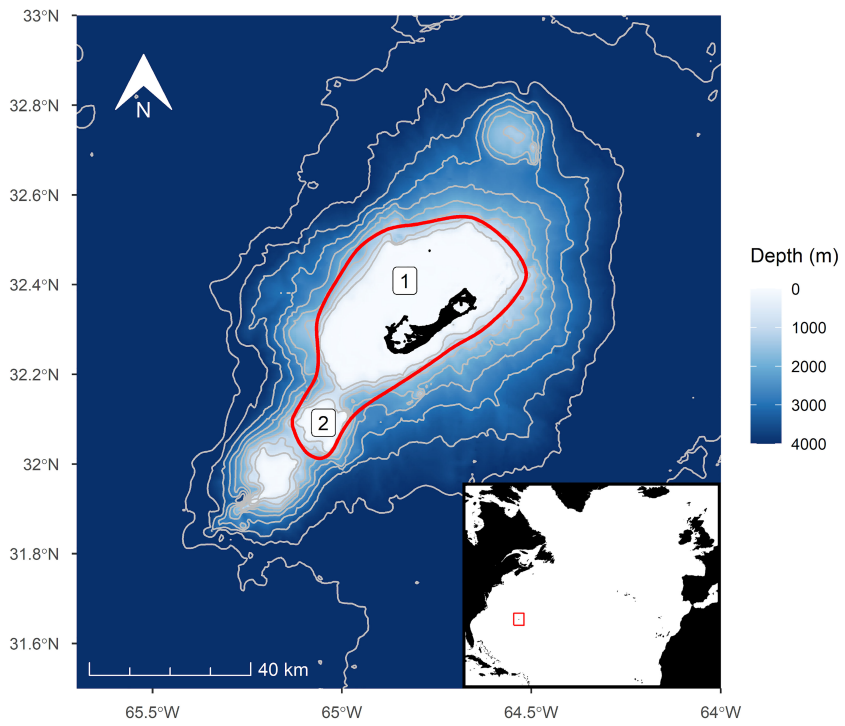

FIGURE 1
Map of the study area, the waters around Bermuda, and its position within the North Atlantic (inset). The approximate search area is denoted by the red line. The study area encompasses two major bathymetric features, 1) the Bermuda Platform and 2) Challenger Bank.

Bermuda has strong migratory connections to other parts of the North Atlantic, with evidence of stopover behavior. Using photo-identification, individuals sighted in Bermuda have been matched to all major feeding grounds, in addition to North Carolina (USA) and Franz Josef Land (Russia); and both Caribbean breeding grounds (Katona and Whitehead, 1981; Stone et al., 1987; A. S., unpublished data; Happywhale[1]). Re-sighting rates suggest that Bermuda is primarily a stopover between the northwest Caribbean and western feeding grounds (Beaudette et al., 2009). Meanwhile, breeding behavior in the form of extensive seasonal singing activity has been recorded at the Bermuda stopover site (Homfeldt et al., 2022), as well as preliminary evidence of foraging (Stone et al., 1987; Hamilton et al., 1997; Stevenson, 2011), aggregation and competitive (Stevenson, pers. comm.) behaviors, during south- and northbound migration.

Due to Bermuda's position along the humpback whale migratory route, the exclusive economic zone was declared a Marine Mammal Sanctuary in 2012, as part of a 'Sister Sanctuary Agreement' with western North Atlantic feeding and breeding areas (NOAA and Government of Bermuda, 2012). However, this designation confers no additional legal protection to humpback whales, and the importance of these waters as a stopover site has not been confirmed through abundance estimates until the present study. With persistent and increasing levels of regional human activity, particularly large vessel traffic (Roberts, 2011; Halpern et al., 2015; Širović et al., 2016), and the announcement of a Blue Economy Strategy for Bermuda (Bermuda Ocean Prosperity Programme, 2021), such evidence could underpin future designations that do carry legally binding management measures, such as Particularly Sensitive Sea Areas (PSSAs; Kachel, 2008), to mitigate risks to humpback whales posed by these activities.

Here, we use a CR framework to model the seasonal abundance of humpback whales around Bermuda from 2011 to 2020 using photo-identification sightings. The data set exhibits low inter-seasonal resighting rates and the resulting model framework does not provide an abundance estimate for the first season of data collection (2010). To reduce bias in our abundance estimates, we account for temporal heterogeneity in sighting effort and whale occurrence, and formally test for both transience and IDH in our data to guide subsequent model fitting and selection. We discuss the potential of this time series to inform marine management in Bermudian waters and establish new baselines to monitor changes through the migratory range of North Atlantic humpback whales.

1 Happywhale, https://www.happewhale.com [last accessed 12 September, 2022]

2 Materials and methods

2.1 Data collection

Between December 2009 and May 2020, annual humpback whale photo-identification surveys were conducted from a small vessel (6.5-10 m length) in coastal and offshore waters around Bermuda (Figure 1). Surveys took place between December and May, the period during which humpback whales typically occur (A. S., unpublished data), and were daily whenever possible. In 2020, survey effort was limited by Covid-19 restrictions in Bermuda (Table 1). All surveys were conducted in calm weather (Beaufort Sea State<3, no precipitation, swell<2 m) with good visibility, and typically spanned daylight hours. Surveys followed a haphazard regime to maximize encounters with whales and focused spatially on the southwestern Bermuda Platform and the Challenger Bank seamount (Figure 1; Vogt and Jung, 2007), although survey routes and sighting locations were not consistently recorded. Surveys were conducted in closing mode; whales were approached on detection and a focal follow of variable duration was conducted at each encounter (Altmann, 1974), which generally lasted 20-30 minutes and up to 2 hours. When possible, the ventral side of the tail flukes of each encountered animal was photographed with a digital SLR camera (Nikon D200, 2010-2017; Nikon D700, 2018-2020; 70-300 mm lens).

Images were used for individual photo-identification *via* scarring patterns and coloration, following Calambokidis et al. (2001). Briefly, two trained researchers independently assigned each image a score of highest quality (1) to lowest quality (5) for five variables against photographic archetypes: proportion of fluke visible, fluke angle (relative to the water), lateral angle of the photographer, sharpness, and lighting. Scores from both researchers were then compared: where there was a discrepancy, the lowest quality (highest score) was retained. We adopted a conservative approach wherein photographs with a score of ≥4 in any category were rejected. Photographs were analyzed independently by two teams and matches detected by only one team were verified by the other.

Data were processed in two ways. For simplicity, each December-May season was named according to the January-May calendar year (e.g., the 2010 season refers to the period December 2009-May 2010). First, to explore residency and support existing evidence that Bermuda is used as a stopover site (a transitory stop, used by whales during long-distance migration for days to weeks), we determined the number of animals that were re-sighted within each season. We calculated the duration (in days) between first and last sightings for each animal within each season, which can be used to infer the minimum residence time in Bermuda. Because Bermuda is thought to encompass south- and north-bound migrations, we removed any durations greater than 20 days. Second, for capture-recapture modeling, each animal was recorded as present or absent for each season, resulting in a summary record of seasonal sighting histories. This was used to determine the number of inter-seasonal re-sights each season (from all previous seasons within the study period) and estimate abundance.

2.2 Model construction

Abundance trends were derived from annual sighting histories using capture-recapture (CR) methods (for example:

TABLE 1 Survey effort (absolute and standardized), sightings, inter-seasonal re-sights (from all previous years within the period) and intra-seasonal re-sights for each season (December-May, e.g., the 2010 season corresponds to December 2009-May 2010), determined through photo-identification.

Season	Effort (days)	Standardized effort	No. whales	No. inter-seasonal re-sights	Intra-seasonal re-sights	
					No. whales	Days between sightings
2010	18	4.35	78		6	1-2
2011	25	7.01	104	4	9	1-7
2012	32	8.60	165	16	21	1-7
2013	33	8.37	158	27	21	1-8
2014	29	6.37	103	20	6	1-5
2015	33	8.38	180	26	13	1-6
2016	31	6.81	88	19	10	1-7
2017	27	7.29	122	28	1	1-1
2018	25	6.59	148	22	17	1-11
2019	38	9.81	218	49	26	1-14
2020	13	3.01	71	20	6	1-14

King, 2014; McCrea and Morgan, 2015; Seber and Schofield, 2019; Hammond et al., 2021). Annual abundance was defined as the total number of animals passing through the approximate search area in a single December-May season. All model construction and analyses were performed in *R* (R Core Team, 2020), and outputs were visualized with the *ggplot2* package (Wickham, 2016). CR models were fitted using *MARK* (White and Burnham, 1999), accessed through *R* using the *RMark* package (Laake and Rexstad, 2012).

With the majority of whales only sighted in one season across all survey years, the data set is information-poor, increasing the risk of over-parameterization and limiting the complexity of suitable CR frameworks (Lebreton et al., 1992; Forster, 2000). Therefore, using a two-step approach, we initially fit a modified Cormack-Jolly-Seber (CJS; Lebreton et al., 1992) model to the data, and then used the fitted model estimates to calculate annual abundance (Cubaynes et al., 2010 season). We also investigated the use of the more complex Jolly-Seber-Schwarz-Arnason (JSSA; Jolly, 1965; Seber, 1965; Schwarz and Arnason, 1996) and Pollock's closed robust design (Pollock, 1982) models. However, for these data, both models led to identifiability issues in the estimation of model parameters (associated with boundary estimates) and thus were not investigated further.

The CJS framework provides estimates of apparent survival and detection, from which abundance can be subsequently derived. The model can be modified to account for variable survey effort, transience, and IDH. We defined each year as a single capture occasion. CJS conditions on the first sighting of each animal, so that we are not able to estimate the associated capture probabilities for the first season of the study, which consequently means that abundance estimates cannot be produced for the first capture occasion (i.e., 2010; Cubaynes et al., 2010). Capture histories were modeled as a function of two parameters: apparent survival rate, Φ, and per-animal detection probability, p. Parameters were linked to covariates with an inverse logit function and values were estimated from observed data using a maximum likelihood estimation (MLE) approach. To estimate total annual abundance, we followed Cubaynes et al. (2010) and used a Horvitz-Thompson estimator (Borchers et al, 2002; Horvitz and Thompson, 1952; McDonald and Amstrup, 2001) such that:

$$\hat{N}_i = \frac{n_i}{\hat{p}_i};$$

where $\hat{N}_i$ denotes the estimated annual total abundance, $\hat{p}_i$ the estimated detection probability and n_i the number of sighted animals at occasion i. A stratified bootstrap approach (1000 replicates) was used to calculate 95% confidence intervals for p, Φ and N (Morgan, 2008; King and McCrea, 2019; Worthington et al., 2021). For each bootstrap replicate, the number of animals first sighted in a given year was set equal to the observed value.

Core CJS model assumptions include that each animal has an independent fate; that identifying marks are retained and recorded correctly; and that all emigration is permanent (Lebreton et al., 1992). Calves were excluded from the present study and humpback whales are thought to form only loose, temporary associations (Valsecchi et al., 2002), suggesting that individuals behave independently from one another. The long-term reliability of humpback whale fluke photo-identification has been exhaustively demonstrated (Katona et al., 1979; Katona and Whitehead, 1981; Carlson et al., 1990; Stevick et al., 2001; Franklin et al., 2020). Temporary emigration in this system was defined as animals that did not visit Bermuda for one or more seasons (years). Despite limited information, temporary emigration is thought to occur in humpback whale breeding grounds (Brown et al., 1995; Madon et al., 2013; Kowarski et al., 2018) and may occur at the Bermuda stopover site, which would violate a model assumption and could contribute to a transience signal.

Within the basic CJS framework, Φ and p can be constant or time dependent. Modifications to this framework were considered to account for heterogeneous detection and survival, based on system knowledge and goodness-of-fit testing, to minimize bias of abundance estimates.

2.2.1 Capture effort

Detection probability p is likely to vary between years as a function of seasonal survey effort (Marucco et al., 2009; Monnahan et al., 2019). However, in terms of explaining detection probabilities, the number of survey days is a coarse and perhaps naïve estimate of effort, given that a) the number of whales present changes during a season, with a consistent peak in sightings in March and April across all years; and b) the temporal distribution of effort varies between seasons (Figure 2). To account for this, we derived a standardized effort value for each season i ($effort_{s,i}$). First, we calculated the mean number of whales seen per day (WPD) for a given calendar month m over all seasons (WPD_m), defined as:

$$WPD_m = \frac{sightings_m}{days_m};$$

where $sightings_m$ is the total number of sightings (one sighting is equal to one identifiable whale seen at least once on one day) and $days_m$ is the total number of effort days, for calendar month m across all seasons. We then derived an associated correction factor for each month (cor_m) as:

$$cor_m = \frac{WPD_m}{\sum_m WPD_m}.$$

This correction factor is an empirical distribution of the average WPD across months, and thus takes into account differences over time relating to whale presence in the area.

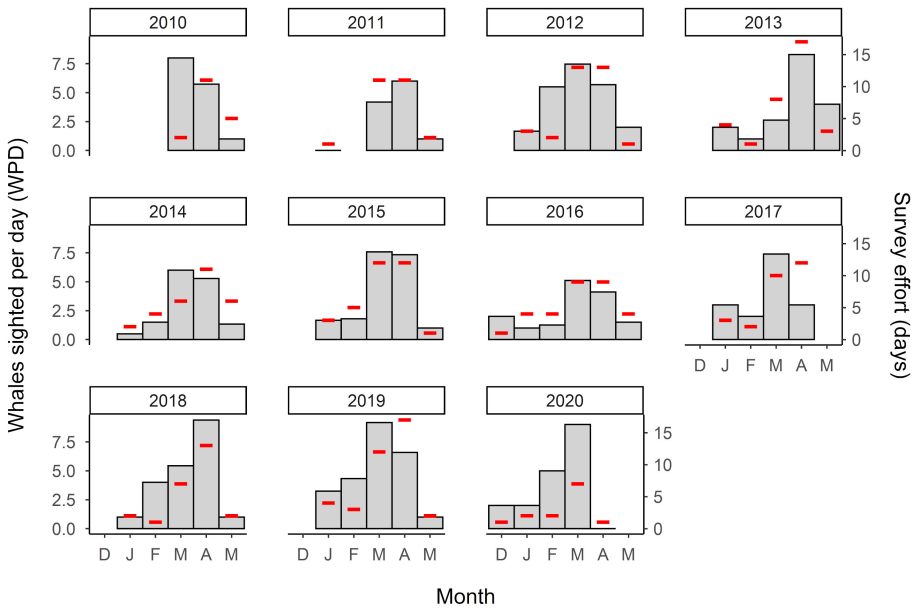

FIGURE 2
Whales sighted per day (WPD; gray bars, left-hand y-axis) and number of days of survey effort (red lines, right-hand y-axis) for each survey month and season.

Finally, we defined the standardized effort ($effort_s$) for season i as:

$$\text{effort}_{s,i} = \sum_m effort_{i,m} \times cor_m ;$$

where $effort_{i,m}$ denotes the number of days of effort for month m in season i. In this way, our standardized effort accounts for intra-seasonal patterns in whale occurrence and the heterogeneous temporal distribution of effort between seasons (years). We considered models in which standardized effort was included as a covariate with p *via* logistic regression.

2.2.2 Transience

We considered the presence of transients, defined as animals that visited Bermuda in only one season during the study period. By definition, transients cannot be observed again and are unavailable for recapture within the study (i.e., have zero "survival" probability; Pradel et al., 1997). Transience has been detected in humpback whale breeding grounds (Constantine et al., 2012; Madon et al., 2013; Chero et al., 2020), although the source of the signal is uncertain. Failure to account for this feature will typically lead to an overestimation of abundance (Madon et al., 2013; Genovart and Pradel, 2019), due to an associated underestimation of capture probability.

We used goodness-of-fit (GoF) testing, implemented through the *R2ucare* package (Choquet et al., 2009; Gimenez et al., 2018), to investigate the presence of transient animals. A significant chi-squared test result ($\chi^2 = 121$, $df = 44$, $p < 0.0001$) suggested a poor fit of the basic CJS model to sighting histories. This test was decomposed to four interpretable components using contingency tables; the TEST 3.SR (Pradel et al., 2005) component yielded a significant result ($Z = 89$, $p < 0.0001$), indicating that newly encountered and previously encountered animals have different probabilities of subsequent re-sighting. This is typically interpreted as a strong signal for transience and removing this component improved goodness of fit considerably ($\chi^2 = 32$, $df = 35$, $p = 0.60$). To account for transience, we followed Pradel et al. (1997) and structured Φ into two age classes ($\Phi \sim transient$), 0 and 1+ years, where 'age' is the time elapsed since first capture and not the actual age of the animal. Φ_0 (model age 0) can be interpreted as the combined apparent survival of 'transient' animals (zero survival probability) and 'resident' animals, and Φ_{1+} (model age 1+) as the survival of residents alone. The proportion of transients among newly sighted animals, τ, was estimated using:

$$\hat{\tau} = 1 - \frac{\hat{\Phi}_0}{\hat{\Phi}_{1+}}.$$

The proportion of transients in the population, T, was then estimated via,

$$\hat{T} = \frac{E(u_i) \times \hat{\tau}}{E(u_i + m_i)},$$

where $E(u_i)$ is the expected number of newly sighted animals and $E(m_i)$ the expected number of re-sighted animals. Following

Perret et al. (2003), we used observed u_i and m_i as estimates for expected values.

We considered models in which Φ_0 and Φ_{1+} were constant (single value) or time-varying in an additive way ($\Phi \sim time + transient$). Additionally, to account for the possibility that temporal variation in Φ was driven by variable transience and not survival, we considered models in which Φ_0 varied over time but Φ_{1+} was constant by using age class as a dummy variable ($\Phi \sim time:transient$; Laake and Rexstad, 2012).

2.2.3 Individual detection heterogeneity

Detectability may also vary between animals as a function of individual attributes, including fluke-up behavior for humpback whales (Barendse et al., 2011) and habitat features, such that each animal within the study system has a unique sighting probability (Cubaynes et al., 2010; Gimenez and Choquet, 2010). Failing to account for individual detection heterogeneity (IDH) can lead to an underestimation of abundance (Hammond, 1990; Hwang and Huggins, 2005; Cubaynes et al., 2010). To test for this feature, following Jeyam et al. (2018), we applied tests of positive association between previous and future encounters using Goodman-Kruskal's gamma. A global version of the test (all capture occasions pooled) was only marginally significant ($\gamma = 0.47$, $p = 0.03$). From occasion-specific tests, only 2013, 2015 and 2016 were (marginally) significant. Therefore, modifications of the detection process p to account for IDH were not included. Of note, in a preliminary analysis, including IDH had little effect on parameter estimates but did lead to some additional identifiability issues.

2.2.4 Model selection

In total, we fitted and compared 16 CJS models, constructed from combinations of the different parameter specifications: three for p (constant, time, standardized effort) and five for Φ (constant, time, transient, time + transient, time:transient). Selection of the final, best-fitting model was achieved with Akaike's Information Criterion corrected for small sample size (AICc; Burnham and Anderson, 2004), where a low score indicates improved model fit offset against model complexity, supplemented with visual inspection of parameter values and associated confidence intervals. The final annual abundance estimates were linearly regressed against time to detect a significant temporal trend. The regression was weighted by the inverse of the variance of each abundance estimate to account for varying precision (Stevick et al., 2003; Kutner et al., 2005; Somerford et al., 2022).

3 Results

In total, 304 days of surveys were conducted between December 2009 and May 2020. Seasonal survey effort ranged from 13 days (2020 season) to 38 days (2019 season; Table 1), with a mean of 27 days (SD = 7.2 days). Seasonal standardized effort, which accounted for intra-seasonal variation in whale sighting rates, varied from 3.01 (2020) to 9.81 (2019), with a mean of 6.96 (SD = 1.95). Out of 2,038 sightings with fluke images, 1,594 sightings on 276 days had images of sufficient quality (a score of ≤3 in all five variables). From these filtered sightings, 1,204 individual whales were identified (Figure 3). The number of identifiable whales per season ranged from 71 (2020) to 218 (2019; Table 1, Figure 3), with a mean of 130 whales (SD = 47 whales). The majority of whales (1,042, 87%) were sighted in only one year, with whales sighted in up to seven different seasons (one whale). The number of animals that were re-sighted between years ranged from 4 (2011) to 49 (2019; Table 1) for each year of re-sighting. Between 1 (2017) and 26 (2019) animals were re-sighted within each season, with a maximum duration of 14 days between first and last sightings (after removing durations >20 days; Table 1).

Candidate CJS models were compared with AICc values (Table 2). The top two models represented 95% of the weight of evidence, had similar AICc values (ΔAICc = 0.6 for second model) and both contained detection p linked to standardized effort and transient Φ. The only difference in model structure was the time dependence of Φ (apparent survival): in the best-fitting model, Φ_0 was time-varying and Φ_{1+} was constant (the apparent survival of non-transient animals did not vary with time), whereas both were time-varying in an additive way in the second best-fitting model. In this way, the best-fitting model, with constant survival following re-sighting, can be regarded as a simpler version of the second best-fitting model. In both these models, the CJS model parameters and associated estimates of abundance are all very similar (Table S1, Figure S1), including substantially overlapping 95% CIs. Thus, in this case we did not compute weighted averages (which would be similar).

From the best-fitting CJS model (constant Φ_{1+}; Figure 4), detection probabilities, p, ranged from 0.05 (95% CI 0.03-0.08) in 2020 to 0.20 (95% CI 0.15-0.28) in 2019. The survival of non-transients, Φ_{1+},was 0.97 (95% CI 0.91-0.98) and the proportion of transients, T, ranged from 0.2 (95% CI 0.04-0.64) in 2019 to 0.8 (95% CI 0.69-0.86) in 2018. The number of transient (N_T) and non-transient (N_R) animals showed differing trends, particularly towards the end of the period, with non-transients increasing and transients decreasing considerably from 2018 to 2019 (Figure 4). Total abundance, N_{tot}, ranged from 786 (95% CI 593-964) in 2016 to 1,434 (95% CI 924-1,908) in 2020, with a non-significant increasing linear trend across the period determined by weighted linear regression ($R^2 = 0.28$, $F = 4.43$, $p = 0.07$). Full model results are available at Grove et al. (2022). Abundance estimates from CJS models with alternative specifications of p (time-varying or linked to unmodified effort) showed similar trends and overlapping confidence intervals (Figure S2).

10.3389/fmars.2022.971801

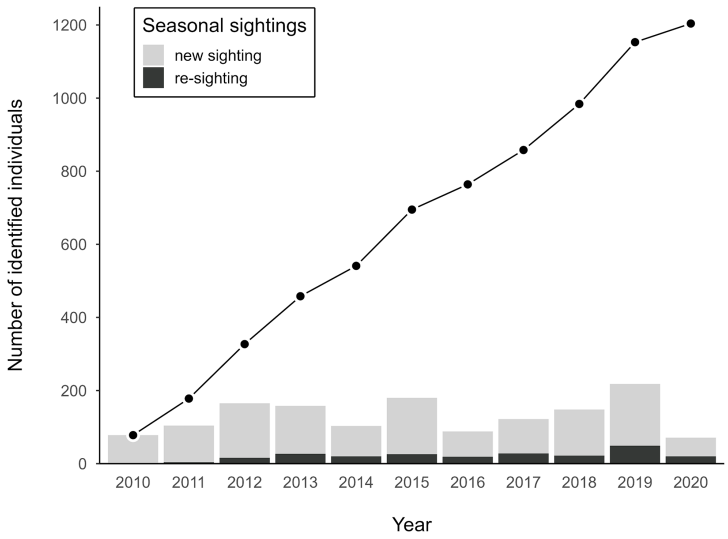

FIGURE 3
Discovery curve of the cumulative number of photo-identified individuals from 2010 to 2020 (points), with bar plots showing the number of new and previously identified (re-sighted) individuals seen each year.

4 Discussion

Abundance estimates for mysticetes are usually derived for feeding and breeding grounds, the endpoints of migration. Here, we provide a ten-year abundance time series at an oceanic, migratory stopover site. According to our best-fitting CR model, up to 1,434 North Atlantic humpback whales (95% CI 924-1,908) visited Bermuda annually between 2011 and 2020, with fluctuations between consecutive years and a slight increase overall. These abundances are comparable with some

TABLE 2 Parameter specification and summary of each candidate CJS model, including AICc score used for model selection.

Apparent survival (Φ)	Detection (p)	Parameters	AICc	ΔAICc	Weight	Deviance
time:transient	**effort**	**13**	**1855.3**	**0**	**0.55**	**300.3**
time + transient	effort	13	1855.9	0.6	0.4	300.9
transient	effort	4	1861	5.8	0.03	324.3
time + transient	time	21	1862.3	7.1	0.02	290.9
time:transient	constant	12	1884.3	29	0	331.3
time + transient	constant	12	1886.5	31.2	0	333.5
transient	constant	3	1890.6	35.4	0	355.9
time:transient	time	20	1891.3	36.1	0	322
constant	effort	3	1921.5	66.3	0	386.8
constant	time	11	1926.1	70.8	0	375.2
transient	time	11	1931	75.7	0	380.1
time	effort	12	1934.1	78.8	0	381.1
time	constant	8	1936.5	81.3	0	391.8
time	time	20	1938.6	83.3	0	369.3
constant	constant	2	1947.7	92.4	0	415

The best-fitting model is in bold. For apparent survival, *transient* denotes that survival is split into two model age classes to account for transient animals; *transient+time* denotes that the two survival values are time-varying; and *time:transient* denotes that Φ_0 is time-varying and Φ_{1+} is constant.

10.3389/fmars.2022.971801

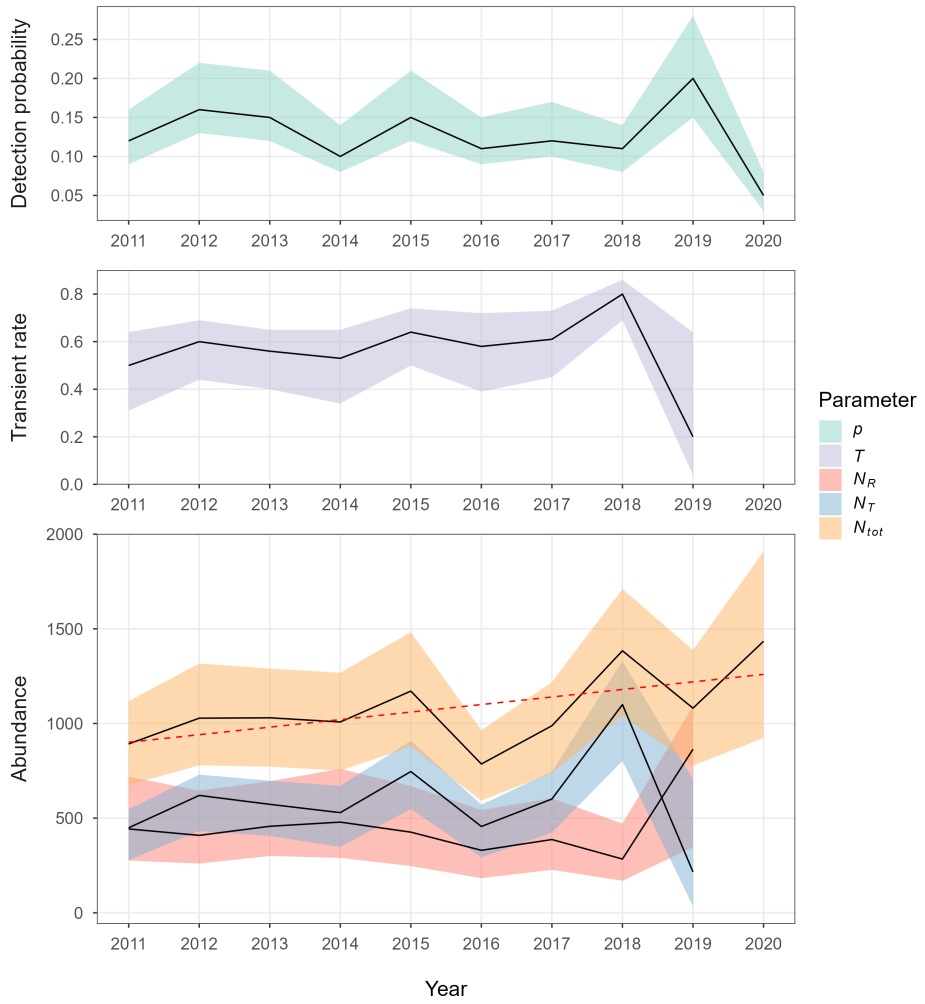

FIGURE 4
Annual estimates for detection probability (p), transient rate (T), abundance of non-transients (N_R), abundance of transients (N_T), and total abundance (N_{tot}), with 95% confidence intervals (CI, shaded regions), for the best-fitting model (effort-dependent p, transient Φ, time-dependent Φ_0, constant Φ_{1+}). The weighted linear trend (non-significant) for total abundance is denoted by the dashed red line.

destination feeding grounds and confirm the contemporary importance of this Marine Mammal Sanctuary as a stopover site. Given the limited protection afforded to humpback whales in Bermudian waters, these estimates should encourage the implementation of area-based management tools to mitigate risks from increasing human activities such as shipping, commercial fishing, and marine wildlife tourism in the waters around Bermuda. Moreover, with Bermuda's migratory connections to both feeding and breeding grounds across the entire North Atlantic, this time series may facilitate population monitoring at a basin scale.

The capture-recapture data set used here is relatively information-poor, with only 13% of whales re-sighted between seasons across the decade. This is unsurprising, given the challenges of monitoring migratory humpback whales around the Bermuda stopover site: inclement weather frequently prevented survey effort, with the number of survey days per December-May season ranging from 13 in 2020 to 38 in 2019 (out of 182 days); Challenger Bank, a major geographical focus of this study, is 15-20 km offshore; and it was often not possible to survey the entire area of interest within a single day. Furthermore, satellite tagging (Kennedy et al., 2014) and historical sightings from whaling ships (Reeves et al., 2004) suggest that North Atlantic humpback whales follow diffuse, poorly defined migration routes from the Caribbean to northern feeding grounds, over several months. The general migration route passing Bermuda may, therefore, be a very wide corridor (hundreds to thousands of kilometers), and the full extent of the stopover site may be greater than the surveyed area, further limiting detectability.

The resulting sparseness of individual sighting histories limits the complexity (number of parameters) of suitable CR models (Lebreton et al., 1992). We derived abundance estimates with a modified CJS model of detection and apparent survival, and a modified Horvitz-Thompson estimator. Using a combination of system knowledge, goodness-of-fit testing, and information criterion, we identified time dependence on detection probabilities, modeled as a function of modified survey effort; as well a considerable time-varying proportion of transients in the population (Figure 4). Strictly, in this study, a transient animal is only present in the study area (waters around Bermuda) for one occasion (season). We acknowledge that sightings data were used twice for model fitting, in terms of capture-recapture data and applying an availability weighting to the catch-effort covariate. However, the latter may be considered a 'long-term average' of monthly sighting rates over the duration of the study period, that is then applied to all years individually. Sensitivity analyses demonstrated that, in practice, the impact of this effort modification on abundance estimates was negligible (Figure S2). Furthermore, a comparable (simple) JSSA model yielded parameter estimates that are broadly similar to those derived from the best-fitting CJS model (Table S2, Figure S3), lending further confidence to our abundance estimates, but the use of JSSA models for these data was strictly limited as a result of associated identifiability issues due to the additional model complexity and parameters to be estimated. Future research could explore the suitability of other CR modeling approaches, such as a recently developed integrated stopover model (Worthington et al., 2019), for this data set.

From the best-fitting CJS model, apparent survival was high (Φ_{1+} = 0.97, 95% CI 0.92-0.98), yet comparable with estimates obtained from other studies, both within and outside the North Atlantic, with such values ranging from 0.9 to 0.99 (Barlow and Clapham, 1997; Mizroch et al., 2004; Ramp et al., 2010; Félix et al., 2011; Hendrix et al., 2012). The modeled proportion of transients, T, was also high between 2011 and 2018 (Figure 4); this was unsurprising, given the high percentage of animals sighted in only one season (87%). However, T declined steeply to 0.2 (95% CI 0.04-0.64) in 2019, which matches a higher inter-seasonal re-sighting rate (Table 1, Figure 3). A transience signal, as defined in this study, has previously been detected at humpback whale breeding grounds (Chero et al., 2020), but, to our knowledge, not feeding grounds or migratory stopovers (Bertulli et al., 2018). Madon et al. (2013) quantified transience using a similar method at a South Pacific breeding ground (New Caledonia), using both photographic and genetic CR. Whilst the values of T were lower from photographic CR (0.19-0.3), values from genetic CR were similar to our results (0.39-0.66; Madon et al., 2013).

The cause of this 'transience' signal and its temporal variability have not been determined for humpback whales (including this study), may not meet the definition of biological transients, and are likely to differ between study systems. The CJS framework is relatively simple and specifies two parameters, p and Φ; therefore, it is unable to distinguish transience from other processes such as temporary emigration. In addition, transience may be confounded with low re-capture probabilities (Genovart and Pradel, 2019), but this is considered unlikely in our model due to the estimation of both low values for p (0.05-0.2) and high transient rates. Alternatively, the 'transience' signal may be driven by several factors. First, animals may not use the same migration route every year. For example, animals may switch breeding or feeding ground and shift migration route in the process (Katona, 1986; Kennedy et al., 2014). However, this is unlikely to be prevalent because exchange rates are very low between breeding grounds (Mattila et al., 1989; Stevick et al., 1999; Stevick et al., 2016) and feeding grounds (Palsbøll et al., 1995; Stevick et al., 2006), particularly between the western and eastern Atlantic. Alternatively, animals may use the same general migration route but be transient in their localized use of Bermuda. Whilst multidecadal route fidelity has been demonstrated for Southwest Atlantic humpback whales (Horton et al., 2020), migratory corridors in the North Atlantic appear to be wide and diffuse between the Caribbean and northern feeding grounds (Reeves et al., 2004; Kennedy et al., 2014). Therefore, animals may follow this corridor annually but be transient in their use of Bermuda as a stopover.

Second, animals may faithfully use the migration route, but not annually. For example, females may take 'rest years' after giving birth, during which they remain in high latitudes and do not visit breeding grounds (Craig et al., 2003). This is supported by a large discrepancy between sex ratios in humpback whale breeding grounds (1.5-2.5 males for every female) and feeding grounds (near to 1:1) around the world (Brown et al., 1995; Craig and Herman, 1997; Chero et al., 2020), including the North Atlantic (Palsbøll et al., 1997; Smith et al., 1999). Furthermore, persistent humpback whale occurrence in North Atlantic feeding grounds in the winter (Kowarski et al., 2018; Martin et al., 2021) suggests that possibly not all animals migrate south every year. This non-annual visitation would constitute temporary 'emigration' from the migration route and not true transience. Temporary emigration can be investigated and characterized using a robust design framework (Pollock, 1982), which structures capture occasions into primary and secondary periods (e.g., Boys et al., 2019). However, this model is more complex, in terms of additional parameters compared to CJS and JSSA, and was unsuitable for our data set, given the low intra- and inter-seasonal re-sighting rates.

To our knowledge, the results presented here provide the most recent abundance time series (2011-2020) for humpback whales within the North Atlantic (Robbins and Pace (2018) provided estimates for the Gulf of Maine up to 2016). From the best-fitting model, annual abundance showed a weak, non-

significant, positive linear trend across the decade (Figure 4). Fluctuations in total abundance were sometimes large between years, with a 34% decrease from 2015 to 2016, and a 40% increase from 2018 to 2019 (Figure 4, Table S1). However, our abundance estimates are imprecise, with largely overlapping confidence intervals (Figure 4), so true inter-annual changes may be far smaller. Nevertheless, these fluctuations may have obscured an underlying temporal trend in abundance (Legendre & Legendre, 2012), and are far greater than the maximum plausible rate of increase in population size for humpback whales (11.8% annually; Zerbini et al., 2010). As such, abundance trends at Bermuda alone should not be used as a proxy for variation in the size of the entire North Atlantic population.

Beyond population size, fluctuations may additionally be explained by (1) annual changes in the number of animals undertaking migration (Gabriele et al., 2017; Cartwright et al., 2019); or (2) annual changes in the migration route itself (Zerbini et al., 2016). The potential drivers of migratory changes are unknown for this stopover site but could include variability in oceanographic conditions and, therefore, habitat suitability, either at distant feeding grounds or Bermuda itself. Prey availability at feeding grounds may influence the likelihood of migration to breeding grounds (Frankel et al., 2022), and there is evidence of both foraging and breeding behavior at the Bermuda stopover (Payne and McVay, 1971; Hamilton et al., 1997; Stevenson, 2011; Homfeldt et al., 2022). Studies in Hawai'i, the principal North Pacific breeding ground, found interannual changes of similar magnitude in humpback whale abundance (Frankel et al., 2022), reproductive rates (Cartwright et al., 2019), and male singing activity (Kügler et al., 2020) in response to the North Pacific Marine Heatwave of 2014-2016. Meanwhile, in North Atlantic feeding grounds, a sharp decline in baleen whale abundance in West Greenland was attributed to species range shifts driven by climate-induced changes in pelagic productivity (Heide-Jørgensen and Laidre, 2015; Hansen et al., 2018); and phenological shifts related to increasing water temperature in the Gulf of Maine (Pendleton et al., 2022). In the Azores, a foraging stopover site in the eastern Atlantic, the seasonal timing of baleen whale sightings (including humpback whales) during northbound migration was related to the timing of the regional spring phytoplankton bloom (Visser et al., 2011). Future work should relate local and regional variation in dynamic oceanography to a Bermuda abundance time series, preferably extended to improve statistical power.

Despite these potential fluctuations, our abundance time series suggests that up to 1,434 whales (95% CI 924-1,908) visited the study area each year, with intra-seasonal sightings demonstrating stopover residency (Table 1). Together, these results confirm the use and importance of Bermuda as a migratory stopover for humpback whales. Due to the lack of recent abundance estimates for North Atlantic feeding and breeding grounds (Kennedy and Clapham, 2017), it is challenging to place these results in the context of the wider North Atlantic and comparisons with outdated abundance estimates should be made cautiously. Total abundance in the primary Caribbean breeding ground was estimated to be 10,752 in 1992-93 (CV = 0.068, Stevick et al., 2003), and it is plausible that the growth rate of 3% has continued (Punt et al., 2006). Abundances for Bermuda are smaller than estimates from some feeding areas, including Iceland (>10,000 during 1995-2007; Víkingsson et al., 2015), and Norway (4,695 during 1996-2001; Øien, 2009), but are comparable with other feeding grounds such as the Gulf of Maine (1,317 in 2016; Robbins and Pace, 2018) and eastern Canada (1,903 in 1982; Katona and Beard, 1990). Therefore, whilst Bermuda is apparently visited by a small proportion of the total North Atlantic population, the island may serve as an important migratory stopover site for individual feeding grounds, particularly in western areas (Beaudette et al., 2009). These feeding grounds are treated as distinct management units at a basin scale (Hayes et al., 2019). Further analysis of the migratory connectivity between Bermuda and other parts of North Atlantic will improve our understanding of Bermuda's role within the wider population.

These results are timely, given the recent announcement of a draft Blue Economy Strategy for Bermuda (Bermuda Ocean Prosperity Programme, 2021) and the lack of specific protection afforded to humpback whales in these waters. The declaration of Bermuda's exclusive economic zone as a Marine Mammal Sanctuary in 2012 formed part of a transboundary network of 'protected areas' (Wenzel et al., 2019) but provided no management measures (NOAA and Government of Bermuda, 2012); the inclusion of humpback whales in Bermuda's Protected Species Act of 2003 broadly prohibits disturbance, harassment and injury (Government of Bermuda, 2003; Government of Bermuda, 2016); and existing whale-watching guidelines are voluntary (Department of Environment and Natural Resources, 2017). Moreover, around Bermuda and the wider Sargasso Sea, anthropogenic activity, particularly large vessel traffic, has increased in recent years and this growth is forecast to continue (Roberts, 2011; Halpern et al., 2015; Širović et al., 2016). As a result, ocean ambient sound is now dominated by shipping in Bermudian waters (Širović et al., 2016). Combined with possible increases in commercial fishing activity and whale-watching tourism (Bermuda Tourism Authority, 2019), any resulting mortality or disturbance may impact whales across the North Atlantic, particularly western feeding grounds and northern Caribbean breeding grounds. Our time series should encourage consideration of area-based management tools to mitigate risks from human activities around Bermuda, such as PSSAs and marine protected areas, as well as a review of existing whale-watching guidelines (Department of Environment and Natural Resources, 2017). Abundance estimates can be combined with current acoustic

monitoring (Homfeldt et al., 2022) and behavioral observation to provide evidence of spatiotemporal patterns in habitat use to guide specific policies (Minton et al., 2011; Rossi-Santos, 2015; Stepanuk et al., 2021). Moreover, such evidence may determine whether Bermuda constitutes critical habitat, defined as areas that are regularly used by a population to perform essential tasks for survival and reproduction (Hoyt, 2011), and may require special consideration for species conservation (Endangered Species Act, 1973).

Beyond Bermuda, the large sightings database (1,204 whales) and ten-year abundance time series may facilitate wider population monitoring on a basin scale (Moore, 2008; Hazen et al., 2019), in conjunction with comparable time series in breeding and feeding grounds (e.g., Robbins and Pace, 2018). Due to Bermuda's unique migratory connections (Katona, 1986) and its role as a stopover site (Payne and McVay, 1971; Stevenson, 2011), changes in abundance around Bermuda may reflect shifts in migratory patterns and population dynamics in distant feeding or breeding grounds across the North Atlantic, and provide extra information on population-level processes. Therefore, we encourage the construction of contemporary, separate abundance time series in other parts of the North Atlantic (especially feeding and breeding grounds), for example, by using existing photo-identification databases, e.g., Happywhale (https://happywhale.com) and the North Atlantic Humpback Whale Catalogue (Katona and Beard, 1990). This aligns with the IWC's recommendation for a range-wide assessment of abundance to replace outdated estimates (International Whaling Commission, 2019). Furthermore, humpback whales are a cosmopolitan marine predator and sensitive to ecosystem change (Cartwright et al., 2019). Better understanding basin-scale population processes, including migratory patterns over space and time, will facilitate assessing the response to environmental change, which may be used as a sentinel for ecosystem monitoring (Simmons et al., 2017; Miloslavich et al., 2018).

Using a capture-recapture framework, guided by goodness-of-fit-testing, we provide an abundance time series for a baleen whale migratory stopover site. Accounting for heterogeneity in survival and detection, we generate robust abundance estimates across a decade and demonstrate the importance of Bermuda for migrating North Atlantic humpback whales. Future marine spatial planning around Bermuda should consider the potential impact that growing anthropogenic pressures, such as vessel traffic and marine wildlife tourism, may have on thousands of humpback whales within potential critical habitat. Furthermore, with Bermuda's migratory connections to feeding and breeding grounds, this time series may facilitate monitoring of population-level processes across the North Atlantic. More generally, we encourage the investigation of whale abundance across a species' range as a potential sentinel for basin-scale ecosystem change. As marine environmental change accelerates across the North Atlantic, sustained photo-identification survey effort in Bermudian waters should be supported to extend this time series.

Data availability statement

The datasets presented in this study can be found in online repositories. The names of the repository/repositories and accession number(s) can be found below: The model outputs generated from this study are available at: https://doi.pangaea.de/10.1594/PANGAEA.945442.

Ethics statement

Ethical review and approval was not required for the animal study because Humpback whales were photographed from a vessel, which did not require any contact or close approach. Nevertheless, WhalesBermuda (Andrew Stevenson) obtained an annual research from the Department of Environmental and Natural Resources, Government of Bermuda, for each year of the study.

Author contributions

L-AH conceptualized the study and acquired funding for analysis and submission. AS conducted all fieldwork and provided resources for data collection. TG and RK designed the study methodology. AS and TG conducted image quality filtering and photo-identification. TG subsequently processed the data, performed analyses, created graphics and led manuscript writing. L-AH and RK supervised the project. RK, AS, and L-AH provided regular feedback; and contributed to and reviewed the manuscript. All authors contributed to the article and approved the submitted version.

Funding

This study received funding from the European Union's Horizon 2020 research and innovation program under grant agreement no. 818123 (iAtlantic). This output reflects only the authors' views and the European Union cannot be held responsible for any use that may be made of the information contained therein. RK was supported by the Leverhulme research fellowship RF-2019-299.

Acknowledgments

On behalf of WhalesBermuda, AS would like to acknowledge support of the Atlantic Conservation Partnership. The authors

are grateful to Olivier Gimenez for providing open-access R code to construct CJS models in RMark and derive abundances. Thank you to Alyssa Stoller for contributing to image scoring for photo-identification, and to Jeff Laake for assistance with JSSA model formulation. All data were collected under an annual Protected Species License issued by the Department of Conservation Services, Government of Bermuda.

Conflict of interest

The authors declare that the research was conducted in the absence of any commercial or financial relationships that could be construed as a potential conflict of interest.

Publisher's note

Supplementary material

The Supplementary Material for this article can be found online at: https://www.frontiersin.org/articles/10.3389/fmars.2022.971801/full#supplementary-material

References

Øien, N. (2009). Distribution and abundance of large whales in Norwegian and adjacent waters based on ship surveys 1995-2001. *NAMMCO Sci. Publ.* 7, 31–47. doi: 10.7557/3.2704

Altmann, J. (1974). Observational study of behavior: sampling methods. *Behaviour* 49, 227–266. doi: 10.1163/156853974X00534

Barendse, J., Best, P. B., Thornton, M., Elwen, S. H., Rosenbaum, H. C., Carvalho, I., et al. (2011). Transit station or destination? attendance patterns, movements and abundance estimate of humpback whales off west south Africa from photographic and genotypic matching. *Afr. J. Mar. Sci.* 33, 353–373. doi: 10.2989/1814232X.2011.637343

Barlow, J., Calambokidis, J., Falcone, E. A., Baker, C. S., Burdin, A. M., Clapham, P. J., et al. (2011). Humpback whale abundance in the north pacific estimated by photographic capture-recapture with bias correction from simulation studies. *Mar. Mammal Sci.* 27, 793–818. doi: 10.1111/j.1748-7692.2010.00444.x

Barlow, J., and Clapham, P. J. (1997). A new birth-interval approach to estimating demographic parameters of humpback whales. *Ecology* 78, 535–546. doi: 10.1890/0012-9658(1997)078[0535:ANBIAT]2.0.CO;2

Beaudette, A., Allen, J., Bort, J., Stevenson, A., Stevick, P., and Stone, G. (2009). "Movement patterns of North Atlantic humpback whales identified at Bermuda," in Quebec City: Presentation at the Biennial Conference of the Society for Marine Mammology Biennial Meeting.

Becker, E. A., Forney, K. A., Redfern, J. V., Barlow, J., Jacox, M. G., Roberts, J. J., et al. (2019). Predicting cetacean abundance and distribution in a changing climate. *Divers. Distrib.* 25, 626–643. doi: 10.1111/ddi.12867

Bermuda Ocean Prosperity Programme (2021) *Blue economy*. Available at: https://www.bermudaoceanprosperity.org/blue-economy (Accessed May 10, 2021).

Bermuda Tourism Authority (2019). *Bermuda National tourism plan 2019-2025* (Hamilton, Bermuda). Available at: https://www.gotobermuda.com/bta/document/national-tourism-plan

Bertulli, C. G., Guéry, L., McGinty, N., Suzuki, A., Brannan, N., Marques, T., et al. (2018). Capture-recapture abundance and survival estimates of three cetacean species in icelandic coastal waters using trained scientist-volunteers. *J. Sea Res.* 131, 22–31. doi: 10.1016/J.SEARES.2017.10.001

Best, P. B. (1993). Increase rates in severely depleted stocks of baleen whales. *ICES J. Mar. Sci.* 50, 169–186. doi: 10.1006/JMSC.1993.1018

Bettridge, S., Baker, C. S., Barlow, J., Clapham, P. J., Ford, M., Gouveia, D., et al. (2015). *Status review of the humpback whale (Megaptera novaeangliae) under the Endangered Species Act. NOAA Technical Memorandum*. NOAA-TM-NMFSSWFSC-540. U.S. Department of Commerce

Borchers, D. L., Buckland, S. T., and Zucchini, W. (2002). *Estimating animal abundance: Closed populations* (New York, NY: Springer).

Boys, R. M., Oliveira, C., Pérez-Jorge, S., Prieto, R., Steiner, L., et al. (2019). Multi-state open robust design applied to opportunistic data reveals dynamics of wide-ranging taxa: the sperm whale case. *Ecosphere* 10, e02610. doi: 10.1002/ecs2.2610

Brown, M. R., Corkeron, P. J., Hale, P. T., Schultz, K. W., and Bryden, M. M. (1995). Evidence for a sex-segregated migration in the humpback whale (*Megaptera novaeangliae*). *Proc. R. Soc B Biol. Sci.* 259, 229–234. doi: 10.1098/rspb.1995.0034

Burnham, K. P., and Anderson, D. R. (2004). Multimodel inference: understanding AIC and BIC in model selection. *Sociol. Methods Res.* 33, 261–304. doi: 10.1177/0049124104268644

Calambokidis, J., Steiger, G. H., Straley, J. M., Herman, L. M., Cerchio, S., Salden, D. R., et al. (2001). Movements and population structure of humpback whales in the north pacific. *Mar. Mammal Sci.* 17, 769–794. doi: 10.1111/j.1748-7692.2001.tb01298.x

Carlson, C. A., Mayo, C. A., and Whitehead, H. (1990). Changes in the ventral fluke pattern of the humpback whale (*Megaptera novaeangliae*), and its effects on matching; evaluation of its significance to photo-identification research. *Rep. Int. Whal. Commun. Special Isue* 12, 105–111.

Cartwright, R., Venema, A., Hernandez, V., Wyels, C., Cesere, J., and Cesere, D. (2019). Fluctuating reproductive rates in hawaii's humpback whales, *Megaptera novaeangliae*, reflect recent climate anomalies in the north pacific. *R. Soc Open Sci.* 6, 181463. doi: 10.1098/rsos.181463

Carwardine, M. (2019). *Handbook of whales, dolphins and porpoises* (London, UK: Bloomsbury Publishing).

Chaloupka, M., Osmond, M., and Kaufman, G. (1999). Estimating seasonal abundance trends and survival probabilities of humpback whales in Hervey Bay (east coast Australia). *Mar. Ecol. Prog. Ser.* 184, 291–301. doi: 10.3354/meps184291

Chero, G., Pradel, R., Derville, S., Bonneville, C., Gimenez, O., and Garrigue, C. (2020). Reproductive capacity of an endangered and recovering population of humpback whales in the Southern Hemisphere. *Mar. Ecol. Prog. Ser.* 643, 219–227. doi: 10.3354/meps13329

Choquet, R., Lebreton, J.-D., Gimenez, O., Reboulet, A.-M., and Pradel, R. (2009). U-CARE: Utilities for performing goodness of fit tests and manipulating CApture-REcapture data. *Ecography.* 32, 1071–1074. doi: 10.1111/j.1600-0587.2009.05968.x

Constantine, R., Jackson, J., Steel, D., Baker, C., Brooks, L., Burns, D., et al. (2012). Abundance of humpback whales in Oceania using photo-identification and microsatellite genotyping. *Mar. Ecol. Prog. Ser.* 453, 249–261. doi: 10.3354/meps09613

Cooke, J. G. (2018). Megaptera novaeangliae. *IUCN Red List Threat. Species* 2018, e.T13006A50362794. doi: 10.2305/IUCN.UK.2018-2.RLTS.T13006A50362794.en

Craig, A. S., and Herman, L. M. (1997). Sex differences in site fidelity and migration of humpback whales (*Megaptera novaeangliae*) to the Hawaiian islands. *Can. J. Zool.* 75, 1923–1933. doi: 10.1139/z97-822

Craig, A. S., Herman, L. M., Gabriele, C. M., and Pack, A. A. (2003). Migratory timing of humpback whales (*Megaptera novaeangliae*) in the Central North Pacific varies with age, sex and reproductive status. *Behaviour* 140, 981–1001. doi: 10.1163/156853903322589605

Cubaynes, S., Pradel, R., Choquet, R., Duchamp, C., Gaillard, J.-M., Lebreton, J.-D., et al. (2010). Importance of accounting for detection heterogeneity when estimating abundance: the case of French wolves. *Conserv. Biol.* 24, 621–626. doi: 10.1111/j.1523-1739.2009.01431.x

Cucuzza, M., Hartman, K., Olio, M., Santos, R. P., Steiner, L., and Stevick, P. T. (2015). "The Azores constitute a migratory stopover for humpback whales in the North Atlantic Ocean," in Malta: *Poster presented at 29th conference of the European Cetacean Society*.

Department of Environment and Natural Resources (2017) *Guidelines for whale watching in Bermuda*. Available at: https://environment.bm/whale-watching-guidelines (Accessed May 20, 2022).

Endangered Species Act (1973). *Endangered species act of 1973* (Washington DC: Department of the Interior, U.S. Fish and Wildlife Service).

Félix, F., Castro, C., Laake, J. L., Haase, B., and Scheidat, M. (2011). Abundance and survival estimates of the southeastern Pacific humpback whale stock from 1991-2006 photo-identification surveys in Ecuador. *J. Cetacean Res. Manage. (Special Issue)* 3, 301–307.

Findlay, K. P., Best, P. B., and Meÿer, M. A. (2011). Migrations of humpback whales past Cape Vidal, South Africa, and an estimate of the population increase rate, (1988–2002). *Afr. J. Mar. Sci.* 33, 375–392. doi: 10.2989/1814232X.2011.637345

Forster, M. R. (2000). Key concepts in model selection: performance and generalizability. *J. Math. Psychol.* 44, 205–231. doi: 10.1006/JMPS.1999.1284

Frankel, A. S., Gabriele, C. M., Yin, S., and Rickards, S. H. (2022). Humpback whale abundance in Hawai'i: Temporal trends and response to climatic drivers. *Mar. Mammal Sci.* 38, 118–138. doi: 10.1111/MMS.12856

Franklin, T., Franklin, W., Brooks, L., Harrison, P., Burns, D., Holmberg, J., et al. (2020). Photo-identification of individual humpback whales (*Megaptera novaeangliae*) using all available natural marks: Implications for misidentification and automated algorithm matching technology. *J. Cetacean Res. Manage.* 21, 71–83. doi: 10.47536/jcrm.v21i1.186

Franklin, T., Franklin, W., Brooks, L., Harrison, P., Pack, A. A., and Clapham, P. J (2021). Social behaviour of humpback whales (*Megaptera novaeangliae*) in hervey bay, Eastern Australia, a preferential female stopover during the southern migration. *Front. Mar. Sci.* 8. doi: 10.3389/FMARS.2021.652147

Gabriele, C. M., Neilson, J. L., Straley, J. M., Scott Baker, C., Cedarleaf, J. A., Saracco, J. F., et al. (2017). Natural history, population dynamics, and habitat use of humpback whales over 30 years on an Alaska feeding ground. *Ecosphere* 8, e01641. doi: 10.1002/ECS2.1641

Genovart, M., and Pradel, R. (2019). Transience effect in capture-recapture studies: The importance of its biological meaning. *PloS One* 14, e0222241. doi: 10.1371/journal.pone.0222241

Gimenez, O., and Choquet, R. (2010). Individual heterogeneity in studies on marked animals using numerical integration: capture–recapture mixed models. *Ecology* 91, 951–957. doi: 10.1890/09-1903.1

Gimenez, O., Lebreton, J., Choquet, R., and Pradel, R. (2018). R2ucare: An r package to perform goodness-of-fit tests for capture–recapture models. *Methods Ecol. Evol.* 9, 1749–1754. doi: 10.1111/2041-210X.13014

Government of Bermuda (2003) *Bermuda Protected species act 2003*. Available at: http://www.bermudalaws.bm/laws/ConsolidatedLaws/ProtectedSpeciesAct2003.pdf (Accessed May 20, 2022).

Government of Bermuda (2016) *Bermuda Protected species amendment order 782 2016. BR4/2016*. Available at: http://www.bermudalaws.bm/laws/Annual%0A783Laws/2016/StatutoryInstruments/ProtectedSpeciesAmendmentOrder2016.pdf (Accessed May 20, 2022).

Grove, T., King, R., Henry, L.-A., and Stevenson, A. (2022). Modelled annual abundance of humpback whales *Megaptera novaeangliae* around Bermuda 2011-2020. *PANGAEA*. doi: 10.1594/PANGAEA.945442

Halpern, B. S., Frazier, M., Potapenko, J., Casey, K. S., Koenig, K., Longo, C., et al. (2015). Spatial and temporal changes in cumulative human impacts on the world's ocean. *Nat. Commun.* 6, 7615. doi: 10.1038/ncomms8615

Hamilton, P. K., Stone, G. S., and Martin, S. M. (1997). Note on a deep humpback whale *Megaptera novaeangliae* dive near Bermuda. *Bull. Mar. Sci.* 61, 491–494.

Hammond, P. S. (1990). Heterogeneity in the Gulf of Maine? estimating humpback whale population size when capture probabilities are not equal. *Rep. Int. Whal. Commun.* 12, 135–139.

Hammond, P. S., Francis, T. B., Heinemann, D., Long, K. J., Moore, J. E., Punt, A. E., et al. (2021). Estimating the abundance of marine mammal populations. *Front. Mar. Sci.* 8. doi: 10.3389/FMARS.2021.735770

Hansen, R. G., Boye, T. K., Larsen, R. S., Nielsen, N. H., Tervo, O., Nielsen, R. D., et al. (2018). Abundance of whales in West and East Greenland in summer 2015. *NAMMCO Sci. Publ.* 11. doi: 10.7557/3.4689

Hayes, S. A., Josephson, E., Maze-Foley, K., and Rosel, P. E. (2019). *US Atlantic and Gulf of Mexico marine mammal stock assessments. NOAA Technical Memorandum*. Woods Hole, MA: U.S. Department of Commerce. doi: 10.25923/ngsq-qc69

Hazen, E. L., Abrahms, B., Brodie, S., Carroll, G., Jacox, M. G., Savoca, M. S., et al. (2019). Marine top predators as climate and ecosystem sentinels. *Front. Ecol. Environ.* 17, 565–574. doi: 10.1002/fee.2125

Heide-Jørgensen, M. P., and Laidre, K. L. (2015). Surfacing time, availability bias and abundance of humpback whales in West Greenland. *J. Cetacean Res. Manage.* 15, 1–8.

Hendrix, A. N., Straley, J., Gabriele, C. M., and Gende, S. M. (2012). Bayesian Estimation of humpback whale (*Megaptera novaeangliae*) population abundance and movement patterns in southeastern Alaska. *Can. J. Fish. Aquat. Sci.* 69, 1783–1797. doi: 10.1139/F2012-101

Homfeldt, T. N., Risch, D., Stevenson, A., and Henry, L.-A. (2022). Seasonal and diel patterns in singing activity of humpback whales migrating through Bermuda. *Front. Mar. Sci.* 9. doi: 10.3389/fmars.2022.941793

Horton, T. W., Zerbini, A. N., Andriolo, A., Danilewicz, D., and Sucunza, F. (2020). Multi-decadal humpback whale migratory route fidelity despite oceanographic and geomagnetic change. *Front. Mar. Sci.* 7. doi: 10.3389/fmars.2020.00414

Horvitz, D. G., and Thompson, D. J. (1952). A generalization of sampling without replacement from a finite universe. *J. Am. Stat. Assoc.* 47, 663–685. doi: 10.1080/01621459.1952.10483446

Hoyt, E. (2011). *Marine protected areas for whales, dolphins and porpoises: A world handbook for cetacean habitat conservation and planning* (London and New York: Earthscan/Taylor & Francis).

Hwang, W.-H., and Huggins, R. (2005). An examination of the effect of heterogeneity on the estimation of population size using capture-recapture data. *Biometrika* 92, 229–233. doi: 10.1093/biomet/92.1.229

International Whaling Commission (2002). Report of the sub committee on the comprehensive assessment of North Atlantic humpback whales. Annex H to the report of the scientific committee. *J. Cetacean Res. Manage.* 4, 230–260.

International Whaling Commission (2009). Report of the scientific committee. Annex E. Report of the standing working group on the aboriginal whaling management procedures. *J. Cetacean Res. Manage.* (Suppl.), 11, 145–168.

International Whaling Commission (2019). Report of the scientific committee. *J. Cetacean Res. Manage.* 20 (Suppl.), 1–78.

Jeyam, A., McCrea, R. S., Bregnballe, T., Frederiksen, M., and Pradel, R. (2018). A test of positive association for detecting heterogeneity in capture for capture–recapture data. *J. Agric. Biol. Environ. Stat.* 23, 1–19. doi: 10.1007/s13253-017-0315-4

Jolly, G. M. (1965). Explicit estimates from capture-recapture data with both death and immigration-stochastic model. *Biometrika* 52, 225–247. doi: 10.2307/2333826

Kachel, M. J. (2008). "Particularly sensitive sea areas," in *Hamburg Studies on Maritime Affairs*, vol. 13, 376. Berlin: Springer. doi: 10.1007/978-3-540-78779-2

Katona, S. K. (1986). "Biogeography of the humpback whale megaptera novaeangliae, in the North Atlantic," in *Pelagic biogeography*, vol. 49 . Eds. A. C. Pierrot-Baits, S. van der Spoel, B. J. Zahuranec and R. K. Johnson (Paris, France: UNESCO Technical Paper in Marine Science), 166–171.

Katona, S., Baxter, B., Brazier, O., Kraus, S., Perkins, J., and Whitehead, H. (1979). "Identification of humpback whales by fluke photographs," in *Behavior of marine animals: Current perspectives in research* (New York, NY: Plenum Press), 33–44.

Katona, S. K., and Beard, J. A. (1990). Population size, migrations and feeding aggregations of the humpback whale (*Megaptera novaeangliae*) in the western North Atlantic Ocean. *Rep. Int. Whal. Commun. Spec. Issue* 12, 295–305.

Katona, S. K., and Whitehead, H. P. (1981). Identifying humpback whales using their natural markings. *Polar Rec.* 20, 439–444. doi: 10.1017/S003224740000365X

Kennedy, A. S., and Clapham, P. J. (2017). From whaling to tagging: The evolution of North Atlantic humpback whale research in the West indies. *Mar. Fish. Rev.* 79, 23–37. doi: 10.7755/MFR.79.2.2

Kennedy, A. S., Zerbini, A. N., Vásquez, O. V., Gandilhon, N., Clapham, P. J., and Adam, O. (2014). Local and migratory movements of humpback whales (*Megaptera novaeangliae*) satellite-tracked in the North Atlantic Ocean. *Can. J. Zool.* 92, 9–18. doi: 10.1139/cjz-2013-0161

King, R. (2014). Statistical ecology. *Annu. Rev. Stat. Its Appl.* 1, 401–426. doi: 10.1146/ANNUREV-STATISTICS-022513-115633

King, R., and Brooks, S. P. (2004). A classical study of catch-effort models for hector's dolphins. *J. Am. Stat. Assoc.* 99, 325–333. doi: 10.1198/016214504000000304

King, R., and McCrea, R. S. (2019). "Capture-recapture methods and models: Estimating population size," in *Handbook of statistics volume 40* (Elsevier), 33–83. doi: 10.1016/bs.host.2018.09.006

Kowarski, K., Evers, C., Moors-Murphy, H., Martin, B., and Denes, S. L. (2018). Singing through winter nights: Seasonal and diel occurrence of humpback whale (*Megaptera novaeangliae*) calls in and around The Gully MPA, offshore eastern Canada. *Mar. Mammal Sci.* 34, 169–189. doi: 10.1111/mms.12447

Kügler, A., Lammers, M. O., Zang, E. J., Kaplan, M. B., and Aran Mooney, T. (2020). Fluctuations in Hawaii's humpback whale *Megaptera novaeangliae* population inferred from male song chorusing off Maui. *Endanger. Species Res.* 43, 421–434. doi: 10.3354/ESR01080

Kutner, M. H., Nachtsheim, C. J., Neter, J., and Li, W. (2005). "Building the regression model III: Remedial measures," in *Applied linear statistical models*. Ed. J. Neter (New York, NY: McGraw-Hill/Irwin), 421–480.

Laake, J., and Rexstad, E. (2012). "Appendix c. RMark–an alternative approach to building linear models in MARK," in *Program MARK: A gentle introduction*. Eds. E. Cooch and G. White (Fort Collins, CO: Colorado State University).

Lawton, J. H. (1993). Range, population abundance and conservation. *Trends Ecol. Evol.* 8, 409–413. doi: 10.1016/0169-5347(93)90043-O

Lebreton, J.-D., Burnham, K. P., Clobert, J., and Anderson, D. R. (1992). Modeling survival and testing biological hypotheses using marked animals: A unified approach with case studies. *Ecol. Monogr.* 62, 67–118. doi: 10.2307/2937171

Legendre, P., and Legendre, L. (2012). "Ecological data series," in *Developments in Environmental Modelling*, 711–783. (Amsterdam: Elsevier) doi: 10.1016/B978-0-444-53868-0.50012-5

Linscott, J. A., and Senner, N. R. (2021). Beyond refueling: Investigating the diversity of functions of migratory stopover events. *Ornithol. Appl.* 123, 1–14. doi: 10.1093/ORNITHAPP/DUAA074

Mace, G. M., Collar, N. J., Gaston, K. J., Hilton-Taylor, C., Akçakaya, H. R., Leader-Williams, N., et al. (2008). Quantification of extinction risk: IUCN's system for classifying threatened species. *Conserv. Biol.* 22, 1424–1442. doi: 10.1111/j.1523-1739.2008.01044.x

Mackintosh, N. A. (1946). The natural history of whalebone whales. *Biol. Rev.* 21, 60–74. doi: 10.1111/j.1469-185X.1946.tb00453.x

Madon, B., Garrigue, C., Pradel, R., and Gimenez, O. (2013). Transience in the humpback whale population of New Caledonia and implications for abundance estimation. *Mar. Mammal Sci.* 29, 669–678. doi: 10.1111/j.1748-7692.2012.00610.x

Martin, S. C., Aniceto, A. S., Ahonen, H., Pedersen, G., and Lindstrøm, U. (2021). Humpback whale (*Megaptera novaeangliae*) song on a subarctic feeding ground. *Front. Mar. Sci.* 8. doi: 10.3389/FMARS.2021.669748

Marucco, F., Pletscher, D. H., Boitani, L., Schwartz, M. K., Pilgrim, K. L., and Lebreton, J. D. (2009). Wolf survival and population trend using non-invasive capture-recapture techniques in the Western Alps. *J. Appl. Ecol.* 46, 1003–1010. doi: 10.1111/j.1365-2664.2009.01696.x

Mattila, D. K., Clapham, P. J., Katona, S. K., and Stone, G. S. (1989). Population composition of humpback whales, *Megaptera novaeangliae*, on Silver Bank 1984. *Can. J. Zool.* 67, 281–285. doi: 10.1139/z89-041

McCrea, R. S., and Morgan, B. J. T. (2015). *Analysis of capture-recapture data* (Boca Raton, FL: CRC Research Press).

McDonald, T. L., and Amstrup, S. C. (2001). Estimation of population size using open capture-recapture models. *J. Agric. Biol. Environ. Stat.* 6, 206–220. doi: 10.1198/108571101750524553

Miloslavich, P., Bax, N. J., Simmons, S. E., Klein, E., Appeltans, W., Aburto-Oropeza, O., et al. (2018). Essential ocean variables for global sustained observations of biodiversity and ecosystem changes. *Glob. Change Biol.* 24, 2416–2433. doi: 10.1111/gcb.14108

Minton, G. T. J. Q., Collins, T., Findlay, K. P., Ersts, P. J., Rosenbaum, H. C., Berggren, P., et al. (2011). Seasonal distribution, abundance, habitat use and population identity of humpback whales in Oman. *J. Cetacean Res. Manage. (Special Issue South. Hemisph. Humpback Whales)* 3, 185–198.

Mizroch, S. A., Herman, L. M., Straley, J. M., Glockner-Ferrari, D. A., Jurasz, C., Darling, J., et al. (2004). Estimating the adult survival rate of Central North Pacific humpback whales (*Megaptera novaeangliae*). *J. Mammal.* 85, 963–972. doi: 10.1644/bos-123

Monnahan, C. C., Acevedo, J., Noble Hendrix, A., Gende, S., Aguayo-Lobo, A., and Martinez, F. (2019). Population trends for humpback whales (*Megaptera novaeangliae*) foraging in the Francisco coloane coastal-marine protected area, Magellan Strait, Chile. *Mar. Mammal Sci.* 35, 1212–1231. doi: 10.1111/mms.12582

Moore, S. E. (2005). "Long-term environmental change and marine mammals," in *Marine mammal research: conservation beyond crisis*. Eds. J. E. Reynolds III, W. F. Perrin, R. R. Reeves, S. Montgomery and T. J. Ragen (Baltimore, MD: John Hopkins University Press), 137–147.

Moore, S. E. (2008). Marine mammals as ecosystem sentinels. *J. Mammal.* 89, 534–540. doi: 10.1644/07-mamm-s-312r1.1

Moore, J. E., and Barlow, J. (2011). Bayesian State-space model of fin whale abundance trends from a 1991-2008 time series of line-transect surveys in the California Current. *J. Appl. Ecol.* 48, 1195–1205. doi: 10.1111/j.1365-2664.2011.02018.x

Morgan, B. J. T. (2008). *Applied stochastic modelling, 2nd edn* (London: Chapman & Hall).

NOAA and Government of Bermuda (2012). *Memorandum of understanding between the united states of America, US department of commerce national oceanic and atmospheric administration, national ocean service, office of marine sanctuaries - and the government of Bermuda, ministry of the environment*.

NOAA (2016). Endangered and Threatened Species; Identification of 14 Distinct Population Segments of the humpback whale (Megaptera novaeangliae) and revision of species-wide listing. *Fed. Regist.* 81, 62259–62320. Available at: https://www.gpo.gov/fdsys/pkg/FR-2016-09-08/pdf/2016-21276.pdf.

Owen, C., Rendell, L., Constantine, R., Noad, M. J., Allen, J., Andrews, O., et al. (2019). Migratory convergence facilitates cultural transmission of humpback whale song. *R. Soc Open Sci.* 6, 190337. doi: 10.1098/RSOS.190337

Palsbøll, P. J., Allen, J., Bérubé, M., Clapham, P. J., Feddersen, T. P., Hammond, P. S., et al. (1997). Genetic tagging of humpback whales. *Nature* 388, 767–769. doi: 10.1038/42005

Palsbøll, P. J., Clapham, P. J., Mattila, D. K., Larsen, F., Sears, R., Siegesmund, H. R., et al. (1995). Distribution of mtDNA haplotypes in North Atlantic humpback whales: the influence of behaviour on population structure. *Mar. Ecol. Prog. Ser.* 116, 1–10. doi: 10.3354/meps116001

Patrician, M. R., and Kenney, R. D. (2010). Using the continuous plankton recorder to investigate the absence of North Atlantic right whales (*Eubalaena glacialis*) from the Roseway Basin foraging ground. *J. Plankton Res.* 32, 1685–1695. doi: 10.1093/plankt/fbq073

Payne, R. S., and McVay, S. (1971). Songs of humpback whales. *Science* 173, 585–597. doi: 10.1126/science.173.3997.585

Pendleton, D. E., Tingley, M. W., Ganley, L. C., Friedland, K. D., Mayo, C., Brown, M. W., et al. (2022). Decadal-scale phenology and seasonal climate drivers of migratory baleen whales in a rapidly warming marine ecosystem. *Glob. Change Biol.* 28, 4989–5005. doi: 10.1111/gcb.16225

Perret, N., Pradel, R., Miaud, C., Grolet, O., and Joly, P. (2003). Transience, dispersal and survival rates in newt patchy populations. *J. Anim. Ecol.* 72, 567–575. doi: 10.1046/j.1365-2656.2003.00726.x

Pike, D. G., Gunnlaugsson, T. H., Øien, N., Desportes, G., Víkingsson, G. A., Paxton, C. G. M., et al. (2005). *Distribution, abundance and trends in abundance of fin and humpback whales in the North Atlantic* (Copenhagen: ICESCM2005/R:12).

Pollock, K. H. (1982). A capture-recapture design robust to unequal probability of capture. *J. Wildl. Manage.* 46, 752–757. doi: 10.2307/3808568

Pradel, R., Gimenez, O., and Lebreton, J.-D. (2005). Principles and interest of GOF tests for multistate capture-recapture models. *Anim. Biodivers. Conserv.* 28, 189–204.

Pradel, R., Hines, J. E., Lebreton, J.-D., and Nichols, J. D. (1997). Capture-recapture survival models taking account of transients. *Biometrics* 53, 60–72. doi: 10.2307/2533097

Punt, A., Friday, N., and Smith, T. (2006). Reconciling data on the trends and abundance of North Atlantic humpback whales within a population modelling framework. *J. Cetacean Res. Manage.* 8, 145–160.

Ramp, C., Bérubé, M., Palsbøll, P., Hagen, W., and Sears, R. (2010). Sex-specific survival in the humpback whale *Megaptera novaeangliae* in the Gulf of St. Lawrence, Canada. *Mar. Ecol. Prog. Ser.* 400, 267–276. doi: 10.3354/meps08426

Ramp, C., Delarue, J., Bérubé, M., Hammond, P., and Sears, R. (2014). Fin whale survival and abundance in the Gulf of St. Lawrence, Canada. *Endanger. Species Res.* 23, 125–132. doi: 10.3354/esr00571

R Core Team (2020) *R: A language and environment for statistical computing*. Available at: https://www.r-project.org/.

Reeves, R. R., Clapham, P. J., and Wetmore, S. E. (2002). Humpback whale (*Megaptera novaeangliae*) occurrence near the Cape Verde Islands, based on American 19th century whaling records. *J. Cetacean Res. Manage.* 4, 235–253.

Reeves, R. R., Smith, T. D., Josephson, E. A., Clapham, P. J., and Woolmer, G. (2004). Historical observations of humpback and blue whales in the North Atlantic Ocean: clues to migratory routes and possibly additional feeding grounds. *Mar. Mammal Sci.* 20, 774–786. doi: 10.1111/j.1748-7692.2004.tb01192.x

Robbins, J., and Pace, R. M. (2018) *Trends in abundance of North Atlantic humpback whales in the gulf of Maine* (Woods Hole, MA: EE133F-17-SE-1320 Task I Contract Report). Available at: https://www.gpo.gov/fdsys/pkg/FR-2016-09-08/pdf/2016-21276.pdf (Accessed May 10, 2021).

Roberts, J. (2011). *Maritime traffic in the Sargasso Sea: An analysis of international shipping activities and their potential environmental impacts* (Hampshire, UK: Report to IUCN Sargasso Sea Alliance Legal Working Group by Coastal & Ocean Management).

Rossi-Santos, M. R. (2015). Oil industry and noise pollution in the humpback whale (*Megaptera novaeangliae*) soundscape ecology of the southwestern Atlantic breeding ground. *J. Coast. Res.* 31, 184–195. doi: 10.2112/JCOASTRES-D-13-00195.1

Ruegg, K., Rosenbaum, H. C., Anderson, E. C., Engel, M., Rothschild, A., Baker, C. S., et al. (2013). Long-term population size of the North Atlantic humpback whale within the context of worldwide population structure. *Conserv. Genet.* 14, 103–114. doi: 10.1007/s10592-012-0432-0

Schleimer, A., Ramp, C., Delarue, J., Carpentier, A., Bérubé, M., Palsbøll, P. J., et al. (2019). Decline in abundance and apparent survival rates of fin whales (*Balaenoptera physalus*) in the northern Gulf of St. Lawrence. *Ecol. Evol.* 9, 4231–4244. doi: 10.1002/ece3.5055

Schwarz, C. J., and Arnason, A. N. (1996). A general methodology for the analysis of capture-recapture experiments in open populations. *Biometrics* 52, 860–873. doi: 10.2307/2533048

Seber, G. A. F. (1965). A note on the multiple-recapture census. *Biometrika* 52, 249–259. doi: 10.2307/2333827

Seber, G. A., and Schofield, M. R. (2019). *Capture-recapture: Parameter estimation for open animal populations* (Cham, Switzerland: Springer).

Simard, Y., Roy, N., Giard, S., and Aulanier, F. (2019). North Atlantic right whale shift to the Gulf of St. Lawrence in 2015, revealed by long-term passive acoustics. *Endanger. Species Res.* 40, 271–284. doi: 10.3354/esr01005

Simmons, S., Bax, N., Costa, D., and Wallace, B. (2017) *Essential ocean variables (EOV) for biology and ecosystems: Marine turtle, bird and mammal abundance and distribution*. Available at: https://www.goosocean.org/index.php?option=com_oe&task=viewDocumentRecord&docID=17511 (Accessed May 10, 2021).

Širović, A., Hildebrand, J. A., and McDonald, M. A. (2016). Ocean ambient sound south of Bermuda and Panama Canal traffic. *J. Acoust. Soc Am.* 139, 2417–2423. doi: 10.1121/1.4947517

Smith, T. D., Allen, J., Clapham, P. J., Hammond, P. S., Katona, S., Larsen, F., et al. (1999). An ocean-basin-wide mark-recapture study of the North Atlantic humpback whale (*Megaptera novaeangliae*). *Mar. Mammal Sci.* 15, 1–32. doi: 10.1111/j.1748-7692.1999.tb00779.x

Smith, T. D., and Reeves, R. R. (2010). Historical catches of humpback whales, *Megaptera novaeangliae*, in the North Atlantic Ocean: Estimates of landings and removals. *Mar. Fish. Rev.* 72, 1–42.

Somerford, T. R., Dawson, S. M., Slooten, E., Guerra, M., Childerhouse, S. J., Richter, C. F., et al. (2022). Long-term decline in abundance of male sperm whales visiting Kaikōura, New Zealand. *Mar. Mammal Sci.* 38, 606–625. doi: 10.1111/MMS.12886

Stepanuk, J. E. F., Heywood, E. I., Lopez, J. F.Jr., DiGiovanni, R. A., and Thorne, L. H. (2021). Age-specific behavior and habitat use in humpback whales: implications for vessel strike. *Mar. Ecol. Prog. Ser.* 663, 209–222. doi: 10.3354/MEPS13638

Stevenson, A. (2011) *Humpback whale research project, bermuda. Sargasso Sea alliance sci. rep. ser.* Available at: http://www.sargassoseacommission.org/storage/documents/No.11_WhaleResearch_HI.pdf (Accessed May 20, 2022).

Stevick, P., Allen, J., Clapham, P., Friday, N., Katona, S., Larsen, F., et al. (2003). North Atlantic humpback whale abundance and rate of increase four decades after protection from whaling. *Mar. Ecol. Prog. Ser.* 258, 263–273. doi: 10.3354/meps258263

Stevick, P. T., Allen, J., Clapham, P. J., Katona, S. K., Larsen, F., Lien, J., et al. (2006). Population spatial structuring on the feeding grounds in North Atlantic humpback whales (*Megaptera novaeangliae*). *J. Zool.* 270, 244–255. doi: 10.1111/j.1469-7998.2006.00128.x

Stevick, P. T., Berrow, S. D., Bérubé, M., Bouveret, L., Broms, F., Jann, B., et al. (2016). There and back again: Multiple and return exchange of humpback whales between breeding habitats separated by an ocean basin. *J. Mar. Biol. Assoc. United Kingdom* 96, 885–890. doi: 10.1017/S0025315416000321

Stevick, P. T., Bouveret, L., Gandilhon, N., Rinaldi, C., Rinaldi, R., Broms, F., et al. (2018). Migratory destinations and timing of humpback whales in the southeastern Caribbean differ from those off the Dominican Republic. *J. Cetacean Res. Manage.* 18, 127–133.

Stevick, P. T., Carlson, C. A., and Balcomb, K. C. (1999). A note on migratory destinations of humpback whales from the eastern Caribbean. *J. Cetacean Res. Manage.* 1, 251–254.

Stevick, P. T., Palsbøll, P. J., Smith, T. D., Bravington, M. V., and Hammond, P. S. (2001). Errors in identification using natural markings: rates, sources, and effects on capture-recapture estimates of abundance. *Can. J. Fish. Aquat. Sci.* 58, 1861–1870. doi: 10.1139/f01-131

Stone, G. S., Katona, S. K., and Tucker, E. B. (1987). History, migration and present status of humpback whales *Megaptera novaeangliae* at Bermuda. *Biol. Conserv.* 42, 133–145. doi: 10.1016/0006-3207(87)90019-X

Taylor, B. L., and Gerrodette, T. (1993). The uses of statistical power in conservation biology: The vaquita and northern spotted owl. *Conserv. Biol.* 7, 489–500. doi: 10.1046/j.1523-1739.1993.07030489.x

Tulloch, V. J. D., Plagányi, É. E., Brown, C., Richardson, A. J., and Matear, R. (2019). Future recovery of baleen whales is imperiled by climate change. *Glob. Change Biol.* 25, 1263–1281. doi: 10.1111/gcb.14573

Valsecchi, E., Hale, P., Corkeron, P., and Amos, W. (2002). Social structure in migrating humpback whales (*Megaptera novaeangliae*). *Mol. Ecol.* 11, 507–518. doi: 10.1046/j.0962-1083.2001.01459.x

Víkingsson, G. A., Pike, D. G., Valdimarsson, H., Schleimer, A., Gunnlaugsson, T., Silva, T., et al. (2015). Distribution, abundance, and feeding ecology of baleen whales in Icelandic waters: have recent environmental changes had an effect? *Front. Ecol. Evol.* 3. doi: 10.3389/fevo.2015.00006

Visser, F., Hartman, K., Pierce, G., Valavanis, V., and Huisman, J. (2011). Timing of migratory baleen whales at the Azores in relation to the North Atlantic spring bloom. *Mar. Ecol. Prog. Ser.* 440, 267–279. doi: 10.3354/meps09349

Vogt, P. R., and Jung, W.-Y. (2007). "Origin of the Bermuda volcanoes and the Bermuda rise: History, observations, models, and puzzles," in *Plates, plumes and planetary processes* (Boulder, CO: Geological Society of America), 553–591. doi: 10.1130/2007.2430(27

Wenzel, F. W., Broms, F., López-Suárez, P., Lopes, K., Veiga, N., Yeoman, K., et al. (2020). Humpback whales (*Megaptera novaeangliae*) in the Cape Verde Islands: Migratory patterns, resightings, and abundance. *Aquat. Mamm.* 46, 21–31. doi: 10.1578/AM.46.1.2020.21

Wenzel, L., Cid, G., Haskell, B., Clark, A., Quiocho, K., Kiene, W., et al. (2019). You *can* choose your relatives: Building marine protected area networks from sister sites. *Aquat. Conserv. Mar. Freshw. Ecosyst.* 29, 152–161. doi: 10.1002/aqc.3041

White, G. C., and Burnham, K. P. (1999). Program MARK: Survival estimation from populations of marked animals. *Bird Study* 46, S120–S139. doi: 10.1080/00063659909477239

Wickham, H. (2016) *ggplot2: Elegant graphics for data analysis* (New York: Springer-Verlag). Available at: https://ggplot2.tidyverse.org (Accessed April 1, 2020).

Worthington, H., King, R., McCrea, R., Smout, S., and Pomeroy, P. (2021). Modeling recruitment of birth cohorts to the breeding population: A hidden Markov model approach. *Front. Ecol. Evol.* 9. doi: 10.3389/fevo.2021.600967

Worthington, H., McCrea, R., King, R., and Griffiths, R. (2019). Estimating abundance from multiple sampling capture-recapture data *via* a multi-state multi-period stopover model. *Ann. Appl. Stat.* 13, 2043–2064. doi: 10.1214/19-AOAS1264

Zerbini, A. N., Clapham, P. J., and Wade, P. R. (2010). Assessing plausible rates of population growth in humpback whales from life-history data. *Mar. Biol.* 157, 1225–1236. doi: 10.1007/s00227-010-1403-y

Zerbini, A. N., Mendez, M., Rosenbaum, H., Sucunza, F., Andriolo, A., Harris, G., et al. (2016). *Tracking southern right whales through the southwest Atlantic: new insights into migratory routes and feeding grounds* (Washington, DC: International Whaling Commission).

frontiers | Frontiers in Marine Science

TYPE Original Research
PUBLISHED 12 April 2023
DOI 10.3389/fmars.2023.1122124

OPEN ACCESS

EDITED BY
Telmo Morato,
University of the Azores, Portugal

REVIEWED BY
Ana Colaço,
Marine Research Institute (IMAR), Portugal
Rachel Elizabeth Boschen-Rose,
Marine Scotland, United Kingdom

*CORRESPONDENCE
Elodie Portanier
elodie.portanier@gmail.com
Didier Jollivet
didier.jollivet@sbr-roscoff.fr

SPECIALTY SECTION
This article was submitted to Deep-Sea Environments and Ecology, a section of the journal Frontiers in Marine Science

RECEIVED 12 December 2022
ACCEPTED 24 March 2023
PUBLISHED 12 April 2023

CITATION
Portanier E, Nicolle A, Rath W, Monnet L, Le Goff G, Le Port A-S, Daguin-Thiébaut C, Morrison CL, Cunha MR, Betters M, Young CM, Van Dover CL, Biastoch A, Thiébaut E and Jollivet D (2023) Coupling large-spatial scale larval dispersal modelling with barcoding to refine the amphi-Atlantic connectivity hypothesis in deep-sea seep mussels.
Front. Mar. Sci. 10:1122124.
doi: 10.3389/fmars.2023.1122124

Coupling large-spatial scale larval dispersal modelling with barcoding to refine the amphi-Atlantic connectivity hypothesis in deep-sea seep mussels

Elodie Portanier[1*], Amandine Nicolle[1,2], Willi Rath[3], Lorraine Monnet[1], Gregoire Le Goff[2], Anne-Sophie Le Port[1], Claire Daguin-Thiébaut[1], Cheryl L. Morrison[4], Marina R. Cunha[5], Melissa Betters[6], Craig M. Young[7], Cindy L. Van Dover[8], Arne Biastoch[3,9], Eric Thiébaut[1] and Didier Jollivet[1*]

[1]Sorbonne Université, Unité Mixte de Recherche 7144, Adaptation et Diversité en Milieu Marin, Station Biologique de Roscoff, Roscoff, France, [2]École Nationale Supérieure de Techniques Avancées (ENSTA) Bretagne, Hydrographie, Océanographie, Positionnement, Brest, France, [3]Research Division 1: Ocean Circulation and Climate Dynamics, GEOMAR Helmholtz Centre for Ocean Research Kiel, Kiel, Germany, [4]U.S. Geological Survey, Eastern Ecological Science Center, Leetown Research Laboratory, Kearneysville, WV, United States, [5]Department of Biology, University of Aveiro, Aveiro, Portugal, [6]Department of Biology, Temple University, Philadelphia, PA, United States, [7]Oregon Institute of Marine Biology, University of Oregon, Eugene, OR, United States, [8]Division of Marine Science and Conservation, Nicholas School of the Environment, Duke University, Beaufort, NC, United States, [9]Christian-Albrechts-Universität, Kiel, Germany

In highly fragmented and relatively stable cold-seep ecosystems, species are expected to exhibit high migration rates and long-distance dispersal of long-lived pelagic larvae to maintain genetic integrity over their range. Accordingly, several species inhabiting cold seeps are widely distributed across the whole Atlantic Ocean, with low genetic divergence between metapopulations on both sides of the Atlantic Equatorial Belt (AEB, i.e. Barbados and African/European margins). Two hypotheses may explain such patterns: (i) the occurrence of present-day gene flow or (ii) incomplete lineage sorting due to large population sizes and low mutation rates. Here, we evaluated the first hypothesis using the cold seep mussels *Gigantidas childressi, G. mauritanicus, Bathymodiolus heckerae* and *B. boomerang*. We combined COI barcoding of 763 individuals with VIKING20X larval dispersal modelling at a large spatial scale not previously investigated. Population genetics supported the parallel evolution of *Gigantidas* and *Bathymodiolus* genera in the Atlantic Ocean and the occurrence of a 1-3 Million-year-old vicariance effect that isolated populations across the Caribbean Sea. Both population genetics and larval dispersal modelling suggested that contemporary gene flow and larval exchanges are possible across the AEB and the Caribbean Sea, although probably rare. When occurring, larval flow was eastward (AEB - only for *B. boomerang*) or northward (Caribbean Sea - only for *G. mauritanicus*). Caution is nevertheless required since

we focused on only one mitochondrial gene, which may underestimate gene flow if a genetic barrier exists. Non-negligible genetic differentiation occurred between Barbados and African populations, so we could not discount the incomplete lineage sorting hypothesis. Larval dispersal modelling simulations supported the genetic findings along the American coast with high amounts of larval flow between the Gulf of Mexico (GoM) and the US Atlantic Margin, although the Blake Ridge population of *B. heckerae* appeared genetically differentiated. Overall, our results suggest that additional studies using nuclear genetic markers and population genomics approaches are needed to clarify the evolutionary history of the Atlantic bathymodioline mussels and to distinguish between ongoing and past processes.

KEYWORDS

COI, population genetics, larval dispersal modelling, long-distance dispersal, cold seep ecosystems, bathymodiolin mussels, Atlantic

1 Introduction

In marine species with a bentho-pelagic life cycle, the maintenance of a single panmictic population over the species range often depends on hydrodynamics, the duration of the pelagic larval phase, the larval behavior, the energetic investment in reproduction, the number of larvae produced, and the availability of suitable habitats (Gaines et al., 2007; Cowen and Sponaugle, 2009). In fragmented and unstable environments, the functioning of a metapopulation depends primarily on an equilibrium between migration and local extinction (Lande, 1988; Harrison and Hastings, 1996) in which the process of habitat recolonization strongly influences the genetic heterogeneity of the species (McCauley, 1991, Pannell and Charlesworth, 1999). Indeed, when local populations become extinct at regular time intervals as may occur in unstable environments, self-recruitment may be insufficient to ensure population and species persistence. Migration then becomes essential, with inward migration contributing to population replenishment and outward migration allowing the colonization of new territories or habitats. In marine environments, such processes are often dependent on the pelagic larval phase (Scheltema, 1986; Roughgarden et al., 1988; Cowen and Sponaugle, 2009; Shanks, 2009). Global changes and anthropogenic impacts have been observed even in the deepest marine ecosystems, and habitat disturbance through climate change, pollution, mining, oil and gas extraction, net trawling, etc. can alter larval connectivity by modifying local hydrodynamics, reducing population sizes and fragmenting habitats (e.g., Baco et al., 2010; Adams et al., 2012; Van Dover, 2014; Levin and Le Bris, 2015; Le Bris et al., 2017; Vilela et al., 2022). It thus appears crucial to investigate larval dispersal and population connectivity and to identify the main corridors of gene flow in order to anticipate the potential impacts of human activities in deep sea ecosystems.

Using a probabilistic model of migration, Hamilton and May (1977) showed that it is always favorable for a species to disperse and establish at a respectable distance from the parental genotypes even when the habitat is stable and more or less continuous. It is, indeed, advantageous for a species to produce a number of migrants greater than half of its descendants in order to make its own genes persist, even if the cost of migration is very high (Hamilton and May, 1977). When the habitat is naturally fragmented and stable, local dynamics needs to be balanced by migration, or the size of patches (and thus their carrying capacity) must be sufficient to support each population: a situation rarely met. As a consequence, the optimal dispersal distance must be large enough to override the degree of habitat aggregation (Hamilton and May, 1977; Levin et al., 1984). Olivieri et al. (1995) pointed out, however, that a predictably perennial habitat with a very low frequency of occurrence may rapidly favor the coexistence of highly dispersive and non-dispersive stages. Indeed, dispersing individuals carrying "high-migration genotypes" will leave local populations and such genotypes will thus be rapidly lost in the local populations while they will be overrepresented in newly colonized sites (Olivieri et al., 1995). The two dispersal strategies may thus co-exist in a metapopulation as a result of opposite selective processes within and between populations. In the specific case of 'nearly-passive' dispersal (e.g. larval dispersal by ocean currents), the number of immigrants is often much smaller than the number of emigrants because a 'long-distance' propagule will have a low probability of finding a suitable settlement site (Shanks, 2009). In such a case, highly dispersive larvae are likely to be rapidly counter-selected for species with low to moderate fecundity living in rare perennial habitats; this might explain why many island-dwelling species have lost their ability to disperse (MacArthur and Wilson, 1967, Lejeusne and Chevaldonné, 2006) and/or have adopted a philopatric behavior (Maes and Volckaert, 2002).

When a habitat is fragmented and locally transient instead of persistent, the risk of local extinction may eventually cause the global extinction of a non-dispersive species. It is then reasonable to assume that the benefits of massive, long-term dispersal far outweigh the costs, especially when the rate of habitat turnover is rapid (McPeek and Holt, 1992). In theory, the migration rate of a

species appears to be positively correlated with the availability of habitat and negatively correlated with its persistence (Doebeli and Ruxton, 1997; Travis and Dytham, 1999) although it is also sensitive to the geographic arrangement of patches in the landscape (Moilanen and Hanski, 1998). Species inhabiting frequently occurring but transient habitats are thus expected to show high migration rates and high dispersal distances (Travis and Dytham, 1999). Dormancy is also another means of survival for species living in fragmented and transient habitats (Levin et al., 1984). In plants, both dispersal and dormancy can confer advantages under different conditions: dormancy, when conditions are unfavorable and dispersal when conditions vary in space, but both are conditioned by natural fluctuations in the environment (Snyder, 2006). In the marine environment, these two processes can be more closely associated if the dormancy phase is integrated with the dispersal phase. An example is the case of the specialized vent worm *Alvinella pompeiana* since its larvae arrest their development until encountering the appropriate thermal conditions for adult survival (Pradillon et al., 2001). High migration rates and dispersal distances coupled with delayed metamorphosis may thus represent one of the most powerful evolutionary strategies for species persistence (Pechenik, 1990).

Cold seeps constitute a fragmented, more or less stable, reduced habitat along active and passive continental margins associated with gas/hydrocarbon or brine resurgence zones in all oceans (Hecker, 1985; Sibuet et al., 1988; MacDonald et al., 1989; Jollivet et al., 1990; Olu et al., 1997; Olu-Le Roy et al., 2004; Yao et al., 2022). These sites are distributed over a wide range of depths from a few hundred to more than 7300 meters (Fujikura et al., 1999), and are often separated by large geographic distances. These deep-sea habitats support a specialized fauna that relies on chemosynthesis with sulfur-oxidizing and/or methanotrophic bacteria (Fisher et al., 1987; Barry et al., 2002; Cordes et al., 2009; Duperron et al., 2012). As an adaptation to fragmentation and instability, species living there are likely to display larval stages favoring long distance dispersal, for instance, planktotrophic larvae that must ascend to the surface to feed (Lutz, 1988; Pond et al., 1997; Herring and Dixon, 1998; Arellano et al., 2014; Yahagi et al., 2017; Kim et al., 2022) or lecithotrophic larvae with large yolk reserves that can develop slowly in the deeper portions of the water column where conditions are oligotrophic and cold (Young, 1994; Chevaldonné et al., 1997; Marsh et al., 2001). They are thus good examples of theoretical predictions promoting long-term dispersal or no dispersal depending on environmental fluctuations and life-history traits constraints. Although many species are endemic to a given geographic area, fine-grained community analysis has shown that many cold-seep species have a relatively wide distribution (Van Dover et al., 2002; Olu et al., 2010; Cowart et al., 2013; LaBella et al., 2017) suggesting putative long-distance dispersal capabilities (Olu-Le Roy et al., 2007; Young et al., 2012; Teixeira et al., 2013; Arellano et al., 2014). In accordance, population genetics and molecular barcoding studies of seep species have suggested the possibility of a shared history between active margin faunas on both sides of the North Atlantic Ocean and/or ongoing connectivity (Andersen et al., 2004; Olu-Le Roy et al., 2007; Cowart et al., 2013; Teixeira et al., 2013; LaBella et al., 2017). The ecological importance of cold seeps as biodiversity hotspots and providers of ecosystem services (Levin et al., 2016) advocates more research on connectivity at ocean scales to assess their vulnerability to environmental changes and precisely define protected areas.

Discriminating between patterns of dispersion and determining how long and where a larva is able to travel in the water column is, however, not an easy task. In general, deep-sea larvae cannot be tracked directly in the field. The inference of dispersal often requires the coupling of several indirect approaches such as larval dispersal modelling using biophysical models, larval rearing in the laboratory and/or the analysis of genetic patterns of populations to estimate gene flow between them (Gilg and Hilbish, 2003; Young et al., 2012; Breusing et al., 2016; Mitarai et al., 2016; Handal et al., 2020; Breusing et al., 2021). To date, studies have not accurately determined the relative contribution of the demographic history of populations and of the contemporary exchanges *via* larval dispersal across the Atlantic Ocean to the genetic structure of species. However, the coupling of present-day population genetic connectivity with the 'large-scale' modelling of larval dispersal at different depths offers particularly promising prospects (Breusing et al., 2016; Breusing et al., 2021). While such coupling approach has been applied along the Mid-Atlantic Ridge (Breusing et al., 2016), no study yet focused on cross-Atlantic exchanges. The Atlantic Ocean monitoring program, through the H2020 iAtlantic project, made such a perspective possible. It allowed the use of both the Parcels v2.0 module (Delandmeter and van Sebille, 2019) of the VIKING20X ocean circulation model developed to investigate the evolution of the Atlantic meridional overturning circulation (AMOC) in the face of global warming (Hirschi et al., 2020; Biastoch et al., 2021) and the barcoding of samples from nearly all the existing collections of cold seep mussels from the American, African and European active margins. The aim of the present study was therefore to test the role of present-day long-term larval migration *via* surface currents in explaining the amphi-Atlantic distribution previously pointed out by Olu-Le Roy et al. (2007) for the two species complexes of seep mussels, namely *Gigantidas childressi*/*G. mauritanicus* (Gustafson et al., 1998; Génio et al., 2008) and *Bathymodioulus boomerang*/*B. heckerae* (Cosel and Olu, 1998; Gustafson et al., 1998). These species seem to be specific to cold seeps and have been sampled only once in seepages located near hydrothermal vents (e.g. Logatchev). They have never been observed in other reduced habitats such as sunken wood or whales falls, although the latter are thought to have played a role in the diversification of bathymodioline mussels creating intermediate habitats that drove evolution from shallow to deep ecosystems (Distel et al., 2000; Lorion et al., 2013). Here we thus aimed to locate putative dispersal corridors between the American and African/European margins and to determine whether long-term larval dispersal represents a viable strategy for population persistence. The distributions and genetic relationships of seep mussels were investigated by molecular barcoding using a portion of the mitochondrial Cytochrome c oxidase 1 gene (COI). This genetic structure was then compared to the expected larval dispersal patterns based on VIKING20X outputs for particles released from the bottom to the surface at several key seep localities with the longest possible pelagic larval duration of one year (as estimated by

Arellano and Young, 2009 for *G. childressi*). While previous studies focused on the northern part of the Atlantic Ocean and/or relied on modelling or genetics only to estimate connectivity (e.g. Cordes et al., 2007; Olu-Le Roy et al., 2007; Young et al., 2012; McVeigh et al., 2017; Gary et al., 2020), we proposed here to combine both approaches at a spatial scale not yet investigated.

2 Material and methods

2.1 Sample collection, DNA extraction, COI amplification and sequencing

A unique collection of cold seep mussels was gathered from 14 different seeps on both side of the Atlantic Ocean (see Table 1 and Figure 1). Samples were collected during several oceanographic cruises that took place between 2006 and 2020 using remotely operated underwater vehicles (ROV) or human occupied underwater vehicles (HOV) (Table 1). Animals were either dissected on board and preserved in 96-100% ethanol or kept frozen at -80°C before being sent to the laboratory (Table 1). DNA was extracted from these frozen or ethanol-preserved tissues of foot, mantle or gills depending on their preservation state and availability. These extractions were performed using a 2% CTAB (Cetyl-trimethyl ammonium bromide)/1% PVP (Poly(n-vinyl-2 pyrolidone) protocol following the modified method of Doyle and Doyle (1987) proposed by Jolly et al. (2003). DNA pellets were then dried using a SpeedVac (ThermoFisher Scientific) and resuspended in 50 to 300µL (according to the size of the pellet) in 0.1X Tris-EDTA buffer. The quality of DNA samples was then checked by electrophoresis using a 0.8% agarose gel.

The COI gene was then amplified using degenerated versions of original Folmer primers (Folmer et al., 1994) that were designed to allow a more efficient amplification of deep-sea mussel species: forward LCO1490Bathspp: 5'-GTTCTACRAAYCATAAAGAYAT TGG-3' and reverse HCO2198Bathspp: 5'-AACYTCTGGRTGV CCRAAAAACCA-3'. Polymerase chain reactions (PCRs) were performed in a final volume of 25 µL with 20-30 ng of DNA, 1X GoTaq® reaction buffer (Promega), 0.05 mg/ml Bovine Serum Albumin, 2 mM MgCl2, 0.12 mM of each dNTP, 0.6 µM of both forward and reverse primers and 1 U of GoTaq ® polymerase. The thermal profile consisted of 3 min of initial denaturation (94°C), followed by 35 cycles of denaturation (30 s, 94°C), annealing (30 s at 50°C) and extension (1 min, 72°C), with a final extension 10 min at 72°C. PCR products was checked on 1.5% agarose gel and sent for Sanger sequencing on both DNA strands at the Eurofins Laboratory (Ebersberg, Germany). For each individual, chromatograms were checked, edited when necessary (e.g. trimmed) and assembled into consensus sequences using CodonCode Aligner 3.6.1 (CodonCode, Dedham, MA, USA). Following this procedure, 248 sequences were obtained and used in subsequent analyses: 16 identified as *B. heckerae*, 30 identified as *B. boomerang*, 137 identified as *G. childressi* and 65 identified as *G. mauritanicus* (see Table 1; Supplementary Table S1; Figure 1 for specific locations and metadata of the samples – see also PANGAEA database, Jollivet et al., 2023 and European Nucleotide Archive database study PRJEB56597). This dataset was enriched with 515 publicly available sequences from GenBank for subsequent analyses (173 for *B. heckerae/B. boomerang*, 342 for *G. childressi/G. mauritanicus*, Table 1; Supplementary Table S1). All sequences (published and amplified from new individuals) were aligned within each species complex using Seaview v.4.7 (Gouy et al., 2010) and the MUSCLE algorithm (Edgar, 2004), and then trimmed to a final length of 449 bp for *G. childressi/G. mauritanicus* and 515 bp for *B. heckerae/ B. boomerang*.

2.2 Species barcoding and population genetics analyses

First, taxonomic units were determined within each species complex using the Assemble-Species-by-Automatic-Partitioning method (ASAP; Puillandre et al., 2021) and the software web interface[1]. ASAP relies on the barcode gap detection approach developed by Puillandre et al. (2012) and uses pairwise distances from single-locus sequence alignments as well as a hierarchical clustering algorithm to identify the most probable partition of individuals in putative species. ASAP analyses were run using default parameter and pairwise distances calculated under the K2P substitution model. Then, haplotypes were determined using DnaSP v.6 (Rozas et al., 2017) and a minimum spanning haplotype network (Bandelt et al., 1999) was constructed using PopArt v.1.7 (Leigh and Bryant, 2015) to visually represent the relationships among haplotypes from different geographic locations within each species complex. DNAsp v.6 was then used to infer haplotype (Hd) and nucleotide (π) diversities for each sampled site within each species complex as well as the number of variable sites (S), the total number of mutations (Eta), the average number of nucleotide differences (k, Tajima, 1983) and the net genetic distances Da (Nei, 1987). Finally, pairwise Fst values from haplotype frequencies were computed between and within species using Arlequin 3.5.2.2 (Excoffier and Lischer, 2010). Significance compared to zero of Fst were assessed using 10 000 permutations. Exact tests of population differentiation with 10 000 dememorization steps and 100 000 steps in the Markov Chain were also performed at a threshold of 0.05. The pairwise Fst matrices were then used to construct heatmaps in R v.4.1.0 (R Core Team, 2021) to help visualizing genetic relationships between populations.

2.3 Estimating divergence time and gene flow

We also used the IMa3 program (Hey et al., 2018) which implements hierarchical Bayesian, Markov-chain Monte Carlo simulations of gene genealogies under an Isolation with Migration model to estimate splitting times, effective population and migration rates between multiple populations. The reference

1 https://bioinfo.mnhn.fr/abi/public/asap/asapweb.html#

population topology (Supplementary Figure S1) used was constructed based on the haplotype networks and ASAP analyses. Four groups of populations could be distinguished (see Results): (1) the Gulf of Mexico (GoM), (2) the US Atlantic margin (US), (3) the African and European margins (Africa-Cadiz) and (4) the populations located on the Barbados Accretionary prism (Barbados-KeJ) (see Table 1 to find the name of localities associated with each group). Because mussels from GoM and US were geographically closer to each other than were individuals from Africa-Cadiz and Barbados-KeJ in both species' complexes, we hypothesized T0 (splitting time between pop 0 and pop 1) to be more recent than T1 (splitting time between pop 2 and pop 3, see Supplementary Figure S1).

Analyses were performed on the whole dataset for *B. heckerae*/*B. boomerang* (GoM $n = 63$, US $n = 62$, Western African Margin $n = 73$, Barbados-KeJ $n = 21$) but, given the heterogeneous sample sizes for *G. childressi*/*G. mauritanicus* (GoM $n = 187$, US $n = 259$, Western African Margin-Cadiz $n = 31$, Barbados-KeJ $n = 67$), we subsampled the GoM and US population groups to $n = 64$ and $n = 66$, respectively. For each *Gigantidas* subsample, 60 individuals were randomly chosen and we then purposely added some individuals to make sure that the frequencies of shared haplotypes remained the same before and after the resampling. Indeed, since both GoM and US datasets were subsampled to around half their initial size, we verified that haplotype frequencies were not shifted after subsampling. The aim of such procedure was to prevent any subsampling-induced bias in parameter estimations, especially migration rates which are directly impacted by the distribution of haplotypes between populations. The *G. childressi* – *G. mauritanicus* intermediate individual (see results) from New England seep was however discarded from the analysis as it may represent a potential hybrid individual with a recombining sequence.

Since our dataset included a single locus, we used one MCMC chain (as recommended in IMa3 manual) with 10 million of sampled genealogies (-L 100 000 and -d 100) and 1 million of burn-in steps (-B). As recommended for mitochondrial loci, we used the HKY substitution model and an inheritance scalar of 0.25 (-h). The generation time was set to one year, as assumed for deep-sea bathymodioline mussels (Faure et al., 2009). For other deep-sea species, the substitution rate was estimated between 0.09% and 0.56% per million years (My) (Chevaldonné et al., 2002; Johnson et al., 2006; Faure et al., 2009; LaBella et al., 2017). We used the value of 0.4% per My to calculate the mutation rate per gene per year needed for IMa3 as (0.004*L)/1000000 with L being the length of the sequences used in IMa3 analyses (i.e. 449 bp for *Gigantidas* spp. and 515 bp for *Bathymodiolus* spp.). Parameter convergence was assessed by checking plots of parameter trends and marginal posterior probability distributions of the parameters, by checking the Effective Sample Size (ESS) and comparing estimates of the first and second halves of the sampled genealogies. We used the -p 3 option to print a histogram of splitting times divided by the prior distribution as recommended when there are two or more splitting times in the model. In order to identify the best uniform prior distribution of values, we started by running numerous tests with alternative maximal values (e.g. using hyperpriors or not and starting with IMa3 manual rules of q=5x, t=2x and m=2/x, with x = the nucleotide diversity of each group estimated from the Watterson's θ using the DNAsp v.6 software). Final prior values used are shown in Table 2.

After fixing prior values, we reran analyses for each species complex in triplicate using different seeds in order to make sure that parameter estimations were similar. For each run, parameter estimates were obtained from the highest posterior probabilities (HiPt) together with the 95% highest posterior density intervals (HPD) as confidence intervals. Final values reported in our results corresponded to the averaged values over the different replicates. Significance of migration rates was determined through log-likelihood-ratio tests implemented in IMa3. When migration rates were significantly different from zero in one run but not another, its significance level was reported in the results.

2.4 Numerical hydrodynamic model description

Modelling was performed using VIKING20X, an updated and expanded version of the VIKING20 ocean general circulation model aiming at hindcast simulations of Atlantic Ocean circulation variability on monthly to multi-decadal timescales and with a spatial resolution sufficient to capture mesoscale processes into subarctic latitudes (see a detailed description in Biastoch et al., 2021). VIKING20X is configured on the ORCA family of tripolar grids. The entire model domain covered the Atlantic Ocean from 33.5°S to ~65°N in latitude and from 100°W to 22°E in longitude with a horizontal resolution of 0.05°, nested into a global ocean-sea-ice model at 0.25° resolution and 46 geopotential z-levels along the depth-axis (Figure 1). The horizontal resolution increased with latitude from 5 km in tropical areas to 3 km in polar regions. Layer thickness increased with depth and varied from 6 m at the surface to 250 m in the deepest layers so that it optimizes the representation of the circulation in surface and subsurface waters at the detriment of the near-bottom circulation. Forced by the atmospheric dataset JRA55-do (Tsujino et al., 2018), VIKING20X has been shown to realistically simulate the large-scale horizontal circulation, the distribution of the mesoscale, overflow and convective processes, and the representation of regional current systems, including the western boundary current systems, in the North and South Atlantic (see Biastoch et al., 2021 and references therein). Five-day average fields of the three-dimensional velocities, potential temperature and salinity for the period 1980-2019 were provided by the model.

2.5 Larval dispersal modelling

Larval trajectories were modeled with the offline 3D Lagrangian code Parcels v2.0 (Probably A Really Computationally Efficient Lagrangian Simulator) based on the 3D velocities provided by the VIKING20X model (Delandmeter and van Sebille, 2019), a technique that is well established for physical and interdisciplinary applications in VIKING20X (e.g., Busch et al., 2021; Schmidt et al., 2021; Fox et al., 2022). Based on the current knowledge on the distribution of the two species complexes of deep-

TABLE 1 Number and locations of all sequences used in analyses. The total numbers per site are reported as well as, within brackets, the number of newly sequenced individuals among this total number.

Site (code for genetic samples)	Location	Lat./Lon. (depth)	Cruise	Chief-scientist (and/or study)	*B. boom.*	*B. heck.*	*G. child.*	*G. mauri.*	Total
Alaminos Canyon (AC)	GoM	26°21'N – 94°30'W (2208 m)	AT26-15 2014 (SEEPC)/RV Atlantis/HOV Alvin	C.L. Van Dover, C.M. Young, R He., D. Eggleston, S. Arellano, (Faure et al., 2015)		3	57 (26)		60
AT340 (AT)	GoM	27°38'N – 88°22'W (2174 m)	AT26-15 2014 (SEEPC)/RV Atlantis/HOV Alvin	C.L. Van Dover, C.M. Young, R He., D. Eggleston, S. Arellano, (Faure et al., 2015)		19			19
Green Canyon (GC)	GoM	27°44'N – 91°13'W (563 m)	AT26-15 2014 (SEEPC)/RV Atlantis/HOV Alvin	C.L. Van Dover, C.M. Young, R He., D. Eggleston, S. Arellano, (Faure et al., 2015; Assié et al., 2016)			61 (20)		61
GB647_697 (GB)	GoM	27°20'N – 92°21'W (965 m)	AT26-15 2014 (SEEPC)/RV Atlantis/HOV Alvin	C.L. Van Dover, C.M. Young, R He., D. Eggleston, S. Arellano, (Faure et al., 2015)			10		10
Mississippi Canyon 853 (MIS)	GoM	28°07'N - 89°08'W (1071 m)	AT42-24 2020/ RV Atlantis/ROV Jason2	C.M. Young, R He., D. Eggleston, S. Arellano, (Faure et al., 2015)			49 (23)		49
Brine Pool (NR1)	GoM	27°43'N – 91°16'W (650 m)	AT26-15 2014 (SEEPC)/RV Atlantis/HOV Alvin	C.L. Van Dover, C.M. Young, R He., D. Eggleston, S. Arellano, (Génio et al., 2008)			10 (7)		10
Chapopote Knoll (Chap)	GoM	21°54N - 93°26'W (2923 m)	Meteor M67/2/ ROV Quest	Sayavedra, direct submission, Raggi et al., 2013)		2			2
Florida Escarpment (FE)	GoM	26°01'N – 84°54'W (3284 m)	AT42-24 2020/ RV Atlantis/ROV Jason2	C.M. Young, R He., D. Eggleston, S. Arellano, (Jones et al., 2006; Olu-Le Roy et al., 2007; Faure et al., 2015, Ball, direct submission)		39(8)			39
Blake Ridge (BR)	US	32°30'N – 76°11'W (2169 m)	AT41 2018/RV Atlantis/HOV Alvin//Cruise RB1903 2019/RV Ron Brown/ROV Jason2//AT42-24 2020/RV Atlantis/ROV Jason2	E. Cordes, C.M. Young, R He., D. Eggleston, S. Arellano, (Ball, direct submission)		34(8)			34
Pick-Up Sticks (PUS)	US	37°34'N –74°16'W (370-410 m)	AT29-04 2015/ RV Atlantis/ HOV Alvin	C.L. Van Dover, (Ball, direct submission)		27			27
Norfolk Canyon (NO)	US	36°52N -74° 29'W (1485-1600 m)	AT41 2018/RV Atlantis/HOV Alvin//Cruise RB1903 2019/RV Ron Brown/ROV Jason2	E. Cordes, (Coykendall et al., 2019; Turner et al., 2020)		1	85		86
Chincoteague (CH)	US	37°32'N – 74°06'W (1020-1060 m)	Cruise 2017/RV Hugh R. Sharp/ ROV Global Explorer//AT42-	C. Ruppel, A. Demopoulos, C.M. Young, R He., D. Eggleston, S. Arellano,			41 (1)		41

(Continued)

TABLE 1 Continued

Site (code for genetic samples)	Location	Lat./Lon. (depth)	Cruise	Chief-scientist (and/or study)	*B. boom.*	*B. heck.*	*G. child.*	*G. mauri.*	Total
			24 2020/RV Atlantis/ROV Jason2	(Coykendall et al., 2019; Turner et al., 2020)					
Baltimore Canyon (BC)	US	38°03'N – 73°49'W (360-430 m)	Cruise 2012/RV Ron Brown/ROV Kraken//Cruise 2013/RV Ron Brown/ROV Jason2//AT42-24 2020/RV Atlantis/ROV Jason2	S. Ross, S. Brooke, C.M. Young, R He., D. Eggleston, S. Arellano, (Coykendall et al., 2019; Turner et al., 2020)			60 (1)	1	61
Shallop Canyon West (SW)	US	39°59'N –69°11'W (360-400 m)	AT29-04 2015/ RV Atlantis/ HOV Alvin	C.L. Van Dover, (Turner et al., 2020)			16 (13)		16
Veatch (VE)	US	39°48'N –69°35'W (1390–1440 m)	AT29-04 2015/ RV Atlantis/ HOV Alvin	C.L. Van Dover, (Turner et al., 2020)			28 (23)		28
New England seep 2 (NE)	US	39°52'N –69°17'W (1380–1440 m)	AT29-04 2015/ RV Atlantis/ HOV Alvin	C.L. Van Dover, (Turner et al., 2020)			28 (23)		28
Milano volcano (BA)	Barbados	11°41'N – 58°33'W (1317 m)	AT21-02 2012/ RV Atlantis/ROV Jason2	C.L. Van Dover, C.M. Young, R He., D. Eggleston, S. Arellano, (Olu-Le Roy et al., 2007; Assié et al., 2016)	4			31 (13)	35
Kick em Jenny (KeJ)	Barbados	11°14'N – 58°22'W (998 -1630 m)	NA054 2014/EV Nautilus/ROV Hercules and Argos	C.L. Van Dover, C.M. Young, R He., D. Eggleston, S. Arellano, (Ball. Direct submission)	17(5)		10	26 (26)	53
Darwin mud volcano (CA)	Cadiz	35°24'N – 7°11'W (1115 m)	TTR10 2003/RV Prof. Logatchev/ TV_grab//JC10 2007/RSS James Cook/ROV Isis	M.R. Cunha, (Génio et al., 2008)				22 (18)	22
West African margin-Ivory (WAM)	WAM	0°53'N – 5° 28'W (1000-1267 m)	–	(Jones et al., 2006)				1	1
Nigerian (NIG) slope	WAM	4°59'N – 4° 08'W, (1700-2100 m)	TDI-Brooks International prospects 2006/ box cores (NCB3008-GSN0892, NCB2001-TGSN0883, NCB2038-TGSN0890)	E. Cordes	17(17)			8 (8)	25
Regab (Regab)	WAM	5°48'S – 9° 43'E (3170 m)	WACS 2011/NO Pourquoi Pas?/ ROV Victor6000	K. Olu, (Olu-Le Roy et al., 2007, Ball, direct submission)	56(8)				56
Total					94	125	455	89	763

GoM, Gulf of Mexico; US, US Atlantic Margin; WAM, West African Margin; Barbados, Barbados Prism; Cadiz, Gulf of Cadiz. See Figure 1 for a map and Supplementary Table S1 for accession numbers.

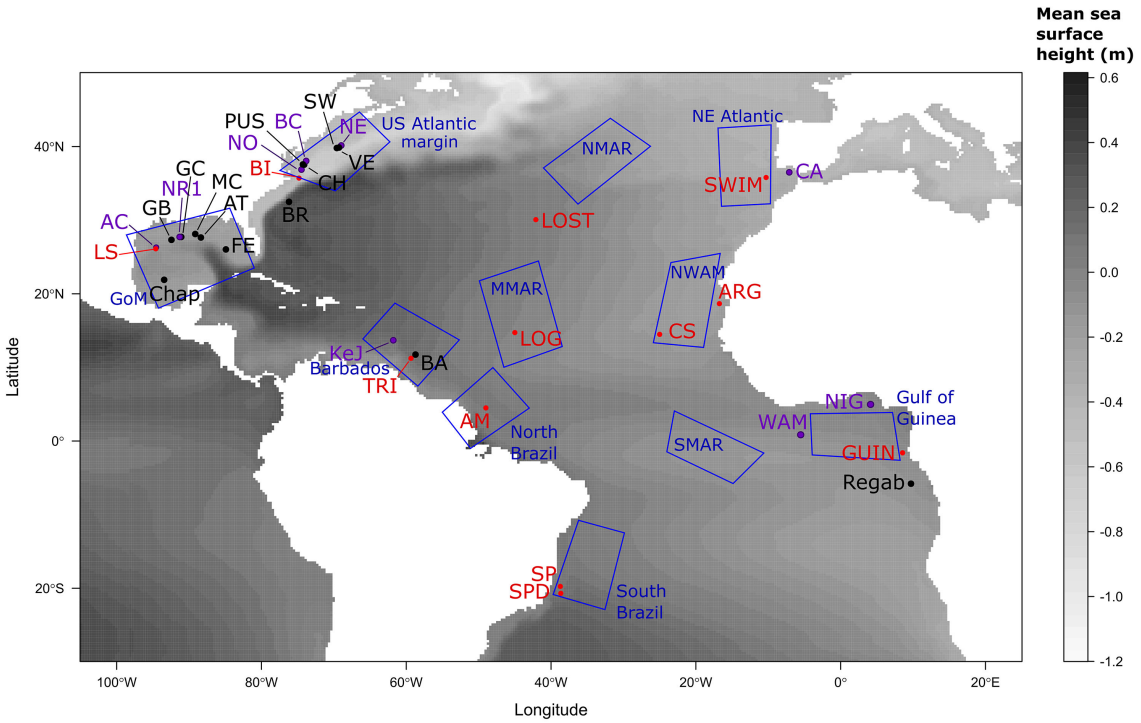

FIGURE 1
Geographic locations of seeps involved in the present study. Sites for which only genetic samples are available are in black, spawning areas used only in larval dispersal modelling are in red, sites used for both genetic and modelling approaches are in purple. Blue polygons represent settlement regions used in the modelling approach. Site abbreviations correspond to NR1, Brine Pool; LS, Louisiana slope; AC, Alaminos canyon; BI, Bodie island; NO, Norfolk canyon; BC, Baltimore canyon; NE, New England seeps; SWIM, SWIM Fault; CA, Gulf of Cadiz; ARG, Arguin bank; CS, Cadamostro seamount; NIG, Nigerian margin; WAM, West African margin; GUIN, Guiness; SP, Sao Paulo seep 1; SPD, Sao Paulo seep 2; AM, Amazon fan; TRI, Trinidad prism; KeJ, Kick em Jenny crater; LOG, Logatchev seep and LOST, Atlantis FZ (Lost City). Abbreviations of the zones for recruitment are: NWAM, North West African margin; NMAR, North Mid-Atlantic Ridge; MMAR, Middle Mid-Atlantic Ridge and SMAR, South Mid-Atlantic Ridge. Genetic samples were either obtained in the present study or included thanks to already published sequences (see Tables 1, 2; Supplementary Table S1).

TABLE 2 Priors and estimates values of IMa3 demographic parameters for the two species complex.

			Gigantidas				*Bathymodiolus*			
Parameter	Biological meaning	Populations	Prior[(a)]	HiPt	HPD95L	HPD95H	Prior	HiPt	HPD95L	HPD95H
t_0	Divergence time between	GoM and US	2	355 791	237 751	575 167	2	153 236	83 981	422 816
t_1		WAM-CA and BA-KeJ	90	576 281	275 612	50 086 303	100	396 440	72 816	48 519 417
t_2		MRCAs of GoM-US and BA-KeJ-WAM -CA	300	584 633	417 595	100 306 236	600	1 019 418	436 893	126 844 660
q_0	Ne	GoM	800	22 438 753	11 414 254	41 146 993	500	10 750 405	2 457 524	48 391 990
q_1		US	1500	23 280 902	13 885 022	39 775 891	100	851 537	127 427	12 129 854
q_2		WAM-CA	70	1 407 990	414 115	3 590 618	300	5 867 718	709 951	34 387 136
q_3		BA-KeJ	70	3 663 697	1 856 208	8 189 727	2	2 063	364	148 180
q_4		GoM-US MRCA	15	33 408	3 132	637 876	5	6 574	0	418 386
q_5		BA-KeJ MRCA	70	954 900	0.000	9 739 003	50	308 455	9 102	5 840 413
q_6		MRCA	70	1 120 546	0.000	9 251 810	1000	424 757	0	121 298 544

(Continued)

TABLE 2 Continued

			Gigantidas				*Bathymodiolus*			
Parameter	Biological meaning	Populations	Prior[(a)]	HiPt	HPD95L	HPD95H	Prior	HiPt	HPD95L	HPD95H
$2N_1m_{1>0}$	Nm from GoM to	US	100	46.41***	19.030	85.030	30	11.967*	0.000	178.100
$2N_2m_{2>0}$		WAM-CA	2	0.020	0.000	3.493	1	0.051	0.000	22.690
$2N_3m_{3>0}$		BA-KeJ	2	0.016	0.000	3.645	9	0.003	0.000	1.156
$2N_0m_{0>1}$	Nm from US to	GoM	100	0.070	0.000	37.030	8	7.507**	0.000	349.000
$2N_2m_{2>1}$		WAM-CA	2	0.021	0.000	3.533	1	0.051	0.000	23.760
$2N_3m_{3>1}$		BA-KeJ	2	0.016	0.000	3.530	4	0.002	0.000	0.866
$2N_0m_{0>2}$	Nm from Af-CA to	GoM	2	0.071	0.000	8.639	1	0.122	0.000	22.100
$2N_1m_{1>2}$		US	4	0.034	0.000	8.606	2	0.031	0.000	14.930
$2N_3m_{3>2}$		BA-KeJ	2	0.225	0.000	5.338	20	0.015**	0.000	2.084
$2N_4m_{4>2}$		GoM-US MRCA	100	0.380	0.000	10.870	4	0.023	0.000	1.324
$2N_0m_{0>3}$	Nm from BA-KeJ to	GoM	4	0.038	0.000	9.918	1	0.123	0.000	33.940
$2N_1m_{1>3}$		US	4	1.375	0.000	11.240	4	0.050	0.000	3.340
$2N_2m_{2>3}$		WAM-CA	2	0.023	0.000	4.095	9	63.239***	0.000	725.300
$2N_4m_{4>3}$		GoM-US MRCA	4	0.014	0.000	2.114	4	0.024	0.000	2.834
$2N_2m_{2>4}$	Nm GoM-US mrca to	WAM-CA	6	0.522	0.000	36.380	4	16.360*	0.000	153.8
$2N_3m_{3>4}$		BA-KeJ	4	0.070	0.000	88.510	8	0.014	0.000	2.467
$2N_5m_{5>4}$		BA-KeJ MRCA	15	0.262	0.000	366.000	4	0.050	0.000	69.920
$2N_4m_{4>5}$	Nm from BA-KeJ mrca to	GoM-US MRCA	15	0.169	0.000	18.720	4	0.005	0.000	3.963

[(a)]priors for migration rates defined for $m_{X>Y}$ and not for 2NM parameters.

GoM, Gulf of Mexico; US, US Atlantic Margin; BA, Barbados; KeJ, Kick em Jenny; WAM, West African Margin; CA, Gulf of Cadiz. Ne, effective size; Nm, effective number of migrants per generation; MRCA, most recent common ancestor; HiPt, histogram bin with the highest posterior probability; HPD95L and HPD95H, 95% low and high HPD, respectively. Time parameters are given in years. As detailed in the main text, HiPt values reported here are mean values over several runs for both species complexes except for q_0, q_1, $2N_1m_{1>0}$, $2N_0m_{0>1}$, $2N_0m_{0>2}$, $2N_1m_{1>2}$, $2N_0m_{0>3}$ and $2N_1m_{1>3}$ in *Gigantidas* for which the best value was used. Asterisks indicate values for which migration rate parameters significantly differed from zero in at least one of the runs (likelihood ratio tests, Supplementary Table S5). HPD95L and HPD95H values reported are the minimal and maximal values observed across runs, respectively. It is noteworthy that in IMa3 $m_{X>Y}$ are expressed in the coalescent, so backward in time. When reading forward in time, $m_{X>Y}$ represents migration from population Y to population X.

sea mussel populations, 17 spawning areas were defined in the North Atlantic along the coasts of North and South America, Europe and Western Africa (Figure 1; Supplementary Table S2). In these sites, the presence of bathymodioline mussels was confirmed or suspected in the present study or elsewhere (Gustafson et al., 1998; Cosel, 2002; Olu-Le Roy et al., 2007; Génio et al., 2008; Faure et al., 2015; Assié et al., 2016; Fujikura et al., 2017; Ketzer et al., 2018; Coykendall et al., 2019; Ruppel et al., 2019; Turner et al., 2020, see Supplementary Table S2 for details). Four additional sites where cold seeps were reported or could be present were added: two along the Mid-Atlantic Ridge (Logatchev and Lost City sites, Gebruk et al., 2000; Brazelton et al., 2006; Proskurowski et al., 2008; LaBella et al., 2017), the Cadamostro Seamount off the Cape Verde Islands, and the South West Iberian Margin Fault Zone (SWIM Fault Zone). Since indices of presence of diffuse hydrothermalism on seamounts were found during iMirabilis2 iAtlantic cruise (2021), these two last sites could act as gateway populations.

The number of released particles during each spawning event needs to be sufficient to properly reproduce distribution of drifting particles including planktonic larvae at regional scale so that no significant changes are reported in the mean characteristics of the dispersal kernel and larval trajectories as the number of particles is increased (Jones et al., 2016; Van Sebille et al., 2018). Preliminary simulations were performed with 1000, 2000, 5000 and 10 000 released larvae on a few spawning areas and showed that spreading of the larval population and maximum larval dispersal distance were not altered when more than 2000 larvae were released. Then, conservatively, for each spawning area defined as a polygon of 0.08° in latitude and longitude, 10 000 larvae were randomly released at each spawning date in near-bottom waters (i.e. specifically at approx. 10 m above the bottom of the simulated Ocean, Table 3). Larvae were released monthly during a unique spawning event that occurred the 1st day of each month from November to March during the natural spawning period of *G. childressi* (Tyler et al., 2007), from 2014 to 2019 to consider year-to-year variations in

TABLE 3 Summary of larval characteristics used in the larval dispersal modelling using VIKING20X.

Number of released larvae	10 000
Depth of release	10 m above the oceanic floor
Spawning dates	1st day of each month from November to March during 5 years (2014-2019)
Duration of spawning	Instantaneous
Pelagic Larval Duration	365 days
Velocity	Vertical swimming at 0.2 $mm.s^{-1}$ until 200 m of depth
Mortality	100% if temperature > 20°C; if not 0%
Measure of connectivity	Percentage of larvae that entered in a settlement region whatever the vertical position

current patterns. Biological characteristics of larvae in terms of Pelagic Larval Duration (PLD), behavior and mortality were defined according to field observations and laboratory experiments performed on *G. childressi* in the GoM. After the spawning, the position of each simulated larva was tracked over one year (i.e. 365 days, Table 3) which corresponds to the maximum PLD of *G. childressi* (Arellano and Young, 2009). The choice of a high value of PLD was made in order to model extreme dispersal events likely to impact genetic structures and promote trans-Atlantic dispersal. After release in the near bottom layer, larvae could swim vertically to reach surface and subsurface waters at a velocity of 0.2 $mm.s^{-1}$ (Table 3), a velocity in agreement with swimming speed of *G. childressi* trochophores observed in experimental chambers (Arellano, 2008). Although no data were available for veligers of *G. childressi* or other bathymodioline species, Chia et al. (1984) reported a mean swimming velocity of 0.2 $mm.s^{-1}$ for bivalve larvae. When they reached a depth of 200 m, larvae stopped swimming. This larval behavior was defined to mimic the vertical distribution of larvae mainly sampled in the first 100 m in the GoM and sometimes up to 550 m deep (Arellano et al., 2014). Laboratory experiments showed that normal larval development occurred between 7 and 15°C and that survival did not differ significantly between 7 and 20°C before decreasing at 25°C (Arellano and Young, 2009; Arellano and Young, 2011; Arellano et al., 2014). Accordingly, we assumed that larvae died when they reached a temperature of 20° C. No other source of larval mortality was considered (Table 3).

Due to the highly aggregated and localized distribution of cold seepage environments and the lack of knowledge about the behavior of bathymodioline mussel larvae during settlement, connectivity was not assessed among cold seeps locations but among 11 large settlement regions of 10^6 km^2. These large regions contained one or more cold seeps locations already documented or are likely to contain cold seeps along the American, African and European active margins and along the mid-Atlantic Ridge. They include the GoM, the US Atlantic margin, the North Eastern Atlantic, the North West African margin, the Gulf of Guinea, the South and North Brazil, the Barbados Prism, the North mid-Atlantic ridge, the Middle mid-Atlantic Ridge and the South mid-Atlantic Ridge (Figure 1). The connectivity, that describes the exchange rate between distant populations, was calculated as the percentage of larvae released from one spawning area (i.e. source population) that entered in a settlement region (i.e. sink region) at the end of the PLD, whatever the vertical position of larvae. The retention rate corresponded to the percentage of larvae released from one spawning area that remains in the settlement region to which the spawning area belongs at the end of the PLD. To analyze the dispersal patterns resulting from our numerical experiments at the end of the PLD, two parameters describing the 2D dispersal kernels, i.e. the density of larvae at a given location normalized by the number of released particles, were retained following Edwards et al. (2007): the mean dispersal distance (D) and the isotropy of the larval population (I). The isotropy depends on the overall inertia which characterizes the variance of the larval distribution around the mean geographic position of the larval population. Inertia can be decomposed into two orthogonal axes representing the maximum (I_{max}) and the minimum (I_{min}) parts of the overall inertia. These parameters were calculated by a principal component analysis performed on the ending positions of larvae. Isotropy was then defined as the square root of the ratio between I_{max} and I_{min}.

3 Results

3.1 Haplotype networks and genetic diversities within groups

Within the *Gigantidas* species complex, 144 haplotypes (among which 42 are new) were identified out of 544 barcoded individuals. Within the *Bathymodiolus* species complex, only 43 haplotypes (among which 10 are new) were evidenced for 219 samples. The number of variable sites (S) was 100 for the former and 38 for the latter, with a total number of mutations of 112 and 39, respectively. The average number of nucleotide differences (k) was also higher in *Gigantidas* spp. than in *Bathymodilus* spp. (k = 5.18 and 3.70, respectively). Accordingly, although haplotype diversity was comparable between *Gigantidas* spp. and *Bathymodilus* spp., nucleotide diversity was almost twice as high in *Gigantidas* spp. for the whole set of samples (Table 4). The haplotype networks showed the presence of two distinct geographic lineages within each species complex (Figures 2, 3). The higher number of nucleotide differences observed between the two *Gigantidas* lineages as compared to the two *Bathymodiolus* lineages was well illustrated by haplotype network reconstructions with 7 and 3 fixed substitutions, respectively (Figures 2, 3). This corresponded to the net genetic distances (Da) we observed since maximal values occurred between lineages, and values were higher between *G. childressi/G. mauritanicus* (≈ 0.02) than between *B. heckerae/B. boomerang* (≈ 0.01, Table 5). The divergence between *B. heckerae/B. boomerang* from the Barbados-KeJ and the US Atlantic margin was, however, slightly lower than that between the African margin and the GoM/US Atlantic margin (Table 5).

Genetic distance within each of the four lineages was low. In the *Gigantidas* species complex, a very low genetic distance of 0.00005

10.3389/fmars.2023.1122124

TABLE 4 Variation of COI nucleotides sequences for each species complex and each sampling site.

		G. childressi/G. mauritanicus				*B. heckerae/B. boomerang*			
		N	h	Hd	π	N	h	Hd	π
GoM	AC	57	26	0.902	0.005	3	1	0	0
	AT					19	2	0.105	0
	MIS	49	22	0.886	0.005				
	NR1	10	5	0.8	0.005				
	FE					39	13	0.623	0.002
	GB	10	7	0.911	0.004				
	GC	61	28	0.859	0.005				
	CHap					2	2	1	0.004
US Atlantic margin	CH	41	21	0.896	0.006				
	NE	28	13	0.825	0.009				
	PUS					27	5	0.553	0.002
	BC	60 (1)	26	0.86	0.005				
	SW	16	6	0.783	0.004				
	NO	85	28	0.83	0.004	1	1	0	0
	VE	28	16	0.915	0.006				
	BR					34	11	0.649	0.002
Barbados-KeJ	BA	(31)	8	0.66	0.003	(4)	2	0.5	0.001
	KeJ	10 (26)	13	0.743	0.003	(17)	2	0.515	0.001
Western African Margin -Cadiz	IV	(1)	1	0.000	0.000				
	NIG	(8)	3	0.464	0.001	(17)	5	0.507	0.002
	Regab					(56)	13	0.538	0.001
	CA	(22)	7	0.645	0.002				
	Overall populations	455 (89)	144	0.900	0.012	125 (94)	43	0.84	0.007

N, number of sequences in each population (*G. childressi* and *B. heckerae* without brackets and *G. mauritanicus* and *B. boomerang* within brackets); h, number of unique haplotypes; Hd, haplotype diversity; π, nucleotide diversity. See Table 1 for population acronyms definition and Figure 1 for a map.

occurred between GoM and the US Atlantic margin while it increases to 0.00225 between Barbados-KeJ and Africa-Cadiz groups (i.e. 45 times higher, Table 5). In *Bathymodiolus* spp., divergence was slightly greater between the GoM and the US Atlantic margin (0.001) due to the slight isolation of the Blake Ridge population (see Figures 3, 4B; Supplementary Table S4) and reached 0.004 between Barbados-KeJ and Western African Margin groups (Table 5). It corresponded to what can be observed in haplotype networks since, in both species complexes, individuals from GoM and the US Atlantic margin populations appeared more genetically similar than individuals from Barbados-KeJ and Africa-Cadiz populations. Numerous *G. childressi* haplotypes were, indeed, shared between the US Atlantic margin canyons and GoM populations (Figure 2). *Bathymodiolus heckerae* haplotypes appeared, nevertheless, more spatially segregated. While few individuals sampled in the Blake Ridge population harbored haplotypes also found in the GoM/Florida Escarpment and Pick Up Sticks populations, most of Blake Ridge samples showed private haplotypes (Figure 3). The Pick-Up Sticks population (located further North on the American margin) exhibited both GoM-derived and Blake Ridge-derived haplotypes.

Barbados-KeJ and Africa-Cadiz populations, although genetically close with no fixed differences, also exhibited a distinguishable geographic structure since haplotypes clustered from each side of the Atlantic Equatorial Belt. Interestingly, in *Bathymodiolus*, haplotypes from Barbados-KeJ were intermediate between GoM-US and African ones (Figure 3). Haplotype networks highlighted peculiar haplotypes. One haplotype from a New England individual had an intermediate position between *G. childressi* and *G. mauritanicus* lineages (individual (a) on Figure 2, accession KX159882 from Turner et al., 2020) and may represent a hybrid individual. Three other ones sampled along the US Atlantic margin (Baltimore Canyon and New England) had a *G. mauritanicus* signature (individuals (b) on Figure 3, accession

10.3389/fmars.2023.1122124

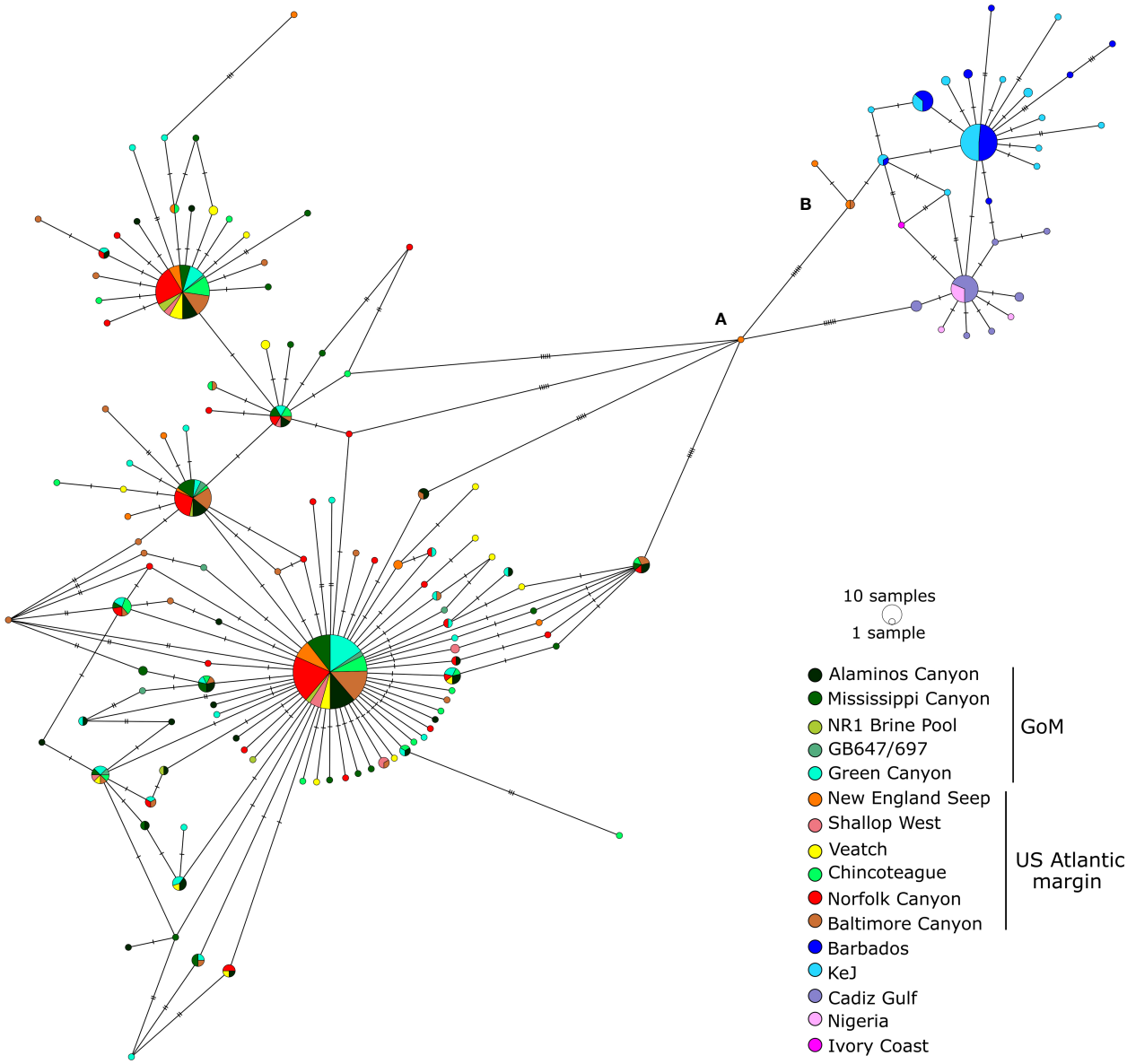

FIGURE 2
Haplotype network for the *G. childressi/G. mauritanicus* species complex. See Table 2 and Supplementary Table S1 for details about sequences included. Individuals (A, B) are highlighted as being the intermediate haplotype between both sides of the Atlantic Ocean (in New England seep) and the three *G. mauritanicus* sampled along the US Atlantic margin (Baltimore Canyon and New England seep), respectively. KeJ: Kick am Jenny, GoM: Gulf of Mexico.

MG519868 from Coykendall et al., 2019 and New England_1553 and New England_1530 from this study, Supplementary Table S1). In *Bathymodiolus*, a unique *B. heckerae* was sampled in the Norfolk canyon (accession MG519869 from Coykendall et al., 2019), within a *G. childressi* population, and a potential *B. boomerang* migrant individual from the Barbados Accretionary Prism was sampled on the Nigerian slope (individual (a) on Figure 3).

3.2 Barcode gap analyses

For both *Gigantidas* and *Bathymodiolus* genera, two distinct OTUs could be distinguished, but these OTUs were not geographically delimited, with one lineage potentially sharing haplotypes across the North Atlantic in both species complexes. Indeed, in the *Gigantidas* species complex, the partition receiving the highest support (lowest ASAP score, Supplementary Figure S2) indicated the presence of two lineages. In accordance, the distribution of pairwise differences was clearly bimodal with two distinct Gaussian distributions with almost no overlap (Supplementary Figure S2). When looking at individual assignments, one lineage grouped all samples from Barbados Accretionary Prism and the African margin plus one individual from the Baltimore Canyon and two from New England Seep (identified as (b) on Figure 2). All these samples were previously identified as *G. mauritanicus* except for 10 individuals from KeJ and

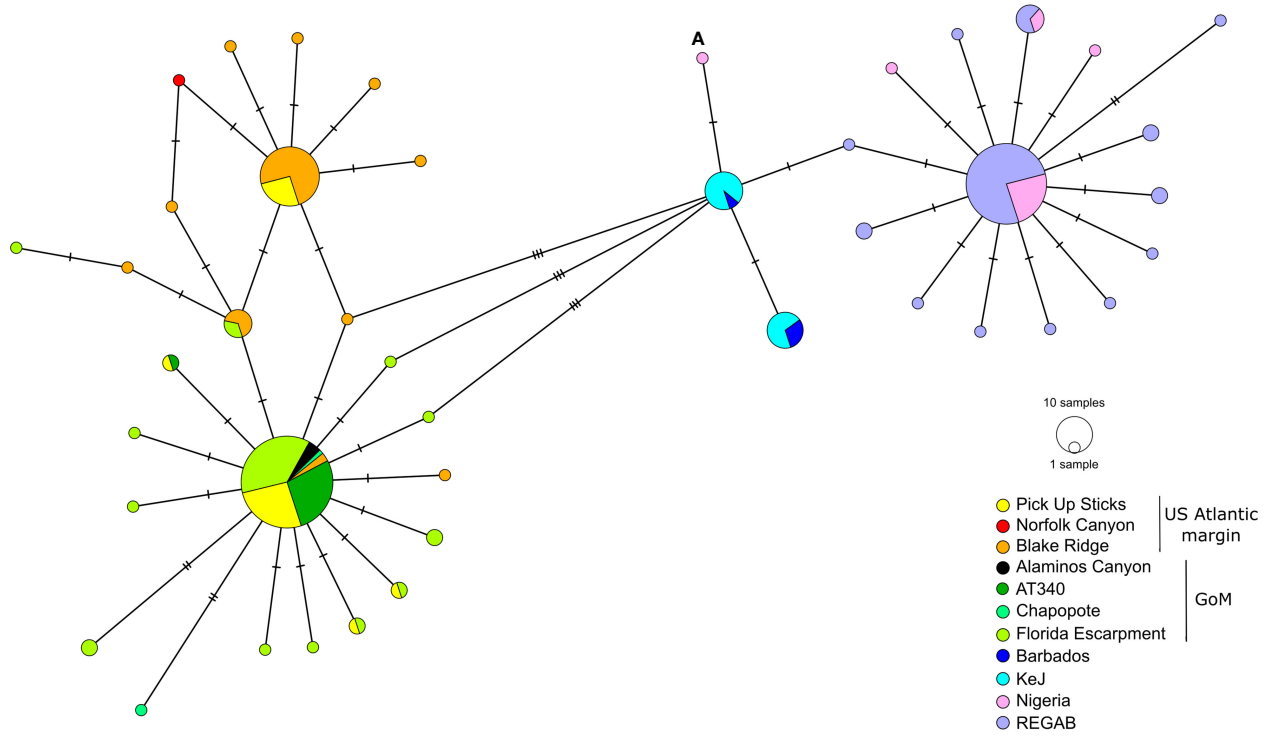

FIGURE 3
Haplotype network for the *B. heckerae/B. boomerang* species complex. See Table 1 and Supplementary Table S1 for details about sequences included. Individual (A) might represent a migrant from Kick em Jenny (KeJ)/Barbados Accretionary Prism to the Nigerian slope. GoM, Gulf of Mexico.

two individuals from New England Seep that were previously affiliated to *G. childressi* based on morphology (Table 1; Supplementary Table S1). This first lineage thus corresponded to *G. mauritanicus*. The second lineage grouped all samples from GoM and US Atlantic margin sites and thus represented *G. childressi*. As recommended by Puillandre et al. (2021), we also examined subsequent partitions. The second-best partition delimited 5 lineages of which composition was identical to the two previously described except that some sequences were isolated in other groups. One group was composed of the sample from the New England seep, which had an intermediate signature between *G. childressi* and *G. mauritanicus* haplotypes groups (individual (a) Figure 2, accession KX159882.1). The two last groups isolated, without apparent biological explanations, one individual from Chincoteague (accession KX159907.1) and one individual from Barbados (DQ513425.1). In the *Bathymodiolus* species complex, the partition receiving the highest support (Supplementary Figure S3) also indicated the presence of two lineages in the dataset. The distribution of pairwise differences was less disjunct than for *Gigantidas* although two peaks can be distinguished (Supplementary Figure S3). One lineage grouped all individuals identified as *B. boomerang* (from Barbados and the African margin) while *B. heckerae* from the GoM and the US Atlantic margin were grouped together in the other lineage. The second-best partition delimited 9 lineages from which no biological significance can be identified.

3.3 Population genetic differentiation

Fst values highlighted a strong to moderate geographic differentiation between three mussel groups within both species'

TABLE 5 Net genetic distance (Da, below the diagonal) and Fst values (above the diagonal) for *Gigantidas sp.* and *Bathymodiolus sp.* calculated between the four populations defined based on haplotype networks and ASAP analyses (see Table 1 for details).

	Gigantidas sp.				*Bathymodiolus* sp.			
	GoM	US	BA-KeJ	WAM-Cadiz	GoM	US	BA-KeJ	WAM
GoM	*	0.00062	**0.20173**	**0.22719**	*	**0.36937**	**0.86440**	**0.89363**
US	0.00005	*	**0.21178**	**0.23759**	0.00115	*	**0.76867**	**0.84742**
BA-KeJ	0.02433	0.02334	*	**0.33111**	0.00807	0.00738	*	**0.76436**
WAM-Cadiz	0.02175	0.02075	0.00225	*	0.01133	0.01070	0.00416	*

Bold values represent significantly different from zero Fst values (exact test of population differentiation).
* symbolized an empty cell in the table.

complexes. These genetic entities corresponded to the populations from (1) GoM/US Atlantic margin, (2) the Barbados accretionary Prism, and (3) European/African margin. As expected, genetic differentiation between *B. heckerae* and *B. boomerang* or *G. childressi* and *G. mauritanicus* was high since nearly all pairwise Fst values between (1) and (2)/(3) were high and significantly different from zero (Figure 4; Table 5). *G. childressi* and *G. mauritanicus* did not display higher Fst values than those obtained between *B. heckerae* and *B.*

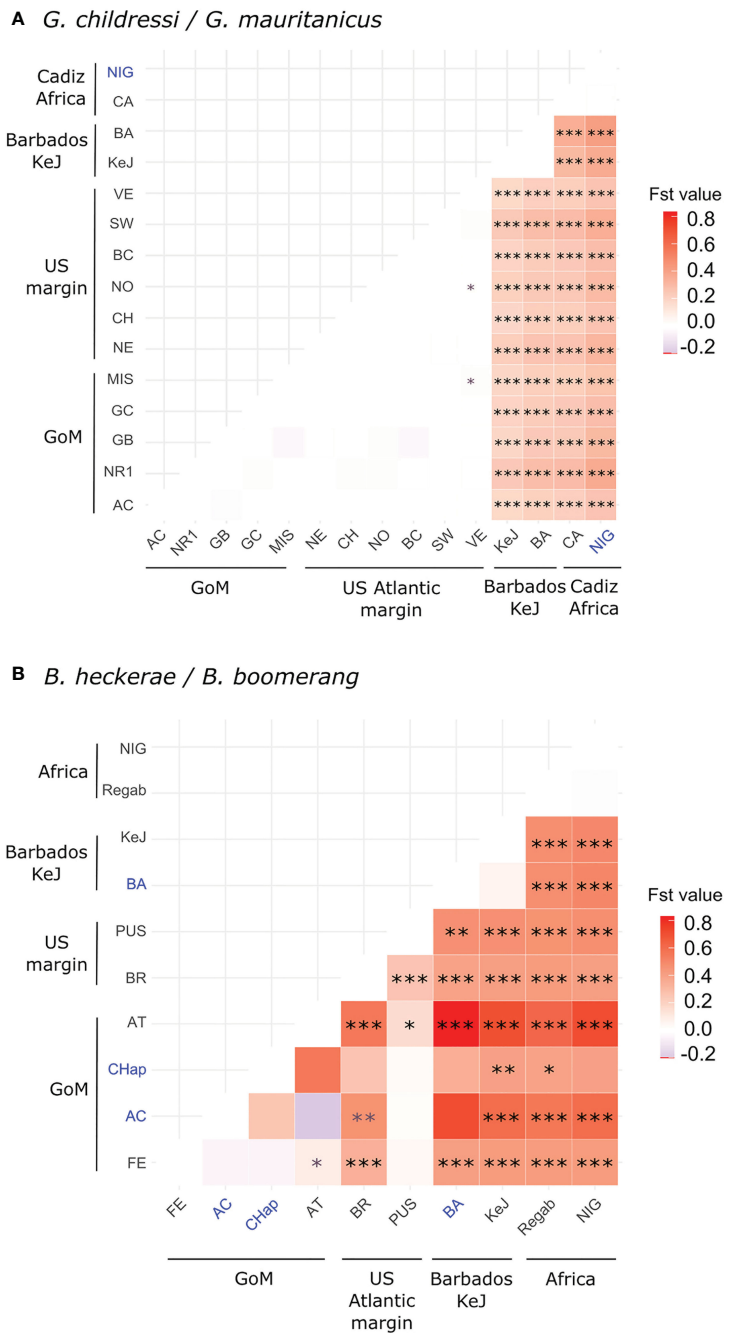

FIGURE 4
Pairwise Fst heatmaps for *G. childressi/G. mauritanicus* **(A)** and *B. heckerae/B. boomerang* **(B)**. Values are color-scaled and significance levels compared to zero are indicated using: *for p-value ≤ 0.05, **p-value ≤ 0.01 and ***p-value ≤ 0.001. Absence of asterisks indicates non-significant values and grey asterisks indicates Fst values for which significance was confirmed using either permutations or exact test of differentiation but not both. Populations for which less than 10 sequences were available are indicated in blue. Values for West African margin-Ivory (WAM) and Norfolk populations for *G. childressi* and *B. boomerang*, respectively, are not displayed since calculations involved only one sequence (see Table 2 for number of samples and population acronyms). GoM, Gulf of Mexico. Exact values and p-values are reported in Supplementary Tables S3, S4.

boomerang (Figure 4; Supplementary Tables S3, S4), as would have been expected since the two *Gigantidas* lineages were separated by a higher number of mutational changes (Figures 2, 3).

Populations of *G. childressi* were almost homogeneous from the GoM to the most northern part of the American margin with all pairwise Fst values between US Atlantic margin and GoM sites being null or very low and not significantly different from zero (except two using exact tests, Figure 4A; Supplementary Table S3). For *B. heckerae*, however, the Blake Ridge population clearly differed from those of the GoM and the Florida Escarpment (Fst = 0.25 to 0.55, Figure 4B; Supplementary Table S4). In *G. mauritanicus* and *B. boomerang* species, high and significant Fst values were observed, especially between African populations and Barbados-KeJ (Figure 4; Supplementary Tables S3, S4). In contrast, Fst values between African populations and that of the Gulf of Cadiz were low and not significantly different from zero (Figure 4; Supplementary Tables S3, S4).

Altogether, pairwise Fst and divergences strongly suggested high levels of gene flow along the European/African margins and weak to almost no gene flow between the African margin and the Barbados Accretionary Prism, but also suggest a strong genetic break between mussel populations from the Barbados Accretionary Prism (South American margin) and those situated in the GoM and further North along the US Atlantic margin.

3.4 Divergence time and gene flow estimates using IMa3

Based on ASAP and Fst analyses, seep mussel populations were sub-divided into 4 distinct geographic groups (i.e. GoM, US Atlantic margin canyons, Barbados accretionary Prism and European/African margin) in order to examine potential gene flow between them. For both species complexes, nearly all replicated runs showed good mixing (plots without trends, large ESS for T1 (all except two > 14 000) and T2 (all > 400 000), and good congruence between first and second halves of the sampled genealogies). For most parameters, marked peaks of posterior probabilities with fairly narrow ranges were observed (Supplementary Figures S4–S8), even for T0 that showed the lowest ESS (<30). For *Gigantidas* spp., we were not able to jointly estimate q_0 and q_1 parameters with $m_{0>1}$ and $m_{1>0}$. Given the good mixing observed in each run and the correspondence of the other estimates (Supplementary Figures S4–S6), estimations of q_0 and q_1 (and thus, 2NM parameters involving N_0 and N_1) were taken from two different runs. For all other parameters, averaged values between runs were calculated after ensuring that good mixing and convergence were obtained for all runs (see Supplementary Figures S4–S6).

The population splitting times separating *G. childressi* and *G. mauritanicus*, on one hand and *B. heckerae* and *B. boomerang*, on the other hand (i.e. T_2) were estimated to have occurred around 585 000 years ago and 1 My ago, respectively (Table 2). For both, the upper boundary of 95% HPD was very large, probably due to the fact that only one locus has been used. Based on Fst and genetic divergence, divergence times between Africa-Cadiz and Barbados-KeJ populations (T1) was expected to be more ancient than divergence between GoM and US Atlantic margin populations (T_0), especially for *Gigantidas* species complex. Accordingly, although quite close, T_1 estimates were 576 281 and 396 440 for *Gigantidas* spp. and *Bathymodiolus* spp., respectively, while T_0 were estimated as 355 791 and 153 236, respectively. Effective sizes of contemporary populations (q_0, q_1, q_2 and q_3) were largely higher in *Gigantidas* spp. than in *Bathymodiolus* spp. except for the Africa-Cadiz population which was four time higher in *B. boomerang* (Table 2). A similar situation was observed for ancestral populations that showed higher sizes in *Gigantidas* spp. although the posterior probabilities distribution of these parameters (especially q_5 and q_6) were quite large (Supplementary Figures S4–S8).

Regarding migration rates, most estimates were close to zero and non-significantly different from it (Table 2). High values significantly different from zero in at least one run were nevertheless observed for $2N_1m_{1>0}$ for both species complexes (*Gigantidas* and *Bathymodiolus*), suggesting efficient migration greater than one individual per generation from GoM to the US Atlantic margin (Table 2). Gene flow in the opposite direction was non-different from zero for *G. childressi* but estimated to be around 7 migrants per generation for *B. heckerae*. It is however noteworthy that for *B. heckerae* both $2N_1m_{1>0}$ and $2N_0m_{0>1}$ HPD95% included zero. Other significantly different from zero values included $2N_3m_{3>2}$ for *B. boomerang*, which represented the number of trans-Atlantic migrants from Western Africa to Barbados-KeJ. This value was, however, very low (less than one individual per generation) and the HPD95% included zero. This contrasted with reverse large and significant *Nm* values of around 60 migrants per generation from Barbados-KeJ to Africa, but also with an ancestral rate of migration of nearly 20 migrants per generation found in *Bathymodiolus* between the American and European/African margins. In the *Gigantidas* species complex, only the *Nm* value from Barbados to the US Atlantic margin was greater than one, but this value was not significantly different from zero. This contemporary flow was confirmed by the sampling of one and two *G. mauritanicus* migrants in the Baltimore Canyon and the New England seep 2, respectively (see (b) in Figure 3).

3.5 Larval dispersal modelling

Despite variations according to the spawning dates (i.e. 5 years with 5 months each), the overall patterns of larval dispersal were generally consistent between dates for each spawning area (see larval simulations in Portanier et al., 2023 and Jollivet et al., 2023) and are summarized in Figures 5, 6; Table 6 at the scale of the whole Atlantic. Larvae released in the GoM (i.e. Alaminos Canyon, Brine Pool, Louisiana Slope) spread throughout the GoM while a significant number of them traveled through the Florida Strait, and dispersed northward along the US Atlantic margin and then eastward off the Mid-Atlantic Bight across the North Atlantic, following the overall North Atlantic gyre (Figures 5, 6; Table 6). Average dispersal distances traveled by larvae varied between

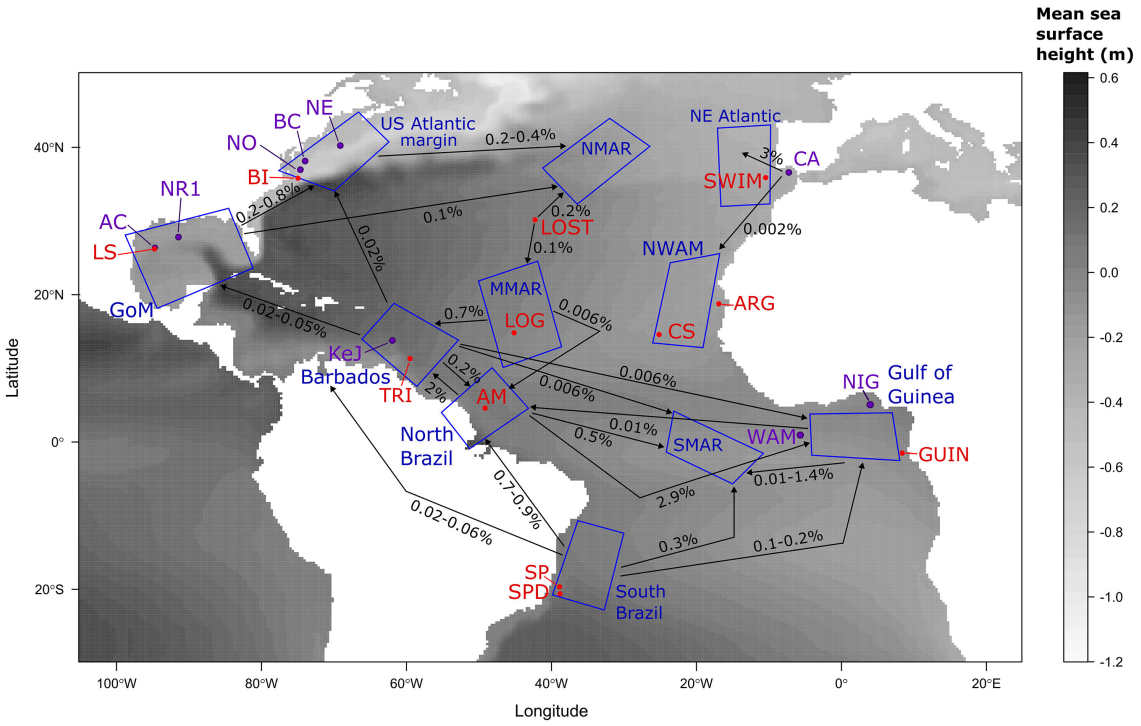

FIGURE 5
Larval dispersal connectivity map obtained using larval dispersal fluxes simulated by the oceanic circulation model VIKING20X. Mean fluxes were calculated between spawning areas (red and purple points) and settlement regions (blue polygons). Arrows show the range of mean values observed for all sites within settlement regions. Details on site per site values can be found in Table 6. See Figure 1 for spawning areas and settlement regions abbreviation definitions.

spawning areas but were higher for larvae released at Brine Pool (Figure 7A). For some spawning dates (e.g. January 2019), most larvae originating from Alaminos Canyon and Louisiana Slope were retained in the GoM and only a few entered the Gulf Stream and dispersed along the US Atlantic margin (Supplementary Figure S9). The average maximal dispersal distance for all spawning dates was also higher for a larval release at Brine Pool (Figure 7B, with some larvae arriving offshore of Ireland, see e.g. Supplementary Figures S10, S11) although extreme distances travelled by some larvae were reported for a larval release at Alaminos Canyon (~ 6500 km, Figure 7B).

Larvae released from the US Atlantic margin (i.e. Bodie Island, Norfolk Canyon, Baltimore Canyon, New England) dispersed along the US Atlantic margin to Nova Scotia, and then eastward across the North Atlantic with low isotropy indices (Figure 6; Table 6, see also Portanier et al., 2023 and Jollivet et al., 2023). The average dispersal distance and the average maximal dispersal distance varied little between sites, between 850 and 1032 km for the former, and between 2787 and 3857 km for the latter (Figure 7). Extreme dispersal distances exceeded more than 4850 km for a larval release at Bodie Island (Figure 7) so that some larvae could reach European waters, South-Western of Ireland (see Supplementary Figures S12, S13).

Larvae originating from the North Eastern Atlantic (i.e. SWIM Fault and Gulf of Cadiz) were transported in different directions (high isotropy indices, Table 6). While some larvae entered the Mediterranean Sea through the Strait of Gibraltar, others were transported northwards along the Portuguese coast or southwards along the coast of Morocco (Figures 5, 6, see also Portanier et al., 2023 and Jollivet et al., 2023). Depending on spawning dates, only a few larvae were transported to latitudes south of the Canary Islands, suggesting that very few larvae could reach the North West African region in the surface layer of the ocean (Table 6). For both sites, the average dispersal distances were low (around 400 km) even though extreme dispersal distances exceeded 2700 km for some larvae entering the Mediterranean Sea (Figure 7, Portanier et al., 2023 and Jollivet et al., 2023).

For a larval release in North West Africa (i.e., Arguin, Cadamostro Seamount), dispersal patterns varied slightly according to the spawning area. For a release at the Arguin site, larvae spread along the coast of North West Africa northwards, southwards to the Cape Verde Peninsula and westwards beyond the Cape Verde archipelago by the Canary and the North Equatorial Currents. For a larval release at the Cadamostro Seamount, larvae were transported westward to a longitude of 30°W but did not reach the Mid-Atlantic Ridge (Table 6; Figures 5, 6, Portanier et al., 2023 and Jollivet et al., 2023). As for larvae originating from the NE

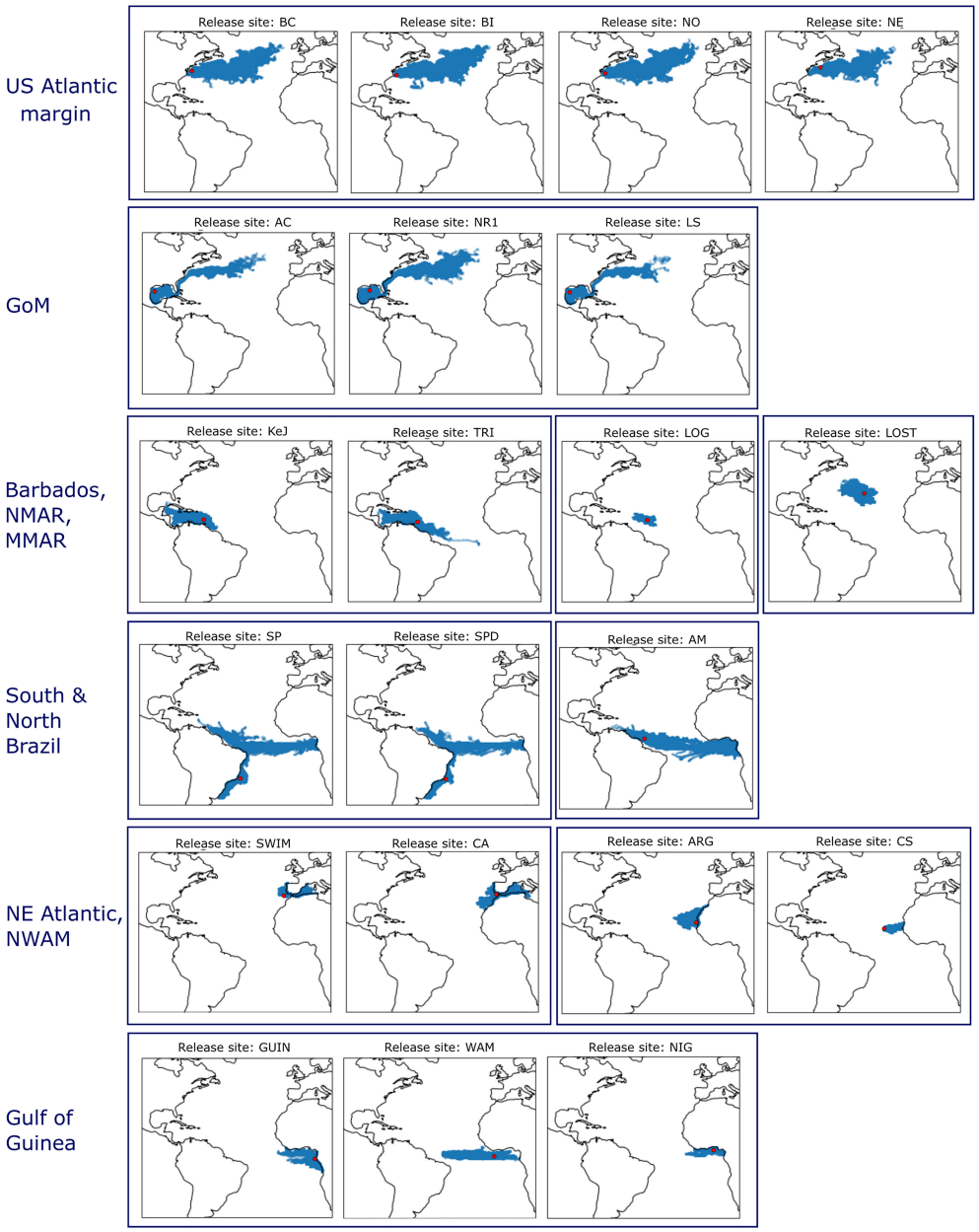

FIGURE 6
Representative patterns of simulated larval distribution after one year following a larval release at one of the 21 seep localities and/or putative stepping stones on the mid-Atlantic Ridge. Release date was January 2017 (see Portanier et al., 2023 and Jollivet et al., 2023 for all 25 release dates simulated). See Figure 1 for spawning areas and settlement regions abbreviation definitions.

Atlantic, the average dispersal distance was low (less than 400 km), and maximal dispersal distance never exceeded 1200 km (Figure 7, Portanier et al., 2023 and Jollivet et al., 2023).

While larvae released from the Gulf of Guinea (i.e. Guiness, Nigeria margin and West African margin) were mainly transported westward, larval dispersal patterns varied among spawning area. Larvae from the Nigeria margin were mainly trapped in the Gulf of Guinea gyre (Figures 5, 6), whereas at some rare spawning dates (Guinea site on Supplementary Figures S14, S15), larvae were transported westward across the Atlantic by the Equatorial South Equatorial Current but did not reach the North Brazil margin (Figure 6; Table 6). While the average dispersal distance was around 400 km, the maximum dispersal distance exceeded 1350 km (Figure 7). Larvae from the West African margin were transported both eastward by the Gulf of Guinea current and westward by the Equatorial South Equatorial Current (Figure 6; Table 6). Larvae from this site reached the North Brazil margin with a maximal dispersal distance of 2715 km (Figures 5, 6; Table 6; Supplementary Figures S14, S15). Larval dispersal following a spawning event from Guiness was highly variable among spawning dates. While larvae could be mainly transported southward along the coasts of Congo, they could also be transported westwards by two branches of the equatorial circulation: the Guinea Current and the Equatorial South

TABLE 6 Mean and maximal (in brackets) percentages of larval exchanges observed between spawning areas and the eleven regions for settlement (see Figure 1 for the mapping of these areas) using larval dispersal simulations of the oceanic circulation model VIKING20X.

Area	Site	US Atlantic margin	GoM	Barbados	South Brazil	NWAM	NE Atlantic	Gulf of Guinea	NMAR	MMAR	SMAR	North Brazil	Isotropy
GoM	NR1	0.8 (5.4)	**14.6 (18.2)**	0.0 (0.0)	0.0 (0.0)	0.0 (0.0)	0.0 (0.0)	0.0 (0.0)	0.1 (2.1)	0.0 (0.0)	0.0 (0.0)	0.0 (0.0)	0.32 ± 0.13
	LS	0.2 (1.6)	**15.8 (18.3)**	0.0 (0.0)	0.0 (0.0)	0.0 (0.0)	0.0 (0.0)	0.0 (0.0)	0.0 (0.0)	0.0 (0.0)	0.0 (0.0)	0.0 (0.0)	0.45 ± 0.15
	AC	0.4 (6.7)	**15.4 (18.2)**	0.0 (0.0)	0.0 (0.0)	0.0 (0.0)	0.0 (0.0)	0.0 (0.0)	0.0 (0.0)	0.0 (0.0)	0.0 (0.0)	0.0 (0.0)	0.47 ± 0.18
US Atlantic margin	BI	**6.3 (17.2)**	0.0 (0.0)	0.0 (0.0)	0.0 (0.0)	0.0 (0.0)	0.0 (0.0)	0.0 (0.0)	0.3 (3.8)	0.0 (0.0)	0.0 (0.0)	0.0 (0.0)	0.23 ± 0.07
	NO	**6.8 (17.0)**	0.0 (0.0)	0.0 (0.0)	0.0 (0.0)	0.0 (0.0)	0.0 (0.0)	0.0 (0.0)	0.2 (2.1)	0.0 (0.0)	0.0 (0.0)	0.0 (0.0)	0.23 ± 0.05
	BC	**9.9 (17.2)**	0.0 (0.0)	0.0 (0.0)	0.0 (0.0)	0.0 (0.0)	0.0 (0.0)	0.0 (0.0)	0.2 (2.9)	0.0 (0.0)	0.0 (0.0)	0.0 (0.0)	0.22 ± 0.06
	NE	**11.3 (17.4)**	0.0 (0.0)	0.0 (0.0)	0.0 (0.0)	0.0 (0.0)	0.0 (0.0)	0.0 (0.0)	0.4 (2.7)	0.0 (0.0)	0.0 (0.0)	0.0 (0.0)	0.24 ± 0.09
NE Atlantic	SWIM	0.0 (0.0)	0.0 (0.0)	0.0 (0.0)	0.0 (0.0)	0.0 (0.0)	**5.2 (17.8)**	0.0 (0.0)	0.0 (0.0)	0.0 (0.0)	0.0 (0.0)	0.0 (0.0)	0.47 ± 0.20
	CA	0.0 (0.0)	0.0 (0.0)	0.0 (0.0)	0.0 (0.0)	0.002 (0.1)	**3.0 (12.2)**	0.0 (0.0)	0.0 (0.0)	0.0 (0.0)	0.0 (0.0)	0.0 (0.0)	0.35 ± 0.14
NWAM	ARG	0.0 (0.0)	0.0 (0.0)	0.0 (0.0)	0.0 (0.0)	**12.4 (16.9)**	0.0 (0.0)	0.0 (0.0)	0.0 (0.0)	0.0 (0.0)	0.0 (0.0)	0.0 (0.0)	0.55 ± 0.20
	CS	0.0 (0.0)	0.0 (0.0)	0.0 (0.0)	0.0 (0.0)	**12.3 (18.2)**	0.0 (0.0)	0.0 (0.0)	0.0 (0.0)	0.0 (0.0)	0.0 (0.0)	0.0 (0.0)	0.49 ± 0.17
Gulf of Guinea	NIG	0.0 (0.0)	0.0 (0.0)	0.0 (0.0)	0.0 (0.0)	0.0 (0.0)	0.0 (0.0)	**6.7 (16.4)**	0.0 (0.0)	0.0 (0.0)	0.01 (0.1)	0.0 (0.0)	0.36 ± 0.12
	WAM	0.0 (0.0)	0.0 (0.0)	0.0 (0.0)	0.0 (0.0)	0.0 (0.0)	0.0 (0.0)	**4.5 (16.6)**	0.0 (0.0)	0.0 (0.0)	1.4 (5.4)	0.01 (0.1)	0.14 ± 0.07
	GUIN	0.0 (0.0)	0.0 (0.0)	0.0 (0.0)	0.0 (0.0)	0.0 (0.0)	0.0 (0.0)	**2.3 (9.1)**	0.0 (0.0)	0.0 (0.0)	0.02 (0.2)	0.0 (0.0)	0.46 ± 0.20
South Brazil	SP	0.0 (0.0)	0.0 (0.0)	0.06 (1.0)	**9.5 (14.7)**	0.0 (0.0)	0.0 (0.0)	0.2 (3.1)	0.0 (0.0)	0.0 (0.0)	0.3 (5.1)	0.9 (5.8)	0.53 ± 0.11
	SPD	0.0 (0.0)	0.0 (0.0)	0.02 (0.1)	**6.4 (15.6)**	0.0 (0.0)	0.0 (0.0)	0.1 (0.3)	0.0 (0.0)	0.0 (0.0)	0.3 (2.2)	0.7 (4.8)	0.41 ± 0.13
North Brazil	AM	0.0 (0.0)	0.0 (0.0)	2.0 (14.8)	0.0 (0.0)	0.0 (0.0)	0.0 (0.0)	2.9 (12.1)	0.0 (0.0)	0.0 (0.0)	0.5 (1.9)	**5.2 (15.6)**	0.18 ± 0.07
Barbados	TRI	0.02 (0.4)	0.05 (0.9)	**12.5 (17.8)**	0.0 (0.0)	0.0 (0.0)	0.0 (0.0)	0.006 (0.1)	0.0 (0.0)	0.0 (0.0)	0.006 (0.1)	0.2 (2.4)	0.3 ± 0.10
	KeJ	0.0 (0.0)	0.02 (0.2)	**11.8 (17.8)**	0.0 (0.0)	0.0 (0.0)	0.0 (0.0)	0.0 (0.0)	0.0 (0.0)	0.0 (0.0)	0.0 (0.0)	0.0 (0.0)	0.29 ± 0.13
MMAR	LOG	0.0 (0.0)	0.0 (0.0)	0.7 (3.4)	0.0 (0.0)	0.0 (0.0)	0.0 (0.0)	0.0 (0.0)	0.0 (0.0)	**9.4 (17.2)**	0.0 (0.0)	0.006 (0.1)	0.36 ± 0.14
NMAR	LOST	0.0 (0.0)	0.0 (0.0)	0.0 (0.0)	0.0 (0.0)	0.0 (0.0)	0.0 (0.0)	0.0 (0.0)	**0.2 (3.7)**	0.1 (2.3)	0.0 (0.0)	0.0 (0.0)	0.53 ± 0.13

The 5-years averaged isotropy values are also reported with their standard deviations. Bold values highlight larval retention in each spawning area. Spawning area abbreviations (lines) correspond to NR1, Brine Pool; LS, Louisiana slope; AC, Alaminos canyon; BI, Bodie island; NO, Norfolk canyon; BC, Baltimore canyon; NE, New England seeps; SWIM, SWIM Fault; CA, Gulf of Cadiz; ARG, Arguin bank; CS, Cadamostro seamount; NIG, Nigerian margin; WAM, West African margin; GUIN, Guiness; SP, Sao Paulo seep 1; SPD, Sao Paulo seep 2; AM, Amazon fan; TRI, Trinidad prism; KeJ, Kick em Jenny crater; LOG, Logatchev seep and LOST, Atlantis FZ (Lost City). Abbreviations of the regions for settlement are: NWAM, North West African margin; NMAR, North Mid-Atlantic Ridge; MMAR, Middle Mid-Atlantic Ridge and SMAR, South Mid-Atlantic Ridge. Non-null values have been highlighted.

10.3389/fmars.2023.1122124

Equatorial Current for the northern branch, and the Central South Equatorial Current for the southern branch (Figure 6; Table 6; Portanier et al., 2023 and Jollivet et al., 2023).

Larvae originating from the South Brazil margin (i.e. Sao Paulo 1 and Sao Paulo 2) were transported southward by the Brazil current to the Rio de la Plata and to a greater extent northward by the highly dynamic North Brazil Under Current and North Brazil Current so that some larvae reached the Barbados Prism (Table 6; Figures 5, 6; Supplementary Figure S15). In parallel, some larvae travelled across the Atlantic Ocean to the Gulf of Guinea by the South Equatorial Current (Table 6; Figures 5, 6, nearly all larval simulations in Portanier et al., 2023 and Jollivet et al., 2023). For a larval release in the North Brazil margin (i.e. Amazon fan), larvae were transported both to the northwest by the North Brazil Current to the Barbados Prism and eastwards by the South Equatorial Current to the Gulf of Guinea (Table 6; Figures 5, 6, nearly all larval simulations in Portanier et al., 2023 and Jollivet et al., 2023) with low isotropy indices (Table 6). For some spawning dates, larvae entered the GoM and traveled through the Florida Strait along the US Atlantic margin (Table 6; Supplementary Figures S15, S16). The larvae emitted along the Brazilian coast are those that travel the greatest distances, with maximum dispersal distances exceeding 5000-6000 km (Figure 7).

Larvae released from the Barbados Prism (i.e. Trinidad and Kick em Jenny crater) were mainly dispersed in the Caribbean Sea (Figure 6, Portanier et al., 2023 and Jollivet et al., 2023). As reported for a larval release in the North Brazil margin, a few larvae reached the entrance of the GoM, and the Florida Escarpment but most of them were entrained along the US Atlantic margin for a few spawning dates (Figures 5, 6; Table 6; Supplementary Figure S9 and larval release from November 2014 to February 2015 in Portanier et al., 2023 and Jollivet et al., 2023). Such transport was more common with some larval releases at Trinidad (Table 6, Supplementary Figure S9). In parallel, larvae released at Trinidad could travel across the Equatorial Atlantic and reached the Gulf of Guinea (Figure 5; Table 6, see e.g. Supplementary Figure S9). On average, mean and extreme dispersal distances of larvae originating from Barbados prism were lower than those of larvae originating from Brazil (Figure 7).

Finally, larvae released from the mid-Atlantic Ridge (i.e. Lost City and Logatchev seeps) were dispersed over short distances with average dispersal distance and maximum dispersal distance of 300-400 km and 960-1400 km, respectively (Figure 7). As the Lost City seep is located in the center of the overall subtropical North Atlantic gyre, outside the main currents, larvae from this site never reached the US Atlantic or African margins and spread in all directions (Figure 6) with high isotropy indices (Table 6). Conversely, some larvae originating from the Logatchev seep could benefit from the North Equatorial Current and the Equatorial Counter Current to reach the Barbados Prism and the North Brazil margin (Figure 5; Table 6, see e.g. Supplementary Figure S9).

In terms of connectivity among the different cold seeps areas in the North and Equatorial Atlantic, there are strong differences between the East and the West margins of the ocean as the result of abrupt differences in the intensity of the general surface circulation (Figure 5). A high northward larval dispersal and connectivity from the South Brazil margin to the US Atlantic margin was simulated. Conversely, no connectivity was reported between the cold seep areas along the East Atlantic, from the Gulf of Cadiz to the Gulf of Guinea (Table 6). Rare and reproducible bidirectional larval exchanges across the Atlantic occurred only in the Atlantic Equatorial Belt (Table 6; Figure 5). In temperate waters, larvae released from the US Atlantic margin travelled across the Atlantic to reach the southwest Ireland but were not able to colonize sites in the south of the Iberian Peninsula. Contrary to our expectations, sites located along the mid-Atlantic Ridge did not seem to play a major role as stepping stones.

4 Discussion

4.1 A shared mitochondrial history between *Gigantidas* and *Bathymodiolus*

The low level of divergence (< 1%) measured in the present study between *G. childressi* and *G. mauritanicus* or between *B. heckerae* and *B. boomerang* corresponded to previous observation made using lower sample sizes (Olu-Le Roy et al., 2007; Génio et al., 2008) and is in the range of differences commonly accepted between populations of the same species or within the grey zone of speciation (Roux et al., 2016). It is similar to what was observed between mussel species that still hybridize (e.g. *B. azoricus*/*B. puteoserpentis* or *B. thermophilus*/*B. antarcticus*, Faure et al., 2009; Johnson et al., 2013) and therefore suggests that geographic species could still exchange genetic material within each genus. Despite a higher number of mutational changes observed between the two *Gigantidas* species when compared with the two *Bathymodiolus* species (Figure 2 vs. 3), genetic distances and population differentiation indices were equivalent in the two species complexes. This gives credit to a shared mitochondrial history of the two genera in the North Atlantic. Indeed, it has been suggested that *G. mauritanicus*/*G. childressi* and *B. boomerang*/*B. heckerae* diverged at similar times, between 1.3 Million years ago (Mya) and 3 Mya (Miyazaki et al., 2010; McCowin et al., 2020). While our estimate of T_2 (population splitting time between MRCAs of GoM-US canyons and Barbados-Africa) corresponded for *Bathymodiolus* spp., it seemed upward biased for *Gigantidas* spp., as also suggested by its proximity with T_1 (divergence between populations from Barbados-KeJ and Africa-Gulf of Cadiz). Such concomitant divergence across the Atlantic and across the Caribbean Sea appeared unlikely given the genetic break identified in the Caribbean Sea for both genera, which instead suggested a complete lineage sorting between *G. childressi*/*G. mauritanicus* and *B. heckerae*/*B. boomerang* and a parallel mitochondrial isolation.

Our results thus tended to validate the hypothesis of a vicariant effect possibly due to an 'old' (1-3 Mya) hydrologic barrier predating the Panama Seaway closure (Knowlton and Weigt, 1998) that separated *B. boomerang* and *B. heckerae* on one hand, and *G. mauritanicus* and *G. childressi* on the other hand (Olu-Le Roy et al., 2007). The change of the Caribbean Sea salinity and of the thermohaline circulation observed around 3 Mya (Haug and Tiedemann, 1998; Haug et al., 2001), which may be linked to the closure of the Panama Seaway (but see Montes et al., 2015), may

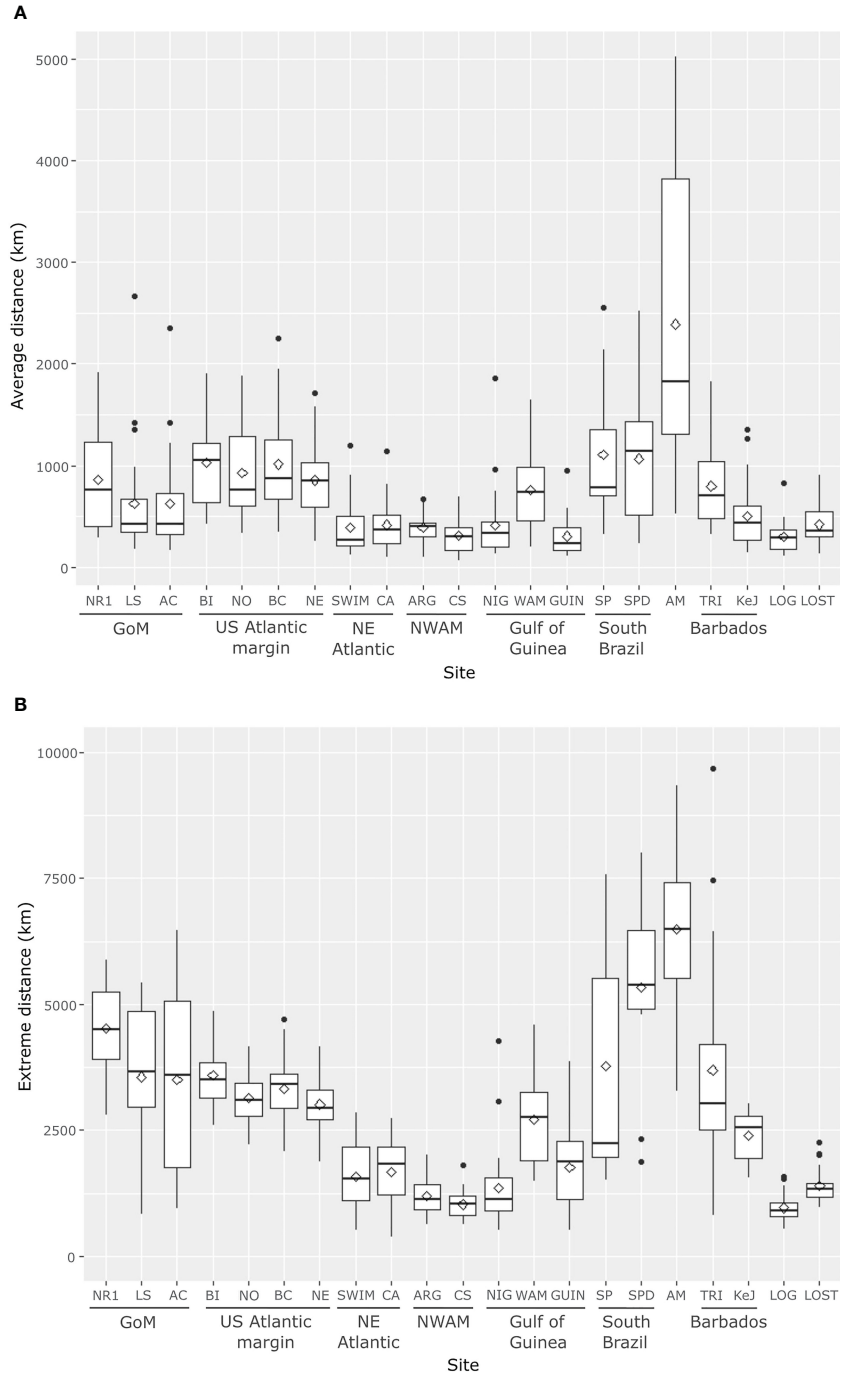

FIGURE 7
Boxplots summarizing mean **(A)** and extreme **(B)** dispersal distances observed for larvae released from the different release sites modeled (white diamonds correspond to means and black dots represent outlier values). See Figure 1 for spawning areas and settlement regions abbreviation definitions.

have impacted the within-Atlantic Ocean circulation. This could have led to a reinforced cross-Atlantic circulation between Barbados and African margins along the Atlantic Equatorial Belt and the diversification of *Bathymodiolus* species (Jones et al., 2006; Olu-Le Roy et al., 2007). Such a scenario may explain how individuals from the same species occur on both sides of the Atlantic and suggest that previously-isolated populations across the Caribbean Sea are currently experiencing a possible secondary contact with the arrival of rare but regular Barbados migrants in the US Atlantic margin waters (see below). Vicariant effects leading to concomitant species divergence at the community scale have also been documented in other deep-sea ecosystems, such as in the back-arc-basins of the South West Pacific (Thaler et al., 2011; Thaler et al., 2014; Lee et al., 2019; Poitrimol et al., 2022; Tran Lu, 2022; Tran Lu Y et al., 2022) or along the East Pacific Rise (Plouviez et al., 2009; Matabos and Jollivet, 2019) in which taxa from several phyla

(Mollusca, Annelida, Crustacea) simultaneously diverged in response to geotectonic rearrangements.

4.2 Contemporary and past gene flow across the Atlantic Equatorial Belt

High faunal similarities between seep communities have been previously depicted on both sides of the Atlantic Ocean (Olu et al., 2010) with very low genetic divergence between siblings (e.g. vestimentiferan tubeworm, Andersen et al., 2004; Cowart et al., 2013; alvinocarid shrimps, vesicomyid bivalves, Teixeira et al., 2013; LaBella et al., 2017; Pereira et al., 2020). In Alvinocarididae shrimps, the level of genetic differentiation was low enough to suggest a high level of contemporary gene flow (Teixeira et al., 2013; Pereira et al., 2020). In the present study, IMa3 analysis, in conjunction with the possible assignment of one Nigerian *B. boomerang* individual to the Barbados genetic group (individual (a) Figure 3), may also suggest the existence of contemporary gene flow across the AEB. For *B. boomerang*, a large and significant proportion of migrants was, indeed, estimated from Barbados to Western African Margin ($2N_2m_{2>3}$ = 63.239), although the HPD95% included zero. Despite the fact that the lower boundary of HPD95% includes zero, gene flow in the opposite direction was not null ($2N_3m_{3>2}$ = 0.015) and gave support to a bi-directional larval exchange between populations. It is noteworthy that migration rates estimated in IMa3 represent migration rates since population divergence. Calculations based on mitochondrial DNA may thus translate to past gene flow. But, in conjunction with the detection of the potential Barbados to Nigeria migrant, the large $2N_2m_{2>3}$ argued in favor of eastward contemporary gene flow. By contrast, IMa3 results did not provide evidence for trans-Atlantic gene flow for *G. mauritanicus* as migration rates were always low (<1) and non-significantly different from zero. It nevertheless supported ancestral gene flow between the US Atlantic and European margins.

The presence of contemporary gene flow across the AEB would assume the existence of teleplanic larvae (or larvae with a long larval life span exceeding several months) and the existence of marine corridors ensuring the transport of larvae by marine currents (e.g. the AMOC, Gary et al., 2020). Such hypothesis is likely for bathymodioline mussels, especially for *G. childressi*, in which larval lifespan is estimated to be more than one year and vertical migration of larvae that then benefit from surface oceanic circulation have been documented, although some larvae have also been collected near the bottom (Arellano and Young, 2009; Arellano and Young, 2011; Young et al., 2012; Arellano et al., 2014; Laming et al., 2018). Overall VIKING20X model results showed a strong larval retention within each geographic region (Table 6) as already observed elsewhere (Young et al., 2012). The maximum distance a larva can achieve during one year (Figure 7) nevertheless suggested that Barbados populations can be directly connected to Africa, although eastward flows were low (0.1% of larvae exchanged at maximum during extreme events, Table 6). In addition, the Amazonian basin (which is geographically close and connected to Barbados and North Brazil, Figure 5) was able to send up to 10% of larvae to Western Africa during extreme events (Table 6). In the opposite direction, the African populations were only able to send a low percentage of larvae to the Amazonian basin (0.1% at maximum during extreme events, Table 6). Although putative Amazonian populations may send a large proportion of larvae to Barbados-KeJ (up to 15%, Table 6), the very low flow from Western Africa to Brazil may prevent, or largely challenge, effective dispersal from Western Africa to Barbados-KeJ.

Altogether, these results suggested that contemporary gene flow across the Atlantic Ocean is possible but rare and occurs most probably from West to East and in surface waters. Interestingly, in our study, the eastward flow was only evidenced for *B. boomerang* and not for *G. mauritanicus*. While a sampling bias cannot be excluded to explain such results, *G. mauritanicus* and *B. boomerang* may also use distinct habitats, making one species able to disperse farther than the other. Usually, *B. boomerang* and *B. heckerae* are present at deeper sites (Olu-Le Roy et al., 2007; Olu et al., 2010; Coykendall et al., 2019 and Table 1). In addition, while both *G. mauritanicus* and *B. boomerang* use a dual symbiosis with both sulfo-oxidizing and methanotrophic bacteria in their gills, *G. mauritanicus* shows dominant methanotrophic phylotypes, suggesting that it requires high methane concentrations and a hard substratum to settle (Sibuet and Olu, 1998; Rodrigues et al., 2013a; Rodrigues et al., 2013b) whereas *B. boomerang* lives buried in soft sediment and may be able to process both methane and sulfide at low flow rates, including peripheral hydrothermal sediments (Olu et al., 1996; Cosel and Olu, 1998; Sibuet and Olu, 1998; Duperron et al., 2011). As a consequence, this latter species is supposed to be adapted to a larger range of environmental conditions when compared to *G. mauritanicus*, which may favor dispersal.

4.3 Contemporary larval flow across the Caribbean Sea

Although IMa3 results supported the presence of a strong genetic break between populations of the Barbados Accretionary Prism and GoM for both genera (all migration rates estimates close to zero), the presence of three *G. mauritanicus* Barbados-KeJ type sampled in the Baltimore Canyon and the New England Seep (US Atlantic margin) (Figure 2) and the IMa3 estimation of 1.4 migrants per generation (not significant) between Barbados and US Atlantic margin gives support for low but existing larval exchanges across the Caribbean Sea. The presence of only a few individuals nevertheless suggested that such dispersal events are rare. This fits well with VIKING20X larval dispersal simulations which suggested low but reproductible larval flows across the Caribbean Sea (max. 0.9% to GoM and 0.4% to the US Atlantic margin during extreme events, Figure 5; Table 6). These larval flows were however much lower than those depicted between the South American and the African margins. In addition, despite no detected larval exchanges along the African coastline, between the Gulf of Cadiz and the Gulf of Guinea (Figure 5; Table 6), *G. mauritanicus* populations in these areas appeared genetically homogeneous (Figure 3). The lack or low genetic connectivity observed between the South American and US Atlantic margins is therefore difficult to explain. The settlement of

large numbers of *G. mauritanicus* and *B. boomerang* in GoM or the US Atlantic margin canyons might be challenging due to differences in environmental conditions (e.g. maladaptation of southern migrants) if the break is due to a well-established genetic barrier (i.e. strong counter-selection of hybrids and the foreign parental form) instead of due to a lack of dispersing larvae. In the opposite direction, both IMa3 estimates and the larval dispersal modelling simulations were unable to detect GoM or US Atlantic margin canyon migrants in the Barbados-KeJ sites.

Larval exchanges between Barbados-KeJ and the US Atlantic margin thus seem to be, as observed between Western Africa and Barbados-KeJ, rare and are likely to occur northward. Cordes et al. (2007) hypothesized that a bidirectional connection may exist between the GoM and Barbados (through the deep Yucatan Strait and the St. Vincent and Dominica passages) but larval dispersal on the bottom appears extremely limited and in contradiction with our genetic data. An indirect way of sending larvae from the US Atlantic margin canyons to the Barbados Accretionary Prism would nevertheless be through the mid-Atlantic Ridge. VIKING20X larval dispersal simulations however weakly support this view but some larvae released in the US Atlantic margin canyons and Blake Ridge were theoretically able to reach the putative cold seeps modelled in NMAR (North Mid-Atlantic Ridge), which were, in turn connected (with a small value) to the central part of MAR and Barbados Accretionary Prism (Figure 5; Table 6).

4.4 Contemporary gene flow between GoM and the US Atlantic margin

As observed elsewhere (Carney et al., 2006; Faure et al., 2015; Coykendall et al., 2019), the *G. childressi* and *B. heckerae* lineages shared numerous haplotypes between GoM and US Atlantic margin canyon populations. This validates that these two regions are highly connected (Figures 2–4). This was especially true for *G. childressi* since all Fst values except ones involving the Shallop West population were close or equal to zero. While also based on COI data, Faure et al. (2015) suggested the occurrence of restricted gene flow between some localities within the GoM, however, we saw evidence of a lack of genetic structure and an apparent panmixia, as observed by Coykendall et al. (2019). The larger sample sizes involved in the present study and Coykendall et al. (2019) may explain this discrepancy. Absence or very low levels of genetic structure have also been observed for other cold seep species within the GoM, such as tubeworms (McMullin et al., 2010; Cowart et al., 2013; Cowart et al., 2014). In accordance with the absence of genetic differentiation observed in *G. childressi*, migration rates estimated with IMa3 between GoM and the US Atlantic margin was not null, but were significantly different from zero and strongly orientated from GoM to the US Atlantic margin canyons ($2N_1m_{1>0}$ = 46.41, $2N_0m_{0>1}$ = 0.070). It is nevertheless noteworthy that the distribution of posterior probabilities of $2N_0m_{0>1}$ exhibited an alternative peak around 15 migrants per generation (Supplementary Figure S6). IMa3 also indicated the occurrence of bidirectional gene flow for *B. heckerae* since both $2N_1m_{1>0}$ and $2N_0M_{0>1}$ were significantly different from zero, although the HPD95% included zero, with values around 10 migrants per generation (Table 2). Accordingly, most Fst values were low and not significantly different from zero between the US Atlantic margin canyons, Pick Up Sticks, and the other GoM seeps (including the Florida Escarpment). However, highly significant genetic differentiation was also found in *B. heckerae* populations between Blake Ridge and the Florida Escarpment, suggesting restricted gene flow between these two populations. These two latter localities have been repeatedly described as peculiar as compared to other GoM and US Atlantic margin canyon seeps and are much deeper (usually less than 2000 m) than the depth range tolerated by *G. childressi*. As a consequence, the distribution of *B. heckerae* is probably more fragmented than that of *G. childressi* (Olu-Le Roy et al., 2007; Olu et al., 2010; Faure et al., 2015; Turner et al., 2020; DeLeo et al., 2022). Sampling *B. heckerae* at the shallower Pick Up Sticks site (400-450 m) is therefore unexpected. The Fst value between Pick Up Sticks and Blake Ridge was lower than other Fst values involving Blake Ridge, so Pick Up Sticks may be also viewed as putatively receiving migrants from both the Blake Ridge and Florida Escarpment seeps.

In accordance with the northward flow depicted by IMa3, larval dispersal simulations evidenced a non-negligible larval transport from GoM/Florida Escarpment towards the US Atlantic margin (up to 6% in extreme events, Table 6). In the meantime, population genetics cannot discard the hypothesis of bidirectional gene flow, although likelihood ratio tests for migration rates are prone to false positives when divergence is weak and sample sizes low (Hey et al., 2015). However, no larvae from the US Atlantic margin canyon seeps were able to reach the GoM (Figure 5; Table 6). Although our simulations included a period of several weeks before larvae reach the surface layers, they fully agreed with previous larval dispersal studies focusing on surface dispersal done by Young et al. (2012); McVeigh et al. (2017), and Gary et al. (2020) for *G. childressi*. By contrast larval transport onto the seafloor led to very limited dispersal distances and a lack of population connectivity between oceanic provinces (results not shown, see also Gary et al., 2020), but physical models on large-scale oceanic circulation do not take the seafloor topology into account with accuracy. Accordingly, if some larvae disperse using bottom currents, these flows may have been overlooked. Such bottom currents often flow in the opposite direction and could explain some unexpected gene flow entering in the GoM (e.g., deep-water current along the Sigsbee Escarpment in the GoM, Hamilton, 2009). To this extent, Cordes et al. (2007) suggested that below 1000 m larvae could be transported southward with the deep western boundary current of the Atlantic, reaching Blake Ridge and going to the Caribbean through the Anagada or the Windward Pass. There, the deepest layers of the Loop Current may take larvae through the Yucatan strait to the GoM. In the GoM, the cyclonic and boundary currents (Furey et al., 2018) may take larvae and ensure mixing between the US Atlantic margin and GoM. Recently, DeLeo et al. (2022) also found evidence of mostly southward gene flow in *G. childressi* along the US Atlantic margin between Baltimore Canyon, Chincoteague and Norfolk Canyon.

The bidirectional gene flow suggested by IMa3 may then result from this double dispersal strategy, using both surface and bottom currents. Moreover, the fact that migration rates seem to be more

balanced for *B. heckerae* may result from its deeper distribution (larvae thus released deeper) and the required time needed to reach the upper layers of the ocean. This could partially explain why *B. heckerae* is more spatially structured than *G. childressi* because, when dispersing at the bottom, larvae travel shorter distances than in surface waters (McVeigh et al., 2017; Gary et al., 2020). It is however noteworthy that such migration routes could result in the presence of *B. heckerae* and/or *G. childressi* in Barbados seeps, while none have been sampled. Their absence may be explained, for example, by the fact that larvae could not cross the Caribbean Sea entirely and may be trapped in the Windward Pass. Alternatively, the apparent absence of *B. heckerae* or *G. childressi* may be erroneous because of the study of mitochondrial DNA only if a genetic barrier exists. Indeed, the *B. heckerae* or *G. childressi* mtDNA types may be counter-selected in Barbados seeps while, actually, hybrids between *B. heckerae*/*B. boomerang* or *G. childressi*/*G. mauritanicus* could exist and would be detectable only using nuclear markers and genomics analyses.

4.5 Incomplete lineage sorting

As discussed above, dispersal events across the AEB and the Caribbean Sea seem to be rare and may fail to explain the lack of divergence observed between populations from both sides of the Atlantic. Indeed, even if occurring, migration seems not efficient enough to homogenize *B. boomerang* and *G. mauritanicus* populations from the Eastern and Western sides of the North Atlantic. Despite being from the same species and showing low divergence, populations of *G. mauritanicus* and *B. boomerang* from Barbados and Western Africa were, indeed, both genetically differentiated with no shared haplotypes and highly significant Fst values (≈ 0.3 and 0.5). Caution must however be taken as rare long-distance mitochondrial migrants might only be rare because of a strong counter-selection against hybrids due to the presence of a genetic barrier, which could be relaxed for neutrally-behaving markers associated with the nuclear genome. In that specific case, cross-Atlantic gene flow could be more important than solely predicted by the mitochondrial genome alone. Nevertheless, in the absence of efficient gene flow, the lack of fixed differences is likely to result from incomplete lineage sorting. In species in which effective size is expected to be very large, the lineage sorting process is slow and usually achieved in a period of time greater than 6*Ne* generations (Rosenberg 2003). In broadcast spawners such as bathymodioline mussels, high effective sizes are expected (e.g. *Ciona savignyi*, Small et al., 2007; *Rimicaris exoculata*, Teixeira et al., 2011). In our study, IMa3 estimates of effective population sizes were very large (often >1 million ind.) for all populations (except *B. boomerang* from Barbados) and 6Ne generations thus represent very large periods of time that greatly exceed the estimated population splitting times T_1 and T_2 estimated using a generation time of one year. Moreover, the lack of fixed differences between Barbados-KeJ and Africa-Cadiz populations in the two lineages *B. boomerang* and *G. mauritanicus* could also be the result of past gene flow and 'old' corridors of colonization. Such a hypothesis can be illustrated by the finding of one intermediate mitochondrial haplotype between *G. childressi* and *G. mauritanicus* sampled at the northernmost US Atlantic margin New England seepage, providing that it is not a recombining haplotype due to local hybridization between these two geographic species. Since this haplotype was closer to Africa-Cadiz haplotypes than to Barbados-KeJ ones, it may trace back a northern pathway of dispersal of *Gigantidas*, possibly relayed by the NMAR/Reykjavik Ridge. This is in accordance with the study of LaBella et al. (2017) on the deep vesicomyid clam *Abyssogena* sp. in which authors detected the presence of Florida Escarpment-derived haplotypes in the Gulf of Guinea populations. These two populations nevertheless did not share haplotypes, suggesting that the genetic signal observed may result from ancient gene flow from US Atlantic margin to Africa. Migration rates estimated by IMa3 (without the intermediate haplotype) however weakly supported this assumption with estimates derived from the ancestral populations of *Gigantidas* being almost null and non-significant. Caution must be taken, however, in extracting past information from our genetic data because of the lack of power associated with our single locus analysis. Multi-locus (e.g. Restriction Site Associated DNA sequencing) analyses may discriminate past from contemporary trans-Atlantic gene flow, making it possible to investigate if hybridization between species occurs, as suggested by the intermediate New England individual.

5 Conclusion and perspectives

Overall, genetic analyses suggested a parallel isolation of *Gigantidas* and *Bathymodiolus* species complexes in the Atlantic Ocean and validated the hypothesis of a vicariant effect resulting from a hydrographic barrier isolating mussel populations across the Caribbean Sea, with a wider and amphi-Atlantic distribution of the southern lineages. Contemporary gene flow between western and eastern margins of the North Atlantic and long-distance larval flow seemed to be rare (at least for the mitochondrial genome), as suggested by the presence of a few putative long-distance migrants (one across the EAB and three across the Caribbean Sea), and the strong spatial segregation of haplotypes indicative of low migration rates. The finding of long-distance migrants, although rare, is however not anecdotic given our sampling sizes and because foreign mitochondrial haplotypes are likely to be counter-selected in the recipient populations in the face of a genetic barrier. When, or if, trans-Atlantic gene flow occurs, it likely was in an eastward direction in surface waters and only for *B. boomerang*. Across the Carribean Sea, from Barbados-KeJ populations to the US Atlantic margin, gene flow seemed to occur northward and only for *G. mauritanicus*. Between the GoM and the US Atlantic margin, bidirectional gene flow may occur for *B. heckerae* but was not detected for *G. childressi* and was not evidenced using larval dispersal modeling.

On the one hand, the differences in migrant detection between species and genera might suggest that *Bathymodiolus* spp. and *Gigantidas* spp. disperse slightly differently. This may be due to

depth, habitat fragmentation and ecological preferences of the two genera in accordance with symbionts requirements: mostly methanotrophic for *Gigantidas* spp. (Duperron et al., 2007; Demopoulos et al., 2019; Coykendall et al., 2019; Turner et al., 2020), while *Bathymodiolus* spp. harbor a dual symbiosis and relies more on sulfide-derived carbon (Prouty et al., 2016; Van Dover et al., 2003; DeLeo et al., 2022). Contrasted levels of spatial genetic sub-structuring and contemporary gene flow between species that went through the same vicariant effects have also been reported in relation with species-specific life history traits and dispersal abilities in several other oceanic regions (Plouviez et al., 2009; Thaler et al., 2014; Poitrimol et al., 2022; Tran Lu Y et al., 2022). In the Atlantic Ocean, two sympatric cold-water corals *Desmophyllum pertusum* and *Madrepora oculata* showed different post-glacial recolonization histories, most probably as a response to contrasted dispersal abilities and ecological requirements (Boavida et al., 2019). It is nevertheless noteworthy that several non-exclusive hypotheses were supported by our results and further studies using nuclear DNA and powerful genomics approaches with larger sample sizes may be informative. This should allow the clarification of the evolutionary and colonization histories of bathymodioline mussels in the Atlantic Ocean and to resolve more precisely the past and current components of effective migration rates. It would also allow determining if the observed genetic structure of *G. mauritanicus*/*B. boomerang* between Barbados and Western Africa is the result of long-term isolation and incomplete lineage sorting or of secondary contact due to the Panama isthmus closure.

Although several sources of bias and variability may be present while modelling larval dispersal (e.g. the effects of long-term exposure to high temperatures on larval survival and development; larval pelagic phase of one year which may be unrealistic for *B. heckerae*, Dixon et al., 2006; the impact of predation on larvae travelling in zooplankton on the probability of long-distance dispersal, Gary et al., 2020; larval vertical distribution and behavior), combining larval dispersal modelling with genetic data highlighted interesting key points. First, the detection of potential gene flow using genetics while not detected using dispersal modelling illustrated the complementarity between these two approaches. The few studies combining genetics and larval dispersal modelling of the deep fauna did not either always fully reconcile gene flow estimates with predicted larval transport (need for 'phantom' stepping stones to explain gene flows, opposite flow directions between the two approaches, Breusing et al., 2016; Breusing et al., 2021). Second, the dual genetics-modelling approach highlighted the importance of "extreme" dispersal events in terms of genetic connectivity. Considering only mean values of larval exchanges may not be sufficient to explain the genetic spatial structure of a given species (e.g. no genetic differentiation observed between the Gulf of Cadiz and African populations of *G. mauritanicus* despite less than 0.1% larval transport between them). Modelling decadal variations in hydrodynamics due to the North Atlantic Oscillation and/or the El Niño Southern Oscillation in future studies may thus provide insights into the impact of such hydrodynamic variations on genetic connectivity at the whole ocean scale. It is nevertheless noteworthy that if such periodic events caused bursts of migration, it should be detectable while investigating the spatial genetic structure. Since our data supported the existence of few migrants and a strong genetic differentiation between the Barbados and African margins, and between these and the GoM or US margin populations, it is more likely that periodic hydrodynamic oscillations only transport a small number of migrants.

Altogether, our study supports the need to combine genomics and larval dispersal modelling approaches in other complexes of species with pan-oceanic or large spatial distribution (Breusing et al., 2016; Breusing et al., 2021; Boavida et al., 2019; Lee et al., 2019). This may improve understanding of species biology, dispersal capabilities and connectivity at whole ocean scales. This is particularly relevant since dispersal is linked to resilience capabilities of deep-sea ecosystems and species which are more and more threatened (Van Dover, 2014; Gross, 2015). Identifying source and sink populations and precisely describing connectivity for different species is necessary to define comprehensive conservation measures such as networks of protected marine areas that will act as refuge zones and genetic diversity reservoirs connected by corridors identified based on biological needs of species (Van Dover, 2014; Gross, 2015; Levin and Le Bris, 2015; Boavida et al., 2019). In the case of conservation strategies for bathymodioline mussel in the Atlantic Ocean, the strong geographic structure and the high rate of larval retention observed in our study suggested that long-distance dispersal is probably not efficient enough to replenish foreign populations, although it may enable the colonization of new territories or the recolonization of territories after local extinction. If larvae disperse using surface currents, as suggested by the results of our combined genetics-modelling approach, then there could be climate change impacts on connectivity and resilience for *Gigantidas* and *Bathymodiolus* species in the Atlantic. Increasing water temperatures may lead to a decrease in pelagic larval duration and an increase of larval mortality for bathymodioline mussels (Yorisue et al., 2013; Arellano and Young, 2009; Arellano and Young, 2011; Arellano et al., 2014; Yahagi et al., 2017), combining to further reduce the apparently low connectivity of these species.

Data availability statement

The datasets presented in this study can be found in online repositories. The names of the repository/repositories and accession number(s) can be found below: https://www.ebi.ac.uk/ena, PRJEB56597, https://www.pangaea.de/, https://doi.pangaea.de/10.1594/PANGAEA.955455, https://figshare.com/, https://figshare.com/articles/figure/Coupling_large-spatial_scale_larval_dispersal_modelling_with_barcoding_to_refine_the_amphi-Atlantic_connectivity_hypothesis_in_deep-sea_seep_mussels/22227670/2.

Author contributions

DJ, ET and AN designed the research. EP, LM, A-SP, MB and CD-T performed laboratory work. GL and AN conducted first modelling analyses and WR provided the whole series of larval simulations over 25 dates. EP and DJ conducted population genetics analyses. AN and ET performed larval dispersal modelling analyses derived from the VIKING20X Atlantic circulation model developed by AB. CM, MC, CY and CV provided samples and scientific advice. EP wrote the first version of the manuscript with the help of ET and DJ. Next versions were improved by all authors who agreed to the published version of the manuscript. All authors contributed to the article and approved the submitted version.

Funding

This study was funded by the European Union's Horizon 2020 research and innovation program under grant agreement No 818123 (iAtlantic, https://www.iatlantic.eu/).

Acknowledgments

We are deeply grateful to all the ship and ROV crews over the years and the world for their time and efforts devoted to collect samples (see Table 1 for a detailed list of cruises involved in the present study). We more particularly warmly thank Clara Rodrigues (CESAM, University of Aveiro, Aveiro, Portugal), Caitlin Plowman (University of Oregon, Eugene, USA), Bernie Ball (University College Dublin, Ireland), Travis Washburn (Duke University, North Carolina, USA), Amanda Demopoulos, Carolyn Ruppel, and Jennifer McClain-Counts (USGS), Andrea Quattrini (Smithsonian Institution, Washington D.C., USA), Erik Cordes (Temple University), James Brooks and Bernie Bernard (TDI Brooks International), Shawn Arellano (Western Washington University), Ryohing He and Dave Eggleston (North Carolina State University) for their involvement in sending and processing samples, as well as Bernie Ball for producing COI sequences from US Atlantic margin samples (see Supplementary Table S1). We also are grateful to Emily Blank and Breda M. Zimkus (Museum of Comparative Zoology, Harvard University) for the MCZ Cryogenic loan of *B. boomerang* (Kick 'em Jenny: lot 380695-99). We thank Stéphane Hourdez and Hayat Guezi for mussel dissection during the WACS cruise. This work benefited from access to the Biogenouest Genomer platform at Station Biologique de Roscoff, and we are grateful to the Roscoff Bioinformatics platform ABiMS and the computing facilities they allowed us to use to perform analyses (http://abims.sb-roscoff.fr). This work also benefitted from the computing facilities of the North German Supercomputing Alliance (HLRN) and the Earth System Modelling Project (ESM) partition of the supercomputer JUWELS at the Jülich Supercomputing Centre (JSC). Part of the samples were obtained thanks to the NSF grant OCE-1851383 and to the Bureau of Ocean Energy Management contract M17PC00009 to TDI Brooks International. Any use of trade, product, or firm names is for descriptive purposes only and does not imply endorsement by the U.S. Government. Finally, we are grateful to the two reviewers for their useful comments that improved the quality of our manuscript.

Conflict of interest

The authors declare that the research was conducted in the absence of any commercial or financial relationships that could be construed as a potential conflict of interest.

Publisher's note

Supplementary material

The Supplementary Material for this article can be found online at: https://www.frontiersin.org/articles/10.3389/fmars.2023.1122124/full#supplementary-material

References

Adams, D. K., Arellano, S. M., and Govenar, B. (2012). Larval dispersal - vent life in the water column. *Oceanography* 25, 256–268. doi: 10.5670/oceanog.2012.24

Andersen, A. C., Hourdez, S., Marie, B., Jollivet, D., Lallier, F. H., and Sibuet, M. (2004). *Escarpia southwardae*, a new species of vestimentiferan tubeworm (Annelida, siboglinidae) from West-African cold seeps. *J. Can. Zool.* 82, 980–999. doi: 10.1139/z04-049

Arellano, S. M. (2008). Embryology, larval ecology, and recruitment of "Bathymodiolus" childressi, a cold-seep mussel from the gulf of Mexico. PhD thesis. (Department of Biology and the Graduate School of the University of Oregon).

Arellano, S. M., Van Gaest, A. L., Johnson, S. B., Vrijenhoek, R. C., and Young, C. M. (2014). Larvae from deep-sea methane seeps disperse in surface waters. *Proc. R. Soc. London B: Biol. Sci.* 281 (1786), 20133276. doi: 10.1098/rspb.2013.3276

Arellano, S. M., and Young, C. M. (2009). Spawning, development, and the duration of larval life in a deep-sea cold-seep mussel. *Biol. Bull.* 216 (2), 149–162. doi: 10.1086/BBLv216n2p149

Arellano, S. M., and Young, C. M. (2011). Temperature and salinity tolerances of embryos and larvae of the deep-sea mytilid mussel '*Bathymodiolus' childressi*. mar. *Biol.* 158, 2481–2493. doi: 10.1007/s00227-011-1749-9

Assié, A., Borowski, C., van der Heijden, K., Raggi, L., Geier, B., Leisch, N., et al. (2016). A specific and widespread association between deep-sea bathymodiolus mussels and a novel family of epsilonproteobacteria. *Environ. Microbiol. Rep.* 8, 805–813. doi: 10.1111/1758-2229.12442

Baco, A. R., Rowden, A. A., Levin, L. A., Smith, C. R., and Bowden, D. A. (2010). Initial characterization of cold seep faunal communities on the new Zealand hikurangi margin. *Mar. Geol.* 272, 251–259. doi: 10.1016/j.margeo.2009.06.015

Bandelt, H., Forster, P., and Röhl, A. (1999). Median-joining networks for inferring intraspecific phylogenies. *Mol. Biol. Evol.* 16, 37–48. doi: 10.1093/oxfordjournals.molbev.a026036

Barry, J. P., Buck, K. R., Kochevar, R. K., Nelson, D. C., Fujiwara, Y., Goffredi, S. K., et al. (2002). Methane-based symbiosis in a mussel, *Bathymodiolus platifrons*, from cold seeps in sagami bay, Japan. *Invertebrate Biol.* 121 (1), 47–54. doi: 10.1111/j.1744-7410.2002.tb00128.x

Biastoch, A., Schwarzkopf, F. U., Getzlaff, K., Rühs, S., Martin, T., Scheinert, M., et al. (2021). Regional imprints of changes in the Atlantic meridional overturning circulation in the eddy-rich ocean model VIKING20X. *Ocean Sci.* 17, 1177–1211. doi: 10.5194/os-17-1177-2021

Boavida, J. R. H., Becheler, R., Choquet, M., Frank, N., Taviani, M., Bourillet, J. F., et al. (2019). Out of the Mediterranean? post-glacial colonization pathways varied among cold-water coral species. *J. Biogeogr.* 46, 915– 931. doi: 10.1111/jbi.13570

Brazelton, W. J., Schrenk, M. O., Kelley, D. S., and Baross, J. A. (2006). Methane-and sulfur-metabolizing microbial communities dominate the lost city hydrothermal field ecosystem. *Appl. Environ. Microbiol.* 72, 6257–6270. doi: 10.1128/AEM.00574-06

Breusing, C., Biastoch, A., Drews, A., Metaxas, A., Jollivet, D., Vrijenhoek, T., et al. (2016). Biophysical and population genetic models predict the presence of "phantom" stepping stones connecting mid-Atlantic ridge vent ecosystems. *Curr. Biol.* 26 (17), 2257–2267. doi: 10.1016/j.cub.2016.06.062

Breusing, C., Johnson, S. B., Mitarai, S., Beinart, R. A., and Tunnicliffe, V. (2021). Differential patterns of connectivity in Western pacific hydrothermal vent metapopulations: A comparison of biophysical and genetic models. *Evolutionary Appl.* 00, 1–14. doi: 10.1111/eva.13326

Busch, K., Taboada, S., Riesgo, A., Koutsouveli, V., Ríos, P., Cristobo, J., et al. (2021). Population connectivity of fan-shaped sponge holobionts in the deep cantabrian Sea. *Deep Sea Res. I* 167, 103427. doi: 10.1016/j.dsr.2020.103427

Carney, S. L., Formica, M. I., Divatia, H., Nelson, K., Fisher, C. R., and Schaeffer, S. W. (2006). Population structure of the mussel "*Bathymodiolus*" childressi from gulf of Mexico hydrocarbon seeps. *Deep Sea Res. I* 53, 1061–1072. doi: 10.1016/j.dsr.2006.03.002

Chevaldonné, P., Jollivet, D., Desbruyères, D., Lutz, R. A., and Vrijenhoek, R. C. (2002). Sister-species of eastern pacific hydrothermal vent worms (Ampharetidae, alvinellidae, vestimentifera) provide new mitochondrial COI clock calibration. *Cahiers Biologie Mar.* 43 (3), 367–370.

Chevaldonné, P., Jollivet, D., Vangriesheim, A., and Desbruyères, D. (1997). Hydrothermal-vent alvinellid polychaete dispersal in the eastern pacific. 1. influence of vent site distribution, bottom currents, and biological patterns. *Limnol. Oceanogr.* 42, 67–80. doi: 10.4319/lo.1997.42.1.0067

Chia, F. S., Buckland-Nicks, J., and Young, C. M. (1984). Locomotion of marine invertebrate larvae: a review. *Can. J. Zool.* 62, 1205–1222. doi: 10.1139/z84-176

Cordes, E. E., Bergquist, D. C., and Fisher, C. R. (2009). Macro-ecology of gulf of Mexico cold seeps. *Annu. Rev. Mar. Sci.* 1 (1), 143–168. doi: 10.1146/annurev.marine.010908.163912

Cordes, E. E., Carney, S. L., Hourdez, S., Carney, R. S., and Brooks, J. M. (2007). Cold seeps of the deep gulf of Mexico: Community structure and biogeographic comparisons to Atlantic equatorial belt seep communities. *Deep-Sea Res. I* 54, 637–653. doi: 10.1016/j.dsr.2007.01.001

Cosel, R. (2002). A new species of bathymodioline mussel (Mollusca, bivalvia, mytilidae) from Mauritania (West Africa), with comments on the genus *Bahymodiolus* kenk and wilso. *Zoosystema* 24, 259–271.

Cosel, V. R., and Olu, K. (1998). Gigantism in mytilidae. a new *Bathymodiolus* from cold seep areas on the Barbados accretionary prism. *Comptes Rendus l'Académie Des. Sci. Paris Série II* 321, 655–663. doi: 10.1016/S0764-4469(98)80005-X

Cowart, D. A., Huang, C., Arnaud-Haond, S., Carney, S. L., Fisher, C. R., and Schaeffer, S. W. (2013). Restriction to large-scale gene flow vs. regional panmixia among cold seep escarpia spp. (Polychaeta, siboglinidae). *Mol. Ecol.* 22 (16), 4147–4162. doi: 10.1111/mec.12379

Cowart, D. A., Halanych, K. M., Schaeffer, S. W., and Fisher, C. R. (2014). Depth-dependent gene flow in gulf of Mexico cold seep lamellibrachia tubeworms (Annelida, siboglinidae). *Hydrobiologia* 736, 139–154. doi: 10.1007/s10750-014-1900-y

Cowen, R. K., and Sponaugle, S. (2009). Larval dispersal and marine population connectivity. *Annu. Rev. Mar. Sci.* 1 (1), 443–466. doi: 10.1146/annurev.marine.010908.163757

Coykendall, D. K., Cornman, R. S., Prouty, N. G., Brooke, S., Demopoulos, A. W. J., and Morrison, C. L. (2019). Molecular characterization of *Bathymodiolus* mussels and gill symbionts associated with chemosynthetic habitats from the U.S. *Atlantic margin. PloS One* 14 (3), e0211616. doi: 10.1371/journal.pone.0211616

Delandmeter, P., and van Sebille, E. (2019). The parcels v2.0 Lagrangian framework: new field interpolation schemes. *Geoscientific Model. Dev.* 12, 3571–3584. doi: 10.5194/gmd-12-3571-2019

DeLeo, D. M., Morrison, C. L., Sei, M., Salamone, V., Demopoulos, A. W., and Quattrini, A. M. (2022). Genetic diversity and connectivity of chemosynthetic cold seep mussels from the US Atlantic margin. *BMC Ecol. Evol.* 22 (1), 1–16. doi: 10.1186/s12862-022-02027-4

Demopoulos, A. W. J., McClain-Counts, J. P., Bourque, J. R., Prouty, N. G., Smith, B. J., Brooke, S., et al. (2019). Examination of bathymodiolus childressi nutritional sources, isotopic niches, and food-web linkages at two seeps in the US Atlantic margin using stable isotope analysis and mixing models. *Deep-Sea Res. I* 148, 53–66. doi: 10.1016/j.dsr.2019.04.002

Distel, D. L., Baco, A. R., Chuang, E., Morrill, W., Cavanaugh, C., and Smith, C. R. (2000). Marine ecology: do mussels take wooden steps to deep-sea vents? *Nature* 403, 725–726. doi: 10.1038/35001667

Dixon, D. R., Lowe, D. M., Miller, P. I., Villemin, G. R., Colaço, A., Serrão-Santos, R., et al. (2006). Evidence of seasonal reproduction in the Atlantic vent mussel *Bathymodiolus azoricus*, and apparent link with the timing of photosynthetic primary production. *J. Mar. Biol. Assoc. United Kingdom* 86, 1363–1371. doi: 10.1017/S0025315406014391

Doebeli, M., and Ruxton, G. D. (1997). Evolution of dispersal rates in metapopulation models: branching and cyclic dynamics in phenotype space. *Evolution* 51 (6), 1730–1741. doi: 10.1111/j.1558-5646.1997.tb05097.x

Doyle, J. J., and Doyle, J. L. (1987). A rapid DNA isolation procedure for small quantities of fresh leaf tissue. *Phytochem. Bull.* 19, 11–15.

Duperron, S., Guezi, H., Gaudron, S. M., Ristova, P. P., Wenzhofer, F., and Boetius, A. (2011). Relative abundances of methane- and sulphur-oxidising symbionts in the gills of a cold seep mussel and link to their potential energy sources. *Geobiology* 9, 481–491. doi: 10.1111/j.1472-4669.2011.00300.x

Duperron, S., Sibuet, M., MacGregor, B. J., Kuypers, M. M. M., Fisher, C. R., and Dubilier, N. (2007). Diversity, relative abundance and metabolic potential of bacterial endosymbionts in three bathymodiolus mussel species from cold seeps in the gulf of Mexico. *Environ. Microbiol.* 9 (6), 1423–1438. doi: 10.1111/j.1462-2920.2007.01259.x

Duperron, S., Rodrigues, C. F., Léger, N., Szafranski, K., Decker, C., Olu, K., et al. (2012). Diversity of symbioses between chemosynthetic bacteria and metazoans at the guiness cold seep site (Gulf of Guinea, West Africa). *Microbiol. Open* 1 (4), 467–480. doi: 10.1002/mbo3.47

Edgar, R. C. (2004). MUSCLE: multiple sequence alignment with high accuracy and high throughput. *Nucleic Acids Res.* 32, 1792–1797. doi: 10.1093/nar/gkh340

Edwards, K. P., Hare, J. A., Werner, F. E., and Seim, H. (2007). Using 2-dimensional dispersal kernels to identify the dominant influences on larval dispersal on continental shelves. *Mar. Ecol. Prog. Ser.* 352, 77–87. doi: 10.3354/meps07169

Excoffier, L., and Lischer, H. E. L. (2010). Arlequin suite ver 3.5: A new series of programs to perform population genetics analyses under Linux and windows. *Mol. Ecol. Resources* 10, 564–567. doi: 10.1111/j.1755-0998.2010.02847.x

Faure, B., Jollivet, D., Tanguy, A., Bonhomme, F., and Bierne, N. (2009). Speciation in the deep sea: Multi-locus analysis of divergence and gene flow between two hybridizing species of hydrothermal vent mussels. *PloS One* 4 (8), e6485. doi: 10.1371/journal.pone.0006485

Faure, B., Schaeffer, S. W., and Fisher, C. R. (2015). Species distribution and population connectivity of deep-Sea mussels at hydrocarbon seeps in the gulf of Mexico. *PloS One* 10 (4), e0118460. doi: 10.1371/journal.pone.0118460

Fisher, C. R., Childress, J. J., Oremland, R. S., and Bidigare, R. R. (1987). The importance of methane and thiosulfate in the metabolism of the bacterial symbionts of two deep-sea mussels. *Mar. Biol.* 96, 59–71. doi: 10.1007/BF00394838

Folmer, O., Black, M., Hoeh, W., and Vrijenhoek, R. C. (1994). DNA Primers for amplification of mitochondrial cytochrome c oxidase subunit I from metazoan invertebrates. *Mol. Mar. Biol. Biotechnol.* 3, 294–299.

Fox, A., Handmann, P., Schmidt, C., Fraser, N., Rühs, S., Sanchez-Franks, A., et al. (2022). Exceptional freshening and cooling in the eastern subpolar north Atlantic caused by reduced Labrador Sea surface heat loss. *Ocean Sci.* 18, 1507–1533. doi: 10.5194/os-18-1507-2022

Fujikura, K., Kojima, S., Tamaki, K., Maki, Y., Hunt, J., and Okutani, T. (1999). The deepest chemosynthesis-based community yet discovered from the hadal zone 7326m deep, in the Japan trench. *Mar. Ecol. Prog. Ser.* 190, 17–26. doi: 10.3354/meps190017

Fujikura, K., Yamanaka, T., Sumida, P. Y. G., Bernardino, A. F., Pereira, O. S., Kanehara, T., et al. (2017). Discovery of asphalt seeps in the deep southwest Atlantic off Brazil. *Deep Sea Res. Part II: Topical Stud. Oceanogr.* 146, 35–44. doi: 10.1016/j.dsr2.2017.04.002

Furey, H., Bower, A., Perez-Brunius, P., Hamilton, P., and Leben, R. (2018). Deep eddies in the gulf of Mexico observed with floats. *J. Phys. Oceanogr.* 48 (11), 2703–2719. doi: 10.1175/JPO-D-17-0245.1

Gaines, S. D., Gaylord, B., Gerber, L. R., Hastings, A., and Kinlan, B. P. (2007). Connecting places: the ecological consequences of dispersal in the sea. *Oceanography* 20, 90–99. doi: 10.5670/oceanog.2007.32

Gary, S. F., Fox, A. D., Biastoch, A., Roberts, J. M., and Cunningham, S. A. (2020). Larval behaviour, dispersal and population connectivity in the deep sea. *Sci. Rep.* 10 (1), 1–12. doi: 10.1038/s41598-020-67503-7

Gebruk, A., Chevaldonné, P., Shank, T., Lutz, R., and Vrijenhoek, R. (2000). Deep-sea hydrothermal vent communities of the logatchev area (14°45′N, mid-Atlantic ridge): Diverse biotopes and high biomass. *J. Mar. Biol. Assoc. United Kingdom* 80 (3), 383–393. doi: 10.1017/S0025315499002088

Génio, L., Johnson, S. B., Vrijenhoek, R. C., Cunha, M. R., Tyler, P. A., Kiel, S., et al. (2008). New record of "*Bathymodiolus*" *mauritanicus* cosel 2002 from the gulf of cadiz (NE Atlantic) mud volcanoes. *J. Shellfish Res.* 27 (1), 53–61. doi: 10.2983/0730-8000(2008)27[53:NROBMC]2.0.CO;2

Gilg, M. R., and Hilbish, T. J. (2003). The geography of marine larval dispersal: coupling genetics with fine-scale physical oceanography. *Ecology* 84 (11), 2989–2998. doi: 10.1890/02-0498

Gouy, M., Guindon, S., and Gascuel, O. (2010). SeaView version 4: A multiplatform graphical user interface for sequence alignment and phylogenetic tree building. *Mol. Biol. Evol.* 27, 221–224. doi: 10.1093/molbev/msp259

Gross, M. (2015). Deep sea in deep trouble? *Curr. Biol.* 25, R1019–R1021. doi: 10.1016/j.cub.2015.10.030

Gustafson, R. G., Turner, R. D., Lutz, R. A., and Vrijenhoek, R. C. (1998). A new genus and five new species of mussels (Bivalvia, mytilidae) from deep-sea sulfide/hydrocarbon seeps in the gulf of Mexico. *Malacologia* 40 (1-2), 63–112.

Hamilton, P. (2009). Topographic rossby waves in the gulf of Mexico. *Prog. Oceanogr.* 82, 1–31. doi: 10.1016/j.pocean.2009.04.019

Hamilton, W. D., and May, R. M. (1977). Dispersal in stable habitats. *Nature* 269 (5629), 578–581. doi: 10.1038/269578a0

Handal, W., Szostek, C., Hold, N., Andrello, M., Thiébaut, E., Harney, E., et al. (2020). New insights on the population genetic structure of the great scallop (*Pecten maximus*) in the English channel, coupling microsatellite data and demogenetic simulations. *Aquat. Conservation: Mar. Freshw. Ecosyst.* 30 (10), 1841–1853. doi: 10.1002/aqc.3316

Harrison, S., and Hastings, A. (1996). Genetic and evolutionary consequences of metapopulation structure. *Trends Ecol. Evol.* 11 (4), 180–183. doi: 10.1016/0169-5347(96)20008-4

Haug, G. H., and Tiedemann, R. (1998). Effect of the formation of the isthmus of Panama on Atlantic ocean thermohaline circulation. *Nature* 393 (6686), 673–676. doi: 10.1038/31447

Haug, G. H., Tiedemann, R., Zahn, R., and Ravelo, A. C. (2001). Role of Panama uplift on oceanic freshwater balance. *Geology* 29, 207–210. doi: 10.1130/0091-7613(2001)029<0207:ROPUOO>2.0.CO;2

Hecker, B. (1985). Fauna from a cold sulfur-seep in the gulf of Mexico: comparison with hydrothermal vent communities and evolutionary implications. *Bull. Biol. Soc. Washington* 6), 465–473.

Herring, P. J., and Dixon, D. R. (1998). Extensive deep-sea dispersal of postlarval shrimp from a hydrothermal vent. *Deep Sea Res. Part I: Oceanogr. Res. Pap.* 45 (12), 2105–2118. doi: 10.1016/S0967-0637(98)00050-8

Hey, J., Chung, Y., and Sethuraman, A. (2015). On the occurrence of false positives in tests of migration under an isolationwith-migration model. *Mol. Ecol.* 24, 5078–5083. doi: 10.1111/mec.13381

Hey, J., Chung, Y., Sethuraman, A., Lachance, J., Tishkoff, S., Sousa, V. C., et al. (2018). Phylogeny estimation by integration over isolation with migration models. *Mol. Biol. Evol.* 35 (11), 2805–2818. doi: 10.1093/molbev/msy162

Hirschi, J. J. M., Barnier, B., Böning, C., Biastoch, A., Blaker, A. T., Coward, A., et al. (2020). The Atlantic meridional overturning circulation in high-resolution models. *J. Geophys. Res.: Oceans* 125 (4), e2019JC015522. doi: 10.1029/2019JC015522

Johnson, S. B., Won, Y. J., Harvey, J. B. J., and Vrikenhoek, R. C. (2013). A hybrid zone between *Bathymodiolus* mussel lineages from eastern pacific hydrothermal vents. *BMC Evolutionary Biol.* 13, 21. doi: 10.1186/1471-2148-13-21

Johnson, S. B., Young, C. R., Jones, W., Waren, A., and Vrikenhoek, R. C. (2006). Migration, isolation, and speciation of hydrothermal vent limpets (Gastropoda; lepetodrilidae) across the blanco transform fault. *Biol. Bull.* 210, 140–157. doi: 10.2307/4134603

Jollivet, D., Faugères, J. C., Griboulard, R., Desbruyères, D., and Blanc, G. (1990). Composition and spatial organization of a cold seep community on the south Barbados accretionnary prism: tectonic, geochemical and sedimentary context. *Prog. Oceanogr.* 24, 25–46. doi: 10.1016/0079-6611(90)90017-V

Jollivet, D., Portanier, E., Nicolle, A., Thiébaut, E., and Biastoch, A. (2023). Atlantic Seep mussels larval dispersal simulations and genetic data. *PANGAEA*. doi: 10.1594/PANGAEA.955455

Jolly, M. T., Viard, F., Weinmayr, G., Gentil, F., Thiébaut, E., and Jollivet, D. (2003). Does the genetic structure of *Pectinaria koreni* (Polychaeta: Pectinariidae) conform to a source–sink metapopulation model at the scale of the baie de seine? *Helgol Mar. Res;* 56, 238–246. doi: 10.1007/s10152-002-0123-1

Jones, B. T., Solow, A., and Ji, R. (2016). Resource allocation for Lagrangian tracking. *J. Atmospheric Oceanic Technol.* 33, 1225–1235. doi: 10.1175/JTECH-D-15-0115.1

Jones, W. J., Won, Y. J., Maas, P. A. Y., Smith, P. J., Lutz, R. A., and Vrijenhoek, R. C. (2006). Evolution of habitat use by deep-sea mussels. *Mar. Biol.* 148, 841–851. doi: 10.1007/s00227-005-0115-1

Ketzer, J. M., Augustin, A., Rodrigues, L. F., Oliveira, R. S., Praeg, D., Gomez Pivel, M. A., et al. (2018). Gas seeps and gas hydrates in the Amazon deep-sea fan. *Geo-Marine Lett.* 38 (5), 429–438. doi: 10.1007/s00367-018-0546-6

Kim, M., Kang, J.-H., and Kim, D. (2022). Holoplanktonic and meroplanktonic larvae in the surface waters of the onnuri vent field in the central Indian ridge. *J. Mar. Sci. Eng.* 10 (2), 158. doi: 10.3390/jmse10020158

Knowlton, N., and Weigt, L. A. (1998). New dates and new rates for divergence across the isthmus of Panama. *Proc. R. Soc. London B* 265, 2257–2263. doi: 10.1098/rspb.1998.0568

LaBella, A. L., Van Dover, C. L., Jollivet, D., and Cunningham, C. W. (2017). Gene flow between Atlantic and pacific ocean basins in three lineages of deep-sea clams (Bivalvia: Vesicomyidae: Pliocardiinae) and subsequent limited gene flow within the Atlantic. *Deep Sea Res. Part II: Topical Stud. Oceanogr.* 137, 307–317. doi: 10.1016/j.dsr2.2016.08.013

Laming, S. R., Gaudron, S. M., and Duperron, S. (2018). Lifecycle ecology of deep-Sea chemosymbiotic mussels: A review. *Front. Mar. Sci.* 5. doi: 10.3389/fmars.2018.00282

Lande, R. (1988). Genetics and demography in biological conservation. *Sci. (Washington)* 241 (4872), 1455–1460. doi: 10.1126/science.3420403

Le Bris, N., Arnaud-Haond, S., Beaulieu, S., Cordes, E., Hilario, A., Rogers, A., et al. (2017). "Hydrothermal vents and cold seeps," in *The first global integrated marine assessment: World ocean assessment I* (Cambridge: Cambridge University Press), 853–862.

Lee, W.-K., Kim, S.-J., Hou, B. K., Van Dover, C. L., and Ju, S.-J. (2019). Population genetic differentiation of the hydrothermal vent crab *Austinograea alayseae* (Crustacea: Bythograeidae) in the southwest pacific ocean. *PloS One* 14 (4), e0215829. doi: 10.1371/journal.pone.0215829

Leigh, J. W., and Bryant, D. (2015). POPART: Full-feature software for haplotype network construction. *Methods Ecol. Evol.* 6, 1110–1116. doi: 10.1111/2041-210X.12410

Lejeusne, C., and Chevaldonné, P. (2006). Brooding crustaceans in a highly fragmented habitat: the genetic structure of Mediterranean marine cave-dwelling mysid populations. *Mol. Ecol.* 15 (13), 4123–4140. doi: 10.1111/j.1365-294X.2006.03101.x

Levin, L. A., Baco, A. R., Bowden, D. A., Colaco, A., Cordes, E. E., Cunha, M. R., et al. (2016). Hydrothermal vents and methane seeps: Rethinking the sphere of influence. *Front.Mar.Sci.* 3, 72. doi: 10.3389/fmars.2016.00072

Levin, S. A., Cohen, D., and Hastings, A. (1984). Dispersal strategies in patchy environments. *Theor. population Biol.* 26 (2), 165–191. doi: 10.1016/0040-5809(84)90028-5

Levin, L. A., and Le Bris, N. (2015). The deep ocean under climate change. *Science* 350, 766–768. doi: 10.1126/science.aad0126

Lorion, J., Kiel, S., Faure, B., Kawato, M., Ho, S. Y. W., Marshall, B., et al. (2013). Adaptive radiation of chemosymbiotic deep-sea mussels. *Proc. R Soc. B* 280, 20131243. doi: 10.1098/rspb.2013.1243

Lutz, R. A. (1988). Dispersal of organisms at deep-sea hydrothermal vents: a review. *Oceanologica Acta Special Issue* 8, 23–30.

MacArthur, R., and Wilson, E. O. (1967). *The theory of island biogeography* (Princeton, USA: Princeton Landmarks in Biology. Princeton University Press), 224p.

MacDonald, I. R., Boland, G. S., Baker, J. S., Brooks, J. M., Kennicutt, M. C., and Bidigare, R. R. (1989). Gulf of Mexico hydrocarbon seep communities. *Mar. Biol.* 101 (2), 235–247. doi: 10.1007/BF00391463

Maes, G. E., and Volckaert, F. A. M. (2002). Clinal genetic variation and isolation by distance in the European eel *Anguilla anguilla* (L.). *Biol. J. Linn. Soc.* 77 (4), 509–521. doi: 10.1046/j.1095-8312.2002.00124.x

Marsh, A. G., Mullineaux, L. S., Young, C. M., and Manahan, D. T. (2001). Larval dispersal potential of the tubeworm *Riftia pachyptila* at deep-sea hydrothermal vents. *Nature* 411 (6833), 77. doi: 10.1038/35075063

Matabos, M., and Jollivet, D. (2019). Revisiting the *Lepetodrilus elevatus* species complex (Vetigastropoda: Lepetodrilidae), using samples from the galápagos and guaymas hydrothermal vent systems. *J. Molluscan Stud.* 85, 154–165. doi: 10.1093/mollus/eyy061

McCauley, D. E. (1991). Genetic consequences of local population extinction and recolonization. *Trends Ecol. Evol.* 6 (1), 5–8. doi: 10.1016/0169-5347(91)90139-O

McCowin, M. F., Feehery, C., and Rouse, G. W. (2020). Spanning the depths or depth-restricted: Three new species of *Bathymodiolus* (Bivalvia, mytilidae) and a new record for the hydrothermal vent *Bathymodiolus thermophilus* at methane seeps along the Costa Rica margin. *Deep–Sea Res. I* 164, 103322. doi: 10.1016/j.dsr.2020.103322

McMullin, E. R., Nelson, K., Fisher, C. R., and Schaeffer, S. W. (2010). Population structure of two deep sea tubeworms, lamellibrachia luymesi and seepiophila jonesi, from the hydrocarbon seeps of the gulf of Mexico. *Deep-Sea Res. I* 57, 1499–1509. doi: 10.1016/j.dsr.2010.07.012

McPeek, M. A., and Holt, R. D. (1992). The evolution of dispersal in spatially and temporally varying environments. *Am. Nat.* 140 (6), 1010–1027. doi: 10.1086/285453

McVeigh, D. M., Eggleston, D. B., Todd, A. C., Young, C. M., and He, R. (2017). The influence of larval migration and dispersal depth on potential larval trajectories of a deep-sea bivalve. *Deep Sea Res. Part I: Oceanogr. Res. Pap.* 127, 57–64. doi: 10.1016/j.dsr.2017.08.002

Mitarai, S., Watanabe, H., Nakajima, Y., Schepetkin, A. F., and McWilliams, J. C. (2016). Quantifying dispersal from hydrothermal vent fields in the western pacific ocean. *Proc. Natl. Acad. Sci.* 113 (11), 2976–2981. doi: 10.1073/pnas.1518395113

Miyazaki, J. I., Martins, L., Fujita, Y., Matsumoto, H., and Fujiwara, Y. (2010). Evolutionary process of deep-Sea *Bathymodiolus* mussels. *PloS One* 5 (4), e10363. doi: 10.1371/journal.pone.0010363

Moilanen, A., and Hanski, I. (1998). Metapopulation dynamics: effects of habitat quality and landscape structure. *Ecology* 79 (7), 2503–2515. doi: 10.1890/0012-9658(1998)079[2503:MDEOHQ]2.0.CO;2

Montes, C., Cardona, A., Jaramillo, C., Pardo, A., Silva, J. C., Valencia, V., et al. (2015). Middle Miocene closure of the central American seaway. *Science* 348, 226–229. doi: 10.1126/science.aaa2815

Nei, M. (1987). *Molecular evolutionary genetics* (New York, NY: Columbia University Press).

Olivieri, I., Michalakis, Y., and Gouyon, P. H. (1995). Metapopulation genetics and the evolution of dispersal. *Am. Nat.* 146 (2), 202–228. doi: 10.1086/285795

Olu, K., Cordes, E. E., Fisher, C. R., Brooks, J. M., Sibuet, M., and Desbruyères, D. (2010). Biogeography and potential exchanges among the Atlantic equatorial belt cold-seep faunas. *PloS One* 5 (8), e11967. doi: 10.1371/journal.pone.0011967

Olu, K., Lance, S., Sibuet, M., Henry, P., Fiala-Médioni, A., and Dinet, A. (1997). Cold seep communities as indicators of fluid expulsion patterns through mud volcanoes seaward of the Barbados accretionary prism. *Deep Sea Res. Part I: Oceanogr. Res. Pap.* 44 (5), 811–841. doi: 10.1016/S0967-0637(96)00123-9

Olu, K., Sibuet, M., Harmegnies, F., Foucher, J. P., and Fiala-Medioni, A. (1996). Spatial distribution of diverse cold seep communities living on various diapiric structures of the southern Barbados prism. *Prog. Oceanogr.* 38, 347–376. doi: 10.1016/S0079-6611(97)00006-2

Olu-Le Roy, K., Sibuet, M., Fiala-Médioni, A., Gofas, S., Salas, C., Mariotti, A., et al. (2004). Cold seep communities in the deep eastern Mediterranean Sea: composition, symbiosis and spatial distribution on mud volcanoes. *Deep Sea Res. Part I: Oceanogr. Res. Pap.* 51 (12), 1915–1936. doi: 10.1016/j.dsr.2004.07.004

Olu-Le Roy, K., Von Cosel, R., Hourdez, S., Carney, S. L., and Jollivet, D. (2007). Amphi-Atlantic cold-seep *Bathymodiolus* species complexes across the equatorial belt. *Deep Sea Res. Part I: Oceanogr. Res. Pap.* 54, 1890–1911. doi: 10.1016/j.dsr.2007.07.004

Pannell, J. R., and Charlesworth, B. (1999). Neutral genetic diversity in a metapopulation with recurrent local extinction and recolonization. *Evolution* 53 (3), 664–676. doi: 10.2307/2640708

Pechenik, J. A. (1990). Delayed metamorphosis by larvae of benthic marine invertebrates: Does it occur? is there a price to pay? *Ophelia* 32 (1–2), 63–94. doi: 10.1080/00785236.1990.10422025

Pereira, O. S., Shimabukuro, M., Bernardino, A. F., and Sumida, P. Y. G. (2020). Molecular affinity of southwest Atlantic *Alvinocaris muricola* with Atlantic equatorial belt populations. *Deep–Sea Res. I* 163, 103343. doi: 10.1016/j.dsr.2020.103343

Plouviez, S., Shank, T. M., Faure, B., Daguin-Thiebaut, C., Viard, F., Lallier, F. H., et al. (2009). Comparative phylogeography among hydrothermal vent species along the East pacific rise reveals vicariant processes and population expansion in the south. *Mol. Ecol.* 18 (18), 3903–3917. doi: 10.1111/j.1365-294X.2009.04325.x

Poitrimol, C., Thiébaut, E., Daguin-Thiébaut, C., Le Port, A.-S., Ballenghien, M., Tran Lu Y, A., et al. (2022). Contrasted phylogeographic patterns of hydrothermal vent gastropods along south West pacific: Woodlark basin, a possible contact zone and/or stepping-stone. *PloS One* 17 (10), e0275638. doi: 10.1371/journal.pone.0275638

Pond, D. W., Segonzac, M., Bell, M. V., Dixon, D. R., Fallick, A. E., and Sargent, J. R. (1997). Lipid and lipid carbon stable isotope composition of the hydrothermal vent shrimp *Mirocaris fortunata*: evidence for nutritional dependence on photosynthetically fixed carbon. *Mar. Ecol. Prog. Ser.* 157, 221–231. doi: 10.3354/meps157221

Portanier, E., Nicolle, A., Thiébaut, E., Jollivet, D., Rath, W., and Biastoch, A. (2023). Atlantic Seep mussels larval dispersal simulations, figshare. *Figure*. doi: 10.6084/m9.figshare.22227670.v2

Pradillon, F., Shillito, B., Young, C. M., and Gaill, F. (2001). Deep-sea ecology: Developmental arrest in vent worm embryos. *Nature* 413 (6857), 698. doi: 10.1038/35099674

Proskurowski, G., Marvin, D. L., Seewald, J. S., Früh-Green, G. L., Olson, E. J., Lupton, J. E., et al. (2008). Abiogenic hydrocarbon production at lost city hydrothermal field. *Science* 319, 604–607. doi: 10.1126/science.1151194

Prouty, N. G., Sahy, D., Ruppel, C. D., Roark, E. B., Condon, D., Brooke, S., et al. (2016). Insights into methane dynamics from analysis of authigenic carbonates and chemosynthetic mussels at newly-discovered Atlantic margin seeps. *Earth Planet. Sci. Lett.* doi: 10.1016/j.epsl.2016.05.023

Puillandre, N., Brouillet, S., and Achaz, G. (2021). ASAP: assemble species by automatic partitioning. *Mol. Ecol. Resour.* 21, 609–620. doi: 10.1111/1755-0998.13281

Puillandre, N., Lambert, A., Brouillet, S., and Achaz, G. J. M. E. (2012). ABGD, automatic barcode gap discovery for primary species delimitation. *Mol. Ecol.* 21 (8), 1864–1877. doi: 10.1111/j.1365-294X.2011.05239.x

R Core Team (2021). *R: A language and environment for statistical computing* (Vienna, Austria: R Foundation for Statistical Computing). Available at: https://www.R-project.org/.

Raggi, L., Schuboltz, F., Hinrichs, K.-U., Dubilier, N., and Petersen, J. M. (2013). Bacterial symbionts of bathymodiolus mussels and escarpia tubeworms from chapopote, an asphalt seep in the southern gulf of Mexico. *Environ. Microbiol.* 15 (7), 1969–1987. doi: 10.1111/1462-2920.12051

Rodrigues, C. F., Cunha, M. R., Génio, L., and Duperron, S. (2013b). A complex picture of associations between two host mussels and symbiotic bacteria in the northeast Atlantic. *Naturwissenschaften* 100, 21–31. doi: 10.1007/s00114-012-0985-2

Rodrigues, C. F., Hilário, A., and Cunha, M. R. (2013a). Chemosymbiotic species from the gulf of cadiz (NE atlantic): distribution, life styles and nutritional patterns. *Biogeosciences* 10, 2569–2581. doi: 10.5194/bg-10-2569-2013

Roughgarden, J., Gaines, S. D., and Possingham, H. (1988). Recruitment dynamics in complex life cycles. *Science* 241, 1460–1466. doi: 10.1126/science.11538249

Roux, C., Fraïsse, C., Romiguier, J., Anciaux, Y., Galtier, N., and Bierne, N. (2016). Shedding light on the grey zone of speciation along a continuum of genomic divergence. *PloS Biol.* 14 (12), e2000234. doi: 10.1371/journal.pbio.2000234

Rozas, J., Ferrer-Mata, A., Sanchez-DelBarrio, J. C., Guirao-Rico, S., Librado, P., Ramos-Onsins, S. E., et al. (2017). DnaSP v6: DNA sequence polymorphism analysis of large datasets. *Mol. Biol. Evol.* 34, 3299–3302. doi: 10.1093/molbev/msx248

Ruppel, C., Skarke, A., and Hoy, S. (2019). "Discoveries at a methane seep field offshore bodie island, north Carolina," in *Windows to the deep 2019: Exploration of the deep-sea habitats of the southeastern united states*. (Washington, USA: National Oceanic and Atmospheric Administration (NOAA) Ocean Exploration, U.S. Department of Commerce). Available at: https://oceanexplorer.noaa.gov/okeanos/explorations/ex1903/logs/july7/july7.html29/09/2022.

Scheltema, R. S. (1986). Long-distance dispersal by planktonic larvae of shoal-water benthic invertebrates among central pacific islands. *Bull. Mar. Sci.* 39 (2), 241–256.

Schmidt, C., Schwarzkopf, F. U., Rühs, S., and Biastoch, A. (2021). Characteristics and robustness of agulhas leakage estimates: an inter-comparison study of Lagrangian methods. *Ocean Sci.* 17, 1067–1080. doi: 10.5194/os-17-1067-2021

Shanks, A. L. (2009). Pelagic larval duration and dispersal distance revisited. *Biol. Bull.* 216 (3), 373–385. doi: 10.1086/BBLv216n3p373

Sibuet, M., Juniper, K. S., and Pautot, G. (1988). Cold-seep benthic communities in the Japan subduction zones: geological control of community development. *J. Mar. Res.* 46 (2), 333–348. doi: 10.1357/002224088785113595

Sibuet, M., and Olu, K. (1998). Biogeography, biodiversity and fluid dependence of deep-sea cold-seep communities at active and passive margins. *Deep-Sea Res. II* 45, 517–567. doi: 10.1016/S0967-0645(97)00074-X

Small, K. S., Brudno, M., Hill, M. W., and Sidow, A. (2007). Extreme genomic variation in a natural population. *PNAS* 104, 5698–5703. doi: 10.1073/pnas.0700890104

Snyder, R. E. (2006). Multiple risk reduction mechanisms: can dormancy substitute for dispersal? *Ecol. Lett.* 9 (10), 1106–1114. doi: 10.1111/j.1461-0248.2006.00962.x

Tajima, F. (1983). Evolutionary relationship of DNA sequences in finite populations. *Genetics* 105, 437–460. doi: 10.1093/genetics/105.2.437

Teixeira, S., Cambon-Bonavita, M. A., Serrao, E. A., Desbruyeres, D., and Arnaud-Haond, S. (2011). Recent population expansion and connectivity in the hydrothermal shrimp *Rimicaris exoculata* along the mid-Atlantic ridge. *J. Biogeography* 38, 564–574. doi: 10.1111/j.1365-2699.2010.02408.x

Teixeira, S., Olu, K., Decker, C., Cunha, R. L., Fuchs, S., Hourdez, S., et al. (2013). High connectivity across the fragmented chemosynthetic ecosystems of the deep Atlantic equatorial belt: efficient dispersal mechanisms or questionable endemism? *Mol. Ecol.* 22 (18), 4663–4680. doi: 10.1111/mec.12419

Thaler, A. D., Plouviez, S., Saleu, W., Alei, F., Jacobson, A., Boyle, E. A., et al. (2014). Comparative population structure of two deep-sea hydrothermal-vent-associated decapods (*Chorocaris* sp. 2 and *Munidopsis lauensis*) from southwestern pacific back-arc basins. *PloS One* 9 (7), e101345. doi: doi: 10.1371/journal.pone.0101345

Thaler, A. D., Zelnio, K., Saleu, W., Schultz, T. F., Carlsson, J., Cunningham, C., et al. (2011). The spatial scale of genetic subdivision in populations of *Ifremeria nautilei*, a hydrothermal-vent gastropod from the southwest pacific. *BMC Evolutionary Biol.* 11 (1), 372. doi: 10.1186/1471-2148-11-372

Tran Lu Y, A. (2022). *La phylogéographie comparée d'espèces hydrothermales du pacifique ouest à l'heure de la génomique des populations* (Montpellier, France: University of Montpellier).

Tran Lu Y, A., Ruault, S., Daguin-Thiébaut, C., Castel, J., Bierne, N., Broquet, T., et al. (2022). Subtle limits to connectivity revealed by outlier loci within two divergent metapopulations of the deep-sea hydrothermal gastropod ifremeria nautilei. *Mol. Ecol.* 31, 2796–2813. doi: 10.1111/mec.16430

Travis, J. M., and Dytham, C. (1999). Habitat persistence, habitat availability and the evolution of dispersal. *Proc. R. Soc. London B: Biol. Sci.* 266 (1420), 723–728. doi: 10.1098/rspb.1999.0696

Turner, P. J., Ball, B., Diana, Z., Fariñas-Bermejo, A., Grace, I., McVeigh, D., et al. (2020). Methane seeps on the US Atlantic margin and their potential importance to populations of the commercially valuable deep-sea red crab, *Chaceon quinquedens*. *Front. Mar. Sci.* 7, 75. doi: 10.3389/fmars.2020.00075

Tsujino, H., Urakawa, S., Nakano, H., Small, R., Kim, W., Yeager, S., et al. (2018). Jra-55 based surface dataset for driving ocean–sea-ice models (jra55 do). *Ocean Model.* 130, 79–139. doi: 10.1016/j.ocemod.2018.07.002

Tyler, P., Young, C. M., Dolan, E., Arellano, S. M., Brooke, S. D., and Baker, M. (2007). Gametogenic periodicity in the chemosynthetic cold-seep mussel "*Bathymodiolus*" *childressi*. *Mar. Biol.* 150, 829–840. doi: 10.1007/s00227-006-0362-9

Van Dover, C. L. (2014). Impacts of anthropogenic disturbances at deep-sea hydrothermal vent ecosystems: A review. *Mar. Environ. Res.* 102, 59e72. doi: 10.1016/j.marenvres.2014.03.008

Van Dover, C. L., Aharon, P., Bernhard, J. M., Caylor, E., Doerries, M., Flickinger, W., et al. (2003). Blake Ridge methane seeps: characterization of a soft-sediment, chemosynthetically based ecosystem. *Deep-Sea Res.* I50, 281–300. doi: 10.1016/S0967-0637(02)00162-0

Van Dover, C. L., German, C. R., Speer, K. G., Parson, L. M., and Vrijenhoek, R. C. (2002). Evolution and biogeography of deep-sea vent and seep invertebrates. *Science* 295 (5558), 1253–1257. doi: 10.1126/science.1067361

Van Sebille, E., Griffies, S. M., Abernathey, R., Adams, T. P., Berloff, P., Biastoch, A., et al. (2018). Lagrangian Ocean analysis: fundamentals and practices. *Ocean Model.* 121, 49–75. doi: 10.1016/j.ocemod.2017.11.008

Vilela, C. L. S., Damasceno, T. L., Thomas, T., and Peixoto, R. S. (2022). Global qualitative and quantitative distribution of micropollutants in the deep sea. *Environ. pollut.* 307, 119414. doi: 10.1016/j.envpol.2022.119414

Yahagi, T., Watanabe, H. K., Kojima, S., and Kano, Y. (2017). Do larvae from deep-sea hydrothermal vents disperse in surface waters? *Ecology* 98 (6), 1524–1534. doi: 10.1002/ecy.1800

Yao, G., Zhang, H., Xiong, P., Jia, H., Shi, Y., and He, M. (2022). Community characteristics and genetic diversity of macrobenthos in haima cold seep. *Front. Mar. Sci* 9, 920327. doi: 10.3389/fmars.2022.920327

Yorisue, T., Kado, R., Watanabe, H., Høeg, J. T., Inoue, K., Kojima, S., et al. (2013). Influence of water temperature on the larval development of neoverruca sp. and ashinkailepas seepiophila – implication for larval dispersal and settlement in the vent and seep environments. *Deep-Sea Res. I.* 71, 33–37. doi: 10.1016/j.dsr.2012.10.007

Young, C. M. (1994). A tale of two dogmas: the early history of deep-sea reproductive biology. *Reproduction, larval biology and recruitment of the deep-sea benthos, in Reproduction, Larval Biology, and Recruitment of the Deep sea Benthos*, (C. M. Young and K. J. Eckelbarger [eds.]), New York, USA: Columbia University Press.

Young, C. M., He, R., Emlet, R. B., Li, Y., Qian, H., Arellano, S. M., et al. (2012). Dispersal of deep-sea larvae from the intra-American seas: simulations of trajectories using ocean models. *Integr. Comp. Biol.* 52, 483–496. doi: 10.1093/icb/ics090

frontiers | Frontiers in Marine Science

TYPE Original Research
PUBLISHED 22 October 2024
DOI 10.3389/fmars.2024.1393385

OPEN ACCESS

EDITED BY
Stefán Áki Ragnarsson,
Marine and Freshwater Research Institute, Iceland

REVIEWED BY
Fanny Girard,
University of Hawaii at Manoa, United States
Didier Alain Jollivet,
Centre National de la Recherche Scientifique (CNRS), France

*CORRESPONDENCE
Cláudia Viegas
cnviegas@gmail.com

RECEIVED 29 February 2024
ACCEPTED 16 August 2024
PUBLISHED 22 October 2024

CITATION
Viegas C, Juliano M and Colaço A (2024) Larval dispersal and physical connectivity of *Pheronema carpenteri* populations in the Azores.
Front. Mar. Sci. 11:1393385.
doi: 10.3389/fmars.2024.1393385

Larval dispersal and physical connectivity of *Pheronema carpenteri* populations in the Azores

Cláudia Viegas[1]*, Manuela Juliano[1,2] and Ana Colaço[1,3]

[1]Institute of Marine Sciences - Okeanos, University of the Azores, Horta, Portugal, [2]Marine Environment and Technology Laboratory, University of Azores, Praia da Vitória, Portugal, [3]Instituto do Mar - IMAR, University of the Azores, Horta, Portugal

The study of larval dispersal and connectivity between deep-sea populations is essential for the effective conservation and management of deep-sea environments and the design and implementation of Marine Protected Areas. Dense sponge aggregations, known as "sponge grounds", are a key component of marine benthic ecosystems, by increasing the structural complexity of the sea floor and providing structure and habitat for many other species. These aggregations are characteristic of the Azores deep-sea environment. These sessile organisms rely primarily on larval dispersal for their reproduction. Connectivity between specific *Pheronema carpenteri* sponge aggregations in the Azores was studied using a 3-D biophysical dispersal model. Different biological trait scenarios were analyzed, considering spawning seasonality and pelagic larval duration. Model results indicate that regional circulation patterns drive larval dispersion, shaping population connectivity of *P. carpenteri* sponge aggregations in the Azores, particularly among aggregations in the Central Group of Azorean islands. Some areas present high retention rates, receiving larvae from several sponge aggregations while also being important larval source aggregations. In contrast, aggregations from the Eastern Group may be isolated from the others. Larval dispersal and connectivity patterns were analyzed concerning the current configuration of Marine Protected Areas (MPAs) in the Azores. The results underscored the importance of maintaining protection efforts in existing MPAs and identified stepping-stone locations and specific sites where additional measures could enhance species connectivity in the Azores.

KEYWORDS

deep-sea sponge, connectivity, larval dispersal, modelling, hydrodynamics, *Pheronema carpenteri*

1 Introduction

Connectivity is a fundamental process driving the persistence of marine populations and influencing the ecosystems' structure, biodiversity, productivity, dynamics and resilience (Kenchington et al., 2019; Busch et al., 2021). In the deep-sea (the ocean below 200 meters depth), connectivity is a key element for spatial management and conservation plans including the establishment of Marine Protected Areas (MPAs) (Lima et al., 2020; Combes et al., 2021).

Many marine organisms rely on the larval phase as the primary means to colonize new areas, making this process crucial for individual survival as well as in population dynamics and persistence (Ross et al., 2020). Some species possess a pelagic larval phase, during which their larvae are transported by ocean currents, facilitating migration between geographically distant populations (Paris et al., 2013). However, despite the pivotal role of the planktonic larval stage and larval dispersal in understanding deep-sea population connectivity, knowledge gaps remain due to challenges in obtaining *in-situ* data (Kenchington et al., 2019). This pelagic larval dispersal phase contributes to (i) population exchanges that aid in the replenishment of populations, population connectivity and the maintenance of well-established communities, and to (ii) the colonization of new territories/habitats, possibly modifying existing communities and associated biodiversity (Adams et al., 2012).

Dense sponge aggregations, known as "sponge grounds", are a key component of marine benthic ecosystems, enhancing, along with corals, the local biodiversity, and acting as feeding, reproductive, nursery and refuge areas for many invertebrates and fish (Pham et al., 2015; Beazley et al., 2021). Deep-sea sponges are thought to play an important role in the deep-sea nutrient cycle, recycling the nutrients, through their capacity of filtering large quantities of water (Leis, 2020). By converting dissolved organic matter (DOM) into detritus, sponges are enable to transfer the energy and nutrients in DOM to higher trophic levels, the so-called sponge loop pathway (Rix et al., 2018). They also contribute to the biogeochemical cycling of dissolved nutrients, such as carbon and nitrogen, and silicate in the case of siliceous sponges like *P. carpenteri*, which belongs to the class of Hexactinella (Maldonado et al., 2016; Ross et al., 2016, 2019; Taranto, 2022).

These deep-sea organisms rely upon a planktonic larval stage for dispersal; thus, studying the environmental patterns responsible for their distribution is critical to inform and support the development of appropriate conservation measures (Maldonado and Young, 1999; Cowen and Sponaugle, 2009; Xavier et al., 2015; Wang et al., 2021).

Deep-sea sponges inhabit multiple areas of the deep-sea, particularly in the North Atlantic (Samuelsen et al., 2022). The hexactinellid *Pheronema carpenteri* forms extensive sponge aggregations, occurring from south of Iceland and west of Scotland, across the Porcupine Seabight, Azores, northern Spain, Portugal, Canary Islands, and off Morocco at 800–1,350 m depth (Maldonado et al., 2016). Some of them are reported to have persistent spicule skeletons (Maldonado et al., 2005). These spicule mats created by the senescence and death of hexactinellid sponges, provide an important substratum that hosts diverse faunal communities (Bett and Rice, 1992) forming biodiversity hotspots (Henry and Roberts, 2014), and may even function as reducers of sediment erosion in the deep-sea (Black et al., 2003). Sponges are also known for establishing complex microbial symbioses being a reservoir of exceptional microbial diversity and major contributors to the total microbial diversity of the world's oceans (Thomas et al., 2016).

P. carpenteri forms the most extensive Hexactinellid aggregations in the North-East Atlantic (Graves et al., 2023), and is a typical organisms of the deep-sea in the Azores (Pham et al., 2015). *P. carpenteri*, is a nest-shaped sponge that likely forms the most extensive sponge aggregations at temperate latitudes, with abundances up to 6 individuals m^{-2} (Maldonado et al., 2016). *P. carpenteri* has been recorded in the northeast Atlantic from the northern Rockall Trough at about 59°37'N north, through the Porcupine Seabight, Bay of Biscay, Portuguese coast and Moroccan coast to the Azores, at depths ranging from 650m to 1600 m (Rice et al., 1990; White, 2003; Howell et al., 2016; Creemers et al., 2019; Colaço et al., 2020; Vieira et al., 2020; Somoza et al., 2021; Taranto, 2022). In the Azores its density can vary between 2 to rarely 56 individuals per squares meter (Colaço pers. observ.).

In the Porcupine Sea Bight, this species occurs in areas with low currents but close to regions where enhanced bottom tidal currents are found (White, 2003). This corroborates the hypothesis of Rice et al. (1990), that these sponges do not tolerate enhanced currents, but may nevertheless be dependent upon the resuspended or undeposited organic matter carried to them from regions of increased tidal energy. In the Azores the same phenomena is observed, with the sponge grounds being present in areas with low intensity currents (Viegas, 2022).

The Azores deep-sea benthos includes a high diversity of sponges and cold-water corals which build rich communities (Pham et al., 2015; Gomes-Pereira et al., 2017; Creemers et al., 2019; Colaço et al., 2020; Morato et al., 2021). *P. carpenteri* is a common taxon in the Azores bathyal environment, forming large aggregations (Colaço et al., 2020) and is considered a vulnerable marine ecosystem (VME) since it meet several of the vulnerability criteria, such as fragility, slow growth rate and low recovery potential (FAO, 2008).

Available data about the biology of hexactinellids sponges results mainly from studies with shallow-water sponges (Barthel et al., 1996; Boury-Esnault et al., 1999), also arctic deep-sea populations (Leys and Lauzon, 1998), and other non-specific glass sponge's case studies (Bett and Rice, 1992; Boury-Esnault et al., 1999; Guillas et al., 2019). The reproductive strategy of *P. carpenteri* is currently unknown (Graves et al., 2023) but Hexactinellids are assumed to reproduce both asexually and sexually with lecithotrophic larvae (Leys and Ereskovsky, 2006; Teixidó et al., 2006). During their life cycle, after hatching, pelagic larvae drifts in the water column for a limited period (Pelagic Larval Duration, PLD), before settling on the seafloor, in a recruitment area, to become sessile juvenile sponges, if the environment conditions are suitable (Maldonado, 2006). Despite their deep-water habitat, hexactinellids sponges may experience seasonality that perhaps influences their reproductive period (Leys and Lauzon, 1998). For the deep-sea species *Geodia* the reproductive season spans from spring to Autumn (Koutsouveli et al., 2020).

The current understanding of deep-sea larval behavior for deep-sea sponges is extremely limited (Busch et al., 2021), mainly due to the inherent difficulty of assessing deep-water habitats (Lopes, 2005), and particularly by the difficulty of collecting larvae of deep-sea organisms. Available data from the shallow-water sponges indicate that most sponge larvae are anchiplanic, with a short planktonic larval duration of minutes to a few days (usually< 2 weeks) (Maldonado, 2006; Ross et al., 2019). However, this short PLD is only reported for shallow-water species and is believed to not be representative of deep-sea water taxa such as *P. carpenteri*. The glass sponge *V. pourtalesii* has an estimated maximum pelagic larval duration of 2 weeks (Wang et al., 2021). Hilário et al. (2015) calculated that the average known PLD of a deep-sea organism is 35 days, which is longer than for their shallow-water counterparts PLD. Wang et al. (2021) used modelling tools to study the fate of glass sponge larvae in the Gulf Stream, hypothesizing a 2-week maximum PLD for deep-sea glass sponge.

Furthermore, it is suggested that sponge larvae may remain in the water column for longer periods, perhaps months (Boury-Esnault et al., 1999; Maldonado, 2006). Environmental factors like seawater temperature can influence the duration of the reproductive period (Maldonado, 2006). Therefore, two different PLDs were tested in this study, a PLD of 15 days (similar as was estimated *V. pourtalesii*), and a PLD of 30 days (similar as was estimated in other deep-sea larvae dispersal studies (Hilário et al., 2015; Vic et al., 2018) (Table 1).

In this work, the potential larval dispersal of *P. carpenteri* deep-sea sponge aggregations in the Azores, it was modeled, as a proxy for the potential larval transport around Azores and evaluate the probability of the current MPAs to maintaining the connectivity of these benthic organism populations.

2 Methodology

2.1 Study area

The Azores archipelago is composed of nine islands, spanning 600 km in the Northeast Atlantic, between 23°W and 33°W and 37° N and 40°N (Figure 1) and divided into three geographical groups. The Mid Atlantic Ridge (MAR) crosses the archipelago. Two islands are located west of the MAR, on the American plate, forming the Western Group (WG), while the other islands are located on the Eurasian plate with 5 islands positioned in the Central Group (CG) of the Archipelago and two islands situated further east (Eastern Group: EG).

2.1.1 *Pheronema carpenteri* in the Azores

The *P. carpenteri* sponge aggregations identified in the scope of the SPONGES Project, due to their frequent observations are the focus of this study. These *P. carpenteri* aggregations are located along the Azores Archipelago (Figure 1), in a bathymetric range from 630 to 1000 meters depth (Table 2). Specifically, they are found over the Mid-Atlantic Ridge (MAR) at Cavala Seamount (L#1) and Gigante Seamount (L#2); in the Central Group (CG), at the Princesa Alice (L#3), Açores Bank (L#4), in the South of Faial (L#6), South of Pico (L#7), and North of Pico (L#8); and in the Eastern Group (EG) L#9 in Mar da Prata, and L#10 in Formigas.

TABLE 1 Literature review for Pelagic larval duration, spawning seasonality, of deep-sea sponges, from different locations and depths, used/obtained in other studies.

Organism/Taxa	PLD	Spawning season	Organism location	Reference
Sponges (generic)	<14 days	n/a	n/a	1)
Sponges (generic)	n/a	phytoplankton blooms (March/autumn)	Several; northwest Atlantic	2)
Demosponge	14 days	After spring bloom	Cantabrian sea	3)
Demosponge *(Geodia barretti)*	n/a	Spring & autumn/phytoplankton blooms	Norwegian fjords, deep continental shelf	4); 5)
Hexactinellida	> 24h (<24h for shallow sponge)	–	North Atlantic	6)
Deep-sea species	Median: 10-310days		Deep-sea (Hydrothermal vents, cold seeps, food falls, Seamounts)	7)
Shallow species	Median: 0.17-293 days		Deep-sea (Hydrothermal vents, cold seeps, food falls, Seamounts)	7)
Hexactinellida	n/a	All year round/ phytoplankton blooms	Fiords, British Columbia	2)
***Vazella pourtalesii* (Hexactinellida)**	2 weeks (value assumed for the model application)	All year round/	282 to 593 meters depth Eastern coast of North America	8)
***Oopsacas minuta* (Hexactinellida)**	n/a	All year round	submarine cave, France	2)
Deep-sea organisms	30-180 days (estimated)	n/a	n/a	9)

1) Maldonado, 2006; 2) Kenchington et al., 2019; 3) Busch et al., 2021; 4) Spetland et al., 2007; 5) (Leys and Lauzon, 1998); 6) Ross et al., 2019; 7) Hilário et al., 2015; 8) Wang et al., 2021; 9) Vic et al., 2018; n/a, no information available or not applicable.

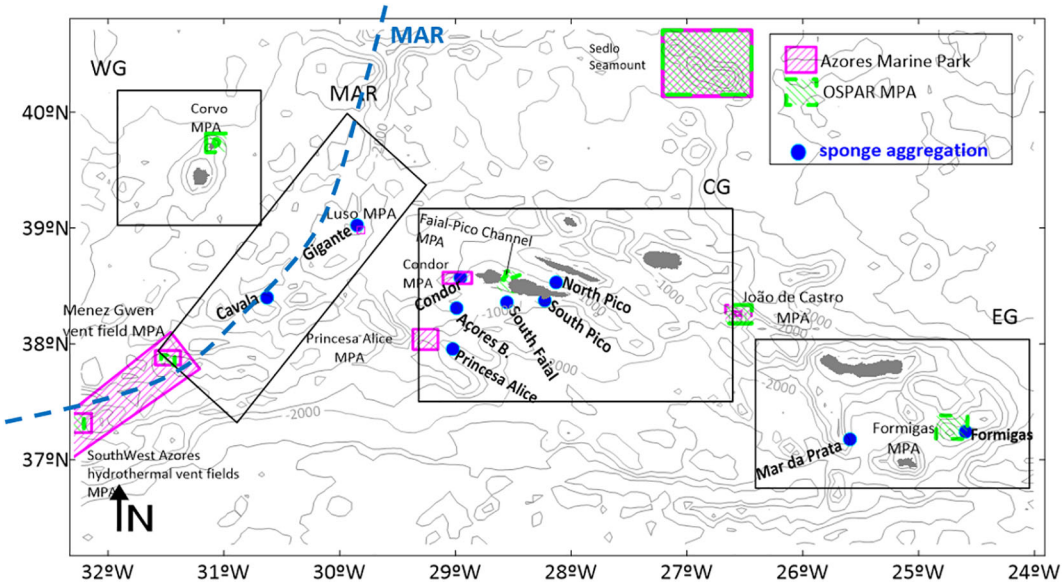

FIGURE 1
Bathymetry of the study area, with the representation of the Mid-Atlantic Ridge (MAR) with a blue dashed line, the 9 islands of the Azores archipelago in grey, the location of the *Pheronema carpenteri* sponge aggregations in the study with blue circles; black polygons depicts the groups in analysis: MAR Group (L#1 Cavala, L#2-Gigante); CG-Central Group (L#3-Princesa Alice, L#4-Açores Bank, L#5-Condor Seamount, L#6-South of Faial, L#7-South of Pico, L#8); EG- Eastern Group (L#9-Mar da Prata, and L#10-Formigas), and representation of the Azores Marine Park and OSPAR Marine Protected Areas, and the Western Group (Flores and Corvo islands), Central Group (Faial, Pico, São Jorge Terceira and Graciosa Islands), and the Eastern Group (São Miguel and Santa Maria islands).

For applying particle-tracking models to study larvae dispersal, it is essential to include information about their biological traits such as spawning seasonality, larval behavior, and pelagic larval duration (Busch et al., 2021). Empirical data about deep-sea sponges biology is very scarce, and specifically regarding *P. carpenteri* it is absent. Previous studies often assume that deep-sea sponges do not experience spawning seasonality, unlike their littoral relatives, because they are too deep to be influenced by light (Barthel et al., 1996). However, further studies pointed out that despite their deep-sea habitat, sponges experience seasonality, which influences their growth rate and perhaps reproductive period, which, in turn, may be regulated by patterns of primary production in the photic zone of the ocean and subsequent sinking of the generated production (Leys and Lauzon, 1998). A number of

TABLE 2 *Pheronema carpenteri* sponge aggregations in the study, their location, depth, source and name/location.

Location	Longitude (°W)	Latitude (°N)	Depth (m)	Name	Group	Source/project
L#1	-30.6701	38.3632	900	Cavala	MAR	emodnet[1]
L#2	-29.88809	38.98353	766	Gigante	MAR	Exp-Fund.Azul [2]
L#3	-29.06232	37.9183	900	Princess Alice	CG1	Biodiaz [3]
L#4	-29.02941	38.273	825	Açores Bank	CG2	Sponges-Observer_2017[4]
L#5	-28.99877	38.53281	775	Condor Seamount South	CG3	IMAR-DOP/UAz (CoralFish, Corazon, Condor) [5]
L#6	-28.59288	38.32531	630	South of Faial	CG4	Sponges-observer_2017[2]
L#7	-28.26657	38.33921	1000	South of Pico	CG5	Sponges-Lula[2]
L#8	-28.1735	38.49624	822	North of Pico	CG	Exp-Fund.Azul[2]
L#9	-25.63083	37.14111	780	Oeste West of São Miguel (Mar da Prata)	EG	IMAR-DOP/UAz (CoralFish, Corazon, Condor) [5]
L#10	-24.63	37.205	904	Formigas	EG	Colecta[6]

[1]http://ipt.vliz.be/eurobis/resource?r=imagedop_video_annotations; [2]Colaço et al., 2020; [3]Institute of Marine Research (IMAR-Azores), Portugal; [4]Department of Oceanography and Fisheries (DOP)-University of the Azores, Portugal, 2017. [5]ImageDOP Bentic Video http://www.vliz.be/en/imis?dasid=4492&doiid=304; [6]DOP/internal unpublished data.

deep-sea species display potential spawning that is linked to organic matter input during seasonal phytoplankton blooms (Mercier et al., 2011; Sun et al., 2011; Mercier et al., 2013; Baillon et al., 2014). In particular, for deep-sea corals, some gametogenic peaks coincided with periods marked by high surface productivity, in spring and autumn (Santos et al., 2013).

The information available regarding deep-sea larval behavior is scarce. Table 1 summarizes the literature review regarding the deep-sea larvae biological traits and specifically for deep-sea sponges larvae. Different scenarios were computed to study the larval dispersal in the Azores. It was considered a yearly release since no information on spawning was available, but since some deep-sea species are believed to experience spawning seasonality, seasonal scenarios were also performed. For the seasonal scenario, a release in March was simulated to represent the spring spawning season, and a release in October to represent the autumn spawning season (Santos et al., 2013). All the scenarios ran with different pelagic larval durations (PLD) of 15 and 30 days (Table 3).

2.1.2 3D Hydrodynamic model using Mohid

The 3-D hydrodynamic modelling system used was MOHID, developed at MARETEC (IST - University of Lisbon) which solves the 3D incompressible primitive equations built and developed using an object-oriented philosophy (IST, 2003; Braunschweig et al., 2004; Leitão et al., 2008). MOHID is an open-source model, available online at https://github.com/Mohid-Water-Modelling-System/Mohid. It is programmed in ANSI FORTRAN 95, following an object-oriented approach allowing the integration of different modules in implicit and explicit ways (IST, 2003). The hydrodynamic model simulates the currents and density fields, fundamental for the Lagrangian and Eulerian transports through advection and/or diffusion processes. The turbulence is solved by the General Ocean Turbulence Model (GOTM) module (Burchard et al., 1999). Model configuration and boundary conditions are described in Table 4.

The model was implemented for the Azores region from 32.4721°N to 42.91211°N, -21.40775°W to -36.2878°W, for the years 2017 and 2018. It has a horizontal resolution of 1/16° horizontal resolution (6 km grid) and a vertical resolution of 50 vertical layers covering the entire water column from the surface to the sea floor (0 – 5940 meters). The first 10 meters of the water column are divided into 7 sigma layers, which change their size based on the tide level evolution. Below these, the water column is divided into 43 Cartesian layers, which are thinner in the upper layers (less than 2 meters in length) and larger in the bottom ones.

For the atmospheric forcing, the boundary conditions are obtained from the Global Forecast System (GFS model), provided by NOAA- America National Ocean and Atmospheric Administration, available at https://www.ncdc.noaa.gov/. This model has hourly fields of surface wind, temperature, relative humidity, pressure, and solar radiation.

Model validation of the selected parameters is detailed in Viegas (2022). Comparison between model results and tide gauge data reveals the capability of the model to accurately simulate sea water level, in the Azores region. Sea surface temperature was validated against remote sensing data and predicted sea water temperature and salinity were compared with *in situ* data from ARGOS floats. Model validation against the ARGO float data for vertical profiles of temperature and salinity showed Pearson correlation coefficients greater than 0.97, with the majority being 0.99 (Viegas, 2022). The outputs of the hydrodynamic model (horizontal and vertical components of the velocity, sea level, temperature, salinity, and density fields) were used to feed the CMS particle tracking model to simulate the plume-dispersal processes in offline mode.

TABLE 3 Scenarios considered in this study, with spawning date and pelagic larval duration and the release length (in days).

Scenario	PLD (days)	Release date	Release length (days)
PLD15_March_2017	15	March 2017	31
PLD15_October_2017	15	October 2017	31
PLD30_March_2017	30	March 2017	31
PLD30_October_2017	30	October 2017	31
PLD15_year_2017	15	January-December 2017	365
PLD30_year_2017	30	January-December 2017	365
PLD15_March_2018	15	March 2018	31
PLD15_October_2018	15	October 2018	31
PLD30_March_2018	30	March 2018	31
PLD30_October_2018	30	October 2018	31

TABLE 4 Hydrodynamic model configuration.

Parameter	MOHID hydrodynamic model
Model dimensions	3D – Baroclinic
Domain	32.472°N to 42.9121°N, and 21.4078°W to 36.288°W
Bathymetry	EMODNET (1/16arc-minutes) [a)]
Horizontal solution	6km
Vertical resolution	50 vertical layers: 7 sigma layers + 43 cartesian layers
Tide	Tide: FES2014b)
Δt	120 seconds
Meteorological forcing	Global Forecast System model (GFS) 0.25° resolution c)
Hydrodynamical forcing	CMEMS Global Ocean Circulation Model (PSY4V3R1) 1/12°resolution[d)]
Model output	3600 seconds
Simulation length	Jan/2017 – Dec/2018

[a]EMODnet Consortium, 2018; [b]Lyard et al., 2021; [c]National Centers for Environmental Prediction, et al., 2015; NOAA, 2015; [d]Lellouche et al., 2018; n/a, not applicable.

2.1.3 Particle tracking model

The CMS-Connectivity Modelling System is an open-source model, freely available online. It was created for the multi-scale tracking of biotic and abiotic particles in the ocean, based on a Lagrangian framework to study complex larval migrations (Paris et al., 2013). This model runs offline, over a 3D hydrodynamic model, applying its velocity fields (u, v, w) to each particle, using a 4th-order Runge–Kutta numerical discretization method (García-Martínez and Flores-Tovar, 1999) to differentiate particle positions through space and time. Modules distributed with the code include mortality, vertical migration, and a connectivity module designed to generate a connectivity matrix output from the source to the final destination of the particles. The model gives a probabilistic estimate of dispersion and oceanographic connectivity, transport and fate of Lagrangian phenomena. The model computes the probability of larval exchange (here in called connectivity), between source and recruitment areas, by dividing the number of larvae that reached each site by the total number of larvae release; mortality, and behavior; providing results over time including particles' location (x, y and depth), water properties, particle status (moving, dead, out of the domain or settled) and also the particles settlement location. For the purpose of the model, there is an assumption that the larvae that reach the recruitment site will settle. However, the successful development of the settled larvae into a new organism, depending on behavioral components and the suitable conditions (e.g., hydrodynamic, environmental conditions, biological and physical processes, competency or predation) (Pineda et al., 2010), is not estimated by the model.

The model can simulate particles settlement in defined recruitment locations (in this case the sponge aggregations in the study). These recruitment locations are defined by a polygon (longitude, latitude and depth). Particle settlement starts after the defined PLD.

In this study, each aggregation is defined by a polygon of 6x6 km (the model resolution). The initial positions for the drift trajectories of each population were the centroids of each one of these areas. Each population is defined by a release location, and Lagrangian tracers represent larvae. A position (longitude, latitude and depth), the number of particles released, the release frequency, and the date characterize each release location. Since there is no information about the fecundity, frequency and seasonality of larval emissions, a hypothetical number was defined (Cowen and Sponaugle, 2009). To standardize this approach, the same number of particles for all the locations was considered, assigning the same hypothetical relevance to all the release points, with the same release size and frequency. The model simulates a release of a total of 150,000 particles per month, in a time step of 1.5 hours, during the entire release period, for all the scenarios. In this study, all the aggregations are simulated with the same number of particles, not reflecting population abundances, size or reproduction rate. Larvae were simulated as passive particles, without any active swimming behavior, being just advected by the hydrodynamics. Model configurations are described in Table 5.

The number of particles was calibrated to provide accurate larvae dispersion results, considering the computational efficiency.

TABLE 5 Biophysical model configuration.

Model parameter	Parameter description
Hydrodynamic model resolution	6×6km
Model time step	720 seconds
Number of release points	10
Release depth	Sea bottom
Number of larvae per release	150000/month/release
Release time step	1.5 hours
Behaviour	Passive (Ross et al., 2019)
Mortality	Half-life (North et al., 2009)
Strata	600 to 1000m (*P.Carpenteri* bathymetric range)
Scenarios	Several considering PLD and seasonality
Simulation length	Jan/2017 – Dec/2018

This calibration was performed using two different methodologies (Viegas, 2022), the Particle Density Distribution, and the evaluation of the fraction of unexplained variation (Simons et al., 2013), and by the analysis of the dispersal pathlength distances saturation (Kough et al., 2013).

The model simulates the larvae dispersal, and larvae settlement after the precompetence period (the PLD). For connectivity studies the model allows defining suitable settlement locations, defined by a polygon (longitude, latitude and depth). In this case, to study connectivity between the sponge aggregations, each sponge aggregation is also a source location and a recruitment area, defined by a polygon of 6x6km (model resolution), and depth (700 to 1000 meters depth). The larvae exchange between different locations will represent connectivity between different sponge aggregations.

Alternatively, to study potential settlement location throughout the Azores region, another methodology was applied, assuming that larvae were able to settle at any location between 700 and 1000 meters depth.

Due to the many uncertainties about deep-sea larval biology, different scenarios were considered, with different pelagic larval durations (PLD), and seasonal scenarios to encompass different potential situations. This is one advantage of using modelling tools, allowing the study of different hypotheses and scenarios (Swearer et al., 2019; Wang and Qiao, 2020).

2.1.4 Data analysis

Larvae were represented by particles, and the model results were analyzed through dispersal maps, larvae positions and larvae exchange between different source and recruitment locations. Connectivity between the sponge aggregations in the study was represented by connectivity matrices, representing the percentage of particles that reach each site, which allows for the analysis of sink and source aggregations. In this study, each particle represents one larva. When

referring to settling particles, it means a particle has reached another location, representing a larva that has settled in a new location and potentially will develop successfully. Connectivity matrices also represent the percentage-recruitment levels. Connectivity between two locations was assumed when, at least, one modelled particle released from one location (source node) reach (also referred as settled in) another location (receiving node), after the PLD. When settling in the same location, it is considered self-recruitment. Source locations are represented as rows (j), and recruitment areas (receiving node) as columns (i), with self-recruitment in each location represented in the matrix diagonal. Colors represent the percentage of particles that reach each locations, calculated by dividing the total number of settled larvae from each source population that settled, at the end of the PLD, in each receiving population, by the total number of larvae released from the source population. Besides the connectivity analysis, the larvae settlement positions throughout the study area were analyzed, to identify other potential larvae settlement positions.

The particle density distribution (PDD) is represented in 2-D vertically integrated maps, where all particles are represented, and each domain grid cell (6km x 6km) correspond to the integrated number of tracers in the entire water column. In contrast, in the particle dispersal maps, particles are not integrated into the water column, and all the particles in each cell are graphed. Some particles can "mask" others, by overlapping. Travel distances were analyzed by the Shapiro-Wilk Normality Test (using Rstudio 2022.02.3), to test if they are normally distributed; and by using histograms to analyze potential travel distances from all the different release points for the different scenarios. These distances were calculated from individual particle trajectories as the sum of straight-line distances between each time step. Additionally, histograms of particle depths were used to analyze how particles are distributed along the water column.

3 Results

3.1 Passive particle drift trajectories

Larvae were simulated as passive particles, being advected by the hydrodynamic currents. The particle density distribution (PDD) illustrates the larval dispersal along the study area, (Figure 2),

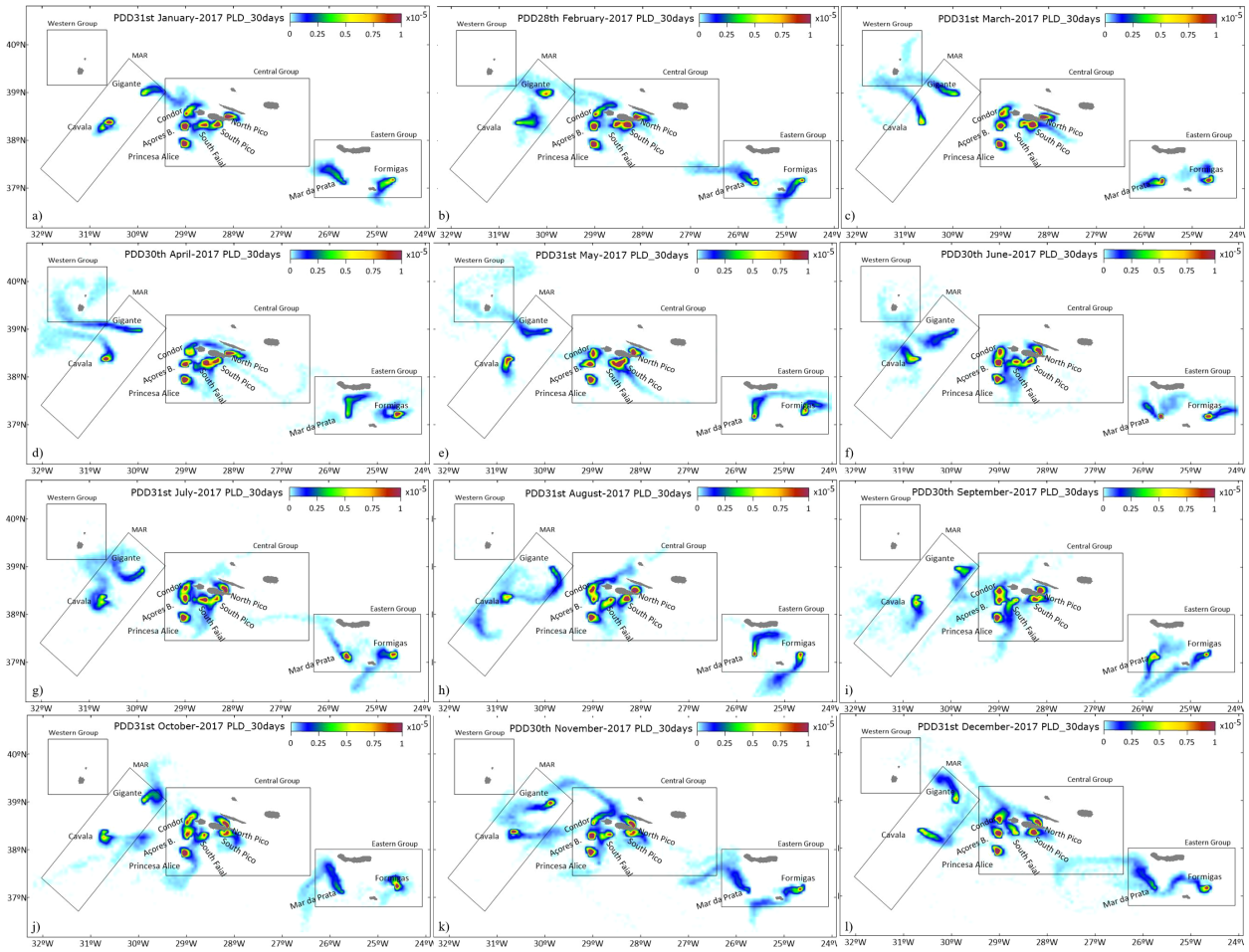

FIGURE 2
Particle density distribution for the annual release with a PLD of 30 days, for 31st January **(A)**: 28th February **(B)**; 31st March **(C)**; 30th April **(D)**; 31st May **(E)**; 30th June **(F)**; 31st July **(G)**; 31st August **(H)**; 30th September **(I)**; 31st October **(J)**; 30th November **(K)**; 31st December **(L)**. Black polygons represent the different location groups: MAR Group (L#1-Cavala, L#2-Gigante); Central Group (L#3-Princesa Alice, L#4-Açores Bank, L#5-Condor Seamount, L#6-South of Faial, L#7- South of Pico, L#8); Eastern Group (L#9)-Mar da Prata, and L#10-Formigas).

indicating the potential particle exchange between different locations. The results reveal a heterogeneous distribution depending on the spawning seasonality. Larvae from the MAR group can reach the Central Group (CG) only during the winter and autumn months (January, February, September, October, November and December). Larval dispersal plumes from the MAR can also reach the Western Group (WG), surrounding Flores and Corvo islands, during March, April, May and June months. Larvae exchange between CG and WG only occurs during July, November and December. However, the low PDD between these groups (Figure 2) indicates a low probability of particle exchange.

In March an eddy is formed between the Western Group and the MAR (Figure 3A), contributing to particle retention in this area. Larvae from the CG mostly remain around the islands. Nevertheless, the low current velocity, (Figure 3), is not sufficient to transport larvae from CG to the EG populations, given the PLD used in these scenarios.

Larvae from the Central Group populations, reach various sponge aggregations. Between the Central and Eastern Group, the hydrodynamic patterns go mainly in the eastward direction during March, Figure 3A, while in October there is a dominant current coming from the east and going westward (Figure 3B). In the northwest part of the study area, currents are stronger during October (Figure 3B) than during March (Figure 3A), and the

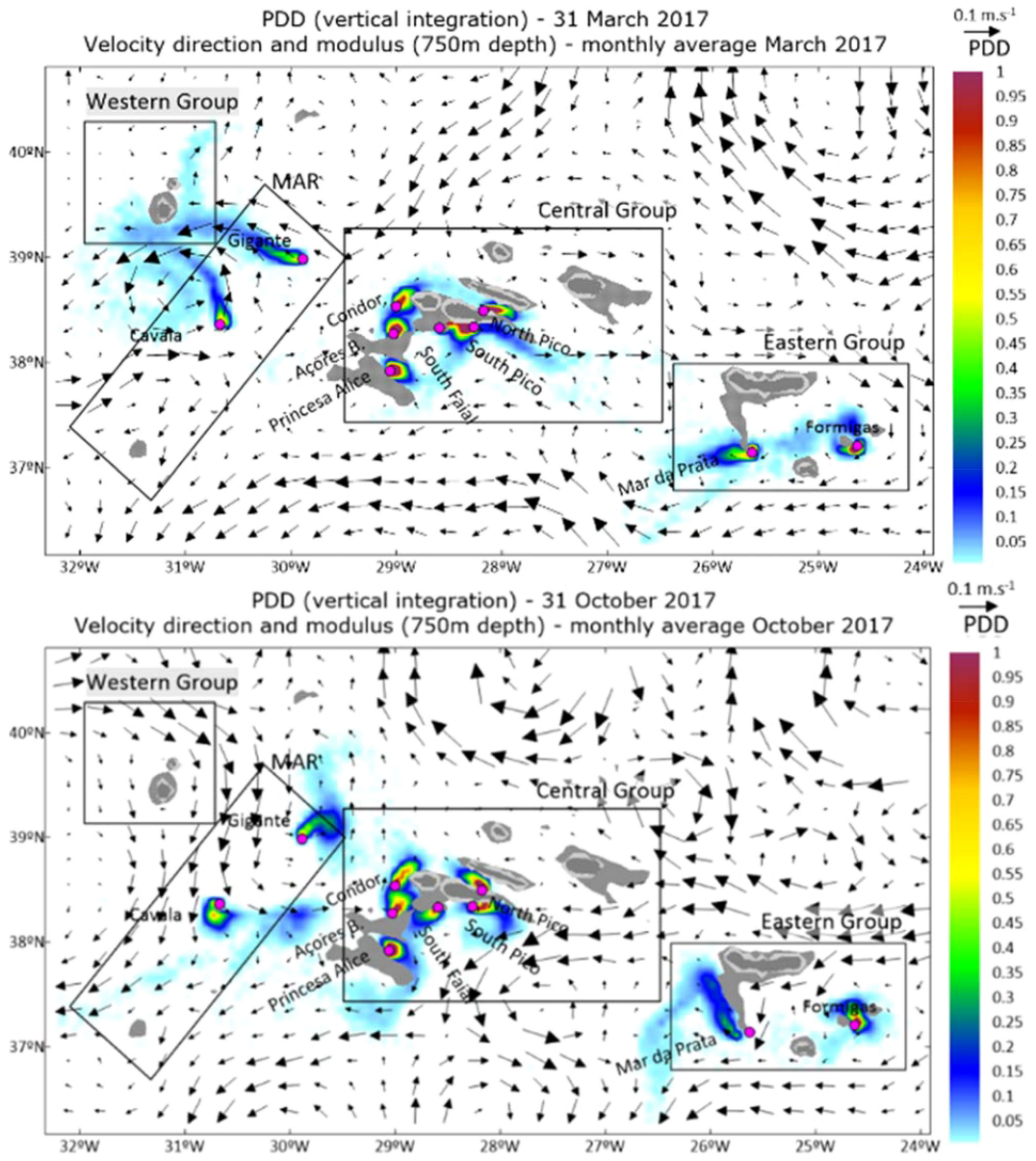

FIGURE 3
Particles density distribution integrated into the entire water column, like presented in Figure 2, with the representation of the velocity vectors at 750 meters depth, for 31 March 2017 (top), and 31 October 2017 (bottom). The PDD is represented with a color scale from blue to red, where 0 is white), vectors represent the monthly average of velocity modulus and direction at 750 meters depth.

10.3389/fmars.2024.1393385

major hydrodynamic fields present another pattern, where the higher velocity (>0.1m/s) matches the absence or reduced particle density, and the higher particle density occurs in locations with lower currents magnitude.

3.2 Particles travel distance

Larvae can travel from a few kilometers to a maximum travelling distance of over 400km (Table 6). Travel distances are highly non-normal, confirmed by the Shapiro-Wilk Normality Test (using Rstudio 2022.02.3). Therefore, rather than considering the average values, the median and the 95th percentile are used for this analysis (Phelps, 2015). Maximum total travel distances are an order of magnitude larger than median distances. Across all March and October scenarios, the longer PLD causes higher travel distances. Median total travel distances for a PLD of 30 days are double the distances with a PLD of 15 days (Table 6). Larval travel distances vary both seasonally and spatially. During March, larvae from the MAR locations: L#1, and L#2, have higher travel distances than those from other locations (with a 95th percentile of 207 and 220 km respectively).

In the Central Group (CG, locations L#3 to L#8), the overall median particle distance in all tested scenarios is lower than in other groups, ranging from 8 to 20 km, which may contribute to higher self-recruitment levels. This lower travel distance is due to the lower current velocities in the region (Figure 3), in contrast to the MAR populations, which are situated in areas with stronger currents.

3.3 Particles depth

Simulated larvae mainly remain close to the bottom at the released bathymetry (Figures 4, 5), despite some travelling through different bathymetric ranges. Histograms of particles' depth along their trajectory are represented in Figure 4 for the March release and in Figure 5 for the October release. In all the locations, larvae remain mostly within the bathymetric range of the release (>40%). A longer PLD contributes to a wider distribution of particles along the water column. The results show no significant difference in particle depth between the March and October releases. This demersal larval dispersal can also lead to higher levels of particle retention at their source locations.

3.4 Connectivity between populations

Results show variation in the level of population connectivity depending on the PLD of 15 or 30 days. Connectivity between the different populations in the study is illustrated by connectivity matrices, and also by connectivity arrows represented on the maps (Figure 6). The matrices depict the percentage of larvae exchanged between different populations, indicating connectivity, or in the case of self-recruitment, the percentage of larvae that settled in the source population after the PLD. A PLD of 30 days enables more connectivity between the different sponge aggregations than a PLD of 15 days (Figure 6). Conversely, a shorter PLD, results in higher self-recruitment levels. There is no connectivity between the EG and the CG or WG, in both PLD scenarios. In the WG, connectivity between Formigas (L#10) and Mar da Prata Seamount (L#9) is unidirectional, with a PLD of 15 days, and bidirectional with a PLD of 30 days. Between the CG and the EG, the larvae exchange is minimal, with no significant larvae exchange among the different populations, as is represented in the connectivity matrices.

This yearly release allows for the analysis of different spawning and hydrodynamic scenarios. The hypothesis of a seasonal spawning release was studied, considering releases of one month in March and one month in October to cover spring and fall scenarios, respectively. The results indicate different connectivity patterns in terms of

TABLE 6 Particle travel distances for the different scenarios.

	Travel distances (kilometres)											
	PLD_15_March			PLD_30_March			PLD_15_October			PLD_30_October		
	max	med	P95	max	med	P95	max	med	P95	max	med	P95
Cavala #1	221	14	126	375	43	207	152	16	73	325	33	138
Gigante #2	285	18	107	462	44	220	179	15	77	334	32	195
Princesa Alice #3	75	8	36	146	16	58	97	7	34	192	15	51
Açores B.#4	83	8	39	186	15	53	132	10	43	314	18	71
Condor B.#5	128	10	55	326	19	80	158	10	61	359	26	168
South Faial #6	205	10	50	436	21	132	196	14	61	385	26	128
South Pico #7	127	9	40	254	20	87	108	9	42	341	20	98
North Pico #8	69	8	38	270	15	55	85	7	39	286	16	63
Mar da Prata #9	118	10	47	264	22	97	176	27	86	406	50	148
Formigas#10	113	11	59	218	24	96	168	11	55	345	23	162

Maximum distance (max); median distance (med) and percentile 95th.

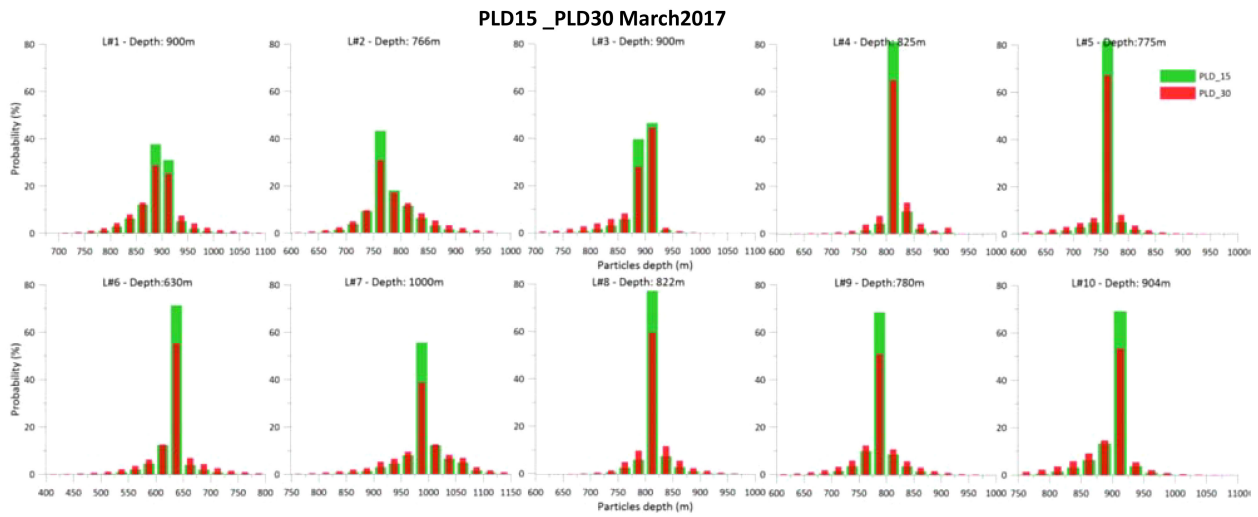

FIGURE 4
Histogram of particles' depth along their trajectory, for each location, for PLD15 and PLD30 days for March 2017 release. The depth of the respective release is detailed at the top of each graph.

seasonality. The October release (Figure 7), generates lower larvae exchange between the different sponge aggregations. Population connectivity between MAR and CG only occurs in the March_PLD_30_2018 scenario, namely between the Azores Bank (L#4) and the Cavala (L#1) and Gigante (L#2) Seamounts. In the other scenarios, there is no connectivity between the different groups. In the CG, the connectivity between different sponge aggregations reveals seasonality, with a higher number of connectivity relations in the March scenarios. The percentage of self-recruitment (Supplementary Tables A3–A6 in the Supplementary Material) is different from March to October, with the releases from CG revealing the highest self-recruitment percentage in October. In different situations, there is neither self-recruitment, nor connectivity between Gigante Seamount (L#2) and any other populations. The same occurs in the Mar da Prata Seamount (L#9), which shows no self-recruitment in October_PLD30_2017.

3.5 Larvae settlement locations

Besides the sponge aggregations in the study, larvae can also settle in other regions of the domain. This study was performed within the defined bathymetric range of 600 to 1000 meters depth. Seasonal dynamics can induce different settlement positions. The yearly release considers all the monthly scenarios, and consequently more settled larvae along the Azores region (Figure 8). Considering

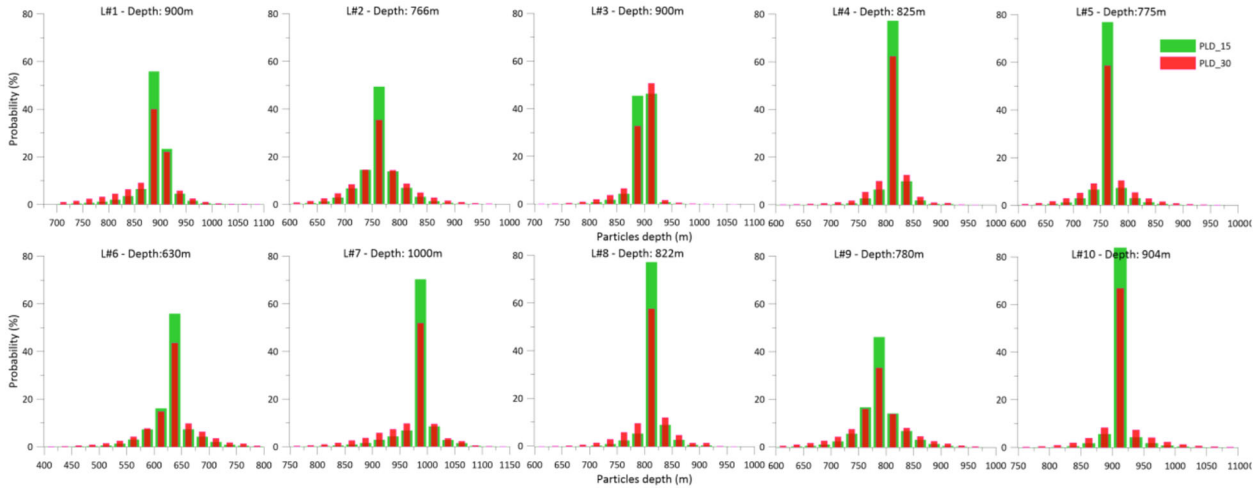

FIGURE 5
Histogram of the particles' depth along their trajectory, for each location, for PLD15 days and a PLD30 for the October 2017 release. The depth of each respective release is detailed at the top of each graph.

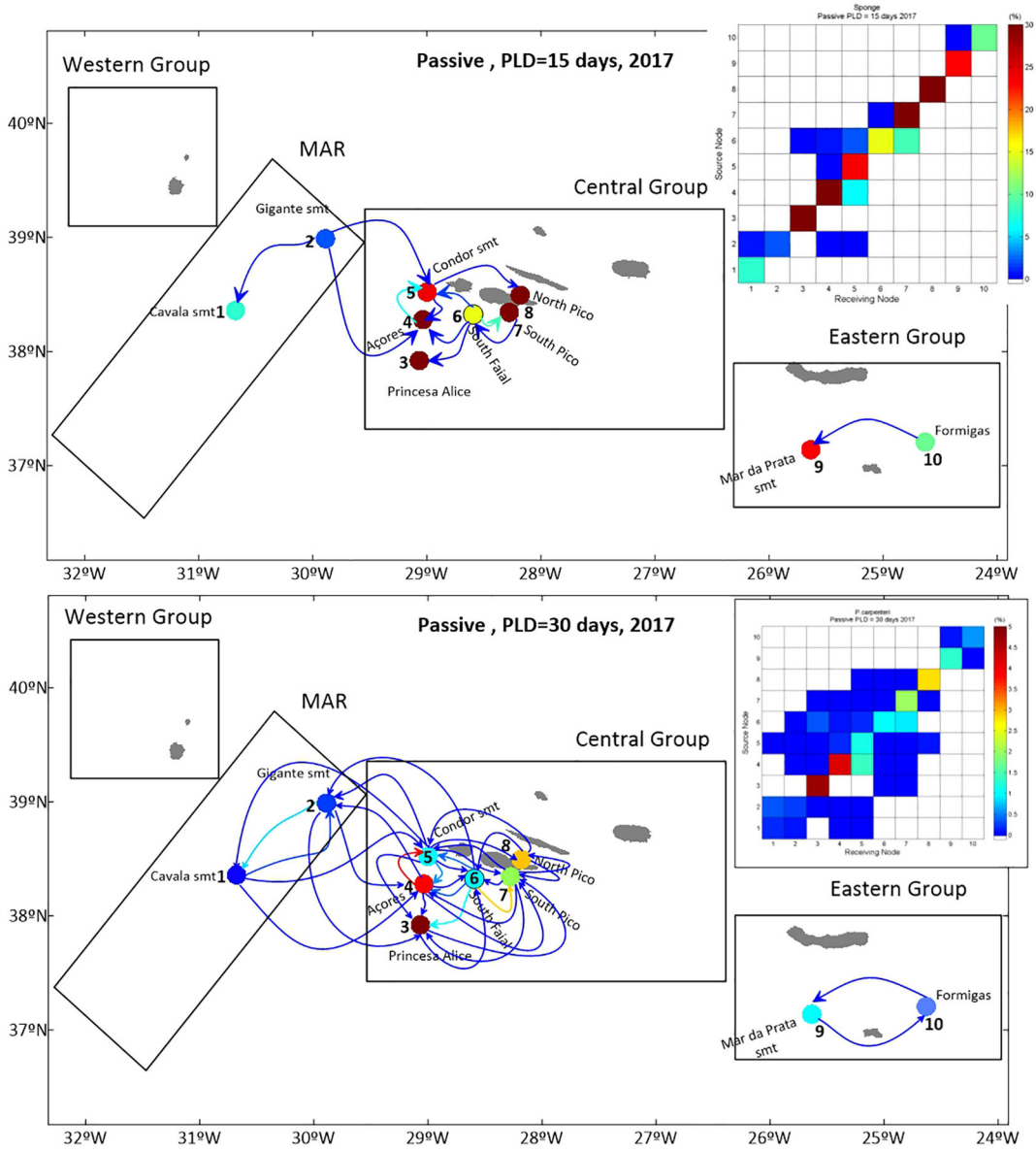

FIGURE 6
Map of connectivity relations, and respective connectivity matrix, for a yearly release (2017) with a PLD of 15 days (top), and PLD of 30 days (bottom), connectivity arrows and auto-recruitment circle colours represent the percentage of settled particles.

the bathymetric range from 600m to 1000m, larvae can settle around all the islands except Terceira island. Larvae settle along the MAR and on seamounts situated on its western and eastern flanks but also at different locations of the CG region'. The Central Group is an important recruitment area. This result highlights the potential connectivity between the populations in the Central Group. Major results show that during the yearly release, larvae from Cavala and Gigante seamounts, settle along the MAR, around Flores and Corvo islands, and along the west slope of the Central Group, but they hardly reach the East part of the Central Group. Gigante Seamount can receive larvae from different locations (Cavala (L#1), Gigante(L#2), Açores Bank (L#4), Condor (L#5), and South of Faial (L#6)), contrasting with the seasonal releases where larvae exchange occurs only during the October scenario, between Gigante (L#2) and Cavala (L#1) seamounts. The larvae from South of Faial (L#6) are the ones with a wider range of settling locations; they can settle along MAR, in the WG, in the CG, in João de Castro bank, and in the EG, in the North of São Miguel (Figure 9F).

4 Discussion

This study aims to use specific sponge aggregations to study the dispersal of their larvae, and the potential connectivity among these different sponge grounds, considering spring and autumn spawning scenarios, and a yearly release, as a first approach to studying the dispersal of deep-sea larvae in the Azores. Given the many knowledge gaps in the reproductive and larval biology of deep-sea sponges, the use of models offers an advantage by allowing the study

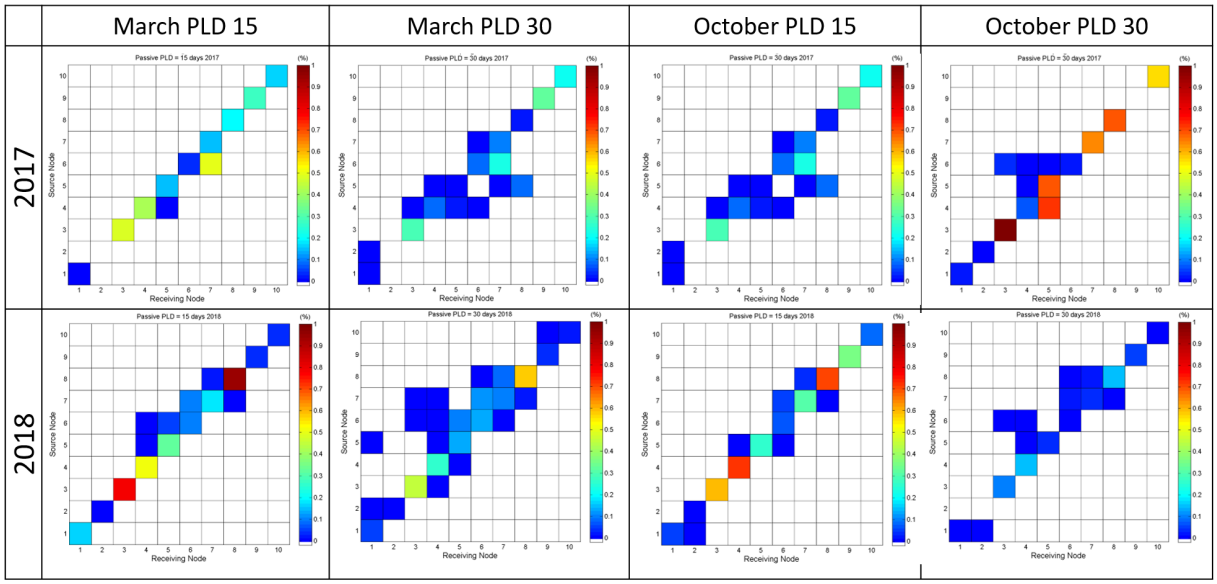

FIGURE 7
Connectivity matrices for the March_PLD15, March_PLD30, October_PLD15 and October_PLD30 for 2017 on top and 2018 on the bottom, connectivity and auto-recruitment colours represent the percentage of settled particles.

of different scenarios. *P. carpenteri* larvae were modelled as passive tracers, similar to other deep-sea sponge larval dispersal modelling studies (Kenchington et al., 2019; Swearer et al., 2019). The few studies of connectivity of sponge grounds in the deep sea in the Northeast Atlantic do not cover the Azores area, but they showed genetically a strong panmixia, and that the observed patterns were very well correlated with the physical drivers and the prevailing currents and topography (Taboada et al., 2023). In the Cantabrian sea, the same pattern emerged from the deep sea fan shaped sponges, where genetically a panmixia was present. However, when applying a virtual particle tracking model to assess oceanographic connectivity it showed a strong retention of larvae in the study area and a variable inter-annual connectivity highly correlated with the current regime (Busch et al., 2021).

Model results show that the hydrodynamic patterns have a strong influence on larval dispersal, causing different distribution patterns depending on the season. Larvae can be advected from a few kilometers to hundreds of kilometers, depending on the PLD and the hydrodynamic currents. The water-mass circulation in the Azores region is highly dynamic, and the influence of the different currents has seasonal effects on larval dispersal. The strong presence of hydrodynamic eddies (Caldeira and Reis, 2017) can contribute to particle retention in different areas, as is the case in March when an eddy forms between the Western Group and the MAR. These results show the importance of studying different spawning season scenarios for larval dispersal. Consequently, due to knowledge gaps in sponge reproductive traits, different seasonal scenarios and PLD were tested. Multiple connectivity relationships exist between the sponge aggregations in the CG, showing a redundancy in connectivity networks is a positive feature as it helps to mitigate recruitment failures by providing alternative connectivity pathways. These multiple connectivity relationships may result from the proximity between these sponge aggregations, but also from the local hydrodynamic patterns characterized by lower velocities. This is in contrast to the strong hydrodynamic patterns that occur between the WG and the MAR in March, and between CG and EG in October.

A significant limitation of this and other deep-sea dispersal models is the lack of information on deep-sea species biological traits (Arellano et al., 2014; Hilário et al., 2015; Graves et al., 2023).

4.1 Connectivity between sponge aggregations and self-recruitment

There are no connectivity studies of benthic organisms in the Azores region. A retention particle study between 0 and 150 meters showed the potential of the different island groups of the Azores to retain particles, and their dependence on the current regime and topography (Sala et al., 2013). Close to the Azores a study of the physical connectivity between the NE Atlantic Seamounts showed self-recruitment abilities and great retention of particles on the seamounts (Lima et al., 2020).

This study shows larval dispersal between different sponge aggregations in the Azores, (Figure 9A–J) namely between the different sponge aggregations located in the same group (MAR, CG and EG), as well as between aggregations located in the MAR and the CG. However, there is no particle exchange between the CG and the EG. Moreover, these Eastern Group sponge aggregations do not exchange larvae with the other populations, and are the most isolated. Therefore, these populations may be spatially fragmented, similar to what was identified in other larval dispersal model studies for deep-sea populations (Hilário et al., 2015).

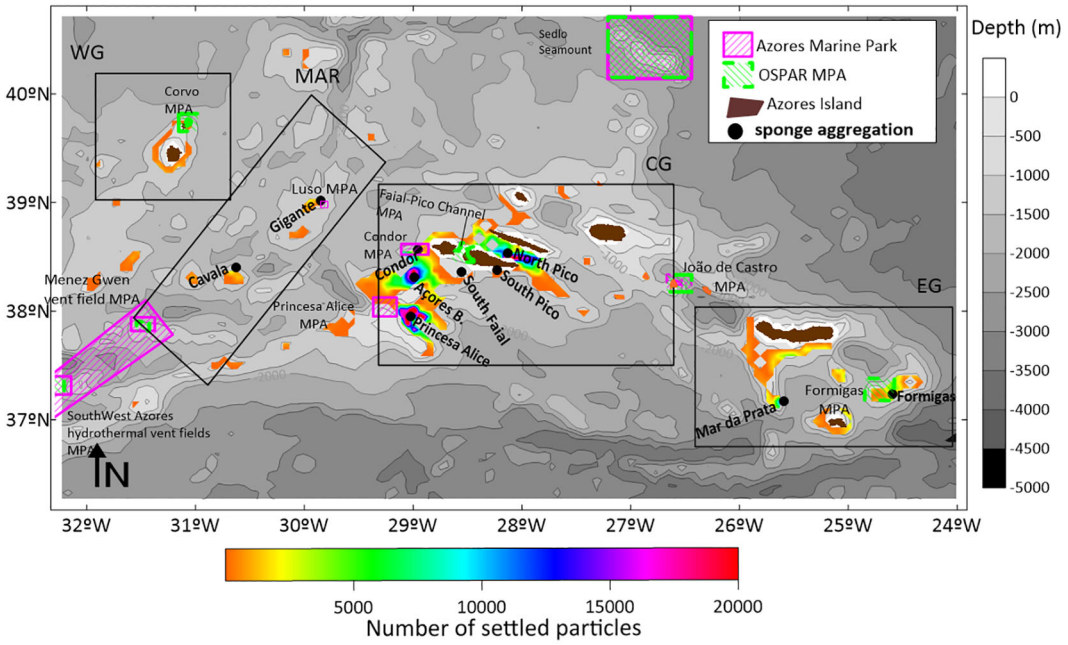

FIGURE 8
Location of settled particles along the domain, in the bathymetric range from 600 to 1000m depth, for the yearly release. Different colours represent number of settled larvae. Bathymetry is represented with a grey colour scale. The Azores islands are represented in dark brown, the Azores Marine Park in pink, and the OSPAR MPAs in green.

The results show that the local ocean currents shape the larval dispersal and connectivity, creating sub-regions not connected, given the studied scenarios. These kind of hydrodynamic barriers were also identified in other modelling approaches for deep-sea larval sponge dispersal on the east coast of North America (Wang et al., 2021). Moreover, this modelling approach also shows that the local eddies can supply and induce local retention of larvae, promoting connectivity and self-recruitment (Wang et al., 2021), as occurs in this case study in the Azores, namely between the WG and the MAR populations. A retention particle study in the Azores at 150 meters also showed the Eastern group isolation and the large capacity of the central area in the Azores to retain particles (Sala et al., 2016), which is coherent with the observed pattern in this study.

4.2 Larval dispersal patterns and connectivity for *P. carpenteri* in the Azores Marine Park

Connectivity among different benthic populations promotes the increase of their genetic diversity (Busch et al., 2021; Wang et al., 2021) and the resilience of the species (Bracco et al., 2019). It is an essential aspect in the development of management and conservation plans for marine ecosystems (Combes et al., 2021). Detailed knowledge of the hydrodynamic patterns and biological interactions that drive the transport of planktonic phases is crucial for improving the effectiveness of the MPAs (Stratoudakis et al., 2019). The model results of larval dispersal and larvae settlement positions for this target species in the Azores were analyzed considering the MPAs from the Azores Marine Park. When MPAs are isolated from each other, they are more vulnerable to local extinction as they cannot be replenished by organisms or larvae from other locations (Stratoudakis et al., 2019). This is especially true for sessile organisms such as deep-sea sponges, which rely on larval dispersal to colonize new habitats (Metaxas and Saunders, 2009), and to support remote populations (Gary et al., 2020). Networks of marine protected areas arranged considering the larval dispersal patterns are considered ideal for the protection of marine species (Steneck et al., 2009). Therefore, studying larval dispersal patterns and identifying the main larval source and sink locations can contribute to the better implementation and management of conservation plans (Combes et al., 2021).

The study of larval dispersal and connectivity of these *P. carpenteri* aggregations serves as a pilot study for the connectivity of deep-sea benthic organisms in the Azores. The current regime and topography have been shown in other studies to be the main drivers of physical connectivity, explaining the genetic connectivity patterns (Busch et al., 2021; Taboada et al., 2023). Using *P. Carpenteri* as a proxy, we can discuss how effective the network of MPA from the Azores Marine Park is from the physical connectivity point of view. Among the 10 deep-sea sponge aggregations in the study, two are located in MPAs: Condor and Formigas populations. The Princesa Alice aggregation is located on the southern slope of the Princesa Alice Seamount, outside but adjacent to the MPA delimitation. Larval dispersal and connectivity results, indicate that Condor is an important source population, exchanging larvae with 8 of the 10 aggregations in the study (Figure 6). In addition, its larvae can achieve different locations in the Central Group, in the Western Group (around the islands of Flores and Corvo), and along the MAR: in the north, at 40.3°N (seamount south of the Kurchatov Fracture Zone); at 39°N in the

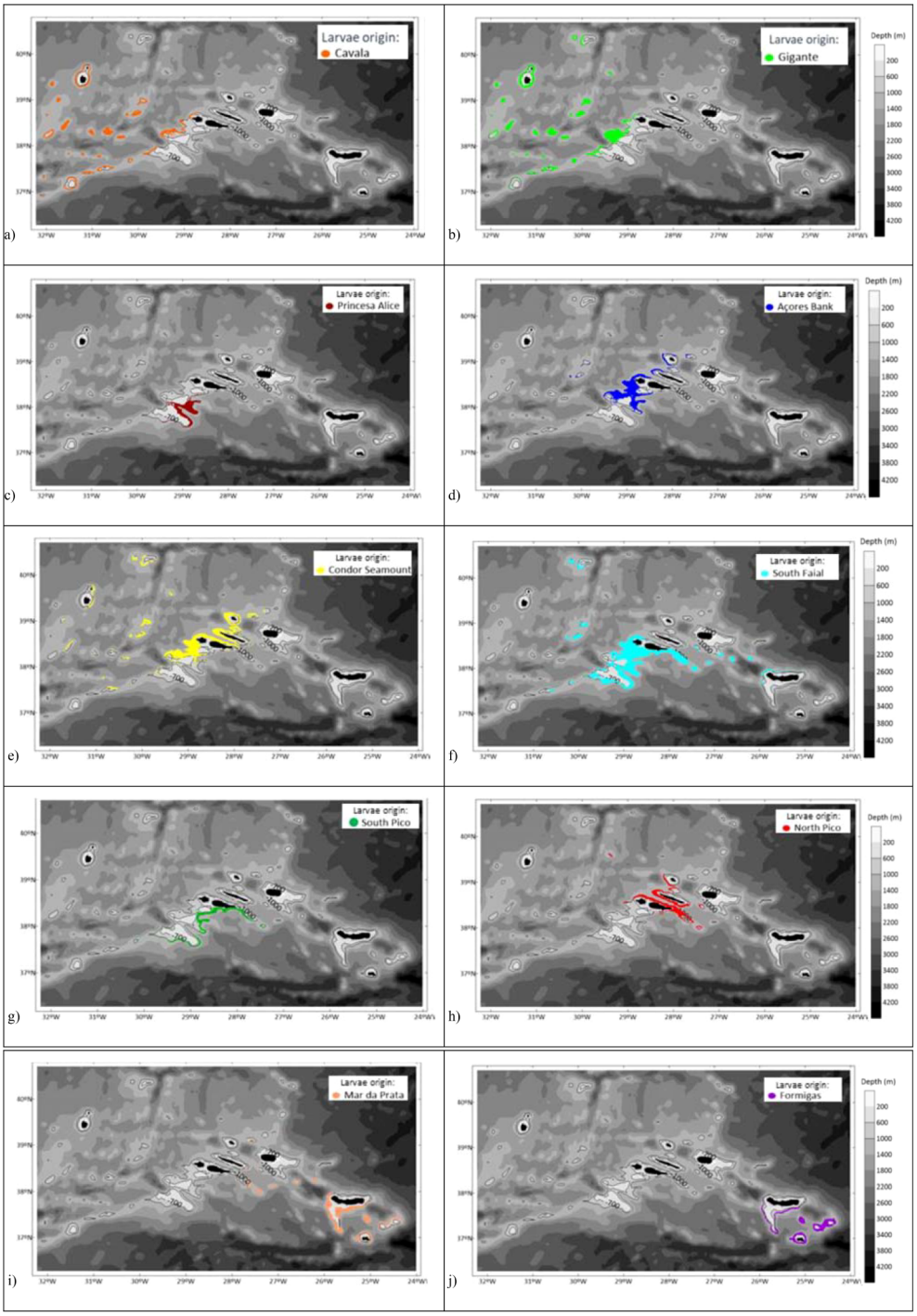

FIGURE 9
Location of settled particles, in the entire domain, in the bathymetric range from 600 to 1000m depth, for the yearly release of 2017 with a PLD of 30 days, for each origin. Different colours represent different releases: **(A)** Cavala; **(B)** Gigante; **(C)** Princesa Alice; **(D)** Açores Bank; **(E)** Condor Seamount; **(F)** South Faial; **(G)** South Pico; **(H)** North Pico, **(I)** Mar da Prata, **(J)** Formigas. Bathymetry is represented in a grey colour scale.

Gigante Seamount; and in the Voador Seamount at 37.5°N (Figure 9E). The MPAs of Princesa Alice and Condor may act as sink locations, once that larvae from different aggregations in the study achieve these locations. These results demonstrate the potential connectivity that sponge populations from Condor may have with different populations in the Azores region.

The Princesa Alice sponge aggregation in the study, adjacent to the limits of the MPA, demonstrates the importance of extending the limits of this MPA as it has the potential to retain larvae from multiple locations in the study: Cavala (Figure 9A), Gigante (Figure 9B) and Condor (Figure 9E) seamounts, and South of Faial (Figure 9F), aggregations.

The main results show a lack of larvae exchange between the EG and the other aggregations in the study (Figures 9I, J), mainly due to its distance from the remaining sponge grounds, but also as a consequence of the hydrodynamic patterns between the CG and the EG, impeding the larvae advection in the westward direction. No larvae exchange was identified between EG and the remaining sponge grounds. Therefore, the protection of an area in Mar da Prata will favor the maintenance of the sponge aggregations on the plateau south of São Miguel island, and both Mar da Prata and Formigas populations, which can be isolated from the remaining archipelago, due to their distance, but also restricted by the hydrodynamic patterns. The vulnerability of Formigas sponge grounds, which face several scenarios with no larvae exchange and the absence of self-recruitment, also reinforces the need to maintain the MPA of Formigas.

The João de Castro Bank MPA can receive larvae from the CG and from the Mar da Prata (in the EG) being an steppingstone location between the Central and the Eastern parts of the archipelago. Therefore, this site is very important for the longer-term protection of these aggregations, by promoting the establishment of a linkage between the CG and the EG. The Gigante Seamount, in the MAR, is a recruitment area for deep-sea sponges, retaining larvae from different sources from the CG (Condor, Açores Bank and South of Faial), as well as from Cavala and Gigante Seamount. The results of larval dispersal also show that larvae from the Gigante seamount can achieve the MAR region, up to seamounts located South of the Kurchatov Fracture Zone (north of the study area), and in seamounts west of the MAR like the Buchanon Seamount. On the other hand, larvae from aggregations of Voador Seamount will favor resilience along the MAR, and South of the Azores EEZ.

This study does not take into account the density of these sponge aggregations. Research by Graves et al. (2023) on the drivers of *P. carpenteri* density suggests that the available environmental data, combined with the scarcity of long-term time series for deep-sea environmental data, do not capture the key factors influencing this species' density. This limitation restricts the ability to model and identify areas where aggregations are likely to occur, particularly those with dense aggregations that could be considered VMEs. Increasing to a multi-year analysis would provide the opportunity to examine variability over the years and test other hypotheses, such as the average temperature variability, which has been identified as an important driver of *P. carpenteri* distribution (Graves et al., 2023).

The application of biological larvae traits and their parameterization in biophysical models presents a challenge (Hilário et al., 2015) even in well studied shallow-water systems (Metaxas and Saunders, 2009). When regarding these biophysical models for deep-sea dispersal, the application of biological traits is even more challenging due to the scarcity of data, and difficulty data collection, observation and model validation (Adams et al., 2012; Ross et al., 2016). So, these mode results can be used as a first approach to study the potential larval dispersal in the Azores, but always considering the associated uncertainties. However, models are always a simplification of the reality and despite all the uncertainty regarding the biological parameters (Simons et al., 2013), the validation of the physical circulation model used in this case study (Viegas, 2022) provides us with the guarantee of the correct physical model component, providing a baseline to study different scenarios, and also to be used to study climate change scenarios hypothesis.

Furthermore, this modelling approach could be used in combination with the species distribution models (Beazley et al., 2021) to construct explicit spatial hypotheses for deep-sea populations connectivity following a seascape framework approach (Kenchington et al., 2006; Kavanaugh et al., 2014; Zeng et al., 2020; Swanborn et al., 2022), in this case for the Azores region. In the future, the possibility of collecting physical samples and performing a population genetic study, will contribute to a deeper knowledge of these populations connectivity (Kool et al., 2011; Selkoe and Toonen, 2011; Antonio Baeza et al., 2019; Wang et al., 2021), and will help to validate our hypothesis.

5 Conclusions and final remarks

The physical connectivity among different deep-sea *P. carpenteri* sponge aggregations in the Azores region was studied using a biophysical particle-tracking model. *P. carpenteri* larvae were modeled as passive tracers (Kenchington et al., 2019; Swearer et al., 2019) under pelagic larval duration (PLD) scenarios of 15 and 30 days and seasonal spawning, based on other deep-sea sponge studies (Kenchington et al., 2019; Ross et al., 2020; Wang et al., 2020, 2021). Model results indicate that PLD and spawning seasonality are crucial for larval dispersal and population connectivity in the Azores. Seasonal effects are mainly driven by the region's dynamic oceanographic conditions. Local hydrodynamic vortices can lead to larval retention, while stronger currents (exceeding 0.1 m/s) between the Western and Central Groups in spring, and between the Central and Western Groups in autumn, hinder larval exchange. Therefore, more information on the species' biological traits, including spawning seasonality, is crucial for understanding effective connectivity across the archipelago.

A PLD of 30 days would enhance population persistence and recovery after disturbances (Cowen and Sponaugle, 2009), whereas a shorter PLD of 15 days could increase population fragmentation. Connectivity and larval dispersal results were analyzed in relation to the current design of the Azores MPAs, demonstrating their effectiveness in promoting connectivity across the archipelago by protecting key sink and source locations. Stepping-stone sites, such as the João de Castro Bank, were identified as critical links between isolated populations of the Eastern Group and the central archipelago. Other locations along the Mid-Atlantic Ridge (MAR), including Gigante, Cavala, Ferradura, and Voador seamounts, also facilitate connectivity, serving as potential sink locations. These locations should be the target of greater protection measures in the design and implementation of protection plans.

This study also identifies potential areas for future exploration, such as João de Castro, Voador, Ferradura, and Buchanan banks, where larvae are predicted to settle. These locations are promising for studying not only *P. carpenteri* but also other deep-sea species cohabitating in these habitats.

This type of investigation highlights the utility of larval dispersal models in designing Marine Protected Areas (MPAs) (Lima et al., 2020), specifically their role in identifying source and

sink locations. It allows the identification of major larval dispersal and connectivity patterns among sponge aggregations in the Azores, providing a framework that can be extended to other deep-sea sponge and coral habitats.

Future studies should include more detailed biological and larval behavior data for deep-sea sponges. Integrating genetic connectivity studies will offer valuable insights into the behavioral dynamics and resilience mechanisms of these organisms within the Azores. Additionally, considering aggregation density and population size in models will provide a more precise quantification of recruitment efficiency. Novel insights into the biology, size, and density of sponge aggregations will be invaluable for understanding the dynamics of this species within the Azorean ecosystem.

Regardless of the lack of information about *P. carpenteri* biological traits, this dispersal modelling approach can provide an overall understanding of deep-sea larval transport in the Azores region, considering the studied PLD scenarios. Moreover, this modelling methodology can therefore be replicated for other species considering these or any other biological traits scenarios, or to study other hypothesis. These results can therefore be used to long-term conservation plans for deep-sea species, and support protection actions for local populations in the Azores.

Data availability statement

The raw data supporting the conclusions of this article will be made available by the authors, without undue reservation.

Author contributions

CV: Conceptualization, Data curation, Formal analysis, Investigation, Methodology, Validation, Writing – original draft, Writing – review & editing. MJ: Data curation, Methodology, Software, Supervision, Writing – original draft, Writing – review & editing. AC: Conceptualization, Funding acquisition, Investigation, Project administration, Resources, Writing – original draft, Writing – review & editing.

Funding

The authors declare financial support was received for the research, authorship, and/or publication of this article. This research is part of the DEEP REST project that was funded through the 2020- 2021 Biodiversa and Water JPI joint call for research projects, under the BiodivRestore ERA-NET Cofund (GA N°101003777), with the EU and the following funding organizations: Agence Nationale de la Recherche (ANR-21-BIRE-0003), France, Ministry of Agriculture, Nature and Food Quality (LNV), Netherlands, Research Foundation -Flanders (FWO), Belgium, German Federal Ministry of Research (BMBF) through VDI/VDE-IT, Germany, Environmental Protection Agency (EPA), Ireland, Fundacão para a Ciência e a Tecnologia (FCT), Portugal, Fundo Regional para a Ciência e Tecnologia (FRCT), Portugal-Azores and State Research Agency (AEI), Spain. CV work was supported by FCT (PhD scholarship) and DEEPREST (M2.2/DEEPREST/004/2022). AC work was supported by FCT/MCTES through national funds in the scope of the CEEC contract CEECIND/00101/2021 (https://doi.org/10.54499/2021.00101.CEECIND/CP1669/CT0001). This work received national funds through the FCT – Foundation for Science and Technology, I.P., under the project UIDB/05634/2020 and UIDP/05634/2020 and through the Regional Government of the Azores through the initiative to support the Research Centers of the University of the Azores and through the project M1.1.A/REEQ.CIENTÍFICO UI&D/2021/010.

Acknowledgments

The authors would like to acknowledge the contributions of many scientists and young researchers that were actively involved in the SPONGES project in the Azores.

Conflict of interest

The authors declare that the research was conducted in the absence of any commercial or financial relationships that could be construed as a potential conflict of interest.

Publisher's note

Supplementary material

The Supplementary Material for this article can be found online at: https://www.frontiersin.org/articles/10.3389/fmars.2024.1393385/full#supplementary-material

SUPPLEMENTARY TABLE 1
Particle travel distances for the different scenarios. Maximum distance (max); median distance (med) and percentile 95th.

SUPPLEMENTARY TABLE 2
Connectivity tables detailing the percentage of particles released particles from each location (rows) that settled in each recruitment area (columns). For the scenario: Annual PLD15.

SUPPLEMENTARY TABLE 3
Connectivity tables detailing the percentage of particles released particles from each location (rows) that settled in each recruitment area (columns). For the scenario: Annual PLD30.

SUPPLEMENTARY TABLE 4
Connectivity tables detailing the percentage of particles released particles from each location (rows) that settled in each recruitment area (columns). For the scenario: March PLD15 2017.

SUPPLEMENTARY TABLE 5
Connectivity tables detailing the percentage of particles released particles from each location (rows) that settled in each recruitment area (columns). For the scenario: March PLD30 2017.

SUPPLEMENTARY TABLE 6
Connectivity tables detailing the percentage of particles released in each location (rows) that settled in each recruitment area (columns). For the scenario October PLD15 2017.

References

Adams, D. K., Arellano, S. M., and Govenar, B. (2012). Larval dispersal, vent life in the water column. *Oceanography* 25, 255–268. doi: 10.5670/oceanog.2012.24

Antonio Baeza, J., Holstein, D., Umaña-Castro, R., and Mejía-Ortíz, L. M. (2019). Population genetics and biophysical modeling inform metapopulation connectivity of the Caribbean king crab Maguimithrax spinosissimus. *Mar. Ecol. Prog. Ser.* 610, 83–97. doi: 10.3354/meps12842

Arellano, S. M., Van Gaest, A. L., Johnson, S. B., Vrijenhoek, R. C., and Youn, C. M. (2014). Larvae from deep-sea methane seeps disperse in surface waters. *Proc. R. Soc B Biol. Sci.* 281, 1–8. doi: 10.1098/rspb.2013.3276

Baillon, S., Hamel, J. F., Wareham, V. E., and Mercier, A. (2014). Seasonality in reproduction of the deep-water pennatulacean coral Anthoptilum grandiflorum. *Mar. Biol.* 161, 29–43. doi: 10.1007/s00227-013-2311-8

Barthel, D., Tendal, O. S., and Thiel, H. (1996). A Wandering Population of the HexactinelIid Sponge Pheronema carpenteri on the Continental Slope off Morocco, Northwest Africa. *Mar. Ecol.* 17, 603–616. doi: 10.1111/j.1439-0485.1996.tb00420.x

Beazley, L., Kenchington, E., Murillo, F. J., Brickman, D., Wang, Z., Davies, A. J., et al. (2021). Climate change winner in the deep sea? predicting the impacts of climate change on the distribution of the glass sponge vazella pourtalesii. *Mar. Ecol. Prog. Ser.* 657, 1–23. doi: 10.3354/meps13566

Bett, B. J., and Rice, A. L. (1992). The influence of hexactinellid sponge (Pheronema carpenteri) spicules on the patchy distribution of macrobenthos in the porcupine seabight (Bathyal ne atlantic). *Ophelia* 36, 217–226. doi: 10.1080/00785326.1992.10430372

Black, K. S., Peppe, O. C., and Gust, G. (2003). Erodibility of pelagic carbonate ooze in the northeast Atlantic. *J. Exp. Mar. Bio. Ecol.* 285–286, 143–163. doi: 10.1016/S0022-0981(02)00524-5

Boury-Esnault, N., Efremova, S., BÉzac, C., and Vacelet, J. (1999). Reproduction of a hexactinellid sponge: First description of gastrulation by cellular delamination in the porifera. *Invertebr. Reprod. Dev.* 35, 187–201. doi: 10.1080/07924259.1999.9652385

Bracco, A., Liu, G., Galaska, M. P., Quattrini, A. M., and Herrera, S. (2019). Integrating physical circulation models and genetic approaches to investigate population connectivity in deep-sea corals. *J. Mar. Syst.* 198, 103189. doi: 10.1016/j.jmarsys.2019.103189

Braunschweig, F., Leitao, P. C., Fernandes, L., Pina, P., and Neves, R. J. J. (2004). The object-oriented design of the integrated water modelling system MOHID. *Dev. Water Sci.* 55, 1079–1090. doi: 10.1016/S0167-5648(04)80126-6

Burchard, H., Bolding, K., and Villarreal, M. (1999). GOTM – a general ocean turbulence model. Theory, applications and test cases.

Busch, K., Taboada, S., Riesgo, A., Koutsouveli, V., Ríos, P., Cristobo, J., et al. (2021). Population connectivity of fan-shaped sponge holobionts in the deep Cantabrian Sea. *Deep. Res. Part I Oceanogr. Res. Pap.* 167, 103427. doi: 10.1016/j.dsr.2020.103427

Caldeira, R. M. A., and Reis, J. C. (2017). The Azores confluence zone. *Front. Mar. Sci.* 4. doi: 10.3389/fmars.2017.00037

Colaço, A., Creemers, M., Mienis, F., Beazley, L., Hanz, U., Bouchard-Marmen, M., et al. (2020). Deliverable D4.5 (SponGES) - Deep-sea Sponge Grounds Ecosystems of the North Atlantic: an integrated approach towards their preservation and sustainable exploitation.

Combes, M., Vaz, S., Grehan, A., Morato, T., Arnaud-Haond, S., Dominguez-Carrió, C., et al. (2021). Systematic conservation planning at an ocean basin scale: identifying a viable network of deep-sea protected areas in the north Atlantic and the Mediterranean. *Front. Mar. Sci.* 8. doi: 10.3389/fmars.2021.611358

Cowen, R. K., and Sponaugle, S. (2009). Larval dispersal and marine population connectivity. *Ann. Rev. Mar. Sci.* 1, 443–466. doi: 10.1146/annurev.marine.010908.163757

Creemers, M. F., Pham, C., Defise, A., Goulard, J., Smith, V., Silva, A. P., et al. (2019). Sponges on the rocks: exploring A new deep-sea sponge ground of the Azores (Portugal). *Deep. Life* 12, 7–8.

EMODnet Consortium. (2018). *EMODnet digital bathymetry (DTM 2018).* doi: 10.12770/18ff0d48-b203-4a65-94a9-5fd8b0ec35f6

FAO. (2008). *International guidelines: Management of deep-sea fisheries in the high seas* (Rome: Food and Agriculture Organization of the United Nations (FAO)).

García-Martínez, R., and Flores-Tovar, H. (1999). Computer modeling of oil spill trajectories with a high accuracy method. *Spill Sci. Technol. Bull.* 5, 323–330. doi: 10.1016/S1353-2561(99)00077-8

Gary, S. F., Fox, A. D., Biastoch, A., Roberts, J. M., and Cunningham, S. A. (2020). Larval behaviour, dispersal and population connectivity in the deep sea. *Sci. Rep.* 10, 1–12. doi: 10.1038/s41598-020-67503-7

Gomes-Pereira, J. N., Carmo, V., Catarino, D., Jakobsen, J., Alvarez, H., Aguilar, R., et al. (2017). Cold-water corals and large hydrozoans provide essential fish habitat for Lappanella fasciata and Benthocometes robustus. *Deep. Res. Part II Top. Stud. Oceanogr.* 145, 33–48. doi: 10.1016/j.dsr2.2017.09.015

Graves, K. P., Bridges, A. E. H., Dabrowski, T., Furey, T., Lyons, K., and Howell, K. L. (2023). Oceanographic variability drives the distribution but not the density of the aggregation forming deep-sea sponge pheronema carpenteri. *Deep. Res. Part I Oceanogr. Res. Pap.* 191, 103917. doi: 10.1016/j.dsr.2022.103917

Guillas, K. C., Kahn, A. S., Grant, N., Archer, S. K., Dunham, A., and Leys, S. P. (2019). Settlement of juvenile glass sponges and other invertebrate cryptofauna on the Hecate Strait glass sponge reefs. *Invertebr. Biol.* 138, 1–11. doi: 10.1111/ivb.12266

Henry, L. A., and Roberts, J. M. (2014). A*pplying the OSPAR habitat definition of deep-sea sponge aggregations to verify suspected records of the habitat in UK waters.* (Peterborough: Joint Nature Conservation Committee Report No 508).

Hilário, A., Metaxas, A., Gaudron, S. M., Howell, K. L., Mercier, A., Mestre, N. C., et al. (2015). Estimating dispersal distance in the deep sea: Challenges and applications to marine reserves. *Front. Mar. Sci.* 2. doi: 10.3389/fmars.2015.00006

Howell, K. L., Piechaud, N., Downie, A. L., and Kenny, A. (2016). The distribution of deep-sea sponge aggregations in the North Atlantic and implications for their effective spatial management. *Deep. Res. Part I Oceanogr. Res. Pap.* 115, 309–320. doi: 10.1016/j.dsr.2016.07.005

IST. (2003). *Water System model Hydrodynamic Module.* (Lisbon: MOHID).

Kavanaugh, M. T., Hales, B., Saraceno, B., Spitz, Y. H., White, A. E., and Letelier, R. M. (2014). Hierarchical and dynamic seascapes: A quantitative framework for scaling pelagic biogeochemistry and ecology. *Prog. Oceanogr.* 120, 291–304. doi: 10.1016/j.pocean.2013.10.013

Kenchington, E. L., Patwary, M. U., Zouros, E. J., and Bird, C. (2006). Genetic differentiation in relation to marine landscape in a broadcast-spawning bivalve mollusc (Placopecten magellanicus). *Mol. Ecol.,* 1781–1796. Available at: https://doi.org/10.1111/j.1365-294X.2006.02915.x

Kenchington, E., Wang, Z., Lirette, C., Murillo, F. J., Guijarro, J., Yashayaev, I., et al. (2019). Connectivity modelling of areas closed to protect vulnerable marine ecosystems in the northwest Atlantic. *Deep. Res. Part I Oceanogr. Res. Pap.* 143, 85–103. doi: 10.1016/j.dsr.2018.11.007

Kool, J. T., Paris, C. B., Barber, P. H., and Cowen, R. K. (2011). Connectivity and the development of population genetic structure in Indo-West Pacific coral reef communities. *Glob. Ecol. Biogeogr.* 20, 695–706. doi: 10.1111/j.1466-8238.2010.00637.x

Kough, A. S., Paris, C. B., and Butler, M. J. IV (2013). Larval connectivity and the international management of fisheries. *PloS One* 8, 1–11. doi: 10.1371/journal.pone.0064970

Koutsouveli, V., Cárdenas, P., Conejero, M., Rapp, H. T., and Riesgo, A. (2020). Reproductive biology of geodia species (Porifera, tetractinellida) from Boreo-Arctic North-Atlantic deep-sea sponge grounds. *Front. Mar. Sci.* 7. doi: 10.3389/fmars.2020.595267

Leis, J. M. (2020). Perspectives on larval behaviour in biophysical modelling of larval dispersal in marine, demersal fishes. *Oceans* 2, 1–25. doi: 10.3390/oceans2010001

Leitão, P. C., Mateus, M., Braunschweig, F., Fernandes, L., and Neves, R. (2008). Modelling coastal systems: the MOHID water numerical lab. *Perspect. Integr. Coast. Zo. Manage. South Am.* 77–88. doi: 10.13140/2.1.1482.4008

Lellouche, J. M., Greiner, E., Le Galloudec, O., Garric, G., Regnier, C., Drevillon, M., et al. (2018). Recent updates to the copernicus marine service global ocean monitoring and forecasting real-time 1g 12° high-resolution system. *Ocean Sci.* 14, 1093–1126. doi: 10.5194/os-14-1093-2018

Leys, S. P., and Lauzon, N. R. J. (1998). Hexactinellid sponge ecology: Growth rates and seasonality in deep water sponges. *J. Exp. Mar. Bio. Ecol.* 230, 111–129. doi: 10.1016/S0022-0981(98)00088-4

Leys, S. P., and Ereskovsky, A. V. (2006). Embryogenesis and larval differentiation in sponges. *Can. J. Zool.* 84, 262–287. doi: 10.1139/z05-170

Lima, M. J., Sala, I., and Caldeira, R. M. A. (2020). Physical connectivity between the NE Atlantic seamounts. *Front. Mar. Sci.* 7. doi: 10.3389/fmars.2020.00238

Lopes, D. (2005). Redescription of two Hexactinosida (Porifera, Hexactinellida) from the southwestern Atlantic, collected by Programme REVIZEE. *Zootaxa*, 43–56.

Lyard, F. H., Allain, D. J., Cancet, M., Carrère, L., and Picot, N. (2021). FES2014 global ocean tides atlas: design and performances florent. *Ocean Sci.* 17, 615–649. doi: 10.5194/os-17-615-2021

Maldonado, M. (2006). The ecology of the sponge larva. *Can. J. Zool.* 84, 175–194. doi: 10.1139/z05-177

Maldonado, M., Aguilar, R., Bannister, R. J., James, J., Conway, K. W., Dayton, P. K., et al. (2016). *Sponge Grounds as Key Marine Habitats : A Synthetic Review of Types, Structure, Functional Roles, and Conservation Concerns Sponge Grounds as Key Marine Habitats : A Synthetic Review of Types, Structure, Functional Roles, and Conservation Concerns*. (Switzerland: Springer International Publishing). doi: 10.1007/978-3-319-17001-5

Maldonado, M., Carmona, M. C., Velásquez, Z., Puig, A., Cruzado, A., López, A., et al. (2005). Siliceous sponges as a silicon sink: An overlooked aspect of benthopelagic coupling in the marine silicon cycle. *Limnol. Oceanogr.* 50, 799–809. doi: 10.4319/lo.2005.50.3.0799

Maldonado, M., and Young, C. M. (1999). Effects of the duration of larval life on postlarval stages of the demosponge Sigmadocia caerulea. *J. Exp. Mar. Bio. Ecol.* 232, 9–21. doi: 10.1016/S0022-0981(98)00076-8

Mercier, A., Sewell, M. A., and Hamel, J. F. (2013). Pelagic propagule duration and developmental mode: Reassessment of a fading link. *Glob. Ecol. Biogeogr.* 22, 517–530. doi: 10.1111/geb.12018

Mercier, A., Sun, Z., and Hamel, J. F. (2011). Reproductive periodicity, spawning and development of the deep-sea scleractinian coral Flabellum angulare. *Mar. Biol.* 158, 371–380. doi: 10.1007/s00227-010-1565-7

Metaxas, A., and Saunders, M. (2009). Quantifying the "Bio-" Components in biophysical models of larval transport in marine benthic invertebrates: advances and pitfalls. *Biol. Bull.* 216, 257–272. doi: 10.1086/bblv216n3p257

Morato, T., Dominguez-Carrió, C., Mohn, C., Ocaña Vicente, O., Ramos, M., Rodrigues, L., et al. (2021). Dense cold-water coral garden of Paragorgia johnsoni suggests the importance of the Mid-Atlantic Ridge for deep-sea biodiversity. *Ecol. Evol.* 11, 16426–16433. doi: 10.1002/%0Aece3.8319

National Centers for Environmental Prediction, National Weather Service, NOAA and U.S. Department of Commerce. (2015). *NCEP GFS 0.25 degree global forecast grids historical archive*. Available online at: https://rda.ucar.edu/datasets/dsd084001/.

NOAA. (2015). *NCEP GFS 0.25 degree global forecast grids historical archive*. doi: 10.5065/D65D8PWK

North, E. W., Gallego, A., Petitgas, P., Ådlandsvik, B., Bartsch, J., Brickman, D., et al. (2009). Manual of recommended practices for modelling physical-biological interactions during fish early life.

Paris, C. B., Helgers, J., van Sebille, E., and Srinivasan, A. (2013). Connectivity Modeling System: A probabilistic modeling tool for the multi-scale tracking of biotic and abiotic variability in the ocean. *Environ. Model. Software* 42, 47–54. doi: 10.1016/j.envsoft.2012.12.006

Pham, C. K., Vandeperre, F., Menezes, G., Porteiro, F., Isidro, E., and Morato, T. (2015). The importance of deep-sea vulnerable marine ecosystems for demersal fish in the Azores. *Deep. Res. Part I Oceanogr. Res. Pap.* 96, 80–88. doi: 10.1016/j.dsr.2014.11.004

Phelps, J. J. C. (2015). *Modelling Hydrodynamic Transport and Larval Dispersal in North-East Atlantic Shelf Seas*. [PhD Thesis]. University of Liverpool.

Pineda, J., Porri, F., Starczak, V., and Blythe, J. (2010). Causes of decoupling between larval supply and settlement and consequences for understanding recruitment and population connectivity. *J. Exp. Mar. Bio. Ecol.* 392, 9–21. doi: 10.1016/j.jembe.2010.04.008

Rice, A. L., Thurston, M. H., and New, A. L. (1990). Dense aggregations of a hexactinellid sponge, Pheronema carpenteri, in the Porcupine Seabight (northeast Atlantic Ocean), and possible causes. *Prog. Oceanogr.* 24, 179–196. doi: 10.1016/0079-6611(90)90029-2

Rix, L., De Goeij, J. M., Van Oevelen, D., Struck, U., Al-Horani, F. A., Wild, C., et al. (2018). Reef sponges facilitate the transfer of coral-derived organic matter to their associated fauna via the sponge loop. *Mar. Ecol. Prog. Ser.* 589, 85–96. doi: 10.3354/meps12443

Ross, R. E., Nimmo-Smith, W. A. M., and Howell, K. L. (2016). Increasing the depth of current understanding: Sensitivity testing of deep-sea larval dispersal models for ecologists. *PloS One* 11, 1–25. doi: 10.1371/journal.pone.0161220

Ross, R. E., Nimmo-Smith, W. A. M., Torres, R., and Howell, K. L. (2020). Comparing deep-sea larval dispersal models: A cautionary tale for ecology and conservation. *Front. Mar. Sci.* 7. doi: 10.3389/fmars.2020.00431

Ross, R. E., Wort, E. J. G., and Howell, K. L. (2019). Combining distribution and dispersal models to identify a particularly vulnerable marine ecosystem. *Front. Mar. Sci.* 6. doi: 10.3389/fmars.2019.00574

Sala, I., Caldeira, R. M. A., Estrada-allis, S. N., Froufe, E., and Couvelard, X. (2013). Lagrangian transport pathways in the northeast Atlantic and their environmental impact. *Limnol. Oceanogr. Fluids Environ.* 3, 40–60. doi: 10.1215/21573689-2152611

Sala, I., Harrison, C. S., and Caldeira, R. M. A. (2016). The role of the azores archipelago in capturing and retaining incoming particles. *J. Mar. Syst.* 154, 146–156. doi: 10.1016/j.jmarsys.2015.10.001

Samuelsen, A., Schrum, C., Yumruktepe, V. Ç., Daewel, U., and Roberts, E. M. (2022). Environmental change at deep-sea sponge habitats over the last half century: A model hindcast study for the age of anthropogenic climate change. *Front. Mar. Sci.* 9. doi: 10.3389/fmars.2022.737164

Santos, M., Moita, M. T., Bashmachnikov, I., Menezes, G. M., Carmo, V., Loureiro, C. M., et al. (2013). Phytoplankton variability and oceanographic conditions at Condor seamount, Azores (NE Atlantic). *Deep. Res. Part II Top. Stud. Oceanogr.* 98, 52–62. doi: 10.1016/j.dsr2.2013.05.037

Selkoe, K. A., and Toonen, R. J. (2011). Marine connectivity: A new look at pelagic larval duration and genetic metrics of dispersal. *Mar. Ecol. Prog. Ser.* 436, 291–305. doi: 10.3354/meps09238

Simons, R. D., Siegel, D. A., and Brown, K. S. (2013). Model sensitivity and robustness in the estimation of larval transport: A study of particle tracking parameters. *J. Mar. Syst.* 119–120, 19–29. doi: 10.1016/j.jmarsys.2013.03.004

Somoza, L., Medialdea, T., González, F. J., Machancoses, S., Candón, J. A., Cid, C., et al. (2021). High-resolution multibeam bathymetry of the northern Mid-Atlantic Ridge at 45–46° N: the Moytirra hydrothermal field. *J. Maps* 17, 184–196. doi: 10.1080/17445647.2021.1898485

Spetland, F., Rapp, H. T., Hoffmann, F., and Tendal, O. S. (2007). Sexual reproduction of Geodia barretti Bowerbank 1858 (Porifera, Astrophorida) in two Scandinavian fjords. *Mus. Nac. Ser. Livros* 1858, 613–620.

Steneck, R. S., Paris, C. B., Arnold, S. N., Ablan-Lagman, M. C., Alcala, A. C., Butler, M. J., et al. (2009). Thinking and managing outside the box: Coalescing connectivity networks to build region-wide resilience in coral reef ecosystems. *Coral Reefs* 28, 367–378. doi: 10.1007/s00338-009-0470-3

Stratoudakis, Y., Hilario, A., Ribeiro, C., Abecasis, D., Gonçalves, E. J., Andrade, F., et al. (2019). Environmental representativity in marine protected area networks over large and partly unexplored seascapes. *Glob. Ecol. Conserv.* 17. doi: 10.1016/j.gecco.2019.e00545

Sun, Z., Hamel, J. F., and Mercier, A. (2011). Planulation, larval biology, and early growth of the deep-sea soft corals Gersemia fruticosa and Duva florida (Octocorallia: Alcyonacea). *Invertebr. Biol.* 130, 91–99. doi: 10.1111/j.1744-7410.2011.00229.x

Swanborn, D. J. B., Huvenne, V. A. I., Pittman, S. J., and Woodall, L. C. (2022). Bringing seascape ecology to the deep seabed: A review and framework for its application. *Limnol. Oceanogr.* 67, 66–88. doi: 10.1002/lno.11976

Swearer, S. E., Treml, E. A., and Shima, J. S. (2019). A review of biophysical models of marine larval dispersal. *Oceanogr. Mar. Biol.* 57, 325–356. doi: 10.1201/9780429026379-7

Taboada, S., Whiting, C., Wang, S., Ríos, P., Davies, A. J., Mienis, F., et al. (2023). Long distance dispersal and oceanographic fronts shape the connectivity of the keystone sponge Phakellia ventilabrum in the deep northeast Atlantic. *Front. Mar. Sci.* 10. doi: 10.3389/fmars.2023.1177106

Taranto, G. H. (2022). Mapping deep-sea biodiversity and good environmental status in the Azores: assisting with the implementation of EU Marine Strategy Framework Directive.

Teixidó, N., Gili, J. M., Uriz, M. J., Gutt, J., and Arntz, W. E. (2006). Observations of asexual reproductive strategies in antarctic hexactinellid sponges from ROV video records. *Deep. Res. Part II Top. Stud. Oceanogr.* 53, 972–984. doi: 10.1016/j.dsr2.2006.02.008

Thomas, T., Moitinho-Silva, L., Lurgi, M., Björk, J. R., Easson, C., Astudillo-García, C., et al. (2016). Diversity, structure and convergent evolution of the global sponge microbiome. *Nat. Commun.* 7, 1–12. doi: 10.1038/ncomms11870

Vic, C., Gula, J., Roullet, G., and Pradillon, F. (2018). Dispersion of deep-sea hydrothermal vent effluents and larvae by submesoscale and tidal currents. *Deep. Res. Part I Oceanogr. Res. Pap.* 133, 1–18. doi: 10.1016/j.dsr.2018.01.001

Viegas, C. (2022). *3-D Biogeochemical and hydrodynamic models in the Azores – A tool to understand marine ecosystems*. [PhD Thesis]. University of the Azores.

Vieira, R. P., Bett, B. J., Jones, D. O. B., Durden, J. M., Morris, K. J., Cunha, M. R., et al. (2020). Deep-sea sponge aggregations (Pheronema carpenteri) in the Porcupine Seabight (NE Atlantic) potentially degraded by demersal fishing. *Prog. Oceanogr.* 183, 102189. doi: 10.1016/j.pocean.2019.102189

Wang, B., Fennel, K., Yu, L., and Gordon, C. (2020). Assessing the value of biogeochemical Argo profiles versus ocean color observations for biogeochemical model optimization in the Gulf of Mexico. *Biogeosciences* 17, 4059–4074. doi: 10.5194/bg-17-4059-2020

Wang, S., Kenchington, E., Wang, Z., and Davies, A. J. (2021). Life in the fast lane: modeling the fate of glass sponge larvae in the gulf stream. *Front. Mar. Sci.* 8, 1–14. doi: 10.3389/fmars.2021.701218

Wang, G., and Qiao, F. (2020). Mirror patterns of physical variables in the ocean. *Clim. Dyn.* 54, 3109–3120. doi: 10.1007/s00382-020-05161-1

White, M. (2003). Comparison of near seabed currents at two locations in the Porcupine Sea Bight - Implications for benthic fauna. *J. Mar. Biol. Assoc. United Kingdom* 83, 683–686. doi: 10.1017/S0025315403007641h

Xavier, J. R., Tojeira, I., and Van Soest, R. W. M. (2015). On a hexactinellid sponge aggregation at the Great Meteor seamount (North-east Atlantic). *J. Mar. Biol. Assoc. United Kingdom* 95, 1389–1394. doi: 10.1017/S0025315415000685

Zeng, C., Rowden, A. A., Clark, M. R., and Gardner, J. P. A. (2020). Species-specific genetic variation in response to deep-sea environmental variation amongst Vulnerable Marine Ecosystem indicator taxa. *Sci. Rep.* 10, 1–15. doi: 10.1038/s41598-020-59210-0c

frontiers | Frontiers in Marine Science

TYPE Original Research
PUBLISHED 21 January 2025
DOI 10.3389/fmars.2024.1456505

OPEN ACCESS

EDITED BY
Manuel Maldonado,
Spanish National Research Council (CSIC), Spain

REVIEWED BY
Jaap Kaandorp,
University of Amsterdam, Netherlands
Fiorella Prada,
Rutgers, The State University of New Jersey, United States

*CORRESPONDENCE
Marta Peña Fernández
m.pena_fernandez@hw.ac.uk
Uwe Wolfram
uwe.wolfram@tu-clausthal.de

RECEIVED 28 June 2024
ACCEPTED 16 December 2024
PUBLISHED 21 January 2025

CITATION
Peña Fernández M, Williams J, Büscher JV, Roberts JM, Hennige SJ and Wolfram U (2025) Morphological analysis of cold-water coral skeletons for evaluating *in silico* mechanical models of reef-scale crumbling. *Front. Mar. Sci.* 11:1456505. doi: 10.3389/fmars.2024.1456505

Morphological analysis of cold-water coral skeletons for evaluating *in silico* mechanical models of reef-scale crumbling

Marta Peña Fernández[1]*, Josh Williams[1], Janina V. Büscher[2,3], J. Murray Roberts[4], Sebastian J. Hennige[4] and Uwe Wolfram[1,5]*

[1]Institute of Mechanical, Process and Energy Engineering, School of Engineering and Physical Sciences, Heriot-Watt University, Edinburgh, United Kingdom, [2]School of Geography and Environmental Sciences, Ulster University, Coleraine, Northern Ireland, [3]Department of Biogeochemistry - Biological Oceanography, GEOMAR Helmholtz Centre for Ocean Research Kiel, Kiel, Germany, [4]Changing Oceans Research Group, School of GeoSciences, University of Edinburgh, Edinburgh, United Kingdom, [5]Institute for Materials Science and Engineering, Clausthal University of Technology, Clausthal-Zellerfeld, Germany

The structural complexity of cold-water corals is threatened by ocean acidification. Increased porosity and thinning in structurally critical parts of the reef framework may lead to rapid physical collapse on an ecosystem scale, reducing their potential for biodiversity support. Understanding the structural-mechanical relationships of reef-forming corals is important to enable the use of *in silico* mechanical models as predictive tools that allow us to determine risk and timescales of reef collapse. Here, we analyze morphological variations of the branching architecture of the cold-water coral species *Lophelia pertusa* to advance mechanical *in silico* models based on their skeletal structure. We identified a critical size of five interbranch lengths that allows using homogenized finite element models to analyze mechanical competence. At smaller length scales, mechanical surrogate models need to explicitly account for the statistical morphological differences in the skeletal structure. We showed large morphological variations between fragments of *L. pertusa* colonies and branches, as well as *dead* and *live* skeletal fragments which are driven by growth and adaptation to environmental stressors, with no clear branching-specific patterns. Future *in silico* mechanical models should statistically model these variations to be used as monitoring tools for predicting risk of cold-water coral reefs crumbling.

KEYWORDS

cold-water corals, *Lophelia pertusa*, ocean acidification, mechanical modelling, 3D morphology

1 Introduction

Cold-water coral (CWC) reefs are important ecosystem engineers, since they support high local biodiversity through the three-dimensionally (3D) complex habitat they make (Roberts et al., 2009, 2006). This structural complexity is at risk from climate-driven shifts, particularly ocean acidification. While *live* coral can continue to calcify under projected temperature and ocean acidification conditions (Büscher et al., 2022; Hennige et al., 2015), the *dead* coral skeletal framework (i.e., erected skeleton no longer covered by soft tissue and exposed to seawater) is prone to dissolution either through direct passive chemical dissolution (Hennige et al., 2015) or increasing rates of bioerosion (Büscher et al., 2022). Dissolution of the dead framework is of particular concern, as the majority of CWC habitat is typically *dead* coral that sits above sediment/rubble (Barnhill et al., 2023; Vad et al., 2017). Ocean acidification induced dissolution may lead to loss of material and increased porosity in structurally critical parts of the *dead* skeletal framework, which can lead to structural weakening and rapid physical habitat collapse on an ecosystem scale (Hennige et al., 2020; Wolfram et al., 2022), reducing the potential for biodiversity support (Barnhill et al., 2023; Kline et al., 2019).

Wolfram et al. (2022) showed that the mechanical mechanisms explaining the collapse of CWCs due to ocean acidification can be described using mathematical and computational models. There, the coral skeleton was modelled as a multiscale, polycrystalline material and the impact of ocean acidification was incorporated as an increase of porosity and a reduction in skeletal thickness (loss of material). With this model, the authors illustrated how changes due to ocean acidification led to a decrease in the loadbearing capacity of the skeleton using image-based finite element (FE) analysis. These high-fidelity image-based models of coral structures represent a powerful tool to assess the risk of collapse in a future ocean and, potentially, to estimate timepoints that are critical to reef-crumbling based on the time they are exposed to acidified water (Hennige et al., 2020). However, the computational cost of this approach together with the reduced availability of 3D image data of these corals and their reef structures restricts its use to small coral colonies and limited timepoints. The development of fast and efficient *in silico* models of real reef structures therefore remains essential. In combination with projections of seawater chemistry changes, such models may allow us to investigate timescales of loadbearing capacity changes as well as the impact of these changes on CWC reefs overall.

Existing models of tropical coral reefs use cantilever beam theory to evaluate the mechanical vulnerability of coral colonies (Madin and Connolly, 2006; Storlazzi et al., 2005). These models on tropical corals consider the skeletal structure uniformly throughout the entire coral colony. While the assumption of a uniform skeletal structure may hold for some tropical coral species and growthforms, it fails to account for the morphological complexity, structural heterogeneities, and skeletal density of branching corals (Chamberlain and Graus, 1975; Graus et al., 1977; Vosburgh, 1982), and in particular CWC branching corals like the cosmopolitan scleractinian species *Lophelia pertusa*, also referred to as *Desmophyllum pertusum* (Addamo et al., 2016). To model future impacts of ocean acidification on *L. pertusa*'s skeletal integrity, it is important to understand its material architecture (Figure 1) and the structural-mechanical relationships across length scales. Whilst the mechanical properties at the microscale have been previously studied (Hennige et al., 2020; Pasquini et al., 2015; Wolfram et al., 2022), little is known about the influence of the corallite branching arrangement on the mechanical behavior of coral colonies. The branching architecture and morphological variations of *L. pertusa* skeletons have important implications not only on their loadbearing capacity but also on their ability to interact with the environment and the organisms they provide shelter for (Caley and St John 1996; Paulay 1997; Cole et al., 2008). Unlike their tropical counterparts, the difficulties in accessing CWC colonies has restricted quantitative analysis of their morphological variations to linear measurements of small coral fragments that have been collected from their environment through ROVs for example, or two-dimensional measurements extracted from video data (Addamo et al., 2015; De Clippele et al., 2018; Gass and Roberts, 2011; Quattrini et al., 2017; Sanna and Freiwald, 2021). Recently, Sanna et al. (2023) demonstrated high structural variations in the shape of *dead L. pertusa* skeletal fragments collected across the mid-Norwegian continental shelf using X-ray computed tomography (CT). However, their analysis was restricted to volume compactness and surface complexity and did not include the shape and size of individual coral branches. To identify critical branch sizes that, in turn, allow us to formulate appropriate surrogate models to capture the mechanical weakening and structural impacts of ocean acidification on exposed CWCs, an analysis of the 3D structural variations of coral skeletons across scales is needed. More importantly, morphological differences in *dead* and *live* skeletons need to be investigated as material loss due to dissolution was observed in skeletons no longer covered by soft tissue (i.e., *dead* coral) (Hennige et al., 2020).

A potential path towards upscaling the mechanical behavior from the structural to reef length scale levels (Figure 1) relies on homogenized FE models (Hollister et al., 1994; Dirrenberger et al., 2019). However, homogenization procedures are only applicable in the case of statistically uniform materials. Therefore, they rely on the existence of a representative volume element (RVE), or at least a close approximation of it, whose analysis yields the effective material properties. As such, the effective mechanical properties of coral colonies can be captured as mean values of apparent properties of RVEs of the underlying skeletal branching structure (Harrigan et al., 1988; Pfeiffer et al., 1997). These *in silico* models require low computational resources and overcome previous assumptions of a uniform homogeneous structure on tropical corals (Madin and Connolly, 2006; Storlazzi et al., 2005). However, whether local effective properties can be defined within *L. pertusa* colonies to account for the heterogeneity of their skeletons depends on the critical size of such RVE. Here, we hypothesize that a critical size of a RVE for *L. pertusa* skeletal structures exists, where for coral colonies larger than such critical size, a homogenized FE approach can be used to investigate the risk of CWC reef collapse. Conversely, for coral colonies smaller than such critical size, the underlying skeletal structure needs to be explicitly modelled. For both approaches, it is important to

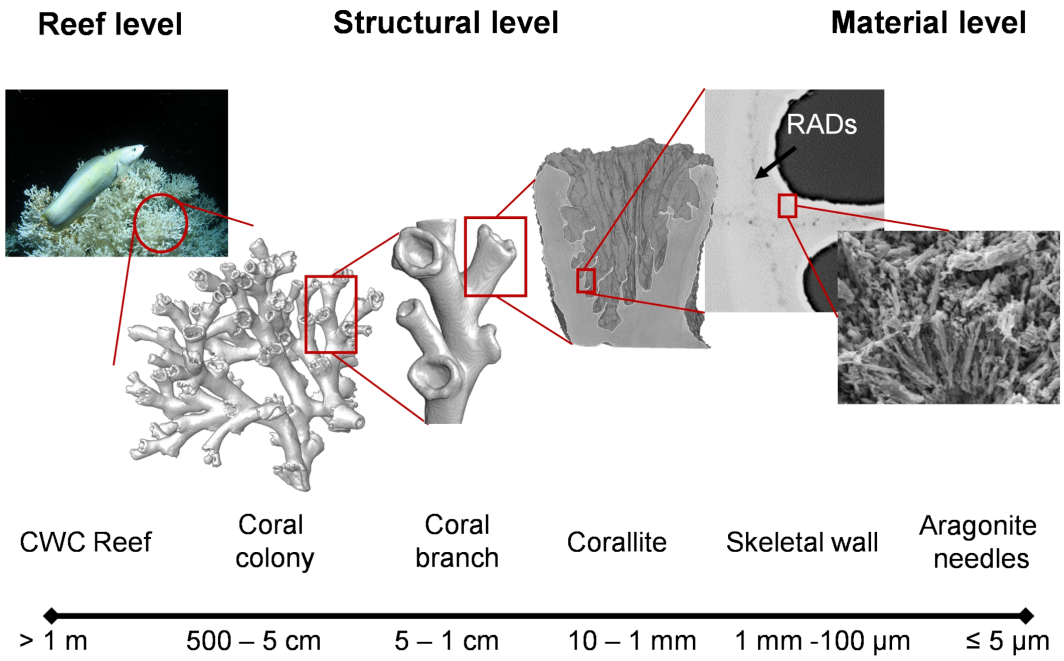

FIGURE 1
The material architecture of the branching cold-water coral (CWC) *L. pertusa* ranges from reef framework to aragonite crystal needles. *L. pertusa* reefs (> 1 m) extend up to 33 m high and several kilometers in diameter (Mortensen et al., 2001; Roberts et al., 2009, 2006). These reefs are formed by coral colonies (< 5 cm) that results from the concurrent growth of multiple coral branches at the structural level (Sanna and Freiwald, 2021), where branches are an assembly of corallites arranged in a fractal-like fashion at the mesoscale (~ 1 cm). The basic structural unit of the corallite's skeletal wall (> 100 µm) is made of aragonite crystals at the material level (~ 5 µm) that protrude from rapid accretion deposits (RADs) forming thickening bands between centers of calcifications (Von Euw et al., 2017).

determine the morphological variations of the underlying skeletal structure as either branch density, arrangements, or morphological features of the branches themselves must be represented.

In this study, we investigate the morphological variations of *dead* and *live L. pertusa* skeletal fragments to advance *in silico* mechanical models of their complex architecture. To achieve this aim, we (i) investigate the critical size of *L. pertusa* skeletal structure that allow us to use a mechanical homogenization approach to investigate crumbling and collapse of whole reef structures; (ii) analyze the morphology of *L. pertusa* skeletal fragments from coral colonies that were *alive* when collected, and *dead* erect coral framework to explain how corals occupy continuous space; and (iii) characterize the branching morphology of *L. pertusa* skeletons to describe size and shapes of individual corallites.

2 Materials and methods

2.1 Cold-water coral specimens

We investigated morphological variations of *L. pertusa* specimens collected by Büscher et al. (2019) from two Norwegian reef sites (Sula Reef Complex at 64°06.32'N, 8°07.1'E and 303 m depth, and Leksa Reef at 63°36.46'N, 9°22.76'E, 157 m depth and 63°36.43'N, 9°22.45'E, 152 m depth). The offshore Sula Reef location consisted of a relatively stable habitat (e.g., constant temperature, pH, and currents), whereas the inshore Leksa Reef location is subjected to strong tidal and currents, leading to a highly variable environment (Büscher et al., 2019; Büscher et al., 2024). *Live* coral colony fragments as well as *dead* erect coral framework fragments were sampled from both sites to provide a better representation of the environmental variability *L. pertusa* corals are found.

To investigate the critical size of a RVE for CWC skeletal structure, we examined two *L. pertusa* specimens collected from Rockall Bank (57°54.9'N, 13°52.296'W, unknown depth) and West Shetland (60°43.188'N, 2°55.788'W, unknown depth), which provided a larger representation of the skeletal structure (Table 1).

2.2 Image acquisition and processing

Computed tomography (CT) images from Büscher et al. (2019) of dried coral fragments from Norwegian reefs were acquired with a Toshiba Aquilion 64 clinical CT (120 kV, 600 mA, 0.351 mm in-plane pixel size, 0.5 mm slice thickness, 0.3 mm slice spacing). Images were reconstructed with a voxel size of 0.351x0.351x0.3 mm^3. For the large specimens, we performed CT with a Siemens Somatom clinical CT (120 kV 80 mA, 0.6 mm slice thickness, 0.35 mm slice spacing). The CT images had an in-plane pixel size of 0.662 mm for the Rockall Bank and 0.445 mm for the West Shetland specimen.

We used Python 3.8 libraries SimpleITK and scikit-image for image post processing. First, we resampled the images to an isotropic voxel size of 0.351 mm^3 for the Norwegian specimens, 0.662 mm^3 for the Rockall Bank specimen, and 0.445 mm^3 for the West of Shetland

TABLE 1 Summary of size characteristics of the analyzed *L. pertusa* specimens.

	Volume in cm^3	Surface area in cm^2	Dry weight in g
Rockall Bank (n=1)	535.0	6495.5	1296.0
West Shetland (n=1)	440.8	4880.1	1214.0
Sula *dead* framework (n=6)	113.4 [90.8, 121.8]	1461.9 [1138.1, 1586.3]	135.5 [93.5, 150.4]
Leksa *dead* framework (n=13)	145.5 [118.0, 160.2]	1728.7 [1482.0, 1902.7]	201.5 [141.7, 226.9]
Sula *live* corals (n=8)	11.4 [6.9, 18.8]	164.7 [93.9, 269.7]	22.3 [13.6, 36.1]
Leksa *live* corals (n=14)	33.2 [12.6, 47.3]	485.5 [213.2, 634.8]	68.1 [22.7, 96.3]

Volume, surface area, and dry weight are reported as median [minimum, maximum].

specimen. We reduced noise using a recursive Gaussian filter with a filter width of σ = 0.3. Thereafter, we segmented coral skeletons and cavities individually. We segmented the coral skeletons using a maximum entropy algorithm and we used a connected component analysis to remove isolated regions that were not attached to the skeleton (Figure 2A, D). We then segmented cavities within the skeleton in three steps. First, we applied a 3D morphological closing filter with a kernel radius of 6 pixels followed by a 3D binary dilation with a kernel radius of two pixels to the segmented coral skeleton to create a coarse mask contour image of the combined coral skeleton and cavities. This mask was then refined using an iterative 3D geodesic active contour (3D-GAC) algorithm (Ohs et al., 2021), which allowed us to identify the external contour of the skeleton (Figure 2B, E). We obtained a binary image containing only the cavities by subtracting the binary coral skeleton from the contour mask image. We labelled individual corallite calices using a hierarchical watershed on the 3D distance map (Figure 2C, F).

To quantify the local size of both the coral skeleton and corallites, we computed the 3D thickness maps (Hildebrand et al., 1999) of the contour and cavities mask images, respectively (Figure 2G, H). We assessed the local shape of the coral skeleton by measuring the 3D ellipsoid factor maps (Doube, 2015) on the contour mask image (Figure 2I). Finally, we computed the mean spacing between skeletal branches (i.e., interbranch lengths) from the 3D spacing maps of the contour images. Thickness (Br.Th), spacing (Br.Sp), and ellipsoid factor (Br.Ef) were computed using BoneJ (Doube et al., 2010) plugin in Fiji (Schindelin et al., 2012).

2.3 Critical size of representative volume element of cold-water corals

A RVE can be defined as the smallest volume element of a heterogeneous structure for which a macroscopic constitutive representation is sufficiently accurate to model the mean constitutive response (Drugan and Willis, 1996). Therefore, an appropriate size of a RVE of the skeletal structure should be found that consider: (i) a large enough number of heterogeneities to be statistically representative of their structure; (ii) a size small enough so that it can still be considered as a material point from a macroscopic point of view. The RVE domain shall comply with the Hill condition (Hill, 1963), which states the necessary and sufficient conditions for equivalence between energetically and mechanically defined properties of elastic materials:

$$\langle \sigma : \varepsilon \rangle = \langle \sigma \rangle : \langle \varepsilon \rangle \quad (1)$$

This means that the average of the product of the stress σ and strain ε tensors (microscale) equals the product of their averages. Similar to trabecular bone (Pahr and Zysset, 2008), we do not strive to find a RVE where (1) is exactly fulfilled but where we can obtain a usable approximation.

Numerical techniques, such as the FE method, can be used to approximate the critical size for a RVE by analyzing the size dependence of the elastic symmetries and properties of the structure (Kanit et al., 2003). These properties can be estimated from the stiffness tensor, S, using a direct mechanics approach through an optimization procedure where the best orthotropic representation of S may be found (van Rietbergen et al., 1995). Here, we approximate the critical size of a RVE for *L. pertusa* skeletal structures by analyzing the convergence of the orthotropy assumption.

2.3.1 Finite element modelling

We virtually extracted a cuboid volume element with edge lengths of 114.2 mm x 58.9 mm x 114.2 mm in x, y, and z direction, respectively, which corresponded to the largest cuboid fully occupied by the structure, from the CT reconstruction of the Rockall Bank and West of Shetland *L. pertusa* specimens (Figure 3). From this, we generated 64 cuboids for each specimen with edge lengths varying from 114.5 mm to 34 mm in the x and z direction while keeping the y direction constant. We created FE models by direct conversion of image voxels into isotropic linear hexahedral elements using previously implemented methods (Peña Fernández et al., 2022). Additionally, we generated a second type of model to investigate larger skeleton sizes than the ones physically available for scanning. We mirrored the original cuboid volume element along x, y, and z axis (Figure 3C) which resulted in a 225 mm cubical volume element. From this cuboid, we generated 217 cuboid volume elements and associated FE models with edge lengths varying from 225 mm to 45 mm.

All models were analyzed using kinematic uniform boundary conditions, where six independent load cases (three uniform longitudinal compressive strains and three uniform shear strains) were applied (Pahr and Zysset, 2008). The tissue material is assumed to be isotropic with a Young's modulus of $E = 65.7GPa$ and Poisson's ratio of $\upsilon = 0.29$ for all models (Wolfram et al., 2022). The apparent stiffness tensor, S, of each model was derived from the FE analysis via the apparent stresses and strains as in (Pahr and Zysset, 2008).

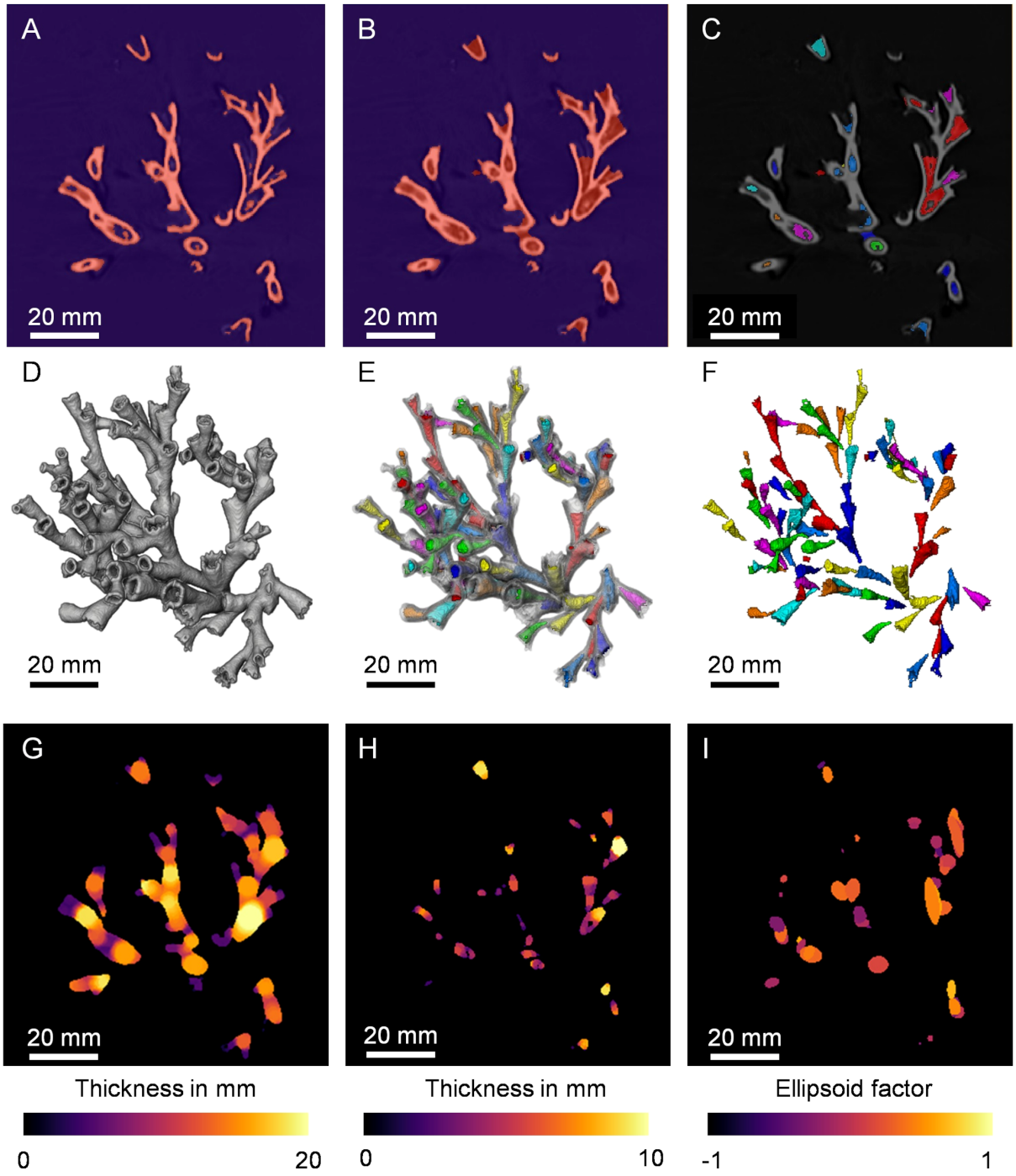

FIGURE 2
Segmentation of skeleton and cavities for an exemplary CWC specimen of the Leksa Reef. A representative CT cross-section and 3D render of the specimen are shown. **(A, D)** Coral skeleton was segmented. **(B, E)** A mask contour image was created by filling the cavities within the skeleton. **(C, F)** Cavities were segmented subtracting the skeleton from the masked contour and individually labelled. **(G, H)** The local diameter of the skeleton and branch thickness were computed from the mask contour image and the cavities image. **(I)** The shape of the coral branches was computed using the ellipsoid factor, where a value of -1 indicates a highly oblate shape and a value of 1 a highly prolate shape.

2.3.2 Determination of orthotropic assumption

We calculated the orientation of the closest orthotropic stiffness tensor by minimizing the objective function defined by:

$$Obj = \frac{\sum_{i,j} c_{ij}^2}{\sum_{i,j} e_{ij}^2} \; with \;\; i,j = 1,\ldots,6 \qquad (2)$$

Where c_{ij} represents the nonorthotropic terms of the stiffness tensor and e_{ij} the orthotropic terms of the transformed stiffness tensor (van Rietbergen et al., 1995). The orientation of the transformed stiffness tensor was obtained through a series of rotations, as defined by the Euler angles, about the coordinate axes x, y, and z. The optimization approach then yielded to the best possible orthotropic representation of the

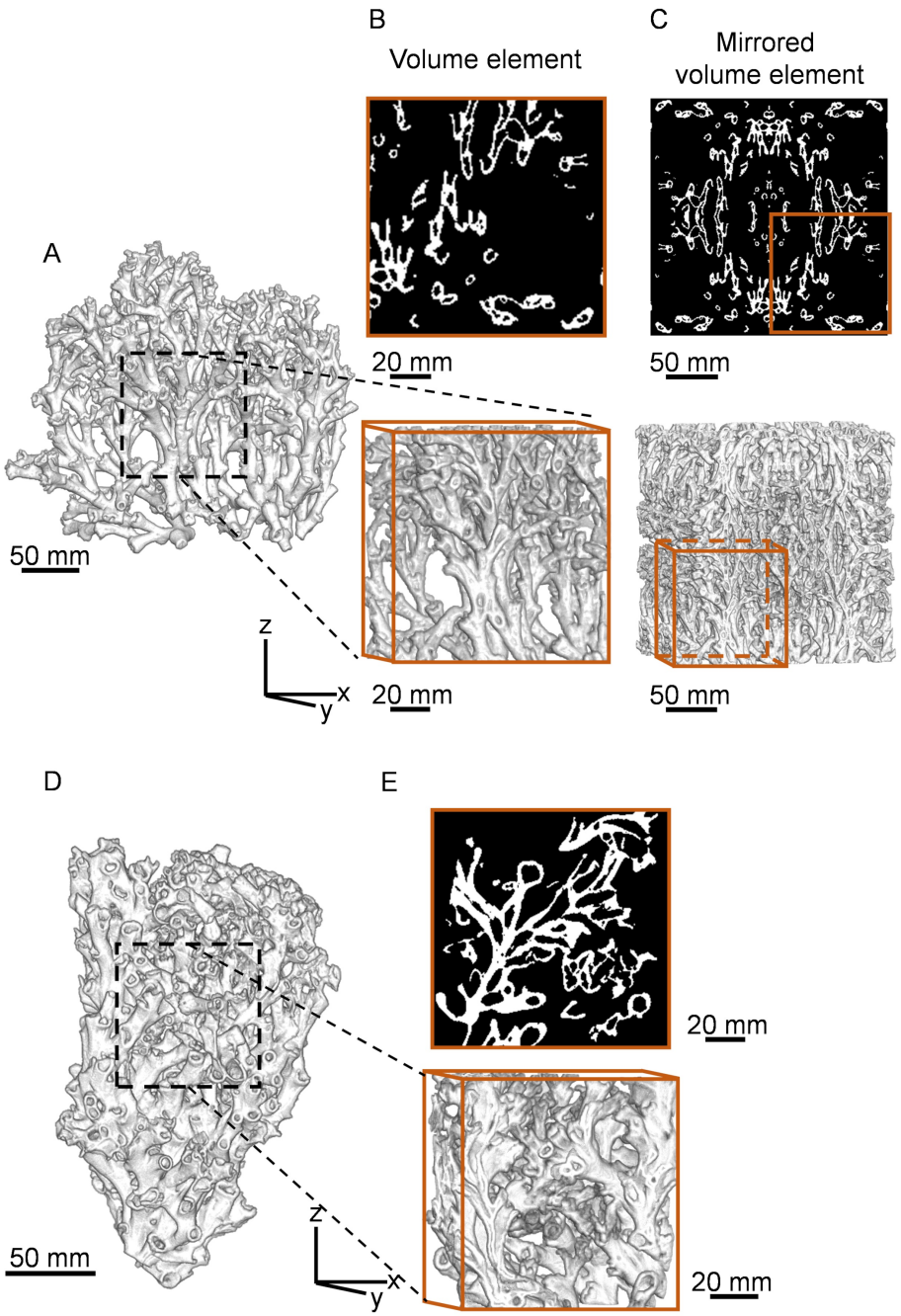

FIGURE 3
Representative volume element of large cold-water coral specimens from Rockall Bank and West Shetland. 3D renders of **(A)** Rockall Bank and **(D)** West Shetland cold-water coral specimens used for finite element analysis. **(B)**, **(E)** 2D cross-sections (top) and 3D volume elements (bottom) with 114.2 mm edge length in x and z axis and **(C)** mirrored model with 225 mm edge length.

stiffness tensor, S^{OPT}. We defined an orthotropic approximation of S^{ORT} by setting the nonorthotropic components to zero. The accuracy of the orthotropic assumption was quantified using the error of the orthotropic approximation (Pahr and Zysset, 2008), defined as:

$$Err = \sqrt{\frac{(S^{OPT}-S^{ORT})::(S^{OPT}-S^{ORT})}{S^{OPT}::S^{OPT}}} \quad (3)$$

We analyzed the convergence of the error with respect to the size of the volume elements expressed as edge length of the volume element and number of interbranch lengths, i.e., edge length over the mean spacing between skeletal branches, Br.Sp. Both S^{OPT} and S^{ORT} were checked to confirm they were positive definite.

2.4 Morphology of *L. pertusa* colony fragments

We introduce six shape variables to quantify the morphology of the *L. pertusa* skeletal fragments at the colony level. We calculated these based on the segmented coral skeleton images (Figures 2A, D) in

Python 3.8.5. We quantified shape through the sphericity and sparsity (capturing volume compactness) and the surface area to volume ratio and fractal dimension (capturing surface complexity) as:

i. Sphericity (S_{ph}) is an invariant measurement of the compactness of an object's volume. S_{ph} is defined as the ratio between the surface area of a sphere with the same skeletal volume (V_S) as the coral colony and the surface area of the coral skeleton (SA).

$$S_{ph} = \frac{\pi^{\frac{1}{3}}(6V_S)^{\frac{2}{3}}}{SA} \tag{4}$$

ii. Sparsity (S) is an invariant measurement of the degree to which there is space between different regions of the coral structure. S is defined as the ratio between the volume of an ellipsoid (V_E) fitting the coral colony and the skeletal volume (V_S) of the coral.

$$S = \frac{V_E}{V_S} \tag{5}$$

iii. Surface area to volume ratio ($SA:Vol$) refers to the amount of surface area (SA) per unit volume of the skeletal volume (V_S) of the coral colony.

$$SA:Vol = \frac{SA}{V_S} \tag{6}$$

iv. Fractal dimension (F_D) captures how the surface of the coral skeletal structure fills space, and it is an estimate of the spatial complexity. F_D is computed as the slope of the number of boxes at a size s that contains part of the coral skeletal structure (N^s) and the size of the boxes (s).

$$F_D = \frac{\Delta log(N^s)}{\Delta log(s)} \tag{7}$$

2.5 Morphology of *L. pertusa* skeletal branches

To quantify morphological variations of the coral specimens at the branch level (i.e., size and shape of the individual and/or group of corallites), we first performed a skeletonization (Kruszyński et al., 2007) of the mask image contour (Figures 3B, E) via a 3D thinning algorithm and we converted the skeletonized image into a graph object (Supplementary Figure S1) using the NetworkX package (Hagberg et al., 2008).

Initially, we assigned a 3D spatial coordinate to each node based on the image coordinates and we then inspected the resulting graphs and manually selected the root (i.e., base) of each skeleton based on the morphology, from where a newly oriented graph was created via a depth-first-search algorithm (Cormen et al., 2001). We added the mean coral branch thickness (Br.Th), length (Br.Len), area (Br.Ar), volume (Br.Vol), taper rate (Br.Tr), and ellipsoid factor (Br.Ef) as nodal attributes to account for the size and shape of each individual branch.

We then introduced four topological descriptors that represent morphological features of the branching coral structure (Khalil et al., 2022). These descriptors associate a function to a given coral skeleton whose independent variable is either the path, δ, or radial, r, distance from the skeletal root (Supplementary Figure S1D).

i. Branching pattern (B_P) quantifies the skeletal complexity of the coral specimens and the distribution of the branches. B_P is related to skeletal growth and spatial arrangement and it can be defined as a function of the radial distance from the root, r, as:

$$B_P(r_i) = \#\{deg_{n_i} \geq 3 | r_i \leq r\} - \#\{deg_{n_i} = 1 | r_i \leq r\} \tag{8}$$

Where # represents the cardinality of each set and r_i the radial distance of i-th node, n_i, to the root.

ii. Terminal branch index (T_{BI}) counts the number of end points that can be reached from a given node. T_{BI} quantifies the hierarchical branching growth of CWC skeletons and it is defined as a function of the path distance, δ, from the root along the branches as:

$$T_{BI}(\delta_i) = \#\{deg_{n_i} = 1 | \delta_i \geq \delta\} \tag{9}$$

Where δ_i represents the path distance from the i-th node to the root.

iii. Tortuosity (τ) is defined as the ratio of the path distance, δ, by the Euclidean distance, ε, between a node and the root. τ is related to the branch growth mechanism, and it is defined as a

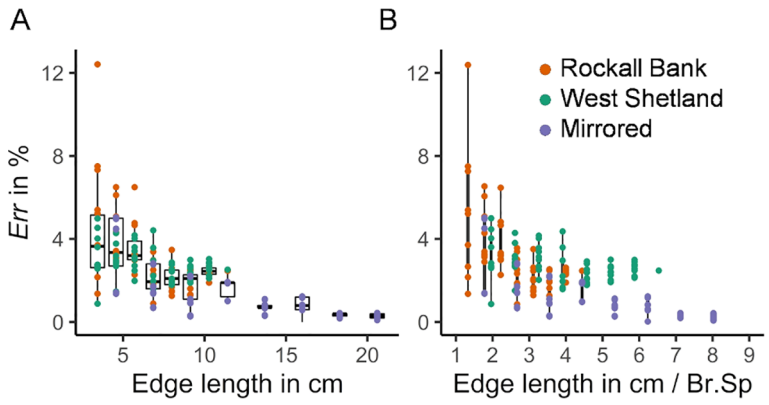

FIGURE 4
Error of orthotropic approximation. Boxplots of the errors for the analyzed volume elements of the Rockall Bank, West Shetland and mirrored models as a function of the **(A)** edge length of the cuboid volume elements and **(B)** number of interbranch spacings, i.e., edge length over mean branch spacing (Br.Sp).

10.3389/fmars.2024.1456505

function of the radial distance from the root, r, as:

$$\tau(r_i) = \frac{\delta_i}{\varepsilon_i} \tag{10}$$

Where ε_i represents the Euclidean distance from the i-th node to the root.

iv. Volume distribution (V_d) gives a measure of how the volumetric mass of the branches are distributed relative to the root. For a given coral skeleton, we consider all its nodes as cloud points in 3D space, $n_i(x_i, y_i, z_i)$, each of them carrying a weight equal to the volume of the branch, v_i. This volume affects the space around them such that each node contributes to a field, V_i, which is normalized to have length v_i and which is of the form:

$$V_i(x, y, z) = v_i \frac{(x-x_i,\ y-y_i,\ z-z_i)}{\varepsilon_i} \tag{11}$$

By superimposition, the node configuration of the skeleton gives rise to a vector field,V, whose magnitude is used as V_d, and it is defined as a function of the radial distance to the root, r, as:

$$V_d(r_i) = \left(\sum_i v_i \frac{x - x_i}{\varepsilon_i}\right)^2 \left(\sum_i v_i \frac{x - x_i}{\varepsilon_i}\right)^2 \left(\sum_i v_i \frac{x - x_i}{\varepsilon_i}\right)^2 \tag{12}$$

To reduce the dimensionality of the proposed descriptors as well as the coral branch attributes (i.e., Br.Th, Br.Len, Br.Ar, Br.Vol, Br.Tr and Br.Ef) we combined those measurements into a vector, V_C, by considering the area under the curve defined by each descriptor, ϕ, as:

$$a(\phi) = \int_0^1 \phi(x)dx \tag{13}$$

Where x is the normalized path, δ_i, or radial, r_i, distance from the skeletal root. The corresponding vector for each coral skeleton, V_C, is:

$$V_C = \left\langle \begin{array}{r} a(B_P), a(T_{BI}), a(V_d), a(Br\,.\,Vol), a(Br\,.\,Ar), a(Br\,.\,Len), \\ a(Br\,.\,Tr), a(Br\,.\,Th), a(Br\,.\,Ef), a(\tau) \end{array} \right\rangle$$

This vectorization allows us to optimize classification of the data (Khalil et al., 2022).

2.6 Analysis of morphological parameters

We compared morphological differences between *dead* and *live* skeletal fragments as well as Sula and Leksa locations at both colony and branch level. For each specimen a distribution of branch morphological parameter was obtained and statistical information calculated. Thereafter, statistical analysis was based on the median values of such parameters.

Statistical analyses of morphological parameters coral skeletons were conducted in RStudio (Version 1.1.456). We used quantile–quantile plots and Shapiro–Wilk *post-hoc* tests to test normal distribution of data. If normality was given, we compared groups using Student's t-tests. Where data were non-normal, we used Wilcoxon rank sum tests. We assumed a significance level of $p = 0.05$.

We used principal component analysis (PCA) to visualize patterns of morphological variations at the colony and branch level. We standardized variables with a mean of zero and unit variance to reduce the influence of variable scale on the projection. We used score plots to visualize the projection of each coral specimen onto the span of the two first principal components and how each group relates to each other. We used confidence ellipsoids around the main points of dead/live classes to illustrate data points lying within the multivariate distributions. A 95% confidence level defined the size of the ellipsoids, whereas the shape was determined by the covariance matrix. Finally, we investigated the relationships between the first two principal components and the original morphological variables using loading plots.

3 Results

3.1 Critical size of representative volume element *L. pertusa*

The error of the orthotropic approximation of the stiffness tensor decreases with increasing specimen size (Figure 4A). The error decreased significantly after 6 cm edge length and converged to less than 3% at ~9 cm edge length. Considering that the mean Br.Sp was 2.57 cm for the Rockall Bank coral specimen and 1.75 cm for the West Shetland specimen, the error converged at four to five Br.Sp (Figure 4B). The size of the volume element influenced the Young's and shear modulus but had minimal influence in the Poisson's ratio (Supplementary Figure S2). Overall, the Rockall Bank specimen displayed lower elastic and shear modulus compared to the West Shetland specimen as a result of its lower skeletal volume fraction, $^{V_S}/_{V_T}$ (Supplementary Figure S3). The underlaying structure had little influence on the error of the orthotropic approximation, with $Err < 3\,\%$ observed for $^{V_S}/_{V_T}$ ranging between 5% to 20%, and a wide range of branching and terminal nodes (Supplementary Figure S3). Similar convergence was observed for the mirrored models ($Err < 3\,\%$ at ~9 cm edge length, ~4 Br.Sp). The imposed orthotropic structure in those models resulted in $Err < 1.5\,\%$ and lower standard deviation for extracted volume elements >13 cm. Therefore, a critical size of ~13 cm (five to seven Br.Sp), should provide sufficiently averaged continuum quantities, thus, allowing for a mechanical homogenization approach for *L. pertusa* skeletal structures.

3.2 Morphology of *L. pertusa* colony fragments

Live coral fragments exhibited significantly greater SA: Vol (Figure 5A), while *dead* fragments displayed a less compact structure (i.e., lower sphericity and sparsity) (Figures 5C, D). Both sphericity and sparsity were significantly larger for *live* Sula fragments (Figures 5C, D). The complexity of the *dead* coral framework was demonstrated through the higher fractal dimension (Figure 5B). *Live* coral specimens showed larger variability of the shape parameters and greater differences between specimens from Leksa and Sula reef.

3.3 Morphology of *L. pertusa* skeletal branches

Live corals contained significantly larger branches compared to the *dead* coral fragments (Figure 6B), yet median branch areas and volume were not significantly different (Figures 6A, D). *Dead* coral framework branches were significantly thicker than those from *live* specimens (Figure 6E). The larger values of the ellipsoid factor and taper rate for *live* corals indicate a more prolate shape and wider opening of their branches (Figures 6C, F). Median branch length and thickness of *live* corals from Leksa reef were significantly lower than those from Sula reef (Figures 6B, E). Overall, skeletal branch morphology was highly variable within each specimen (Figure 7; Supplementary Tables S1-S3), as demonstrated when pooling all analyzed branches (Supplementary Figure S4).

Skeletonization of the coral structure demonstrated no significant differences in the number of branches and nodes per unit of skeletal volume between *live* and *dead* skeletal fragments (Figures 6G-I). *Live* fragments from Leksa reef had significantly more branches and branching nodes per unit of skeletal volume compared to those specimens from Sula Reef, however, the number of terminal nodes per unit of skeletal volume was not significantly different.

3.4 Topological descriptors

B_P decreased with increasing radial distance (Figure 8A). Such a decrease was faster for the *dead* fragments. This illustrates that for the *live* specimens, newer polyps appear further from the initial base. Similarly, the distribution of T_{BI} (Figure 8B) showed a faster decrease for *live* coral fragments, that is, the path to reach the end points of the structure is more direct than for the *dead* fragments. The higher complexity of the skeletal structure of *dead* fragments results in increased τ (Figure 8C), as well as a larger V_d (Figure 8D), which decreased for the more distant branches, as a consequence of the dense packing of the structure (Figure 5).

3.5 Principal component analysis

At the colony fragment length scale, the first principal component (PC1) of the PCA explained 47.3% of variation (Figures 9A, B). The projection of *live* coral fragments from Leksa reef in the score plots was largely aligned in the direction of PC1 (Figure 9A), which was primarily contributed by the branching descriptors (i.e., number of branches, branching nodes, and terminal nodes per unit of volume) (Figure 9B). The second principal component (PC2) explained 34.5% of variation, with a major contribution of the fractal dimension and sparsity. A clear positive correlation between the branching parameters, as well as a negative correlation between fractal dimension and sparsity, sphericity and SA: Vol. SA: Vol had the lowest contribution on both PCs. At the skeletal branch level, PC1 explained 76.1% of the variation, whereas the PC2 explained only 11.1% of the variation (Figures 9C, D). B_P and Br.Tr were positively correlated and largely aligned with PC1, while showing a negative correlation with Br.Th, Br.Len, Br.Ar, T_{BI} and τ. The confidence ellipsoids demonstrate that *dead* specimens showed the lowest variance of the morphometric parameters at the colony

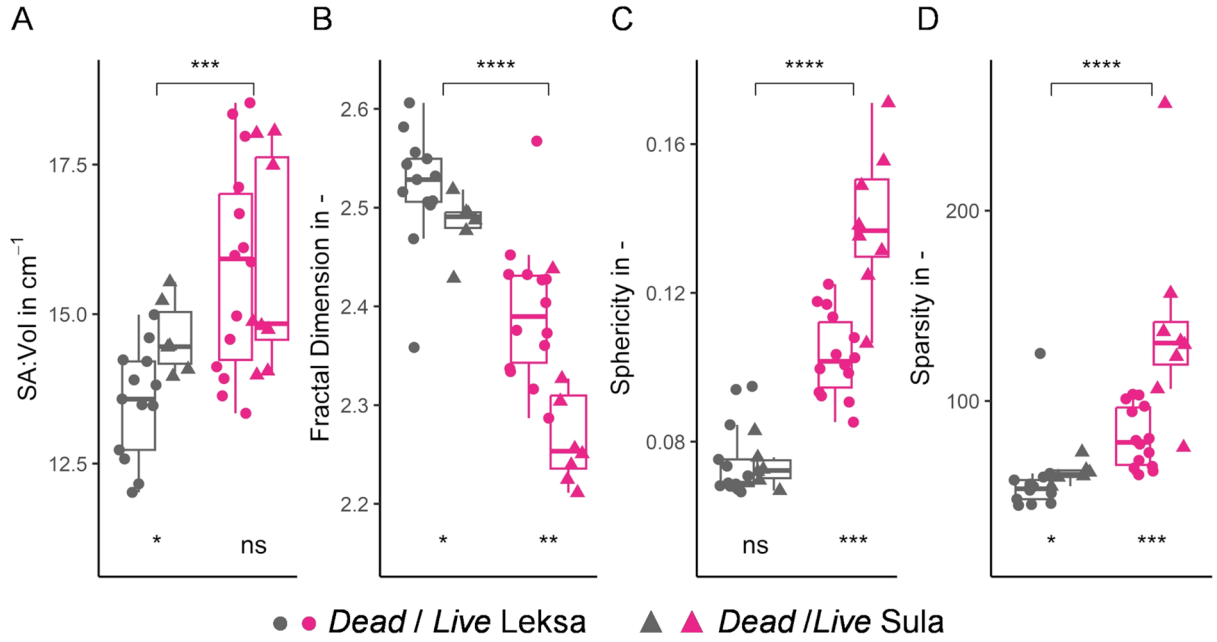

FIGURE 5
Morphological parameters of *L. pertusa* coral colonies. Boxplots of **(A)** surface area to volume ratio (SA: Vol), **(B)** fractal dimension, **(C)** sphericity and **(D)** sparsity for dead and live coral fragments are shown in grey and pink colors, respectively. '●' and '▲' symbols correspond to specimens from Leksa and Sula reef, respectively. Significance levels between dead and live fragments are indicated at the top of each boxplot and those between Leksa and Sula at the bottom. ns: non-significant, *p < 0.05, **p < 0.01, ***p < 0.001, ****p < 0.0001.

10.3389/fmars.2024.1456505

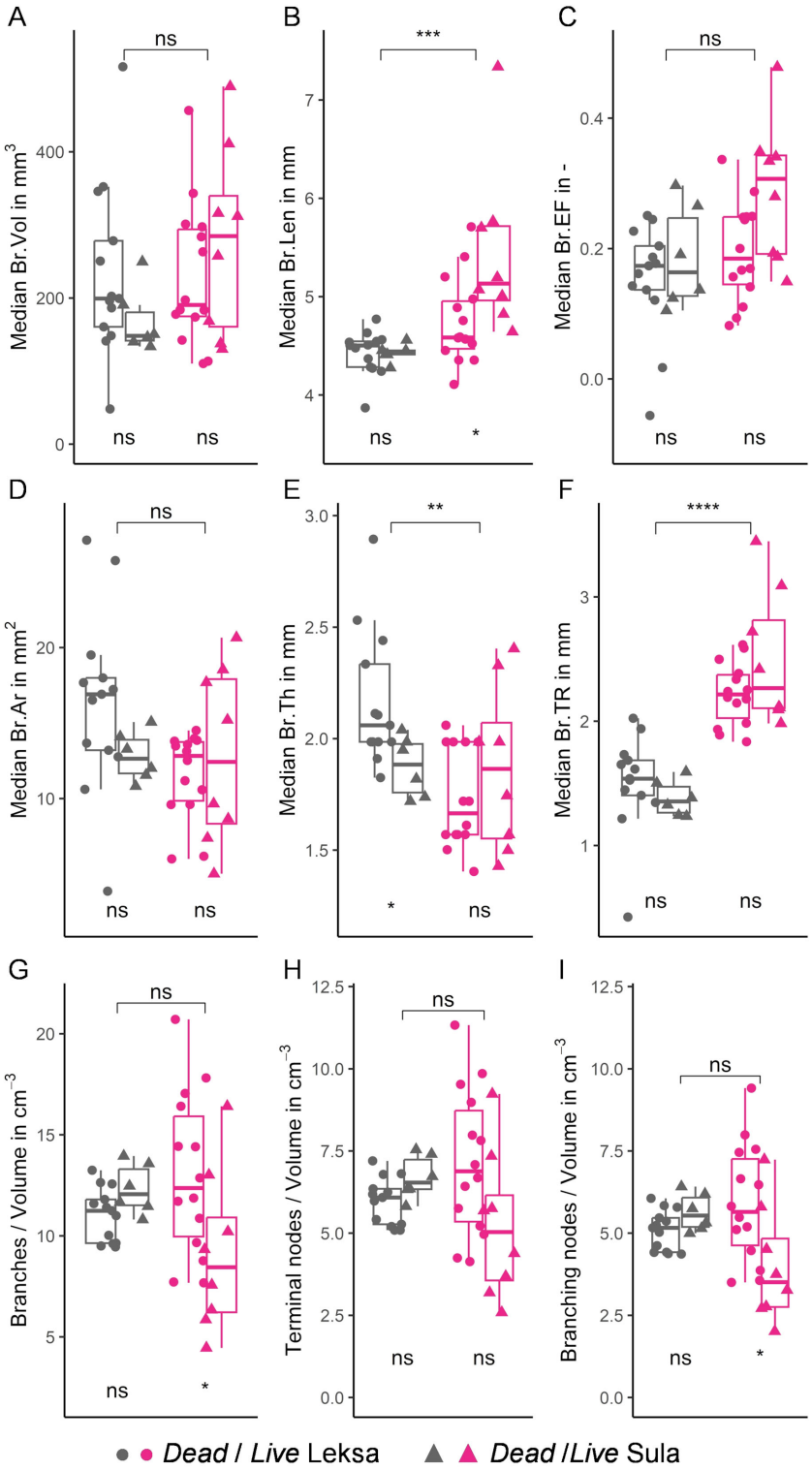

FIGURE 6
Morphological parameters of L. pertusa coral branches. Boxplots of **(A)** median branch volume (Br.Vol), **(B)** area (Br.Ar), **(C)** length (Br.Len), **(D)** thickness (Br.Th), **(E)** ellipsoid factor (Br.Ef), **(F)** taper rate (Br.Tr), **(G)** number of branches per unit volume, **(H)** terminal nodes per unit volume, and **(I)** branching nodes per unit volume for dead and live coral fragments are shown in grey and pink colors, respectively. '●' and '▲' symbols correspond to specimensfrom Leksa and Sula reef, respectively. Significance levels between dead and live fragments are indicated at the top of each boxplot and those between Leksa and Sula at the bottom. ns: non-significant, *p < 0.05, **p < 0.01, ***p < 0.001, ****p < 0.0001.

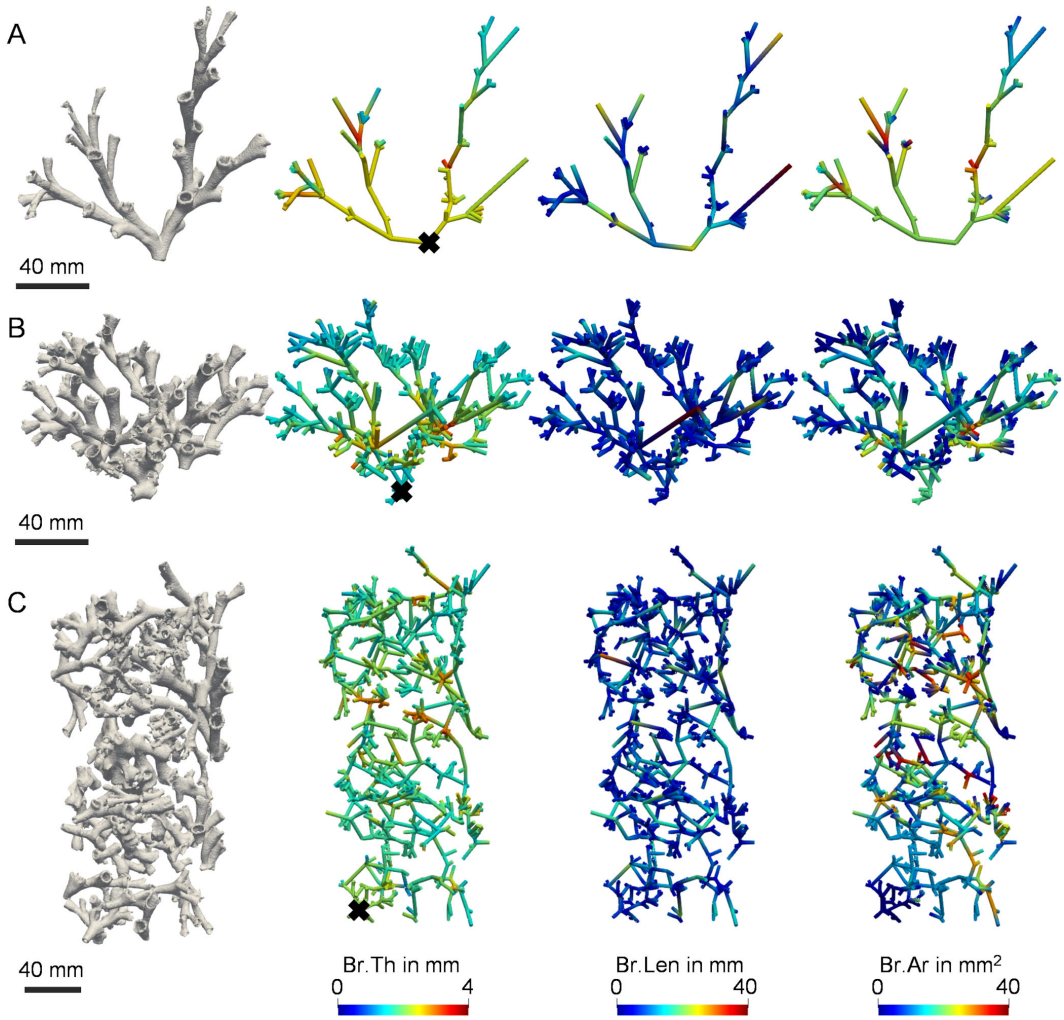

FIGURE 7
Local morphometry of *L. pertusa skeletal* branches. 3D graphical representation of branch thickness (Br.Th), length (Br.Len), and area (Br.Ar) of the individual branches for three representative *L. pertusa* specimens with increasing levels of complexity; **(A)** *Live* coral fragment from Leksa reef, **(B)** *Live* coral fragment from Sula reef, and **(C)** *dead* coral fragment from Sula reef. Please note the fusion of multiple coral origins in the dead coral fragment **(C)**. 'x' symbols correspond to the defined skeletal root (base).

fragment level (Figure 9A), but highest variance at the skeletal branch level (Figure 9C).

4 Discussion

4.1 Critical size for *Lophelia pertusa* skeletons

We performed a preliminary investigation on the critical size of *L. pertusa* skeletal structure that allows us to use a mechanical homogenization approach to study the mechanical vulnerability of CWCs to ocean acidification. We built upon concepts developed for porous structures such as trabecular bone, where similar challenges are present (e.g., trabecular thickness and connectivity depending on age/disease and their influence on bone fracture). We showed that the orthotropic approximation of the stiffness tensor for the coral skeletal structure converges at ~13 cm edge length, which reflects the RVE size for the estimation of macroscopic properties of *L. pertusa* skeletons at the structural level. This critical size corresponds to five to seven times the mean spacing between skeletal branches (i.e., interbranch length) and over 20 times the mean thickness of the branches. Thus, averaging the mechanical properties over less than five interbranch lengths does not provide sufficient continuum quantities, and the homogenization approach must be replaced by statistical models of the underlaying structure. Similar results are seen in other material architectures, such as trabecular bone, in which average mechanical properties are sufficient when considering volume elements over five intertrabecular lengths (Harrigan et al., 1988) or carbon reinforce polymers, where RVEs larger than 15-16 times the heterogeneity size (i.e., fiber thickness) fulfil the Hill criteria (Khisaeva and Ostoja-Starzewski, 2006; Trias et al., 2006). Here, we limited our investigation to two specimens from different locations due to the unavailability of 3D data on large coral colonies. While this low number of specimens is likely insufficient to provide a

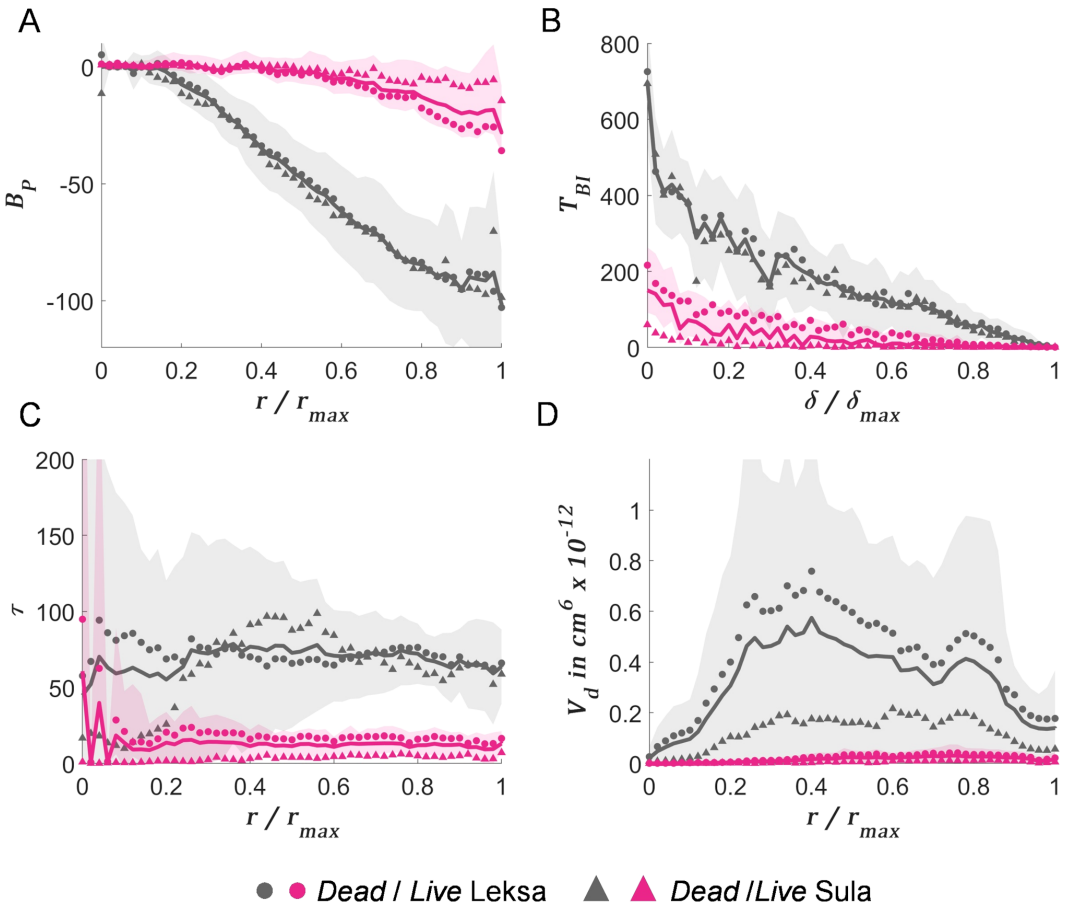

FIGURE 8
Topological descriptors for *L. pertusa* fragments. **(A)** Branching pattern (B_P), **(B)** terminal branch index (T_{BI}), **(C)** tortuosity (τ), and **(D)** volume distribution (V_d) as a function of the radial, r, or path distance, δ, from the skeletal root. Solid lines indicate the mean values, while shaded areas show the mean ± standard deviation for *dead* and *live* coral fragments in grey and pink colors, respectively. '●' and '▲' symbols correspond to mean values for specimens from Leksa and Sula reef, respectively.

representation of the elastic properties of *L. pertusa* skeletal structure across many locations, it illustrates the variability which can be found in skeletal structure from specimens from relatively close sites. Indeed, we observe that the lower skeletal density of the Rockall Bank specimen led to lower elastic and shear modulus compared to the West Shetland specimen, yet the error of the orthotropic assumption was not dependent on such skeletal density or the branch distribution (Supplementary Figure S3). While larger number of specimens will be needed to derive the relationships between the effective elastic properties at the macroscale and underlying structure, our convergence study demonstrates that the determined critical sizes are robust and applicable to other coral skeletal fragments. In addition to this, we demonstrate the applicability of the methodology so that our results can be easily confirmed as larger samples become accessible.

4.2 Morphological variability of *L. pertusa* skeletal structure

The structural complexity of *L. pertusa* reefs makes it difficult to standardize the sampling, which resulted in a large range of specimen sizes and aspect ratios (Table 1; Supplementary Figure S5), with *dead* coral fragments bigger than *live* ones. For this reason, a comparison of size morphometric variables of the colonies, such as volume or area, is not legitimate. Therefore, we used four shape variables to describe how *L. pertusa* colonies occupy the space. Variations in volume compactness capture a gradient from *dead* to *live* coral specimens (Figure 9). This is indicative of the open branching structure of *live* colonies, which is optimized for food particle capture, opposite to the dense structure of the *dead* framework resulting from the packing and fusion of several branches as they thicken when aging. Moreover, the ability for building reef frameworks increases for colonies with high compactness (Rasser and Riegl, 2002). However, compactness constrained surface complexity, as previously shown by Zawada et al. (2019b). Thus, *live* colonies with higher levels of compactness tended to be smooth (i.e., higher SA: Vol and lower fractal dimension). The increased SA: Vol of *live* colonies also implies increased exposure to the environment. Indeed, variation in surface complexity relates to competition and resource use (Zawada et al., 2019a), where colonies with higher structural complexity have less access to those resources (e.g., nutrients), but can have more polyps packed within a

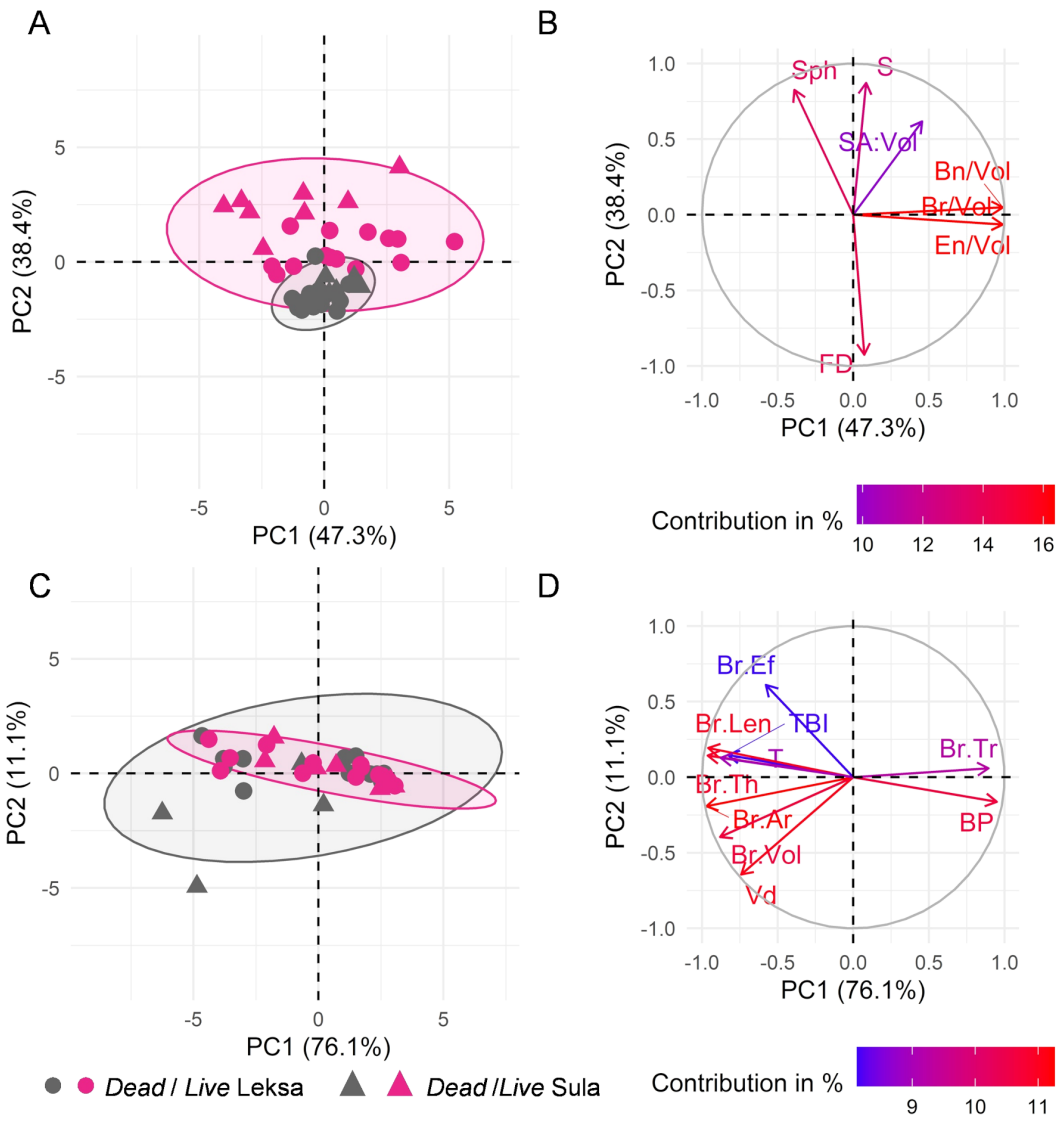

FIGURE 9
Principal component analysis. **(A, C)** Score and **(B, D)** loading plots resulting from PCA for the morphological analysis at **(A, B)** colony and **(C, D)** skeletal branch level. Points in **(A, C)** represent the projection of the analyzed *dead* and *live* coral fragments in grey and pink color, respectively. '●' and '▲' symbols in **(A, C)** correspond to specimens from Leksa and Sula reef, respectively. Confidence ellipsoids centered at the mean value of *dead*/*live* labels are also shown. Arrows in **(B, D)** indicate variable loadings. S_{ph}, sphericity; *S*, sparsity; *SA* : *Vol*, surface area to volume ratio; F_D, fractal dimension; *Br*/*Vol*, number of branches; B_n/*Vol*, branching nodes; E_n/*Vol*, ending nodes; B_P, branching pattern; T_{BI}, terminal branch index; V_d, volume distribution; τ, tortuosity; *Br* . *Vol*, branch volume; *Br* . *Ar*, branch area; *Br* . *Len*, branch length; *Br* . *Th*, branch thickness; *Br* . *Ef*, branch ellipsoid factor; *Br* . *Tr*: branch taper rate.

given space (Wangpraseurt et al., 2012). From a mechanical perspective, the highly packed structure of the *dead* framework serves to support living colonies by sustaining external loads.

When comparing these shape variables between specimens from Leksa and Sula Reef we observed higher surface complexity (i.e., fractal dimension) in *dead* and *live* fragments from Leksa Reef, which agrees with data from Sanna et al. (2023) in *dead* skeletal framework of *L. pertusa*. However, in contrast to Sanna et al. (2023), we obtained higher compactness values (i.e., sphericity and sparsity) in colony fragments from Sula Reef. These differences were especially significant for *live* coral fragments (Figure 6), and may be driven by current flows (Sanna et al., 2023). This would also explain the higher diversity pattern observed by Mortensen and Fossâ (2006) in mid-Norwegian inshore reefs (including Leksa) compared to reefs at Sula, as increased surface complexity and reduced compactness creates niches for other associated organisms (Zawada et al., 2019b).

We quantified the morphology of *L. pertusa* skeletal branches based on a skeletonization of 3D CT images, as first proposed by Kruszyński et al. (2007) for the tropical scleractinian coral *Madracis mirabilis*. While the authors focused on branch diameters and spacings, which are controlled by a combination of hydrodynamics and genetics (Sebens et al., 1997), we extended the analysis to other parameters that may influence the load-bearing capacity of *L. pertusa* reefs, such as wall thickness, branch length, cross-sectional area, and volume. Some of these parameters (e.g., thickness and length) have only been quantified using linear measurements from small coral fragments (Gass and

Roberts, 2011; Sanna and Freiwald, 2021), consequently, restricting the analysis to a small number of corallites. However, *L. pertusa* colonies are made up of hundreds to thousands of corallites. Thus, the method we present here provides an efficient tool to assess intraspecific morphological variations in coral skeletal branches. In line with Gass and Roberts (2011) and Sanna and Freiwald (2021), we showed a large variation in size and shape for the analyzed branches (Supplementary Figure S4). These local architectural variations both within the same coral fragment and in between fragments may reflect an adaptive response of *L. pertusa* to environmental stressors, where the size and shape of branches adapt to minimize mechanical stresses on the coral skeletons while optimizing food capture. *Live* fragments from the Sula Reef Complex displayed significantly shorter branches, yet more branches per unit of volume. This confirms findings from Büscher et al. (2019) who hypothesized such difference may reflect the more stable environment in this offshore location, which allows *L. pertusa* skeletal branches to grow longer without risk of fracture. An aspect that was unresolved here was the growth time before death of the *dead* skeletal material, and hence time for the older polyps to radially thicken while alive. Interestingly, *dead* skeletal fragments from Leksa reef displayed significantly higher median thickness compared to fragments from Sula reef, which may be due to higher bioerosion rates found in the Sula reef (Büscher et al., 2019).

An additional unknown variable that remains a challenge for *live* coral research is the ability to store and transfer nutrients within and between individual coral polyps (Georgoulas et al., 2023). We assume that energetic reserves are maintained within each coral polyp unit – while this is assured if connective tissue is lost between polyps, where connective tissue is retained, are energetic reserves partly mobile? To compound this challenging point further, as coral branches come into contact, there is fusion of tissue and skeletal material (Figure 8C) – complete with regards to individual and closely genetically related (sibling) colonies (Hennige et al., 2014). From a mechanical perspective, the fusion of skeletal branches likely contributes to the stiffness of the coral structure. Indeed, other studies have shown that increased connectivity of network-like structures such as fibrous networks or trabecular bone led to higher elastic modulus (Davoodi Kermani et al., 2021; Maquer et al., 2015). While our methodological approach does not allow us to determine the occurrence of such fusions, we evaluated the density of branching nodes as a surrogate of connectivity (Figure 6I). Those branching nodes account not only for the fused branches but also the "split" of branches as they grow.

The measured mean taper rate (i.e., difference in diameter between top and bottom of the corallite) and areas aligns well with previous studies (Farber et al., 2016; Gass and Roberts, 2011; Sanna and Freiwald, 2021), highlighting that our CT image-based approach is able to capture slight variations of branch morphology. However, we reported thicker wall values, which may be explained by differences in the employed methodology, where we consider the mean thickness of the entire branch based on the CT data as opposite to the linear measurement of the thinner wall at the top of the corallites in Gass and Roberts, 2011 and Sanna and Freiwald, 2021. Accurate measurements of the wall thickness in CWC skeletons is important as ocean acidification induces dissolution of the skeletal wall material, decreasing the load bearing capacity of the entire structure (Hennige et al., 2020, 2015; Wolfram et al., 2022).

In addition to the skeletal branch size and shape, we analyzed four topological descriptors that describe the branching characteristics of *L. pertusa* structures and their distribution in the 3D space. These descriptors confirmed the higher complexity of the *dead* framework, as seen in the increased tortuosity and volume distribution, which may be a consequence of dense packing of several colony fragments. Although the increased volume distributions (i.e., higher mass density) may represent an advantage of the *dead* framework to support living colonies under mechanical stressors, the bare *dead* coral skeleton, which lacks protection by organic tissue or defense mechanisms (Beuck et al., 2010), is more vulnerable to dissolution (Hennige et al., 2020) and bioerosion (Büscher et al., 2019; Wisshak et al., 2012), and consequently, mechanical damage (Vad et al., 2017). Therefore, degradation of skeletal branches in the *dead* framework may compromise the stability of the entire colony, leading to a rapid collapse and, consequently, loss of biodiversity support (Hennige et al., 2020). The environmental conditions of the analyzed location are reflected in these descriptors, where lower complexity (i.e., branching pattern, tortuosity) is seen for *live* fragments from the Sula Reef complex (relatively stable currents) compared to fragments from Leksa. Similarly, the higher volume distribution of *dead* fragments in Leksa reflect the higher compactness of the inshore corals to withstand stronger currents.

Our principal component analysis did not point to clear branching pattern-specific differences in branch morphology between *dead* and *live* skeletal fragments (Figure 9). This suggests that we cannot simply skip morphological features when developing *in silico* mechanical models. Nevertheless, reduced morphological variation was observed for *live* coral specimens compared to *dead* framework at the skeletal branch level.

4.3 Towards reef-scale modelling of cold-water corals

The investigation of timescales for reef crumbling relies on the development of computational tools that are able to provide accurate and efficient predictions of the mechanical behavior based on the time *L. pertusa* coral reefs are exposed to acidified waters (Hennige et al., 2020; Wolfram et al., 2022). These tools are currently non-existent, partially due to the lack of information on the structure-function relationships of corals at the structural level (Figure 1). Here, we showed that homogenized FE models of coral colonies may be used to estimate the risk of crumbling of coral reefs when these surpass the identified critical size of five interbranch lengths. Similarly to previous studies in other multiscale structures such as bone (Cowin, 1986, 1985; Pahr and Zysset, 2009), the stiffness and strength of the individual finite elements can account for the skeletal volume fraction and architectural information (Figure 10A). This approach outperforms current models that considered a uniform homogeneous coral skeletal structure (Madin and Connolly, 2006; Storlazzi et al., 2005), thus, missing the influence of *L. pertusa* branching structure and composition (i.e., *live* or *dead* skeleton) on the mechanical response. However, CWC reefs comprise hundreds to thousands of colonies of varying sizes and shapes which are mostly related to variations in the

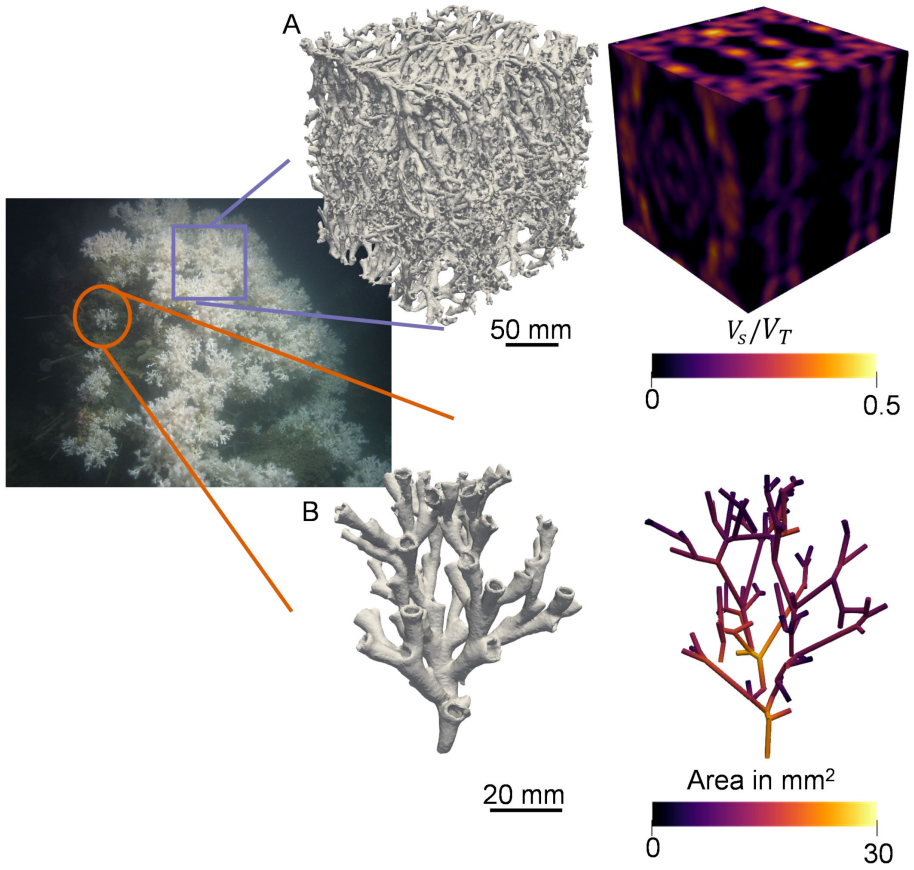

FIGURE 10
Realms of *in silico* models for *L. pertusa* skeletal structure. **(A)** Large coral colonies (> 13 cm, 5 interbranch lengths or 800 branches) may be modelled using homogenized finite element models based on density (i.e., skeletal volume fraction, V_S/V_T) and/or fabric information. **(B)** The morphology of the skeletal branches needs to be considered modelling smaller coral colonies, using, for example, nonlinear beams.

substrate and local hydrodynamics (De Clippele et al., 2018), meaning they are subjected to diverse loading conditions. As the size of some of those colonies may be smaller than the critical size we determined (e.g. on Tisler Reef (Norway) almost 60% of colonies have sizes smaller than 30 cm (De Clippele et al., 2018)), homogenized FE models would be unsuitable and must be replaced by explicit models of the branching structure of *L. pertusa* skeletons.

The 3D graph representation we presented here may serve to define *in silico* mechanical models of these smaller colonies consisting of nonlinear beams (Figure 10B). Beam FE models have demonstrated to predict the mechanical properties of complex structures in an accurate and computational efficient manner (Pothuaud et al., 2004; Stauber et al., 2004). Since at small length scales *L. pertusa* skeletal structure is not random, the properties of each beam (i.e., skeletal branch) may account for the statistical information of the morphological analysis we introduce here. Future analyses would need to validate the use of such specimen-specific beam FE models against image-based FE models to confirm its applicability for predictions of the risk of crumbling of *L. pertusa* skeletal structures.

The expected reduced computational cost of the models we identified here can ease the translation from the mechanical response at the structural level to entire reefs, facilitating *in silico* models at the reef scale to investigate the mechanical vulnerability of CWC reefs to ocean acidification. Most importantly, we could model the increased dissolution in the *dead* framework observed from increasing aragonite concentration (Hennige et al., 2020) as a decrease in the skeletal volume fraction in our homogenized models or a reduced branch thickness in our beam models.

Our study points to some important gaps in knowledge. Although we provide a detailed morphological evaluation of a large number of *L. pertusa* skeletal fragments, these only represent a fraction of the colony from two unique sites in Norway. While these two locations represent different environmental conditions, future analysis should focus on the characterization of morphological variations of skeletal fragments collected from other regions to better understand the impact of local environmental stressors on *L. pertusa* structure. To date, monitoring reef corals largely relies on 2D measurements of colony size or colony cover (De Clippele et al., 2018; Vad et al., 2017), thus lacking high-resolution volumetric information. To investigate the risk of crumbling of larger colonies we need to investigate new techniques that allow us to infer 3D volumetric information from planar data (House et al., 2018). The most crucial gap is potentially the lack of information on time estimates for

morphological changes due to exposure to ocean acidification and consequent increasing rates of bioerosion (Büscher et al., 2022). This will require extension of previous mesocosm experiments (Hennige et al., 2020) to different acidification conditions over long time-scales and complementary *in situ* measurements of seawater chemistry to establish an exposure trajectory of aragonite concentrations and the relationships with ocean acidification induced dissolution. This data would allow us to use the proposed surrogate models as predictive tools to investigate timescales of loadbearing capacity changes as well as the impact of those changes based on the time CWCs are exposed to acidified waters, and if combined with models detailing *where* corals of the future may be (Cordes et al., 2023), we can also start to assess the habitat *quality* of these reefs into the future.

5 Conclusion

We here investigated the critical size of a representative volume element of *L. pertusa* skeletons based on morphological variations to evaluate mechanical surrogate models of their skeletal structure. We proposed a size limit of five interbranch lengths that allows the determination of the type of model to be used based on the characteristic material architecture of coral skeletons. Our morphological analyses point to large variations between *L. pertusa* skeletal fragments and branches, as well as *dead* and *live* skeletal structures which are driven by growth and adaptation to environmental stressors. Spatially large colonies may be modelled using homogenized FE models by averaging the mechanical properties over five interbranch lengths, whereas small colonies may be modelled using specimen-specific beam-like FE models. Both approaches may allow us to efficiently scale up the analysis to entire reef systems to investigate reef crumbling due to the time they are exposed to acidified waters. Ultimately, this will support future conservation and management efforts by indicating which marine ecosystems are at greatest risk, when they will be at risk, and how much of an impact this will have on the biodiversity they support.

Data availability statement

The original contributions presented in the study are included in the article/Supplementary Material. Further inquiries can be directed to the corresponding authors.

Author contributions

MPF: Conceptualization, Data curation, Formal analysis, Investigation, Methodology, Validation, Visualization, Writing – original draft, Writing – review & editing. JW: Methodology, Writing – review & editing. JB: Data curation, Investigation, Writing – review & editing. JMR: Funding acquisition, Writing – review & editing. SH: Conceptualization, Funding acquisition, Project administration, Resources, Supervision, Writing – review & editing. UW: Conceptualization, Funding acquisition, Project administration, Resources, Supervision, Writing – review & editing.

Funding

The author(s) declare financial support was received for the research, authorship, and/or publication of this article. This work was supported by a Leverhulme Trust Research Project Grant to UW (RPG-2020-215) and an Independent Research Fellowships to SH (NE/K009028/1, NE/K009028/2). Norwegian coral samples were collected as part of the German coordinated BMBF (Federal Ministry of Education and Research)-funded project BIOACID II (FKZ 03F0655A). This paper is a contribution to the European Union's Horizon 2020 research and innovation program under grant agreement no. 678760 (ATLAS) and no. 818123 (iAtlantic), and the UKRI GCRF One Ocean Hub (NE/S008950/1). It reflects the authors' views, and the European Union is not responsible for any use that may be made of the information it contains.

Acknowledgments

The authors acknowledge Dr Jürgen Titschack for providing the CT datasets. We would also like to thank Dr Carola Daniel for her assistance during CT imaging at the University of Edinburgh and captains and crews of research cruises POS455 (2013) and POS473 (2014) with RV POSEIDON during which Norwegian samples were collected.

Conflict of interest

The authors declare that the research was conducted in the absence of any commercial or financial relationships that could be construed as a potential conflict of interest.

The author(s) declared that they were an editorial board member of Frontiers, at the time of submission. This had no impact on the peer review process and the final decision.

Publisher's note

Supplementary material

The Supplementary Material for this article can be found online at: https://www.frontiersin.org/articles/10.3389/fmars.2024.1456505/full#supplementary-material

References

Addamo, A. M., Martínez-Baraldés, I., Vertino, A., López-González, P. J., Taviani, M., and Machordom, A. (2015). Morphological polymorphism of Desmophyllum dianthus (Anthozoa: Hexacorallia) over a wide ecological and biogeographic range: Stability in deep habitats? *Zool Anz* 259, 113–130. doi: 10.1016/j.jcz.2015.10.004

Addamo, A. M., Vertino, A., Stolarski, J., García-Jiménez, R., Taviani, M., and Machordom, A. (2016). Merging scleractinian genera: The overwhelming genetic similarity between solitary Desmophyllum and colonial Lophelia. *BMC Evol. Biol.* 16, 108. doi: 10.1186/s12862-016-0654-8

Barnhill, K. A., Roberts, J. M., Myers-Smith, I., Williams, M., Dexter, K. G., Ryan, C., et al. (2023). Incorporating dead material in ecosystem assessments and projections. *Nat. Clim Chang* 13, 113–115. doi: 10.1038/s41558-022-01565-5

Beuck, L., Freiwald, A., and Taviani, M. (2010). Spatiotemporal bioerosion patterns in deep-water scleractinians from off Santa Maria di Leuca (Apulia, Ionian Sea). *Deep Res. Part II Top. Stud. Oceanogr* 57, 458–470. doi: 10.1016/j.dsr2.2009.08.019

Büscher, J. V., Form, A. U., Wisshak, M., Kiko, R., and Riebesell, U. (2022). Cold-water coral ecosystems under future ocean change: Live coral performance vs. framework dissolution and bioerosion. *Limnol Oceanogr.* 67, 2497–2515. doi: 10.1002/lno.12217

Büscher, J. V., Juva, K., Flögel, S., Wisshak, M., Rüggeberg, A., Riebesell, U., et al. (2024). Water mass characteristics and hydrodynamics at an inshore versus an offshore mid-Norwegian cold-water coral reef habitat. *Front. Mar. Sci.* 11, 1363542. doi: 10.3389/fmars.2024.1363542

Büscher, J. V., Wisshak, M., Form, A. U., Titschack, J., Nachtigall, K., and Riebesell, U. (2019). *In situ* growth and bioerosion rates of Lophelia pertusa in a Norwegian fjord and open shelf cold-water coral habitat. *PeerJ* 2019, 1–36. doi: 10.7717/peerj.7586

Caley, M. J., and St John, J. (1996). Refuge Availability Structures Assemblages of Tropical Reef Fishes. *Journal of Animal Ecology* 65(4), 414–428. doi: 10.2307/5777

Chamberlain, J., and Graus, R. R. R. (1975). Water flow and hydromechanical adaptations of branched reef corals. *Bull. Mar. Sci.* 25, 112–125.

Cole, A. J., Pratchett, M. S., and Jones, G. P. (2008). Diversity and functional importance of coral-feeding fishes on tropical coral reefs. *Fish and Fisheries* 9, 286–307. doi: 10.1111/j.1467-2979.2008.00290.x

Cordes, E. E., Mienis, F., Gasbarro, R., Davies, A., Baco, A. R., Bernardino, A. F., et al. (2023). "A global view of the cold-water coral reefs of the world BT - cold-water coral reefs of the world,". Eds. E. Cordes and F. Mienis (Cham: Springer International Publishing) 19, 1–30. doi: 10.1007/978-3-031-40897-7_1

Cormen, T. H., Leiserson, C. E., Rivest, R. L., and Stein, C. (2001). *Introduction to algorithms. 2nd ed.* (Cambridge, MA: MIT Press and McGraw-Hill).

Cowin, S. C. (1985). The relationship between the elasticity tensor and the fabric tensor. *Mech. Mater* 4, 137–147. doi: 10.1016/0167-6636(85)90012-2

Cowin, S. C. (1986). Fabric dependence of an anisotropic strength criterion. *Mech. Mater* 5, 251–260. doi: 10.1016/0167-6636(86)90022-0

Davoodi Kermani, I., Schmitter, M., Eichinger, J. F., Aydin, R. C., and Cyron, C. J. (2021). Computational study of the geometric properties governing the linear mechanical behavior of fiber networks. *Comput. Mater Sci.* 199, 110711. doi: 10.1016/j.commatsci.2021.110711

De Clippele, L. H., Huvenne, V. A. I., Orejas, C., Lundälv, T., Fox, A., Hennige, S. J., et al. (2018). The effect of local hydrodynamics on the spatial extent and morphology of cold-water coral habitats at Tisler Reef, Norway. *Coral Reefs* 37, 253–266. doi: 10.1007/s00338-017-1653-y

Dirrenberger, J., Forest, S., and Jeulin, D. (2019). Computational Homogenization of Architectured Materials. In: Estrin, Y., Bréchet, Y., Dunlop, J., and Fratzl, P. (eds) Architectured Materials in Nature and Engineering. Springer Series in Materials Science, vol 282. Springer, Cham, Switzerland. doi: 10.1007/978-3-030-11942-3_4

Doube, M. (2015). The ellipsoid factor for quantification of rods, plates, and intermediate forms in 3D geometries. *Front. Endocrinol. (Lausanne)* 6. doi: 10.3389/fendo.2015.00015

Doube, M., Klosowski, M. M., Arganda-Carreras, I., Cordelières, F. P., Dougherty, R. P., Jackson, J. S., et al. (2010). BoneJ: Free and extensible bone image analysis in ImageJ. *Bone* 47, 1076–1079. doi: 10.1016/j.bone.2010.08.023

Drugan, W. J., and Willis, J. R. (1996). A micromechanics-based nonlocal constitutive equation and estimates of representative volume element size for elastic composites. *J. Mech. Phys. Solids* 44, 497–524. doi: 10.1016/0022-5096(96)00007-5

Farber, C., Titschack, J., Hanna Lydia Schönberg, C., Ehrig, K., Boos, K., Baum, D., et al. (2016). Long-term macrobioerosion in the Mediterranean Sea assessed by micro-computed tomography. *Biogeosciences* 13, 3461–3474. doi: 10.5194/bg-13-3461-2016

Gass, S. E., and Roberts, J. M. (2011). Growth and branching patterns of Lophelia pertusa (Scleractinia) from the North Sea. *J. Mar. Biol. Assoc. United Kingdom* 91, 831–835. doi: 10.1017/S002531541000055X

Georgoulas, K., Hennige, S., and Lee, Y. C. (2023). Smoothed particle hydrodynamics for modelling cold-water coral habitats in changing oceans. *J. Sea Res.* 192, 102358. doi: 10.1016/j.seares.2023.102358

Graus, R. R. Jr, Chamberlain, J. A., and Boker, A. M. M. (1977). Structural modification of corals in relation to waves and currents. *Stud. Geol* 4, 135–153.

Hagberg, A., Swart P, S., and Chult, D. (2008). Exploring Network Structure, Dynamics, and Function using NetworkX. *Proceedings of the Python in Science Conference.*

Harrigan, T. P., Jasty, M., Mann, R. W., and Harris, W. H. (1988). Limitations of the continuum assumption in cancellous bone. *J. Biomech* 21, 269–275. doi: 10.1016/0021-9290(88)90257-6

Hennige, S. J., Morrison, C. L., Form, A. U., Büscher, J., Kamenos, N. A., and Roberts, J. M. (2014). Self-recognition in corals facilitates deep-sea habitat engineering. *Sci. Rep.* 4, 6782. doi: 10.1038/srep06782

Hennige, S. J., Wicks, L. C., Kamenos, N. A., Perna, G., Findlay, H. S., and Roberts, J. M. (2015). Hidden impacts of ocean acidification to live and dead coral framework. *Proc. R Soc. B Biol. Sci.* 282, 28220150990. doi: 10.1098/rspb.2015.0990

Hennige, S. J., Wolfram, U., Wickes, L., Murray, F., Roberts, J. M., Kamenos, N. A., et al. (2020). Crumbling reefs and cold-water coral habitat loss in a future ocean: evidence of "Coralporosis" as an indicator of habitat integrity. *Front. Mar. Sci.* 7. doi: 10.3389/fmars.2020.00668

Hildebrand, T., Laib, A., Müller, R., Dequeker, J., Rüegsegger, P., Ller, R. M., et al. (1999). Direct three-dimensional morphometric analysis of human cancellous bone: microstructural data from spine, femur, iliac crest, and calcaneus. *J. Bone Miner Res.* 14, 1167–1174. doi: 10.1359/jbmr.1999.14.7.1167

Hill, R. (1963). Elastic properties of reinforced solids: Some theoretical principles. *J. Mech. Phys. Solids* 11, 357–372. doi: 10.1016/0022-5096(63)90036-X

Hollister, S. J., Brennan, J. M., and Kikuchi, N. (1994). A homogenization sampling procedure for calculating trabecular bone effective stiffness and tissue level stress. *J. Biomech* 27, 433–444. doi: 10.1016/0021-9290(94)90019-1

House, J. E., Brambilla, V., Bidaut, L. M., Christie, A. P., Pizarro, O., Madin, J. S., et al. (2018). Moving to 3D: Relationships between coral planar area, surface area and volume. *PeerJ* 6, e4280. doi: 10.7717/peerj.4280

Kanit, T., Forest, S., Galliet, I., Mounoury, V., and Jeulin, D. (2003). Determination of the size of the representative volume element for random composites: statistical and numerical approach. *Int. J. Solids Struct.* 40, 3647–3679. doi: 10.1016/S0020-7683(03)00143-4

Khalil, R., Kallel, S., Farhat, A., and Dlotko, P. (2022). Topological Sholl descriptors for neuronal clustering and classification. *PloS Comput. Biol.* 18, e1010229. doi: 10.1371/journal.pcbi.1010229

Khisaeva, Z. F., and Ostoja-Starzewski, M. (2006). On the size of RVE in finite elasticity of random composites. *J. Elast* 85, 153–173. doi: 10.1007/s10659-006-9076-y

Kline, D. I., Teneva, L., Okamoto, D. K., Schneider, K., Caldeira, K., Miard, T., et al. (2019). Living coral tissue slows skeletal dissolution related to ocean acidification. *Nat. Ecol. Evol.* 3, 1438–1444. doi: 10.1038/s41559-019-0988-x

Kruszyński, K. J., Kaandorp, J. A., and van Liere, R. (2007). A computational method for quantifying morphological variation in scleractinian corals. *Coral Reefs* 26, 831–840. doi: 10.1007/s00338-007-0270-6

Madin, J. S., and Connolly, S. R. (2006). Ecological consequences of major hydrodynamic disturbances on coral reefs. *Nature* 444, 477–480. doi: 10.1038/nature05328

Maquer, G., Musy, S. N., Wandel, J., Gross, T., and Zysset, P. K. (2015). Bone volume fraction and fabric anisotropy are better determinants of trabecular bone stiffness than other morphological variables. *J. Bone Miner Res.* 30, 1000–1008. doi: 10.1002/jbmr.2437

Mortensen, P. B., and Fossâ, J. H. (2006). *Species diversity and spatial distribution of invertebrates on deep-water Lophelia reefs in Norway*, Vol. 1868. 1849–1868.

Mortensen, P. B., Hovland, T., Fossâ, J. H., and Furevik, D. M. (2001). Distribution, abundance and size of Lophelia pertusa coral reefs in mid-Norway in relation to seabed characteristics. *J. Mar. Biol. Assoc. United Kingdom* 81 (4), 581–597. doi: 10.1017/S002531540100426X

Ohs, N., Collins, C. J., Tourolle, D. C., Atkins, P. R., Schroeder, B. J., Blauth, M., et al. (2021). Automated segmentation of fractured distal radii by 3D geodesic active contouring of *in vivo* HR-pQCT images. *Bone* 147, 115930. doi: 10.1016/j.bone.2021.115930

Pahr, D. H., and Zysset, P. K. (2008). Influence of boundary conditions on computed apparent elastic properties of cancellous bone. *Biomech Model. Mechanobiol* 7, 463–476. doi: 10.1007/s10237-007-0109-7

Pahr, D. H., and Zysset, P. K. (2009). A comparison of enhanced continuum FE with micro FE models of human vertebral bodies. *J. Biomech* 42, 455–462. doi: 10.1016/j.jbiomech.2008.11.028

Paulay, G. (1997). Diversity and distribution of reef organisms. in C. E. Birkeland, editor. *Life and death of coral reefs.* (New York, New York, USA: Chapman & Hall), 298–353.

Pasquini, L., Molinari, A., Fantazzini, P., Dauphen, Y., Cuif, J. P., Levy, O., et al. (2015). Isotropic microscale mechanical properties of coral skeletons. *J. R Soc. Interface* 12, 1–9. doi: 10.1098/rsif.2015.0168

Peña Fernández, M., Sasso, S. J., McPhee, S., Black, C., Kanczler, J., Tozzi, G., et al. (2022). Nonlinear micro finite element models based on digital volume correlation measurements predict early microdamage in newly formed bone. *J. Mech. Behav. BioMed. Mater* 132, 105303. doi: 10.1016/j.jmbbm.2022.105303

Pfeiffer, F., Rammerstorfer, F. G., and Salençon, J. (1997). *Continuum micromechanics* (Vienna: Springer Vienna). doi: 10.1007/978-3-7091-2662-2

Pothuaud, L., van Rietbergen, B., Charlot, C., Ozhinsky, E., and Majumdar, S. (2004). A new computational efficient approach for trabecular bone analysis using beam models generated with skeletonized graph technique. *Comput. Methods Biomech BioMed. Engin* 7, 205–213. doi: 10.1080/10255840412331285943

Quattrini, A. M., Gómez, C. E., and Cordes, E. E. (2017). Environmental filtering and neutral processes shape octocoral community assembly in the deep sea. *Oecologia* 183, 221–236. doi: 10.1007/s00442-016-3765-4

Rasser, M. W., and Riegl, B. (2002). Holocene coral reef rubble and its binding agents. *Coral Reefs* 21, 57–72. doi: 10.1007/s00338-001-0206-5

Roberts, J. M., Wheeler, A. J., and Freiwald, A. (2006). Reefs of the deep: The biology and geology of cold-water coral ecosystems. *Sci. (80-)* 312, 543–547. doi: 10.1126/science.1119861

Roberts, J. M., Wheeler, A., Freiwald, A., and Cairns, S. (2009). *Cold-water corals: the biology and geology of deep-sea coral habitats* (Cambridge: Cambridge University Press). doi: 10.1017/CBO9780511581588

Sanna, G., Büscher, J. V., and Freiwald, A. (2023). Cold-water coral framework architecture is selectively shaped by bottom current flow. *Coral Reefs* 42, 483–495. doi: 10.1007/s00338-023-02361-z

Sanna, G., and Freiwald, A. (2021). Deciphering the composite morphological diversity of Lophelia pertusa, a cosmopolitan deep-water ecosystem engineer. *Ecosphere* 12 (11), e03802. doi: 10.1002/ecs2.3802

Schindelin, J., Arganda-Carreras, I., Frise, E., Kaynig, V., Longair, M., Pietzsch, T., et al. (2012). Fiji: an open-source platform for biological-image analysis. *Nat. Meth* 9, 676–682. doi: 10.1038/nmeth.2019

Sebens, K. P., Witting, J., and Helmuth, B. (1997). Effects of water flow and branch spacing on particle capture by the reef coral Madracis mirabilis (Duchassaing and Michelotti). *J. Exp. Mar. Bio Ecol.* 211, 1–28. doi: 10.1016/S0022-0981(96)02636-6

Stauber, M., Huber, M., van Lenthe, G. H., Boyd, S. K., and Müller, R. (2004). A finite element beam-model for efficient simulation of large-scale porous structures. *Comput. Methods Biomech BioMed. Engin* 7, 9–16. doi: 10.1080/10255840410001656408

Storlazzi, C. D., Brown, E. K., Field, M. E., Rodgers, K., and Jokiel, P. L. (2005). A model for wave control on coral breakage and species distribution in the Hawaiian Islands. *Coral Reefs* 24, 43–55. doi: 10.1007/s00338-004-0430-x

Trias, D., Costa, J., Turon, A., and Hurtado, J. E. (2006). Determination of the critical size of a statistical representative volume element (SRVE) for carbon reinforced polymers. *Acta Mater* 54, 3471–3484. doi: 10.1016/j.actamat.2006.03.042

Vad, J., Orejas, C., Moreno-Navas, J., Findlay, H. S., and Roberts, J. M. (2017). Assessing the living and dead proportions of cold-water coral colonies: Implications for deep-water Marine Protected Area monitoring in a changing ocean. *PeerJ* 2017, 1–20. doi: 10.7717/peerj.3705

van Rietbergen, B., Weinans, H., Huiskes, R., and Odgaard, A. (1995). A new method to determine trabecular bone elastic properties and loading using micromechanical finite-element models. *J. Biomech* 28, 69–81. doi: 10.1016/0021-9290(95)80008-5

Von Euw, S., Zhang, Q., Manichev, V., Murali, N., Gross, J., Feldman, L. C., et al. (2017). Biological control of aragonite formation in stony corals. *Sci. (80-)* 356, 933–938. doi: 10.1126/science.aam6371

Vosburgh, F. (1982). Acropora reticulata : structure, mechanics and ecology of a reef coral. *Proc. R Soc. London Ser. B Biol. Sci.* 214, 481–499. doi: 10.1098/rspb.1982.0023

Wangpraseurt, D., Larkum, A. W. D., Ralph, P. J., and Kühl, M. (2012). Light gradients and optical microniches in coral tissues. *Front. Microbiol.* 3. doi: 10.3389/fmicb.2012.00316

Wisshak, M., Schönberg, C. H. L., Form, A., and Freiwald, A. (2012). Ocean acidification accelerates reef bioerosion. *PloS One* 7, e45124. doi: 10.1371/journal.pone.0045124

Wolfram, U., Peña Fernández, M., McPhee, S., Smith, E., Beck, R. J., Shephard, J. D., et al. (2022). Multiscale mechanical consequences of ocean acidification for cold-water corals. *Sci. Rep.* 12, 1–17. doi: 10.1038/s41598-022-11266-w

Zawada Kyle, J. A., Dornelas, M., and Madin, J. S. (2019b). Quantifying coral morphology. *Coral Reefs* 38, 1281–1292. doi: 10.1007/s00338-019-01842-4

Zawada Kyle, J. A., Dornelas, M., Madin, J. S., Baird, A. H., and Bridge, T. C. L. (2019a). *Morphological traits can track coral reef responses to the Anthropocene*. 33, 962–975. doi: 10.1111/1365-2435.13358

frontiers | Frontiers in Marine Science

TYPE Original Research
PUBLISHED 31 March 2025
DOI 10.3389/fmars.2025.1458014

OPEN ACCESS

EDITED BY
Jose Angel Alvarez Perez,
Universidade do Vale do Itajaí, Brazil

REVIEWED BY
Vadim Mokievsky,
P.P. Shirshov Institute of Oceanology (RAS), Russia
Teng Zhou,
Hainan University, China

*CORRESPONDENCE
Luciana Erika Yaginuma
luciana.yaginuma@unifesp.br

RECEIVED 01 July 2024
ACCEPTED 10 March 2025
PUBLISHED 31 March 2025

CITATION
Yaginuma LE, Gallucci F, Vieira DC, Gheller PF, Brito de Jesus S, Corbisier TN and Fonseca G (2025) Hybrid machine learning algorithms accurately predict marine ecological communities. *Front. Mar. Sci.* 12:1458014. doi: 10.3389/fmars.2025.1458014

Hybrid machine learning algorithms accurately predict marine ecological communities

Luciana Erika Yaginuma[1,2]*, Fabiane Gallucci[2], Danilo Cândido Vieira[2], Paula Foltran Gheller[1], Simone Brito de Jesus[2], Thais Navajas Corbisier[1] and Gustavo Fonseca[2]

[1]Instituto Oceanográfico, Universidade de São Paulo, São Paulo, Brazil, [2]Instituto do Mar, Universidade Federal de São Paulo, Santos, Brazil

Predicting ecological communities is highly challenging but necessary to establish effective conservation and monitoring programs. This study aims to predict the spatial distribution of nematode associations from 25 m to 2500 m water depth over an area of 350,000 km² and understand the major oceanographic processes influencing them. The study considered data from 245 nematode genera and 44 environmental parameters from 100 stations. Data was analyzed by means of a hybrid machine learning (ML) approach, which combines unsupervised and supervised methods. The unsupervised phase detected that the nematodes were geographically structured in six associations, each with representative genera. In the supervised stage, these associations were modeled as a function of the environmental features by five supervised algorithms (Support Vector Machine, Random Forest, k-Nearest Neighbors, Naive Bayes, and Stochastic Gradient Boosting), using 80% of the samples for training, leaving the remaining for testing. Among them, the random forest was the best model with an accuracy of 86.4% in the test portion. The Random Forest (RF) model recognized 8 environmental features as significant in predicting the associations. Depth, the concentration of dissolved oxygen in the water near the bottom, the quality and quantity of phytodetritus, the proportion of coarse sand and carbonate, the sediment skewness, pH, and redox potential were the most important features structuring them. The inference of each association across the whole study area was based on the modeling results of the 8 significant environmental features. This model still correctly classified 90% of test data. Such findings demonstrated that it is possible to infer the spatial distribution of the nematode associations using only a small set of environmental features. The recommendation is thus to permanently monitor these environmental variables and run the ML models. Implementing ML approaches in monitoring programs of benthic systems will increase our prediction capacity, reduce monitoring costs, and, ultimately, support the conservation of marine systems.

KEYWORDS

nematodes, marine environment, artificial intelligence, supervised learning, unsupervised learning, baseline, environmental monitoring

1 Introduction

Monitoring and predicting the state of marine ecosystems are essential for baseline studies, management actions, and conservation programs (Nichols and Williams, 2006). Assessing the state of ecosystems requires knowing the biological communities, their variability in space and time, and their response to environmental changes. Nevertheless, modeling the species composition of communities is still a challenge. It has been traditionally done based on classical statistical methods, such as canonical and redundancy analysis, which frequently return a low proportion of the explained variance (Makarenkov and Legendre, 2002; Vieira et al., 2019) and whose predictions are rarely explored. Part of this limitation is related to model assumptions and the nature of the data, such as a large number of zeros, unbalanced designs, multi-normal distribution, and missing data (Xu and Jackson, 2019). Machine learning (ML) modeling handles some of these limitations (Olden et al., 2008; Fonseca and Vieira, 2023). Furthermore, the principle of ML is to evaluate the model's predictive performance, a desirable aspect in the context of monitoring programs to anticipate undesirable environmental changes (Schuwirth et al., 2019).

There are various ML techniques with different degrees of learning complexity (Joshi, 2020). Each approach must be used considering the nature of the data and the problem itself (Zhou, 2012; Stupariu et al., 2022). In some specific tasks, to enhance model performance, a combination of complementary ML algorithms is performed in a sequence of analytical steps, commonly termed hybrid models (Ippolito et al., 2020; Bastille-Rousseau and Wittemyer, 2021; Kruk et al., 2022; He et al., 2023). A common approach among them is to reduce the dimensionality of a multivariate dataset based on an unsupervised learning method and then use the obtained groups as the response variable in a supervised learning method (Krueger et al., 2020; Carcillo et al., 2021; Pinto et al., 2021). In community ecology, such a two-phase hybrid approach could be useful. The first phase would consist of detecting distinct taxonomic groups, a common practice among ecologists (Clarke et al., 2014), followed by a supervised learning phase where the environmental data are used to predict the occurrence of the groups.

For oceanographic studies, ML holds promise (Rubbens et al., 2023). Environmental data like bathymetry, temperature, and surface primary productivity are obtained in high spatial-temporal resolution with sonars and satellite images, while biodiversity data are sparse and logistically challenging to obtain (Balmford and Gaston, 1999; Heink and Kowarik, 2010), particularly offshore. Accurate inferences of biodiversity based on environmental data are crucial for marine ecosystem monitoring and conservation (Guisan and Zimmermann, 2000; Guisan and Thuiller, 2005; Holon et al., 2018). One challenge of modeling marine biodiversity is that oceanographic processes are dynamic, differ in spatial extent, and interact with each other (Sonnewald et al., 2021). As such, while accurate predictions are needed, it is also important to extract the model features and the interactions within environmental data (Murdoch et al., 2019). It is based on the response of biological data and interactions between environmental variables that the major oceanographic processes can be understood and monitored.

The objective of this study is to predict, through a hybrid model, the spatial distribution of nematode associations from 25 m to 2500 m water depth over an area of approximately 350,000 km^2 along the Brazilian continental margin and understand the major oceanographic processes influencing them. Free-living marine nematodes are microscopic organisms mostly smaller than 0.5 mm that belong to the meiofauna (Giere, 2009). In marine sediments, nematodes are usually the most abundant component of the meiofauna. They are known as one of the best ecological indicators due to their ubiquitous presence in diverse ecosystems, with high abundance, diversity, and sensitivity to multiple environmental changes (Ridall and Ingels, 2021).

2 Methods

2.1 Study area and sampling design

The Santos Basin (SB) is located in the southeastern region of the Brazilian margin between the Campos Basin and Pelotas Basin. It is limited to the north by Cabo Frio High (22°S) and to the south by Florianopolis High (28.5°S). The basin occupies an area of approximately 350,000 km^2, bordering four Brazilian states along 271 km of the southeast coast and reaching down to 3000 m water depth in the São Paulo Plateau. The continental shelf is narrower (70 km) in the Cabo Frio region (Rio de Janeiro state, RJ) and wider off Santos city (230 km), in São Paulo state (SP), with declivity ranging from 1:600 to 1:1300 and shelf break depth varying from 120 m to 180 m (Mahiques et al., 2010).

Environmental and nematode assemblage data were obtained from sediment samples of the Santos Project – Santos Basin Environmental Characterization – by PETROBRAS/CENPES (Moreira et al., 2023). A total of 100 sampling stations were distributed in eight transects perpendicular to the coast and at 11 isobaths (25 m, 50 m, 75 m, 100 m, 150 m, 400 m, 700 m, 1000 m, 1300 m, 1900 m, and 2400 m). Twelve additional stations were sampled within the São Paulo Plateau region, between 1900 m and 2400 m, where most of the oil and gas production takes place. Sampling cruises were conducted in July 2019 at the continental slope and plateau (isobaths from 400 m to 2400 m) and in November 2019 at the continental shelf (from 25 m to 150 m).

2.2 Sampling and sample processing

Sediment samples were taken in three replicates with a spade-type box corer (0.25 m^2 surface area) or a modified Van Veen grab (231 L, 0.75 m^2 surface area), depending on the grain size of the sediment. Sampling was incomplete in stations P1 and B5, with only 2 successful replicates; in A7, H4, and G9, with only one successful replicate; and in G11 with no successful sampling. The nematode samples were taken from the larger samplers with a cylindrical corer

(5 cm diameter, 10 cm high, 19.63 cm^2 area), and were stored and fixed with 10% buffered formalin. Samples for 38 environmental variables were obtained from the same box corer or Van Veen. The variables were related to the content of phytopigments, organic matter, and carbonates, and the granulometry of the sediment and were analyzed by other research parties. Details of the variables such abbreviation, name, analytical method, and the reference for more information are provided in the Supplementary Table S1. Additionally, six variables related to bottom water's physicochemical properties and topographic characteristics were measured at each sampling station, totaling 44 environmental variables. More details about sampling and methodological analyses of the environmental variables are available in Moreira et al. (2023).

In the laboratory, nematodes were extracted from the sediment by density flotation technique (Somerfield et al., 2005) with Ludox TM 50 (Sigma-Aldrich) adjusted to the specific gravity of 1.18 g/cm^3, repeated 3x with each sample. Organisms were then transferred to 10% formalin and stained with Rose Bengal. Nematodes were counted in a Dollfus plate and abundances were adjusted to no. individuals/10 cm^2. For the genus identification, 200 specimens were randomly separated to be mounted on glass slides for identification, after a diafanization process with glycerol 5% (Seinhorst, 1962; De Grisse, 1965). After mounting, nematodes were identified to genus level or family level, in case the genus could not be identified, using the Nemys database (Nemys Eds, 2023) and pertinent nematode taxonomic literature. The nematode slides were deposited in the Biological Collection "Prof. Edmundo F. Nonato" (ColBIO-IOUSP, 2023). Identification counts were adjusted to sample abundance. The abundance, Shannon evenness, and relative dominance (abundance of the most abundant genus divided by the total number of individuals) were calculated per station. After sample processing, the mean abundance data of 261 Nematoda genera from 99 samples were used for analysis.

2.3 Data preprocessing

The proposed hybrid model combined unsupervised and supervised machine learning methods (Fonseca and Vieira, 2023). A total of 27 analytical steps, which were separated into five phases, were performed in this pipeline (Figure 1). The first phase consisted

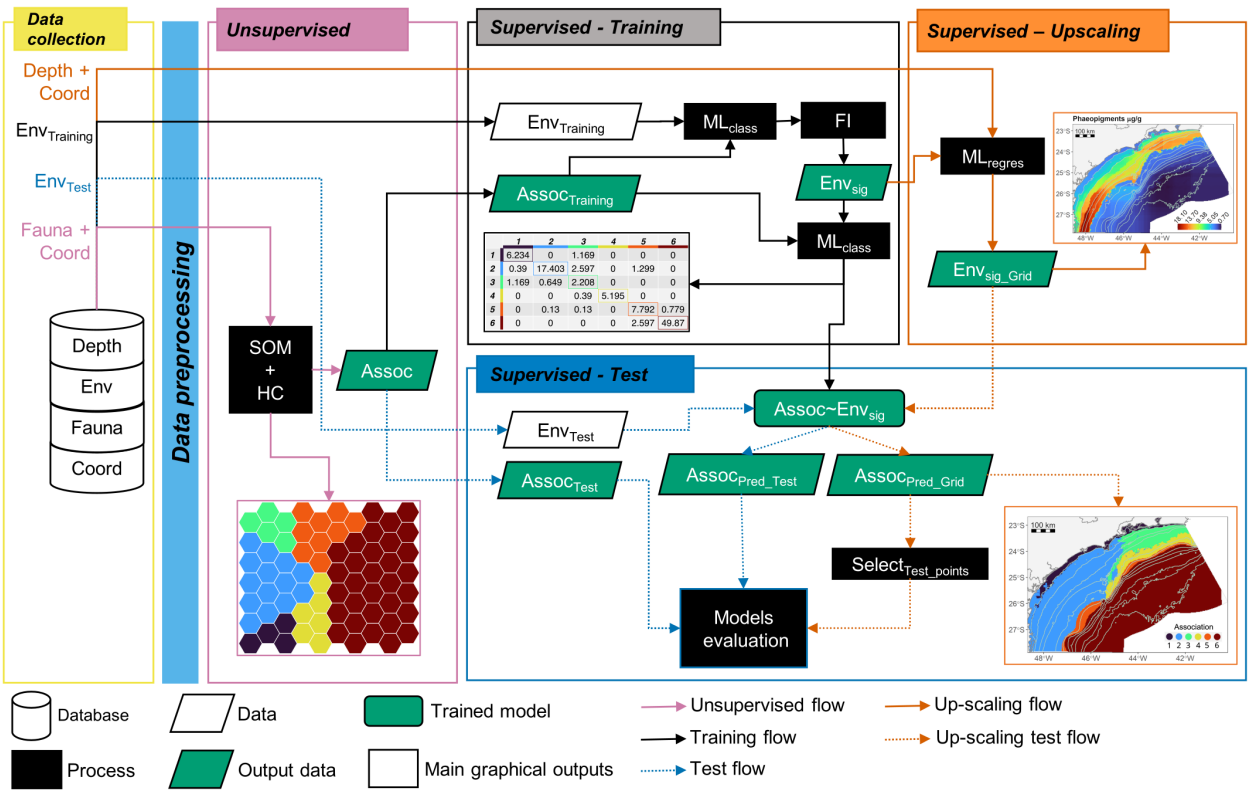

FIGURE 1
Analytical workflow highlighting the hybrid modeling approach implemented for the nematode assemblage data and the main outcomes. The analytical scheme is represented in five phases: Data collection, Unsupervised, Supervised-Training, Supervised Up-scaling, and Supervised-Test. Geometric forms represent the analytical processes and outputs, while the arrows represent the sequence of analytical steps. Depth, bathymetric data; Env, environmental data; Fauna, nematode genera data; Coord, coordinates data; SOM, Self Organizing Map analysis; HC, Hierarchical Clustering analysis; Assoc, taxonomic association data; ML_{class}, classification Machine Learning training model; FI, Feature Importance analysis; Env_{sig}, significant environmental features data; ML_{regres}, regression Machine Learning training model; Env_{sig_Grid}, significant environmental features modeled in a higher resolution grid data; Assoc~Env_{sig}, the trained model of the associations as function of the significant environmental features; $Assoc_{Pred\_*}$, Associations predicted using the Env_{Test} (*$_{Test}$) or the Env_{Sig_Grid} (*$_{Grid}$) as predictors; $Select_{Test\_points}$, selection of the gridded data to the points of the Test dataset.

of the data collection (yellow contour color in Figure 1) and the pre-processing steps (light blue rectangle in Figure 1). At this stage, imputation was used to fill in missing environmental data using a bagged tree model for each variable (as a function of all the others; Fonseca and Vieira, 2023). Also, highly correlated environmental variables were removed (cut off = 0.75), considering the largest mean absolute values of pairwise Spearman correlations (Kuhn, 2008; Supplementary Figure S1). After removing those variables, 24 features remained in the environmental data (Supplementary Figure S2). Hereafter, they are referred to as features since they have become input variables in the model. For the nematode data, a logarithm (log_{10}) transformation was applied.

2.4 Unsupervised phase

The second phase concerns the unsupervised analysis (light purple contour color in Figure 1), which involved a self-organizing map followed by a hierarchical clustering analysis (process box SOM + HC in Figure 1), to access and reduce the multivariate structure of the fauna into clusters (Assoc parallelogram in Figure 1). The self-organizing map (SOM) analysis is an unsupervised neural network method (Kohonen, 2001) used to aggregate similar samples into neurons, also termed map units (Best-Matching units – BMU). Here, we employed a SOM version with multiple layers (Wehrens and Buydens, 2007; Wehrens and Kruisselbrink, 2018). The dimensions of the grid was 7 x 10 neurons, with a hexagonal topology and a non-toroidal grid. The neighborhood function used was the Gaussian. The first layer was the nematode genera data with a weight of 0.95 and based on the Bray-curtis similarity index. The second layer was their respective coordinates, with a weight of 0.05 and based on the Euclidean distance. The second layer was implemented to account for potential spatial correlation between samples. For training, the complete dataset was presented 500 times to the network. Each neuron of the final map is composed of a weighted list of species termed codebook, meaning that all samples within a neuron will share the same codebook. Using the codebook provided by the SOM analysis, a hierarchical clustering (based on the Ward method with squared differences, "Ward2") was applied to group similar BMUs and their respective samples. To choose the number of groups formed by the clustering analysis a split moving window analysis was performed to detect a discontinuity in the relation between the number of groups and the within-cluster sum of squares (WSS). The groups of neurons are referred to hereafter as taxonomic associations (Assoc, Figure 1) and used as a descriptor of the fauna. The abundance, evenness, and relative dominance of each association were compared among the associations through analysis of variance (ANOVA). The ANOVA tests were performed in R language.

2.5 Supervised training

Following the unsupervised step of the hybrid model, each taxonomic association (Assoc, Figure 1) was further used as a response variable in the Supervised Training phase (black contour color in Figure 1). This phase aims to use the best set of environmental features to model and predict those clusters through machine-learning classification algorithms. First, samples were split for validation purposes in a way that ensured a balanced partition among the associations. The training dataset (80% of the data) was used for model fitting and the test dataset (20%) for further evaluation. Then, multiple machine learning classification algorithms were performed and compared: Naïve Bayes (NB), Support Vector Machine (SVM) Learning (linear and radial), K-nearest neighbor (knn), Random Forest (RF), and Stochastic Gradient Boosting Regression Trees (sgboost). Before running the SVM and knn algorithm, the environmental features were scaled by the root mean square. All the algorithms were performed using a cross-validation method with 5 folds and 10 repetitions, and a maximum of 10 tuning combinations were chosen, except for the sgboost. For each algorithm, the highest accuracy value was used to select the optimal model among the tuning combinations. The RF models were based on 500 trees. For the sgboost models, parameter shrinkage (or learning rate) was set at 0.1 and 0.05, the minimal number of observations in the terminal nodes of the trees was 10, the number of trees was 250 and 500 and the interaction depth was performed with 1 and 2. The model with the highest accuracy and Kappa metrics was selected to be used in the following steps (process box ML_{class} in Figure 1).

The significant environmental features (Env_{sig} parallelogram in Figure 1) from the most accurate model were retrieved using a feature importance analysis (box FI in Figure 1). Except for the RF algorithm, the importance of each feature of the environmental model was obtained by random permutation of the feature/variable while the others were kept unchanged (Breiman, 2001). This process disrupts the relationship between the feature and the target variable (Assoc). Permutations were repeated 100 times, corresponding to the null normally distributed population, and the observed metric (non-permuted model) was compared to it. The statistical significance (p-value) was obtained by retrieving the proportion of extreme permuted values higher than the observed one. For the RF algorithm, the significant environmental features were obtained using the randomForestExplainer package (Jiang et al., 2020). To get a more efficient model (Assoc~Env_{sig} in Figure 1), only the significant environmental features (Env_{sig}) data were then used to train the model of the associations ($Assoc_{training}$ parallelogram in Figure 1) using the same ML_{class} algorithm selected before. Additionally, boxplots of the environmental features were performed to understand the differences in the environmental conditions among the associations.

2.6 Supervised upscaling

Once the model Assoc~Env_{sig} had been trained, the next step was to predict the taxonomic associations in a 2 km x 2 km grid (orange contour color in Figure 1). To achieve this, we first modeled each significant environmental feature (Env_{sig}) obtained from the feature importance analysis (FI) as a function of water depth and geographical coordinates. The most accurate regression ML

algorithms among the SVM Learning (linear and radial), knn, RF, and sgboost were used to build each model. The hyperparameters of the algorithms used in this phase were the same as those used in the Supervised Training phase. After running all the models, we obtained 100,555 data points for each significant environmental feature (Env_{sig_Grid} parallelogram in Figure 1). This newly created dataset was then used as predictors for the Assoc~Env_{sig} model (orange dotted arrows in Figure 1) to obtain the predictions of the taxonomic associations in a 2 km x 2 km grid ($Assoc_{Pred\_Grid}$ parallelogram in Figure 1).

2.7 Supervised test

To evaluate the performance of our predictions (blue contour color in Figure 1), the observed associations separated for test ($Assoc_{Test}$, Figure 1) were compared to those inferred from the environmental features from the test dataset ($Assoc_{Pred\_test}$ parallelogram in Figure 1) and those inferred from the environmental features modeled in the upscaling phase ($Assoc_{Pred\_Grid}$ parallelogram in Figure 1). Both comparisons were made based on a confusion matrix, performance metrics (accuracy and Kappa coefficient), and individual predictions at each sampling station. Based on these outcomes, it is possible to determine how much information is lost, or not, when inferring the community associations solely based on the inferences from the environmental models.

2.8 Software

All the analytical steps and outputs were done in the iMESc - An Interactive Machine Learning App for Environmental Science, which is an open-source application built on R language (Vieira et al., 2025) that can be downloaded at https://zenodo.org/record/7278042. A user guide to the application is available at https://danilocvieira.github.io/iMESc_help/#introduction. The dataset and the analysis are accessible by downloading the Savepoints at https://github.com/DaniloCVieira/imesc_savepoints and restoring them following the guide "Savepoint" at the help page of the iMESc. The selection of points from the gridded data to the points of the test data (box $Select_{Test\_points}$ in Figure 1) and the calculation of metrics between the predictions of the Test data and the gridded data (box Models evaluation in Figure 1) were made using R language. The code script can also be download at the provided link for the Savepoints. More information about the iMESc application is available in Vieira et al. (2025).

3 Results

3.1 Unsupervised phase of the hybrid model

3.1.1 Nematode associations

A total of 245 nematode genera were identified. The most abundant genera were *Sabatieria*, *Halalaimus*, *Acantholaimus*, and *Microlaimus*, representing 14.1%, 5.3%, 4.2%, and 4.2% of all individuals, respectively. The SOM analysis stabilized after a learning rate of around 0.045 for the nematode data and 0.06 for the coordinate data. The SOM network explained 75.65% of the data variance with a mean topographic error of 0.41 (Table 1). The hierarchical clustering analysis revealed that the optimal number of taxonomic associations (Assoc) was 6, with association number 6 being the most different (Figure 2A) and with more samples (Figure 2B). The spatial distribution of the associations followed a depth pattern throughout the basin and a north-south pattern on the continental shelf, where each association showed a distinct spatial extent (Figure 2D). Association 1 occurred in the shallowest region along the basin, Associations 3 and 4 occurred in the northern region of the continental shelf, while Association 2 occurred in the southern. Associations 5 and 6 were respectively restricted to the slope and plateau regions along the whole basin. The most abundant genus, *Sabatieria*, was dominant in Associations 2, 3, 4, and 5 (Table 2). Association 1 was characterized by higher abundances of *Chomadorina*, *Microlaimus*, *Daptonema*, and *Sabatieria*. In Association 6, *Monhystrella* and *Acantholaimus* predominated.

3.1.2 Univariate descriptors of the nematode associations

Abundance per station varied from 40 to 1,758 individual/10 cm^2 (mean = 511 ± 392 individual/10 cm^2), genus richness from 43 to 105 genera, evenness from 0.64 to 0.88 (mean value = 0.80 ± 0.04), and relative dominance from 0.07 to 0.43 (mean value = 0.18 ± 0.06). All measures varied significantly among the associations (Supplementary Table S2). Abundance was higher in Association 3, followed by Associations 1, 2, and 5, and lower in Associations 4 and 6 (Figure 2C). Associations 1 and 5 showed higher richness than Associations 2 and 6. Association 2 differed from Associations 1, 3, 5, and 6 by showing lower evenness, and Association 1 showed higher evenness than Associations 2 and 4. The relative dominance of Associations 2 and 4 was significantly higher than that of Associations 1, 5, and 6.

3.2 Nematoda associations model

The accuracy of the training models of the six ML algorithms varied from 0.80 to 0.88 and the kappa index from 0.69 to 0.83 (Table 3). The Random Forest (RF) algorithm was the most

TABLE 1 Quality measures of the nematode and coordinate layer and the mean value of the trained SOM.

	Nematoda	Coordinates	Mean
Quantization error	50.89	0.77	25.83
Percentage of explained variance	66.87	84.42	75.65
Topographic error	0.01	0.82	0.41
Kaski-Lagus error	11.85	3.06	7.46
Neuron Utilization error	0.24		

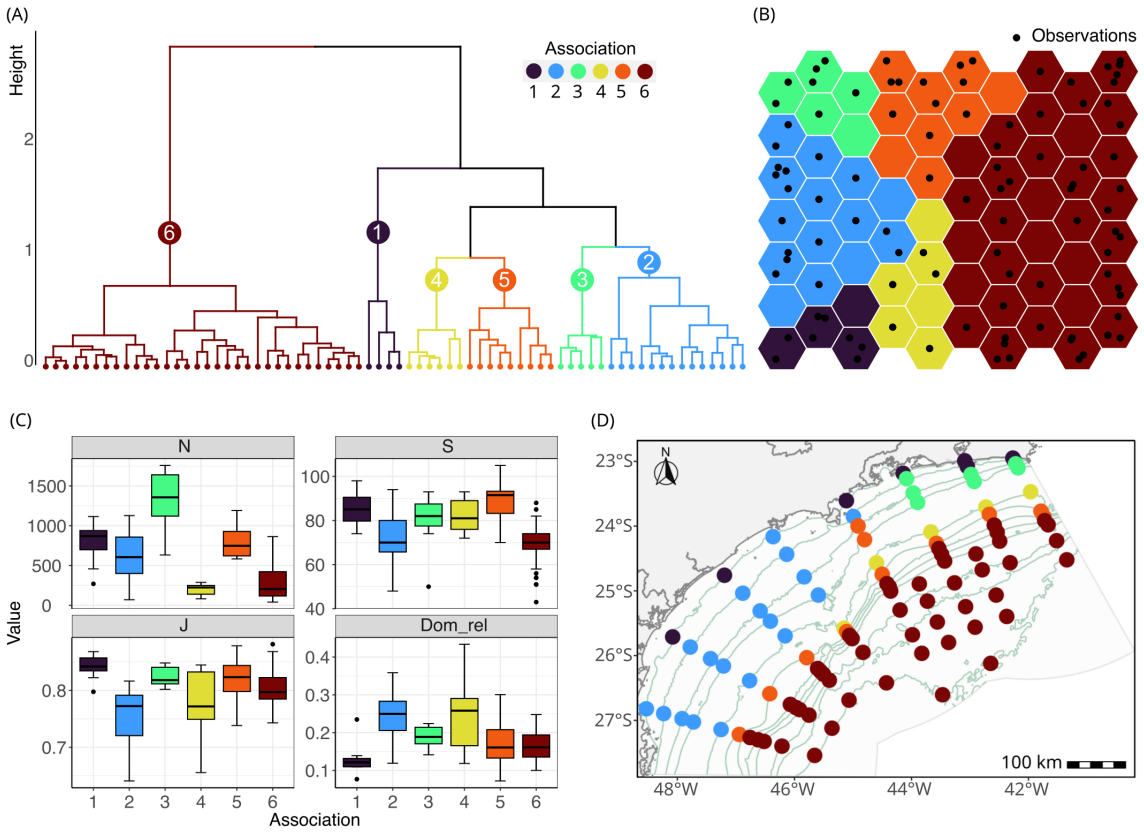

FIGURE 2
Nematode associations from the unsupervised phase of the hybrid model. **(A)** Dendrogram obtained by the hierarchical clustering of the neurons from the Self Organizing Map (SOM); **(B)** SOM with neurons grouped by the respective clusters; **(C)** box-plot of Richness, Abundance, Evenness, and Relative Dominance of each association, with the whiskers representing the minimum and maximum, the box the 25% and 75% quartiles, the line the median value and the dots the outliers; **(D)** map of the associations at each sampling station at the Santos Basin.

TABLE 2 Mean abundance, standard deviation (± SD) and relative abundance (%) of the most abundant genera (mean relative abundance >2% in at least one association) by each association.

Genus	1		2		3		4		5		6	
	Mean ± SD	%	Mean ± SD	%	Mean ± SD	%	Mean ± SD	%	Mean ± SD	%	Mean ± SD	%
Sabatieria	36.2 ± 29.2	**4.6**	127.9 ± 60.1	**20.9**	249.2 ± 89.2	**18.8**	47.1 ± 37	**24**	132.7 ± 54.3	**16.7**	19.5 ± 25	**7.1**
Monhystrella	0.3 ± 0.8	0	0.7 ± 1.8	0.1	1.1 ± 1.6	0.1	1.5 ± 1.1	0.8	22.6 ± 22.5	**2.8**	33.4 ± 23.6	**12.1**
Acantholaimus	6.9 ± 15	0.9	1.7 ± 3.1	0.3	1 ± 1.6	0.1	4.8 ± 3.1	2.4	34 ± 24.7	**4.3**	32.9 ± 21.9	**12**
Microlaimus	42.3 ± 41	**5.4**	57.5 ± 66.3	**9.4**	50.2 ± 39.3	**3.8**	3.7 ± 3.9	1.9	12.2 ± 9.2	1.5	4.8 ± 4.9	1.7
Halalaimus	15.4 ± 10.5	2	14.7 ± 8.5	2.4	52.8 ± 21.2	**4**	11.2 ± 6.3	**5.7**	50.2 ± 15.9	**6.3**	25.4 ± 18.7	**9.3**
Richtersia	29.9 ± 41.2	**3.8**	23.3 ± 32.5	**3.8**	49.1 ± 14.5	**3.7**	14.2 ± 19.1	**7.2**	9.1 ± 13.7	1.1	0 ± 0.1	0
Cervonema	1.1 ± 2	0.1	4.4 ± 3.4	0.7	23.3 ± 9.9	1.8	1.1 ± 0.8	0.5	48.1 ± 28.3	**6**	9.4 ± 12.2	**3.4**
Chromadorina	43.2 ± 42	**5.5**	0.5 ± 1.1	0.1	7.4 ± 7.7	0.6	1.4 ± 1.2	0.7	1.9 ± 3.4	0.2	0.4 ± 1.2	0.1
Terschellingia	7.4 ± 10.8	0.9	31.4 ± 67.1	**5.1**	21 ± 17.8	1.6	0.4 ± 0.4	0.2	4 ± 3.4	0.5	0.4 ± 0.5	0.2
Daptonema	36.4 ± 63.4	**4.6**	15.1 ± 14.7	2.5	35.2 ± 29.4	2.7	4.7 ± 3.6	2.4	17.9 ± 5.9	2.2	5.3 ± 7.3	1.9

(Continued)

10.3389/fmars.2025.1458014

TABLE 2 Continued

Genus	1		2		3		4		5		6	
	Mean ± SD	%	Mean ± SD	%	Mean ± SD	%	Mean ± SD	%	Mean ± SD	%	Mean ± SD	%
Desmoscolex	9.1 ± 7.3	1.2	1.2 ± 1.8	0.2	28.6 ± 18.5	2.2	7.9 ± 1	**4**	17 ± 13.1	2.1	5.8 ± 5.1	2.1
Molgolaimus	11.6 ± 11.6	1.5	23.5 ± 35.9	**3.8**	31.7 ± 18.4	2.4	1.6 ± 0.5	0.8	19.4 ± 23.2	2.4	1.4 ± 1.8	0.5
Neotonchus	4.2 ± 6.4	0.5	10.6 ± 8.3	1.7	44.2 ± 36.9	**3.3**	2.5 ± 4.6	1.3	7.3 ± 8.9	0.9	0.1 ± 0.3	0
Pseudometachromadora	0.8 ± 1.4	0.1	4.7 ± 7.7	0.8	42.4 ± 46.5	3.2	2.4 ± 4.6	1.2	5.2 ± 9.3	0.7	0 ± 0.2	0
Metasphaerolaimus	0.3 ± 0.7	0	1.2 ± 1.3	0.2	18 ± 19.1	1.4	0.3 ± 0.4	0.2	12.7 ± 10.8	1.6	7.9 ± 8.4	2.9
Comesoma	22.6 ± 32.7	2.9	1.1 ± 4.7	0.2	6.3 ± 11.4	0.5	0.1 ± 0.2	0.1	2.6 ± 6.4	0.3	0 ± 0	0
Thalassomonhystera	1.6 ± 3.7	0.2	0.3 ± 0.6	0	0.7 ± 1.3	0.1	1.2 ± 1.4	0.6	9.6 ± 9.8	1.2	7.4 ± 5.6	2.7
Pselionema	7.2 ± 4.8	0.9	13.5 ± 12.3	2.2	32.6 ± 25.1	2.5	1.5 ± 1.5	0.8	8.9 ± 5.3	1.1	2.8 ± 2.7	1
Paramonohystera	8.4 ± 14.4	1.1	14.3 ± 14.7	2.3	19.7 ± 13.9	1.5	0.4 ± 0.5	0.2	6.4 ± 3.8	0.8	2.2 ± 2.4	0.8
Rhynchonema	18 ± 13.8	2.3	0.9 ± 3.3	0.1	0 ± 0	0	0.1 ± 0.2	0	0.1 ± 0.4	0	0 ± 0	0
Paramphimonhystrella	0 ± 0	0	5.6 ± 7.5	0.9	11.2 ± 20	0.8	2.1 ± 2.2	1.1	18.1 ± 14.2	2.3	3.8 ± 4.5	1.4
Odontophora	5.6 ± 4.2	0.7	8.2 ± 12.3	1.3	29.6 ± 24.6	2.2	0 ± 0	0	0.5 ± 1.7	0.1	0 ± 0.1	0
Echinodesmodora	17.1 ± 15.2	2.2	0.6 ± 1.6	0.1	1.3 ± 2.3	0.1	3.5 ± 5.1	1.8	1.3 ± 4.4	0.2	0 ± 0.1	0
Leptolaimus	5.7 ± 7.9	0.7	13.1 ± 10.7	2.1	14.1 ± 18.6	1.1	2.7 ± 1.1	1.4	16.8 ± 12.1	2.1	5.9 ± 4.7	2.1
Amphimonhystrella	0.1 ± 0.3	0	1.7 ± 2.4	0.3	7.3 ± 13.2	0.6	1.5 ± 1.2	0.7	11.8 ± 15.2	1.5	5.7 ± 6.8	2.1
Syringolaimus	0 ± 0	0	0.1 ± 0.3	0	0 ± 0	0	2.6 ± 2.7	1.3	7 ± 6.3	0.9	5.7 ± 6.2	2.1
Campylaimus	3.7 ± 5.3	0.5	12.6 ± 15	2.1	24.4 ± 15.5	1.8	0.7 ± 0.6	0.3	4.8 ± 2.7	0.6	1.2 ± 1.1	0.4

The relative abundance of the four or five most abundant genera in each association are highlighted in bold. Number of observations in Associations 1 to 6 was 8, 18, 7, 5, 12, and 49, respectively.

accurate and the radial Support Vector Machine (SVM radial) was the least accurate. Considering the test part of the data, the Random Forest (RF) showed the best performance, with an accuracy of 0.91 and a Kappa index of 0.88 (Table 3), and was selected as the best model (ML_{class}) to be used in the following steps of the analytical workflow. Among the 24 environmental features, eight were significant (significance level = 0.05; Figure 3A) selected by the RF model. Among them, water column depth (Depth) was the most important feature with a mean minimal depth of 1.29, followed in decreasing order by the Chlorophyll-a/Phaeopigments ratio (Chloa_Phaeo), sediment redox potential (Redox), content of carbonates (Carbonates), angle of the slope, content of coarse sand (CSand), sediment pH, and concentration of phaeopigments (Phaeo) in the sediment. Recalculating the model based solely on

TABLE 3 Accuracy and Kappa index of the six models for the training and test sets.

Model		Training				Test	
		Accuracy	Kappa	Accuracy SD	Kappa SD	Accuracy	Kappa
RF		0.884	0.825	0.059	0.094	0.909	0.875
sgboost		0.844	0.763	0.071	0.108	0.818	0.740
SVM*	linear	0.814	0.725	0.090	0.140	0.818	0.743
SVM*	radial	0.798	0.688	0.070	0.110	0.682	0.543
knn*		0.798	0.690	0.081	0.133	0.773	0.677
NB		0.823	0.737	0.077	0.115	0.864	0.809

SD, standard deviation; NB, Naïve Bayes; SVM, Support Vector Machine; knn, K-nearest neighbor; RF, Random Forest; sgboost, Stochastic Gradient Boosting Trees. *environmental features data was scaled by the root mean square. Training set: 77 samples; Test set: 22 samples.

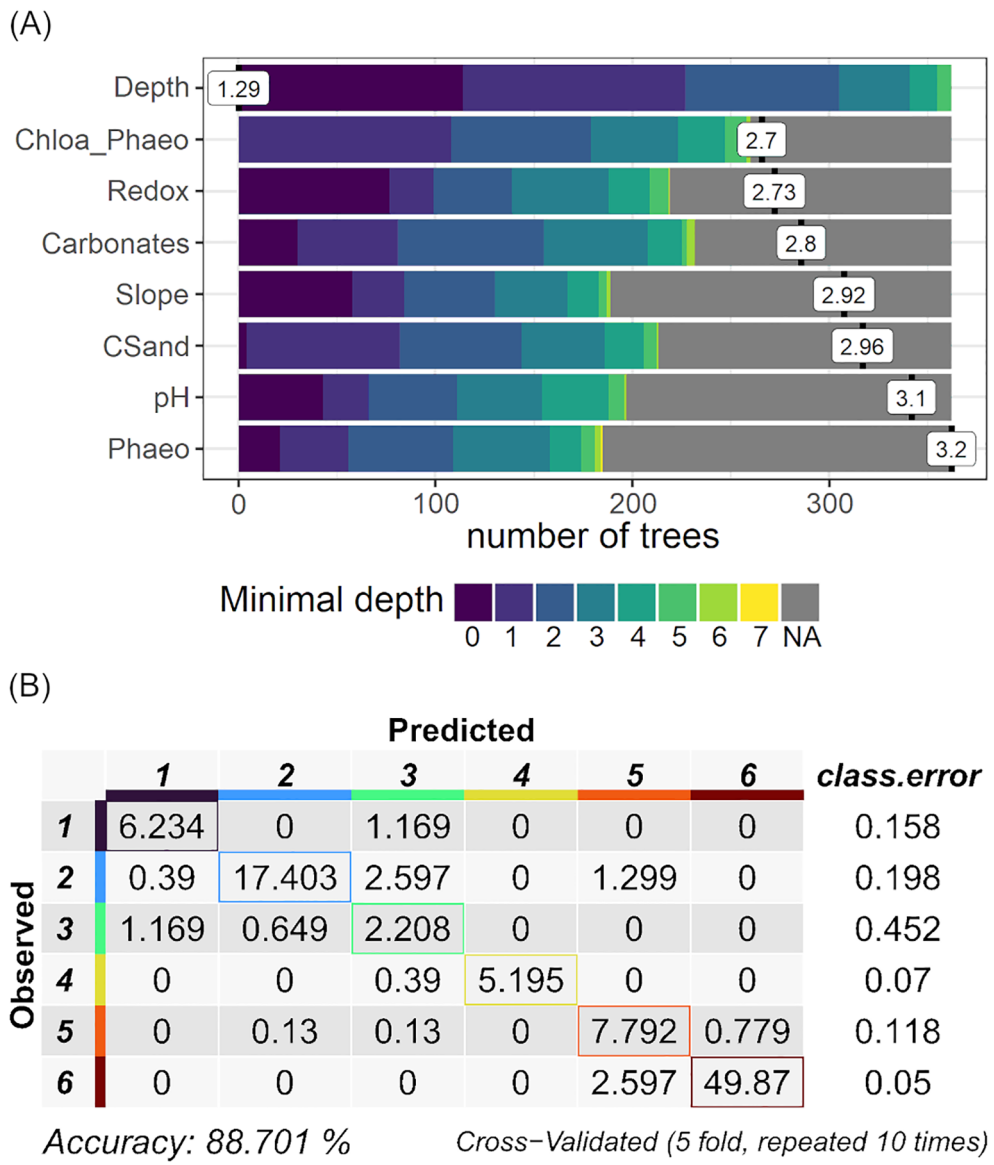

FIGURE 3
The Minimal Depth distribution **(A)** of the eight significant environmental features and **(B)** the confusion matrix from the training of the Random Forest model based on the significant environmental features. Depth: water column depth (m); Chloa_Phaeo: chlorophyll-a/phaeopigments ratio; Redox: sediment redox potential (mV); Carbonates: sediment content of carbonate; Slope: angle of the slope (°); CSand, sediment content of coarse sand; pH, sediment pH; Phaeo, sediment concentration of phaeopigments (µg/g).

those significant environmental features, the accuracy slightly raised to 0.89 (± 0.06) and the kappa index to 0.83 (± 0.09). Association 3 showed the highest error (0.45), misclassifying part of the samples as Association 1 or 2 (Figure 3B).

3.3 Simulated environmental features

The accuracy of the RF models (ML_{regres}) of the significant environmental features (Env_{sig}) as a function of the depth, latitude, and longitude varied from 0.45 for coarse sand to 0.74 for carbonate (Table 4). The spatial distribution of the environmental features showed that the ocean floor of the basin was heterogeneous (Figure 4). The sediment in the northern region of the continental shelf showed a higher content of coarse sand (Figure 4F). In this region, samples were classified as Associations 1 and 3 (Figure 2D) and were characterized by coarser sediment (Supplementary Figure S3D). The concentration of phaeopigments was higher on the continental shelf, with maximum values around the isobaths of 75 m and 100 m (Figure 4H). Samples of those isobaths were classified as Association 2 in the south and Association 3 in the north (Figure 2D), and presented the highest concentration of phaeopigments in the sediment (Supplementary Figure S3F). However, values were slightly higher in the shelf southern region, reflecting a lower proportion of fresh phytopigments, compared to the north, the slope, and the plateau (Figure 4B, Supplementary Figure S3A). The carbonate content was

TABLE 4 Results of the regression RF models of the significant environmental features (Env_{sig}) in predicting the nematode associations.

Variable	Training						Test		
	RMSE	R^2	MAE	RMSE SD	R^2 SD	MAE SD	RMSE	R^2	MAE
Chloa_Phaeo	0.07	0.64	0.06	0.01	0.13	0.01	0.06	0.84	0.04
Redox	101.58	0.51	71.27	17.65	0.15	12.56	64.77	0.75	48.61
Carbonates	0.11	0.74	0.08	0.02	0.10	0.02	0.08	0.78	0.06
Slope	0.76	0.60	0.49	0.17	0.15	0.11	1.48	0.24	0.98
CSand	0.08	0.45	0.06	0.02	0.26	0.01	0.07	0.28	0.05
pH	0.18	0.70	0.13	0.05	0.13	0.03	0.18	0.66	0.13
Phaeo	2.96	0.68	1.83	0.96	0.17	0.46	2.44	0.80	1.45

RMSE, root mean square error; R^2, percentage of variance explained; MAE, mean absolute error; SD, standard deviation. Chloa_Phaeo, chlorophyll-a/phaeopigments ratio; Redox, sediment redox potential (mV); Carbonates, sediment content of carbonate; Slope, angle of the slope (°); CSand, sediment content of coarse sand; pH, sediment pH; Phaeo, sediment concentration of phaeopigments (µg/g).

lower near the coast and increased towards the deep, though marked by a high peak around the 150 m isobath (Figure 4D). This peak matches the location of samples from Association 4 (Figure 2D), which exhibited a high carbonate content in the sediment (Supplementary Figure S3C). Both the redox potential and the pH of the sediment revealed an evident difference between the continental shelf and the slope and plateau, with lower values in the first region (Figures 4C, H).

3.4 Association predictions and model validations

The results of the model of the associations ($Assoc \sim Env_{sig}$) using the simulated significant environmental features in the 2 km x 2 km resolution grid (Env_{sig_Grid}) evidenced the depth-related arrangement of the taxonomic associations (Figure 5A) and the difference along the continental shelf between the South and North. Association 1 occupied the shallowest region, restricted by the 25 m isobath, along the entire basin. The continental shelf was occupied by Association 2 in the southern region and Associations 3 and 4 in the northern region. Association 5 occurred along the whole basin in a narrow band on the upper slope, around the 400 m isobath. Finally, Association 6 occupied the deeper region of the basin, from the middle slope to the plateau.

Comparing the observed association of the test dataset ($Assoc_{Test}$ in Figure 1) with the predictions of the supervised model based on the unseen environmental features ($Assoc_{Pred\_Test}$ in Figure 1) and the simulated significant environmental features ($Assoc_{Pred\_Grid}$; Figure 1) showed that both models classified all the associations of the test samples equally (Figure 5B). The total accuracy was 0.91 and the kappa index was 0.87. Specifically, both models misclassified only two of the 22 samples (Figure 5B).

4 Discussion

The proposed hybrid model predicted with 91% accuracy the spatial distribution of nematode associations as a function of a small set of important environmental features. From a theoretical standpoint, the reduction of dimensionality of the nematode data into associations, along with accurate predictions, suggests that the Basin is formed by distinct local communities, constituting a metacommunity (Wilson, 1992; Leibold et al., 2004). As shown by the feature importance analysis, these local communities are probably structured by depth, supply of potential food sources, such as Chlorophyll-*a* and Phaeopigments, topography, and the properties of the sediments, as well as other environmental variables that were highly correlated with them (Supplementary Figure S1).

Although depth is a key variable in predicting nematode associations, it is not, *per se*, an environmental driver of community structure; instead, it is a geographical variable that reflects a strong environmental gradient. Towards the deep, as we move away from the continental sources of sediments and organic matter and into less energetic environments, the granulometric characteristics of the sediment change, as well as its physicochemical properties and food availability (Suess, 1980; Mahiques et al., 1999; Restreppo et al., 2020). Along the Santos Basin, this was not different. On the continental shelf, sediment was coarser, with lower redox and pH values, and a higher contribution of fresher organic matter (Carreira et al., 2023; Figueiredo Jr. et al., 2023). On the other hand, muddy sediments extended over the slope and plateau, where the organic matter was scarcer and less fresh (Carreira et al., 2023; Figueiredo et al., 2023). The contrasting environmental conditions between the continental shelf and slope were also reflected in the fauna. The food-rich conditions of the continental shelf supported higher abundances of nematodes, as observed for Associations 1, 2, and 3 in contrast to Associations 4 and 6. The differences are also present in the taxonomic composition. For instance, Associations 1, 2, and 3 showed a greater abundance of typical genera from continental shelves worldwide, like *Sabatiera*, *Microlaimus*, and *Daptonema* (Muthumbi et al., 2004; Vanreusel et al., 2010; Muthumbi et al., 2011). In contrast, Association 6 was dominated by *Acantholaimus*, *Monhystrella*, and *Halalaimus*, common genera from slopes and

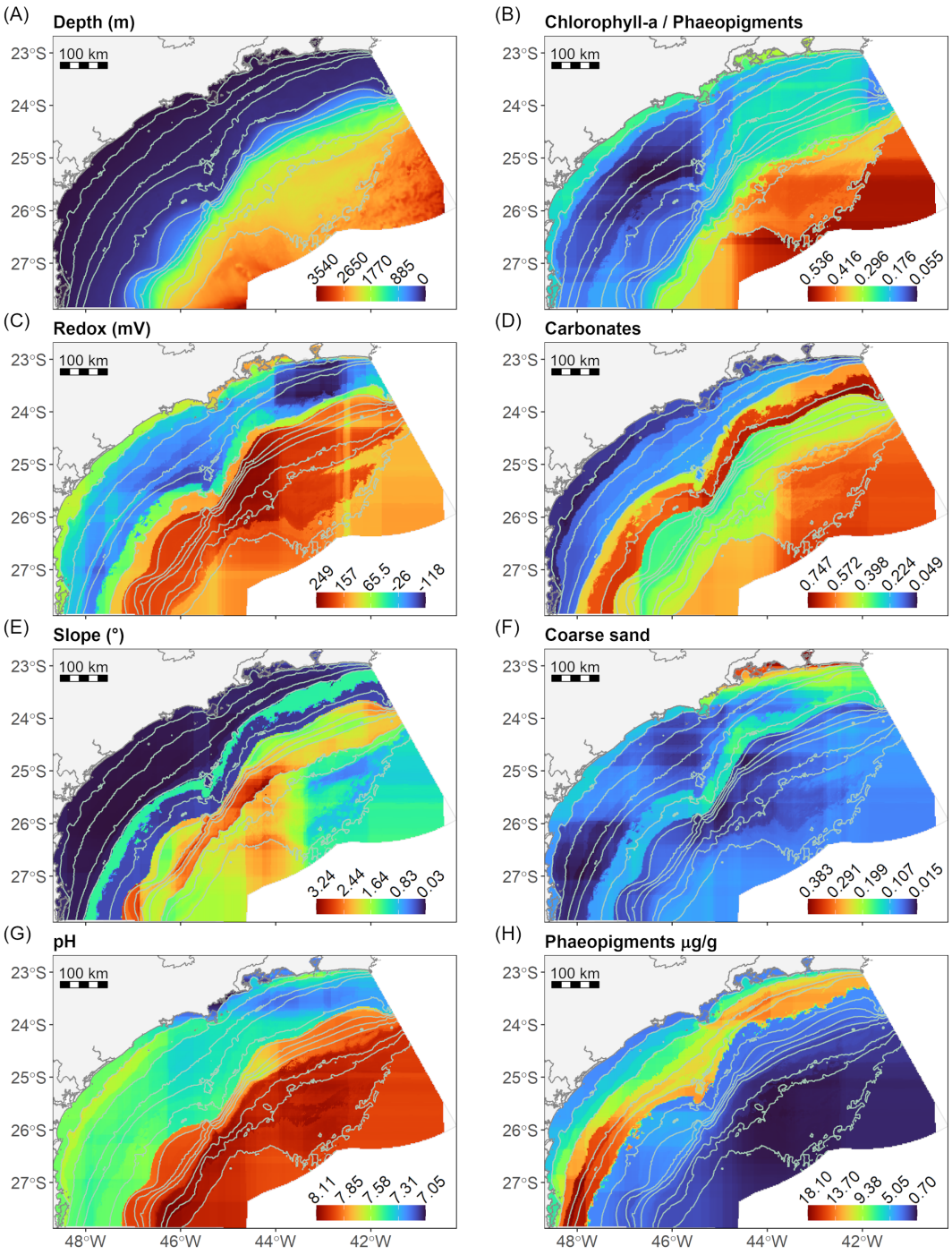

FIGURE 4
Spatial distribution maps of the significant environmental features (Env_{sig}) in predicting the nematode associations. Values plotted in the maps are the predictions of the random forest models of the environmental features as a function of depth and geographical coordinates in a 2 km x 2 km grid. **(A)** Depth: water column depth (m); **(B)** Chlorophyll-a/Phaeopigments ratio; **(C)** Redox: sediment redox potential (mV); **(D)** Carbonates: sediment content of carbonate; **(E)** Slope: angle of the slope (°);**(F)** Coarse Sand: sediment content of coarse sand grain fraction; **(G)** pH: sediment pH; **(H)** Phaeopigments: sediment concentration of phaeopigments (µg/g).

deep-sea habitats (Vanreusel et al., 2010; Macheriotou et al., 2021; Armenteros et al., 2022, 2024).

In the continental shelf, the north-south pattern was evidenced by Association 2 in the south and Associations 3 and 4 in the north. Such a pattern results from the boundary between two sedimentation zones related to different oceanographic processes (Mahiques et al., 1999). The south receives low-salinity and cold nutrient-rich waters from the Sub-Antarctic Argentinian shelf, the La Plata River runoff, and the Patos Lagoon (Piola et al., 2000; de Souza and Robinson, 2004; Brandini et al., 2018). The interaction of

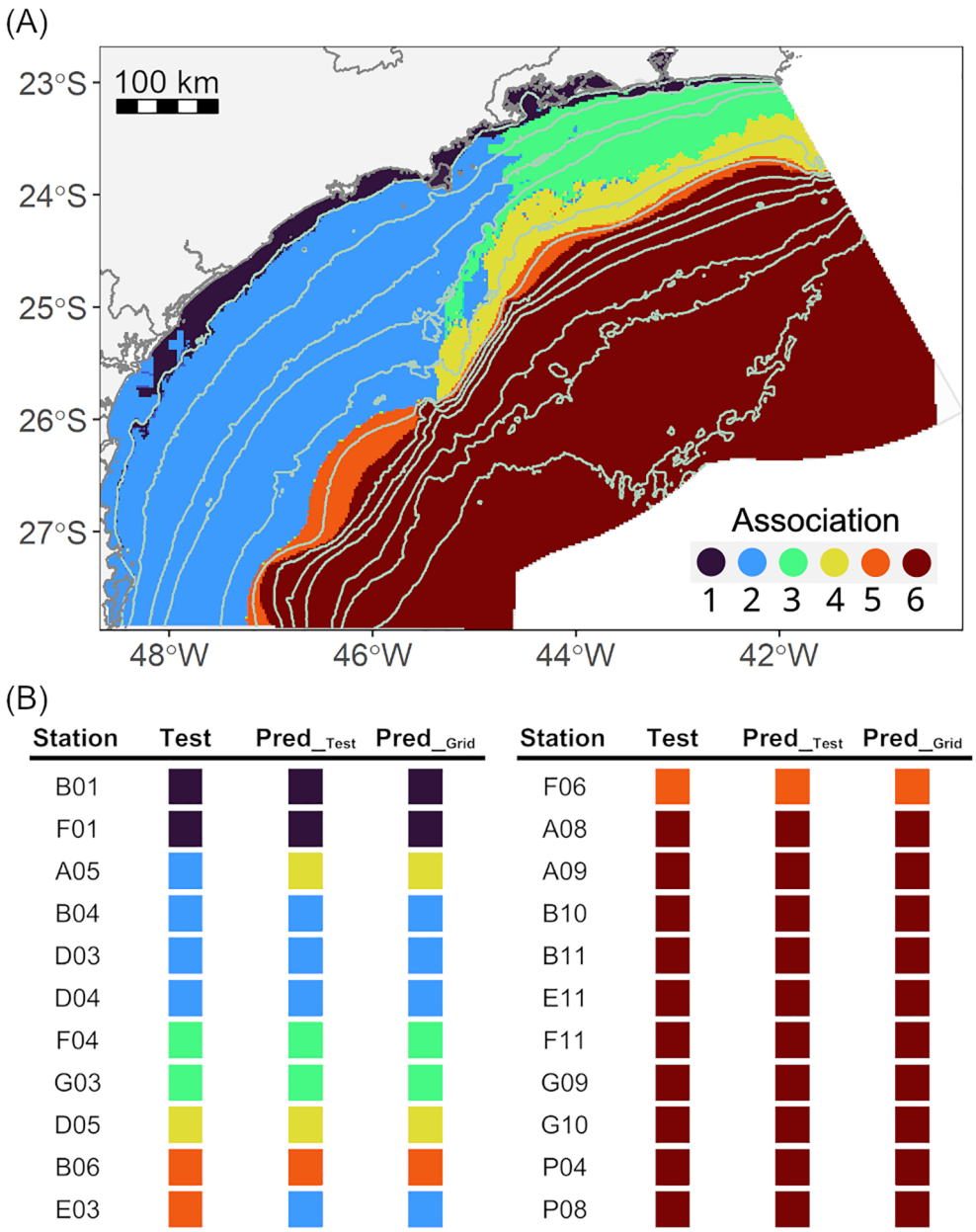

FIGURE 5
(A) Predicted spatial distribution map of the nematode associations of the hybrid model: values plotted in the maps are the predictions of the six associations as a function of the simulated environmental features on a bathymetric grid of 2 km x 2 km ($Assoc_{Pred\_Grid}$ in Figure 1); **(B)** Observed (Test) and predicted ($Pred_{\_Test}$, $Pred_{\_Grid}$) associations of the test samples: $Pred_{\_Test}$ was predicted using the environmental features from the test dataset as predictors and $Pred_{\_Grid}$ using the simulated environmental features in a 2 km x 2 km grid.

those waters with the meandering of the Brazil Current and the morphology of the shelf increases the productivity and sedimentation rates, resulting in the predominance of finer and homogeneous sediments with an accumulation of organic matter (Carreira et al., 2023; Mahiques et al., 2010). High organic matter inputs in sediments stimulate bacterial activity, which leads to a reduced environment (Li et al., 2022). Genera like *Sabatieria*, *Microlaimus*, and *Terschellingia*, which were the most abundant of Association 2, are known to dominate sediments under such conditions (Van Gaever et al., 2009; Vanreusel et al., 2010). In the northern portion of the basin, high productivity events also occur here due to the onshore motion in the mid-shelf and the coastal upwelling of the South Atlantic Central Water (SACW). It promotes the deposition of higher-quality organic matter to the bottom (Brandini et al., 2018), impacting the benthic systems (Sumida et al., 2005; De Léo and Pires-Vanin, 2006). However, sediments are coarser and more heterogeneous in this region due to the complex hydrodynamics associated with the coastline shape and

narrower shelf (Mahiques et al., 1999, 2010; Figueiredo et al., 2023). Though genera like *Sabatieira* and *Microlaimus* remained abundant in Associations 3 and 4, typical genera of coarser sediment, like *Richtersia*, and deeper areas, like *Halalaimus*, become more abundant. Particularly for Association 4, characterized by carbonates from bioconstruction fields (Figueiredo et al., 2023), the abundance of *Desmoscolex* increased. This taxon is known for its affinity to habitats with carbonated structures (Vanreusel et al., 2010). As we go deeper, towards the slope and plateau, environments with muddy sediments and scarce organic matter dominate (Carreira et al., 2023). While Association 5 showed a transition in taxa composition between the shelf and the deeper stations, Association 6 was typical from deep seas worldwide, with low abundances and dominance of typical deep-sea genera (Vanreusel et al., 2010; Lins et al., 2017).

The results of this study improve our understanding of the spatial structure of the benthic community of the Basin. Our study provided a comprehensive analysis of the entire Santos Basin, different from studies with macrofaunal and foraminiferal communities in the same basin which were restricted to the shelf or slope and plateau areas (Araújo et al., 2023; Moura et al., 2023). As suggested by meiofauna higher taxa data, the upwelling of the South Atlantic Central Water (SACW) and the intrusion of waters from the south with the contribution of the La Plata River are the main processes structuring the benthos in the continental shelf (Gallucci et al., 2023; Moura et al., 2023). Compared with the patterns observed for the meiofauna, the present study analytically confirmed the existence of 6 benthic zones in the Basin. Both studies recognized the Lower Slope and Plateau, the Upper and Mid-Slope, and the Upwelling as unique zones. Nonetheless, while the meiofauna study separated the southern portion of the continental shelf in two, observing a tradeoff in the abundances of kinorhynch, polychaete, and copepods associated with the concentrations of phytodetritus (Gallucci et al., 2023), the nematode genera data separated a coastal area (Association 1) from the rest of the southern portion of the continental shelf (Association 2). It is suggestive that copepods, kinorhynchs, and polychaetes are more sensitive to changes in phytodetritus deposition (Landers et al., 2020; Pruski et al., 2021), while nematodes to changes in granulometric properties of the sediment. The differences in responses between nematodes and other meiofauna taxa have already been reported (e.g. Stark et al., 2020). Such findings demonstrate the importance of monitoring multiple ecological indicators since each may respond differently to environmental changes.

Compared to traditional analytical tools commonly applied in community ecology, our hybrid approach offers at least three advantages. The first is the possibility of making accurate predictions; the second is the selection of the essential environmental variables to make the predictions, and the third is the possibility of continuous learning with the increment of new data. Accurate predictions are essential in regions with limited data, especially regarding biodiversity data. Since human activities are constantly pressuring the systems, knowing ahead of the biodiversity of an unsampled location gives us better support for management decisions. As some data are less laborious and expensive to obtain than others, such as granulometry versus biodiversity data, selecting a set of predictors by the hybrid model permits optimizing sampling strategies, data processing, and ultimately, the efficiency of monitoring programs. Particularly for the Santos Basin, it is crucial now to include additional variability, such as temporal variation or data from unsampled regions, to validate the model's performance and enhance our understanding of the system. This can be done continually, allowing the model to improve with each new income (Fonseca and Vieira, 2023). The hybrid model approach can be applied to any scenario involving the simultaneous analysis of multiple species along with a set of environmental variables. By employing such a methodology, we move from the traditional hypothesis testing approach commonly applied to community ecology to a predictive modeling approach. Comprehensive baseline studies coupled with robust predictive models are the first steps toward implementing effective monitoring programs (Lindenmayer and Likens, 2010; Fonseca and Vieira, 2023). Based on them it is possible to predict the response of multiple ecological indicators to environmental changes and therefore build a roadmap for the validation of monitoring programs. This is a significant step towards the conservation of natural ecosystems.

Data availability statement

The datasets presented in this study can be found in online repositories. The names of the repository/repositories and accession number(s) can be found in the article/Supplementary Material.

Ethics statement

The manuscript presents research on animals that do not require ethical approval for their study.

Author contributions

LY: Conceptualization, Formal analysis, Investigation, Methodology, Writing – original draft, Writing – review & editing, Visualization. FG: Conceptualization, Funding acquisition, Investigation, Project administration, Resources, Supervision, Writing – review & editing. DV: Conceptualization, Formal analysis, Investigation, Methodology, Software, Visualization, Writing – review & editing. PG: Data curation, Investigation, Writing – review & editing. SB: Data curation, Investigation, Writing – review & editing. TC: Funding acquisition, Project administration, Resources, Supervision, Writing – review & editing. GF: Conceptualization, Formal analysis, Investigation, Methodology, Supervision, Writing – original draft, Writing – review & editing.

Funding

The author(s) declare that financial support was received for the research and/or publication of this article. Data used in this study were provided by the Santos Project - PCR-BS, which was funded, promoted, and executed by Petrobras. Petrobras was not involved in the analysis and interpretation of data, the writing of this article, or the decision to submit it for publication. GF receives support from CNPQ under grant number 306780/2022-4.

Acknowledgments

The authors acknowledge Petrobras for promoting and executing the Santos Project - PCR-BS, Daniel Moreira for coordinating the PCR-BS project, and Silvia Helena de Mello e Souza for coordinating the subproject "Benthos". We would also like to thank Prof. Alberto Figueiredo, Prof. Renato Carreira, and Prof. Cízia Mara Hercos for making environmental data available. We are grateful to the members of the meiofauna team for their valuable help and commitment to sample processing and Prof. Wandrey Watanabe for his valuable physical oceanography consultancy and help with graphical items. Gustavo Fonseca acknowledges the support of CNPQ under grant number 306780/2022-4.

Conflict of interest

The authors declare that the research was conducted in the absence of any commercial or financial relationships that could be construed as a potential conflict of interest.

Publisher's note

All claims expressed in this article are solely those of the authors and do not necessarily represent those of their affiliated organizations, or those of the publisher, the editors and the reviewers. Any product that may be evaluated in this article, or claim that may be made by its manufacturer, is not guaranteed or endorsed by the publisher.

Supplementary material

The Supplementary Material for this article can be found online at: https://www.frontiersin.org/articles/10.3389/fmars.2025.1458014/full#supplementary-material

References

Araújo, B. D., Yamashita, C., Santarosa, A. C. A., Rocha, A. V., Vicente, T. M., Mendes, R. N. M., et al. (2023). Deep-sea living (stained) benthic foraminifera from the continental slope and São Paulo Plateau, Santos Basin (SW Atlantic): ecological insights. *Ocean Coast. Res.* 71, e23025. doi: 10.1590/2675-2824071.22080bda

Armenteros, M., Marzo-Pérez, D., Pérez-García, J. A., Schwing, P. T., Ruiz-Abierno, A., Díaz-Asencio, M., et al. (2024). Setting an environmental baseline for the deep-sea slope offshore northwestern Cuba (Southeastern Gulf of Mexico) using sediments and nematode diversity. *Thalass. Int. J. Mar. Sci* 40, 931–945. doi: 10.1007/s41208-024-00691-5

Armenteros, M., Quintanar-Retama, O., and Gracia, A. (2022). Depth-related patterns and regional diversity of free-living nematodes in the deep-sea Southwestern Gulf of Mexico. *Front. Mar. Sci.* 9. doi: 10.3389/fmars.2022.1023996

Balmford, A., and Gaston, K. J. (1999). Why biodiversity surveys are good value. *Nature* 398, 204–205. doi: 10.1038/18339

Bastille-Rousseau, G., and Wittemyer, G. (2021). Characterizing the landscape of movement to identify critical wildlife habitat and corridors. *Conserv. Biol.* 35, 346–359. doi: 10.1111/cobi.13519

Brandini, F. P., Tura, P. M., and Santos, P. P. G. M. (2018). Ecosystem responses to biogeochemical fronts in the South Brazil Bight. *Prog. Oceanogr.* 164, 52–62. doi: 10.1016/j.pocean.2018.04.012

Breiman, L. (2001). Random forests. *Mach. Learn.* 45, 5–32. doi: 10.1023/A:1010933404324

Carcillo, F., Le Borgne, Y.-A., Caelen, O., Kessaci, Y., Oblé, F., and Bontempi, G. (2021). Combining unsupervised and supervised learning in credit card fraud detection. *Inf. Sci.* 557, 317–331. doi: 10.1016/j.ins.2019.05.042

Carreira, R. S., Lazzari, L., Ceccopieri, M., Rozo, L., Martins, D., Fonseca, G., et al. (2023). Sedimentary organic matter accumulation provinces in the Santos Basin, SW Atlantic: insights from multiple bulk proxies. *Ocean Coast. Res.* 71, e23030. doi: 10.1590/2675-2824071.22061rsc

Clarke, K. R., Gorley, R. N., Somerfield, P. J., and Warwick, R. M. (2014). *Change in marine communities: an approach to statistical analysis and interpretation. 3rd ed* (Plymouth: Primer-E Ltd).

ColBIO-IOUSP (2023). *Coleção Biológica Prof. Edmundo F. Nonato*. São Paulo, Brazil: Instituto Oceanográfico da Universidade de São Paulo.

De Grisse, A. (1965). A labour-saving method for fixing and transferring eelworms to anhydrous glycerin. *Landbouw Hogesch. OpzoekStns—Leerstoel Dierkd. Gent*. 4.

De Léo, F. C., and Pires-Vanin, A. M. S. (2006). Benthic megafauna communities under the influence of the South Atlantic Central Water intrusion onto the Brazilian SE shelf: A comparison between an upwelling and a non-upwelling ecosystem. *J. Mar. Syst.* 60, 268–284. doi: 10.1016/j.jmarsys.2006.02.002

de Souza, R. B., and Robinson, I. S. (2004). Lagrangian and satellite observations of the Brazilian Coastal Current. *Cont. Shelf Res.* 24, 241–262. doi: 10.1016/j.csr.2003.10.001

Figueiredo, J. A. G., Carneiro, J. C., and dos Santos Filho, J. R. (2023). Santos Basin continental shelf morphology, sedimentology, and slope sediment distribution. *Ocean Coast. Res.* 71, e23007. doi: 10.1590/2675-2824071.22064agfj

Fonseca, G., and Vieira, D. C. (2023). Overcoming the challenges of data integration in ecosystem studies with machine learning workflows: an example from the Santos project. *Ocean Coast. Res.* 71, e23021. doi: 10.1590/2675-2824071.22044gf

Gallucci, F., Fonseca, G., Vieira, D. C., Yaginuma, L. E., Gheller, P. F., Brito, S., et al. (2023). Predicting large-scale spatial patterns of marine meiofauna: implications for environmental monitoring. *Ocean Coast. Res.* 71, e23037. doi: 10.1590/2675-2824071.22070fg

Giere, O. (2009). *Meiobenthology: The Microscopic Motile Fauna of Aquatic Sediments. 2nd ed* (Berlin, Heidelberg: Springer). doi: 10.1007/978-3-540-68661-3

Guisan, A., and Thuiller, W. (2005). Predicting species distribution: offering more than simple habitat models. *Ecol. Lett.* 8, 993–1009. doi: 10.1111/j.1461-0248.2005.00792.x

Guisan, A., and Zimmermann, N. E. (2000). Predictive habitat distribution models in ecology. *Ecol. Model.* 135, 147–186. doi: 10.1016/S0304-3800(00)00354-9

He, B., Zhao, Y., Liu, S., Ahmad, S., and Mao, W. (2023). Mapping seagrass habitats of potential suitability using a hybrid machine learning model. *Front. Ecol. Evol.* 11. doi: 10.3389/fevo.2023.1116083

Heink, U., and Kowarik, I. (2010). What criteria should be used to select biodiversity indicators? *Biodivers. Conserv.* 19, 3769–3797. doi: 10.1007/s10531-010-9926-6

Holon, F., Marre, G., Parravicini, V., Mouquet, N., Bockel, T., Descamp, P., et al. (2018). A predictive model based on multiple coastal anthropogenic pressures explains

the degradation status of a marine ecosystem: Implications for management and conservation. *Biol. Conserv.* 222, 125–135. doi: 10.1016/j.biocon.2018.04.006

Ippolito, M., Ferguson, J., and Jenson, F. (2020). Improving facies prediction by combining supervised and unsupervised learning methods. *J. Pet. Sci. Eng.* 200, 108300. doi: 10.1016/j.petrol.2020.108300

Jiang, Y., Biecek, P., Paluszyńska, O., and Kobylinska, K. (2020). ModelOriented/randomForestExplainer: CRAN release 0.10.1 (v0.10.1). *Zenodo*. doi: 10.5281/zenodo.3941250

Joshi, A. V. (2020). *Machine Learning and Artificial Intelligence* (Cham: Springer International Publishing). doi: 10.1007/978-3-030-26622-6

Kohonen, T. (2001). *Self-Organizing Maps, Springer Series in Information Sciences* (Berlin, Heidelberg: Springer). doi: 10.1007/978-3-642-56927-2

Krueger, R., Beyer, J., Jang, W.-D., Kim, N. W., Sokolov, A., Sorger, P. K., et al. (2020). Facetto: combining unsupervised and supervised learning for hierarchical phenotype analysis in multi-channel image data. *IEEE Trans. Vis. Comput. Graph.* 26, 227–237. doi: 10.1109/TVCG.2019.2934547

Kruk, M., Goździejewska, A. M., and Artiemjew, P. (2022). Predicting the effects of winter water warming in artificial lakes on zooplankton and its environment using combined machine learning models. *Sci. Rep.* 12, 16145. doi: 10.1038/s41598-022-20604-x

Kuhn, M. (2008). Building predictive models in R using the caret package. *J. Stat. Software* 28, 1–26. doi: 10.18637/jss.v028.i05

Landers, S. C., Bassham, R. D., Miller, J. M., Ingels, J., Sánchez, N., and Sørensen, M. V. (2020). Kinorhynch communities from Alabama coastal waters. *Mar. Biol. Res.* 16, 494–504. doi: 10.1080/17451000.2020.1789660

Leibold, M. A., Holyoak, M., Mouquet, N., Amarasekare, P., Chase, J. M., Hoopes, M. F., et al. (2004). The metacommunity concept: a framework for multi-scale community ecology: The metacommunity concept. *Ecol. Lett.* 7, 601–613. doi: 10.1111/j.1461-0248.2004.00608.x

Li, S., Fang, J., Zhu, X., Spencer, R. G. M., Álvarez-Salgado, X. A., Deng, Y., et al. (2022). Properties of sediment dissolved organic matter respond to eutrophication and interact with bacterial communities in a plateau lake. *Environ. pollut.* 301, 118996. doi: 10.1016/j.envpol.2022.118996

Lindenmayer, D. B., and Likens, G. E. (2010). The science and application of ecological monitoring. *Biol. Conserv.* 143, 1317–1328. doi: 10.1016/j.biocon.2010.02.013

Lins, L., Leliaert, F., Riehl, T., Pinto Ramalho, S., Alfaro Cordova, E., Morgado Esteves, A., et al. (2017). Evaluating environmental drivers of spatial variability in free-living nematode assemblages along the Portuguese margin. *Biogeosciences* 14, 651–669. doi: 10.5194/bg-14-651-2017

Macheriotou, L., Rigaux, A., Olu, K., Zeppilli, D., Derycke, S., and Vanreusel, A. (2021). Deep-sea nematodes of the Mozambique channel: evidence of random community assembly dynamics in seep sediments. *Front. Mar. Sci.* 8. doi: 10.3389/fmars.2021.549834

Mahiques, M. M., Mishima, Y., and Rodrigues, M. (1999). Characteristics of the sedimentary organic matter on the inner and middle continental shelf between Guanabara Bay and São Francisco do Sul, southeastern Brazilian margin. *Cont. Shelf Res.* 19, 775–798. doi: 10.1016/S0278-4343(98)00105-8

Mahiques, M. M. D., Sousa, S.H.D.M.E., Furtado, V. V., Tessler, M. G., Toledo, F. A. D. L., Burone, L., et al. (2010). The Southern Brazilian shelf: general characteristics, quaternary evolution and sediment distribution. *Braz. J. Oceanogr.* 58, 25–34. doi: 10.1590/S1679-87592010000600004

Makarenkov, V., and Legendre, P. (2002). Nonlinear redundancy analysis and canonical correspondence analysis based on polynomial regression. *Ecology* 83, 1146–1161. doi: 10.1890/0012-9658(2002)083[1146:NRAACC]2.0.CO;2

Moreira, D. L., Dalto, A. G., Figueiredo, A. G. Jr., Valerio, A. M., Detoni, A. M. S., Bonecker, A. C. T., et al. (2023). Multidisciplinary scientific cruises for environmental characterization in the Santos Basin – methods and sampling design. *Ocean Coast. Res.* 71, e23022. doi: 10.1590/2675-2824071.22072dlm

Moura, R. B. D., Dalto, A. G., Sallorenzo, I. D. A., Moreira, D. L., and Lavrado, H. P. (2023). Community structure of the benthic macrofauna along the continental slope of Santos Basin and São Paulo plateau, SW Atlantic. *Ocean Coast. Res.* 71, e23032. doi: 10.1590/2675-2824071.22091rbdm

Murdoch, W. J., Singh, C., Kumbier, K., Abbasi-Asl, R., and Yu, B. (2019). Definitions, methods, and applications in interpretable machine learning. *Proc. Natl. Acad. Sci.* 116, 22071–22080. doi: 10.1073/pnas.1900654116

Muthumbi, A. W., Vanreusel, A., Duineveld, G., Soetaert, K., and Vincx, M. (2004). Nematode Community Structure along the Continental Slope off the Kenyan Coast, Western Indian Ocean. *Int. Rev. Hydrobiol.* 89, 188–205. doi: 10.1002/iroh.200310689

Muthumbi, W. A., Vanreusel, A., and Vincx, M. (2011). Taxon-related diversity patterns from the continental shelf to the slope: a case study on nematodes from the Western Indian Ocean. *Mar. Ecol.- Evol. Perspect.* 32, 453–467. doi: 10.1111/j.1439-0485.2011.00449.x

Nemys Eds. (2023). *Nemys: World Database of Nematodes*. Available online at: https://nemys.ugent.be (Accessed August 18, 2023).

Nichols, J. D., and Williams, B. K. (2006). Monitoring for conservation. *Trends Ecol. Evol.* 21, 668–673. doi: 10.1016/j.tree.2006.08.007

Olden, J. D., Lawler, J. J., and Poff, N. L. (2008). Machine learning methods without tears: A primer for ecologists. *Q. Rev. Biol.* 83, 171–193. doi: 10.1086/587826

Pinto, A., Pereira, S., Meier, R., Wiest, R., Alves, V., Reyes, M., et al. (2021). Combining unsupervised and supervised learning for predicting the final stroke lesion. *Med. Image Anal.* 69, 101888. doi: 10.1016/j.media.2020.101888

Piola, A. R., Campos, E. J. D., Möller, J. O. O., Charo, M., and Martinez, C. (2000). Subtropical Shelf Front off eastern South America. *J. Geophys. Res. Oceans* 105, 6565–6578. doi: 10.1029/1999JC000300

Pruski, A. M., Rzeznik-Orignac, J., Kerhervé, P., Vétion, G., Bourgeois, S., Péru, E., et al. (2021). Dynamic of organic matter and meiofaunal community on a river-dominated shelf (Rhône prodelta, NW Mediterranean Sea): Responses to river regime. *Estuar. Coast. Shelf Sci.* 253, 107274. doi: 10.1016/j.ecss.2021.107274

Restreppo, G. A., Wood, W. T., and Phrampus, B. J. (2020). Oceanic sediment accumulation rates predicted via machine learning algorithm: towards sediment characterization on a global scale. *Geo-Mar. Lett.* 40, 755–763. doi: 10.1007/s00367-020-00669-1

Ridall, A., and Ingels, J. (2021). Suitability of free-living marine nematodes as bioindicators: status and future considerations. *Front. Mar. Sci.* 8. doi: 10.3389/fmars.2021.685327

Rubbens, P., Brodie, S., Cordier, T., Destro Barcellos, D., Devos, P., Fernandes-Salvador, J. A., et al. (2023). Machine learning in marine ecology: an overview of techniques and applications. *ICES J. Mar. Sci.* 80, 1829–1853. doi: 10.1093/icesjms/fsad100

Schuwirth, N., Borgwardt, F., Domisch, S., Friedrichs, M., Kattwinkel, M., Kneis, D., et al. (2019). How to make ecological models useful for environmental management. *Ecol. Model.* 411, 108784. doi: 10.1016/j.ecolmodel.2019.108784

Seinhorst, J. W. (1962). Modifications of the elutriation method for extracting nematodes from soil. *Nematologica* 8, 117–128. doi: 10.1163/187529262X00332

Somerfield, P. J., Warwick, R. M., and Moens, T. (2005). "Meiofauna techniques," in *Methods for the Study of Marine Benthos. 3rd Edition*, A. Eleftheriou and A. McIntyre (Oxford: Blackwell), 229–272. doi: 10.1002/9780470995129.ch6

Sonnewald, M., Lguensat, R., Jones, D. C., Dueben, P. D., Brajard, J., and Balaji, V. (2021). Bridging observations, theory and numerical simulation of the ocean using machine learning. *Environ. Res. Lett.* 16, 073008. doi: 10.1088/1748-9326/ac0eb0

Stark, J. S., Mohammad, M., McMinn, A., and Ingels, J. (2020). Diversity, abundance, spatial variation, and human impacts in marine meiobenthic nematode and copepod communities at Casey Station, East Antarctica. *Front. Mar. Sci.* 7. doi: 10.3389/fmars.2020.00480

Stupariu, M.-S., Cushman, S. A., Pleşoianu, A.-I., Pătru-Stupariu, I., and Fürst, C. (2022). Machine learning in landscape ecological analysis: a review of recent approaches. *Landsc. Ecol.* 37, 1227–1250. doi: 10.1007/s10980-021-01366-9

Suess, E. (1980). Particulate organic carbon flux in the oceans - Surface productivity and oxygen utilization. *Nature* 288, 260–263. doi: 10.1038/288260a0

Sumida, P. Y. G., Yoshinaga, M. Y., Ciotti, Á.M., and Gaeta, S. A. (2005). Benthic response to upwelling events off the SE Brazilian coast. *Mar. Ecol. Prog. Ser.* 291, 35–42. doi: 10.3354/meps291035

Van Gaever, S., Galéron, J., Sibuet, M., and Vanreusel, A. (2009). Deep-sea habitat heterogeneity influence on meiofaunal communities in the Gulf of Guinea. *Deep Sea Res. Part II Top. Stud. Oceanogr.* 56, 2259–2269. doi: 10.1016/j.dsr2.2009.04.008

Vanreusel, A., Fonseca, G., Danovaro, R., Da Silva, M. C., Esteves, A. M., Ferrero, T., et al. (2010). The contribution of deep-sea macrohabitat heterogeneity to global nematode diversity: Nematode diversity and habitat heterogeneity. *Mar. Ecol.* 31, 6–20. doi: 10.1111/j.1439-0485.2009.00352.x

Vieira, D. C., Brustolin, M. C., Ferreira, F. C., and Fonseca, G. (2019). segRDA: An r package for performing piecewise redundancy analysis. *Methods Ecol. Evol.* 10, 2189–2194. doi: 10.1111/2041-210X.13300

Vieira, D. C., Paula, F. S., Yaginuma, L. E., and Fonseca, G. (2025). iMESc – an interactive machine learning app for environmental sciences. *Front. Environ. Sci.* 13. doi: 10.3389/fenvs.2025.1533292

Wehrens, R., and Buydens, L. M. C. (2007). Self- and super-organizing maps in R: the kohonen package. *J. Stat. Software* 21, 1–19. doi: 10.18637/jss.v021.i05

Wehrens, R., and Kruisselbrink, J. (2018). Flexible self-organizing maps in kohonen 3.0. *J. Stat. Software* 87, 1–18. doi: 10.18637/jss.v087.i07

Wilson, D. S. (1992). Complex interactions in metacommunities, with implications for biodiversity and higher levels of selection. *Ecology* 73, 1984–2000. doi: 10.2307/1941449

Xu, C., and Jackson, S. A. (2019). Machine learning and complex biological data. *Genome Biol.* 20, 76. doi: 10.1186/s13059-019-1689-0

Zhou, Z.-H. (2012). *Ensemble Methods: Foundations and Algorithms*. (New York: Chapman and Hall/CRC). doi: 10.1201/b12207

Frontiers in Marine Science

Explores ocean-based solutions for emerging global challenges

The third most-cited marine and freshwater biology journal, advancing our understanding of marine systems and addressing global challenges including overfishing, pollution, and climate change.

Discover the latest Research Topics

See more →

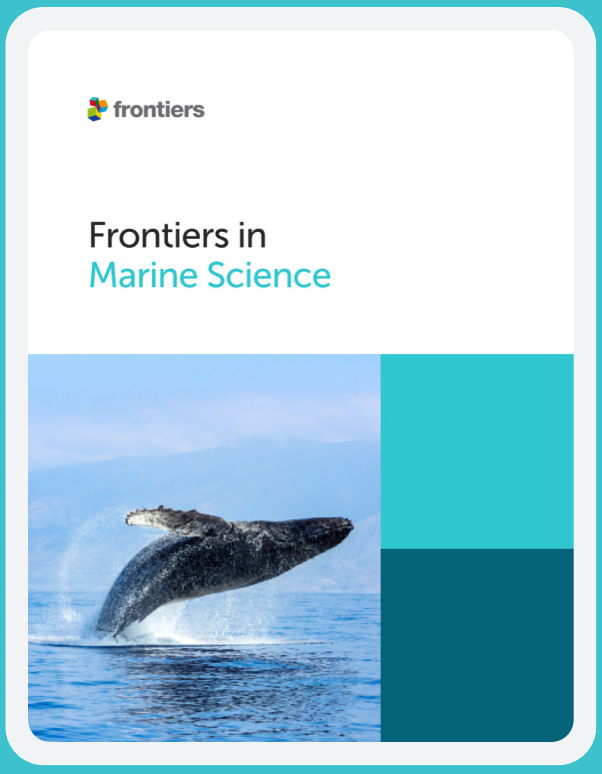

Frontiers

Avenue du Tribunal-Fédéral 34
1005 Lausanne, Switzerland
frontiersin.org

Contact us

+41 (0)21 510 17 00
frontiersin.org/about/contact